Geological Framework of the Mineral Deposits of the Collahuasi district, Región de Tarapacá, Chile

Timothy Ireland B.Sc.(Hons)

Submitted in fulfilment of the requirements of the degree of
Doctor of Philosophy

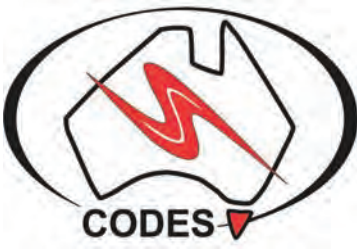

CODES ARC Centre of Excellence in Ore Deposits

University of Tasmania, Hobart, Australia

October, 2010

Declaration and Statement on Authority and Access.

This thesis claims originality for no material which has been accepted for a degree or diploma by the University or any other institution and, to the best of my knowledge and belief, contains no material that has been published or written by another person except where due acknowledgement is made in the text of this thesis.

Timothy Ireland

Date:

Confidentiality Statement:

This thesis is not to be made available for loan and copying until 2/04/2011.

Following that time, this thesis may be made available for loan and limited copying in accordance with the Copyright Act 1968.

This page is intentionally blank

Abstract

The Collahuasi district, Chile (21ºS, 68º45'W) is the northernmost of four major Eocene-Oligocene porphyry-epithermal mineral camps distributed along a 650 km-long segment of the central Andean margin. The district hosts the Rosario, Ujina, Quebrada Blanca and Copaquire porphyry copper-molybdenum deposits, which together account for a global resource of ~77 Mt of Cu and ~6,500 Mlb of Mo. The copper-rich La Grande high sulfidation epithermal vein system, adjacent to the Rosario porphyry, contains a further ~8 Mt of Cu. The district also contains small Au- and Ag-bearing epithermal deposits and exotic copper deposits. Collahuasi is unique among the northern Chilean porphyry copper districts in that the deposits are primarily hosted within the Carboniferous to Triassic volcano-sedimentary units (The Peine Group) that formed the basement to the Paleogene arc.

New mapping of ~120 km^2 (60%) of the district, petrology, whole rock chemistry, 26 new laser ablation zircon U-Pb ages and six new $^{40}Ar/^{39}Ar$ step heating ages constrain a detailed new Permian to Eocene stratigraphy and intrusive history that is coherent across the district. The Peine Group stratigraphy at Collahuasi is here divided into 43 lithostratigraphic members, which comprise four broad facies associations. The stratigraphy and related intrusive rocks reflect distinct periods of accommodation of deposited materials and petrogenesis during Peine Group time. The lowermost Peine Group (~310-290 Ma) records explosive, mostly subaerial eruptions that resulted in the formation of voluminous dacitic to rhyolitic ignimbrites. A significant period of creation of sedimentary accommodation space commenced at ~290 Ma, and was accompanied by effusive subaqueous eruption of basaltic andesites in the Rosario-La Grande area. Polylithic epiclastic conglomerates and granular sandstones interbedded with the basaltic andesites were deposited as local mass flows entered the adjacent subbasin. By about 285 Ma, the early basin had filled, and creation of accommodation space shifted westward across the Monctezuma Fault. Dacitic, and lesser andesitic lavas were erupted, followed by voluminous dacitic and rhyodacitic ignimbrites. During periods of volcanic quiescence, laminated microbial limestones and minor evaporites were deposited in a lacustrine environment. The same time coincides with a change in the bulk magma chemistry after which younger magmas

are commonly reddish rather than grey and contain little magmatic ilmenite.

A volcanic hiatus between 270 and 260 Ma coincided with intrusion of voluminous equigranular medium grained intermediate to felsic plutons. Disharmonic open, upright 'crumple' folding of the Peine group was associated with the emplacement of these intrusions. The uppermost Peine Group was erupted in the earliest Triassic (~248 Ma) and includes various felsic domes, flows and proximal explosive volcaniclastic facies. These formed at two centres, interpreted to be located on the Domeyko Fault and the northern Monctezuma Fault, respectively. At around the same time, rare, thick dykes of porphyritic monzogranite, and a swarm of relatively primitive basaltic andesite dykes were emplaced in the eastern half of the district. These record the onset of slab rollback and the waning of magmatism in the Choyoi Arc. Thickness variations and movement of deposcentres relative to major faults imply that all of the faults that define the modern fracture architecture of the Collahuasi district originated as growth faults during deposition of the Peine Group.

Faults and vein arrays were mapped at 1:300-500 in selected domains across and/or around the perimeter of each of the six principal mineral deposits, and in trenches and excavations adjacent to the deposits. The relative timing of successive events is constrained by the hydrothermal vein, fault and breccia paragenesis in each system. There is a broad distinction between the structural architecture of two pairs of deposits formed approximately two million years apart. The 37-36 Ma Copaquire and Quebrada Blanca porphyries are located on NNE trending second-order faults that splay from the 1000 km-long Domeyko Fault. Accommodation of intrusions, breccias, and early stage alteration and mineralisation occurred along this generation of faults, as well as on 3rd order ENE-trending splays at Quebrada Blanca. Early stage veining in both deposits includes important sheeted or subhorizontal sets. These mineralised complexes are therefore interpreted to have intruded during dextral transpression along the Domeyko Fault. In contrast, the ~35 Ma Ujina, and ~34 Ma Rosario deposits are located near the intersection of major NNW-trending Triassic dykes with multiple second order Peine-age faults. At Ujina, vein arrays are strongly influenced by older fracture sets, but define grossly concentric arrays indicative of formation during conditions of very low differential horizontal stress.

At Rosario, main stage stockwork veins dip steeply and generally strike parallel to a NNW-trending fault segment (the Lulu Fault) that dissects the deposit and appears to be a Tertiary stepover between strands of a larger, older NNE-trending fault. The strain recorded by the veins and faults implies formation during WSW-directed extension, i.e. during relaxation of the stress imparted by continental convergence. Epithermal mineralisation occurred at La Grande ~1.8 m.y. after porphyry formation, and is partly telescoped onto the Rosario deposit. Telescoping of the porphyry and epithermal environments was facilitated by tectonic escape of a block bound by the Lulu fault, and records a change from mild extension to sinistral transtension along arc-subparallel faults. As a whole, the metallogenic event spans a fundamental change from dextral to sinistral along-arc shear in the Central Andes.

Zircon (U-Th)/He thermochronometry was used to constrain the magnitude and timing of fault displacements. Samples yielded younger average ages (Oligocene) to the west of the arc-parallel Domeyko Fault than to the east of it (Late Eocene). This implies relative post-Eocene uplift of the western block, contrary to that implied by the relative ages of rocks on either side of the fault. A coarse three-stage history is suggested by integration of district mapping with the thermochronometry and field observations. Uplift of the Domeyko Cordillera occurred during the main stage Incaic orogeny (44-38 Ma) during which time the bounding Domeyko fault experienced principally reverse movement. Toward the end of this compressive event, the Domeyko Fault underwent dextral shear under ductile conditions. Striae on brittle, younger segments of the Domeyko Fault are uniformly subhorizontal and indicate sinistral shear. This most recent major stage of fault movement was achieved by major low angle oblique sinistral-(normal) slip. This history coincides closely with that implied by the mineral deposit mapping, such that Copaquire and Quebrada Blanca formed during waning dextral transpression, and Ujina formed during-, and Rosario after the onset of along-arc sinistral shear.

The magmatic chemistry of the barren and mineralised Paleogene magmatic rocks was investigated to elucidate possible tectonic controls on mineralisation. New whole rock analyses were performed on samples of the Eocene, Cretaceous intrusive suites at Collahuasi, and existing data was compiled for the Central Andes and for

other porphyry Cu camps in the Central Andes and the SW Pacific. The chemistry of background arc magmas differs between terranes primarily because of variations in availability and assimilation of radiogenic felsic material. In contrast, there is general similarity between the composition of mineralised suites between several porphyry copper camps in the Andes, and between these fertile continental arc suites and mineralised suites from several oceanic arcs in the SW Pacific. At Collahuasi the syn-mineralisation suites are the most primitive intermediate to felsic rocks, suggesting that they ascended into the shallow crust from their melt source with minimal contamination. Convex-shaped Harker diagram patterns for the high field strength- and rare earth elements also distinguish Paleogene magmas from normal Andean volcanic rocks. These patterns preclude evolution by fractional crystallisation, and instead suggest that the mineralised suites form by low degree partial melting of an amphibolitic source rock; most probably in the continental mantle lithosphere. Barren syn-mineralisation rocks elsewhere in northern Chile appear to be higher-degree partial melt equivalents of the mineralised suites. Likewise, the pre-mineralisation Icanche Formation shares a similar origin but appears to have assimilated substantial amounts of crustal material, consistent with abundant Paleozoic zircon xenocrysts in these rocks at Collahuasi. Fertile petrogenesis is therefore favoured by tectonic scenarios during which thick amphibolitic lithosphere forms, and is subsequently re-melted. Highly specialised structural architecture and deformation regimes are required to permit ascent into the shallow crust of small volumes of fertile intermediate-felsic magma.

The Late Eocene to Early Oligocene porphyry copper event in the Central Andes coincided with the onset of flat subduction in the Central Andes, and with bending of the Bolivian Orocline. These phenomena are interpreted, respectively, to have prompted melting of the mantle lithosphere, and to have permitted efficient ascent of magmas by way of driving the change in along-arc shear sense. Mineral explorers might therefore target areas and periods of geological time characterised by rapidly changing style and rate of intra-arc deformation, irrespective of the causes of that deformation. At district scale, the intersections of second order structures, especially major dykes that formed during basement extension appear to be particularly favorable for shallow emplacement of low-volume magmas related to mineralisation.

Acknowledgements

Financial sponsorship for this project drew from the six corporate sponsors of AMIRA International project P765: Anglo American plc, AngloGold Ashanti Ltd., Gold Fields, Newcrest Mining Ltd., Newmont Mining Corporation, Placer Dome Inc., and Teck Cominco. The Australian Research Council also provided critical support via provision of an Australian Postgraduate Award scholarship to the author. I thank all these organisations for their committment to scientific research, and their recognition that postgraduate research requires strong financial backing in a competitive marketplace. I also thank the Society of Economic Geologists' McKinstry Grant for providing funds that were used for thermochronological (U-Th/He) analyses. Raw ASTER images were kindly donated by Bob Agar, then at Newmont. I give special thanks to Grigore Simon, David A. Groves, Miles McAlister and Brian Levet at Newmont Mining Corporation; individuals who trusted me enough to give me a job with the flexibility to finish my studies concurrently. In addition to Hobart, parts of this thesis were written on five continents.

Anglo American plc was a sponsor of P765 and provided additional logistical support through their partly owned subsidiary and operator of the Rosario and Ujina mines, la Compañía Minera Doña Inés de Collahuasi (CMDIC). To Chris Carlon, Mike Buchanan and Graeme Lyall at Anglo, and Kevin Olshefsky at (partner company, then) Falconbridge I give most sincere thanks. CMDIC geologists Ingrid Smoje, Jorge (Floro) Zamorano, Sergio (GG) Giglio, Pedro Apablaza, Claudio Ahumada, Patricio Osorio, Marcial Vergara, and Alejandro Sanhueza were also involved in the project. On site, Patricio Muñoz, Sergio Abarca, Eduardo Kong, Hector Cortez and Carlos Lopez generously gave their assistance at various times with project logistics. I give my greatest thanks to Jean-Philippe Desrochers and Martin LaPointe at Aur Resources (Quebrada Blanca) for their enthusiasm and efforts regarding on site project facilitation: efforts that were made largely out of compassion and courtesy, as Aur Resources was not part of AMIRA P765.

Ron Berry and Dave Cooke oversaw this project and have both contributed many pearls of wisdom and much pragmatic commentary toward its completion. The final manuscript has benefited substantially from their patient reviews. In the final days,

Dave worked some small miracles that testify to his particular committment and dedication as a research supervisor.

This was however a broad project, and it has seen me knocking on many different doors asking for professional assistance, ad-hoc training, and every now and again, a game of tennis. I give special thanks to those kind people who have donated their time, expertise and enthusiasm: Neville Alley, Jocelyn McPhie, Pat Quilty, and Stuart Bull (Volcanology and Sedimentology); Enrique Chait, Felipe Urzua, Loreto Lazcano and Carolina Acevedo (logística e amistád en Chile); Pete Hollings, Leonid Danyushevsky and Tony Crawford (Geochemistry); Brett Davies and Gordon Lister (Structural Geology and Tectonics); Sebastien Meffre, Pete Reiners, Alan Clark, Doug Archibald, and Amelia Rainbow (Geochronology); Mike Roach, Bob Agar and Ayşegul Domaç (GIS and geophysics); Dave Braxton, Jean-Philippe Desrochers and Martin LaPointe (encouragement and outstanding critical discussion); and my partner Anna Lazarova, who, amongst many other things, patiently attributed countless thousands of map elements and cleaned up the map topology so that sooner rather than later, Zhara might have a dad not permanently attached to a computer.

Ultimately, I wish to thank my friends. Without you, this project has otherwise given me cause to feel tired and lonely. Though it's typically been a long time between meetings, I thank you all most sincerely, for distracting me enough through the years to keep me sane, smiling, and at times, dancing. Thank you for believing in me.

"You see I've been climbing stairs, but mostly stumbling down,
I've been reaching high, but always losing ground.
You see I've conquered hills, I still have mountains to climb.

At this point in my life, I'd like to live...as if redemption was in sight,
as if the search to live honestly was all that anyone needs,
no matter if you find it."

Tracy Chapman, At This Point In My Life (1995).

Table of Contents

List of Figures

CHAPTER 5.

CHAPTER 6.

APPENDICES.

List of Tables

CHAPTER 5.

CHAPTER 6.

APPENDICES.

Chapter 1.

INTRODUCTION

1.1 Preamble

Porphyry Cu-(Mo)-(Au) deposits, a group of generally low grade, bulk tonnage deposits related to intrusion-driven hydrothermal systems, were widely recognised and defined as a major deposit class and exploration target in the 1970s (Lowell and Guilbert, 1970; Sillitoe, 1973; Moore and Nash, 1974; Gustafson and Hunt, 1975). They have been the subject of advanced research attention over the subsequent three

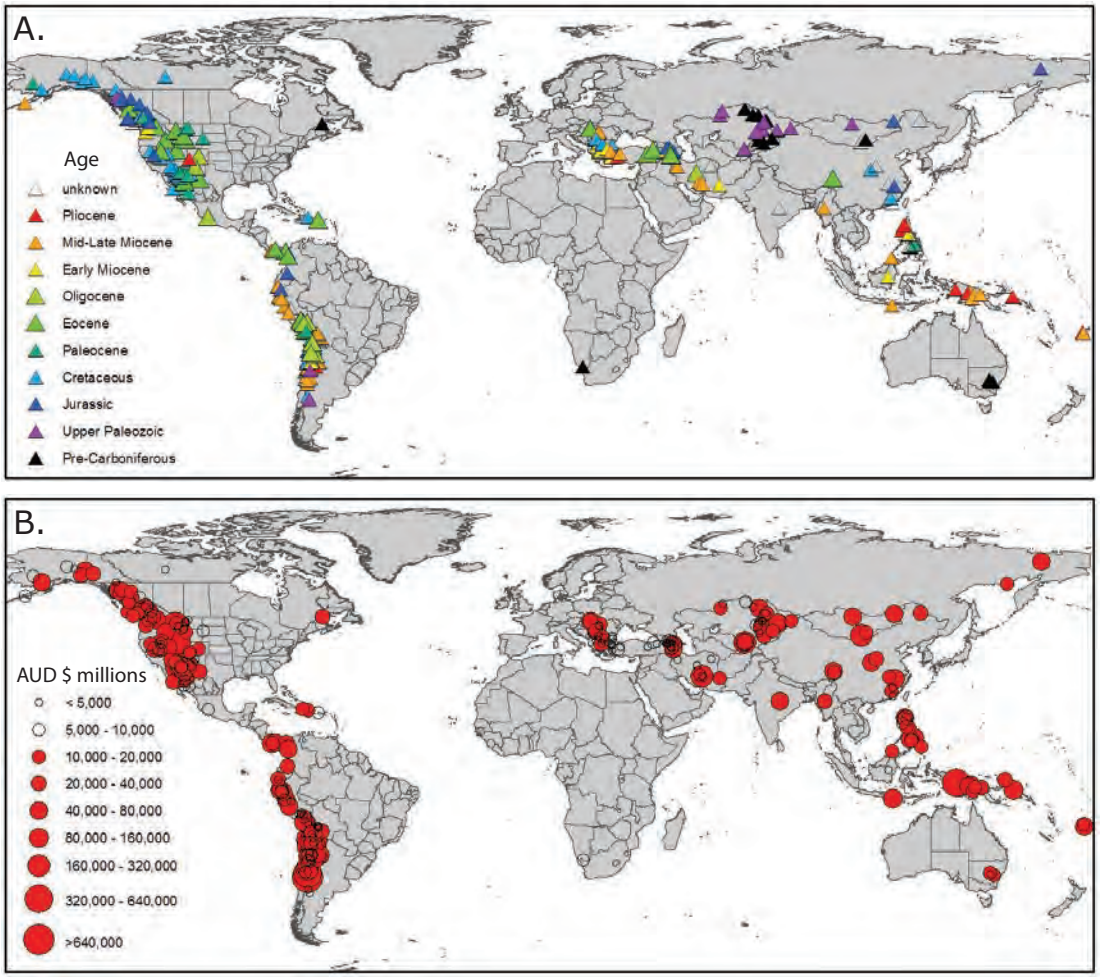

Figure 1.1. Global distribution of porphyry and related magmatic-hydrothermal deposits including Cu, Zn or Au skarns/mantos, and high-, intermediate-, and alkaline low sulfidation epithermal deposits, graduated by (A) mineralization age, and (B) cumulative monetary value of pre mining global resources of Cu+Au+Mo at July 2009, Based on Mutschler et al. (2000) and Singer et al., 2005, with minor additions from Lilov and Chipchakova (1999), Strashimirov et al. (2002), Von Quadt et al. (2002), Camus (2002; 2003), Perelló et al. (2003), Hou et al. (2003), and various corporate websites.

decades (see Seedorff et al., 2005 for a recent summary). Porphyry- and related mineral deposits occur worldwide, almost exclusively in preserved convergent margin magmatic arcs (e.g., Mutschler et al., 2000: Fig. 1.1).

Deposit-scale studies have been conducted both by academics seeking to understand generative processes, and within corporations that seek to improve the efficiency of mining and exploration activities. These studies have confirmed the spatial and temporal recurrence of major mineralisation processes and products, but have also highlighted the individuality of some porphyry and associated epithermal deposits (Sillitoe, 1973; Gustafson and Hunt, 1975; Brimhall, 1977; Titley et al., 1978; Titley and Beane, 1980; Sillitioe and Gappe, 1984; Norman et al., 1991; Vila et al., 1991; Ossandon and Zentilli, 1997; Gustafson et al., 1999; Dilles et al., 2000; Garwin, 2000; Perelló et al., 2003; Richards et al., 2001a; Camus, 2003; Seedorff and Einaudi, 2004a; 2004b). For the very large deposits that have motivated on-going research, there has been repeated re-organisation and refinement of ideas on mineralisation controls and processes, such as those at Chuquicamata (Lindsay et al., 1995; Zentilli et al., 1995; Ossandon and Zentilli, 1997; Reynolds et al., 1998; Ossandon et al., 2001; Arnott and Zentilli, 2003) and El Salvador, Chile (Gustafson and Hunt, 1975; Mpodozis et al., 1994; Tomlinson et al., 1994; Cornejo et al., 1997; Watanabe and Hedenquist, 2001). Such bodies of work have led to the development of increasingly refined empirical and partly theoretical models on which explorers base some of their decision making (economic and sovereign risk concerns notwithstanding). Nonetheless, Sillitoe (1995) concluded that discoveries of major mineral deposits during the period 1990-1995 in the circum-Pacific occurred primarily by chance, and that the discoveries "defy rational analysis and categorisation". As the exploration business becomes increasingly concerned with risk mitigation (e.g., Enders and Levielle, 2004), there is still ample room for improvement of our understanding of the controls on deposit formation and localisation.

There are more than 64 porphyry Cu-(Mo)-(Au) deposits in the Central Andes, including 11 of 20 giants in the Circum-Pacific region (Kelley et al., 2003; Cooke et al., 2005). These deposits furnish Chile and Peru with an impressive Cu endowment that has made the central Andes the subject of intense mineral exploration. In 2007

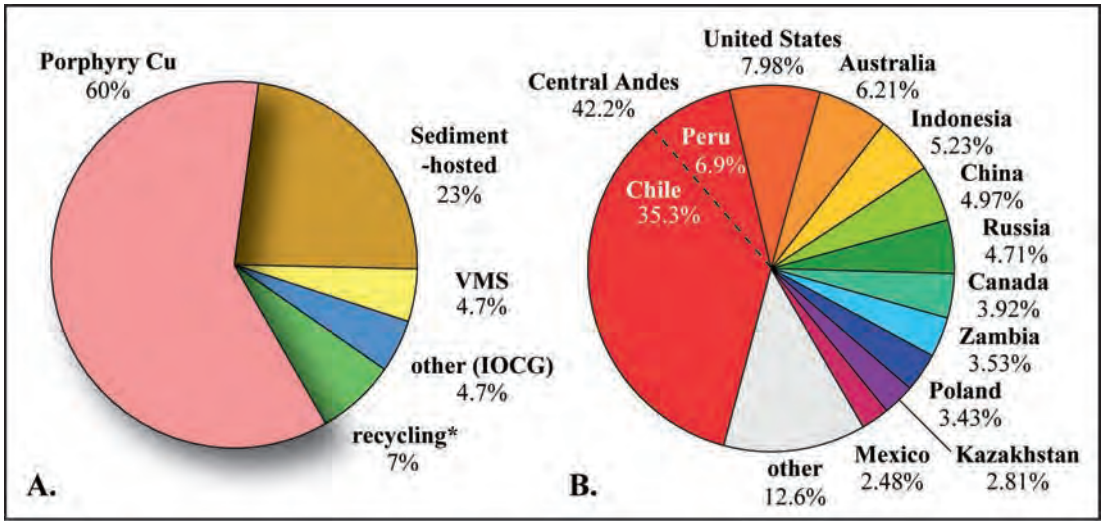

Figure 1.2. Pie charts indicating the global primacy of porphyry Cu deposits and the central Andean porphyry terranes. A) approximate bulk Cu production by deposit style in the year to July 2004 (Edelstein, 2004), and B) bulk Cu production by country in the year to January 2007 (USGS, 2007). * US only, data for 2006-7 from the USGS (2007).

this region accounted for ~42% of world copper production (Fig. 1.2). The minerals industry in Chile is approaching maturity, with a growing perception that most of the significant deposits exposed at surface have already been identified (Heather and Bissig, 2003; Kelley et al., 2003; 2006). This perception is increasingly driving explorers to pursue blind deposits in known mineralised districts, with considerable success (e.g., Sillitoe, 2004; Rivera et al., 2006b; Toro et al., 2006; Rivera, 2007; Holliday and Cooke, 2007). In general, broad alteration halos and localisation adjacent to long-lived fault systems characterise most porphyry deposits (Lowell and Guilbert, 1970; Titley and Heidrick, 1978; Seedorff et al., 2005). In addition to the demonstrated efficacy of field observation and mapping (Sillitoe, 2004; Brimhall et al., 2006), the discovery of covered deposits is also likely to include a better understanding of the nature of the tectonic environment favourable for mineralisation, and of the pre- and syn-mineral structural architecture that favoured shallow crustal magma emplacement and fluid flow. It will also require the courage of exploration managers and company directors to drill targets based on these inferred, or interpreted geological characteristics. Only then can the nature and zonation of alteration facies, toward which so much investigative attention has been directed, be applied to exploration for covered deposits.

1.2 Location and Environment

Porphyry copper deposits typically occur in spatial clusters (Camus, 2002; Cooke et al., 2005), wherein each of the deposits is much closer to the next deposit than it is to the next cluster. The Collahuasi district is defined here as the area that contains the Ujina, Rosario, Quebrada Blanca and Copaquire porphyries, and related alteration. It is the northernmost of the four major Eocene-Oligocene porphyry copper districts in Chile. The district is centred at 20°58'S, 68°43'W, approximately 250 km by road southeast of Iquique, a coastal city 1300 km north of Santiago (Fig. 1.3) and the administrative centre of the Tarapacá region. Access is by sealed road from the Pan American Highway 100 km to the west, and then by unsealed roads that connect to the eastern part of the district via Pozo Almonte township, and to the western part via the village of Pintados.

The ~40 x 20 km district comprises part of the Domeyko Cordillera (Fig. 1.3), an incised, uplifted block that currently stands between 3,800 and 4,900 m. It is bound to the west by steeply dissected terrain that leads down into the Longitudinal Valley. The eastern boundary is defined by the salt lake-filled intermontane Preandean Depression and the active Andean volcanic front. Stratovolcanoes of the 'Western' Cordillera rise to between 5,000 and 6,200 m. adjacent to the Collahuasi district and the watershed marks the Bolivian border (Fig. 1.3). This physiography and the cold Humbolt Current of the eastern Pacific Ocean cause the hyperaridity that characterises the Chilean part of the Atacama Desert (Fig 1.4). Annual precipitation in the district averages just 150 mm/yr, and is concentrated during the summer months when thunderstorms form over the Western Cordillera and move southwest across the district, bringing localised heavy rain and hail. Temperatures follow normal southern hemisphere seasonality with summer average maxima 10 to 15°C and winter average maxima +5 to –5°C. Vegetation is restricted to highly specialised spiny "bunch grasses" (dominated by *Stipa ichu*) and low heath species (such as the crying button plant "Llareta" *Azorella compacta;* Fig 1.4 c). Fauna in the area is include domestic llama, and wild vicuña, guanaco and vizcacha.

The atmosphere at 4,000 m elevation (the average of the Rosario-Ujina-Qda Blanca operations) has ~60% of the oxygen as it does at sea level, and altitude sickness

Figure 1.3. Location map of northern Chile showing location of the Collahuasi district relative to major physiographic elements, porphyry Cu-Mo deposits and districts, and regional service towns. Background is the digital SRTM 90 m-pixel digital elevation with a NE sunshade.

is the commonest occupational health hazard. Of the various symptoms attributed to altitude sickness (combined with very low humidity), the author experienced insomnia, headaches and skin irritation.

1.3 Mineral Resources, Discovery and Corporate Structure

The ore deposits of the greater Collahuasi district include six porphyry Cu-Mo deposits, some of which are spatially associated with epithermal Cu-Ag-(As)-(Au) and Ag-Mn-Au vein systems, as well as palaeogravel-hosted exotic Cu deposits, and minor placer Au deposits. This section offers a brief history of exploration and mining in the Collahuasi district, compiled largely from Hunt (1985), DeBeer and Dick (1994), and Masterman and Moore (2002).

Vein systems in the district were worked for precious metals by indigenous miners as early as 1400 A.D., and intermittently thereafter, with the most significant production

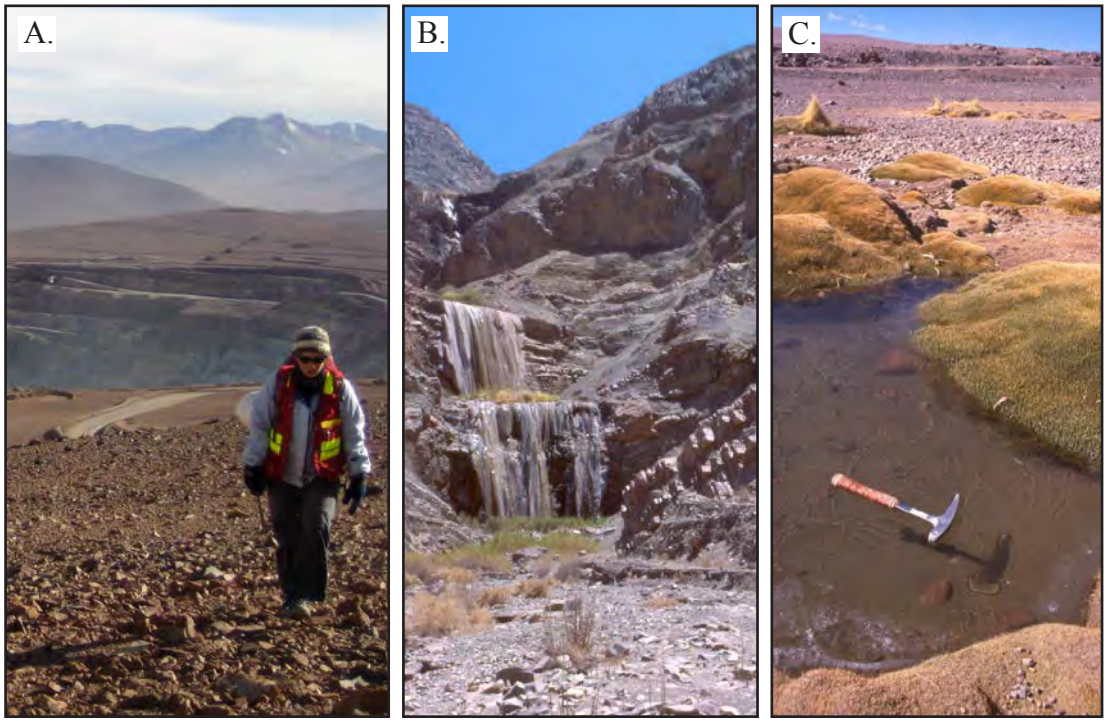

Figure 1.4. Landscape and environment photos of parts the study area. A) View to the northeast across the Rosario open pit showing typical deflation lag scree-covered terrain of the Domeyko Cordillera in the study area. Volcán Irrutupunctu (6,153 m) on the Bolivian border dominates the skyline. B) Tributary of the Quebrada Guatacondo with external stalagtites built on limestone waterfall terraces during prolonged arid climatic conditions of the Atacama Desert. C) Frozen groundwater seep near Rosario revealing the cold temperature and clear sky that characterise the spring and autumn climate in the study area. Button plants (*Azorella compacta*) and spiny grasses (*Stipa Ichu, background*) inhabit the immediate area.

occurring between 1870 and 1930. Historic production centred on the outcropping high grade vein systems of Cerro La Grande, which collectively produced ~300,000 tonnes of ore averaging 25% Cu, 180 g/t Ag, and 2 g/t Au. Interest in the region as prospective for bulk tonnage, lower grade mineralisation began in 1936, when a reconnaisance sampling visit to Quebrada Blanca was made by two independent geologists. There appears to be no record of the locations of their sampling (Fam, 1974), and interest was not renewed until 1958 (Villemur, 1963; Fam, 1974; Ware et al., 1981). At that time, the surface exposures suggested geology and alteration that proved to be consistent with the generic porphyry Cu model subsequently published by Lowell and Guilbert (1970). Initially discovered by the Chilean branch of Anaconda, delineation of the Quebrada Blanca resource (1977-82) and subsequent discovery of Rosario (1979) and Ujina (1991) were achieved by a series of joint ventures between North American oil and base metal companies that resulted from repeated corporate amalgamation and streamlining. The complex and dynamic

Table 1.1 Pre-mining Cu and Mo reserves for mineral deposits of the Collahuasi district.

	Ore			Metal		Proportions	
Orebody	Mt ore	% Cu	% Mo	Mt Cu	Mlb Mo	Cu	Mo
Copaquire hypogene	957	0.10	0.046	0.96	977	2.36	30.33
Quebrada Blanca supergene	400	0.83	0.015	3.3	132	8.20	4.10
Quebrada Blanca hypogene	1,030	0.50	0.020	5.2	453	12.72	14.07
Rosario hypogene	2,161	0.88	0.027	19.0	1284	47.03	39.85
Rosario supergene	225	0.99	0.010	2.2	50	5.51	1.54
Rosario Oeste supergene	248	1.48	-	3.7	-	9.07	-
La Grande supergene[a]	0.3	25.00	-	0.08	-	0.19	-
Ujina supergene	741	0.81	0.020	6.0	326	14.83	10.12
Huinquintipa exotic[b]	2	2.00	-	0.04	-	0.10	-
Total[c]	5,764	0.70	0.025	40.49	3,221		

a) historical production

b) BOTE estimations from generalised dimensions, density and common grades. No figures are available

c) average grades are the bulk contained metal / the bulk tonnage of all resources in cases where more than one reserve category is listed in the data source.

Compiled and calculated from Moore and Masterman, 2002; Camus, 2003; www.angloamerican.com; www.internationalpbx.com; www.teckcominco.com and www.xstrata.com. For Rosario, figures were calculated from remaining reserves at Jan 2007 plus production 2003-2006, and does not include remaining inferred and indicated resources as equivalent figures are not available for the other deposits. "Supergene" denotes all ore subsets in which supergene mineralisation is the dominant contribution to the bulk grade.

corporate history surrounding exploration successes in the district demonstrates the value of perserverance and intelligent management in a highly prospective geological terrane (Masterman and Moore, 2002).

During this study Rosario was operated by, and Ujina was under care and maintenance of, the Compañia Minera Doña Inés de Collahuasi (CMDIC) that is currently owned by Xstrata (44%, previously Falconbridge Ltd.), Anglo American plc (44%), and a consortium led by Mitsui Corporation (12%). Quebrada Blanca was operated by the Compañia Minera Quebrada Blanca Ltd., that is co-owned by Teck Cominco (76.5 %, previously Aur Resources Ltd.), the Sociedad Minera Pudahuel Ltd. (13.5%) and Enami (10%). The licences covering the Copaquire deposit were acquired by junior explorer International PBX Ventures in 2005 following dramatic increases in copper and molybdenum prices during the course of this study.

Total reserves plus production for the district amounts to ~5,500 Mt at 0.73% Cu, and 0.025% Mo (Table 1.1). In mid-2005, prior to its takeover by Xstrata, Falconbridge released a preliminary resource estimate of 248 Mt @ 1.48% Cu for the supergene enrichment of a previously unrecognised northern extension of the La Grande high sulfidation system (re-named Rosario West as it overlaps with the southwestern margin of the Rosario porphyry). Drilling was in progress at Copaquire at the time of writing, and has underpinned a measured reserve of 957 Mt @ 0.0464 % Mo and 0.10 % Cu. These two recent brownfields exploration programs added 9.2% to the Cu, and ~30% to the Mo inventories of the district, respectively. Further, the Xstrata website lists inferred and indicated resources at Rosario of 3,587 million tonnes @ 0.79% Cu and 0.030 % Mo, which if realised would add a further 71% and 78% to the Cu and Mo inventories, respectively. Enders and Levielle (2004) point out that 80% of the Cu “discovered” in the period 1996-2002 was in near-mine environments, which appears to have been the continuing trend at Collahuasi.

1.4 Thesis Scope and Outline

This thesis presents the results of a broad range of geological techniques applied across the ~375 km^2 area surrounding the main porphyry and epithermal mineral deposits of the Collahuasi district. The primary goal was to investigate the structural architecture of mineralisation at deposit- and district scales. To do that effectively, the

project broadened to include lithostratigraphic and alteration mapping of the district, targeted geochronology, thermochronology and magmatic chemistry. Several other techniques were used to a lesser extent and a large amount of data was compiled from published and especially unpublished sources. This research forms part of an on-going research effort into South American Cu-Mo-(Au) deposits at CODES, the Australian Research Council's Centre of Excellence in Ore Deposits at the University of Tasmania. It contributes to AMIRA International project P765, "Transitions and Zoning in Porphyry-Epithermal Mineral Districts". The work was principally financed by Anglo American plc, AngloGold Ashanti Ltd., Gold Fields, Newcrest Mining Ltd., Newmont Mining Corporation, Placer Dome Inc., and Teck Cominco through their sponsorship of the collaborative AMIRA P765 research project, and by the Australian Reasearch Council through an Australian Postgraduate Award scholarship provided to the author.

1.4.1 Thesis Outline

Chapter 2 is a review of the tectonic and metallogenic evolution of the Andes Cordillera.

Chapter 3 presents the results of district mapping and describes in detail the stratigraphy of the district with particular emphasis on the Late Paleozoic Peine Group, the major host to Paleogene Cu-Mo mineralisation. U-Pb and $^{40}Ar/^{39}Ar$ geochronology underpins the stratigraphic interpretations presented. The magmatic chemistry of the Peine Group is revisited via a compilation of new and existing data.

Chapter 4 investigates the relationships between structural geology and mineralisation. In the first section, interpretations are made of the structural architecture of the district based on the stratigraphy and map patterns. The second section presents the results of detailed deposit-scale structural mapping. This work relies on the sequence of hydrothermal vein events and reviews the vein and intrusion paragenesis of each deposit, with some critical additions.

Chapter 5 presents the results of U-Th/He thermochronology that constrains the relative Tertiary uplift history across the major faults in the district. Integration of this data with structural mapping permit interpretations of the strike-slip history along the Domeyko Fault.

Chapter 6 provides new whole rock geochemistry for three suites of Late Cretaceous to Eocene magmatic rocks. Compilation and comparison of this data with published Central Andean datasets is used to make interpretations of the tectonic environments that characterised key stages of the geological history. By comparison with existing magmatic chemistry datasets for porphyry copper camps in the SW Pacific, a hypothesis is put forward for fertile magma petrogenesis that is independent of crustal thickness. Tectonic scenarios that favour this petrogenesis are discussed.

Chapter 7 provides a summary and conclusions, and recommendations for mineral exploration and future research.

1.5 Previous Research in the Collahuasi district

Mapping by the Instituto de Invesigaciones Geológicas at 1:50,000 (Vergara, 1978; Vergara and Thomas, 1984) and subsequently compiled by the Chilean national geological survey at 1:250,000 (Tomlinson et al., 2001a) were the first coherent studies of the district's geology. Subsequent mapping has been done largely in-house as part of ongoing exploration, of which the Collahuasi – Quebrada Blanca district compilation of Ware et al. (1981) and the Rosario-La Grande area report and map of Munchmeyer et al. (1984) stand out as summaries that indicate the level of geological knowledge around the time of discovery of the principal porphyry copper deposits (Fig. 1.5).

At the deposit-scale, the Quebrada Blanca and Rosario porphyry copper deposits have been studied in detail, and the other deposits and prospects have been subject to only limited research. Comprehensive descriptions of the geology and mineralisation at Quebrada Blanca were presented following its discovery by members of the exploration team (Ware et al., 1981; Hunt et al., 1983), and the magmatic and hydrothermal evolution dissected in the PhD thesis of Rowland (1998). Selected detail of vein paragenesis and evolution of the hydrothermal system was published by Rowland and Wilkinson (1999), and aspects of the breccia and vein parageneses are described in the honours theses of Fam (1974), Lehmann (1980) and Martini (1984). Apatite U-Th/He thermochronological contraints on the uplift and exhumation history of the Domeyko Fault System (FS) between Quebrada Blanca

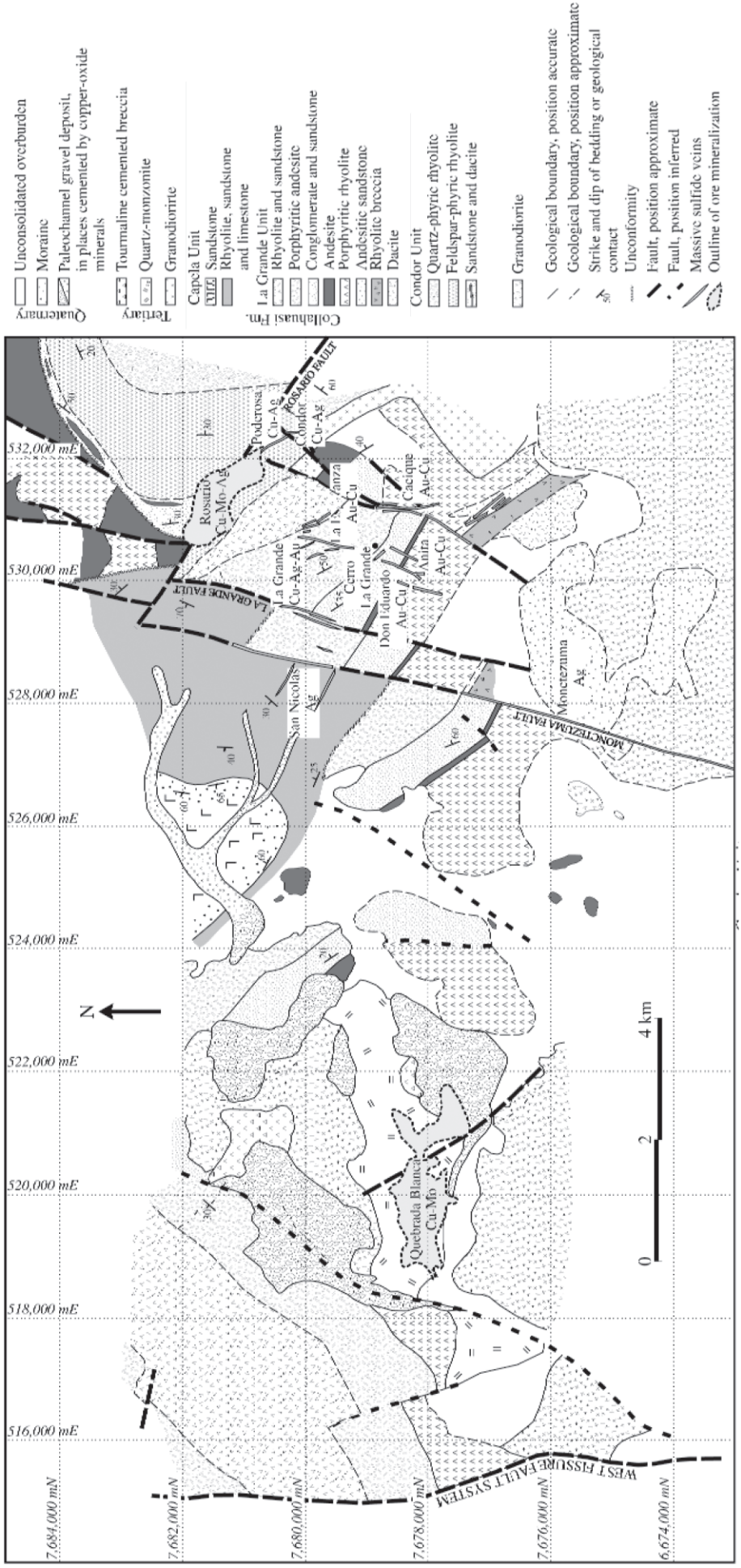

Figure 1.5. Collahuasi district geology map, originally drawn at 1:50,000 by Ware et al. (1981), redrafted in Munchmeyer et al. (1984) and Masterman et al. (2005), from which this version is taken. The position of the major structural elements is generally well defined, although several key structures are not marked (*cf* Chapter 5). The broadlithostratigraphy is consistent with the findings of this study (Chapter 3), however the relationships between stratigraphy in the Quebrada Blanca, Capella and Condor sectors is ambiguous.

and Chuquicamata were the subject of the honours thesis of Olivares (2001).

Mineralogy and paragenesis of the Rosario Cu-Ag-(As) vein system was described from surface exposures by DeBeer and Dick (1994) and from two exploratory underground drives in the Masters thesis of Lee (1994). A geological and structural comparison of the Rosario and Ujina deposits was published by Bisso et al. (1998), who described some of the major diffences between these deposits and highlighted the need for better constraint of the structural evolution of the district. The PhD thesis of Masterman (2003) is a detailed geological and geochemical study of the Rosario porphyry deposit with additional data concerning the mineralogy and alteration of the La Grande vein system and the geochronology of the Ujina porphyry deposit. His study significantly refined the understanding of the local structural and stratigraphic geometry and developed an integrated genetic model for the Rosario hydrothermal systems (Masterman et al., 2004; 2005).

The geology and economic molybdenum potential of the Copaquire porphyry has been investigated several times as an exploration prospect (Villemur, 1963; Camus and Fam, 1971; Munchmeyer, 1972; Sillitoe and Neumann, 1972; Hollister and Bernstein, 1975; Arias Farias et al., 1988), but these studies all lean toward economic evaluation. The geology of the Ujina deposit has not been studied in any detail outside the operating company and the comparative work of Masterman (2003). Variations of a simplified Ujina mine section presented by DeBeer and Dick (1994) are repeated in the subsequent literature (Bisso et al., 1998; Masterman and Moore, 2002; Masterman et al., 2005).

The Collahuasi district has featured in numerous regional studies, notably those of Maksaev (1990) and Maksaev and Zentilli (1999), who used samples from Copaquire and Quebrada Blanca in studies of central Andean metallogeny, uplift and thermochronology. Tomlinson and Blanco (1997a, b) made structural and stratigraphic reconstructions across the Domeyko Fault between Quebrada Blanca and Copaquire. Recent investigations of the interplay of deformation and intrusion along the Domeyko Fault included the Guatacondo section in the westernmost Collahuasi district (McClay et al., 2002; Amilibia and Skarmeta, 2003; Skarmeta et al., 2003; Amilibia et al., 2008). By extrapolation of their deposit-scale findings,

Bisso et al. (1998), Masterman (2003), and Masterman et al. (2005) placed the Rosario, Ujina and the La Grande veins into a district and regional context, whilst recognising the need for more concerted evaluation of the district as a whole. This study follows directly from those and attempts to bridge a variety of scales; from investigation of the detailed structure of key mineralised- and high strain areas, to the district geological evolution, toward recognition of the interplay of regional tectonomagmatic events and mineralisation in the district.

1.6 Work Completed in this Study

1.6.1 Reviewed Literature

As the Central Andes is the end member example of Phanerozoic continental convergent margins and is also prolifically mineralised there is a rich and diverse body of previous research. The literature reviewed and cited in the study was largely sourced from the University of Tasmania Science and Technology library in Hobart, and from the collections of the author and of several members of staff at the University of Tasmania. The author also visited the Chilean Geological Survey (SERNAGEOMIN) library in Santiago for two weeks to access Latin American literature that is largely unavailable in Australia or online. The extended abstracts volumes from the triennial Congreso Geológico Chileno proved a particularly rich source of relevant literature not published elsewhere. Numerous unpublished resources were also acquired from the in-house libraries of the companies working in the project area. All literature sources are cited at appropriate locations in the text.

1.6.2 Field Work

Field work was carried out by the author over three visits to the Collahuasi district for a total of eight months based at Collahuasi, three weeks at Quebrada Blanca, and two weeks in the Quebrada Guatacondo-Copaquire area. Total field activity included detailed (1:200-500) mapping of ~5 km of excavated faces along roads and in open pits (Fig. 1.6), 1:5,000 scale district mapping of approximately 150 km^2 (a 30 x 5 km belt) and graphic logging of more than 15 kms of diamond drill core.

Work completed between March and June 2004, included graphic logging of drill

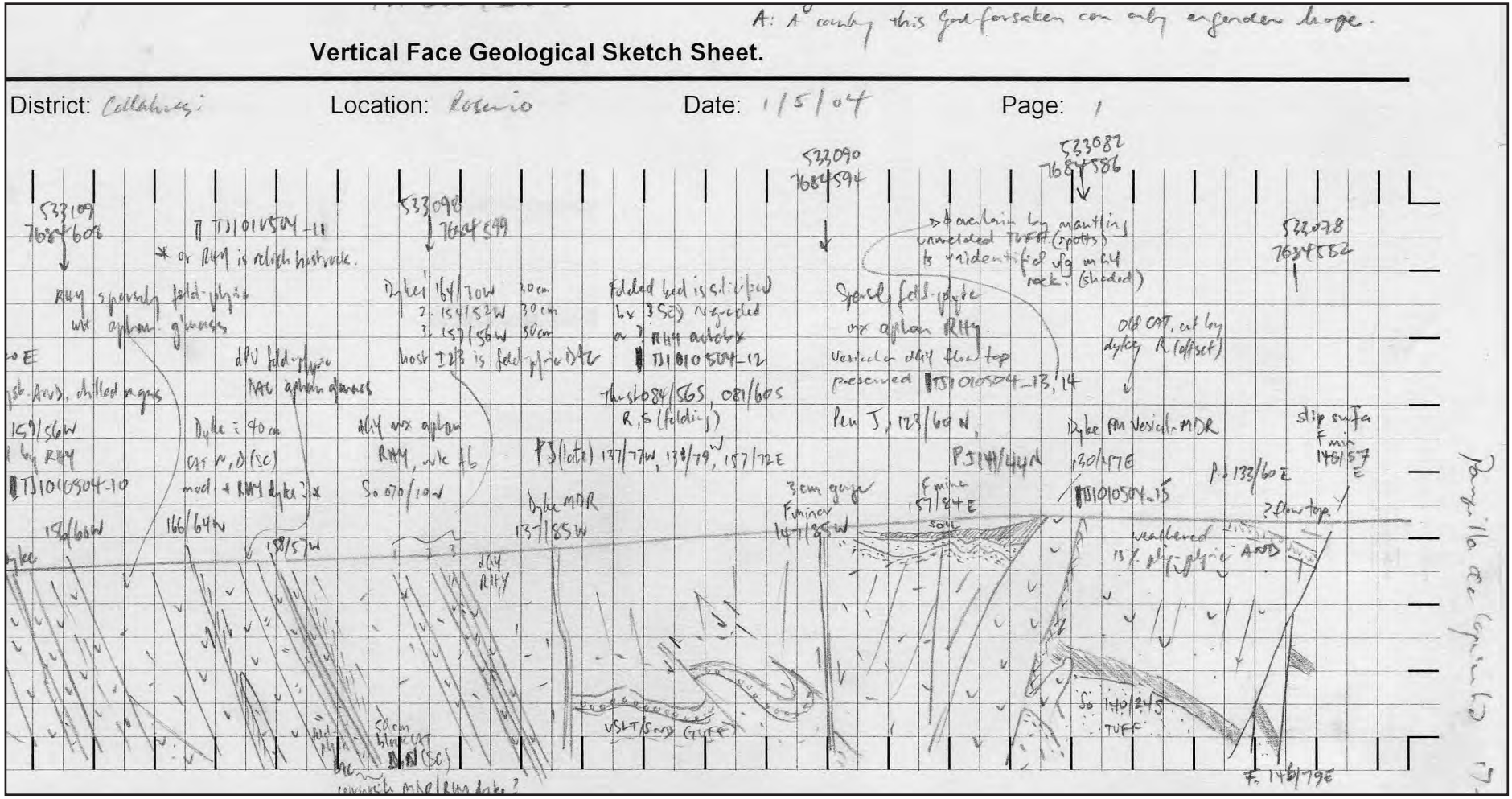

Figure 1.6. An example of methods of raw data collection for this thesis, showing a vertical face sketch map of a road cut section along the main access road between the Collahuasi camp and the Rosario Mine. In this complex section, aspects of the volcanology of the upper La Grande formation are evident, as well as Permo-Triassic faults and Early Triassic dykes that were emplaced in the terminal magmatic event of the Choiyoi Arc (Chapters 3 and 4).

core, and structural mapping in the Rosario and Ujina open pits and of new road and conveyor cuts in the eastern part of the district. The roads between Coposa, Ujina and Rosario mines and a new 12 km-long cutting for the Rosario – Ujina conveyor provided exposures that added significantly to the stratigraphic and structural information available. Regional (sterilisation) drill holes were re-logged in detail to augment locally sparse outcrop evidence of the relationships and correlations between units.

Work conducted between October and December 2004 included traverse mapping of the Domeyko FS in the Quebrada Guatacondo, regional mapping at Quebrada Yabricoyita, Cerro Chigliuno, on-going detailed structural mapping in the Rosario, Ujina and Quebrada Blanca open pit mines, and logging of oriented core at Cerro La Grande. The Rosario Pit was an extremely dangerous site throughout the study period and access was limited for safety reasons. The supergene resource at Ujina had been extracted by this time and the Ujina Pit was actively being backfilled, which also restricted access in some cases.

1.6.3 Map Compilation and Cartography

Map data compilation was done by the author between 2005-06. The mapping incorporates all the existing map data available in 2004-05, as well as the lithological data collected from drill holes logged in this study, and the mineralogical data from the entire CMDIC exploration database. The stratigraphic and structural geometry presented is the simplest that satisfies the field data.

Cartography was done by the author in 2007-09 using ESRI ArcGIS 9.2 software with technical assistance from Willy Lynch at ESRI and Aysegul Domac at Newmont Altin Madencilik. A reduced-scale version of the new district geology map sheet is presented in Chapter 3, and a poster-size version with greater detail is included as an insert at the back of the thesis.

1.6.4 Petrography

Hand specimen and thin section petrography underpins the stratigraphic correlations presented in Chapter 3, and a table of petrographic descriptions is contained in the appendices. Petrography was conducted by the author at the University of Tasmania,

using a standard petrological microscope. Approximately 250 thin sections were investigated in this study, a small subset of which derived from Masterman's PhD study (Masterman, 2003). The results of the microscopic investigation were used routinely to clarify or constrain more general hand specimen descriptions made by the author while mapping in the field.

1.6.5 U-Pb Geochronology

Zircon U-Pb geochronology provides a temporal framework for the mapped stratigraphy presented in Chapter 3, and constrains the interpretation of previous geochronological studies that utilised other methods. Heavy mineral separation and laser ablation ICP-MS geochronology was performed by the author in July 2004 and June 2006, with a small number of samples prepared and analysed by Dr. Sebastien Meffre at CODES in May 2005.

1.6.6 Geochronology $^{40}Ar/^{39}Ar$

$^{40}Ar/^{39}Ar$ geochronology was used in this study to date magmatic emplacement of rock units that lack abundant zircon and to date hydrothermal events. Hornblende and illite separations were performed by Amelia Rainbow at Queens University, Kingston, Ontario. Geochronolgical analyses were performed by the author in September, 2005, under the supervision of Dr. Doug Archibald at Queens University.

1.6.7 Electron Microprobe

Electron microprobe analyses were undertaken during this study to determine the potassium content of samples used in $^{40}Ar/^{39}Ar$ geochronology and to investigate the chemistry of minor accessory phases in some magmatic rocks. Analyses were performed by the author under the supervision of Dr. Karsten Goemann at the Central Science Laboratories, University of Tasmania, in late 2006.

1.6.8 Structural Analysis

The results of structural mapping are presented in Chapter 4. Structural analysis was done by the author during field mapping and intermittently thereafter at the University of Tasmania. There are few published examples of the analysis of stockwork vein geometries such as that attempted in this study, and interpretation

has relied heavily on the results of several fundamental works on brittle structural geology and transpressive fault systems (Etchecopar et al., 1981; Sanderson and Marchini, 1984; Hancock, 1985; Dunne and Hancock, 1994; Tikoff and Teyssier, 1994; Jones and Tanner, 1995; Jones et al., 1997; Casas et al., 2001; Jones et al., 2004).

1.6.9 U-Th/He Thermochronology

U-Th/He thermogeochronology is used in this study to place constraints on the magnitude and timing of relative vertical displacements across principal faults. Grain picking and analyses were performed by members of Dr. Peter Reiners' team, then at Yale University, Connecticut, USA, during late 2005 and early 2006. Interpretation of the geological significance of the data was done by the author.

1.6.10 Whole Rock Geochemistry

Whole rock geochemistry of least-altered magmatic rocks is used in this study to constrain the tectonic environment of basement volcanism and sedimentation and to make inferences about the tectonic environment of fertile magma generation (Chapter 5). X-ray fluroescence (XRF) and laser ablation ICP-MS analyses were performed by Dr. Phil Robinson at CODES in August 2004, May 2005, and July 2006. Further LA ICP-MS and XRF geochemistry was done at the Ontario Geoscience Laboratories, Thunder Bay, Ontario (OGS), in collaboration with Dr. Peter Hollings at Lakehead University.

1.6.11 Advanced Spaceborne Thermal Emission and Reflection Radiometer (ASTER) mineral mapping

ASTER spectral filter mineral maps were made during this study as a comparator to alteration mapped in drilling and at surface (Chapter 4). ASTER data was generously donated by Bob Agar, a consultant to Newmont Asia Pacific, in Perth, Australia. The data was processed by the author in August 2007, but the raw imagery is younger than the mining operations, so spectral anomalies in the vicinity of the major deposits (notably over cover sequences east of Ujina) are likely to be anthropogenic. Little of geological value could therefore be drawn from this work and the results are not presented.

1.6.12 Concurrent and Subsequent Studies

This study ran in parallel with the broader goals of AMIRA International project P765. It is therefore associated with-, and provides important background to investigations of wholerock geochemistry of altered rocks and the trace element chemistry of alunite, enargite and epidote that were important aspects of that broader research project.

Shortly before this study commenced, Anglo American had sponsored the PhD project of Esteban Urqueta, that dealt primarily with surface lithogeochemical mapping across the eastern Collahuasi district. Publications related to this study include the conference abstract of Oates et al. (2007), and Urqueta et al.'s (2009) paper concerning the major results of their lithogeochemical study.

During field work for this thesis, Professors Victor Maksaev and Fransisco Munizaga at the University of Chile in Santiago were working on a regional Re-Os geochronology and Os isotope study of Chilean porphyry belts, although the results are yet to be published. Subsequent to reporting of mapping and geochronology results contained in this thesis, Munizaga et al. (2008) published 13 SHRIMP zircon U-Pb ages for the Peine Group. However, these authors failed to constrain the stratigraphic position of their samples and appear to have repeatedly dated the lowermost part of the package. This is perhaps not surprising since it comprises erosionally resistant felsic ingmibrites that are widespread and distinctive. During 2008, CMDIC also commissioned a study of the magmatic chemistry of the mineralised intrusive rocks at Collahuasi. This work largely duplicates results reported to AMIRA P765 sponsors in December 2006, but together the datasets provide a more statistically robust data population on which petrogenetic interpretations may be made (e.g., Selles et al., 2009).

1.7 Terminology

Abbreviations, translations and relevant geological nomenclature conventions are contained in Appendix I for reference. Common and regional names have been translated in keeping with previous authors, but local place names have been kept in their original form.

Chapter 2.

TECTONIC EVOLUTION AND METALLOGENY OF THE CENTRAL ANDES; A REVIEW.

2.1 Introduction

The tectonic setting of the Central Andes cordillera has been the focus of much research over the past 35 years, including important contributions from Mortimer and Saric (1975), Lopez-Escobar et al. (1979), Maksaev (1979), Coira et al. (1982), Tosdal et al. (1984), Ramos et al. (1986), Woerner et al. (1992a), Kay and Mahlburg-Kay (1993), Grocott et al. (1994), Scheuber et al. (1994), Kay et al. (1995), Sandeman et al. (1995); James and Sacks (1999), Kay et al. (1999); Maksaev and Zentilli (1999), Tassara (2005), Arevalo (2006), and Oncken et al. (2006). Much of the research has necessarily investigated the Andean margin at spatial and temporal scales that are too broad for precise conclusions to be made that are relevant to the interpretation of the regional metallogeny. Understanding of how the metallogeny relates to tectonic events that can be inferred from mappable geology remains interpretive and field work-intensive, and is the subject of considerable debate (Zentilli and Maksaev, 1995; Kay et al., 1999; Maksaev, 2000; Tosdal and Richards, 2001; Haschke et al., 2002a; McClay et al., 2002; Amilibia and Skarmeta, 2003; Skarmeta et al., 2003; Matthews and Cornejo, 2003; Richards, 2003; Cooke et al., 2005; Gow and Walshe, 2005; Perelló and Posso, 2007; Amilibia et al., 2008). There is general consensus however that because of the nature of crustal permeability, fluid flow and mineralisation accompany deformation (e.g., Cox, 2005). The spatial relationships between mineralised Late Miocene-Quaternary arc segments and subduction of thickened oceanic crust (e.g., Cooke et al., 2005; Rosenbaum et al., 2005) further suggests that although subduction zones may be generally dynamic, mineralisation accompanies relatively short periods of deformation of unusual geometry and/or intensity.

This chapter is a review of the tectonic and geologic framework of the Chilean Andes as currently understood, presented as background and context for the detailed study

of the Collahuasi district to follow. In this regard it is similar to previous reviews (e.g., Ramos and Aleman, 2000; Hollings et al., 2003), but attempts to emphasise the geological evidence for the standing interpretations. It is divided into three sections that describe periods of similar prevailing tectonic regime: the 'Hercynian Cycle' of terrane accretion and westward continental growth from the Cambrian to the Mississippian (e.g., Ramos and Aleman, 2000); the 'Gondwanan Cycle' of oblique sinistral subduction and related extensional volcanism and sedimentation from the Pennsylvanian to mid-Cretaceous (e.g., Scheuber et al., 1994); and the 'Andean Cycle' of mildly oblique dextral subduction convergence and concommitant east-migrating arc magmatism and orogenic compression from the late Cretaceous to the present. The western South American margin did not evolve through this time in isolation, and many of the events discussed here occurred along much or all of the western margin of Gondwana (Fig. 2.1: Ramos, 1988).

Figure 2.1. Tectonic diagram of Gondwana during the Late Paleozoic-Jurassic showing arc-related (-), and extensional felsic (=) and mafic (v) magmatic provinces associated with western margin of Gondwana. Re-drafted from Herve (1988). Abbreviations: Carb. = Carboniferous; P = Permian; Tr = Triassic, J = Jurassic.

Genetic models for many major mineral deposit styles, including porphyry Cu deposits, involve an appreciation that a series of favourable conditions for mineralisation typically coincide in one (or rarely more) tectonic setting (e.g., Sillitoe, 1972; Tosdal and Richards, 2001; Groves and Bierlein, 2007). Understanding regional tectonic evolution is therefore a key element of terrane selection for mineral exploration, and metallogenic events are included in this chapter in the context of their tectonic setting.

2.2 Tectono-Geologic History of the Andes Cordillera

2.2.1 Hercynian Cycle

The late Proterozoic and early Cambrian was marked by rifting along the entire southern margin of Pangaea from the Argentine to Australian cratons (Glen and Walshe, 1999; Omarini et al., 1999), culminating with inversion of these basins at about 530 Ma. (Table 2.1; Pampean and Delamerian Orogenies: Omarini et al., 1999; Glen et al., 2007). In the western part of the orogen, rifting generated a core complex comprised of Precambrian aluminous metamorphics of the Amazon and Argentine (Pampia) cratons, and caused detachment of discrete crustal slivers from the Pangaean margin (Ramos, 1988; Tosdal, 1996; Bahlburg et al., 2000; Bahlburg, 2003; Finney et al., 2003a). Cratonic rocks are rare to the south and southwest of this margin, and the basement in this region is comprised of several lithologically, chronologically and chemically distinct terranes (Fig. 2.2). Some of these terranes are semi-autochthonous and were rifted from the continent during the late Proterozoic (e.g., Arequipa-Antofalla: Lucassen et al., 2000; Ramos and Aleman, 2000) contemporaneous with widespread sedimentation (Griem-Klee and Neimeyer, 2006). Other terranes share little or no affinity with cratonic South America (Famatina, Chilenia: Coira et al., 1982; Ramos et al., 1986; Ramos, 1994; Miller et al., 2003, and Arequipa-Antofalla according to Loewy et al., 2004). A coarse fabric of NW-trending crustal-scale fault zones and coincident magmatic axes (Coughlin et al., 1995; Seggiaro, 2006) that traverse the modern Andes Cordillera is interpreted to reflect crustal structures that formed or were transposed into that orientation during suturing of these terranes (“lineaments” of Salfity, 1985; Ramos, 1994; Richards, 2000). Widespread

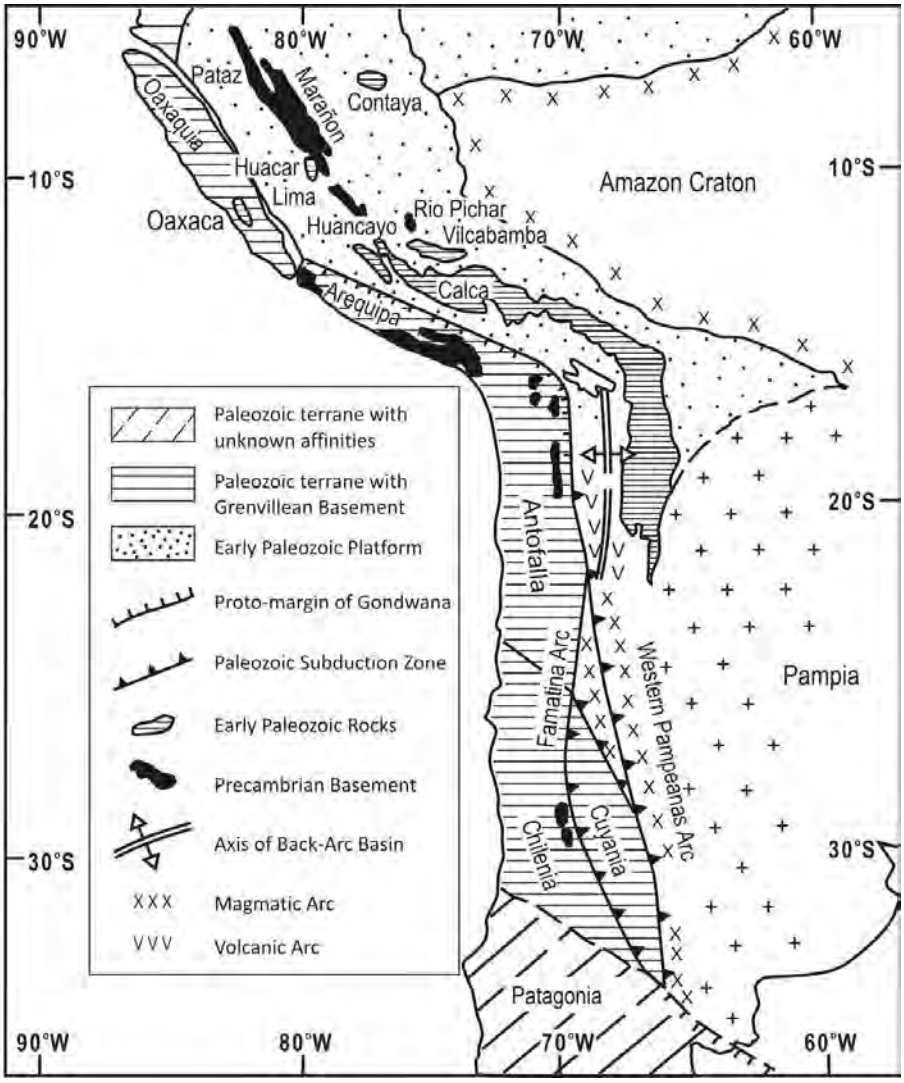

Figure 2.2. Simplified geological map showing the present location of rock units that relate to Lower Paleozoic tectonic elements of southwestern South America. Redrafted from Ramos and Aleman (2000), with additional details from Ramos (1986; 1988), and Mpodozis and Kay (1992).

distribution of post-Devonian strata imply that the accretionary events related to amalgamation of the Central and Southern Andean basement terranes occurred before the Late Devonian (Coira et al., 1982; Ramos et al., 1986).

Continent-directed subduction began along the continental margin, as well as along a bimodal calc-alkaline island arc outboard of the margin of Gondwana during the Cambrian (Famatina Arc: Aceñolaza and Toselli, 1976; Mangano and Buatois, 1996; Toselli et al., 1996; Miller et al., 2003). Collision of the Pampia cratonic 'sliver' and the Famatinian island arc with mainland Pangaea occurred at about 450 Ma and caused intense compressive deformation, including development of a fold-and-thrust belt, metamorphism and syn-kinematic granitoid emplacement in the Sierras

Pampeanas (Ocloyic I tectonic event: Fig. 2.3, Table 2.1, e.g., Coira et al., 1982). Docking of the semi-autochthonous Arequipa-Antofalla and Cuyania terranes approximately 20 m.y. later caused renewed compressive deformation of a similar style along a broader section of the continental margin as far north (modern coordinates) as central Peru (Ocloyic II tectonic event: Fig. 2.3, Table 2.1, e.g., Turner et al., 1979). These two events coincide closely in time with two episodes of deformation attributed to the accretionary Benambran Orogeny in eastern Australia (Vandenberg, 1999; Glen et al., 2007) suggesting the possibility of contemporaneous accretion-related deformation along the entire southern margin of Pangaea. Structurally-controlled orogenic gold deposits formed in turbiditic marine sedimentary packages of the Famatina back arc during this event (Zappettini and Segal, 1998), and major gold deposits of this type formed in eastern Pangaea (Victoria, Australia: Berlein and Maher, 2001). Shallow marine (shelf) deposition then dominated a relatively passive continental margin during the Siluro-Devonian. Another compressive tectonic phase affected NW Argentina, Bolivia and SE Peru at ~350 Ma. (the Chanic event: Bahlburg et al., 2000), broadly coincident with accretion of the Chilenia Terrane into an east-dipping subduction zone further south (Coira et al., 1982; "Gondwanan Orogen", Heredia et al., 2006). Continental and shallow marine strata of Mississippian age (Damm et al., 1990, Busquets et al., 2005) and younger volcano-sedimentary marine facies (e.g., Bahlburg and Breitkreuz, 1991) overlie an unconformity across the accreted terranes of southwestern South America and mark the end of the Hercynian Cycle (Ramos et al., 1986).

2.2.2 Gondwanan Cycle, part I: Carboniferous to middle Triassic

Bimodal calc-alkaline arc magmatism, arguably related to a subduction zone, recommenced along the southwestern margin of Pangaea during the early Pennsylvanian (Choiyoi Arc, Fig. 2.3: Bahlburg and Breitkreuz, 1991, 1993; Breitkreuz and Zeil, 1994; Munizaga et al., 2008). The onset of magmatism may have been driven by decreased drift of Gondwana related to its collision with Laurasia (e.g., Stampfli and Borel, 2002). Highly oblique sinistral convergence between the Aluk (Phoenix) plate and the continental plate (Zonenshayn et al., 1984) generated tensional conditions and sedimentary accommodation along the magmatic arc (Jarrard, 1986; Bahlburg

and Breitkreuz, 1991; Scheuber et al., 1994) such that the volcanic and dominantly epiclastic shallow marine strata of the lower Peine Group are intercalated (Breitkreuz and Zeil, 1994; Bahlburg and Herve, 1997). The 'arc graben' persisted through the Permian, deepening in southern Peru where the volcanics of the Púcara Group is subordinate to intercalated marine carbonates (Kontak et al., 1985; Clark et al., 1990a; Rosas et al., 2003). Magmatism in northern Chile related both to subduction processes and crustal anatexis, and may have become more anatectic in character in the latest Permian and Triassic (Kay et al., 1989; Brown, 1991; Depine et al., 2005). The Gondwanan margin at this time is interpreted to have been a transtensional subduction zone in which the continental basement was thin and hot (Scheuber et al., 1994; Mpodozis and Cornejo, 2003).

Volcanism along the Choiyoi Arc ceased during the middle Triassic, and a reduction in arc volcanic productivity is marked by the general absence of volcaniclastic facies in the uppermost Peine Group (Breitkreuz and Zeil, 1994). Pronounced regression in the Peruvian sector culminated in the deposition of evaporites in the upper Púcara Group (Ramos et al., 1996b; Rosas et al., 2003). Decline of the Choiyoi Arc is attributed to the San Rafael compressional tectonic event around the Permian-Triassic boundary (Llambias and Sato, 1990; Mpodozis and Kay, 1992; Fernandez Seveso et al., 1993; Ramos et al., 1996a). Tectonism and subsequent westward relocation of the arc front has been variously interpreted as a result of increased mantle convection under Gondwanaland with associated slab rollback (Breitkreuz and Zeil, 1994), subduction of an oceanic plateau (Parada et al., 1991), or accretion of an unidentified

Figure 2.3. (adjacent page) Generalised time-space diagram and upper crustal sections for northern Chile (21º-25ºS) showing the key stages in the development of the greater Andes Cordillera and the relationship between magmato-tectonic cycles and mineralization. The spatial distribution of magmatic products is based on a compilation of radiometric ages by Scheuber et al. (1994). Crustal sections are modified from Ramos and Aleman (2000). Additional details were compiled from Aceñolaza and Toselli (1976), Coira et al. (1982), Tosdal et al. (1984), Zonenshayn et al. (1984), Chong Diaz and Reutter (1985), Herve (1988), Bogdanic et al. (1990), Clark et al. (1990a), Scheuber and Andriessen, (1990), Bahlburg and Breitkreuz (1991), Scheuber and Hammerschmidt (1991), Hammerschmidt et al. (1992), Scheuber and Reutter (1992), Breitkreuz and Zeil (1994), Charrier and Muñoz (1994), Prinz et al. (1994), Sandeman et al. (1995), Scheuber et al. (1995), Toselli et al. (1996), Bahlburg and Herve (1997), Tomlinson and Blanco (1997a, b), Lucassen et al. (1999a, b), Richards et al. (2001), Haschke et al. (2002b), Miller et al. (2003); Franz et al. (2006). Abbreviations for mineralisation: PCD = porphyry Cu-(Mo-Au); IOCG = iron oxide copper gold; HSE = high sulfidation epithermal; XCU = exotic Cu; SCU = supergene Cu enrichment. Abbreviations for geological time: Neocom.=Neocomian; Apt.=Aptian; Cenom.= Cenomanian; Tur.= Turonian; Maast.= Maastrichtian.

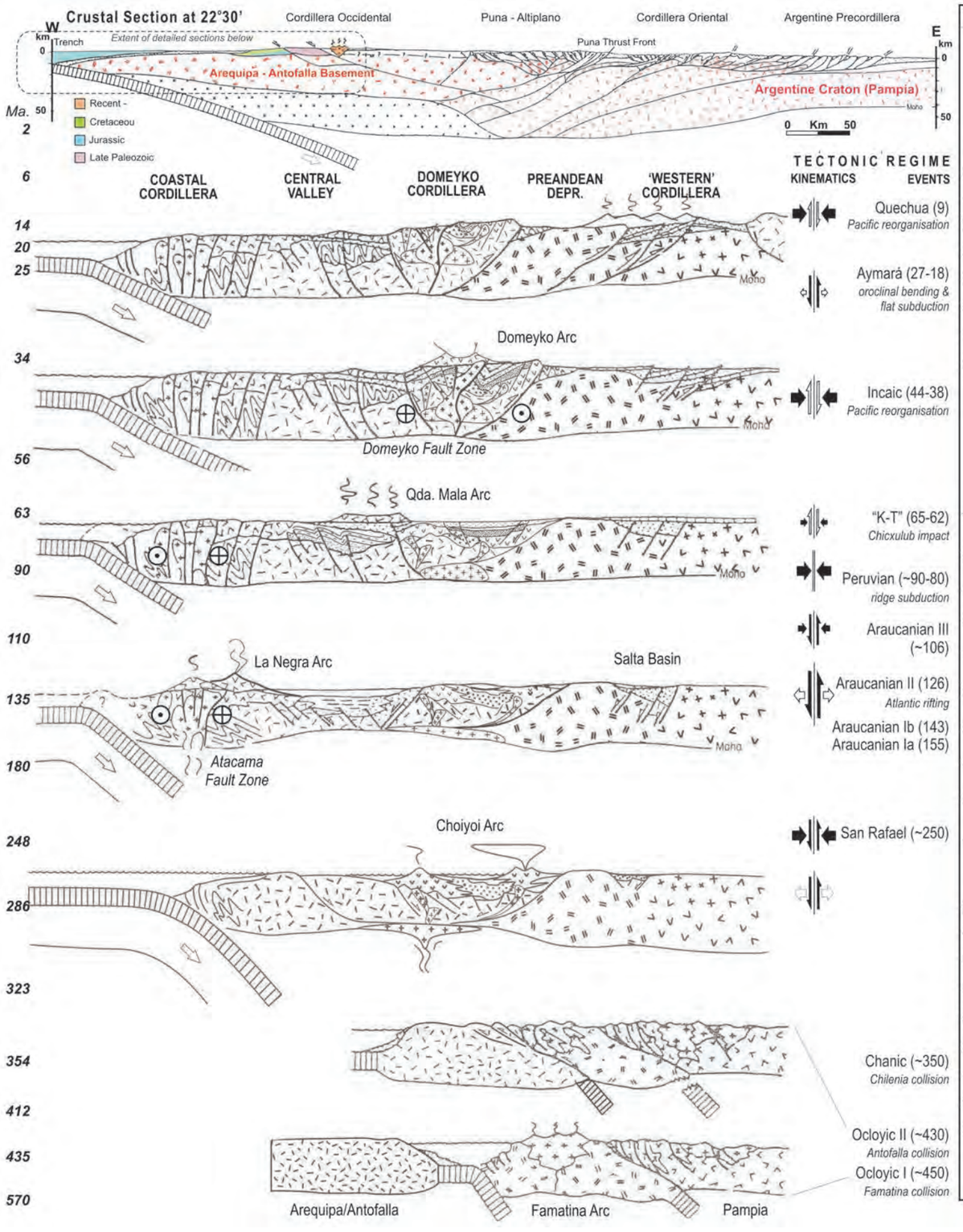
Crustal Section at 22°30'
Cordillera Occidental
Puna - Altiplano
Cordillera Oriental
Argentine Precordillera
W
E
km
Trench
Extent of detailed sections below
Arequipa - Antofalla Basement
Puna Thrust Front
Argentine Craton (Pampia)
Moho
0 Km 50
Recent -
Cretaceou
Jurassic
Late Paleozoic
Ma.
COASTAL CORDILLERA
CENTRAL VALLEY
DOMEYKO CORDILLERA
PREANDEAN DEPR.
'WESTERN' CORDILLERA
TECTONIC REGIME
KINEMATICS
EVENTS
Quechua (9)
Pacific reorganisation
Aymará (27-18)
oroclinal bending & flat subduction
Domeyko Arc
Domeyko Fault Zone
Incaic (44-38)
Pacific reorganisation
Qda. Mala Arc
"K-T" (65-62)
Chicxulub impact
Peruvian (~90-80)
ridge subduction
Araucanian III (~106)
La Negra Arc
Salta Basin
Araucanian II (126)
Atlantic rifting
Araucanian Ib (143)
Araucanian Ia (155)
Atacama Fault Zone
Choiyoi Arc
San Rafael (~250)
Chanic (~350)
Chilenia collision
Ocloyic II (~430)
Antofalla collision
Ocloyic I (~450)
Famatina collision
Arequipa/Antofalla
Famatina Arc
Pampia
AGE
CENOZOIC
MESOZOIC
PALEOZOIC
QUATERNARY
TERTIARY
CRETACEOUS
JUR.
TRIASSIC
PERM.
CARBONIFEROUS
DEV.
SIL.
C.-O.
Recent
Pleist.
Pliocene
Miocene
Oligocene
Eocene
Paleocene
Tur.-Maast.
Apt.-Cenom.
Neocom.
Pensylvanian
Mississippian

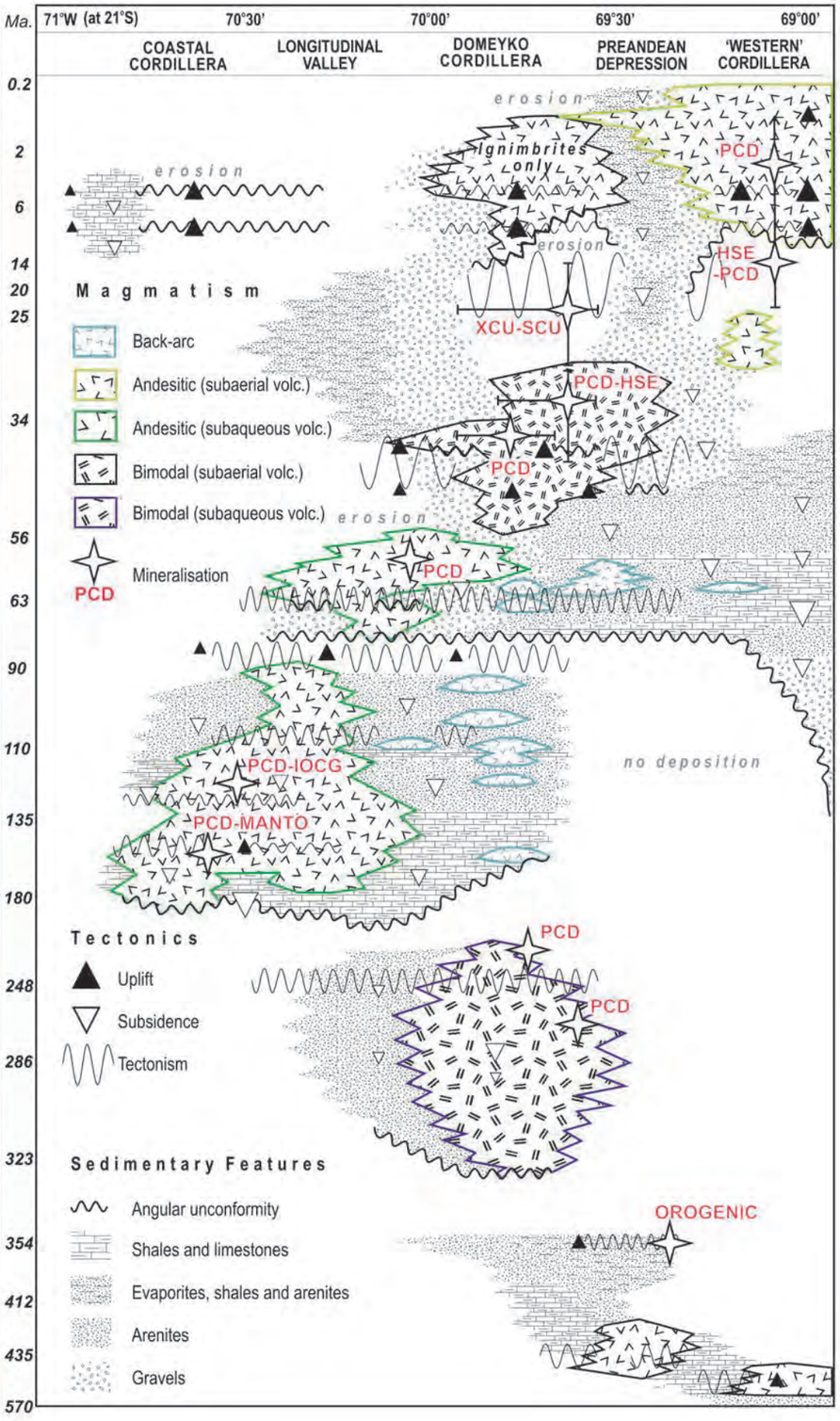
Ma.
71°W (at 21°S)
70°30'
70°00'
69°30'
69°00'
COASTAL CORDILLERA
LONGITUDINAL VALLEY
DOMEYKO CORDILLERA
PREANDEAN DEPRESSION
'WESTERN' CORDILLERA
erosion
Ignimbrites only
PCD
HSE -PCD
XCU-SCU
PCD-HSE
PCD-IOCG
PCD-MANTO
no deposition
Magmatism
Back-arc
Andesitic (subaerial volc.)
Andesitic (subaqueous volc.)
Bimodal (subaerial volc.)
Bimodal (subaqueous volc.)
Mineralisation
Tectonics
Uplift
Subsidence
Tectonism
Sedimentary Features
Angular unconformity
Shales and limestones
Evaporites, shales and arenites
Arenites
Gravels
OROGENIC

Figure 2.3. Generalised time-space diagram and upper crustal sections for northern Chile (21º-25ºS). The key stages in the development of the greater Andes Cordillera and the relationship between magmato-tectonic cycles and mineralization are . The spatial distribution of magmatic products is based on a compilation of radiometric ages by Scheuber et al. (1994). Crustal sections are modified from Ramos and Aleman (2000). Additional details were compiled from Aceñolaza and Toselli (1976), Coira et al. (1982), Tosdal et al. (1984), Zonenshayn et al. (1984), Chong Diaz and Reutter (1985), Hervé (1988), Bogdanic et al. (1990), Clark et al. (1990a), Scheuber and Andriessen (1990), Bahlburg and Breitkreuz (1991), Scheuber and Hammerschmidt (1991), Hammerschmidt et al. (1992), Scheuber and Reutter (1992), Breitkreuz and Zeil (1994), Charrier and Muñoz (1994), Prinz et al. (1994), Sandeman et al. (1995), Scheuber et al. (1995), Toselli et al. (1996), Bahlburg and Herve (1997), Tomlinson and Blanco (1997a, b), Lucassen et al. (1999a), Richards et al. (2001a), Haschke et al. (2002a, 2002b), and Miller et al. (2003). Abbreviations for mineralisation: PCD = porphyry Cu-(Mo-Au); IOCG = iron oxide copper gold; HSE = high sulfidation epithermal; XCU = exotic Cu; SCU = supergene Cu enrichment. Abbreviations for geological time: Neocom.=Neocomian; Apt.=Aptian; Cenom.= Cenomanian; Tur.= Turonian; Maast.= Maastrichian.

microplate "X" (Mpodozis and Kay, 1992). Minor localised magmatism persisted along the arc at least 20 m.y. after the cessation major widespread volcanism, and was associated with the formation of the younger members of a series of small, low grade porphyry Cu-Mo centres. These occur along the eastern part of the arc between 20º and 40ºS and formed in three magmatic-hydrothermal epochs at around 284, 243 and 210 Ma (Fig. 2.4, Sillitoe, 1977; Baeza and Alfaro, 1994; Marquardt et al., 1997; Camus, 2003; Sillitoe and Perelló, 2005; Cornejo et al., 2006).

2.2.3 Gondwanan Cycle, part II: Triassic to middle Cretaceous

Mafic-intermediate arc magmatism re-established in the Jurassic, along a steep Mariana-type subduction zone (Uyeda and Kanamori, 1979) some 200-300 km west of the older arc front (La Negra Arc: Charrier and Muñoz, 1994; Pichowiak, 1994; Scheuber et al., 1994). A transtensional regime again prevailed along the arc front (Davidson et al., 1976; Naranjo and Puig, 1984; Roessling et al., 1986), and the Jurassic arc was characterised by a strong arc-back arc couple that developed an elongate extensional basin in the back arc (Figs. 2.3 and 2.5, the Tarapacá Basin of Prinz et al., 1994). Sedimentation in the back-arc was dominated by marine shales and limestones throughout the Jurassic (Charrier and Muñoz, 1994). Pronounced along-arc segmentation split the back arc basin into five discrete and persistent depo-centres coincident with Paleozoic crustal-scale fault zones (Prinz et al., 1994).

Sinistral transcurrent displacement was articulated along the trench-parallel Atacama FS (Arabasz, 1971; Scheuber and Hammerschmidt, 1991). This 20 to 100 km-wide structural zone focussed magmatic emplacement (Grocott et al., 1994) and hydrothermal fluid flow related to a series of structurally controlled and stratabound, intrusion-related manto copper-silver deposits between 170 and 150 Ma. (Espinoza, 1986; Sillitoe, 1990; Vidal et al., 1990; Trista-Aguilera et al., 2006). In the southernmost Peruvian arc segment, porphyry Cu deposits formed at this time (Sillitoe and Perello, 2005). Sheeted mafic dykes were emplaced into the Atacama FS during an oscillatory transtensional-transpressional event in the latest Jurassic (Araucanian I event, 155-143 Ma.: Riccardi, 1988; Scheuber and Gonzalez, 1999), and accompanied the formation of porphyry Cu deposits (Fig. 2.4: Antucoya, Puntillas, Galenosa) and the breccia-hosted intrusion-related Mantos Blancos Cu

deposit in the Tocopilla-Antofagasta region of northern Chile (Maksaev et al., 2006; Ramirez et al., 2006). Intense ductile strain and mylonite formation occurred along the Atacama FS during the Neocomian (Araucanian II event, 130-125 Ma.: Naranjo et al., 1984; Scheuber and Andriessen, 1990; Scheuber and Hammerschmidt, 1991; Scheuber et al., 1995; Cembrano et al., 2003). Mylonitisation was associated with local uplift of the proto-Cordillera de la Costa (Maksaev et al., 1988) and contemporaneous with partial inversion of the back-arc basin (Fig. 2.5: Charrier and Muñoz, 1994). The event coincided with a pulse of pronounced rifting in the incipient South Atlantic Ocean at ~127 Ma. (Ramos and Ramos, 1979; Turner et al., 1994; Oyarzun et al., 2003).

Magmatism along the La Negra Arc persisted into the Neocomian, accompanied by complex metallogeny including porphyry copper deposits (Camus, 2002; Sillitoe and Perello, 2005) and hematitic, commonly intrusion-related Cu deposits associated with a broader iron oxide-apatite mineralisation event along the Atacama FS (121-111 Ma.: Espinoza, 1981; Ménard et al., 1990; Oyarzun et al., 1996; Marschik et al., 1997; Oyarzun et al., 1999; Fox et al., 2001; Marschik and Fontboté, 2001; Mathur et al., 2002; Barton et al., 2005; Arévalo et al., 2006). The Cretaceous porphyry activity appears to have stepped southwards along the arc front, occurring at 132-118 Ma in northern Chile, at 106-91 Ma in north-central Chile, and at 90-73 Ma in central Chile (Fig. 2.4: Camus, 2002). A further pulse of Atlantic spreading and a shift in the absolute motion of the South American plate occurred between 110-106 Ma and caused a compressional event recorded by constriction of the La Negra Arc (Araucanian III event, Figs. 2.3 and 2.5, Table 2.1: Ramos and Ramos, 1979; Ramos and Alemán, 2000). The northern and north-central groups of Cretaceous porphyries formed contemporaneous with-, or immediately after the Araucanian II and III tectonic phases, respectively (Camus, 2003). After this tectonism, magmatism was restricted to the eastern half of what had once been a much broader arc front, but became more common along the back-arc (Fig. 2.3, e.g., Pichowiak, 1994).

→

Figure 2.4. Metallogenic and geologic sketch map of the central Andes showing the spatial and temporal distribution of porphyry, epithermal and other intrusion-related mineral deposits and districts (age of mineralisation in parentheses). Major structural discontinuitie, "lineaments" and fault systems are also shown. Compiled from DeWit et al., 1988; Clark et al., 1990a; 1990b; Cunningham et al., 1994; Mutschler et al., 2000; Richards, 2000; Camus, 2002; Perello et al., 2003; Sillitoe and Perello, 2005; Bertens et al., 2006; Palacios et al., 2006, Ramirez et al., 2006; and Trista-Aguilera et al., 2006.

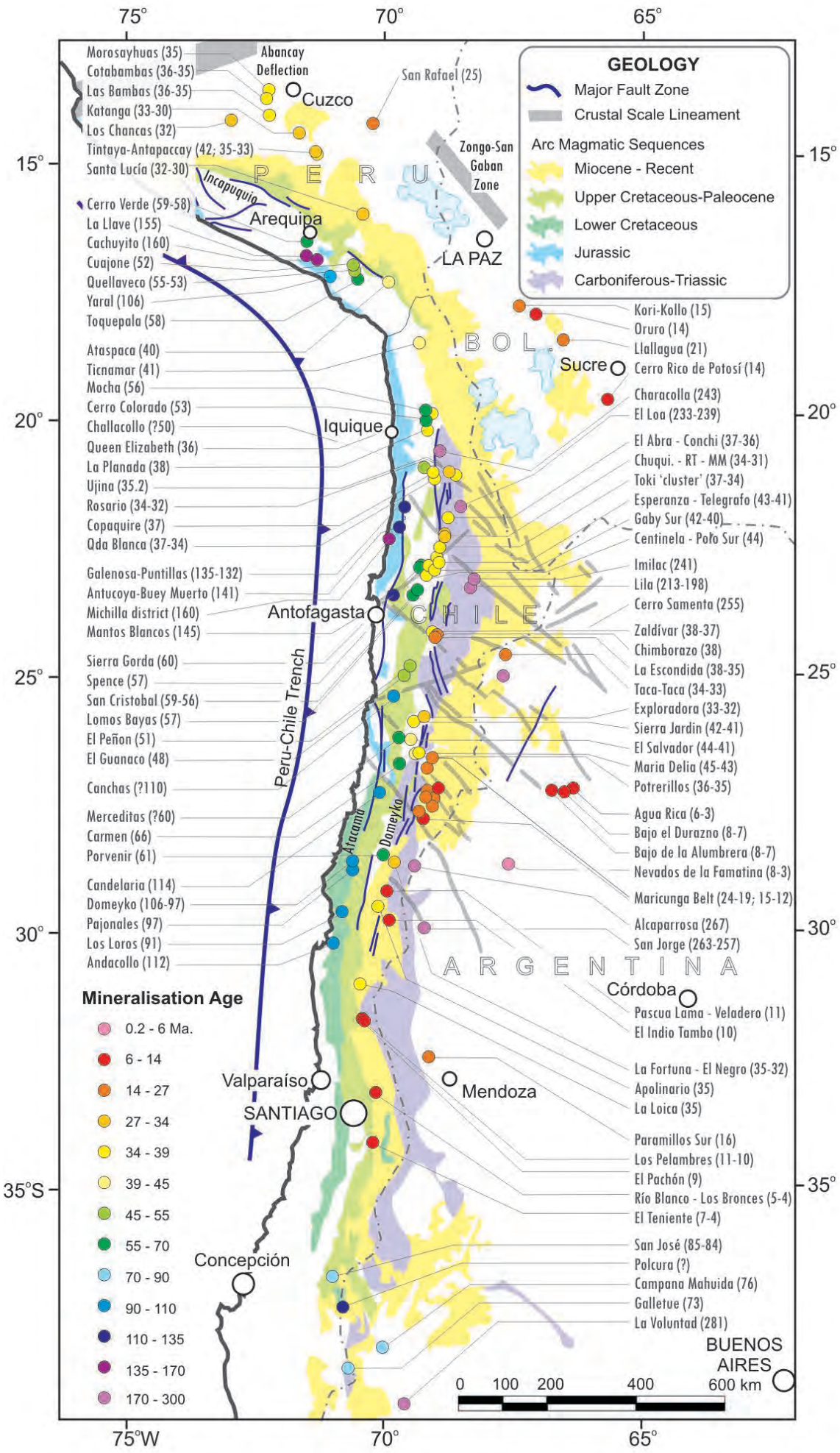
GEOLOGY
Major Fault Zone
Crustal Scale Lineament
Arc Magmatic Sequences
Miocene - Recent
Upper Cretaceous-Paleocene
Lower Cretaceous
Jurassic
Carboniferous-Triassic
Mineralisation Age
0.2 - 6 Ma.
6 - 14
14 - 27
27 - 34
34 - 39
39 - 45
45 - 55
55 - 70
70 - 90
90 - 110
110 - 135
135 - 170
170 - 300
Morosayhuas (35)
Cotabambas (36-35)
Las Bambas (36-35)
Katanga (33-30)
Los Chancas (32)
Tintaya-Antapaccay (42; 35-33)
Santa Lucía (32-30)
Cerro Verde (59-58)
La Llave (155)
Cachuyito (160)
Cuajone (52)
Quellaveco (55-53)
Yaral (106)
Toquepala (58)
Ataspaca (40)
Ticnamar (41)
Mocha (56)
Cerro Colorado (53)
Challacollo (?50)
Queen Elizabeth (36)
La Planada (38)
Ujina (35.2)
Rosario (34-32)
Copaquire (37)
Qda Blanca (37-34)
Galenosa-Puntillas (135-132)
Antucoya-Buey Muerto (141)
Michilla district (160)
Mantos Blancos (145)
Sierra Gorda (60)
Spence (57)
San Cristobal (59-56)
Lomos Bayas (57)
El Peñon (51)
El Guanaco (48)
Canchas (?110)
Merceditas (?60)
Carmen (66)
Porvenir (61)
Candelaria (114)
Domeyko (106-97)
Pajonales (97)
Los Loros (91)
Andacollo (112)
Kori-Kollo (15)
Oruro (14)
Llallagua (21)
Cerro Rico de Potosí (14)
Characolla (243)
El Loa (233-239)
El Abra - Conchi (37-36)
Chuqui. - RT - MM (34-31)
Toki 'cluster' (37-34)
Esperanza - Telegrafo (43-41)
Gaby Sur (42-40)
Centinela - Polo Sur (44)
Imilac (241)
Lila (213-198)
Cerro Samenta (255)
Zaldívar (38-37)
Chimborazo (38)
La Escondida (38-35)
Taca-Taca (34-33)
Exploradora (33-32)
Sierra Jardin (42-41)
El Salvador (44-41)
Maria Delia (45-43)
Potrerillos (36-35)
Agua Rica (6-3)
Bajo el Durazno (8-7)
Bajo de la Alumbrera (8-7)
Nevados de la Famatina (8-3)
Maricunga Belt (24-19; 15-12)
Alcaparrosa (267)
San Jorge (263-257)
Pascua Lama - Veladero (11)
El Indio Tambo (10)
La Fortuna - El Negro (35-32)
Apolinario (35)
La Loica (35)
Paramillos Sur (16)
Los Pelambres (11-10)
El Pachón (9)
Río Blanco - Los Bronces (5-4)
El Teniente (7-4)
San José (85-84)
Polcura (?)
Campana Mahuida (76)
Galletue (73)
La Voluntad (281)
San Rafael (25)
Abancay Deflection
Incapuquio
Zongo-San Gaban Zone
Peru-Chile Trench
Atacama
Domeyko
PERU
BOL.
CHILE
ARGENTINA
Cuzco
Arequipa
LA PAZ
Sucre
Iquique
Antofagasta
Valparaíso
SANTIAGO
Mendoza
Córdoba
Concepción
BUENOS AIRES
0 100 200 400 600 km
75°
70°
65°
15°
20°
25°
30°
35°S
75°W

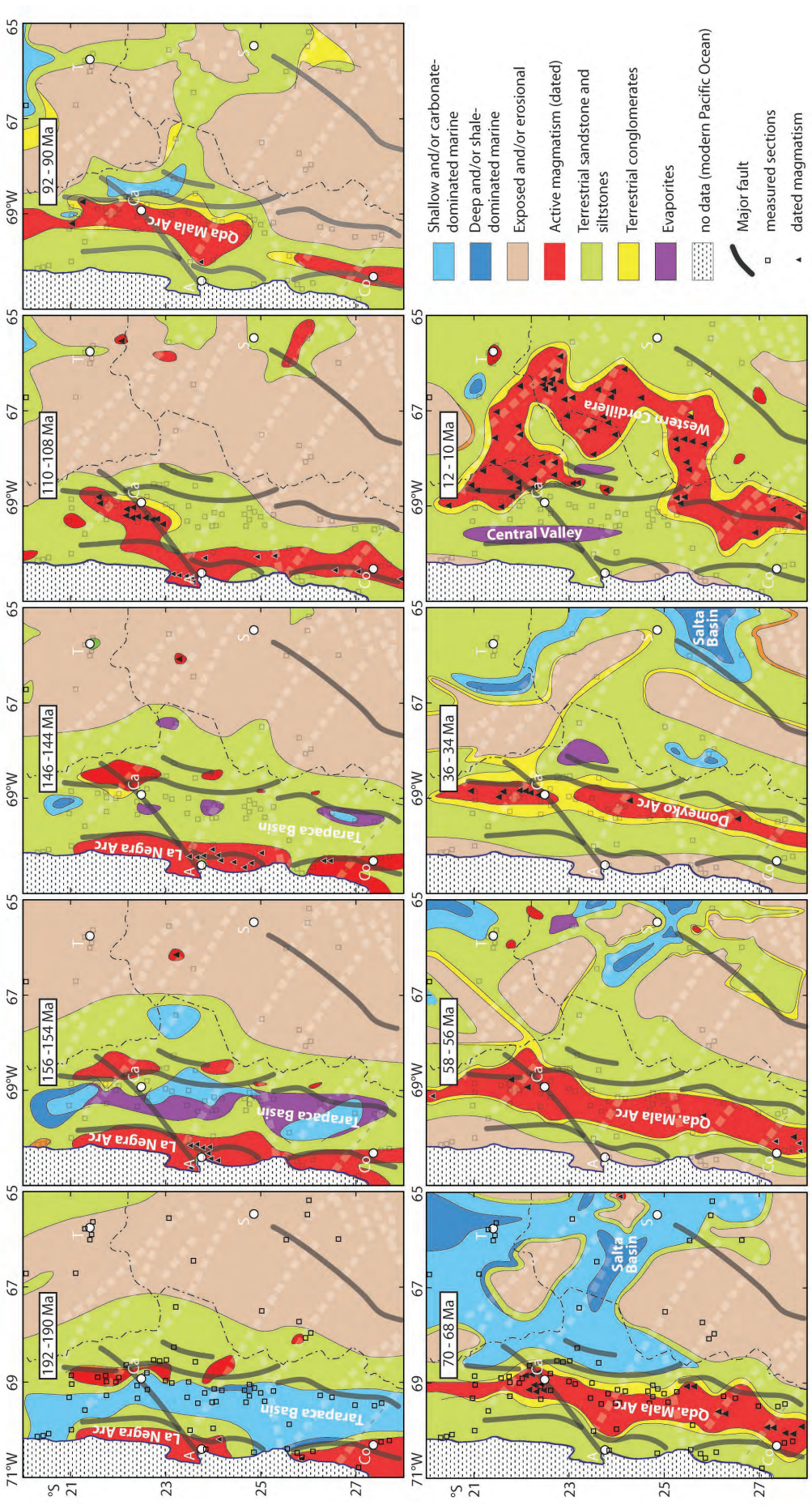

Figure 2.5. Simplified sedimentary facies and magmatism maps of the southern Central Andes for nine, two million year intervals from the Jurassic to the Middle Miocene. Reconstructions are redrafted from Arcuri and Brimhall (2002) and were drawn based on available measured stratigraphic sections (small squares in left-most panels) and geochronolgical data (black triangles), and account for known periods of tectonism and global eustatic sea level changes. Overlaid are the major regional fault systems observable in surface geology (from Richards, 2000, and Palacios et al., 2007), and interpreted lineaments (Salfity, 1985; Richards 2000b). Locally there is good spatial coincidence

... (continued on next page)

Major compressive deformation of the Peruvian Tectonic Phase affected the arc during the Turonian (Steinmann, 1929; e.g., Clark et al., 1990a) as the Aluk-Farallón spreading ridge migrated southward along the subduction zone (Scheuber et al., 1994). Deformation occurred at 87-83 Ma in central Peru (Harland et al., 1990), and had finished by 78 Ma in northern Chile (Maksaev et al., 1988). The La Negra Arc was completely attenuated at this time and the forearc underwent significant folding and thrust shortening. Inboard of the arc, shortening was accommodated by block faulting and epeiric uplift articulated on inverted back-arc growth structures (Bogdanic and Doebel, 1990). Migration of the spreading ridge beyond continental South America caused a fundamental change in the far-field stress regime: from >45° sinistral transtension (Aluk subduction) to <30° dextral transpression (Farallón subduction: Zonenshayn et al., 1984; Scheuber et al., 1994). This marks the end of the Gondwanan cycle along the Andean continental margin. Magmatic quiescence followed in northern Chile until 72 Ma when a magmatic arc was re-established 50-100 km to the east in the position of the modern eastern Valle Central and Domeyko Cordillera (Quebrada Mala Arc, Fig. 2.3: Scheuber and Reutter, 1992; Charrier and Muñoz, 1994).

2.2.4 Andean Cycle, part I: Late Cretaceous to Upper Oligocene

Andesitic volcanism of the Quebrada Mala Arc occurred until ~65 Ma on a substrate of Jurassic-Turonian back-arc sedimentary rocks. Continental extension accommodated extensive sedimentation in a contemporaneous back arc basin along the proto-Preandean Depression. This basin deepened southward and became shallow marine to the south of Calama (Purilactis Group: Charrier and Reutter, 1994). Continental extension further inland caused subsidence and marine incursion into the Argentine Salta Basin (Fig. 2.3). A compressive tectonic event at 65-62 Ma caused local uplift of basement blocks along the proto-Domeyko Cordillera (Andriessen and Reutter, 1994) and partial inversion of the back-arc basin (Fig. 2.5). This prompted a change to bimodal explosive volcanism along the arc and increased plutonism in the back

←

Figure 2.5. *continued from previous page)...* between these structural elements and the lithofacies, elsewhere there is no relationship. Yellow triangles in the youngest panel are Pliocene volcanic centres along the Archibarca Lineament (e.g., Richards and Villeneuve, 2001; Richards et al., 2006). Abbreviations: Co = Copiapo, Ca = Calama, T = Tupiza, A = Antofagasta, S = Salta. Dark grey fine dashed line are the international borders.

arc ("K-T" event: Cornejo et al., 2003; Table 3.1). Subdued magmatism during, and especially after this event was associated with formation of major porphyry copper deposits in central-northern Chile (66-57 Ma) and in northernmost Chile and southern Peru 59-52 Ma (Clark et al., 1990a; Zweng and Clark, 1995; Concha and Valle, 1999; Mattos and Valle, 1999; Camus, 2002; Sillitoe and Perelló, 2005). Mild extension followed in the late Paleocene and earliest Eocene, accompanied by minor rhyolitic dome eruptions. Low sulfidation epithermal Au-Ag vein mineralisation post-dates, but appears spatially related to these rhyolites (Carrasco and Chong-Diaz, 1985; Warren, 2005; Arancibia et al., 2006b).

Magmatism was re-established by 48 Ma, in a narrow 50 km-wide front in the position of the modern Domeyko Cordillera (Fig. 2.5: Domeyko Arc: Scheuber et al., 1994). This zone straddled a series of soft-linked basement faults that originated in the early Mesozoic back-arc (Prinz et al., 1994) and was bound on its eastern margin by growth faults of the Maastrichtian-Paleocene back-arc (Charrier and Reutter, 1994). Global tectonic reorganisation (e.g., Clague and Jarrard, 1973; cf. Norton, 1995) and/or incipient flattening of the subducting slab (James and Sacks, 1999) likely prompted a major compressive tectonic phase recorded throughout the arc and back-arc by numerous unconformity surfaces and fission track data between 45-38 Ma (Incaic Phase, Table 2.1: Noble et al., 1979). Deformation amounting to ~25% net shortening was characterised by inversion of, and thrust-related folding along two arc-parallel fault systems with opposite vergence that caused the pop-up style uplift of elongate basement slivers that comprise the Domeyko Cordillera (Chong and Reutter, 1985; Charrier and Reutter, 1994).

Early in the Incaic event, segments of a Jurassic age arc-parallel basement fault array underwent sinistral displacements (Mpodozis et al., 1993; Tomlinson et al., 1994), but toward the end of the Incaic event, had coalesced to form a hard-linked continental wrench fault, the Domeyko FS (known as the West Fissure or Falla Oeste in the Chuquicamata area), along which dextral offsets of up to 2 km reflect the far-field transpressive regime (e.g., Tomlinson and Blanco, 1997a). The major porphyry copper (and high sulfidation epithermal) event in the northern Chilean Andes was associated with syn- and post-tectonic low-volume intermediate-felsic plutonism along the Domeyko Arc between 43 and 31 Ma (Zentilli and Maksaev,

Table 2.1. Tectonic and metallogenic events of the Central Andes cordillera, with summaries of supporting geological evidence.

Event	Timing	Tectonic Relationships	Stress Regime	Mineralisation	Geological Relationships
Andean Cycle					
Daguita[1, 2]	6-4 Ma.	Spreading shift from the Galapagos Rise to the East Pacific Rise[6], Subduction of the Nazca and Juan Fernandez aseisemic ridges, fast convergence[7,8] and shallow subduction[9].	Compressional in the Central Andes[10,11], transtensional in the Southern Andes[12].	Major porphyry Cu-Mo, Au-Cu and epithermal Au mineralisation in northern Peru and central Chile. No known mineralisation in northern Chile[13-16].	Rejuvenation by epeiric uplift all the principal cordillera[17,18], with ~3 km of vertical offset on the Tucucaro segment of the Rio Loa fault[19,20]. Development of the fold and thrust belt in the Argentine Precordillera[20,21]. Major porphyry and epithermal mineralisation spatially associated with ridge subduction and slab flattening[22,23].
Quechua[2, cf. 3-5]	9-8 Ma.				
Aymara[2]	27-18 Ma.	Bending of the Bolivian Orocline[22,24-28], acceleration of convergence rate, incipient aseismic ridge subduction and flat slab subduction under the Central Andes[2,22,29].	Sinistral transtension with strong strain partitioning[20,25,30,31].	Early stages of porphyry and epithermal Au-Cu mineralisation in belts the northern Peru[32] and central Chile[15,16]. Porphyry Sn-Ag mineralisation in the Bolivian retro arc[32].	Attenuation of magmatism except sporadic explosive felsic eruptions. Unconformity at the base of late Miocene gravels deposited during epeiric uplift and peneplanation of the Pampa de Tamarugal and Llanuras Costeranas surfaces[22,33,34]. Thrusting in the Cordillera Oriental[35], sinistral meso-scale offsets on the Rio Loa[34] and the Atacama[36] fault systems, and kilometre-scale offset along the Domeyko fault system[25,37-39], with related transtensional basin formation[40]. Lower Miocene ignimbrites do not show paleomagnetic rotation common to older rocks[26-28].
Incaic[3,41]	45-34 Ma., peak at 38.5 Ma[34,37,42-46].	Kinematic changes of the Pacific[47-49, cf.50,51] and the African Plate[52]. Acceleration of the South American Plate[7]. Incipient subduction of the pacific-Farallon spreading ridge under western North America[54].	Oscillating transpression, shear strain partitioning into the Domeyko Fault[37,55-57].	Major porphyry Cu-Mo and high sulfidation epithermal Cu-Ag mineralisation along 1300 km arc segment[13,14,58].	Uplift of the Domeyko Cordillera, by hard-linking and inversion of Mesozoic arc-parallel growth faults (Domeyko and Rio Loa)[34,59-61]. Around the Salar de Atacama these show local dextral shear folds[62,63] and truncate Eocene volcanics[37,46]. E-vergent thrusting and volcanism in the Peruvian and Bolivian Cordillera Oriental[2] including a non-magmatic thermal event in the Zongo-San Gaban Zone[64]. W-vergent thrusts along the western Preandean Depression[20,63,65] are covered by undeformed Miocene strata (Challo Fault)[20,42,45]. Attentuation of arc magmatism, PCD emplacement and exhumation within 15 m.y.[60]. Intraformational unconformities among terrestrial sediments (Sichal and Purilactis F)[40,63]. Erosion of 4-5 km between 50 and 30 Ma. indicated by apatite FT ages[38,59].
"K-T"[66,67]	65-62 Ma.	Minor global plate reorganisation indicated by rotation of the E European Dinarides and Idria Plate[68], potentially triggered by the Chicxulub Impact Event[69].	Dextral transpression with restricted shear strain partitioning[17].	Porphyry Cu-Mo (Peru-N Chile), Porphyry Cu-Mo-(Au) and epithermal styles (N Chile)[14,70-72].	Attenuation of arc magmatism, narrowing and eastward shift of the arc front[34]. Change in magmatic mineralogy from 'dry' pyroxene-bearing to 'wet' amphibole-bearing products[46.] Syn-kinematic pluton emplacement, with foliation development, and unconformities at the base of the Paleocene volcanics[46,66], and among the Salar de Atacama sedimentary sequence[67]. Variation in the degree of deformation across the K-T boundary[73]. Inversion of mid-K growth faults (Sierra del Buitre) and antithetic break-outs (Agua Amarga) along the eastern Central Valley[66,74].
Gondwanan Cycle					
Peruvian[3,43].	~90 Ma. (Peru)[33,43]; 86-83 Ma. (Chile)[5,59,75]	Subduction of the S-migrating Aluk - Farallon spreading ridge[34,76] and subsequent transient flat slab subduction[22].	Dextral transpression and inversion[34].	No mineralisation known	Uplift and tight folding of the forearc (including La Negra volcanic arc rocks). Strong attenuation of arc magmatism and final closure of the back arc basin with open folding of these sequences[34]. Thrusting and inversion of basin-bounding faults along the proto-Domeyko Fault Zone, with uplift of basement horsts such as the Sierra de Moreno[40].
Araucanian[77].	Stage III: 115-106 Ma.[78]	Change in absolute motion of the South American Plate[79].	uncertain, ?sinistral transpression	Andacollo PCD, Candelaria skarn-hosted Cu-Au[80] and associated belt of intrusion-related deposits[72,81-83].	Thrusting and uplift in the Coastal Cordillera and attenuation of arc magmatism[78]. Regression in the back arc basin[34]. Unconformity separates the back arc strata from the subsequent volcanic arc[62].
	Stage II: 125-130 Ma.[60,84-87]	Mantle plume activity under Gondwanaland, including pronounced Atlantic rifting[76,88].	Change from extension to sinistral transpression[89,90].	Minor porphyry Cu mineralisation in N Chile[71].	Evolution of mylonites with sinistral porphyroclast and S-C systematics[85,87,89,91] and emplacement of syn-kinematic granitoids[92] along the trench-parallel Atacama fault Zone.
	Stage I: >152; 143 Ma.[84]	Global plate reorganisation[93]: rotation of Laurentia and major thrusting in SW USA-Mexico[94,95].	Sinistral transpression (Atacama Fault Zone)[79,87].	Porphyry Cu-Mo and Manto Cu-Ag deposits in N Chile[96,97].	Uplift of the Cordillera de la Costa, formation of an angular unconformity surface therein and change to terrestrial conglomeratic deposition (Caleta Coloso Formation)[85].
San Rafael[9].	250-220 Ma.[34]	?Subduction of an unidentified terrane[98,99] or accelerated mantle plume activity under Gondwana[34].	uncertain	Small, low-grade porphyry Cu deposits[100].	Closure of the Choiyoi 'arc graben' with inversion of NE trending faults in the modern Domeyko Cordillera[34].
Hercynian Cycle					
Chanic[101].	400-350 Ma.[101-103]	Accretion of Chilenia Terrane[101-106].	compression (all Hercynian events)	No mineralisation known	Inversion of a shallow marine Siluro-Devonian basin between the Puna Arc arc the Argentine Cratonic continent[101].
Ocloyic[107].	Stage II: ~430 Ma.[101]	Final docking of the Arequipa and Antofalla Terranes[101,102,108,109].		Orogenic slate-hosted Au deposits in the foreland fold-and-thrust belt[110].	Thrust-related folding and syn-kinematic granitoid emplacement in the Argenitine Pampia Terrane[101,102,107]. Metamorphism of the Choja Formation basement migmatites[40].
	Stage I: ~450 Ma.[107]	Accretion of the Famatina Terrane and Puna Arc[79,101,111,112].			
Pampean[113].	~530 Ma.	Original collision of Arequipa and Antofalla terranes with cratonic Argentina., followed by rifting[114].		No mineralisation known	Thrusts and syn-kinematic granitoids of the western Pampia Terrane (Argentine Craton)[113]. Metamorphism of mid-proterozoic to cambrian clastic sediments and mafic volcanics[40].

Table 2.1. FOLD OUT

Reference Index:

1. Jordan and Alonso (1987)
2. Sandeman et al. (1995)
3. Steinmann (1929)
4. Maksaev (1979)
5. Mégard (1984)
6. Rea (1978)
7. Pardo-Casas and Molnar (1987)
8. Cande and Haxby (1991)
9. Ramos et al. (1996b)
10. Scheuber et al. (1994)
11. Norabuena et al. (1998)
12. Melnick et al. (2006)
13. Ruiz et al. (1965)
14. Sillitoe (1988)
15. Vila et al. (1991)
16. Noble and McKee (1999)
17. Maksaev (1990)
18. Farias et al. (2003)
19. Niemeyer (1984)
20. Wilkes and Goerler (1994)
20. Reinhardt et al. (1990)
21. Kley and Reinhardt (1994)
22. James and Sacks (1999)
23. Kay et al. (1999)
24. Creager et al. (1995)
25. Tomlinson and Blanco (1997b)
26. Roperch et al. (2000)
27. Roperch et al. (2002)
28. Arriagada et al. (2003)
29. Somoza (1998)
30. Baby et al. (1990)
31. Herail et al.(1996)
32. Sillitoe et al. (1998)
33. Tosdal et al. (1984)
34. Breitkreuz and Zeil (1994)
35. Kussmaul et al. (1975)
36. Armijo and Thiele (1990)
37. Tomlinson and Blanco (1997a),
38. Maksaev and Zentilli (1999)
39. Dilles et al. (1997)
40. Tomlinson et al. (2001b)
41. Noble et al. (1979)
42. Perelló and Muller (1984)
43. Clark et al. (1990a)
44. Hammerschmidt et al. (1992),
45. Tomlinson et al. (1994)
46. Cornejo et al. (1997)
47. Claque and Jarrard (1973)
48. Veevers (2000)
49. Wessel et al. (2002)
50. Norton (1995)
51. Rowley (1996)
53. Harada and Nemoto (2003)
54. Hamilton and Dostal (2000)
55. Mpodozis et al. (1993)
56. Lindsay et al. (1995)
57. Richards et al. (2001a)
58. Gustafson and Hunt (1975)
59. Maksaev et al. (1988)
60. Maksaev and Zentilli (1999)
61. Reutter et al. (1991)
62. Charrier and Muñoz (1994)
63. Charrier and Reutter (1994)
64. Farrar et al. (1988)
65. Amilibia and Skarmeta (2003)
66. Cornejo et al. (2003)
67. Mpodozis et al. (2005)
68. Marton et al. (1998)
69. Stueben et al. (2005)
70. Clark et al. (1990b)
71. Camus (2003)
72. Sillitoe and Perello (2005)
73. Marinovic and Garcia (1999b)
74. Andriessen and Reutter (1994)
75. Harland et al. (1990)
76. Oyarzun et al. (2003)
77. Riccardi (1988)
78. Mpodozis and Ramos (1990)
79. Ramos and Aleman (2000)
80. Mathur et al. (2002)
81. Espinoza (1986)
82. Reyes et al. (1990)
83. Oyarzun et al. (1996)
84. Scheuber and Hammerschmidt (1991)
85. Arévalo et al. (2003)
86. Naranjo et al. (1984)
87. Scheuber and Andriessen (1990)
88. Turner et al. (1994)
89. Scheuber and Gonzales (1999)
90. Grocott and Taylor (2002)
91. Arabasz (1971)
92. Grocott et al. (1994)
93. Radelli et al. (1993)
94. Schweickert et al. (1984)
95. Carillo et al. (2001)
96. Maksaev et al. (2006)
97. Ramirez et al. (2006)
98. Parada et al. (1991)
99. Mpodozis and Kay (1992)
100. Sillitoe (1977)
101. Coira et al. (1982)
102. Ramos et al. (1986)
103. Limarino et al. (1996; 1999)
104. Megard et al. (1971)
105. Fernando Seveso et al. (1993)
106. Diaz Martinez (1996)
107. Turner et al. (1979)
108. Finney et al. (2003a)
109. Finney et al. (2003b)
110. Zappettini and Segal (1999)
111. Rapalini et al. (1999)
112. Miller et al. (2003)
113. Omarini et al. (1999)
114. Ramos (1988)

1995; Camus, 2002). The deposits are hosted within a 1300 km-long x 30 km-wide belt between 14 and 31ºS (Camus, 2002; Perelló et al., 2003), clustering at the intersection of major NW and NE- trending crustal-scale fault zones and magmatic axes (Fig. 2.4: Salfity, 1985; Richards, 2000; Camus, 2002; Rivera et al., 2006a; Seggiaro, 2006; Palacios et al., 2007). The location of each of the major Eocene porphyry Cu camps also coincides with arc-orthogonal regional magnetic lows (Behn et al., 2001) which perhaps reflect the geometry of major sub-arc magma storages (e.g. Tamura et al., 2002). These districts commonly also have late-stage high sulfidation epithermal mineralisation and alteration (e.g., DeBeer and Dick., 1994; Dick et al., 1994; Ossandon et al., 2001; Richards et al., 2001a; Masterman et al., 2005). Epithermal veins and alteration in this belt commonly overprint the porphyries due to rapid post-Incaic erosion and unroofing of the shallow intrusive rocks (e.g., Sillitoe, 1999; 2000). To the south of 28ºS and north of 20ºS there is an increase in the Au grade, but a decrease in the contained metal of Eocene-Oligocene porphyry deposits (Mpodozis and Perelló, 2003) that accompanies decreasing crustal thickness (e.g., Oncken et al., 2006; Tassara et al., 2006). The southernmost part of the belt hosts a higher proportion of related epithermal mineralisation and explosive felsic volcanic products dominate, whereas the northern part is characterised by more abundant skarn mineralisation and exposure of the pre-Eocene stratigraphy (Cornejo et al., 1997; Richards et al., 1999; Mpodozis and Perelló, 2003; Sillitoe and Perelló, 2005).

2.2.5 Andean Cycle, part II: Mid-Oligocene-Recent

The central Andean margin was largely non-volcanic through the Oligocene and lower Miocene, although extension occurred in the southern Andean arc and forearc at 28-25 Ma. This affected the entire Andean margin south of 18ºS (Jordan et al., 2001) and may have been a response to changes in athenospheric flow caused by acceleration of the Nazca plate velocity (Tebbens and Cande, 1997). It is plausibly the event in which the Central Valley and Preandean Depression basins developed to

←

Table 2.1. Tectonic and metallogenic events recognised in the Central Andes, including summaries of key geological relationships that have been used to define each period of tectonism. References are indexed in order of appearance (top left to bottom right):

approximately their modern extent. In the Late Oligocene, flat subduction conditions prevailed in response to strong interplate coupling (Oncken et al., 2006) that arose from rapid convergence (Somoza, 1998) driven by acceleration of the westward drift of the South American continent (Silver et al., 1998), and enhanced by the drying climate and lower trenchward sediment flux (Lamb and Davis, 2003). Related shortening and uplift are recorded as unconformities in central (Moquequa Fn.) and southern Peru (Tacazá Fn.), and also in the Bolivian Altiplano, and collectively define the Aymara Tectonic Phase (25-18 Ma; Table 2.1, Sandeman et al., 1995). Facilitated by the flat subduction regime (Creager et al., 1995), clockwise rotation of northern Chile about the Arica Bend occurred between the Eocene and Early Miocene (MacFadden et al., 1995; Arriagada et al., 2000). Bending was a geometric necessity of bulk shortening gradients along the arc (Oncken et al., 2006), with maxiumum shortening measured in the axis of the orocline (Allmendinger et al., 2003). Along-arc shortening gradients were accomodated by major arc-parallel strike slip fault zones, recorded, for example by post-Paleocene sinistral throw of ~37 km on the Domeyko FS (Dilles, 1997; Tomlinson and Blanco, 1997b; Maksaev and Zentilli, 1999; Campbell et al., 2006). Arc-parallel strike-slip shear was associated with subsidence along intermontaone basins such as the Preandean Depression (Scheuber et al., 1994; Tomlinson and Blanco, 1997b).

Extensive erosion of the uplifted Domeyko Arc and foreland through this period is recorded by the Pampa de Tamarugál (northern Chile) and Llanuras Costeranas (southern Peru) pediplains (Mortimer and Saric, 1975; Sillitoe et al., 1968; Sandeman et al., 1995; Reutter et al., 1996; Digert et al., 2003). Semi-arid climate and high denudation rates in the Domeyko Cordillera promoted the formation of supergene enriched mineralisation blankets over the unroofed Paleogene porphyry and epithermal deposits (Alpers and Brimhall, 1989; Sillitoe and McKee, 1996; Bouzari and Clark, 2002; Arancibia et al., 2006a). At the same time, copper leached from the regolith of these deposits was transported laterally in the groundwater and deposited as exotic copper oxide- and copper silicate-facies concentrations in active terrestrial gravels (Munchmeyer, 1994) via a bacteriogenic mechanism (Nelson et al., 2009). Deposits of this type are spatially associated with the major porphyry copper deposits of the Domeyko Cordillera, including Mina Sur (Chuquicamata), Huinquintipa

(Collahuasi), and Damaina (El Salvador).

Andesitic arc volcanism was re-established along a broad front east of the Preandean Depression at ~17 Ma and has continued in that position to the present day (Fig. 2.5: Western Cordillera). This sequence is intercalated with major felsic pyroclastic units that extend at least 50 km west of the arc front (Naranjo and Puig, 1984; Vergara and Thomas, 1984; Scheuber et al., 1994; Kay et al., 2003) although the calderas from which they are thought to originate are commonly located on the continent-ward (Bolivian) side of the arc (Francis and Baker, 1978; Hildyard et al., 2001; Lindsay et al., 2001; Richards and Villeneuve, 2002; Milner et al., 2003).

Major epithermal and porphyry gold mineralisation occurred during two stages

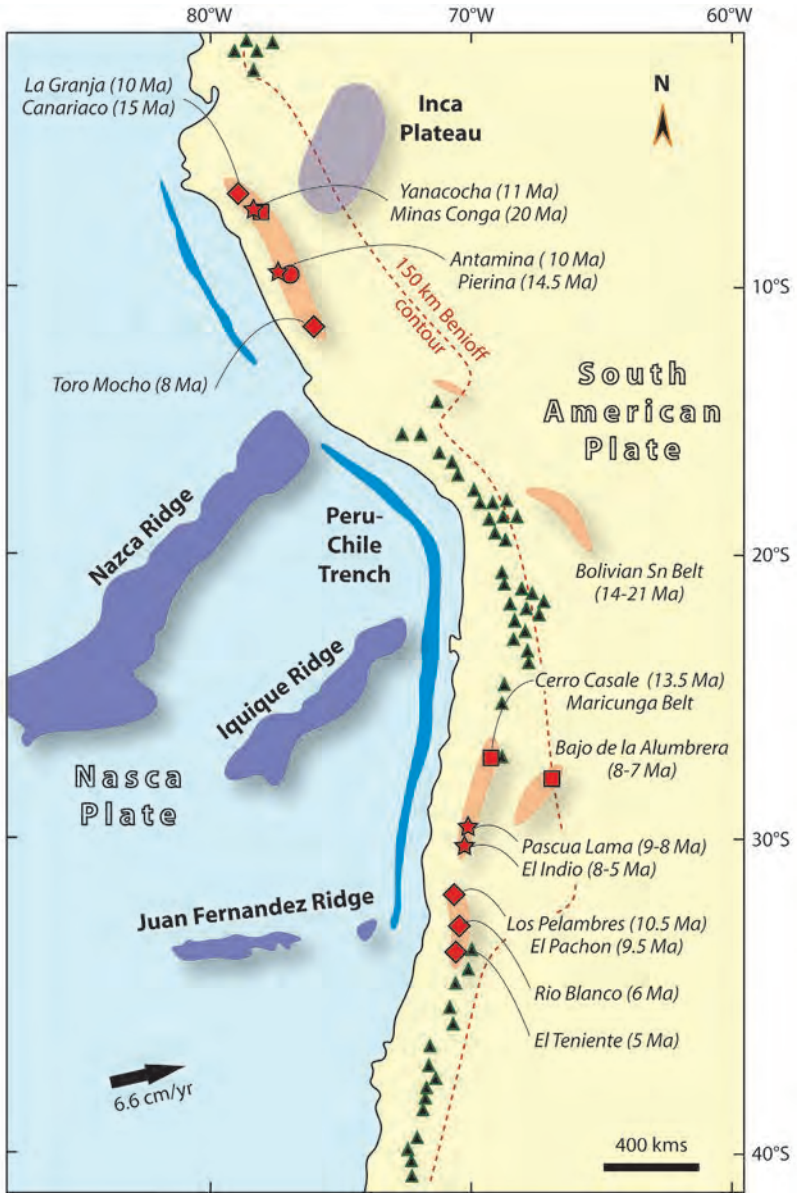

Figure 2.6. Map of the key tectonic elements of the western South American convergent margin, showing the position of the Peru-Chile trench, the major aseismic ridges and plateaux of the Nazca Plate, the 150 km depth contour of the Benioff Zone and the locations of active volcanoes (triangles). Selected major mineral deposits and belts (pink) of the Miocene metallogenic epoch are shown (square = Cu-Au porphyry, diamond = Cu-Mo porphyry, star = epithermal; circle = skarn). Eastward steps in the Benioff contour indicate slab flattening and coincide spatially with the subduction of the Inca Plateau-Nazca Ridge in Peru and the Juan Fernandez Ridge in Chile. These zones have little or no modern volcanism and host the bulk of Miocene mineralisation. The Iquique Ridge has yet to be begin subduction. Diagram compiled from Jordan et al. (1983), Sasso and Clark (1998), Gutscher et al. (1999; 2000), Cooke et al. (2005), and Rosenbaum et al. (2005).

during the early and late Miocene in the central Chilean Maricunga and El Indio belts (Fig. 2.6: 20-6 Ma: considered one belt by Mpodozis and Kay, 2003), and in central and northern Peru (27º-29ºS, Fig. 2.4: Noble and McKee, 1999). Major porphyry-related tin-silver-(bismuth) mineralisation formed inboard of the main arc, in the Bolivian Cordillera Oriental during part of the same period (23-12 Ma: Sillitoe et al., 1998). Two discrete phases of mineralisation in the central Chilean belt migrated southward in time between 24-12 Ma, against the plate convergence vector (Vila et al., 1991; Kay et al., 1999; Bissig et al., 2000; Mpodozis and Kay, 2003) whereas those in Peru proceeded ahead of the margins of the subducting Nazca Ridge (Rosenbaum et al., 2005). Two of the largest deposits formed during the Quechua Tectonic Phase (Antamina, 9.8 Ma; Love et al., 2000; Yanacocha, 8.2-13.6 Ma; Longo, 2006). Regolith copper-enrichment processes that had occurred from the upper Eocene to lower Miocene did not affect the Neogene deposits because the establishment of the Antarctic ice cap and the northward progression of the cold Humboldt Current caused a regional climate change to hyperarid conditions in the Andes during the Lower - Middle Miocene (Alpers and Brimhall, 1988, Carrizo et al., 2007; 19-13 Ma: Rech et al., 2006).

Neogene magmatism in the Western Cordillera was interrupted by two compressive tectonic phases at 9-8 Ma (Quechua Tectonic Phase) and 5-4 Ma (Daguita Tectonic Phase: Jordan and Alonso, 1987; Scheuber et al., 1994; Sandeman et al., 1995). These events may have been related to transfer of Pacific oceanic spreading from the Galapagos to the East Pacific Rise (Herron, 1972; Herron et al., 1979; Mammerickx et al., 1980). However, the Central Andean plateau has been sustained by ongoing shortening throughout the Neogene, such that these events represent bursts of accelerated shortening superimposed on the broader plateau orogeny (e.g., Oncken et al., 2006). Both phases occurred under near-orthogonal arc convergence (Pardo-Casas and Molnar, 1987). They primarily caused reactivation of pre-existing structures in western parts of the orogen such as the Domeyko Cordillera (Scheuber et al., 1994; Muñoz and Charrier, 1996) and domal and epeiric uplift in the ‘Western’ Cordillera and western Altiplano (e.g., Schildgen et al., 2007) that was facilitiated by thin-skinned thrusting along the eastern orogen margin (e.g., Müller et al., 2002). Estimates of Neogene net vertical displacements are 2.0 - 3.5 kilometres (Wilkes

and Goerler, 1994; Farias et al., 2003; Garzione et al., 2006; Schildgen et al., 2007). Accounting for the likely Paleogene and post-Miocene uplift and erosion, these Late Miocene-early Pliocene tectonic events therefore generated 50 - 70% of the modern Andean physiographic relief.

Miocene-Pliocene metallogeny in the Andes is spatially associated with the onset of flat slab subduction (Fig. 2.6: Kay et al., 1999; Camus, 2002; Hollings et al., 2005; Cooke et al., 2005; Rosenbaum et al., 2005). Major porphyry Cu mineralization occurred between 12 and 4 Ma in a short belt in central Chile (Fig. 2.6). The time-space distribution of these deposits has been interpreted as younging southward in front of the subducting Juan Fernandez Ridge (Kay et al., 1999; Hollings et al., 2005). However, the age distribution is also bimodal, with the northern group of deposits all formed at approximately 12-10 Ma, and the southern group at 6.5-4 Ma (Toro et al., 2006). Prior to the Miocene, subduction of the Juan-Fernandez Ridge was not associated with a reduction in volcanic productivity, nor with shallow subduction or mineralisation (Trumbull et al., 2006). Therefore metallogeny in this belt may ultimately be controlled in time by the dynamics of the Mio-Pliocene compressive tectonism, and localised in space by deformation relating to the position of the subducting aseismic ridge.

Porphyry Cu-Au and epithermal Au mineralization also formed east of the arc front in the Bajo de la Alumbrera and Famatina districts, western Argentina, during the Late Miocene and Pliocene, respectively (Figs. 2.4 and 2.6: Losada-Calderon and McPhail, 1994; Losada Calderon et al., 1996; Proffett, 2003; Harris et al., 2004). These represent the most recent known mineralisation event in this part of the orogen and appear to comprise a discrete belt of mineralisation inboard of the main arc, rather than implying an eastward step of the arc front (Sasso and Clark, 1998). The Bajo de la Alumbrera district is situated on a proposed basement terrane boundary represented by the NW-trending Culampaja lineament that is also coincident with the El Salvador porphyry district (Salfity, 1985; Richards, 2000). This tectonic and structural relationship may explain why these are two of the more Au-rich porphyry systems in the Andes outside the Maricunga Belt (Shatwell, 1995).

Eastward subduction of the Nazca Plate beneath western South America continues

to the present, at around 6 cm per year (Angermann et al., 1999); about half of the rate during inception of the Incaic and Quechua tectonic phases (Pardo Casas and Molnar, 1987). In the Central Andes the continental margin is dominated by near-orthogonal compression, whereas the Southern Andes is primarily a dextral transtensional domain (e.g., Yáñez et al., 2002; Melnick et al., 2006). Of that convergence in the central Andes, as much as 85% is absorbed by westward growth of the central Andean forearc (Clift et al., 2007) and the bulk of the remainder manifests as shortening in the foreland fold and thrust belts of Bolivia, Argentina and eastern Peru (Norabuena et al., 1998). Elsewhere, crustal deformation is dominated by shortening along foreland fold belts, locally associated with low volume alkalic and adakitic magmatism in back-arc positions. This magmatism is spatially related to subduction of the Nazca Ridge in Peru (e.g., Gutscher et al., 1999: James and Sacks, 1999; Espurt et al., 2007), the Juan Fernandez Ridge in central Chile (Kay et al., 1989; Cahill, 1990; Laursen et al., 2002; Kay et al., 2006), the Carnegie Ridge in Ecuador (Beate et al., 2001) and the actively spreading Chile Ridge in southern Chile (e.g., Gerbault et al., 2005). Calc-alkaline arc magmatism occurs along the arc front of the remainder of the Peruvian and Chilean segments of the South American margin. Magmatism extends into the back arc environment and locally traces long-lived structural corridors (Fig. 2.5: Schreiber and Schwab, 1991; Matteini et al., 2001; Seggiaro, 2006), some of which show evidence of active hydrothermal systems (Richards and Villeneuve, 2002; Richards et al., 2006a). Present rates of erosion (e.g., Barnes and Pelletier, 2006) and likely depths of emplacement (e.g., McInnes et al., 2005) imply that any porphyry mineralisation forming in the southern Central Andes today might be exposed sometime in the next 3 - 7 million years.

Chapter 3.

STRATIGRAPHY, INTRUSIVE HISTORY AND GEOCHRONOLOGY.

3.1 Introduction

This chapter presents the results of detailed litho- and chronstratigraphic mapping of the Collahuasi district. This forms the basis for interpretations of the longevity and nature of key structural elements that can then be assessed in terms of their influence on the localisation of porphyry-style mineralisation discussed in Chapter 4. The Mesozoic and Tertiary stratigraphy is also reviewed and revised in accordance with the results of new mapping and U-Pb geochronology. Throughout this chapter, geochronology results listed in section headings are new data, and relevant pre-existing data are discussed in the text. The magmatic geochemistry, petrogenesis and tectonic significance of the Peine Group is also dicsussed, based on new whole rock geochemistry.

The Collahuasi district is unique among the major Eocene-Oligocene porphyry districts in Chile in that Paleozoic volcanosedimentary rocks are both the major host to porphyry mineralisation, and are well exposed. In the other porphyry districts of that age, either Mesozoic and Paleogene sedimentary and magmatic rocks host the Cu deposits, or Paleozoic stratigraphy is poorly exposed and/or treated as an ambient 'basement' (Gustafson and Hunt, 1975; Ossandon and Zentilli, 1997; Richards et al., 2001a). Collahuasi therefore provides an excellent opportunity to investigate the evolution of the Late Paleozoic sequences and their influence, if any, on the younger mineralisation.

Across the Collahuasi district, outcropping Late Paleozoic felsic to andesitic volcanics have been labelled the Collahuasi Formation by previous workers (Vergara, 1978; Vergara and Thomas, 1984). This sequence of rocks includes all volcanic and sedimentary units deposited along the Choiyoi Arc (Chapter 2) and is more appropriately called the Peine Group (Bahlburg and Breitkreuz, 1991). Peine Group rocks occur throughout the northern Chilean Precordillera, and include

sequences referred to variously as the Cas, Pular, La Tabla, Bardas, Tuina, Agua Verde, Quipisca and Estratos el Borde Formations (Ramirez and Gardeweg, 1982; Marinovic and Lahsen, 1984; Naranjo and Puig, 1984; Gardeweg, 1988; Maksaev et al., 1991; Breitkreuz and Zeil, 1994; Smoje and Marinovic, 1994; Marinovic and Garcia, 1999a; Marinovic and Garcia, 1999b; Tomlinson et al., 2001). Outside the mineralised districts there has been investigation of the tectonic significance of the Peine Group, as it marks the transition between the accretionary Gondwanan Phase and the constructional Andean Phase of evolution of the western South American margin (Chapter 2; Breitkreuz et al., 1990).

The geology of the Collahuasi district is dominated by an arc-parallel inlier approximately 20 kilometers wide that is comprised largely of Peine Group stratigraphy (Fig. 3.1). This inlier contains the most extensive and continuous exposure of Permo-Triassic strata in northern Chile (Tomlinson et al., 2001a). The

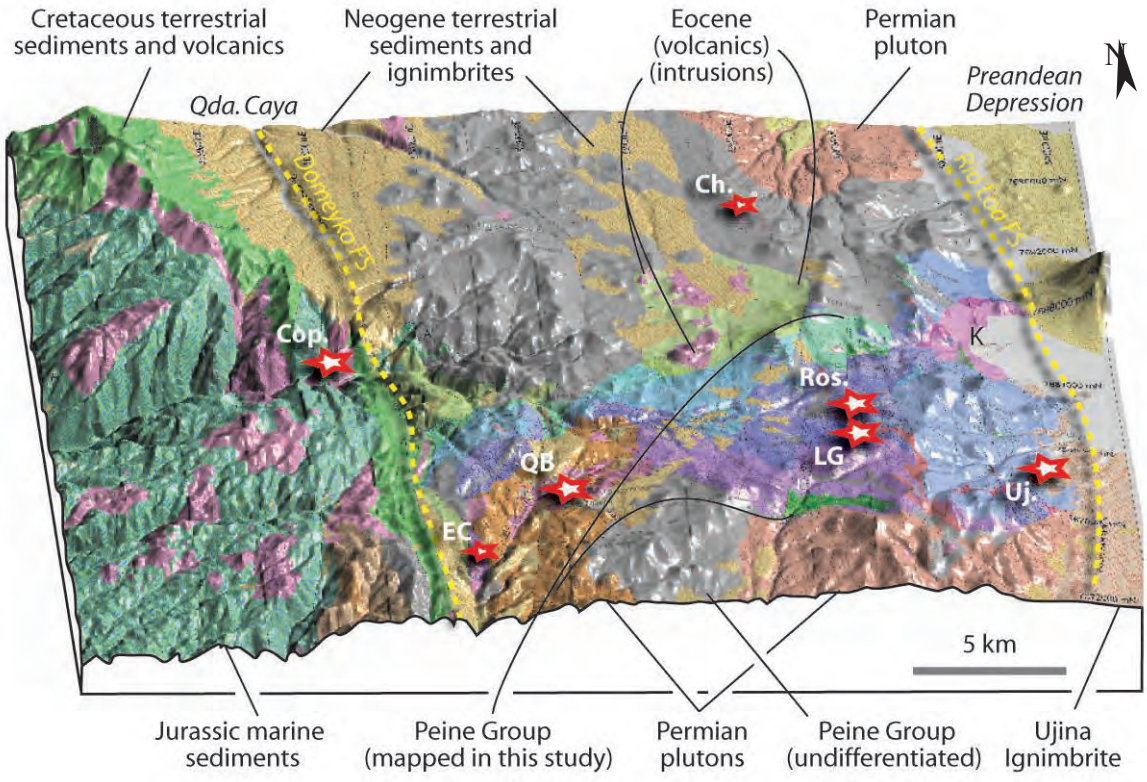

Figure 3.1. Interpreted litholostratigraphic map of the greater Collahuasi district draped over the SRTM 90m pixel elevation model with vertical exaggeration = 2, illuminated from the east. Key stratigraphic subdivisions are indicated. Peine Group stratigraphy resolved in this study coloured aqua green through mauve. Pink areas in the western sector are Eocene dioritic stocks. Mineral deposits (stars) and major terrane-bounding faults are marked (FS = fault system, Cop. = Copaquire, EC = El Colorado, QB = Quebrada Blanca, Ch. = Characolla, Ros. = Rosario, LG = La Grande, Uj. = Ujina)

western margin of the inlier is defined by the Domeyko fault system, a multiply reactivated, continental-scale arc-parallel fault system (e.g., Tomlinson et al., 1997b; Amilibia et al., 2008). The eastern margin is also interpreted to be structurally controlled, but the Rio Loa fault system is covered by Oligocene to Quaternary sediments and ignimbrites throughout the district (Vergara, 1978; Vergara and Thomas, 1984; Tomlinson et al., 2001a).

Jurassic to Late Cretaceous marine sedimentary sequences of the back arc Tarapacá Basin occur in the western Collahuasi district, to the west of the Domeyko fault system (Smoje, 1989; Prinz et al., 1994). This regional fault is commonly interpreted to have originated as a marginal growth fault of the Tarapacá Basin (Prinz et al., 1994; Tomlinson et al., 1997a). During a series of compressive tectonic events between the Maastrichian and the Pliocene (Chapter 2) shortening in the Collahuasi district was largely accommodated by a west-vergent, basement-involved fold and thrust belt that includes and extends west of the Domeyko fault system (Fig. 3.1, Maksaev, 1990; Amilibia and Skarmeta, 2003; Amilibia et al., 2008). The Peine Group stratigraphy has therefore largely escaped strong ductile deformation (Vergara, 1978; Vergara and Thomas, 1984). and has not undergone significant widespread regional metamorphism (Breitkreuz and Schmidt, 1993; Breitkreuz et al. 1994a, 1994b).

Paleogene to Recent sediments are accommodated in intramontane basins along both margins of, and locally within the Paleozoic inlier (Quebrada Caya and the Preandean Depression, Fig. 3.1: Tomlinson et al., 2001). Many of these basins appear to have originated or undergone major subsidence in the Oligocene during a phase of regional extension (Jordan et al., 2001) or associated with transtensional block rotations driven by bending of the Bolivian Orocline (e.g., Arriagada et al., 2003), or both. Neogene ignimbrites comprise a signficant part of the fill in these basins and completely obscure large areas of both margins of the Paleozoic sequence in the Collahuasi district (Baker et al., 1978; Vergara, 1978; Vergara and Thomas, 1984). Nonetheless, the Peine Group stratigraphy remains well exposed over an area of at least 20 x 10 km, and importantly, there are good exposures in the vicinity of the major Eocene mineral deposits.

3.2 Methods

Mapping for this project was conducted at 1:5,000 in areas of aerial photo coverage and at 1:10,000 outside those areas. The distribution of new data points, outcrops mapped, and base map coverages are shown in Figure 3.2. The principal map sources that existed prior to this work are the 1:5,000 surface lithology mapping of Aur Resources at Quebrada Blanca (J-P. Desrochers, unpublished data), the 1:10,000 lithology and structural mapping of CMDIC at La Grande (Ware et al., 1981; Munchmeyer et al., 1984), and the 1:50,000 regional lithological mapping of SERNAGEOMIN (Vergara, 1978; Vergara and Thomas, 1984; Tomlinson et al., 2001). The new and pre-existing data have been integrated to create new geological maps and sections.

Correlations between outcrops and drill intercepts were made using field relationships, U-Pb geochronology, geochemical composition (Chapter 5), texture, phenocryst, xenocryst, and xenolith assemblages, allowing for common lateral facies changes described in volcanosedimentary environments by McPhie et al. (1993). The interpreted lithology map incorporates constraints from surface mapping and drill core logging by the author. As outcrop is limited and large sections of the area are covered by Neogene terrestrial sediments and ignimbrites, the lithological boundaries are necessarily approximate in many locations. Where fault offsets mapped in areas of good exposure are covered elsewhere, the offset has been inferred to be continue under cover.

Hierarchical stratigraphic nomenclature has been applied in this study. Subdivisions of the Peine Group have therefore been called formations. They should not be confused with the informal use of the term “Collahuasi Formation” to refer to the same sequence of rocks elsewhere in the literature (Fig. 3.3; Ware et al., 1981; Munchmeyer et al., 1984; Vergara and Thomas, 1984; DeBeer and Dick, 1994; Dick et al., 1994; Bisso et al., 1998; Lee, 1994; Tomlinson et al., 2001; Masterman et al., 2005). In the text, existing stratigraphic names are shown with the stratigraphic level capitalised (e.g., Quehuita Formation), whereas new proposed names are shown with the stratigraphic level in lower case (e.g., Huinquintipa formation).

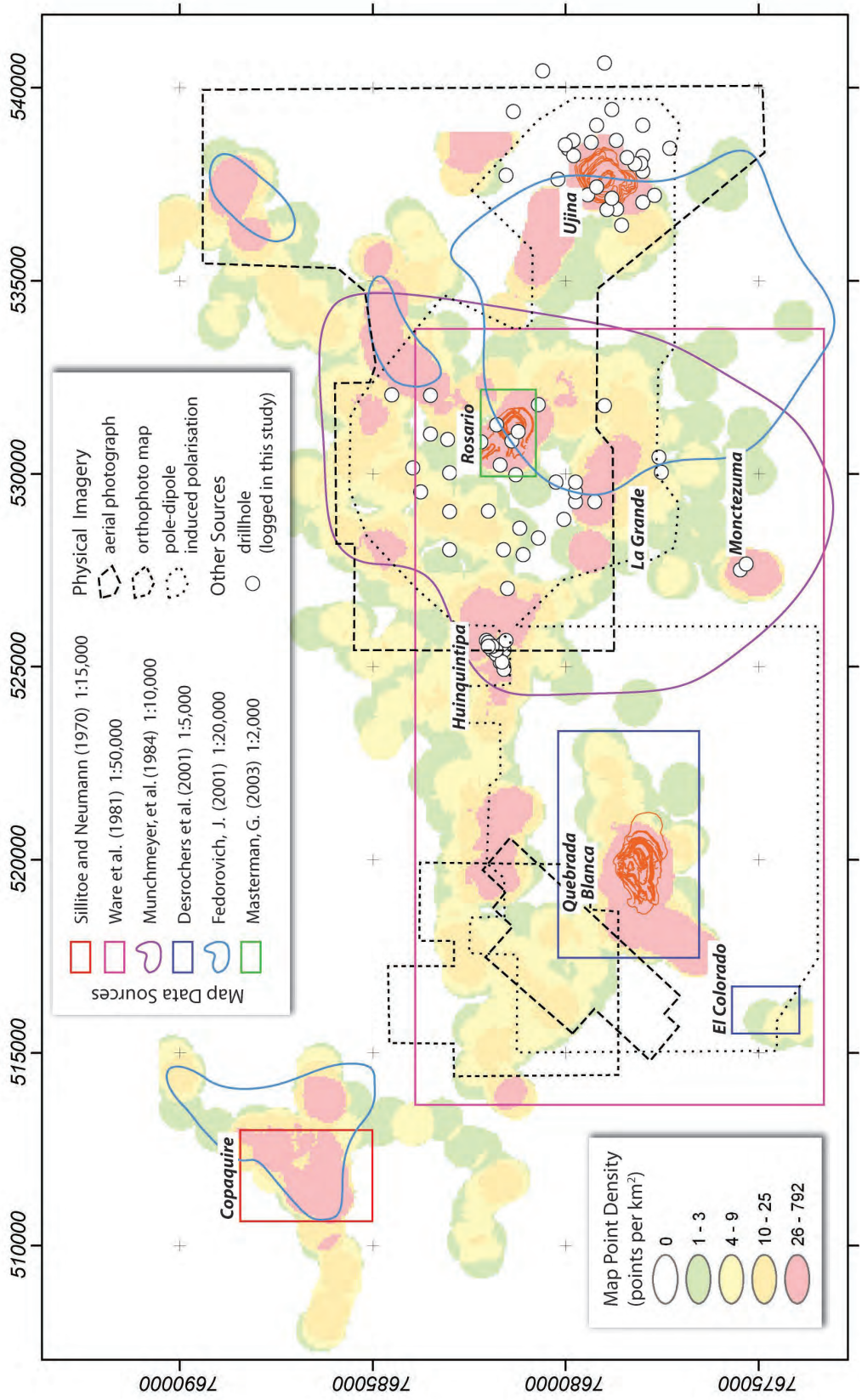

Figure 3.2. Map of the Collahuasi district showing the distribtuion of base map imagery and pre-existing geological map data. SERNAGEOMIN 1:50,000 geological mapping is not shown as it covers the entire area. The extent of new data collection is indicated by the desity distribution of new map data points and drillholes logged. The area if new map point data briadly coincides with an area for which outcrop distribution was accurately mapped (not shown for clarity). Digital topographic contour maps, Landsat and Geoscan images were also used as mapping bases outside the extent of aerial photography.

3.3 Stratigraphy of the Peine Group

3.3.1 Regional Extent and Stratigraphic Limits

The Peine Group includes all of the predominantly volcanic strata deposited along the Choyoi Arc (Coira et al., 1982), at least some of which have been interpreted as the products of major caldera-forming exposive eruptions (e.g., Davidson et al., 1985). These rocks rest unconformably on lower Carboniferous (or older) basement and are locally overlain by Mezosoic sedimentary strata (Fig. 3.3; Davidson et al., 1981; Mpodozis et al., 1983; Bahlburg and Breitkreuz, 1991). The Peine Group comprises a NNW-trending belt that traverses the modern Andean volcanic arc at low angle from Neuquen in southern Argentina, through the Argentine Cordillera Frontal to the Domeyko Cordillera (Chilean Precordillera) at the latitude of Iquique in northern Chile (Fig. 2.4). In the project area, it has experienced subtle regional metamorphism (Djouka-Fonkwe et al., 2008) and retains abundant primary sedimentary and volcanic textures. The sequence is at least 5 km thick and dips moderately northward in the study area such that the exposure provides an approximate E-W section through the stratigraphy (Figs. 3.1 and 3.4).

The Peine Group is overlain in the west by Jurassic redbeds assigned to the Quehuita Group ("Guatacondo Formation" of Smoje, 1989). These crop out in a structural window adjacent to the Domeyko Fault system and are not observed elsewhere in the map area (Fig. 3.4). The Tarapacá Basin in which they were deposited (Fig. 2.5) is interpreted to have been bound on its eastern margin by the proto-Domeyko fault system, and Jurassic strata may never have covered much of the Collahuasi district east of this structure (Breitkreuz and Zeil, 1994; Prinz et al., 1994). Elsewhere

Figure 3.3. Simplified regional time-space diagram in longsection S to N along the Permo-Carboniferous magmatic arc. Patterns indicate lithology if unspecified. Selected radiometric ages in parentheses. Non-linear time scale. Many of the broad stratigraphic groups are semi-continuous along the arc, but have typically been assigned different names in each district. Note that the Salar de Atacama section is located approximately 60 kms further from the trench than the other sectors. Compiled largely from Scheuber et al 1994; Tomlinson et al 2001; Cornejo et al 2003; Clark et al 1990a; Mpodozis and Perello, 2003, Marinovic and Lahsen, 1984, this study. Abbreviations: Fn. = Formation; mb. = member; rhy. = rhyolite; dac.= dacite; and. = andesite; volc. = volcanic; ig. = collective pyroclastic facies; cgl.= conglomerate; snd. = sandstone; shl. = shale; sst. = siltstone; lms. = limestone; sed. = sedimentary rocks; terr. = terrigenous; Missis. = Mississippian; Pennsyl.= Pennsylvanian; Neocom.= Neocomian; Apt.= Aptian; Cen. = Cenomanian; Tur. =Turonian; Maast.= Maastrichian; PLEIST.= Pleistocene; REC.= Recent.

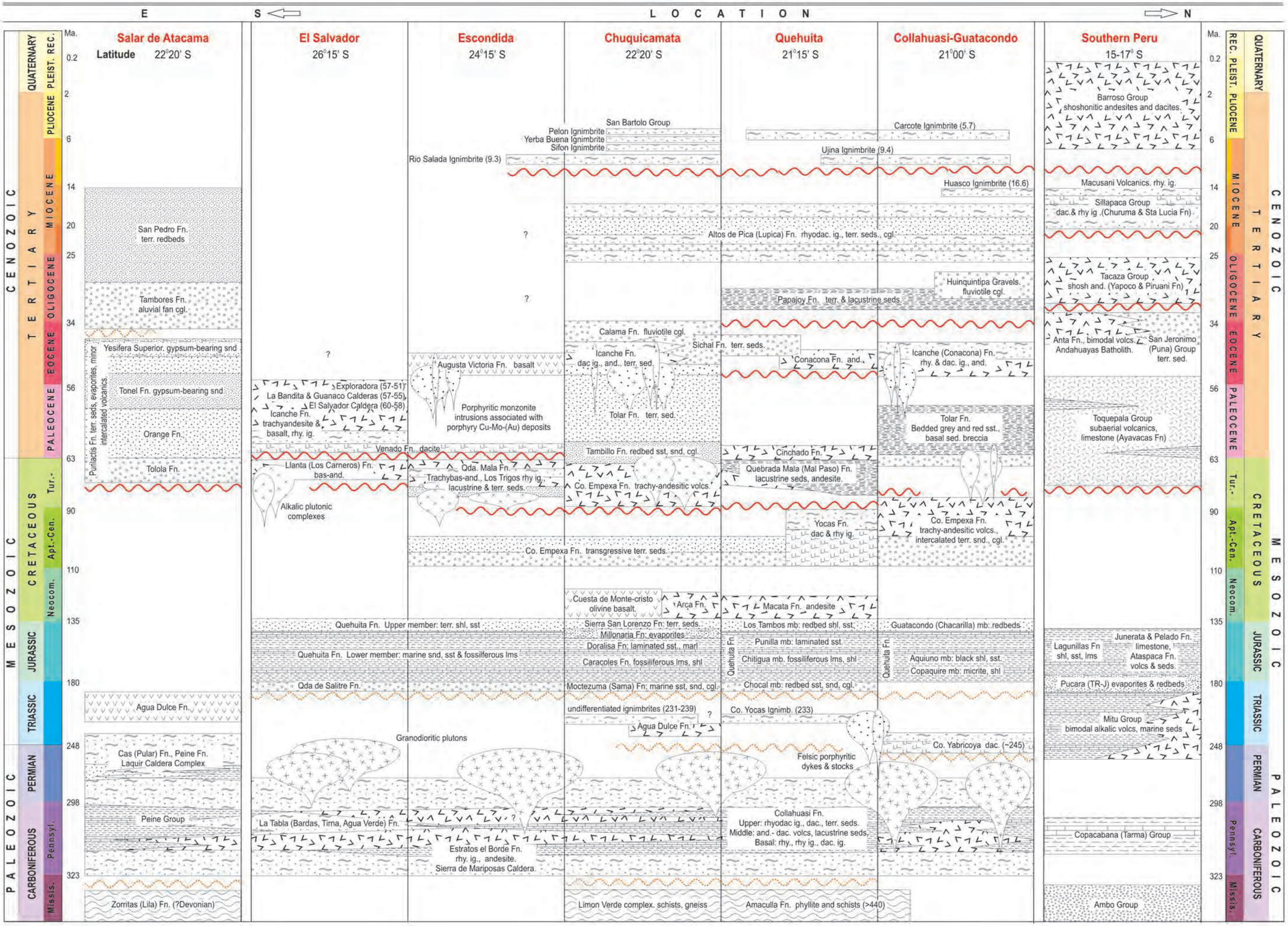
E
S
L O C A T I O N
N
Salar de Atacama
Latitude 22°20' S
El Salvador
26°15' S
Escondida
24°15' S
Chuquicamata
22°20' S
Quehuita
21°15' S
Collahuasi-Guatacondo
21°00' S
Southern Peru
15-17° S
Ma.
CENOZOIC
TERTIARY
QUATERNARY
PLEIST. REC.
PLIOCENE
MIOCENE
OLIGOCENE
EOCENE
PALEOCENE
MESOZOIC
CRETACEOUS
Tur.-
Apt.-Cen.
Neocom.
JURASSIC
TRIASSIC
PALEOZOIC
PERMIAN
CARBONIFEROUS
Pennsyl.
Missis.
San Pedro Fn. terr. redbeds
Tambores Fn. aluvial fan cgl.
Yesifera Superior. gypsum-bearing snd
Tonel Fn. gypsum-bearing snd
Purilactis Fn. terr. seds, evaporites, minor intercalated volcanics.
Orange Fn.
Tolola Fn.
Agua Dulce Fn.
Cas (Pular) Fn., Peine Fn. Laquir Caldera Complex
Peine Group
Zorritas (Lila) Fn. (?Devonian)
San Bartolo Group
Pelon Ignimbrite
Yerba Buena Ignimbrite
Sifon Ignimbrite
Rio Salada Ignimbrite (9.3)
Exploradora (57-51)
La Bandita & Guanaco Calderas (57-55)
El Salvador Caldera (60-58)
Icanche Fn. trachyandesite & basalt, rhy. ig.
Venado Fn. dacite
Llanta (Los Carneros) Fn. bas-and.
Alkalic plutonic complexes
Quehuita Fn. Upper member: terr. shl, sst
Quehuita Fn. Lower member: marine snd, sst & fossilferous lms
Qda de Salitre Fn.
Granodioritic plutons
La Tabla (Bardas, Tirna, Agua Verde) Fn.
Augusta Victoria Fn. basalt
Porphyritic monzonite intrusions associated with porphyry Cu-Mo-(Au) deposits
Qda. Mala Fn.
Trachybas-and., Los Trigos rhy ig., lacustrine & terr. seds.
Co. Empexa Fn. transgressive terr. seds.
Estratos el Borde Fn. rhy. ig., andesite. Sierra de Mariposas Caldera.
Huasco Ignimbrite (16.6)
Altos de Pica (Lupica) Fn. rhyodac. ig., terr. seds., cgl.
Calama Fn. fluviotile cgl.
Icanche Fn. dac ig., and., terr. sed.
Tolar Fn. terr. sed.
Tambillo Fn. redbed sst, snd, cgl.
Co. Empexa Fn. trachy-andesitic volcs.
Cuesta de Monte-cristo olivine basalt.
Arca Fn.
Sierra San Lorenzo Fn: terr. seds.
Millonaria Fn: evaporites
Doralisa Fn: laminated sst., marl
Caracoles Fn. fossiliferous lms, shl
Moctezuma (Sama) Fn: marine sst, snd, cgl.
undifferentiated ignimbrites (231-239)
Agua Dulce Fn.
Limon Verde complex. schists, gneiss
Carcote Ignimbrite (5.7)
Ujina Ignimbrite (9.4)
Huinquintipa Gravels. fluviotile cgl.
Papajoy Fn. terr. & lacustrine seds.
Sichal Fn. terr. seds.
Conacona Fn. and.
Cinchado Fn.
Quebrada Mala (Mal Paso) Fn. lacustrine seds, andesite.
Yocas Fn. dac & rhy ig.
Macata Fn. andesite
Los Tambos mb: redbed shl, sst.
Punilla mb: laminated sst.
Chitigua mb. fossiliferous lms, shl
Chocal mb: redbed sst, snd, cgl.
Co. Yocas Ignimb. (233)
Felsic porphyritic dykes & stocks
Collahuasi Fn. Upper: rhyodac ig., dac., terr. seds. Middle: and.- dac. volcs, lacustrine seds, Basal: rhy., rhy ig., dac. ig.
Amaculla Fn. phyllite and schists (>440)
Quehuita Fn.
Icanche (Conacona) Fn. rhy. & dac. ig., and.
Tolar Fn. Bedded grey and red sst., basal sed. breccia
Co. Empexa Fn. trachy-andesitic volcs., intercalated terr. snd., cgl.
Huinquintipa Gravels. fluviotile cgl.
Guatacondo (Chacarilla) mb: redbeds
Aquiuno mb: black shl, sst.
Copaquire mb: micrite, shl
Co. Yabricoya dac. (~245)
Barroso Group shoshonitic andesites and dacites.
Macusani Volcanics. rhy. ig.
Sillapaca Group dac.& rhy ig .(Churuma & Sta Lucia Fn)
Tacaza Group shosh and. (Yapoco & Piruani Fn)
Anta Fn., bimodal volcs. Andahuayas Batholith.
San Jeronimo (Puna) Group terr. sed.
Toquepala Group subaerial volcanics, limestone (Ayavacas Fn)
Lagunillas Fn shl, sst, lms
Junerata & Pelado Fn. limestone, Ataspaca Fn. volcs & seds.
Pucara (TR-J) evaporites & redbeds
Mitu Group bimodal alkalic volcs, marine seds
Copacabana (Tarma) Group
Ambo Group

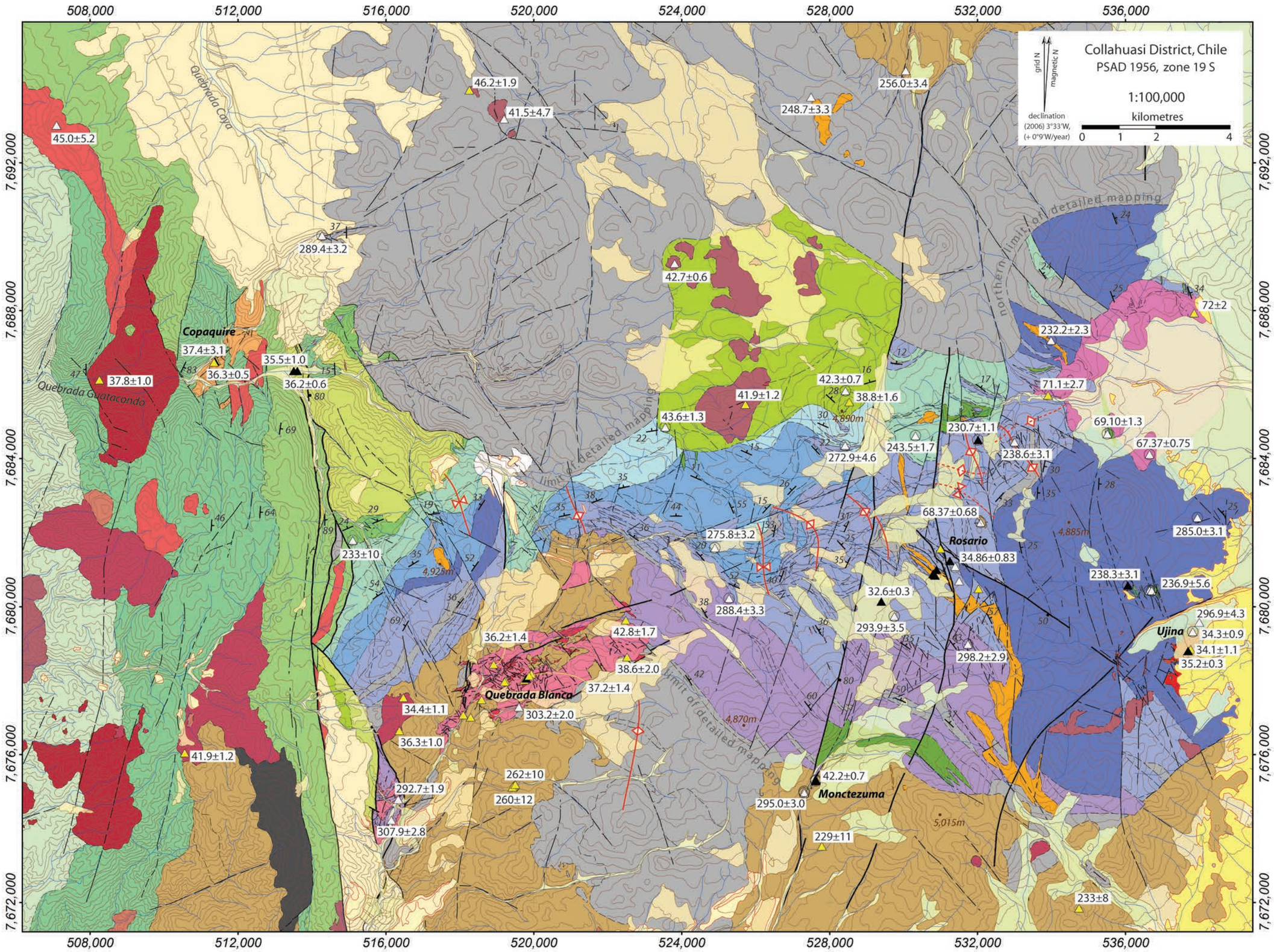
Collahuasi District, Chile
PSAD 1956, zone 19 S
1:100,000
kilometres
0 1 2 4
grid N
magnetic N
declination (2006) 3°33'W, (+ 0°9'W/year)
508,000
512,000
516,000
520,000
524,000
528,000
532,000
536,000
7,692,000
7,688,000
7,684,000
7,680,000
7,676,000
7,672,000
Quebrada Cayo
Quebrada Guatacondo
Copaquire
Quebrada Blanca
Rosario
Ujina
Monctezuma
limit of detailed mapping
northern limit of detailed mapping
45.0±5.2
46.2±1.9
41.5±4.7
248.7±3.3
256.0±3.4
289.4±3.2
42.7±0.6
37.4±3.1
35.5±1.0
36.3±0.5
36.2±0.6
37.8±1.0
41.9±1.2
42.3±0.7
38.8±1.6
43.6±1.3
4,890m
230.7±1.1
243.5±1.7
272.9±4.6
238.6±3.1
71.1±2.7
69.10±1.3
67.37±0.75
72±2
232.2±2.3
68.37±0.68
275.8±3.2
285.0±3.1
34.86±0.83
238.3±3.1
236.9±5.6
32.6±0.3
288.4±3.3
293.9±3.5
296.9±4.3
34.3±0.9
34.1±1.1
35.2±0.3
298.2±2.9
233±10
4,925m
36.2±1.4
42.8±1.7
38.6±2.0
37.2±1.4
34.4±1.1
303.2±2.0
36.3±1.0
41.9±1.2
262±10
260±12
292.7±1.9
307.9±2.8
4,870m
42.2±0.7
295.0±3.0
5,015m
229±11
233±8

in northern Chile, the Peine Group is overlain unconformably by localised post-middle Cretaceous volcanics and ubiquitous Neogene terrestrial sediments (Ware et al., 1981; Munchmeyer et al., 1984). In the Chuquicamata, Salar de Atacama and Escondida areas the lower and middle Peine Group and semi-contemporaneous intrusions are overlain by a Triassic volcano-sedimentary sequence called the Agua Dulce Formation (Fig. 3.3: Wilkes and Goerler, 1994; Richards et al., 2001a; Tomlinson et al., 2001).

The basal contact of the Peine Group is unknown at Collahuasi. The lowermost part of the sequence occurs in the southern part of the study area where it has been intruded by Permian granitoids (Figs. 3.1 and 3.4). It is generally assumed that the Peine Group rests unconformably on greenschist facies Devonian metapelites of the Amaculla Formation (Breitkreuz and Zeil, 1994), which crop out in a fault-bound inlier associated with the Domeyko fault system in the southeast of the map area (Fig

Figure 3.4. Map of the simplified geology of the Collahuasi district (1:100,000; opposite page) showing solid geology, principal structures, representative structural measurements, and geochronology. New map data (collected at 1:5,000) is integrated with all available existing map sheets. The distribution of Neogene cover packages is largely taken from Tomlinson et al. (2001a), and does not include ubiquitous shallow colluvium that obscures much of the area. A larger, more detailed version of this map is presented as a insert #1 at the back of this thesis.

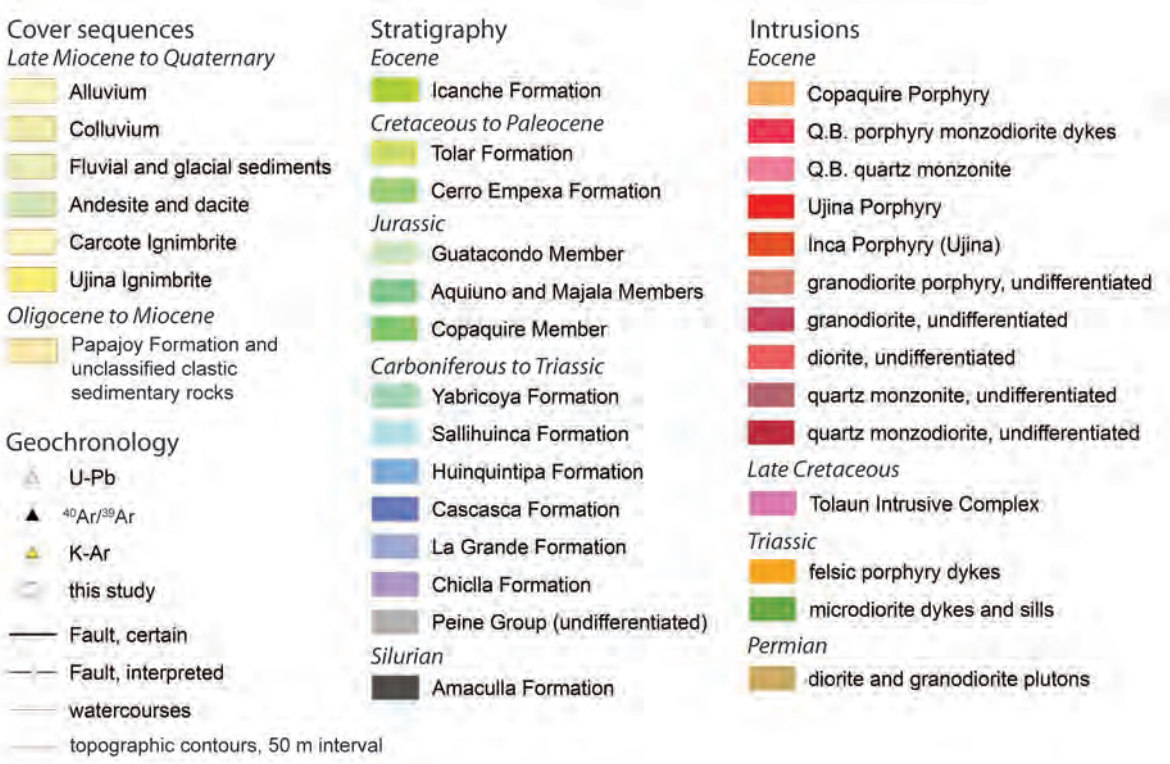

3.4; Vergara and Thomas, 1984; Tomlinson et al., 2001a). Just outside the Collahuasi district, Mesoproterozoic amphibolite facies metavolcanic and metasedimentary rocks are exposed in the Quebrada Choja (southwest of the map area in Fig. 3.4; e.g., Damm et al., 1990). These are part of a major crystalline basement terrane (Antofalla-Arequipa) that occurs throughout northern Chile and southern Peru (Ramos, 1988; Bahlburg and Herve, 1997; Tomlinson et al., 2001a) and likely also underlies the Collahuasi district.

The Peine Group is here subdivided into six formations (Fig. 3.4; Table 3.1) that are separated from each other by unconformities and/or major lithofacies changes. The formations are themselves subdivided into 43 mappable geologic units (equivalent to members). The most widespread and distinctive of these units have been assigned informal names. The majority remain unnamed and have been allocated systematic alpha-numeric codes based on their ages and stratigraphic positions (Table 3.1).

Sections 3.4 to 3.9 provide lithological descriptions and stratigraphic relationships of the detailed Peine Group stratigraphy from lowermost to uppermost (approximately south to north) across the district. The numerous lithfacies units comprise nine lithofacies associations that provide the basis for interpretation of the volcano-sedimentary environments of deposition in this part of the Choyoi Arc. Petrological details are encapsulated in Table 3.1, which also incorporates new geochronological data generated in this study and discussed in Section 3.16. Petrological descriptions are contained in Appendix II. Individual lithofacies units are described after summary description of their host formation.

3.4 Chiclla Formation

The Chiclla Formation comprises the lowermost part of the Peine Group exposed across the southern part of the Collahuasi district (Fig. 3.5). It is dominated by a sequence of grey, subaerial felsic domes and pyroclastic deposits (Fig. 3.6) that attain a maximum thickness of ~2 km in the Monctezuma sector. The Chiclla Formation is conformably overlain by, and locally intercalated with the subaqueous, andesitic lower parts of the La Grande Formation.

TABLE 3.1. (part 1) Compilation of stratigraphic facies associations and lithofacies unit descriptions for the upper Peine Group.

Facies Association	Lithofacies / Stratigraphy[a]	Rock Characteristics	Crystal and Clast Characteristics[b,c]	Genetic Interpretation	References
Andesitic volcanic facies association.	*Yabricoya Formation*				
	TRa1. Andesite lava. Tabular flows <5 m thick.	Dark grey, massive, fine to medium grained, plag-phyric coherent andesite and lesser monomict blocky andesite breccia	Plag: 16-30%, 2-3 mm	Effusive subaerially eruptions, fissure vent source (?)	Vergara, 1978.
	Quebrada Pino andesite. TRa2.	Mid brown-grey, fine to medium grained, subvitreous amphibole-phyric coherent andesite	Amph: 20-30%, 1-3 mm, bronze-coloured and submetallic due to hematitic reaction rims		〃
Oxidised rhyolitic-dacitic volcanic and volcaniclastic facies association.	*TRy1.* Rhyolite tuff.	Light grey, pumiceous, kfs-qtz phyric, polymict lithic lapilli-bearing, ashy rhyolitic ignimbrite	Pum: 3%, <4 cm; Lith: 2-10%, <3 mm; Kfs: 6%, 1-2 mm; Qtz: 4%, 2-3 mm	Ash-rich pyroclastic flows	Munchmeyer et al.,1984 (Sub. 17-19)
	Yabricoya crystal ignimbrite. TRy2. Laterally extensive sheet, <350 m thick.	Red-brown, thick bedded, well-sorted medium-grained, variably quartzose, feldspar rich, lithic, welded crystal ignimbrite, rhyolitic at base, dacitic at top	Plag: 16-45% subh. 2-3 mm, An8-36; Kfs: 4-28%, 1-3 mm; Qtz: 7-34% embayed xls 1-3 mm; Lith: 0-16%, 0.5-4 cm, brown dacite; Cpx: 2%, 1-2 mm, altered and rimmed by hematite; Mtx: deformed glassy shards	High density, crystal-rich (medial ?) pyroclastic flow (surge ?) deposits, associated with localised effusive lava dome eruption	
	Yabricoya dacite. TRy3. 244 Ma. Domal flows <250m thick.	Dark brown-red, coarsely plag-(cpx-qtz)-phyric coherent dacite; fine phaneritic groundmass	Plag: 14-20%, 5-7 mm, An34-37 + albitic rims; Qtz: 4-6%, embayed xls 3-4 mm; Amph: 4%, 0.3-0.5 mm; Cpx: 1% <0.2 mm		Munchmeyer et al., 1984 (Sub. 16)
	Ornajuno rhyolite breccia. TRy4. 242 Ma. <350 m thick.	Grey-brown, very poorly sorted, moderately compacted, strongly polymict boulder-lapilli lithic dacite to rhyolite volcanic breccia	Lith: 15-65%, 1-10 cm; feldspars: 5-20%, 2-3 mm; Qtz: 1-10%, 2-4 mm; Mtx: 30% axiolitic glassy shards <300 μm	Block and ash flow deposits. Laterally E-directed flow (Ornajuno sector), unidentified explosive source	
	TRy5. Conglomerate. Channelised deposits <10 m thick.	Brown, weakly stratified, poorly sorted, polymict dacite-dominated subrounded cobble conglomerate	Lith: 75%, 1-25 cm, dacite TRy3	Proximal fluvial channel deposits	
	TRy6 . Rhyolite lava. Domal flows <100 m thick.	Mid red-brown, fine to medium grained, finely flow banded , qtz-(plag)-phyric rhyolite	Qtz: 8%, 1-2 mm; Plag: 6%, 2-3 mm	Minor subaerial effusive eruption	
Reduced rhyolitic-dacitic volcaniclastic facies association.	*Sallhuinca Formation*				
	Pzps1. Rhyolitic ignimbrite.	Light grey, pumiceous, ashy feldspar-qtz phyric rhyolitic ignimbrite	Pum: 3%, <2 cm; Qtz: 4%, 0.5-1 mm; feldspar: 7%, 1-2 mm, white	Repeated small laterally-directed ash-rich pyroclastic flows	
	Pzps3. R hyodacitic ignimbrite. Laterally attenuated sheet <200 m thick.	Dark grey, bedded, pumiceous, mod. compacted, plag-(qtz) phyric, rhyodacitic ignimbrite	Pum: 5%, <3 cm; Plag: 10%, 1-3 mm; Qtz: 1%, 0.5-1 mm		
	Pzps2. Rhyolite lava. 273 Ma. Irregular domal flows <200 m thick.	Light grey to dark brown, aphanitic, strongly undulose flow banded rhyolite and rhyolite dykes	Aphanitic, massive	Effusive subaerially erupted lavas and subvolcanic feeder dykes	
	Huinquintipa Formation				
	Pzph6. Platy rhyolitic ignimbrite. Laterally attenuated, <850 m thick.	Mid grey, pumiceous, strongly compacted, platy, kfs-qtz phyric rhyolitic ignimbrite	Pum: ?20%, 1-8 cm, indistinct; Kfs: 6-8%, 2-5 mm, pink; Qtz: 4-12%, 1-5 mm	Hot, laterally-directed ash-rich pyroclastic flows. Deposits underwent strong welding compaction.	Munchmeyer et al., 1984 (Sub. 10C)
	Pzph6a. Rhyolitic ignimbrite. Laterally restricted zone <80 m thick.	dark brown, pumiceous, moderately compacted, kfs-qtz phyric rhyolitic ignimbrite	Pum: 1%, <4 cm; Kfs: 11% 2-4mm, pink; Qtz: 6% 1-7mm eyes	Explosive volcanic centre unidentified	
	Pzph7 and Pzph7b. Rhyodacitic ignimbrite. Laterally restricted, <400 m thick.	Grey to mauve, polymict lithic, locally pumiceous, strongly plag-(amph-qtz) phyric dacitic ignimbrite and breccia	Lith: 2-10%, <4 cm, Pzpg.5 dacite (accessory); Pum: 0-25%, 1-10 cm; Plag: 15-35%, 2-3mm; Kfs: 3-5%, 0.5-1 mm; Qtz: 4%, 0.5-1 mm; Amph: 1-4%, 0.5-1 mm. Mtx: str relict shard textures	High density, vertically- or laterally directed pyroclastic flows. Explosive volcanic centre unidentified	〃
	Chigliuno rhyolitic ignimbrite. Pzph9 and Pzph9b. Laterally attenuated sheet <400 m thick.	Light grey, vitreous, strongly compacted, weakly qtz-(kfs) phyric welded ashy rhyolitic ignimbrite	Pum: 0-5%, 1-4 cm; Qtz: 5-6%, 2-3mm; Kfs: 1-4%, 2-3 mm	Hot, laterally-directed ash-rich pyroclastic flows. Explosive volcanic centre unidentified	〃
Oxidised felsic volcanic facies association.	*Huinquintipa dacite. Pzpg5* [d]. 276 Ma. Tabular flows <150 m thick	Dark brown to biege, massive to weakly flow banded plag phyric dacite and lesser dacite breccia	Plag: 10-20%, 1-3 mm, An29; Kfs: 5% 0.5-1 mm; Amph: 2-4%, 0.5-1 mm	Effusive to weakly explosive subaerial eruption	Munchmeyer et al., 1984 (Sub. 9)
	Pzph10 . Dacite lava. Domal flows <250 m thick	Brown, coarsely plag-phyric, aphanitic groundmass dacite	Feldspar: 12%, 1-6 mm, white lath aggregates	〃	(Sub. 10B)
	Pzph11. Rhyolite lava. Domal flows <250 m thick	Dark brown, vitreous, weakly qtz-(kfs) phyric rhyolite, masive to finely flow banded rhyolite	Qtz: 8% 0.5-1.5 mm; Kfs: 3% 1-2 mm, laths	〃	(Sub. 9)
Oxidised dacitic to rhyolitic volcanic and volcaniclastic facies association.	*Cascasa Formation*				
	Cascasa rhyolitic ignimbrite Pzpa1. 285 Ma. Laterally attenuated sheet <1250 m thick.	Pink-grey, vitreous, strongly compacted, welded, pumiceous, qtz-phyric rhyolitic ignimbrite	Pum: 6-14%,1-6 cm; Qtz: 7%, 3-6 mm; Kfs: 8% 1-2 mm; Mtx: poor stacked shard textures	Major laterally-directed ash-rich pyroclastic flow. Explosive source unidentified	Munchmeyer et al., 1984 (Sub. 13)
	Pzpa2. Dacite lava. Laterally attenuated sheet <350 m thick.	Purple to brown, finely planar flow-banded, weakly plag-phyric dacite and minor associated dacite breccia	Plag: 6% 0.5-1.5 mm, An8, fragmented. Qtz: 2% 0.5-1 mm; Oxides: 2%, <0.2 mm, equant	Effusive to weakly explosive subaerial eruption	Munchmeyer et al., 1984 (Sub. 12)
	Chusquina dacite. Pzpa3. Domal flow complex <1000 m thick	Black to purple, massive, plag-phyric dacite	Plag: 35% 3-4 mm, An38	Effusive eruption and shallow subvolcanic intrusion	
	La Grande Formation (partial)				
	Pzpg1. Rhyodacitic ignimbrite. Laterally extensive sheet <400 m thick.	Dark brown-red, fine to medium grained, moderately compacted, pumiceous feldspar-(qtz) phyric rhyodacitic ignimbrite	Pum: 7%, <2 cm; Lith: 0-4% ; Plag: 26%, 0.5-1.5 mm, An7. Kfs: 4%, 0.5-1 mm. Qtz: 1%, <0.5 mm. Opx: 2%, 0.5-1.5 mm	Vertically- or laterally-directed crystal rich pyroclastic flow. Explosive source unidentified	Munchmeyer et al., 1984 (Porfido Ines); Masterman, 2003.
	Inés dacitic ignimbrite. Pzpg3. Laterally attenuated sheet <150m thick.	Dark purple-brown, fine to medium grained, moderately compacted, pumiceous feldspar-phyric welded dacitic ignimbrite	Pum: 5-20 %, 2-5 cm; Plag: 10-15%, 0.5-2 mm; Kfs: 3-5%, 0.5-1.5 mm; Mtx: weak stacked shard textures	〃	

a.) Stratigraphic subdivision is based on mapped sedimentary or volcanic hiatuses (Fig 3.3b, 3.19b), and is partly independent of changes in lithofacies associations. Sequence of lithofacies nomenclature reflects the position of the occurrence of the greatest thickness of a given lithofacies unit and does not exclude local intercalation contrary to the sequence described. Radiometric ages are those produced in this study, rounded to the nearest million years, ignoring errors. Thicknesses given are maxima recorded in the district.

b.) % are average volume percent determined by visual estimation in hand specimen and/or in thin section under transmitted light. Dimensions are the long axis of elongate forms.

c.) Mineral compositions determined by electron microprobe and/or extinction angle (Michel-Levy test for plagioclase)

Abbreviations: Pum = pumice; Lith = lithic fragments; Plag = plagioclase; Kfs = orthoclase; Qtz = quartz; Amph = amphibole; Bt = biotite; Cpx = clinopyroxene; Opx = orthopyroxene; Mtx: matrix; An = anorthosite fraction of plagioclase; Sub.=subunit (subunidad).

TABLE 3.1. (part 2) Compilation of stratigraphic facies associations and lithofacies unit descriptions for the lower Peine Group

Facies Association	Lithofacies / Stratigraphy[a]	Rock Characteristics	Crystal and Clast Characteristics[b,c]	Genetic Interpretation	References
	La Grande Formation (continued)				
Subaerial volcanic and terrestrial evaporitic sedimentary facies association.	*Pzpg2.* Redbed siltstones and sandstones.	Red-brown, thin-bedded, evaporite-bearing plane laminated siltstones, and normally graded fine to granular lithic sandstones; minor chert	Evaporites: 0-25%, globular aggregates 2-35 mm concentrated in discrete beds	Locally-derived restricted-basin terrigenous fluviotile and lacustrine sediments. Cherts ?exhalative	Munchmeyer et al., 1984 (Sub. 8, 10A)
	Pzpg4. Andesite lava. Tabular flows <40 m thick.	Dark red-brown, fine to medium grained andesite and monomict andesite breccia	Commonly equigranular. Plag: 55-75%, 1-3 mm; Amph: 20-25%, 1-3 mm	Subaerial effusive eruption from multiple small centres	〃
	Huinquintipa dacite. Pzpg5[d] and *Pzpg5a.* Tabular and domal flow complexes <400 m thick.	Dark brown to biege, massive to weakly flow banded plag phyric dacite and lesser monomict lithic dacite breccia	Plag: 10-20%, 1-3 mm, An29; Kfs: 5%, 0.5-1 mm; Amph: 2-4%, 0.5-1 mm	〃	〃
	Pzpg6. Rhyolitic ignimbrite. Laterally attenuated sheet <250 m thick.	Light grey, fine to medium grained, qtz-phyric welded ashy rhyolitic ignimbrite	Qtz: 6-12%, 2-3 mm; Feldspar: 4-10%, 1-3 mm, white; Lith: 2-6%, <2 cm, polymict subangular	Subaerial pyroclastic flow deposits that underwent welding upon deposition. Explosive volcanic centre unidentified	
Subaqueous bimodal volcano-sedimentary facies association.	*Pzpg7.* Rhyolite lava. Domal flows <150 m thick.	Pale coloured, massive, aphanitic to weakly feldspar-phyric coherent rhyolite and lesser monomic rhyolite breccia	Plag: 3-5% 0.5-1.5 mm, An 8-10. Kfs: <1%, 0.5-1 mm; Qtz: 1-2% 0.5-1 mm; Oxides: 1%, <0.5 mm, equant	Subaerial effusive eruption from multiple small centres	
	Pzpg8. Marl and limestone.	Black and grey crenular laminated micritic limestone, green massive to poorly laminated arkosic marl and minor jasperoid chert	Granular sand: 2-15%, dominated by feldspar crystal fragments	Restricted-basin microbially-mediated chemical sediments with locally derived clastic input	
	Pzpg9 . Andesite lava. Tabular flows <10 m thick.	Black, aphanitic, magnetic, andesite and lesser monomict andesite breccia	Commonly equigranular	Effusive subaqueous eruption with minor phreatomagmatic explosivity. Possible fissure vent along the Rosario Fault Zone	Vergara, 1978; Munchmeyer et al., 1984 (Sub. 6A-7); Breitkreuz and Zeil, 1994; Masterman, 2003.
	Ocoita andesite. Pzpg10. Tabular flows <60 m thick.	Dark grey, plag-megacrystic amygdaloidal andesite, monomict andesite breccia, and minor sandstone-matrix andesite peperite	Plag: 10-40%, 4-16 mm, An 36-38. Amygdales: 0-40%, <6 mm, concentrated in brecciated flow margins		
	La Grande andesite. Pzpg13 . Tabular flow complexes <80 m thick.	Black to grey, weakly magnetic, plag-phyric andesite & monomict andesite breccia. Minor andesite-sandstone peperite	Plag: 30-70%, 0.5-3 mm, An31-37; Oxides: 2-4%, <0.5 mm, equant; Cpx: 0-2%, 0.2-0.5 mm. Amygdales: 0-20%,<5 mm, concentrated in brecciated flow margins	〃	
	Pzpg12. Sedimentary breccia and granular sandstone. ?lobate flows and fans.	Massive to weakly graded, mosaic-textured polymict pebble breccias & granular sandstones	Lith: 30-70% aphanitic andesite, thermally oxidised, red; 30-50% feldspar-(qtz) phyric felsic rocks, light grey; Plag: 10-20% broken crystals; Mtx: 50% feldspathic bubble-wall shards	Amalgamated mass flow sediments, with variable contrib-ution of locally-derived juvenile epiclastic clasts. Possibly related to basin subsidence events	〃
	Pzpg11. Dacitic ignimbrite. Laterally extensive sheets <150 m thick.	Grey, variably compacted, pumiceous, polymict lithic, locally welded feldspar-(qtz)-phyric rhyodacite tuff	Pum: 15-50%, 0.5-3 cm; Lith: 0-5%, <1 cm; Feldspar: 4-10%, 1-3 mm	Subaerial pyroclastic flow deposits emplaced into water	〃
	Chiclla Formation				
Reduced subaerial felsic volcanic and volcaniclastic facies association.	*Pzpc1.* Dacitic ignimbrite. 289 Ma. Laterally extensive sheets <100 m thick.	Grey, polymict lithic, plag-(amph-qtz) phyric dacitic ignimbrite	Plag: 35% 0.5-1.5 mm, An6-8. Lith: 10-25%, 0.5-3 cm, dacite and andesite; Hbl: 2%, 0.2-0.3 mm; Qtz: 0-1%, 0.3-0.6 mm	Major subaerial pyroclastic flow deposit that underwent welding upon deposition	
	Pzpc3. Conglomerate. ?channelised deposits and lobate flows <120 m thick.	weakly strat, moderately sorted, subang, polymict, conglomerate to granular sandstone	Lith: 60-85%, 0.5-5 cm, subangular felsic-dacitic volcanics	Amalgamated terrigenous mass flow sediments. Possibly related to incipient subsidence	
	Pzpc4. Andesite lava. Tabular flow complexes <150m thick.	dgn to grey, f to cg, strongly zoned plag to phyric andesite	Plag: 22% 4-7 mm, An40. Amygdales: 1% 1-3 mm	Localised subaerial effusive eruption	Munchmeyer et al., 1984 (Sub. 3)
	El Colorado rhyolite. Pzpc2. 288 Ma. Domes complexes <400 m thick.	Grey to pink, weakly flow banded qtz-phyric vitreous rhyolite	Qtz: 8-16%, 2-3 mm; Feldspar: 3% 1-2 mm	Major vertically directed ash-rich subaerial pyroclastic flow deposit and ?related flow-dome eruptions on multiple centres	Munchmeyer et al., 1984 (Sub. 5)
	Chiclla rhyolitic ignimbrite. Pzpc5. 298Ma. Laterally extensive sheet <1100 m thick.	Dark grey, subvitreous, weakly lithic polymict, weakly pumiceous, strongly qtz phyric rhyolitic ignimbrite. Minor intercalated andesite	QTZ: 13% embayed and melt-inclusion-rich subhedral broken xls <5 mm. PLAG: 8% broken subhedral xls <5 mm, An35. Spherules: <1% radial fragments 0.5-1 mm; Mtx: abundant deformed shards		Munchmeyer et al., 1984 (Sub. 4)
	Monctezuma dacite. Pzpc6. Domal flow complexes <400 m thick	Dark grey, plag-phyric, strongly plane flow-banded dacite, and lesser finely crenular flow-banded mid grey dacite	Flow bands: 5-20%, 1-3 mm wide, qtz-muscovite, pink; Plag: 4-10%, 1-1.5 mm, white	Effusive subaerial eruption	Munchmeyer et al., 1984 (Sub. 2)
	Pzpc9. Rhyolite and dacite lava. 295 Ma. Domes and small flows <300 m thick.	Monomic volcanic breccias: pink rhyolite (Monctezuma) and gn to grey dacite (El Colorado)	Aphanitic (Monctezuma), weakly feldspar-phyric (El Colorado)	Effusive subaerial to locally subaqueous eruption	Munchmeyer et al., 1984 (Sub. 1)
	Pzpc10. Rhyolitic ignimbrite. Laterally extensive sheets <120 m thick.	Pale grey, fine to medium grained, pumiceous qtz-feldspar-phyric ashy rhyolitic ignimbrite	Plag: 10-14%, 1-3 mm; Pum: 4-12%, 0.5-3 cm; Qtz: 4-8%, 1-2 mm	Ashy-crystal rich pyroclastic fall deposit	Desrochers et al., 2001
	Pzpc10a. Rhyodacitic ignimbrite. Laterally extensive sheets <30 m thick.	Pale grey, fine to medium grained, pumiceous feldspar-(qtz) phyric ashy rhyodacitic ignimbrite	Plag: 10-18%, 1-3 mm; Pum: 4-20%, 0.5-3 cm; Qtz: 1-4%, 1-2 mm	〃	〃

a.) Stratigraphic subdivision is based on mapped sedimentary or volcanic hiatuses (Fig 3.3b, 3.19b), and is partly independent of changes in lithofacies associations. Sequence of lithofacies nomenclature reflects the position of the occurrence of the greatest thickness of a given lithofacies unit and does not exclude local intercalation contrary to the sequence described. Radiometric ages are those produced in this study, rounded to the nearest million years, ignoring errors. Thicknesses given are maxima recorded in the district.

b.) % are average volume percent determined by visual estimation in hand specimen and/or in thin section under transmitted light. Dimensions are the long axis of elongate forms.

c.) Mineral compositions determined by electron microprobe and/or extinction angle (Michel-Levy test for plagioclase)

d.) The Pzpg.5 lithofacies occurs sporadically throughout the higher parts of the upper Collahuasi Formation (Fig. 3.3A, B).

Abbreviations: Pum = pumice; Lith = lithic fragments; Plag = plagioclase; Kfs = orthoclase; Qtz = quartz; Amph = amphibole; Bt = biotite; Cpx = clinopyroxene; Opx = orthopyroxene; Mtx: matrix; An = anorthosite fraction

3.4.1 Rhyolitic ignimbrite (Pzpc10, Pzpc10a)

Vitriclastic rhyolitic and lesser rhyodacitic ignimbrite occur as a weakly stratified sequence 100-150 m thick in the El Colorado sector southwest of Quebrada Blanca (Figs. 3.4, 3.5). These strata define a tight S-vergent, moderately N-plunging syncline-anticline pair between strands of the Domeyko fault system. The entire fault block is strongly affected by leaching related to supergene oxidation of the El Colorado hydrothermal system and petrographic detail is largely destroyed. Sparse, locally preserved fragmental texture is dominated by lens-shaped clasts interpreted to be compacted pumice clasts. Small equant quartz phenocrysts vary in abundance up to 7 volume percent and define stratification within the unit that can be traced over more than one kilometre. The fragmental texture, clast and crystal components and strong lateral bed continuity suggest a pyroclastic origin. The inferred position of this unit at the base of the Peine Group stratigraphy has been independently confirmed by SHRIMP zircon U-Pb geochronology (Munizaga et al., 2008). These authors reported ages of ~308 Ma, the oldest anywhere in the district, from the El Colorado prospect and from host rhyolitic rocks 600 m below surface at Rosario. The latter demands that these lowermost felsic pyroclastic deposits extended across the district.

3.4.2 Rhyolite and dacite (Pzpc9, 295.1 ± 3.1 Ma)

Small domes and flows of rhyolite and dacite occur localised along major faults in the Monctezuma and El Colorado sectors, respectively. Coherent facies are subordinate to monomictic volcanic breccias. At El Colorado strong curviplanar clast morphologies and partial jigsaw-fit textures are interpreted as products of quench fragmentation. Occurences at Monctezuma are dominated by blocky matrix-supported chaotic breccia geometries and are interpreted to have erupted subaerially. A sample of this material dated during this study yielded an age within error of a SHRIMP zircon U-Pb age for dacite from the El Colorado sector (298.8 ± 2.2 Ma: Munizaga et al., 2008).

3.4.3 Monctezuma dacite (Pzpc6)

A thick package of distinctive strongly flow banded dark grey, weakly plagioclase-phyric dacites occurs between the Monctezuma and La Grande sectors. This unit

is a major host to epithermal mineralisation at Monctezuma, where flow banding is locally dense and crenulated (Fig. 3.6a) or more commonly planar, with 1-2 mm-wide pale pink-bands that occur at a frequency of ~2/cm (Fig. 3.6b). Surface exposure of the Monctezuma dacite is offset in a sinistral sense ~1750 m along the Monctezuma Fault, but its continuity further west has not been investigated beyond the limits of mineralisation.

3.4.4 Chiclla rhyolitic ignimbrite (Pzpc5, 298.5 ± 2.1 Ma)

Extensive outcrops of massive, strongly quartz-phyric, vitreous rhyolite define a strike-parallel topographic ridge between Cerro Chiclla (SE) and Cerro Escorial (NW). Rare moderately compacted pink and grey fiamme (Fig. 3.6c,d), combined with textural evidence for plastic deformation of abundant glassy shards in the matrix (Fig. 3.6e,f) are interpreted to indicate a pyroclastic origin and depositional welding of the Chiclla rhyolitic ignimbrite. It extends at least 12 km across the district, and is only absent in the El Colorado section adjacent to the Domeyko fault system. Minor undifferentiated andesites are intercalated with the rhyolitic ignimbrite (Fig. 3.4) and indicate that it is a composite of at least two separate pyroclastic depositional events in which the crystal and clast populations are similar. Based on a simple geometric

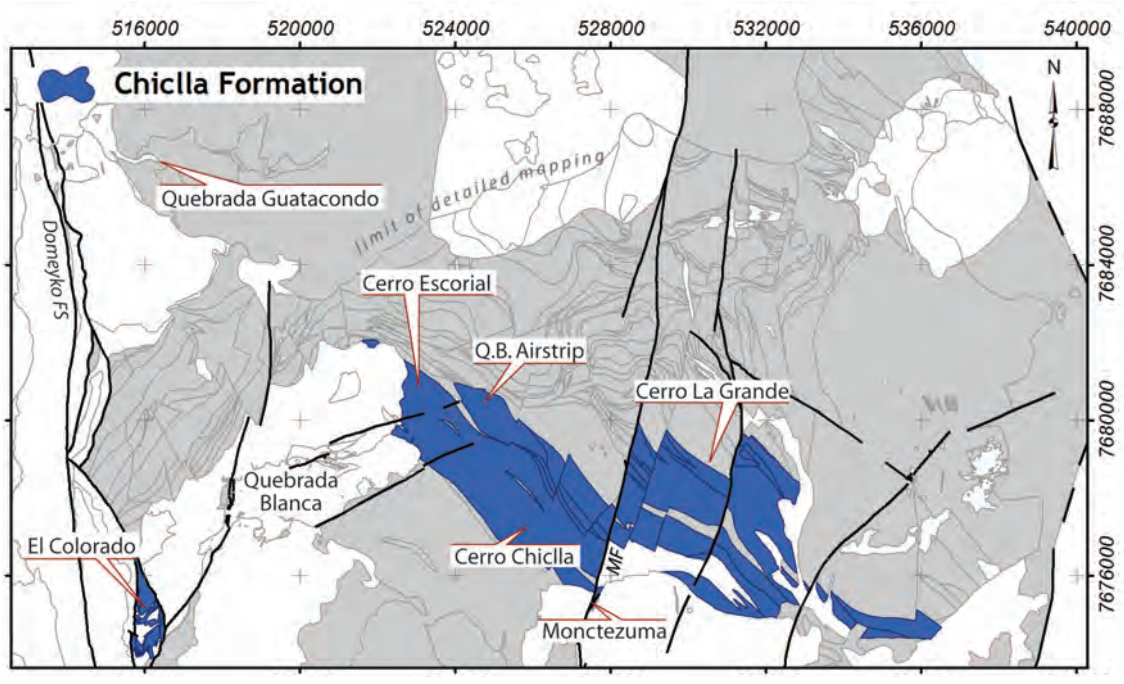

Figure 3.5. 1:100,000 map showing the distrubtion of the Chiclla Formation in the Collahuasi district. Light grey area depicts the extent of Peine Group rocks in the district. Black linework indicates major faults. Landmarks mentionned in the text are indicated. Abbreviations: FS = fault system, MF = Monctezuma Fault. Grid divisions are 2 kilometres.

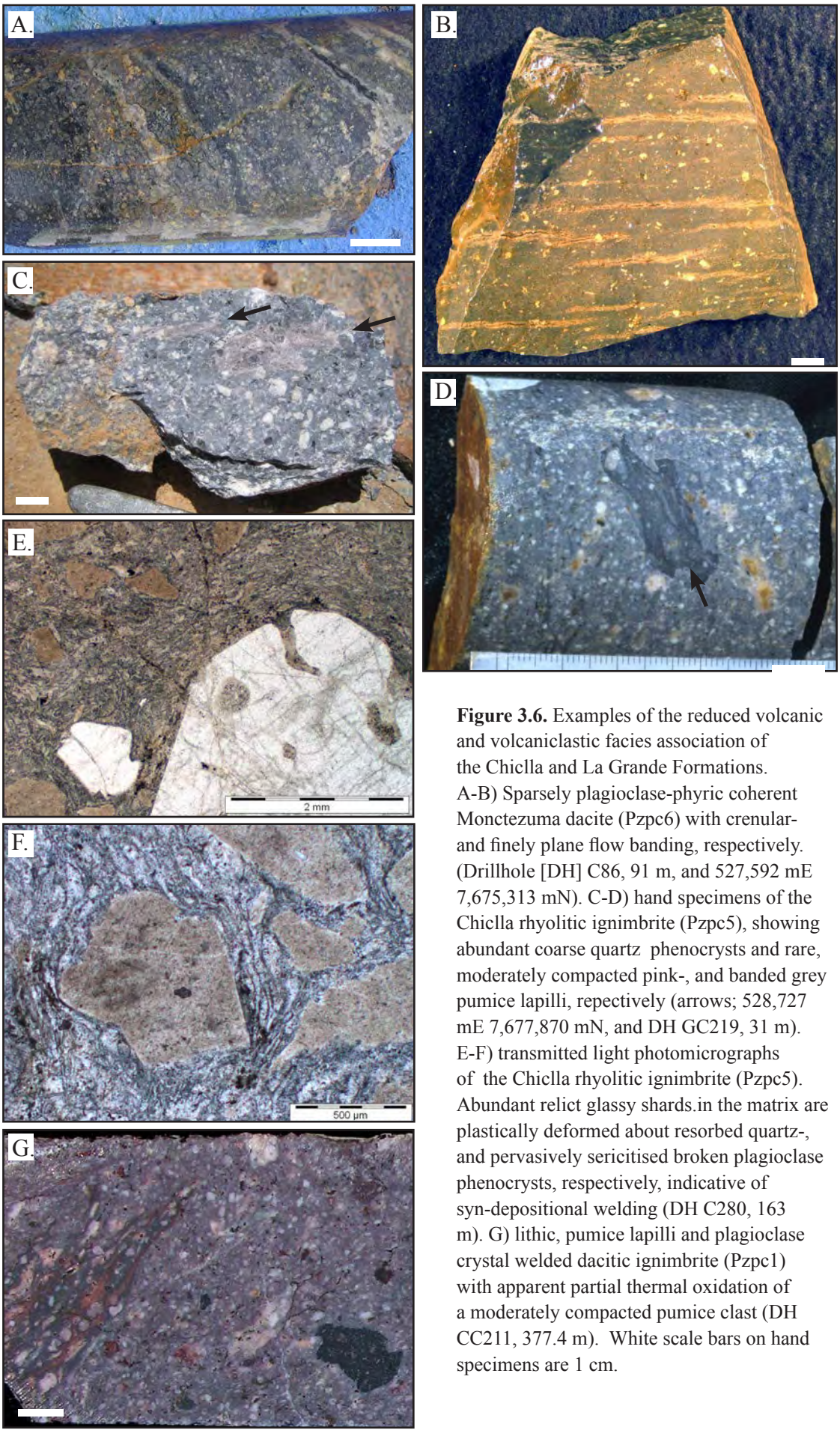

Figure 3.6. Examples of the reduced volcanic and volcaniclastic facies association of the Chiclla and La Grande Formations. A-B) Sparsely plagioclase-phyric coherent Monctezuma dacite (Pzpc6) with crenular- and finely plane flow banding, respectively. (Drillhole [DH] C86, 91 m, and 527,592 mE 7,675,313 mN). C-D) hand specimens of the Chiclla rhyolitic ignimbrite (Pzpc5), showing abundant coarse quartz phenocrysts and rare, moderately compacted pink-, and banded grey pumice lapilli, repectively (arrows; 528,727 mE 7,677,870 mN, and DH GC219, 31 m). E-F) transmitted light photomicrographs of the Chiclla rhyolitic ignimbrite (Pzpc5). Abundant relict glassy shards.in the matrix are plastically deformed about resorbed quartz-, and pervasively sericitised broken plagioclase phenocrysts, respectively, indicative of syn-depositional welding (DH C280, 163 m). G) lithic, pumice lapilli and plagioclase crystal welded dacitic ignimbrite (Pzpc1) with apparent partial thermal oxidation of a moderately compacted pumice clast (DH CC211, 377.4 m). White scale bars on hand specimens are 1 cm.

approximation (specifically a 12 km diameter, circular disc-shaped body 0.9 km thick and compacted to 50% of its original volume) this equates to an erupted volume of ~200 km^3, which is the same order of magnitude as the larger individual ignimbrites erupted in the Taupo Volcanic Zone of New Zealand, e.g., the 140 Ka Mamaku Ignimbrite and 320-340 Ka Whakamaru Ignimbrites (Wilson et al., 1984; Brown et al., 1998; Milner et al., 2003).

3.4.5 Andesite (Pzpc4)

Thin, laterally discontinuous lenses of strongly plagioclase-phyric andesite overlie the Chiclla rhyolitic ignimbrite locally in the La Grande and Cerro Chiclla areas. These are distinguished by coarse grained equant euhedral plagioclase phenocrysts with strong compositional zonation that is visible in hand specimen and commonly accentuated by hydrothermal alteration.

3.4.6 Lithic conglomerate and sandstone (Pzpc3)

Conglomerates and granular sandstones composed of subangular felsic and lesser andesite clasts overlie Pzpc4 or the Chiclla rhyolitic ignimbrite. These proximal sedimentary facies extend laterally for several kilometres south of Cerro La Grande (Fig. 3.4) but individual beds or flows cannot be traced between drillholes or outcrops. Sedimentary facies appear to be absent in the easternmost part of the district (El Colorado).

3.4.7 QB airstrip rhyolite (Pzpc2, 288.6 ± 3.3 Ma)

Grey to beige, quartz-phyric rhyolite crops out extensively in the northern part of the El Colorado sector. The unit is composed of numerous small (< 10 m) domes that show weak internal textural zonation parallel to the dome margins and narrow feeder dykes. The small domes are interdigitated like large pillows. Various monomictic rhyolite breccias occur between adjacent domes.

Pink-brown, vitreous, weakly flow-banded quartz-phyric rhyolite and monomictic rhyolite breccia occurs as a single large body adjacent to the old Quebrada Blanca airstrip. The distribution of coherent and breccia facies is unknown, as exposure is poor and breccia textures are only revealed in thin section. However, it has a high

aspect ratio and short lateral continuity suggestive of dome morphology. Further isolated small quartz-phyric rhyolites occur at the same stratigraphic interval in a structurally complex zone north of Quebrada Blanca. Breccia facies are absent in this area and these occurrences may be cryptodomes.

3.4.8 Dacitic ignimbrite (Pzpc1, 289.7 ± 3.1 Ma)

Massive light grey crystal-rich lithic lapilli dacitic ignimbrites (Fig. 3.6g) appear to onlap the QB airstrip rhyolite in the vicinity of the contact. Locally these ignimbrites have poor lateral continuity, and may have infilled topography at the time of their eruption. Similar ignimbritic rocks comprise rampart outcrops in the upper reaches of the Quebrada Guatacondo. In this sector the strata dip to the southwest (Fig. 3.4) suggesting that the generally N-dipping strata in the area of detailed mapping is the southern limb of a broad E-trending basement syncline.

3.5 La Grande Formation

The La Grande Formation conformably overlies the Chiclla Formation (Fig. 3.4, Table 3.1) and records an abrupt lower Permian transgression followed by gradual regression and basin infilling of the central Collahuasi district. It extends across

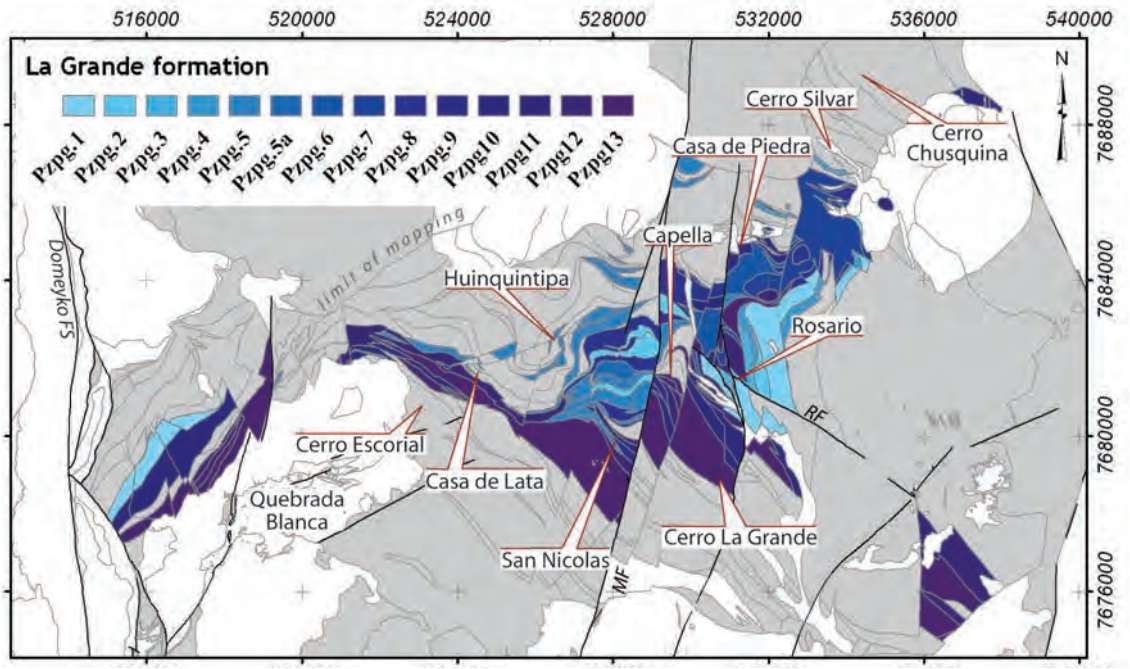

Figure 3.7. Distrubtion of the La Grande Formation in the Collahuasi district. Landmarks mentionned in the text are indicated. All other map elements and abbreviations as per figure 3.5. Grid divisions are 2 kilometres.

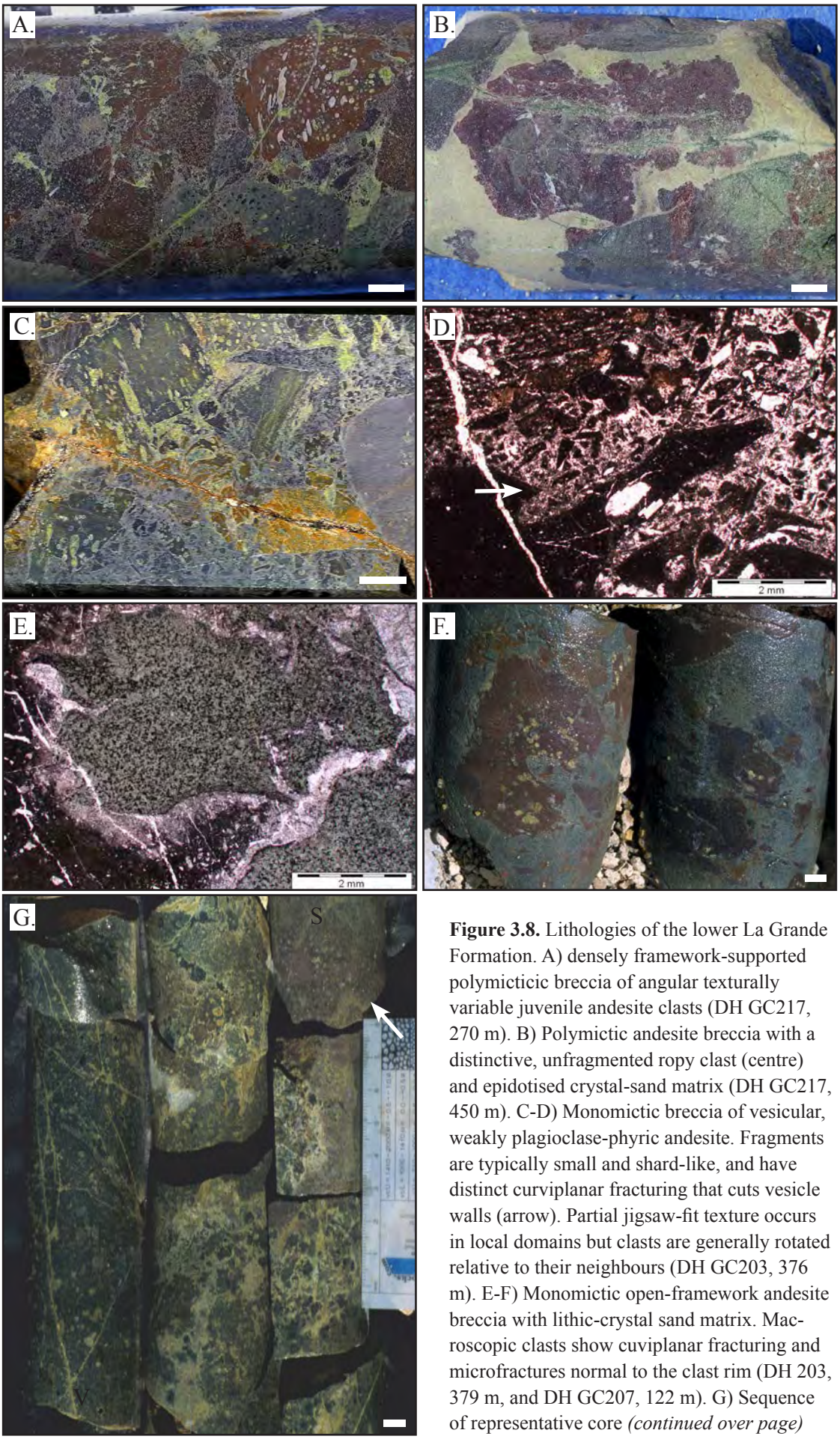

Figure 3.8. Lithologies of the lower La Grande Formation. A) densely framework-supported polymicticic breccia of angular texturally variable juvenile andesite clasts (DH GC217, 270 m). B) Polymictic andesite breccia with a distinctive, unfragmented ropy clast (centre) and epidotised crystal-sand matrix (DH GC217, 450 m). C-D) Monomictic breccia of vesicular, weakly plagioclase-phyric andesite. Fragments are typically small and shard-like, and have distinct curviplanar fracturing that cuts vesicle walls (arrow). Partial jigsaw-fit texture occurs in local domains but clasts are generally rotated relative to their neighbours (DH GC203, 376 m). E-F) Monomictic open-framework andesite breccia with lithic-crystal sand matrix. Macroscopic clasts show cuviplanar fracturing and microfractures normal to the clast rim (DH 203, 379 m, and DH GC207, 122 m). G) Sequence of representative core *(continued over page)*

the district from west to east and reaches a maximum true thickness of 2.4 km in the section between Casa de Piedra and La Grande (Fig. 3.7). The lower part is dominated by andesitic volcanics and mass flow clastic sediments. These likely formed in response to mass wasting from volcanic edifices and from marginal escarpments following basin subsidence. A similar association of sedimentary and andesitic volcanic facies is described as the "middle member" (Miembro Medio) of the three broad regional subdivisions of the Peine Group described by previous workers (Fig. 3.3: Vergara, 1978; Ware et al., 1981; Davidson et al., 1985; Pichowiak et al., 1987; Gardeweg, 1988; Bahlburg and Breitkreuz, 1991; Breitkreuz and Zeil, 1994; Tomlinson et al., 2001a). Rhyolite and dacite volcanics are dominant in the upper parts of the section and are intercalated with calcareous sediments, evaporite-bearing redbeds and subaerial felsic volcaniclastics. Aqueous depositional environments of the Miembro Medio basin are described variously as marine and limnic on the basis of scarce fossil evidence (Munchmeyer et al., 1984; Osorio and Riviano, 1985; Breitkreuz and Zeil, 1994). Localised attenuation of La Grande Formation stratigraphy and discordance of bedding between the La Grande and overlying members (Fig. 3.4) suggest that a period of erosional valley incision followed deposition of the pyroclastic Inés porphyry, possibly associated with inversion of the Miebro Medio basin at this time.

3.5.1 Cerro La Grande andesite (Pzpg13)

Black to grey, magnetic, moderately plagioclase-phyric andesites are the most distinctive lithofacies of the La Grande Formation (Fig. 3.8). Fragmental facies commonly account for more than 70% of the volume of andesitic material (Fig. 3.9). These include andesitic breccias in which clasts are dominantly blocky and subangular, and commonly strongly vesicular (Fig. 3.8a). Clasts with fluidal shapes are present in some breccias, and are inferred to be primary ejecta (Fig. 3.8b). Locally, monomictic breccias composed of angular curviplanar shard-like fragments are preserved. The primary fragmentation that generated these clasts traversed

...fragments across the basal contact of an andesite flow. The bedded crystal-lithic sandstone (S, arrow parallel to bedding) substrate becomes matrix to a 10-100 cm-thick zone of peperite that grades into coherent andesite (V). DH GC219, 228-229 m downhole.

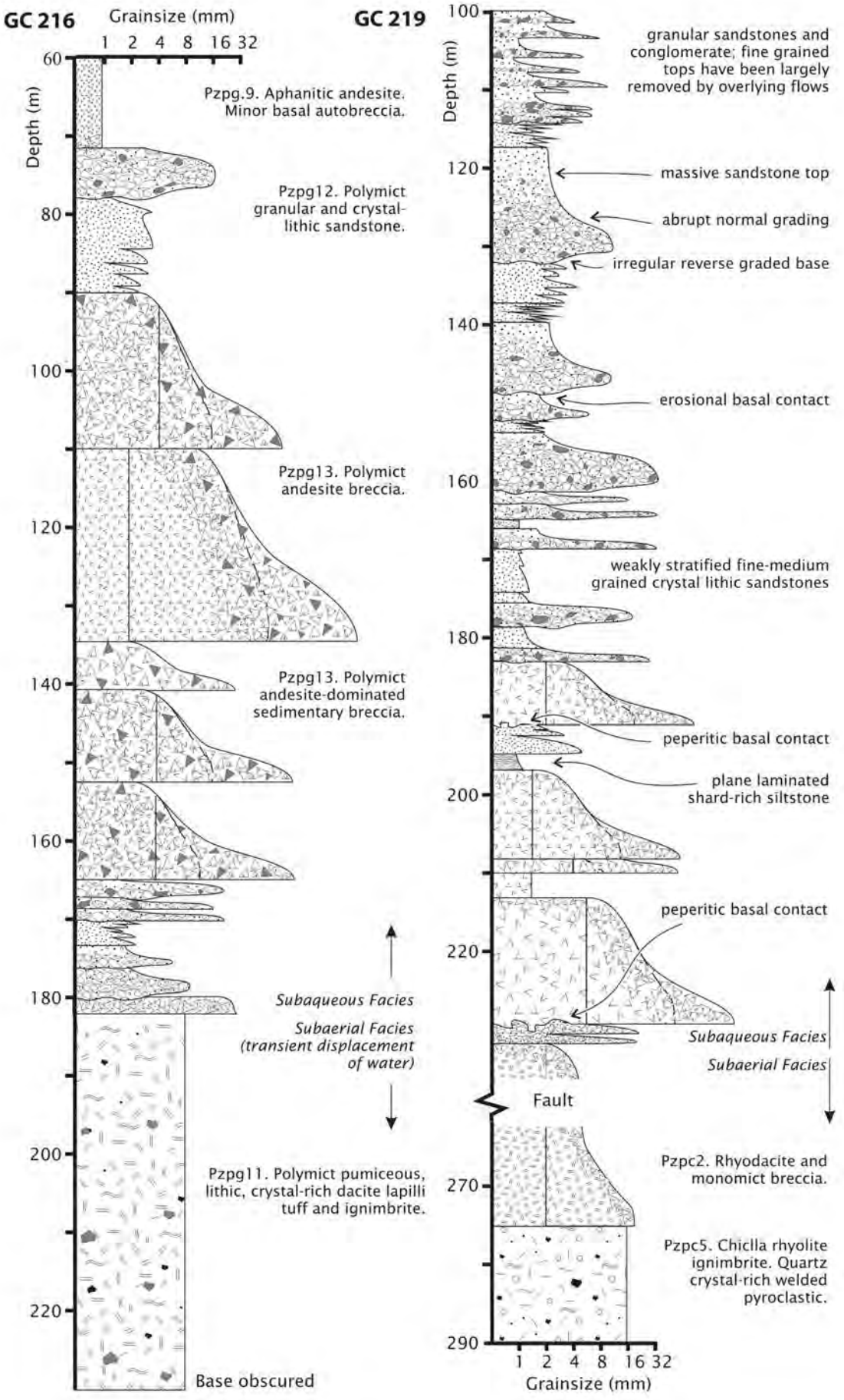
GC 216
Grainsize (mm)
1 2 4 8 16 32
Depth (m)
60
80
100
120
140
160
180
200
220
Pzpg.9. Aphanitic andesite. Minor basal autobreccia.
Pzpg12. Polymict granular and crystal-lithic sandstone.
Pzpg13. Polymict andesite breccia.
Pzpg13. Polymict andesite-dominated sedimentary breccia.
Subaqueous Facies
Subaerial Facies (transient displacement of water)
Pzpg11. Polymict pumiceous, lithic, crystal-rich dacite lapilli tuff and ignimbrite.
Base obscured
GC 219
Depth (m)
100
120
140
160
180
200
220
270
290
granular sandstones and conglomerate; fine grained tops have been largely removed by overlying flows
massive sandstone top
abrupt normal grading
irregular reverse graded base
erosional basal contact
weakly stratified fine-medium grained crystal lithic sandstones
peperitic basal contact
plane laminated shard-rich siltstone
peperitic basal contact
Subaqueous Facies
Subaerial Facies
Fault
Pzpc2. Rhyodacite and monomict breccia.
Pzpc5. Chiclla rhyolite ignimbrite. Quartz crystal-rich welded pyroclastic.
1 2 4 8 16 32
Grainsize (mm)

vesicle walls (Figs. 3.8c,d) and created small arcuate fractures sub-perpendicular to the clast margins (Fig. 3.8e). The andesite fragments are variably plagioclase-phyric and have a massive, very fine grained groundmass that is opaque in thin section. The groundmass cannot therefore be shown to be glassy, however the textural detail (above) is consistent with post-vesiculation quench fragmentation in an aqueous environment (Yamagishi, 1979; McPhie et al., 1993). Breccias comprised of clasts of quench fragmented andesite and matrices of polymictic lithic-crystal sandstone (Fig. 3.8 e, f) occur along the bases of many andesite flows (Fig. 3.8 g), and rarely on both margins of narrow sills. These textural and spatial relationships indicate subaqueous andesite eruption onto, or emplacement into an unconsolidated sedimentary substrate (Busby-Spera and White, 1987; Gifkins et al., 2002; Skilling et al., 2002; Squire and McPhie, 2002).

3.5.2 Lithic sandstone and conglomerate (Pzpg12)

Crowded "mosaic-textured" pebble conglomerates and granular sandstones (Fig. 3.10a,b) are the dominant sedimentary lithofacies associated with andesitic volcanics in the lower La Grande Formation. These are made up of subangular to subrounded clasts of andesite and rhyolitic volcanic lithologies in variable proportions, suggesting mixed provenance from the immediate volcanic environment and from the basin margins. Andesitic clasts have undergone varying degrees of thermal oxidation, resulting in red-black hues. The volumetrically minor sandstone matrices consist of plagioclase crystals and devitrified bubble-wall shards. Bedding is commonly defined by internal grainsize variations within massive erosionally amalgamated beds (Fig. 3.10b). Where preserved, basal contacts of coarse conglomeratic lenses are weakly reverse graded. Above the main conglomerate bed, they grade upward into poorly stratified granular sands (Fig. 3.9). Thin beds of matrix-supported pebble-sand breccias and plane-laminated crystal ash turbidites are preserved locally (Fig. 3.10c).

Figure 3.9. Representative 1:1,000 vertical scale graphic logs of selected intervals of the lower La Grande Formation stratigraphy in drillholes GC216 and GC219. The logs are drawn to demonstrate relationships between volcanic and sedimentary lithofacies described in the text and in Table 3.1. Bedding-core axis intersection angles are high throughout the holes such that downhole thicknesses approximate true bed thicknesses. Vertical lines across some beds indicate the grainsize of the groundmass or matrix. Lobate extensions of some beds to coarse grainsizes reflects the expected lateral facies changes as coherent units develop fragmental carapaces and margins.

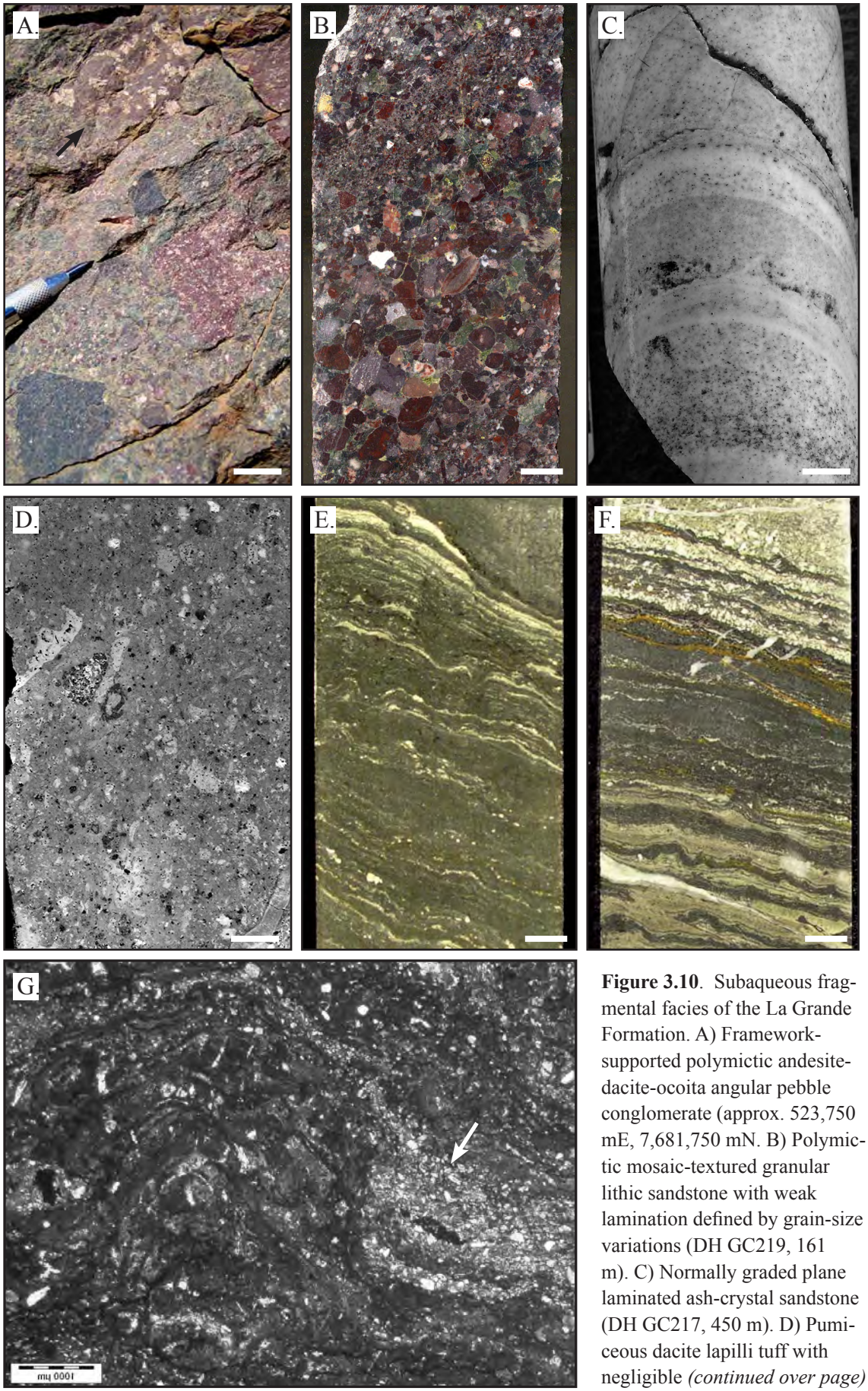

Figure 3.10. Subaqueous fragmental facies of the La Grande Formation. A) Framework-supported polymictic andesite-dacite-ocoita angular pebble conglomerate (approx. 523,750 mE, 7,681,750 mN. B) Polymictic mosaic-textured granular lithic sandstone with weak lamination defined by grain-size variations (DH GC219, 161 m). C) Normally graded plane laminated ash-crystal sandstone (DH GC217, 450 m). D) Pumiceous dacite lapilli tuff with negligible *(continued over page)*

These bedforms and internal characteristics of this sequence are consistent with formation by energetic mass flow processes in a sub-wave base aqueous environment (e.g., Sohn, 2000; Felix and Peakall, 2006).

3.5.3 Dacite lapilli tuff (Pzpg11).

Pumiceous lapilli-rich dacitic pyroclastic deposits (Fig. 3.10d) are locally intercalated with sedimentary and andesitic volcanic units. These show rapid lateral attenuation over distances of < 500 m and are best developed in the La Grande and San Nicolas areas (Fig. 3.7). The degree of compaction of pumice clasts is variable and in some cases no compaction is apparent (Fig. 3.10e). This may indicate that juvenile pyroclasts were cool prior to deposition, consistent with either primary emplacement into water or resedimentation (e.g., McPhie et al., 1993). Internal stratification is absent and these rocks are interpreted as primary pyroclastic deposits.

3.5.4 Ocoita Andesite (Pzpg10).

Strongly plagioclase megacrystic andesites known locally as 'ocoita' have been described previously from the Collahuasi district (Vergara, 1978; Ware et al., 1981; Masterman, 2003). Similar coherent and fragmental facies are present, as for the Cerro La Grande andesite (Pzpg13). Megacrystic andesites occur sporadically throughout the La Grande Formation, but appear to be concentrated toward the top of the main andesitic package on the northern flank of Cerro La Grande (Fig. 3.7). Localised flow complexes in the upper La Grande Formation crop out immediately below the unconformity between the La Grande and Yabricoya Members in the Casa de Piedra area, and along the margins of the Cretaceous intrusive complex southeast of Cerro Silvar and Cerro Chusquina (Fig. 3.7).

3.5.5 Andesite (Pzpg9)

Fine grained, magnetic, black, massive basaltic andesite is a minor component of the lower La Grande Formation. Oxide phases are abundant (5-10 volume %) and

...compaction (529,516 mE, 7,676,277 mN). E) Crenular laminated dark grey limestone (DH C265, 56 m). F) Variably plane- and crenular laminated green-grey marl with feldspar-rich crystal sand laminae (DH C265, 61 m). G) Microscopic biohermal structure in E with kerogenous laminations and clastic sediment accumulation in its lee (arrow).

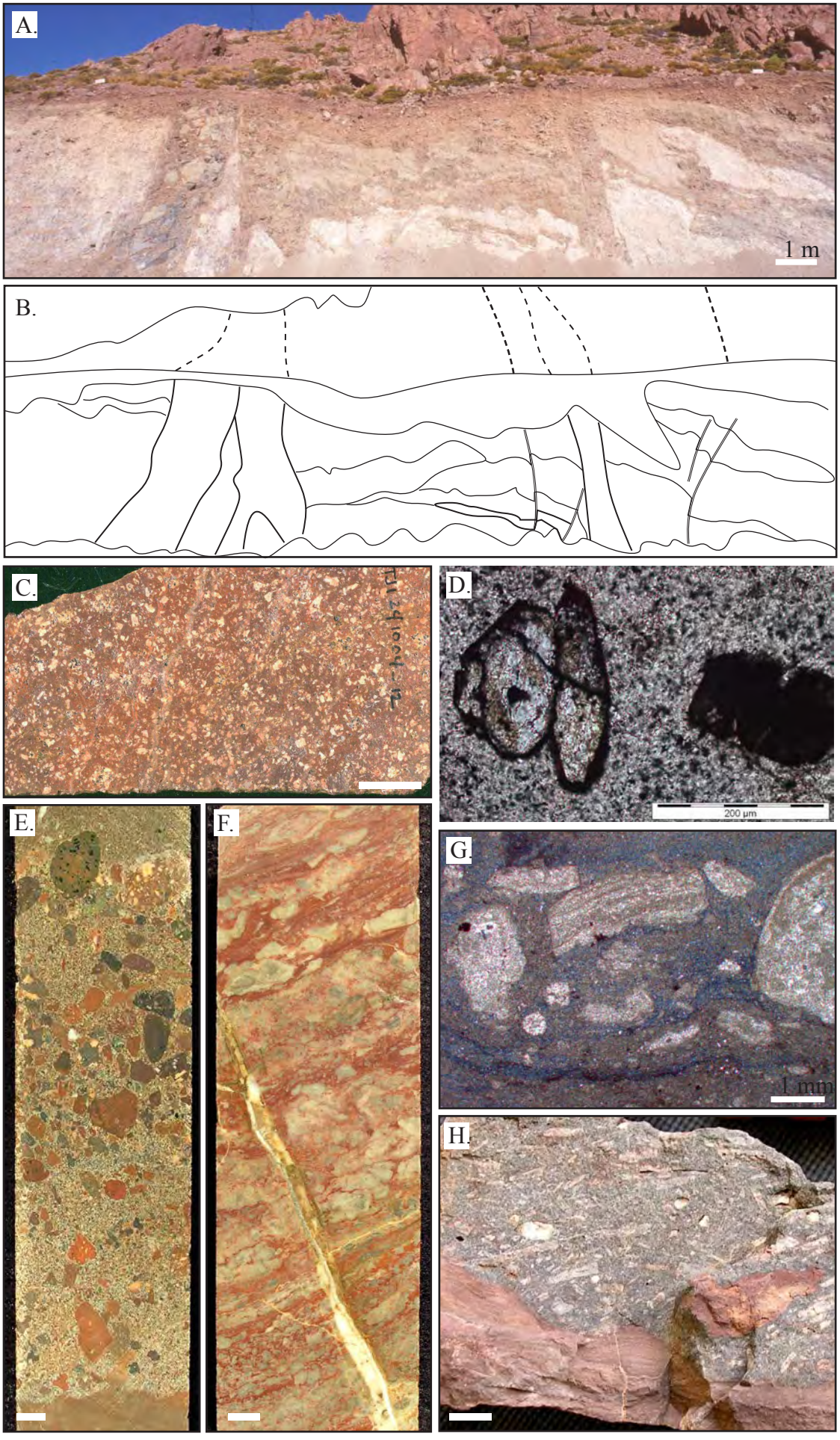
A.
1 m
B.
C.
D.
200 µm
E.
F.
G.
1 mm
H.

some examples are completely opaque in thin section. This facies is best developed in the basal part of the sequence north of Cerro Escorial (Fig. 3.7). Breccia facies are generally less abundant than in other andesite varieties.

3.5.6 Capella Member (Pzpg8)

Black and grey-green crenular laminated micritic limestones occur intercalated with coarse clastic mass flow deposits and rhyolitic and dacitic volcanics throughout the upper parts of the La Grande Formation. Primary sedimentary features are best preserved in the poorly exposed central part of the map area between the Capella and Casa de Piedra sectors. The Capella Member does not occur (i.e. does not crop out and has not been intersected in drilling) west of Casa de Lata (Figs. 3.4, 3.7). Rheological contrasts between these strata and crystalline volcanic units appear to have caused preferential strain accommodation and disharmonic dome-and-basin folding of the calcareous stratigraphy (Fig. 3.4). Epidote-garnet-magnetite-pyrite-(chalcopyrite) skarns are developed in this lithofacies unit in the northeastern part of the Rosario deposit (Masterman, 2003). Calcareous beds adjacent to Triassic and Laramide intrusions are commonly metamorphosed to epidote-garnet-wollastonite-albite skarn.

Thin-bedded limestones, marls and sandstones are traceable over distances of up to 3 km between drillholes and outcrops. These units commonly show upward-coarsening (shallowing) cycles of limestone-marl-arenite sedimentation and appear to onlap onto dacitic volcanics that were apparently constructional edifices (Fig. 3.12). Sedimentary textures include massive, flaser bedded and laminated varieties

Figure 3.11. Relationships and textures in the upper La Grande Formation. A-B) Photo and linework interpretation of a roadcut northeast of Rosario (533,070 mE 7,684,580 mN, looking south) showing interdigitated small andesite flows (Pzpg.9) and irregular blocky bodies of rhyolite and rhyolite breccia (Pzpg.7). Triassic andesitic dykes (TRmdd) have intruded steeply dipping faults. C) Typical red-brown feldspar-phyric weakly flow banded Huinquintipa Dacite (Pzpg5; DH HC06, 20m). D) Plane light photomicrograph of C showing oxide corona (left) and replacement (right) of euhedral amphibole phenocrysts. E) Reverse graded pebbly lithic debris flow conglomerate dominated by brown dacite clasts (DH C272, 78 m). F) Nodular carbonate-replaced evaporites in laminated red siltstone. Sample is cut by a late calcite veinlet (DH C265, 163 m). G) Detail in crossed polars of an intraclast breccia of laminated evaporite crusts (same sample as F). Photo appears grainy due to pervasive fine grained sparry calcite replacement of the original mineralogy. H) Accidental lithic clast of locally derived sandstone in Ocoita Andesite, Casa de Piedra area. Note the absence of any contact brecciation or peperite and the ripple-marked basal contact that has not been disturbed by the andesite. Surficial lithification appears to have occurred prior to eruption (531,075 mE, 7,684,355 mN). Unmarked white bars are 1 cm.

that include microbial laminites, crenular and micro-biohermal forms (Fig. 3.10e,f) and clastic detrital laminae (Fig. 3.10f,g). Outcrops in the San Nicolas area (Fig. 3.7) show intimate intercalation of coarse mass flow clastic deposits and fine crenulated micritic limestones indicative of sub-wave base conditions. Abundant kerogenous material is visible in thin section, but oxalic acid whole rock dissolution tests conducted during this study failed to yield recogniseable microfossils.

Thin intervals (1-2 m) of massive to plane laminated white, pale grey and red variably pyritic jasperoid chert occur locally throughout the calcareous sections. Given the high-energy nature of the dominant associated sedimentary facies it seems unlikely that the generally shallow Miembro Medio basin transiently attained the depth and stability for the occurrence of biologically-mediated chemical sedimentation. Instead, the broad association of these chert beds with evaporitic conditions (indicated by Pzpg2) and active volcanism is consistent with their abiogenic formation in a strongly saline, alkaline lacustrine environment as described for the modern sediments of Lake Magadi, Kenya (Eugster, 1969) and the Permian Bolzano Volcanic Complex, Italy (Krainer and Spoetl, 1998). Chemical sedimentation was also inferred for the equivalent Peine Group sequence at 24ºS that includes a similar facies association (Davidson et al., 1985).

3.5.7 Camino Rosario rhyolite (Pzpg7)

Massive light coloured vitreous rhyolite is exposed as common blocky outcrops along the access road northeast of Rosario. The unit stands in erosional relief and field relationships with other units are typically obscured by colluvial cover at surface. One road cut exposes metre-scale intercalations of this rhyolite, dominated by monomictic rhyolite breccias, with andesites (Fig. 3.11a,b). The unit dominates stratigraphy immediately south of Cerro Silvar and appears to comprise a complex of small flows that thins to the southwest (Fig. 3.4).

3.5.8 Rhyolitic ignimbrite (Pzpg6)

A pale-coloured fine to medium grained, quartz-phyric rhyolite occurs with localised sedimentary intercalations in the Casa de Piedra area (Figs. 3.4, 3.7), where it overlies massive rhyolites. The rhyolite has a vitriclastic matrix in which

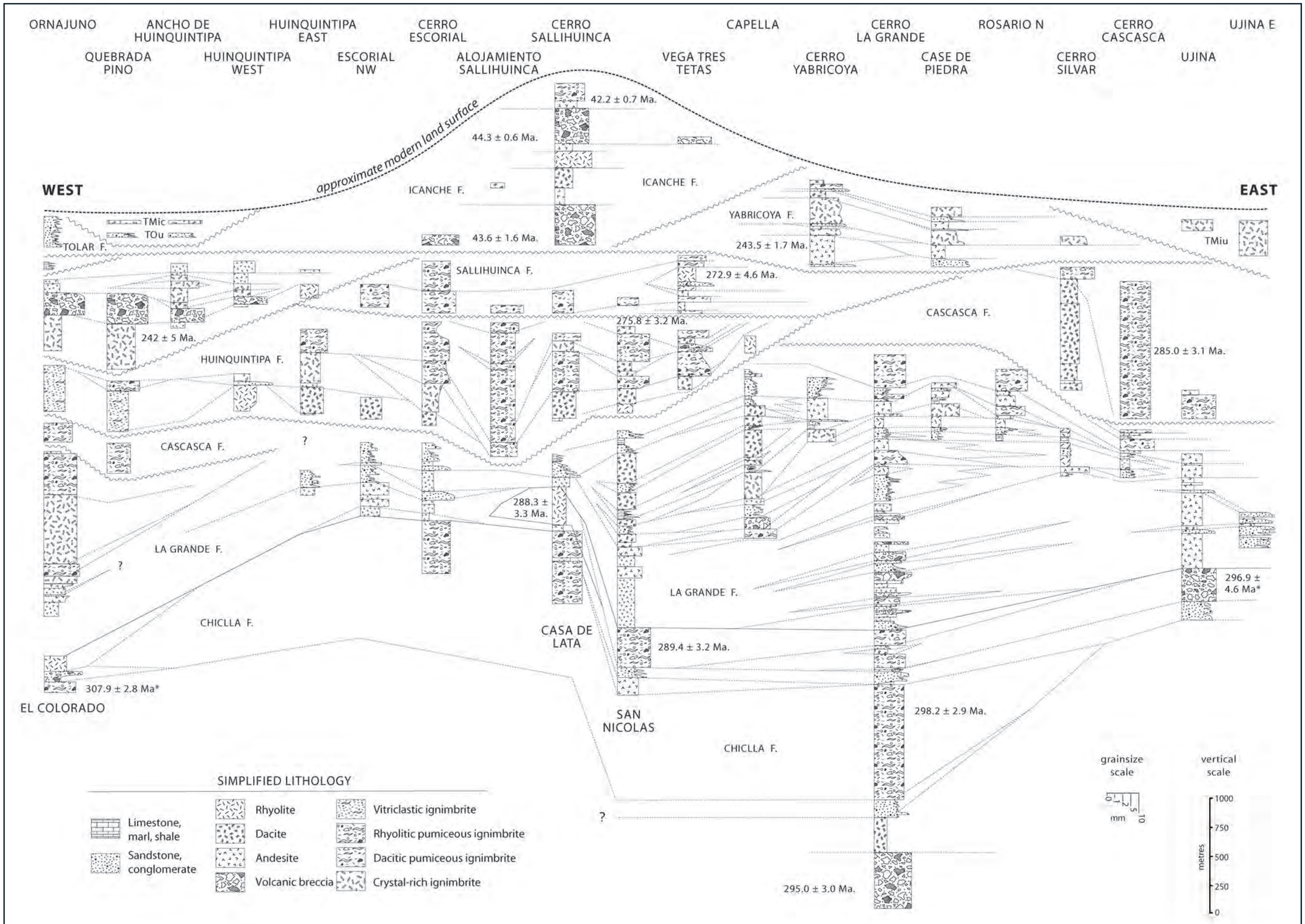
ORNAJUNO
ANCHO DE HUINQUINTIPA
HUINQUINTIPA EAST
CERRO ESCORIAL
CERRO SALLIHUINCA
CAPELLA
CERRO LA GRANDE
ROSARIO N
CERRO CASCASCA
UJINA E
QUEBRADA PINO
HUINQUINTIPA WEST
ESCORIAL NW
ALOJAMIENTO SALLIHUINCA
VEGA TRES TETAS
CERRO YABRICOYA
CASE DE PIEDRA
CERRO SILVAR
UJINA
approximate modern land surface
WEST
EAST
42.2 ± 0.7 Ma.
44.3 ± 0.6 Ma.
ICANCHE F.
ICANCHE F.
YABRICOYA F.
TMic
TOu
TOLAR F.
43.6 ± 1.6 Ma.
243.5 ± 1.7 Ma.
TMiu
SALLIHUINCA F.
272.9 ± 4.6 Ma.
275.8 ± 3.2 Ma.
CASCASCA F.
242 ± 5 Ma.
HUINQUINTIPA F.
285.0 ± 3.1 Ma.
CASCASCA F.
?
288.3 ± 3.3 Ma.
LA GRANDE F.
?
LA GRANDE F.
296.9 ± 4.6 Ma*
CHICLLA F.
CASA DE LATA
289.4 ± 3.2 Ma.
307.9 ± 2.8 Ma*
EL COLORADO
SAN NICOLAS
298.2 ± 2.9 Ma.
CHICLLA F.
?
295.0 ± 3.0 Ma.
SIMPLIFIED LITHOLOGY
Limestone, marl, shale
Sandstone, conglomerate
Rhyolite
Dacite
Andesite
Volcanic breccia
Vitriclastic ignimbrite
Rhyolitic pumiceous ignimbrite
Dacitic pumiceous ignimbrite
Crystal-rich ignimbrite
grainsize scale
0
1
2
5
10
mm
vertical scale
1000
750
500
250
0
metres

Figure 3.12. Stratigraphic correlation diagram. Section locations are shown below.

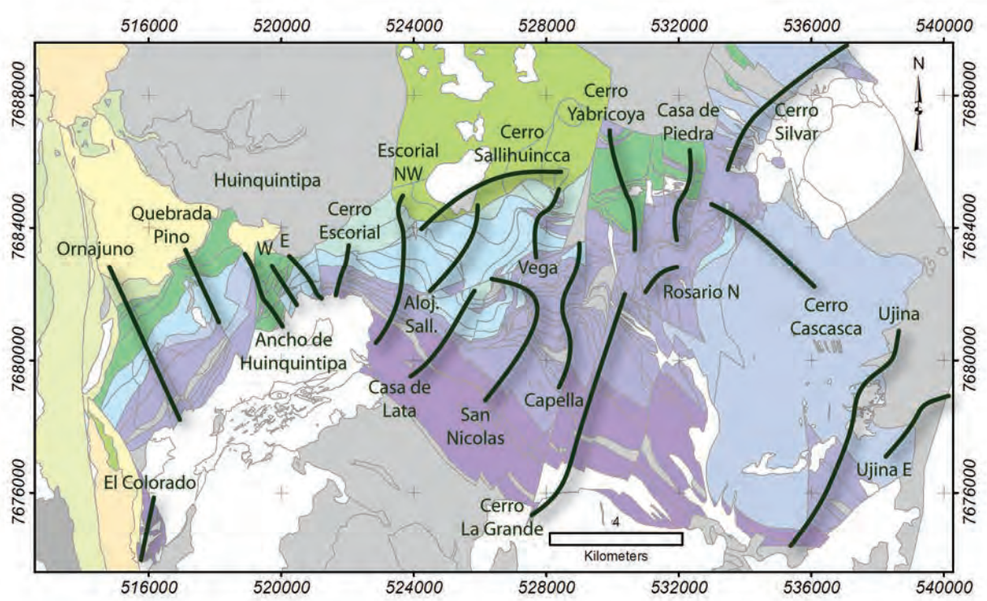

Generalised Stratigraphy

- Papajoy Formation
- Icanche Formation
- Tolar Formation
- Cerro Empexa - Tolar Formation
- Cerro Empexa Formation
- Quehuita Formation
- Yabricoya Formation
- Sallihuinca Formation
- Huinquintipa Formation
- Cascasca Formation
- La Grande Formation
- Chiclla Formation
- Peine Group (undifferentiated)
- Amaculla Formation

A) Simplified version at 1:32,000 vertical scale. B) A0-format detailed version at 1:10,000 vertical scale (insert at back of thesis). Measured columns depict best estimates of true thicknesses, based on 1:5,000 field mapping, existing larger scale mapping, and drillholes logged in this study (eastern half of the district, Appendix II). Section locations are shown above. Vertical exaggeration is approximately three times. Correlations are based on lithology (including phenocryst, xenocryst, and xenolith assemblages, and allowing for lateral facies changes), field relationships, and U-Pb geochronology. Correlation lines are projected beyond the limits of exposure to indicate the likely lateral extent of units for which there are no direct correlates in adjacent sections. Disconformable erosional surfaces are indicated by dashed sinusoidal lines. Breaks in apparently conformable sections reflect poor outcrop and/or incomplete drill coverage. Internal thickness, grainsize and compositional variation is depicted truly for volcaniclastic units, but are stylised to indicate the nature of bedding for sedimentary units. Rock unit descriptions are provided in the text. Ages shown are new zircon U-Pb data presented in this chapter, except three dates from Munizaga et al. (2008; marked with an asterisk). Abbreviations: Co. = Cerro, HQT = Huinquintipa, W = west, E = east, N = north, NW = northwest.

glassy shards have undergone strong plastic deformation. On that basis this unit is interpreted as a welded rhyolitic ignimbrite. It is tentatively correlated with similar rocks encountered in drilling north of Rosario (drillholes C268 and C336), but has not been found elsewhere and appears to be restricted to the central part of the district (Fig. 3.12).

3.5.9 Huinquintipa Dacite (Pzpg5)

Dark brown to beige, massive to weakly flow banded plagioclase-amphibole-phyric dacites (Fig. 3.11c) occur throughout the upper members of the Peine Group. The thickest accumulation occurs in the upper La Grande Formation around the Huinquintipa mine (Fig. 3.13: San Nicolas sector), where several flow complexes up to 300 m thick are separated by sedimentary intercalations (Figs. 3.4, 3.12). These rocks appear restricted to the central part of the map area at this stratigraphic level, whereas higher in the sequence, isolated flows 1-30 m thick occur across the district (Fig. 3.13). Breccia facies of the Huinquintipa Dacite (Pzpg5a) are rare, but occur locally in the Capella area and were intersected in resource drilling at Huinquintipa. These typically comprise framework-supported angular blocks of variably textured dacite hosted by aphanitic brown dacite.

The Huinquintipa Dacite marks an important change in the Peine Group stratigraphy from the grey and black-coloured lower part, to the reddish brown-coloured upper part. This difference in colouration persists at depth in drilling and appears unrelated to surface processes. In thin section the red-brown rocks show strong oxide alteration of ferromagnesian phases (Fig. 3.11d) that bear no obvious spatial relationship to hydrothermal alteration or mineralisation.

3.5.10 Red andesite (Pzpg4)

Laterally restricted, dark red-brown, fine to medium grained equigranular andesite and lesser monomictic andesite breccia occur locally to the east and northeast of Rosario.

3.5.11 Inés Dacitic Ignimbrite (Pzpg3)

Dark purple-brown, massive plagioclase-phyric dacite is a major host to

mineralisation at Rosario. Once interpreted as a porphyritic intrusive (Munchmeyer et al., 1984), it has been shown to contain fiamme of compacted pumice and have a matrix of plastically deformed glassy shards indicating a welded pyroclastic origin (Masterman et al., 2005). This ignimbrite has limited distribution in the environs of the Rosario deposit and appears to have infilled topography at the time of its emplacement.

3.5.12 Casa de Piedra Member (Pzpg2)

Thin intervals of red-brown, planar-laminated, locally calcareous and/or evaporitic, fine grained sandstones and intercalated lithic granular and pebbly mass flow units (Fig. 3.11d) occur commonly in the upper La Grande Formation. Nodular (Fig 3.11e) and rarely prismatic (Fig. 3.11f) crystal aggregates of calcite occur with crenular carbonate laminae in diffuse zones of fine sand and siltstone among generally coarser sandstone. Thin beds of intraclast breccia composed entirely of fragments of laminated crystalline calcite (Fig. 3.11g) suggest periodic dessication of the substrate. The base of an andesite flow at Casa de Piedra includes rare angular accidental xenoliths and has not distrurbed ripple marks on the basal sandstone contact (Fig 3.11h), further suggesting periodic exposure. This is consistent with an evaporitic origin for the nodular textures, which are morphologically similar to modern anhydrite evaporites from supratidal environments (e.g., Warren, 1986).

3.5.13 Rhyodacitic ignimbrite (Pzpg1)

A dark brown-purple, weakly pumiceous welded rhyodacitic ignimbrite visually similar to the Inés Dacitic ignimbrite but containing a few percent quartz comprises a laterally extensive sheet that overlies evaporitic sediments north and west of Rosario. A rhyodacitic pyroclastic unit considered to correlate with Pzpg1 (on the basis of similaries in lithology and stratigraphic position relative above to Pzpg12) crops out along the Quebrada Ornajuno (Fig. 3.7), suggesting that this unit may once have extended across the district.

3.6 Cascasca Formation

The Cascasca Formation comprises major rhyolitic ignimbrite(s) and dacite lavas that dominate the eastern map area (Fig. 3.13). In the west and northeast it is largely

concordant with the upper La Grande Formation, but appears to become increasingly discordant in the southeast where it is structurally juxtaposed against the underlying stratigraphy (Fig. 3.4).

3.6.1 Dacite (Pzpa3)

Subcrop along the lower slopes of eastern Cerro Chusquina (Fig. 3.13) comprise a massive dark purple-brown, strongly plagioclase-phyric dacite. A similar unit occurs over a small area adjacent to the Cerro Silvar porphyry dyke on Cerro Silvar. The basal contact is not exposed, but these dacites appear to discordantly overlie La Grande Formation rocks in a structurally disrupted area east of Cerro Chusquina and also on the southern slopes of Cerro Silvar (Fig. 3.13).

3.6.2 Chusquina Dacite (Pzpa2)

The upper eastern flanks of Cerro Chusquina are dominated by a distinctive purple to brown, sparsely plagioclase-phyric, finely planar flow-banded dacite and rare monomictic dacite breccias. This unit overlies, and is overlain by Pzpa3, and is therefore likely to be transitional with it.

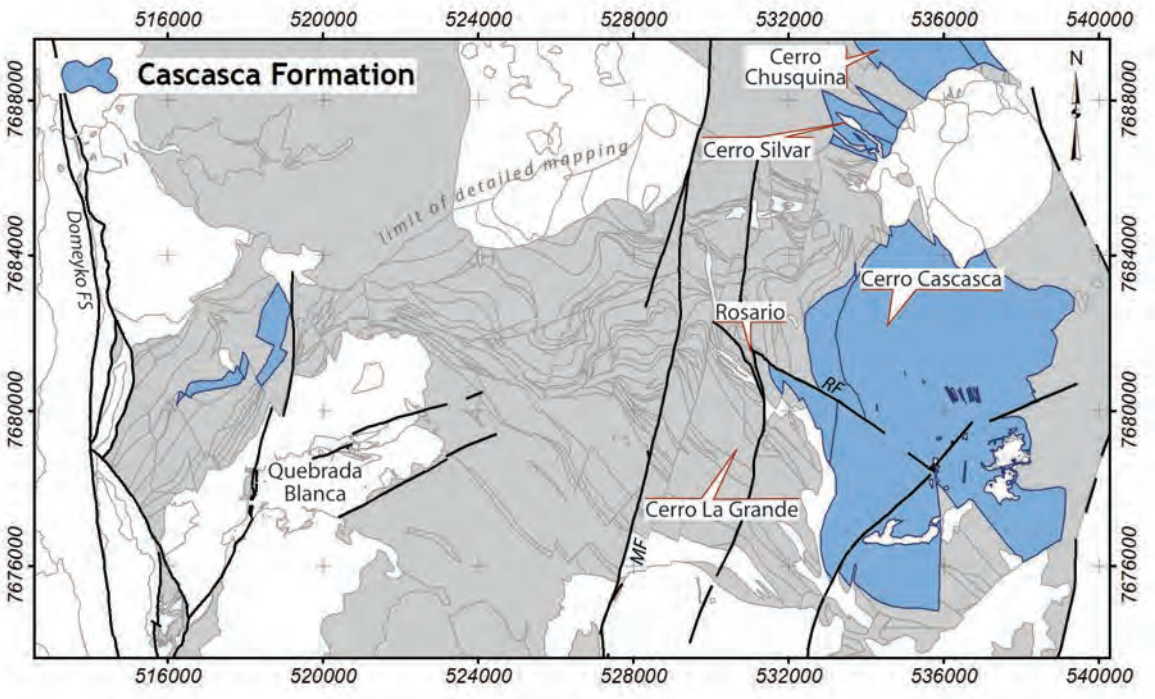

Figure 3.13. Distrubtion of the Cascasca Formation in the Collahuasi district. Light grey area depicts the extent of Peine Group rocks in the district. Black linework indicates major faults. Landmarks mentioned in the text are indicated. Abbreviations: FS = fault system, MF = Monctezuma Fault, RS = Rosario Fault. Grid divisions are 2 kilometres.

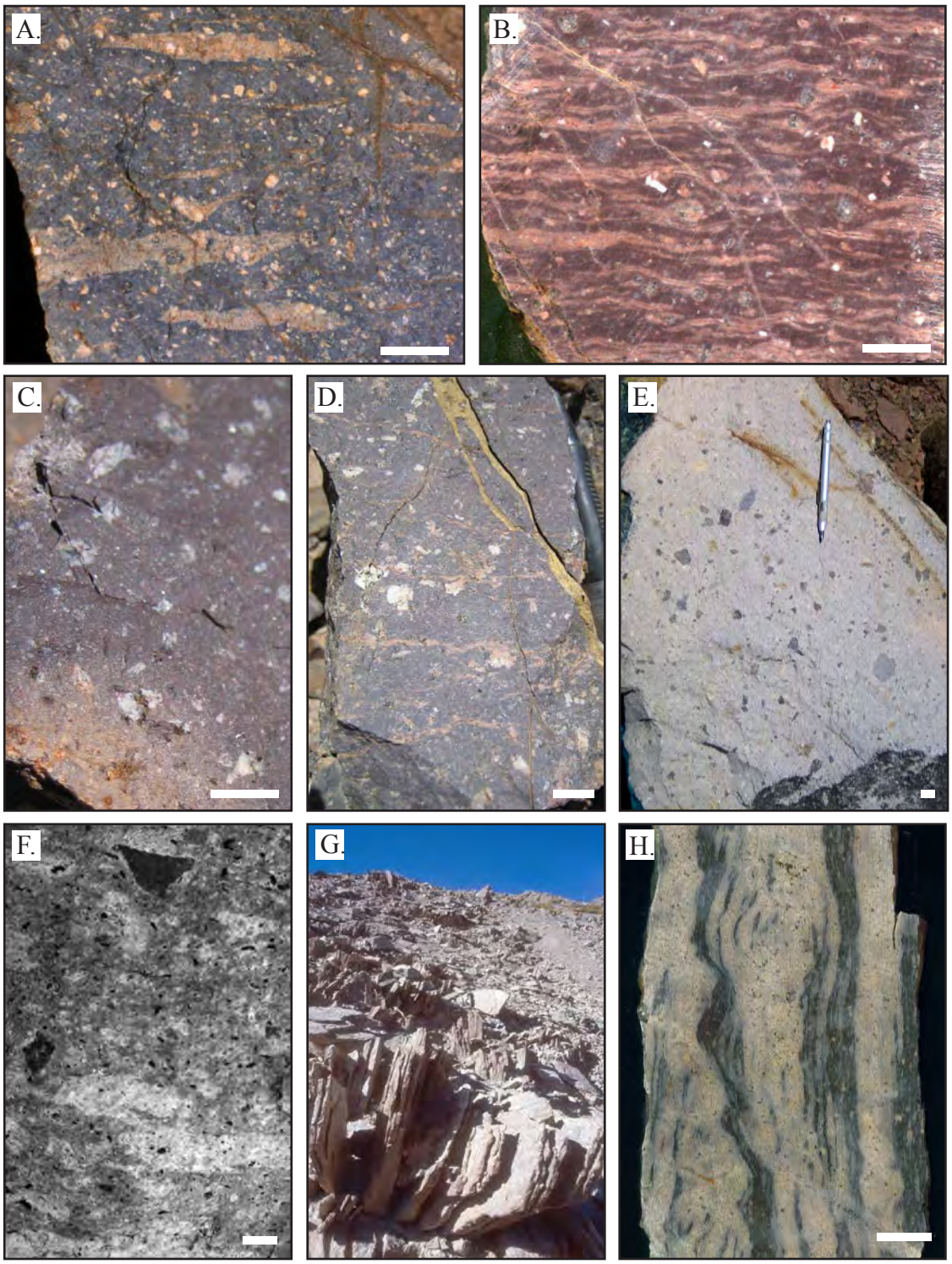

Figure 3.14. Rocks of the Cascasca and Huinquintipa Formations: A) Weathered surface of the Cascasca rhyolitic ignimbrite (Pzpa1) from Cerro Cascasca (537,983 mE, 7,682,319 mN) showing pale pink, strongly compacted fiamme and grey quartz eyes. B) Strongly pumiceous quartz-eye rhyolitic ignimbrite from the equivalent stratigraphic position to A, but in the western part of the district (515,643 mE 7,680,713 mN). C) Coarsely plagioclase-phyric dacite (Pzph10) from a laterally continuous flow south of Casa de Lata (524,410 mE, 7,681,590 mN). D) Coarsely plagioclase- and sparsely quartz-phyric dacite (Pzph10; 520,835 mE, 7,682,155 mN). E) Lithic lapilli-rich part of the Huinquintipa rhyodacitic ignimbrite (Pzph7; approx. 525,570 mE, 7,681,290 mN). F) Pumiceous zone in the Huinquintipa rhyolitic ignimbrite (Pzph7; approx. 526,290 mE, 7,682,635 mN) shown in black and white with contrast enhancement to accentuate the fiamme. G.) Characteristic tabular outcrop texture *(continued over page)*

3.6.3 Cascasca rhyolitic ignimbrite (Pzpa1, 286.3 ± 1.9 Ma)

Pink-grey, fiammé-rich (pumiceous) rhyolitic ignimbrite with obvious large quartz eyes (Fig. 3.14a) is the dominant unit across a large part of the eastern map area including Cerro Cascasca (Figs. 3.4, 3.13). Making the geometric assumption that the thickness of the observed section approximates the maximum thickness for this unit, then the Cascasca rhyolitic ignimbrite represents an erupted volume of 25 km^3 in the eastern map area. A similar, strongly compacted, fiamme-rich quartz-eye rhyolitic ignimbrite (Fig. 3.14b) occurs at the equivalent stratigraphic level of a concordant section in the area immediately north of Quebrada Blanca (Figs. 3.4, 3.13). In this area it is attenuated against a major N-S fault and is not present in the central part of the map area. It is uncertain if the eastern and western units are direct correlates or represent discrete explosive volcanic events that are approximately equivalent in time. The absence of the Cascasca rhyolitic ignimbrite from the Cerro Chusquina section (Fig. 3.12) suggests that it is younger than the Chusquina dacite, and infilled topography around a dacitic volcanic edifice in the vicinity of Cerro Chusquina.

3.7 Huinquintipa Formation (Pzph)

The Huinquintipa Formation comprises a thick section of felsic lavas and pyroclastic deposits in the central-northern map area (Fig. 3.15). It concordantly overlies the Cascasca Formation in the west, but more commonly overlies the upper-, and locally middle La Grande Formation. This suggests a depositional hiatus and possible erosional removal of the intervening laterally extensive units prior to eruption of the basal Huinquintipa Formation.

3.7.1 Brown Flow Banded Rhyolite (Pzph11)

Quartz-phyric, red to dark brown variously massive to flow banded rhyolite occurs in the central map area as isolated small high aspect ratio flows with limited lateral extent overlying sedimentary strata of the upper La Grande Formation (Fig. 3.4).

←

... of platy rhyolitic ignimbrite (Pzph6) foreground field of view is 2 m (526,555 mE, 7,682,468 mN). H) Example of strongly flow banded aphyric rhyolite (Pzps2) from southeast of Cerro Sallihuinca (528,424 mE, 7,684,353 mN). Unmarked white bars are 1 cm.

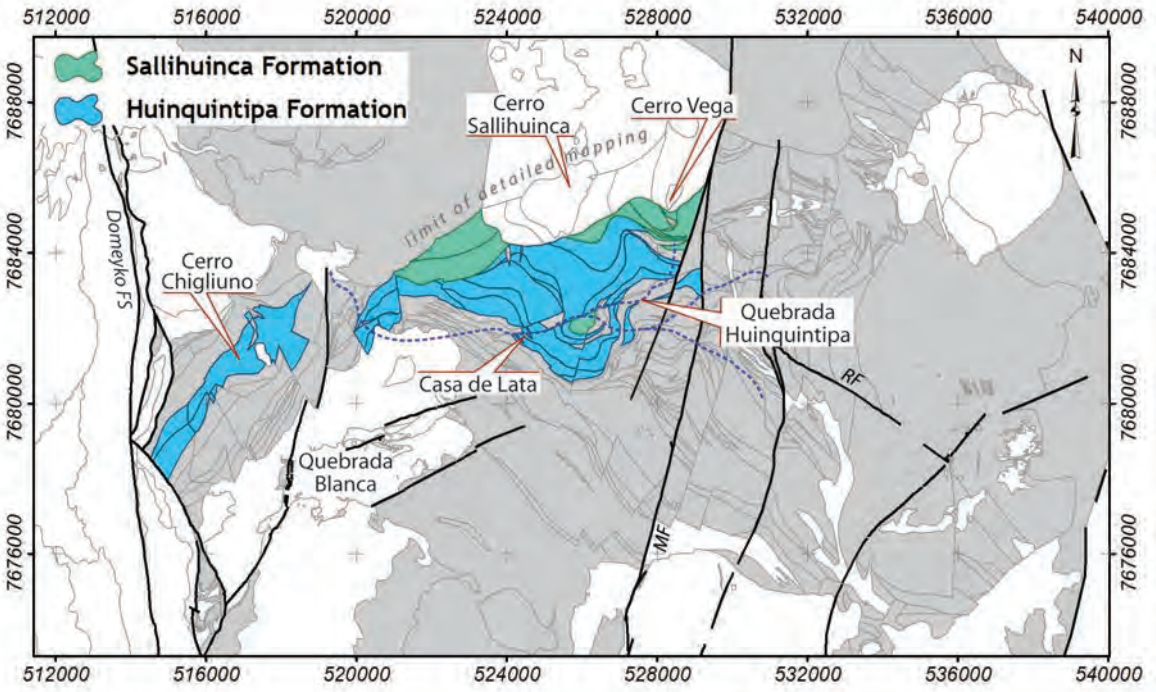

Figure 3.15. Distrubtion of the Huinquintipa and Sallihuinca Formations in the Collahuasi district. Light grey area depicts the extent of Peine Group rocks in the district. Black linework indicates major faults, and dashed blue lines are selected drainages. Landmarks mentioned in the text are indicated. Abbreviations: FS = fault system, MF = Monctezuma Fault, RS = Rosario Fault. Grid divisions are 2 kilometres.

These rhyolites are commonly associated with flow units of the Huinquintipa Dacite (Pzpg5) and may represent a more evolved comagmatic product.

3.7.2 Brown Megacrystic Dacite (Pzph10, 275.7 ± 3.2 Ma)

Brown, coarsely plagioclase-phyric holocrystalline dacite (Fig. 3.14c) occurs as a thick monotonous flows in the Casa de Lata area at approximately the same stratigraphic level as rhyolites of Pzph11. Discrete beds of weakly flow banded dark grey-brown dacite that contains rare, fine-grained quartz phenocrysts (Fig. 3.14d) occurs at the same stratigraphic level northwest of Casa de Lata.

3.7.3 Chigliuno Rhyolitic Ignimbrite (Pzph9, Pzph9b)

Cerro Chugliuno, northwest of Quebrada Blanca (Fig. 3.15), is dominated by a massive, erosionally resistant pale grey sparsely quartz-feldspar-phyric rock that was originally described as an “intrusive rhyolite” (Munchmeyer et al., 1984). However, outcrops on the western flank of Cerro Chigliuno contain rare, strongly compacted, pale pink fiamme that indicate a pyroclastic origin for this unit. A distinct variety

that contains abundant cognate lithic fragments (Pzph9b) occurs as a laterally discontinuous lens on the northern flanks of the same hill. Along strike to the northeast the Chigliuno rhyolitic ignimbrite thins markedly and is not present in the Huinquintipa Formation stratigraphy of the central map area.

3.7.4 Amphibole-bearing grey dacitic ignimbrite (Pzph7, Pzph7a)

Grey pyroclastic rocks comprise the bulk of the Huinquintipa Formation in the central map area. A distinctive crystal and accessory lithic-rich amphibole-bearing dacitic ignimbrite (Fig 3.14e) forms a laterally continuous sheet that overlies red-brown dacites in the syncline near Casa de Lata (Figs. 3.4, 3.15). Strongly compacted pumiceous variants of this unit occur locally but appear to only have limited extents (Fig. 3.14f).

3.7.5 Foliated rhyolitic ignimbrite (Pzph6, Pzph6a)

A large area south of Cerro Sallihuinca to Casa de Lata (Fig. 3.15) is dominated by an erosionally recessive vitriclastic quartz-orthoclase phyric rhyolitic ignimbrite that has a pronounced, locally developed compaction foliation (Fig. 3.14g). Similar pyroclastic materials were apparently deposited in at least two events, separated in the stratigraphy by a narrow discontinuous interval of subvitreous, dark brown, strongly quartz-phyric pumiceous rhyolitic ignimbrite (Pzph6a). These units together attain thicknesses in excess of 1 km locally, but have extremely limited lateral continuity. Pinchouts coincide spatially with major district faults (Fig. 3.4) and these uppermost Huinquintipa Formation pyroclastic deposits probably infilled a local subbasin or valley.

3.8 Sallihuinca Formation (Pzps)

The Sallihuinca Formation comprises grey pyroclastic rocks similar to the Huinquintipa Formation and a partly intrusive brown rhyolite. It overlies the Huinquintipa formation in subtle angular discordance (Figs, 3.12, 3.15), suggesting a depositional hiatus between the two. The rhyolite member cuts the upper Huinquintipa Formation but is partly overlain by the uppermost pyroclastic member of the Sallihuinca Formation. The upper margin of the Sallihuinca Formation is

unknown as it is overlain by shallowly-dipping volcanic strata of the Eocene Icanche Formation (Fig. 3.4)

3.8.1 Rhyodacitic ignimbrite (Pzps3)

The basal Sallihuinca Formation comprises a dark grey, bedded, rhyodacitic ignimbrite that forms buttress outcrops in the core of the Casa de Lata syncline along the Quebrada Huinquintipa (Figs. 3.4, 3.15). That valley traces an interpreted fault with relative uplift of the northern block such that the Pzps3 ignimbrite is truncated and does not occur on the north side of the valley. This ignimbrite also crops out along a series of low hills immediately southwest of Cerro Sallihuinca.

3.8.2 Flow banded rhyolite (Pzps2, 272.5 ± 4.7 Ma)

Strongly flow banded cream-brown rhyolite lava with abundant laterally continuous folded flow banding (Fig. 3.14h) has intruded bedded volcaniclastic rocks on Cerro Vega (Fig. 3.15). This locality is adjacent to a colluvium-filled valley that marks the likely northern extension of the Monctezuma Fault (Fig. 3.4). The Sallihuinca Formation is not recognised to the east of this regional structure.

3.8.3 Pumiceous rhyolitic ignimbrite (Pzps1)

West of Cerro Sallihuinca the dacitic ignimbrite (Pzps3) is conformably overlain by a paler, weakly bedded, more siliceous and pumiceous ignimbrite. A similar ignimbrite with abundant ?cognate lithic fragments on the southern knoll of Cerro Vega is tentatively correlated with Pzps.3. In this location the ignimbrite partly overlies flow banded rhyolites and therefore the two pyroclastic members of the Sallihuinca Formation bracket eruption of the flow banded rhyolite.

3.9 Yabricoya Formation (TRy, TRa)

The Yabricoya Formation comprises red-brown and rare grey rhyolitic volcaniclastic and lesser dacitic volcanic rocks and coarse terrestrial sediments. These occur on the southern flanks of Cerro Yabricoya, north of Rosario (Fig. 3.16), and unconformably overlie the upper La Grande Formation. Direct correlates that crop out extensively north of Quebrada Blanca conformably overly the upper Huinquintipa Formation

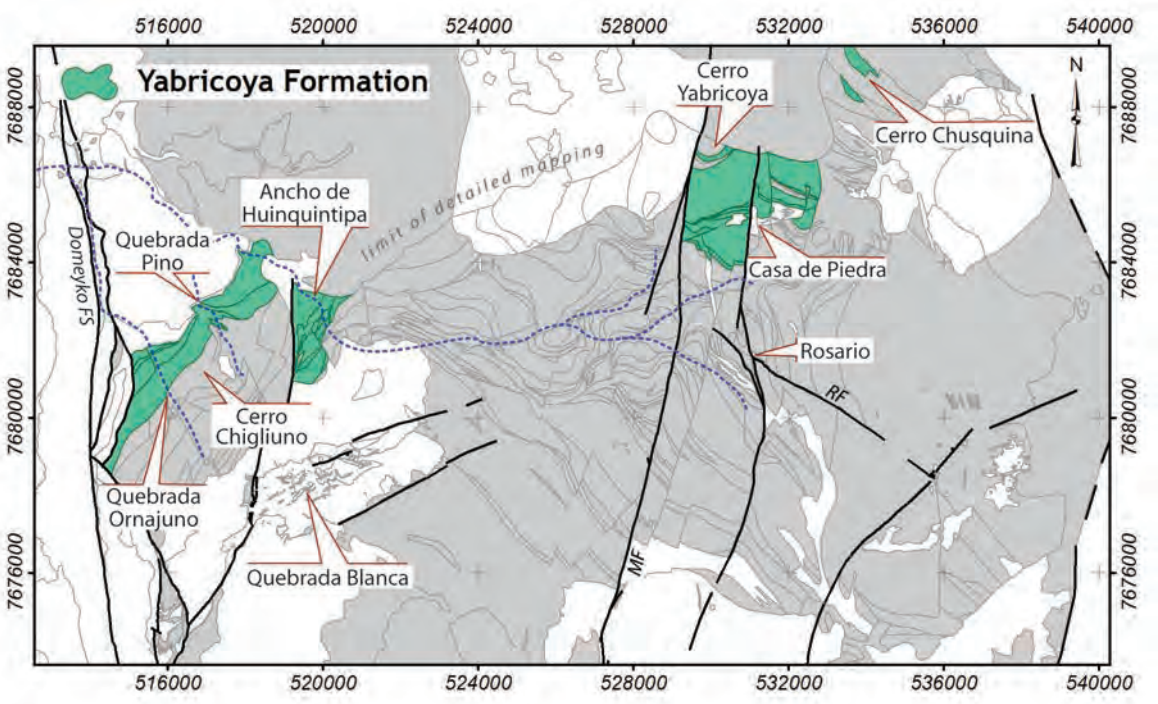

Figure 3.16. Distrubtion of the Yabricoya Formation in the Collahuasi district. Light grey area depicts the extent of Peine Group rocks in the district. Black linework indicates major faults, and dashed blue lines are selected drainages. Landmarks mentioned in the text are indicated. Abbreviations: FS = fault system, MF = Monctezuma Fault, RS = Rosario Fault. Grid divisions are 2 kilometres.

(Fig. 3.12). The Yabricoya Formation forms the uppermost Peine Group in the Collahuasi district and is unconformably overlain by redbed sandstones of the Jurassic Quehuita Formation or conglomerates of the Tolar and Papajoy Formations.

3.9.1 Rhyolite (TRy6)

Fine to medium grained, finely flow banded red-brown rhyolite occurs as an isolated flow in the structurally complex area east of Ancho de Huinquintipa.This unit is apparently conformable with the upper Huinquintipa Formation. The distinction between the two is based on the abrupt colour change of volcanic materials.

3.9.2 Polymicticic conglomerate (TRy5)

Minor conglomerates dominated by rounded to subrounded clasts of red-brown rhyolite and dacite occur among the basal parts of the Yabricoya Formation. These conglomerates are commonly unstratified and strongly channelised, with limited lateral continuity in outcrop. Where present, stratification is planar and beds defined by different clast sizes are generally less than 1 m thick.

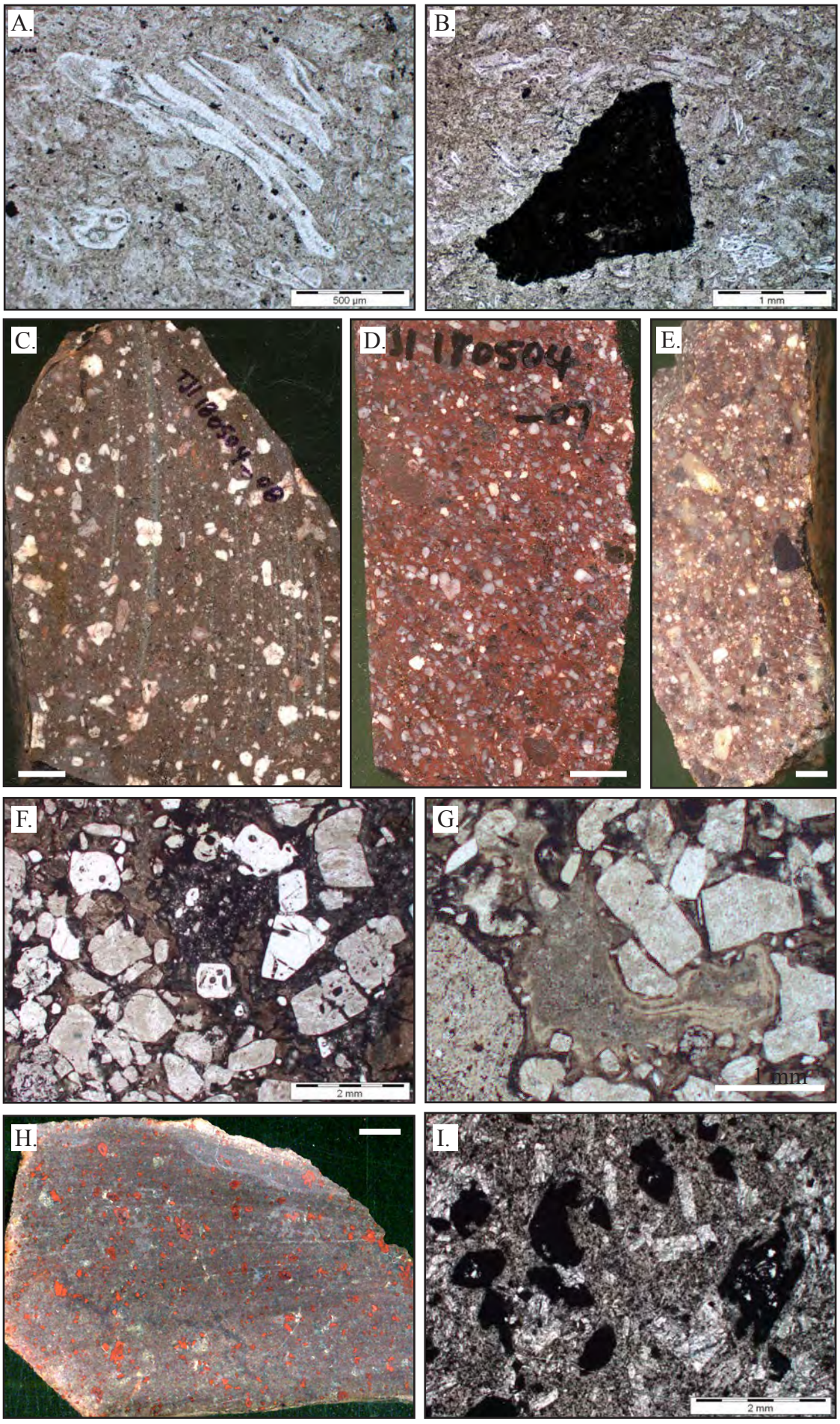
A.
500 µm
B.
1 mm
C.
D.
E.
F.
2 mm
G.
1 mm
H.
I.
2 mm

3.9.3 Ornajuno rhyolite breccia (TRy4, 242.4 ± 5.1 Ma)

Grey-brown, very poorly sorted, strongly polymictic boulder to lapilli-bearing lithic volcanic breccia is a major component of the Yabricoya Formation in the northwestern part of the district (Fig. 3.16). The breccia comprises bulky outcrops along the Quebrada Ornajuno and along strike on the northern flanks of Cerro Chigliuno. Clasts are subangular and include a variety of porphyritic felsic lithologies and rare fine grained andesites. The matrix consists of quartz crystal fragments and abundant glassy shards (Fig. 3.17a). These shards are not deformed, even where lithic fragments impinge against them (Fig. 3.17b). As plastic deformation of primary pyroclasts is one of the principal criteria for welding (Smith, 1960; Guest and Rogers, 1967; Riehle et al., 1995), preservation of shard morphology indicates that this unit did not weld upon deposition. The unit thins to the east, but possibly correlates with a poorly exposed grey lithic dacite breccia near the base of the Yabricoya Formation north of Rosario. Further east, an ashy grey rhyolite tuff that uncornformably overlies the Chusquina dacite on Cerro Chusquina (Fig. 3.4) is a possible distal manifestation of the same pyroclastic event. If this correlation is correct, then the unit thins, and the size of lithic fragments decreases to the east, indicating that the explosive vent was most likely located somewhere west of the limit of present day Peine Group exposure.

3.9.4 Yabricoya dacite (TRy3, 243.7 ± 1.5 Ma)

A distinctive dark brown-grey coarsely plagioclase-(clinopyroxene-quartz)-phyric dacite (Fig. 3.17c) occurs as low blocky outcrops immediately west of Casa de

Figure 3.17. (facing page) Key lithofacies units of the Yabricoya Formation. A-B) Unwelded glassy shard-rich matrix of polymictic lithic tuff (TRy4; 515,104 mE, 7,681,796 mN), showing rigid behaviour of shards in contact with a lithic fragment. C) Yabricoya dacite (TRy3; 530,323 mE, 7,684,616 mN) showing coarse white plagioclase phenocrysts and holocrystalline groundmass (vertical striping are saw blade marks). D) Yabricoya crystal ignimbrite (TRy2; 7,685,962 mN, 529,601 mE) showing the packed equigranular crystal populations typical of this unit. E) Lithic lapilli-rich variant of the Yabricoya rhyolitic ignimbrite from north of Cerro Chigliuno (517,932 mE, 7,682,854 mN). F) Crystal ignimbrite from Cerro Yabricoya (D) showing embayed subhedral quartz crystals in the ignimbrite and morphologically similar crystals a cognate lithic fragment (dark matrix, right of frame). G) Plastically deformed rare ?pumiceous lithic fragment with adjacent crystals impressed into the clast margin (same sample as D). H) Specimen of the Quebrada Pino andesite showing oxidative submetallic orange coloration of amphiboles on a cut surface (519,440 mE, 7,682,318). I) Plane light photomicrograph of H showing near complete oxide replacement of euhedral amphibole phenocrysts. Unmarked white bars are 1 cm.

Piedra, south of Cerro Yabricoya (Fig. 3.16). It is commonly coherent, but locally occurs as monomictic breccia facies. It is slightly more coarse-grained than, but generally petrographically similar to the Pzph10 lithofacies unit, but new geochronology (Fig. 3.12, Section 3.16) indicate that it belongs to the uppermost Peine Group stratigraphy.

3.9.5 Yabricoya crystal ignimbrite (TRy2)

Red brown strongly crystal-rich rhyolite to rhyodacitic ignimbrites (Fig. 3.17d) comprise a sheet-like deposit, variations of which occur intermittently across the district from Quebrada Ornajuno to Cerro Chusquina (Figs. 3.4, 3.12). Weak bedding is defined by the variable proportions of quartz and feldspar crystals (the lower part is generally more quartz-rich), and abundance of brown lithic lapilli (up to 15 volume percent). A lithic and pumice-rich variety (Fig. 3.17e) occurs in a small area north of Cerro Chigliuno. Lithics include accessory fragments of the Huinquintipa Dacite (Pzpg5) and cognate fragments of a rhyolite (Fig. 3.17f) that has not been recognised in outcrop. Rare pumiceous fragments (Fig. 3.17g) and bubble wall shards show plastic deformation indicating welding upon deposition (Smith, 1960; Guest and Rogers, 1967; Riehle et al., 1995).

3.9.6 Rhyolite tuff (TRy1)

A pale grey, pumiceous, polymictic lithic lapilli-bearing rhyolitic tuffaceous rock occurs toward the top of Cerro Yabricoya (Fig. 3.16), intercalated with thin flows and monomicticic breccia bodies of a brown dacite that macroscopically resembles the Huinquintipa Dacite. Lithic clasts in the tuff include a variety of middle and lower Peine Group rock types. The matrix is shard-rich and rare pumice clasts are weakly compacted. On the basis of these tectures, this unit is interpreted as an unwelded primary pyroclastic deposit, though its original spatial extent is unclear.

3.9.7 Quebrada Pino andesite (TRa1, TRa2)

Tabular one to two m-thick flows of mid-grey to brown dacitic andesite overlie the pyroclastic lower Yabricoya lithofacies units in the area north of Cerro Chigliuno (Fig. 3.16). These include a distinctive amphibole-phyric facies (TRa2: Fig. 3.17h) in

which amphibole phenocrysts have very strong submetallic orange hematite reaction rims (Fig. 3.17i). A dark grey plagioclase-phyric facies (TRa1) occurs intercalated with the distinctive amphibole-bearing variety.

3.10 Mesozoic Stratigraphy

The Mesozoic stratigraphy of the Domeyko Cordillera includes two principal subdivisions: Jurassic to Lower Cretaceous back arc sedimentary and lesser subaqueous volcanic rocks, and Late Cretaceous to Paleocene back arc terrestrial sedimentary and volcanic rocks. These strata comprise the Precordilleran fold and thrust belt that occurs along the western margin of the Collahuasi district and is best exposed along the Quebrada Guatacondo (Fig. 3.18; Amilibia and Skarmeta, 2003; Amilibia et al., 2008). These rocks have been extensively studied by previous workers (e.g., Perelló and Muller, 1984; Smoje, 1989; Orrego G., 1992; Charrier and Muñoz, 1994; Pichowiak et al., 1994; Prinz et al., 1994; Tomlinson et al., 2001a) and only a brief review of that work is provided here.

3.10.1 Quehuita Formation

The name Quehuita Formation is used here to refer to all marine sediments of the Tarapacá basin (e.g., Prinz et al., 1994). The basin was initiated during the Late Triassic as the back-arc to the La Negra volcanic arc (e.g., Pichowiak et al., 1994) and continued to accumulate marine sediments throughout the Jurassic. Smoje (1989) provides the most detailed investigation of the Jurassic stratigraphy in the Collahuasi district and defines five “formations” that are here treated as members in accordance with Tomlinson et al. (2001a). Between 20º30’S and 21º30’S the Quehuita Group is approximately six kilometres thick and spans Liassic to Kimmeridgian time (Smoje, 1989). It is structurally juxtaposed against the Peine Group along the Domeyko Fault (Smoje, 1989; Tomlinson et al., 2001a; Amilibia and Skarmeta, 2003; Amilibia et al., 2008). The basal section that records transgression in the nascent Tarapacá Basin (Sama Formation: Orrego, 1992) is not known in this area. Age constraints among the Jurassic stratigraphy are typically assigned on the basis of fossil assemblages that are dominated by fish and ammonoid species (Bogdanic and Chong, 1985; Prinz et al., 1994; Tomlinson et al., 2001).

Copaquire Member (Jqc. ?Liassic). The Copaquire Member crops out along the Quebrada Copaquire, east of the Domeyko fault zone (Figs. 3.4, 3.18). It comprises siliceous grey marine shales and minor marls that attain maximum thickness of 570 m. These are overlain by up to 140 m of intercalated coarse-grained quartz sandstones and lesser black shales (Smoje, 1989).

Aquiuno Member (Jqa. ?Dogger). The Aquiuno Member conformably overlies the Copaquire Member and occurs throughout the upper Quebrada Guatacondo, west of the confluence with Quebrada Copaquire (Fig. 3.18). It comprises a basal ~75 m-thick sequence of marine bioturbated black shales overlain by almost 700 m of massive black shales, siltstones and minor intercalated quartz sandstones (Smoje, 1989).

Quehuita Member (Jqq. ?Callovian). The Quehuita Member (in the sense of Smoje, 1989) conformably overlies the Aquiuno Member and is best exposed in anticlinal cores in the Quebrada Sipuca southwest of the Collahuasi district. It comprises a laterally extensive basal conglomerate and up to 2,000 m of marine micritic limestones and subordinate siltstones that increase in abundance up-section (Smoje, 1989).

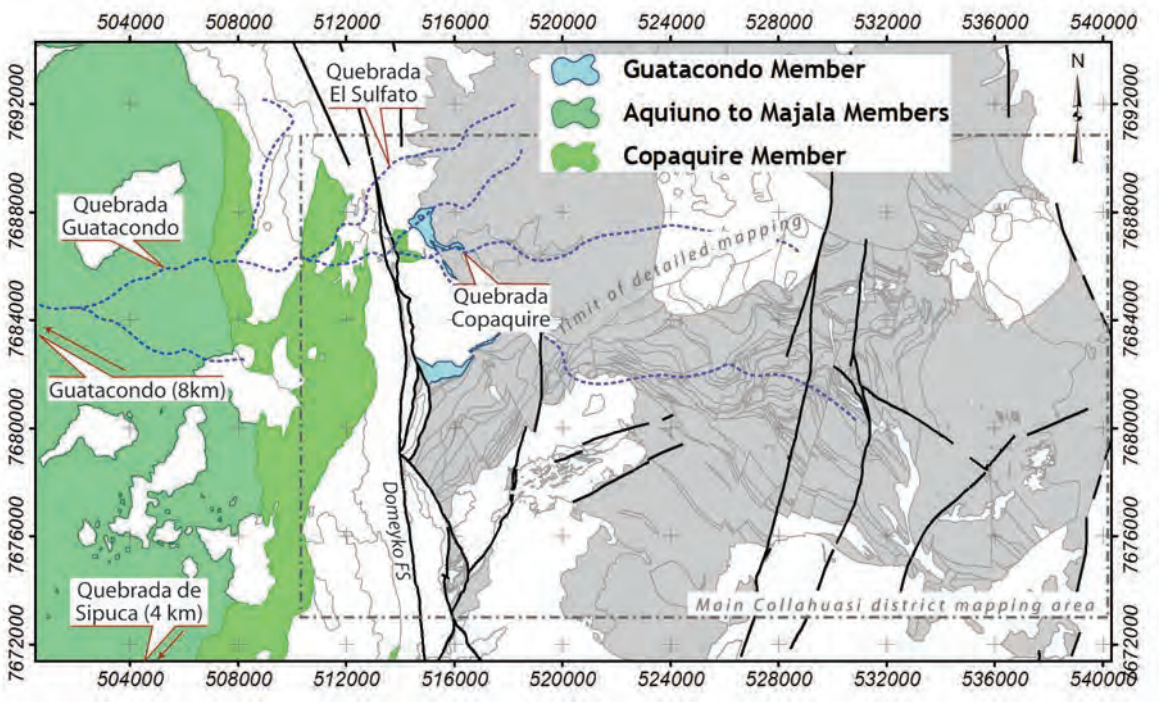

Figure 3.18. Distrubtion of the Jurassic Quehuita Formation in the greater Collahuasi district. Light grey area depicts the extent of Peine Group rocks in the district. Black linework indicates major faults, and dashed blue lines are selected drainages. Landmarks mentioned in the text are indicated. Abbreviations: FS = fault system; km = kilometres. Grid divisions are 2 kilometres.

Majala Member (Jqm). The Majala Member conformably overlies the Quehuita Member and occurs in anticlinal cores exposed near the Guatacondo village (west of the area shown in Fig. 3.18). It comprises a sequence of intercalated green-grey marine shales, marls and fine sandstones that is commonly a few hundreds of metres thick, but reaches 1,600 m thick locally (Smoje, 1989).

Guatacondo Member (Jqg. ?Kimmeridgian). The Guatacondo Member records terrestrial sedimentation in the Tarapacá Basin, and disconformably overlies the Majala Member. It comprises ~1,500 m of intercalated red shales, marls and quartz sandstones, overlain by ~1,300 m of laminated red-brown shales that crop out widely in the vicinity of the Guatacondo village (Smoje, 1989). Laminated red sandstones that unconformably overlie the Peine Group in the Quebrada Copaquire area (Fig. 3.18) are tentatively correlated with the Guatacondo Member.

A sequence of laminated red sandstones known informally as the Chacarilla Beds occurs approximately 20 kilmetres north of Guatacondo (Galli, 1957). These are also correlated with the Guatacondo Member as they preserve various late Jurassic sauropod footprints (e.g., Moreno et al., 2000)

3.10.2 Cerro Empexa Formation (Ktei)

The Cerro Empexa Formation (Galli, 1957) comprises green-grey to black andesitic terrestrial sediments and subaerial lavas that record a migration of the Late Cretaceous volcanic arc toward the back arc. Detailed stratigraphy and paleogeographic reconstructions are provided by Tomlinson et al. (2001a), and radiometric ages compiled therein range from 63.8 – 72.2 Ma. In the Collahuasi district the Cerro Empexa Formation occurs as fault-bound belt that is limited on its eastern margin by the Domeyko fault system (Fig. 3.19). Massive fine grained blue-grey to green-black andesites and lesser boulder conglomerates ascribed to the Cerro Empexa Formation crop out along the western side of the Quebrada Ornajuno.

3.10.3 Tolar Formation (Ktes)

The Tolar Formation (Maksaev, 1978) is a sequence of red-brown terrestrial clastic sedimentary rocks that unconformably overlie the Cerro Empexa Formation and are locally intercalated with the basal Icanche Formation. Based on detailed

stratigraphy and mapping between Collahuasi and Chuquicamata, Tomlinson et al. (2001a) interpret that the Tolar Formation was deposited as fluvial infill of localised intermontane basins that formed to the east of the proto-Domeyko Cordillera.
The Tolar Formation overlies the Peine Group with slight angular discordance. At Collahuasi it occurs predominantly in fault-bound blocks along the Domeyko fault zone, east of Copaquire and adjacent to El Colorado (Fig. 3.19).

3.11 Icanche Formation

The Icanche Formation (Maksaev, 1978) is a widespread, loosely defined package of subaerial volcanics and terrestrial volcanogenic sediments erupted along an Eocene volcanic arc coincident with the Domeyko Cordillera (~55-43 Ma: Tomlinson et al., 2001a). It has been recognised in the other major porphyry districts in northern Chile (Fig. 3.3; Huete et al., 1977; Maksaev, 1978; Maksaev and Zentilli, 1990; Hammerschmidt et al., 1992; Tomlinson and Blanco, 1997b; Tomlinson et al., 2001a, and SERNAGEOMIN map references therein). In the area immediately

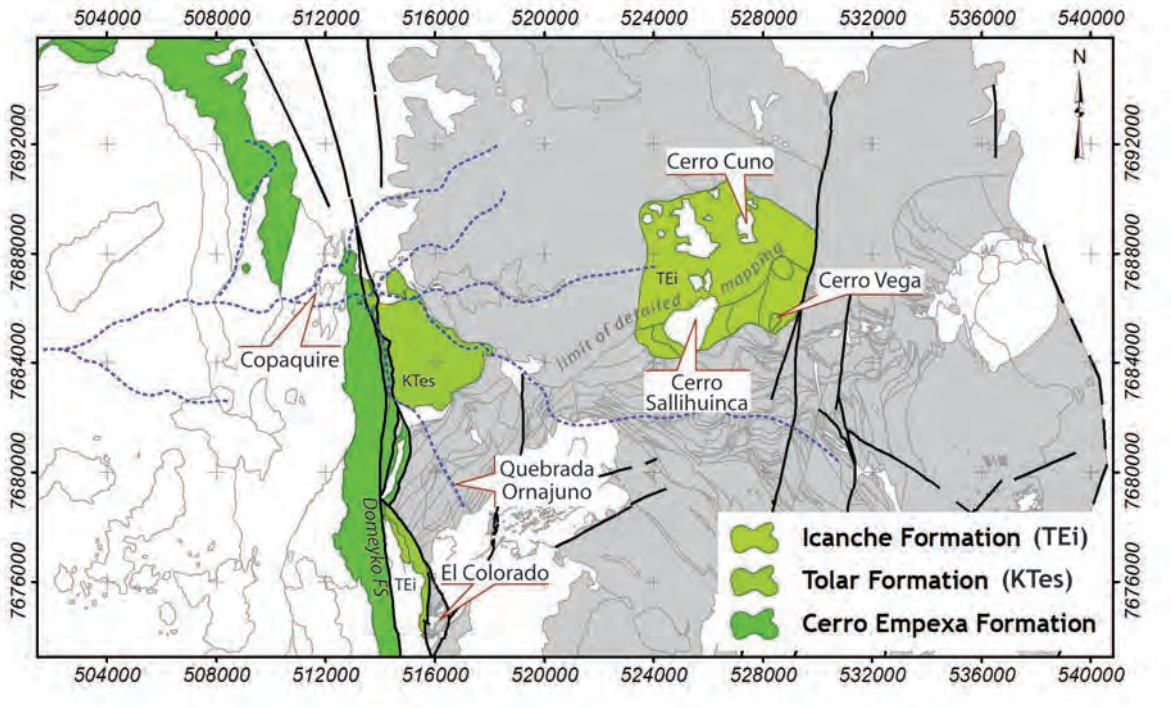

Figure 3.19. Distrubtion of Cretaceous and Paleogene units in the greater Collahuasi district. Light grey area depicts the extent of Peine Group rocks in the district. Black linework indicates major faults, and dashed blue lines are selected drainages. Landmarks mentioned in the text are indicated. Abbreviations: FS = fault system. Grid divisions are 2 kilometres.

north of Chuquicamata the Icanche Formation is intercalated with the lower parts of the fluvial and lacustrine Sichal Formation (Fig. 3.1; Maksaev, 1978). This study provides the first record of the Icanche Formation at Collahuasi, but the Sichal Formation appears to be absent.

The Icanche Formation crops out in the north-central part of the Collahuasi district, around the Cerro Sallihuinca Stock (Fig. 3.19). Outcrops in this location were previously mapped as Cerro Empexa Formation (Munchmeyer et al., 1984) despite a biotite K-Ar age of 38.8 ± 1.6 Ma from the uppermost member (Ware et al., 1981). Here this package of rocks is attributed to the Icanche Formation on the basis of new geochronology (Fig. 3.12, Section 3.16) and the dominance of felsic lithologies that are uncommon in the Cerro Empexa Formation (Table 3.2). Eocene volcanic rocks are interpreted to extend to the north (beyond the limit of detailed mapping in this study) to surround a cluster of Eocene stocks at Cerro Cuno (Fig. 3.19). The Icanche Formation also comprises a fault-bound sliver along the Domeyko Fault northwest of El Colorado (Maksaev, 1978).

3.11.1 Sallihuinca Breccia (TEi7, 43.6 ± 1.3 Ma)

The basal member of the Icanche Formation is a polymictic matrix-supported cobble breccia with strong compaction foliation. Macroscopic fragments are subrounded to subangular and are dominated by texturally variable dacite and andesite, whereas the ash-crystal matrix includes common embayed medium to coarse-grained anhedral quartz crystals and lesser fine grained plagioclase crystals. Reworked fragments of quartz-calcite veins are a minor component, suggesting some hydrothermal activity prior to eruption. The groundmass is composed of stacked, plastically deformed glassy shards and broken quartz and plagioclase crystals. These textures are consistent with a pyroclastic origin and depositional welding for this unit (e.g., Smith, 1960; Guest and Rogers, 1967; Riehle et al., 1995). The abundance and variety of accessory lithic fragments could suggest that subsurface explosions may have accompanied eruptions.

3.11.2 Dacite and andesite (TEi4)

Coherent, strongly porphyritic khaki-grey dacite and andesite crop out sporadically

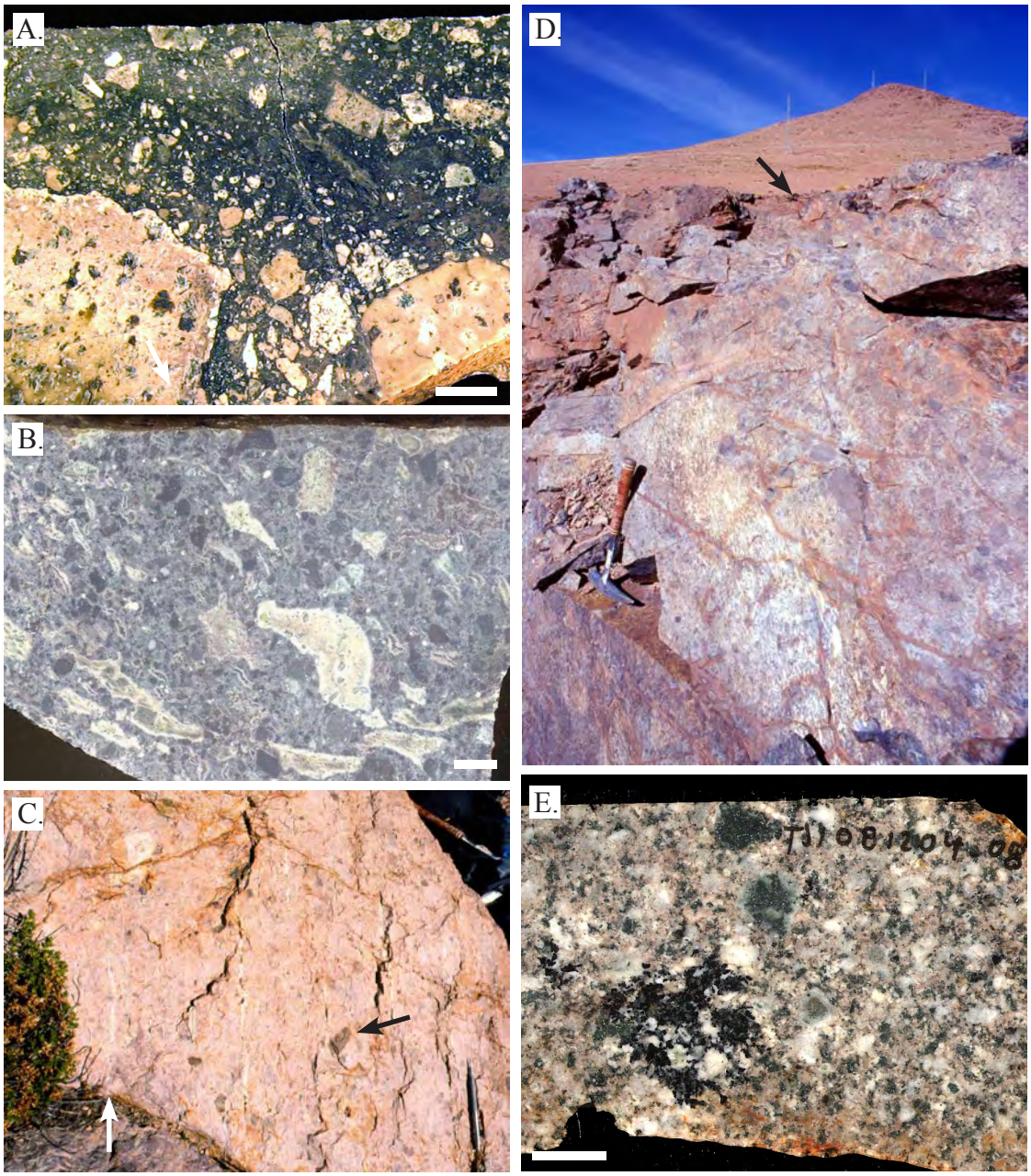

Figure 3.20. Photographs of the Icanche Formation and related rocks (unmarked white bars are 1 cm). A) Polymictic rhyolite breccia (TEi3; 526,220 mE, 7,685,443 mN) showing very poorly sorted angular porphyritic andesite, dacite and rhyolite fragments in dark siliceous glass groundmass. Hammer for scale. B) sample detail of pumiceous dacitic ignimbrite in TEi2 showing plastic deformation and moderate compaction of pale pumice lapilli (528,430 mE, 7,685,829 mN). C) Outcrop detail of the rhyolitic ignimbrite TEi1 showing strongly compacted pumice clasts (white arrow) and dark brown accessory dacite lithic fragments of TEi2. Pen for scale. (528,444 mE, 7,685,791 mN). D) Outcrop of fragmental dacitic volcanics of the Icanche Formation (TEi2) on Cerro Vega (photo taken from 528,634 E, 7,686,243 mN, looking SSW). This unit shows abrupt facies variations over short distances including strongly pumiceous polymictic ignimbrites (white arrow). An intraformational angular unconformity (black arrow) separates this moderately dipping unit from the overlying subhorizontal rhyolitic ignimbrite (TEi1). E) Hand specimen of the Cerro Sallihuinca monzonite showing medium to coarse grained weakly seriate texture and dendritic tourmaline-albite mairolitic cavity intergrowth (525,250 mE, 7,684,932 mN).

on the south side of Cerro Sallihuinca (Fig. 3.4). Contacts with other units are obscured by colluvial cover, but similar lithologies occur as accidental lithic fragments in the overlying rhyolite breccia. Two samples chosen for thin section petrography have different phenocryst assemblages and there appears to be considerable phenocryst variability within this unit, between plagioclase-hornblende-(orthoclase)-bearing and biotite-(plagioclase-quartz)-phyric varieties. Magnetite is a common microphenocryst phase in all examples. Poor exposure prohibits any description of the morphology of these units. They could represent either subaerial effusive lavas or shallow subvolcanic intrusions.

3.11.3 Rhyolitic boulder ignimbrite (TEi3)

Uncompacted, matrix-supported, polymictic lithic volcanic breccia with a hyalocrystalline black matrix crops out on the saddle between Cerro Vega and Cerro Sallihuinca (Figs. 3.4, 3.19). Clasts are angular and range from sand to boulder sizes. There is local flow alignment of elongate clasts (Fig. 3.20a), development of which coincides with gradation from very coarse to fine grainsize. Clasts include coherent andesite to rhyolite and rare sandstone derived from the local Icanche Formation substrate and members of the Peine Group. Small broken sodic plagioclase, orthoclase and quartz crystals are minor clast components. The matrix is composed of stacked and plastically deformed glass shards with strong axiolitic, and local micropoikilitic textures.

This unit includes textures common to pyroclastic and coherent volcanic rocks. The abundant lithic clasts, glassy shards and high proportion of broken crystals that characterise the matrix necessitate some kind of explosivity during eruption (e.g., Smith, 1960; McPhie et al., 1993; Allen and McPhie, 2003). In contrast, the spatial relationship between clast alignment and grainsize distribution indicates post-depositional flow (e.g., Wolff and Wright, 1981). Welding of primary pyroclasts is reflected in plastic deformation of glassy shards and the hyalocrystalline matrix (Guest and Rogers, 1967; Riehle et al., 1995). The overall poor sorting, very large size of some lithic fragments, and high temperature required for rheomorphic flow suggests deposition close to the eruption vent (McPhie et al., 1993; Quane and Russel, 2005). This unit is therefore interpreted as a proximal block-and-ash flow

deposit that underwent local rheomorphism and flowed short distances (?tens of metres) post-deposition.

3.11.4 Vega dacite breccia (TEi2, 44.4 ± 0.6 Ma)

Dark brown-grey, texturally variable, fragmental to coherent dacite crops out sparsely across the northern flanks of Cerro Vega (Figs. 3.4, 3.19). Coherent portions of this unit have sparse white plagioclase phenocrysts and rare quartz-phyric lithic fragments set in an aphanitic, subvitreous groundmass composed of aligned feldspar microlites with rare fine quartz-zeolite flow bands. Monomictic angular, framework-supported boulder breccias of this dacite are intercalated with the coherent facies. These grade upward into polymictic fragmental facies composed of weakly bedded pumice-bearing (Fig.3.20b) and pumice-absent varieties of framework-supported angular lithic lapilli breccia, which share gradational contacts and show weak to moderate compaction. Pumice fragments are composed of masses of axiolitic microlites and include common orthoclase phenocrysts.

Based on the intimate spatial relationship of coherent dacite, monomictic breccias and polymictic lithic lapilli breccias, this unit is interpreted as a collection of vent-proximal subaerial eruption products (e.g., Wilson and Walker, 1982). The monomictic breccias are inferred to have formed a carapace to coherent dacite (e.g.McPhie et al., 1993), but the surface exposure does not permit definition of this geometry. The polymictic breccias require some degree of eruptive explosivity, but the moderate grainsize sorting and absence of large clasts might indicate that this activity was limited (e.g., Sparks, 1976). Eruption of the Vega dacite was therefore effusive to weakly explosive.

3.11.5 Vega rhyolitic ignimbrite (TEi1, 42.3 ± 0.7 Ma)

The summit and northern knoll of Cerro Vega are composed of a distinctive pale pink, massive, moderately pumiceous banded lithic lapilli rhyolitic ignimbrite (Fig. 3.20c). Beige banding is caused by strong compaction of pumice clasts that define a pervasive compaction fabric that is deflected around brown-grey dacite lithic clasts. Pumice clasts include the small quartz and feldspar phenocrysts, and have strong axiolitic texture about their margins. The matrix consists of compacted, devitrified

TABLE 3.2. Compilation of stratigraphic and petrographic detail for Phanerozoic stratigraphy of the Collahuasi district.

Lithofacies Unit	Age	Rock Characteristics	Crystal and Clast Characteristics[a,b]	Interpretation	References
Neogene cover sequences					
Alluvium (Qal)	Quaternary	Scree, gravels and sands	Locally derived angular to subrounded lithic and crystal fragments	Active alluvial and colluvial deposits	Vergara, 1978
Terrigenous clastics (PPlg)	Pliocene	Poorly sorted gravels and lesser sands	Volcanic lithic and crystal fragments, locally with faceted surfaces and straie	Alluvial and glaciotile deposits	Vergara, 1978; Munchmeyer et al., 1984
Western Cordillera volcanic and epiclastic deposits (QTMv)	Miocene-Recent	Andesite, subordinate basalt and dacite, and associated monomict breccias	Highly variable regionally; flows on western Cerro Pabellon del Inca are fine to medium grained, vesicular and strongly plagioclase-homblende phyric	Subaerial andesitic effusive to mild explosive stratovolcano eruptions.	Vergara, 1978; Feeley et al., 1993; Woerner et al., 1992
Carcote Ignimbrite (Tmic)	5.8 Ma	Variably welded dacitic lithic-pumiceous lapilli crystal ignimbrite; 10-30 m thick regionally, <2 m at Collahuasi	Plag: 25-30% euhedral broken <2.5 mm; Bt: 2-6% subhedral <2 mm; Shards: 15-20%; Pum: 0-6% angular lapilli; Lith: 0-3% angular Peine Group lapilli	Highly energetic laterally directed pyroclastic flow deposit; distal facies	Baker, 1977; Baker and Francis, 1978; Tomlinson et al., 2001a
Ujina Ignimbrite (Tmiu)	9.2 Ma	Moderately to strongly welded dacitic crystal-ash ignimbrite; thickness up to ~300 m controlled by paleotopography	Plag: 35-50% euhedral broken <3 mm; Cpx: 3-6% subhedral <2 mm; Hbl: 2-4% subhedral <1 mm; Bt: 1-2% subhedral <1 mm; Shards: 15-20%; Pum: <1% irregular 10-60 mm	Highly energetic laterally directed pyroclastic flow deposit	
Altos de Pica Formation (Tsap5)	Miocene	Poorly consolidated, poorly sorted gravels and granular sands, and minor dacitic ash-crystal tuffs	Angular to subangular locally derived lithic fragments dominated by Mesozoic sedimentary- and Eocene intrusive lithologies	Alluvial and colluvial deposits and intercalated minor pyroclastic deposits	Tomlinson et al., 2001a
Papajoy Formation (Tou)	Oligocene	Channelised polymict conglomerates and subordinate local plane laminated sandstone and carbonaceous siltstone; coarse facies locally host to exotic Cu mineralisation	Subangular to rounded lithics, dominated by Peine Group and related intrusive lithologies. Fine-grained facies are quartzose	Alluvial and lacustrine deposits restricted to localised extensional and transtensional basins	Vergara, 1978; Tomlinson and Blanco 1997b
Icanche Formation					Maksaev, 1978
Vega rhyolite ignimbrite (TEi1)	42.7 Ma.	Light pink, banded, strongly compacted, pumiceous lithic lapilli rhyolite ignimbrite	Plag: 1-3% euhedral broken <2 mm, An2-6; Lith: 2% angular <30 mm, of qtz-phyric granophyric volcanics. G'mass: very fine microlitic mass of oriented dominantly ?feldspar xls. Banding is defined by discontinuous lenses of granophyric qtz or radial zeolites <20 mm long and <1 mm wide	Vent-distal pyroclastic flow and/or column collapse deposits that underwent compaction and welding upon deposition	this study
Vega dacite breccia (TEi2)	44.3 Ma.	Dark brown-grey bedded strongly polymict lithic pumiceous weakly compacted dacite breccia and subordinate coherent dacite	Pum: 5-20% <30 mm, kfs-phyric, axiolitic; Lith: 10-20% angular to subrounded fragments < 10 mm of plag-phyric and amygdaloidal dacite and andesite; Kfs: 12% subhedral <2mm. Plag: 3% subhedral <1 mm	Block and ash flows and associated lava dome eruption	this study
Sallihuinca rhyolite breccia (TEi3)	-	Black, strongly polymict accessory > cognate lithic subvitreous rhyolite rheoignimbrite breccia	Lith: 15% angular to subangular 5 mm - 2 m, andesite and rhyolite; Plag: 3% euhedral broken <2mm, An10. Kfs: 1% euhedral <3mm. Qtz: 1% anhedral embayed broken <2 mm. Mt: 2% subhedral <1mm. G'mass: deformed glass shards, axiolitic	Vent-proximal explosive eruptions; block and ash flows with significant sub-surface explosivity and post-depositional flow	this study
Dacite and andesite (TEi4)	-	Undifferentiated, brown-grey porphyritic plagioclase-hornblende phyric dacites and andesite	Plag: 14-20% subhedral 1-4 mm, zoned An48-28; Kfs: 5% subhedral resorbed <5 mm; Hbl & Bt: 0-10% subhedral elongate <3 mm; Mt: 4-8% anhedral 5-200 mm; G'mass: plag>hbl-bt>mt-qtz	Effusively erupted small domes and lobate flows	this study
Sallihuinca breccia (TEi7)	43.9 Ma.	Polymict accessory > cognate lithic, matrix supported, poorly sorted, moderately to strongly compacted welded volcanic breccia	Lith: 10-30% subrounded-subangular polymict volcanics <20 cm; Qtz: 7% angular to subround embayed <4 mm; Plag: 4% angular <1 mm. Vein Qtz-Calcite: 3% subrounded fragments <4 mm; G'mass: stacked deformed glass shards	Vent-proximal explosive eruptions; block and ash flows with significant sub-surface explosivity and strong post-depositional compaction	this study
Tolar Formation					
undifferentiated. KTes	-	Medium to thin bedded, polymict lithic fine to coarse-grained clastic sediments; basal conglomerate is dark green-grey and poorly sorted; upper red sandstones are plane laminated, and locally cross bedded	see Tomlinson et al., 2001a	Fluviotile channels and overbank deposits, shallow lacustrine sediments with minor turbiditic mass flow sedimentation	Maksaev, 1978; Tomlinson et al., 2001a; this study
Cerro Empexa Formation.					
undifferentiated. KTei	73-64 Ma.	Andesite, minor monomict andesite breccia and basal epiclastic sandstones and conglomerates	see Tomlinson et al., 2001a	Epiclastic alluvial fan deposits and subaerial effusive lave flows	Galli, 1957
Quehuita Formation					
Guatacondo Member (J.cb)	?Kimmer-idgian.	Red-brown, plane laminated shale and siltstone and thin bedded, well sorted quartzose fine sandstones; rare sauropod print fossils	see Smoje, 1989	Shallow lacustrine sediments, fluvial sheetflood and overbank deposits	Galli, 1957; Vergara and Thomas, 1984; Smoje, 1989; Orrego G., 1992; Moreno, 2000; Tomlinson et al., 2001a; this study
Majala Member[c]	?	Green-grey interbedded shale, marl and sandstone		Regressive shallow carbonate platform marine sediments	
Quehuita Member[c]	?Callovian	Mid-grey bedded micritic limestone and subordinate siltstone; basal conglomerate			
Aquiuno Member (Jaq)	?Dogger	Dark green to black, massive to rhythmically plane-laminated siltstone, carbonaceous mudstone and subordinate fine sandstone		Transgressive shallow to moderate depth marine basin sediments; carbonaceous mudtsones of the Aquiuno member record the maximum flooding surface of the Tarapaca Basin.	
Copaquire Member (Jcq)	?Liassic	Interbedded thin-thick bedded grey shales, marls and intercalated sandstones; rare ammonoid fossils			

a.) % are average volume percent determined by visual estimation in hand specimen and/or in thin section under transmitted light. Dimensions are the long axis of elongate forms.

b.) Mineral compositions determined by electron microprobe and/or extinction angle (Michel-Levy test for plagioclase)

c.) These units are not recognised in the Collahuasi District map (Fig. 3.4), but are described from nearby occurrences.

Abbreviations: Pum = pumice; Lith = lithic fragments; Plag = plagioclase; Kfs = orthoclase; Qtz = quartz; Amph = amphibole; Bt = biotite; Cpx = clinopyroxene; Opx = orthopyroxene; Mtx: matrix; An = anorthosite fraction of plagioclase; Sub.=subunit (subunidad).

Table 3.2 Phanerozoic stratigraphy and petrography.

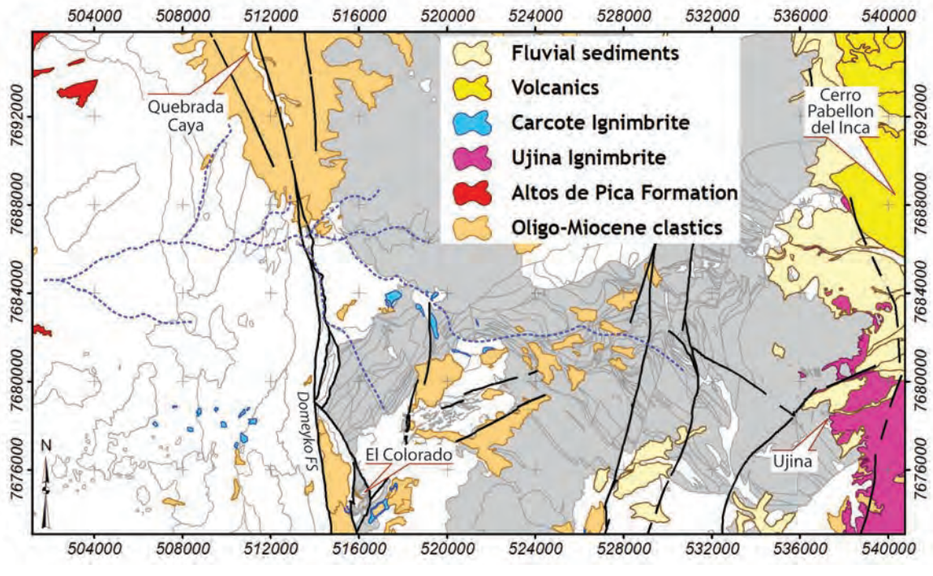

Figure 3.21 Distrubtion of Neogene units in the greater Collahuasi district. Areas denominated "Oligo-Miocene clastics" include the Oligocene Papajoy formation along the Domeyko FS and the Quebrada Caya. "Fluvial desiments" includes glaciofluvial deposits that occur as a common cover sequence southwest of Ujina. Light grey area depicts the extent of Peine Group rocks in the district. Black linework indicates major faults. Dashed blue lines are selected drainages. Abbreviations: FS = fault system. Grid divisions are 2 kilometres.

glass shards and lesser small broken quartz and feldspar crystals. The fragmental components and strong compaction are consistent with a pyroclastic origin for this unit (e.g., Wilson and Walker, 1982). However, devitrification has obscured the detail of shard morphology, and therefore clear evidence of depositional welding could not be established (e.g Smith, 1960). The absence of bedding and dominance of fine-grained fragmental components are inconsistent with deposition in a vent-proximal position (e.g., Sparks 1976) as suggested for the underlying strata. The Vega rhyolitic ignimbrite was therefore apparently erupted from another, as yet unknown, middle Eocene volcanic centre in the vicinity of the Collahuasi district.

Mild local deformation and erosion appears to have occured between eruption of the Vega dacite (TEi2) and the Vega rhyolitic ignimbrite (TEi1). Compaction fabrics in the two units define angular discordance of 15º to 20º (Fig. 3.20d).

3.12 Cenozoic Terrestrial Sedimentary Rocks

Oligocene to Recent terrestrial gravels and minor lacustrine sedimentary rocks (and equivalent unconsolidated sediments) are common throughout the Domeyko Cordillera (Tomlinson et al., 2001a). Of note at Collahuasi, weakly consolidated polylithic conglomerate and agglomerate hosts exotic Cu mineralisation at Huinquintipa (Munchmeyer et al., 1984). These rocks were not investigated in detail in this study, and the description provided is largely a review of previous work supplemented by some additional observations and interpretation.

3.12.1 Papajoy Formation (Oligocene)

The Papajoy Formation comprises a series of terrestrial conglomerates and sandstones deposited in highly localised sub-basins up to 320 m deep along the trace of the Domeyko fault system (Vergara, 1978). In the Collahuasi district, the Papajoy Formation comprises poorly bedded polymictic pebble conglomerates with rounded clasts that have filled an elongate basin immediately south-southwest of El Colorado (Fig. 3.21). The formation is juxtaposed against Eocene intrusions and the Peine Group by a brittle sinistral strand of the Domeyko fault system. Tomlinson et al (2001a) suggest that deposition occurred during sinistral motion along the Domeyko fault system, which they bracketed between late stage alteration at Chuquicamata at

around 31 Ma and eruption of ignimbrites assigned to the Altos de Pica Formation at around 25 Ma. Given that these ignimbrites are also known from drilling in the Quebrada Caya (Fig. 3.21; Tomlinson et al., 2001a), it seems likely then that some of the deeper fill in that basin may also correlate with the Papajoy Formation.

3.12.2 Altos de Pica Formation (Late Oligocene)

Poorly consolidated terrestrial gravels and widespread crystal-rich dacitic ignimbrites accumulated along the western margin of the Domeyko Cordillera and throughout the Central Valley in the uppermost Oligocene (Tomlinson et al., 2001a, and references therein). These units do not crop out in the Collahuasi district proper, but remain as erosional remnants on the west-facing slopes northwest of the Quebrada Caya (Fig. 3.21). They are an important stratigraphic marker among Tertiary units in that area.

3.12.3 Huinquintipa conglomerate (Oligocene to Miocene)

Throughout the Tertiary porphyry Cu districts of northern Chile, subsidiary "exotic" concentrations of copper oxides, primarily chrysocolla, atacamite and copper wad, formed as grain coatings and low-temperature hydrothermal cement among fluviotile conglomerates adjacent to eroded hypogene copper deposits (Brimhall et al., 1985; Alpers and Brimhall, 1988; Munchmeyer, 1994; Cuadra and Camus, 1998; Ossandon et al., 2001). At Collahuasi, exotic mineralisation is hosted by a series of green-grey bedded pebble conglomerates and granular lithic sandstones that occupy steep-walled structurally controlled W-draining paleovalleys at Huinquintipa (Figs. 3.4, 3.21; Ware et al., 1981). Munchmeyer (1994) concluded that exotic mineralisation occurs largely at the same time as fluvial sedimentation, and so the timing of deposition of the Huinquintipa conglomerates is bracketed between earliest Oligocene hypogene mineralisation at Rosario (Masterman et al., 2004) and Middle Miocene climatic changes that dramatically slowed weathering processes in the Domeyko Cordillera (Alpers and Brimhall, 1988). These deposits are therefore likely to correlate with the Papajoy or Altos de Pica Formations (Fig. 3.3; Tomlinson et al., 2001a, and references therein).

Similar fluviotile and lesser lacustrine sediments occur widely across the Collahuasi district, especially in the vicinity of the Quebrada Blanca copper deposit (Figs. 3.4,

3.21). Of note, thin bedded sands and black siltstones accumulated in mesoscopic half-grabens articulated on NW-trending nornal faults that cut the deposit. These are exposed in the southern walls of the Quebrada Blanca open pit mine.

3.13 Neogene Volcanics

3.13.1 Ignimbrites (TMiu and TMic, Late Miocene)

Pale coloured, sheet-like, variably welded plagioclase ± clinopyroxene ± hornblende ± biotite crystal-rich dacitic ignimbrites that infill topography are common throughout northern Chile (Baker, 1977; Francis and Baker, 1978; Lindsay et al., 2001; Richards and Villeneuve, 2002; Quang et al., 2005; Ramelow et al., 2006). These ignimbrites are generally distributed toward the landward side of the volcanic axis and extend into Bolivia and Argentina. Large, approximately circular salt lakes in these areas have been interpreted as the surface expression of caldera vents from which these ignimbrites were erupted (e.g., Baker, 1977). In the Collahuasi district there are two principal examples: the Ujina Ignimbrite (*TMiu*, 9.7 Ma: Baker, 1977; Vergara, 1978) and the Carcote Ignimbrite (*TMic*, 5.8 Ma: Baker 1977; Tomlinson et al., 2001a).

The Ujina ignimbrite occurs as infill of the Preandean Depression south of the Pabellón del Inca volcano (Figs. 3.4, 3.21), and onlaps onto the eastern margin of the Paleozoic inlier that comprises the Domeyko Cordillera. It extends westward along local paleovalleys near Ujina (Fig. 3.4), and prior to mining covered most of the alteration and mineralisation that had been exposed by Oligocene to Middle Miocene erosion (Ware et al., 1981). The pumiceous lithic Carcote Ignimbrite occurs over large areas 25-60 kilometres south of Collahuasi (Baker and Francis, 1978). The Collahuasi district contains the northernmost exposures of the Carcote Ignimbrite, wherein it is restricted to isolated, thin valley fill remnants that have largely been removed by subsequent valley incision (Figs. 3.4, 3.21).

3.13.2 Stratovolcanoes of the Western Cordillera (QTMv, Miocene to Recent)

The eastern margin of the Collahuasi district is ~10 kilometres west of the main volcanic axis of the Miocene-Recent Western Cordillera (Lopez-Escobar et al.,

1979; Hawkesworth et al., 1982; Rogers and Hawkesworth, 1989; Wörner et al., 1992a; Wörner et al., 1992b; Feeley et al., 1993; McMillan et al., 1993; Wörner et al., 1994; Wörner et al., 2000; Grunder et al., 2006; Klemetti and Grunder, 2008), and is separated from it by the Preandean Depression. The Cerro Pabellón del Inca is an isolated volcano situated approximately six kilometres west of the main arc front. Dacite and andesite lava flows on its western side onlap onto the Domeyko Cordillera (Vergara, 1978). Occurrence of this volcano inboard of the arc front is interpreted to reflect a penentrative crustal structure in this location, equivalent to structures invoked by Matteini et al. (2002) and Richards and Villeneuve (2002) for volcanoes outboard of the arc several hundred kilometres to the south.

3.14 Permo-Triassic Intrusive Rocks

Permo-Triassic intrusive rocks occupy approximately 15% of the mapped Collahuasi district. Petrographic characteristics are presented in Table 3.3.

3.14.1 Diorite, granodiorite and monzonite plutons (Pzdio, Pzgd, Pzqmnz)

Voluminous medium to coarse-grained, intermediate to felsic plutons have intruded the upper Paleozoic sequences througout northern Chile (Huete et al., 1977;

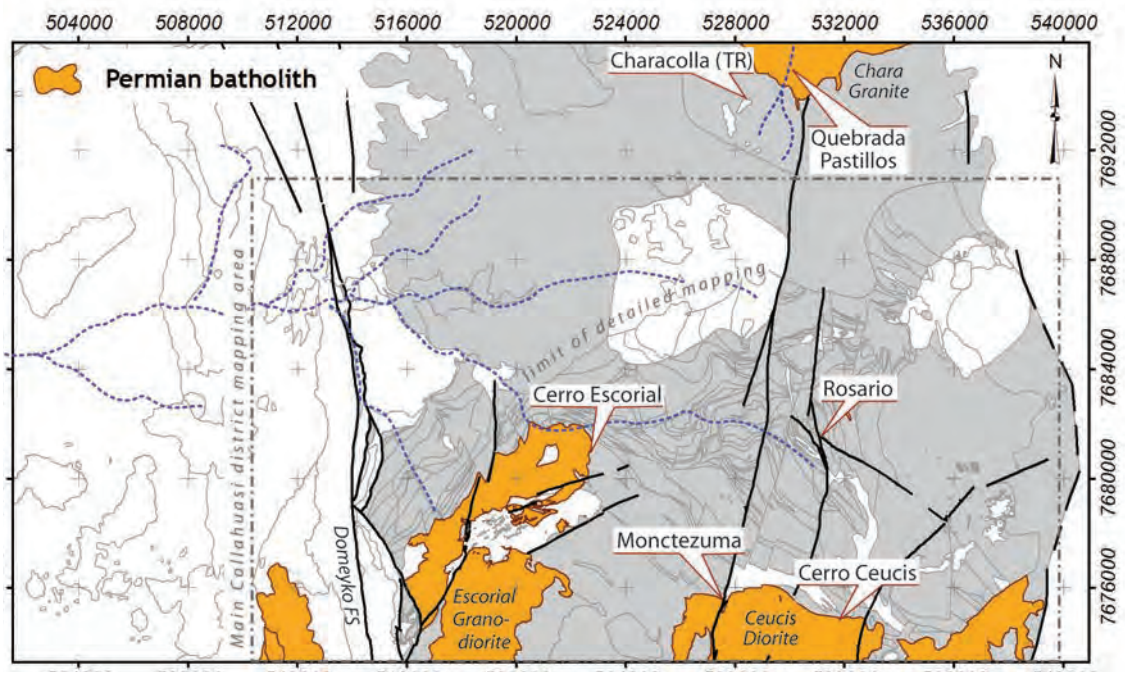

Figure 3.22. Distribution of Permian plutonic rocks in the greater Collahuasi district. Other map elements as per figure 3.21. Locations mentioned in the text are indicated. Abbreviations: FS = fault system. Grid divisions are 2 kilometres.

TABLE 3.3. Petrographic characteristics of Late Paleozoic and Triassic intrusions.

Lithofacies[a]	Crystal Characteristics[b,c]	References
Plutons		
Pzdio[d] (Pzgd, Pzqmnz). ~256 Ma.† Equigranular to weakly seriate grey-green to grey diorite, granodiorite and quartz monzonite.	PLAG: 70-80 % subhedral 1-3 mm, An_{37-41}; HBL: 10-20 % anhedral 0.2-1 mm; BT: 5-7 % subhedral 0.2-1 mm, chloritised; CPX: 1-2 % anhedral 0.1-0.5 mm; MT: 5-7 % subhedral xls 0.1-0.4 mm.	Huete et al., 1977; Vergara, 1978; Ware et al., 1981; †Damm et al.,
Dykes and Stocks		
TR.pco. ~245 Ma.^ Collahuasi Porphyry. Biege to pink strongly porphyritic granodiorite.	PLAG: 30 % euhedral xls with weak oscilliatory zoning, 0.6-8 mm, An_{0-5}; QTZ: 15-20 % rounded and resorbed "eyes" ≤7 mm; KFS: 10-15 %, 0.5-5 mm; MT: <1 % 0.2-1 mm. G'MASS: aphanitic to aplitic 20-400 μm, qtz-kfs>plag>>zirc-ap.	Ware et al., 1981; Vergara and Thomas, 1984; ^ Masterman 2003.
TR.pch. ~243 Ma.* Characolla Porphyry. Light grey quartz monzodiorite.	PLAG: 6-10 %, subhedral laths 2-4 mm, An_{34} with thin albitic rims; G'MASS: holocrystalline 300-500 μm plag>qtz>>shreddy biotite-euhedral magnetite>>apatite-zircon.	*V. Maksaev, written commun. 2005; this study.
TR.pcs. ~232 Ma. Co. Silvar Porphyry. Biege strongly porphyritic alkali feldspar granite.	QTZ: 12% euhedral to embayed xls 2-5 mm; PLAG: 6% subhedral xls 3-6 mm, An_{12}; KFS: 7% subhedral xls 2-4 mm. G'MASS: granophyric 200-300 μm kfs>qtz>>zircon-apatite>oxides.	this study.
TR.pur. Undifferentiated biege to pink, vitreous, strongly porphyritic felsic dykes and stocks.	QTZ: 4-18% rounded and embayed xls 1-5 mm; FELDSPARS: 8-14 % subhedral xls 2-4 mm. G'MASS: subvitreous, aphanitic 50-200 μm kfs-qtz>>zircon-apatite-oxides.	this study.
TRmdd. ~237 Ma. Cascasa Dyke Swarm. Equigranular to strongly porphyritic green-grey microdiorite dykes.	PLAG: 0-12 % subhedral laths $An_{32-36;}$ AMPH: 2-10 %, subhedral prismatic xls; MT: 5-10 % subhedral xls 0.1-1 mm; CPX: 0-4 % euhedral xls 0.5-2 mm. G'MASS: holocrystalline 100-800 μm plag>amph>cpx-bt.	this study.

a.) Radiometric ages are rounded to the nearest million years, ignoring errors, and include new data and various literature and in-house sources.
b.) Modal percentages are average visual volume percent in hand specimen and/or in thin section under transmitted light. Dimensions are the crystal C- axis.
c.) Plagioclase compositions determined by extinction angle (Michel-Levy test)
d.) Pzdio description taken from the intrusion south of Monctezuma, in the southern central map area.

Abbreviations: xls = crystals; PLAG = plagioclase; KFS = orthoclase; QTZ = quartz; AMPH = amphibole; BT = biotite; CPX = clinopyroxene; MT; G'MASS: groundmass; An = anorthosite fraction of plagioclase; zirc = zircon; ap = apatite.

Lopez-Escobar et al., 1979; Brown, 1991; Tomlinson et al., 2001a, and references therein). These plutons typically have spatial extents on the order of 50 km^2. Two such plutons, the Escorial Granodiorite and the Ceucis Diorite, occupy the southern margin of the Collahuasi district (Fig. 3.22; Huete et al., 1977; Vergara, 1978; Ware et al., 1981; Munchmeyer et al., 1984; Vergara and Thomas, 1984). Another, the Chara 'Granite' (which is in fact a quartz monzonite) is exposed along the Quebrada Pastillos some 16 km north of Rosario (Fig. 3.22; Damm et al., 1986).

These plutonic rocks are typically medium-grained, equigranular and are not hydrothermally altered beyond the immediate area of Tertiary intrusions. Exposures in the Monctezuma area show Neogene glacial striaie, consistent with unconsolidated till that covers parts of the southern central map area (Munchmeyer et al., 1984). In this location the Ceucis Diorite is an equigranular, medium grained plagioclase-hornblende-biotite-magnetite diorite. The Escorial Granodiorite is a composite pluton that ranges in composition from granodiorite to diorite and includes rare, large enclaves of fine grained diorite.

3.14.2 Collahuasi Porphyry (TRpco, Early Triassic)

The beige-pink alkali granite Collahuasi Porphyry is a major host rock to Cu-Mo mineralisation at Rosario and has been described in previous studies (Ware et al., 1981; Vergara and Thomas, 1984; Masterman, 2003; Masterman et al., 2005). It comprises a structurally disrupted dyke up to 300 m wide that extends at least 9 kilometres NNW-SSE from northwest of Rosario to the limit of mapping southwest of Ujina (Fig. 3.23; Vergara, 1978; Ware et al., 1981). The dip of the main dyke is poorly constrained, but faults and joints associated with it are commonly subvertical. Masterman et al. (2005) described the modal mineralogy as quartz-albite-orthoclase >> biotite-hornblende > magnetite. Another biotite granite, the La Profunda 'stock', is known from limited drilling southeast of Ujina (Fig. 3.23). This intrusion was also emplaced at ~245 Ma (Munizaga et al., 2008) although its geometry is unknown.

3.14.3 Characolla porphyry (TRpch, Early Triassic)

The name Characolla (previously Ralfito Lorenzito) refers to a porphyry copper prospect some 12.5 kilometres NNW of Rosario associated with a group of small

porphyritic intrusions (Fig. 3.22). These intrusions are marked as Tertiary on existing maps (Tomlinson et al., 2001a, and references therein), probably based on their spatial association with porphyry copper mineralisation. However, recent geochronology has shown that zircons in the porphyry intrusion crystallised at around 245 Ma (Munizaga et al., 2008), and illite in the hydrothermal alteration zone is a couple of million years younger (A. H. Clark, written commun. 2007).

3.14.4 Cascasca dyke swarm (TRmdd, ~237 Ma)

Narrow (0.5-8 m wide) dark grey-green dykes of andesitic composition occur sporadically across the Collahuasi district (Ware et al., 1981). They occur among the immediate host rocks to the mineralised Quebrada Blanca, Rosario and Ujina intrusions (this study). All three mining operations, and the road- and conveyor cuttings in the eastern part of the district expose numerous dykes (n ~200). Given the limited distribution of excavations, this is anticipated to be a small fraction of the total.

The Cascasca Dykes are most abundant in a steeply W-dipping, NNW-trending zone through Cerro Cascasca (Fig. 3.23, Chapter 4). The dyke swarm has not been traced

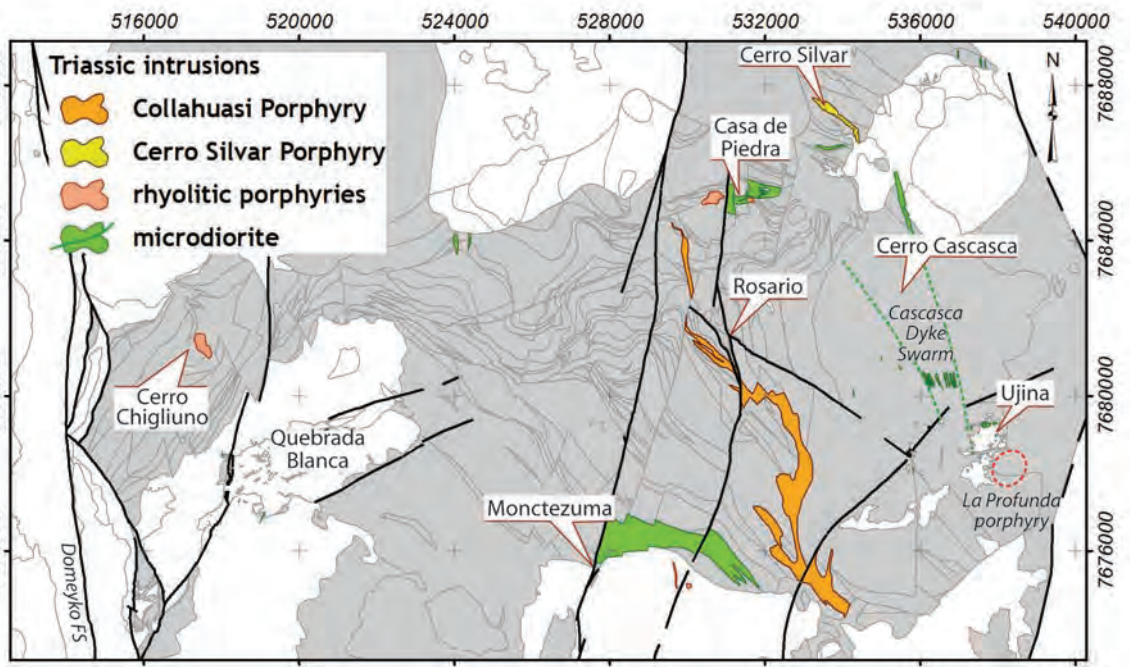

Figure 3.23. Distribution of Triassic intrusive rocks in the Collahuasi district. Light grey area depicts the extent of Peine Group rocks in the district. Black linework indicates major faults. Red dashed line indicates the surface projection (but not shape) of the La Profunda biotite granite. Locations mentioned in the text are indicated. Abbreviations: FS = fault system. Grid divisions are 2 kilometres.

southeast of the Ujina porphyry, but “andesites” make up a disporportionate amount of the wallrocks to mineralisation compared to the felsic Cascasca Formation that is ubiquitous in the area. At its northern extent, the dyke swarm become irregular and appears to be replaced by a thick sill in the Casa de Piedra area (Fig. 3.23). It may have served as a volcanic feeder to the uppermost, andesitic member of the Yabricoya Formation.

The dykes vary from fresh to completely weathered in near-surface exposures and most of them are erosionally recessive and produce limited, or no outcrop. They appear to weather quickly, as they are not a common component of the colluvial cover even where road cuttings show them to be abundant. In the vicinity of porphyry copper hydrothermal systems they commonly show strong selective biotite (proximal) or epidote-chlorite (distal) alteration.

An equigranular dark grey holocrystalline rock comprised of plagioclase and clinopyroxene occupies the lower Chiclla Formation stratigraphy near Monctezuma (Figs. 3.4, 3.23). This rock is interpreted to be a sill related to the Cascasca dykes as it does not show any volcanic textures and is petrographically more similar to the dykes than to andesites of the Peine Group.

3.14.5 Cerro Silvar porphyry (TRpcs, 232.4 ± 2.3 Ma)

This cream-colored, strongly quartz-orthoclase-albite porphyritic alkali granite crops out over a strike length of two kilometres as a 100-200 m-wide, NW-trending dyke along the main ridge of Cerro Silvar (Fig. 3.23). At its southern end it is truncated by the Cretaceous Tolaun intrusive complex, and in the north it may extend under colluvial cover (Fig. 3.4).

3.14.6 Undifferentiated rhyolite porphyries (TRpur)

Small, localised stocks of beige to pink quartz-feldspar porphyry with massive aphanitic vitreous groundmass have intruded the Huinquintipa Formation on Cerro Chigliuno and the Yabricoya Formation in the Casa de Piedra area (Fig. 3.23). In this latter area, petrographic distinction between intrusive (and possibly coherent extrusive) porphyry and the Yabricoya Crystal Ignimbrite (TRy2) is indistinct and the

two may be cogenetic. Crosscutting relations with the Yabricoya dacite imply that this intrusion is no older than earliest Triassic.

3.15 Cretaceous to Paleogene Intrusive rocks

There have been several previous studies of Paleogene intrusive rocks in the Collahuasi district, owing to the common genetic association between Eocene intrusions and mineralisation in northern Chile (e.g., Ware et al., 1981; Munchmeyer et al., 1984; Hunt, 1985; DeBeer and Dick, 1994; Dick et al., 1994; Lee, 1994; Clark et al., 1998; Masterman, 2003; Masterman et al., 2005). Consequently, the current study has not further investigated these intrusions in detail, and descriptions here focus on those intrusions for which only limited published information was available prior to this study. The key characteristics of the Cretaceous intrusions are compiled in Table 3.4, and of the Eocene-Oligocene intrusions in Table 3.5. The chemistry of Cretaceous and Paleogene magmatic rocks is the subject of Chapter 7.

3.15.1 Tolaun intrusive complex (KL-, ~67-71 Ma)

A prominent ridge of small hills between the Pabellón del Inca volcano and Cerro

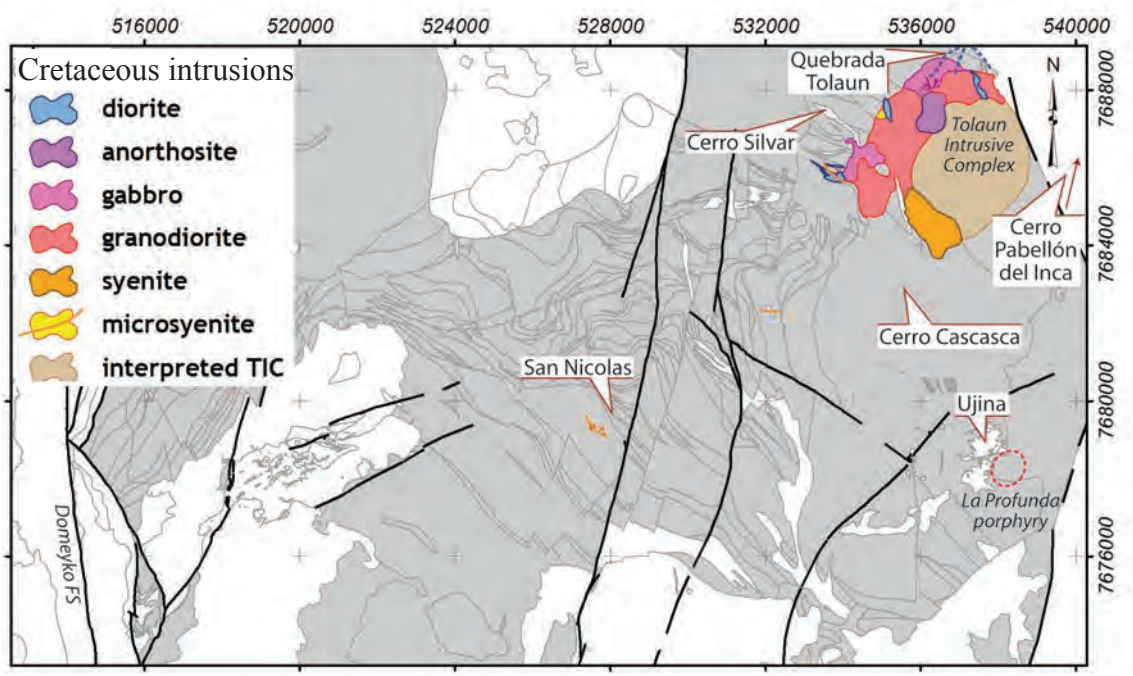

Figure 3.24. Distribution of Late Cretaceous intrusive rocks in the Collahuasi district. Background and line map elements are the same as Figure 3.21. Locations mentioned in the text are indicated. The blind, Triassic, La Profunda stock appears to host Late Cretaceous hydrothermal alteration (geochronology of Masterman et al., 2004). Abbreviations: FS = fault system. Grid divisions are 2 km.

TABLE 3.4. Petrological characteristics of the Cretaceous intrusive rocks of the Collahuasi district.

Lithofacies[a] / Age[a] / Geometry	Crystal Characteristics[b,c]	References
La Profunda Porphyry		
KC.ppr. 80.4 Ma.*. Medium to coarse grained weakly porphyritic biotite granite. Known in drilling only.	not investigated in this study.	Masterman et al., 2004.
Tolaun Intrusive Complex		Vergara and Thomas, 1984
KLgdb. ?~71 Ma.[d] Medium to coarse grained, locally seriate, mid grey labradorite-biotite granodiorite.	PLAG: 45% subhedral <2.5 mm, An_{30}, albitic rims. KFS: 3% anhedral <1.5 mm. BT: 6% euhedral <2 mm. CPX: 3% euhedral <1 mm. MT: 2% subhedral <0.3 mm.	this study
KLgbr. ?~71 Ma.[d] Medium to coarse grained, black-grey, magnetic, plagioclase-pyroxene-amphibole-phyric gabbro. Irregular stocks <2 km^2.	PLAG: 4% subhedral prismatic <4 mm, An_{60}, dominates g'mass; CPX: 3% subhedral poikilitic <1.5 mm, abundant in g'mass. HBL: 1% subhedral <1 mm. MT: 2% aggregate euhedral xls <0.5 mm.	this study
KLdio. ?~71 Ma.[d] Medium grained, grey, magnetic, plagioclase-pyroxene phyric diorite. Irregular small elongate stocks and dykes <0.2 km^2.	PLAG: 8% euhedral aggregate xls <4.5 mm, zoned An_{47-30}, dominates g'mass; MT: 3% euhedral bipyramids <0.5 mm. CPX: 10% anhedral equant to prismatic <1 mm; HBL: 4% prismatic; BT: 4% partial replacements of cpx & hbl.	this study
KLant. ?~71 Ma.[d] Coarse grained equigranular anorthosite. Dumbbell-shaped stock, 0.5 km^2.	PLAG:85% subhedral 1-5 mm, An_{45}; KFS: 7% in g'mass, BT: 5% in g'mass; MT: 3% subhedral equant <0.5 mm.	this study
KLsyn. 68 Ma.[e] Medium to coarse grained light brown-grey seriate quartz syenite. Discrete oblong stock >2 km^2.	KFS: 25% subhedral locally perthitic <8 mm; PLAG: 10%, An_{10} anhedral <2 mm. G'mass: kfs>plag>>qtz-mt-bt	this study
KLmsy. 68 Ma.[e] Fine to very fine grained saccharoidal to weakly porphyritic white to beige quartz micro-syenite. Laterally discontinuous dykes 0.5-2 m wide.	KFS: 2-20% subhedral <2.5 mm; QTZ: 1-8% anhedral pokilitic <1 mm; BT: 0-4% anhedral <1 mm; MT: 0-3% subhedral <0.4 mm; PLAG: 2% subhedral <2 mm, An_{0-8}; HBL: 0-1% subhedral prismatic <0.5 mm. G'MASS: kfs-plag>qtz>bt.	this study

Footnotes a.), b.) and c.), and abbreviations are the same as Tables 3.1, 3.2 and 3.3.

d.) The ~71 Ma age is estimated from apparent inheritance recorded in zircon grain populations of the younger Tolaun Complex intrusions.

e.) Radiometric ages of the coarse and fine grained syenitic phases of the Tolaun Intrusive Complex are within error, but dykes cut the stock.

Silvar in the northeastern part of the study area (Fig. 3.24) defines the southern margin of the Quebrada Tolaun catchment. The ridge is composed of unaltered medium to coarse grained intrusive rocks that were assigned a Cretaceous age by Vergara (1978) on the basis of one K-Ar age reported by Baker et al. (1977). Intrusive rocks similar to these occur as a semicircular polyphase complex that extends five kilometres south to the northern slopes of Cerro Cascasca, and may extend east under the Ujina Ignimbrite (Fig. 3.24).

The earliest and most widespread phase in the complex is a distinctive seriate blue-grey plagioclase-biotite-(orthoclase) granodiorite which shows strong labradorescence (KLgdr). In the north and west of this area the granodiorite is intruded by irregular pods <1 km wide of black, magnetic, fine to coarse grained, variably porphyritic plagioclase-hornblende-clinopyroxene gabbro (KLgbr). The gabbros are in turn intruded by small, elongate < 200 m-wide bodies of equigranular dark grey diorite (KLdio). A discrete coarse-grained plug of equigranular dark grey anorthosite truncates the gabbro-diorite complex in the north-central part of the complex (KLant), and the south of the complex is dominated by a coarse grained beige biotite syenite (KLsyn; Fig. 3.24).

Highly localised epidote-garnet-albite exoskarn is developed about the margins of the Tolaun intrusive complex in andesites and calcareous sedimentary units. There is no other hydrothermal alteration associated with these intrusions.

3.15.2 Microsyenite dykes (KLmsy, 68.4 ± 0.7 Ma, and 69.5 ± 1.2 Ma)

Narrow (< 2 m wide) saccharoidal to fine grained equigranular white to beige-pink, orthoclase ± quartz ± biotite microsyenite dykes cut the Tolaun intrusive complex and occur commonly across the entire Collahuasi district (Figs. 3.4, 3.24). They typically occur as isolated intrusions, except for a dense cluster of irregular, laterally discontinuous dykes south of the abandoned San Nicolas mine workings (Fig. 3.24).

3.15.3 Cerro Sallihuinca stock (TEmnzq, Lutetian)

Cerro Sallihuinca is located in the northern central map area (Fig. 3.25). It is composed largely of a medium to coarse-grained seriate plagioclase-phyric beige quartz monzonite. The southwestern part of the stock is characterised by sparse

aplitic vein-dykes and common 1-10 cm-diameter patches of black and white tourmaline-quartz alteration with arborescent form (Fig. 3.20e). Sparse mesoscopic aplite dyke-veins. In thin section the tourmaline is strongly pleochroic brown-blue.

These Cerro Sallihuinca stock, as well as stocks exposed to the north on Cerro Cuno and Cerro remedios, were all emplaced at around 42 Ma (Damm et al., 1986; Tomlinson et al., 2001a). Intrusion of the stocks was therefore approximately contemporaneous with eruption of the youngest known Icanche Formation volcanic facies. The relatively coarse grainsize (4-6 mm) of the Sallihuinca and Cerro Cuno stocks (Table 3.5) suggests that they cooled more slowly than- and were probably emplaced more deeply than the finer-grained porphyritic stocks for which fluid inclusion data suggest emplacement depths of 1-2 kms (Rowland and Wilkinson, 1999; Masterman et al, 2005). This implies that the present day distribution of the

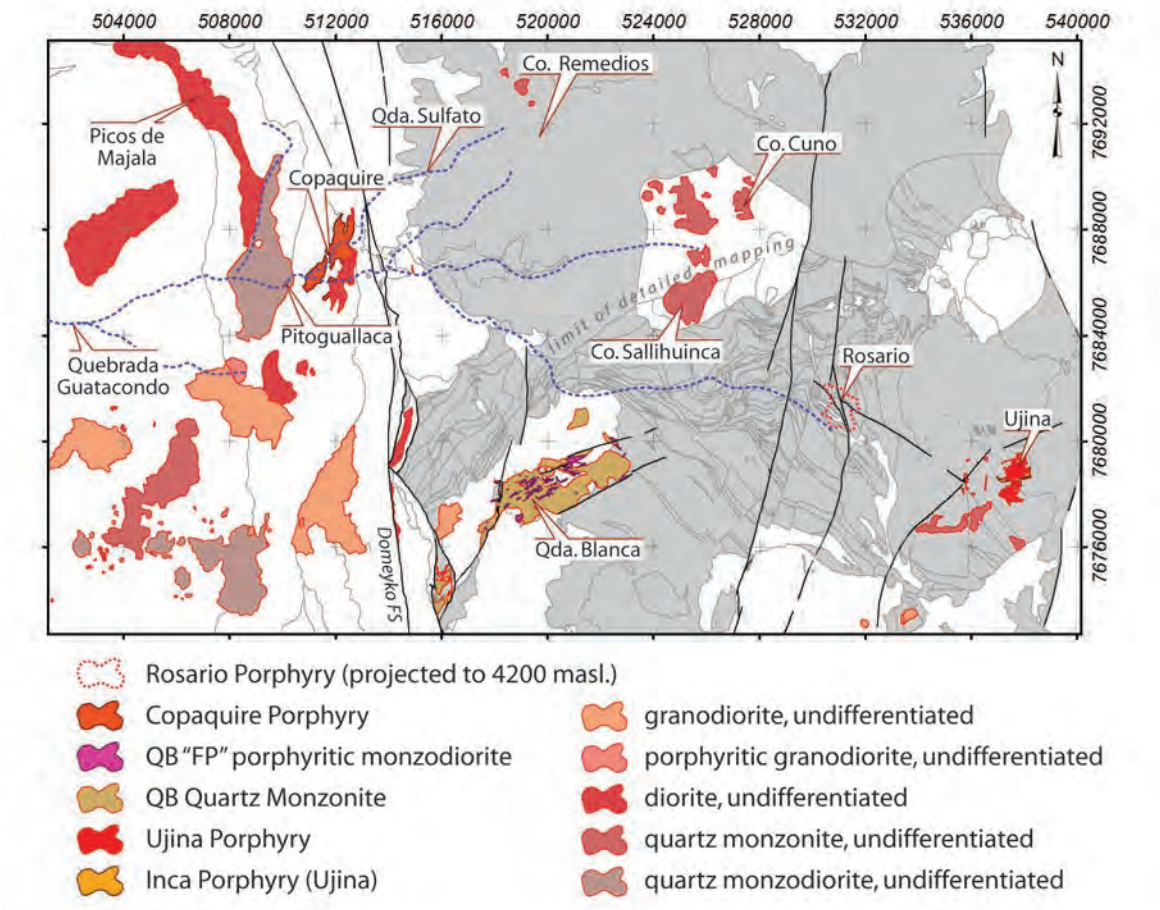

Figure 3.25. Distribution of Eocene to earliest Oligocene intrusive rocks in the Collahuasi district. Background and line map elements are the same as Figure 3.21. Dashed red linework indicates surface projection of the Rosario porphyry at ~4200 masl. Locations mentioned in the text are indicated. Abbreviations: FS = fault system, Co. = Cerro, Qda. = Quebrada. Grid divisions are 2 km.

Icanche Formation in the Collahuasi district is the basal remnant of an originally much thicker volcanic sequence.

3.15.4 Pitoguallaca stock (TEmzdq, Bartonian)

A seriate medium to coarse-grained brown-grey quartz monzodiorite crops out in the central Quebrada Guatacondo and hosts a small abandoned mine called Pitoguallaca. It is approximately 2.5 km wide and extends almost 7 kilometres N-S and has subvertical lateral margins. Intrusion of the stock truncated the Picos de Majala diorite (Tomlinson et al., 2001a).

At the current level of exposure Pitoguallaca is the largest of several dozen Middle Eocene intermediate stocks that were emplaced in the fold-and-thrust belt to the west of the Domeyko Fault (Vergara and Thomas, 1984; Damm et al., 1986; Maksaev, 1990; Tomlinson et al., 2001a). A mesoscopic block of strongly brecciated and pervasively epidotised rock near the eastern margin of the stock is likely a roof pendant of the calcareous lower Jurassic strata. Patchy, epidote-pyrite-garnet endoskarn developed locally along the eastern margin of the intrusion, but no other hydrothermal alteration is known to be associated with this intrusion.

3.15.5 Quebrada Blanca intrusive complex (TEqbfp and TEpqm, Priabonian)

The Quebrada Blanca (QB) intrusive complex (Figs. 3.4, 3.25) comprises three principal stages: a voluminous equigranular to weakly porphyritic pink-beige quartz monzonite (TEpqm) which is cut by mid- to dark grey quartz-present and quartz-absent varieties of strongly porphyritic monzonodiorite dykes (TEqbfp). These plagioclase-(quartz-biotite) phyric dykes show systematic preferred orientation (Chapter 4) and are considered to be intimately related to development of the Quebrada Blanca hydrothermal system (Fam, 1974; Lehmann, 1980; Hunt et al., 1983; Martini Vargas, 1984; Hunt, 1985; Rowland, 1998). Rowland (1998) suggested that intrusion of some andesitic dykes in the Quebrada Blanca area was broadly contemporaneous with emplacement of the main complex, although field relationships to support or deny this assertion were not observed in this study.

3.15.6 Copaquire intrusive complex (TEpcq, Priabonian)

The polyphase Copaquire intrusive complex crops out intermittently around the

TABLE 3.5. Petrological characteristics of the Late Eocene intrusive rocks of the Collahuasi district (*continues on next page*).

Lithofacies[a] / Age[a] / Geometry	Crystal Characteristics[b,c]	References
Copaquire Intrusive Complex		
Tonalite. TE.pcq. 36.1 Ma.‡^˜ [d]. Fine to medium-grained plagioclase-quartz-biotite phyric tonalite. Elongate irregular stock >3 km^2.	PLAG: 35-50% subhedral <3.5 mm, zoned An_{12-35}. KFS: 2-6% subhedral xls <3 mm. QTZ: 5-7% anhedral xls <3 mm. BT: 2-8% anhedral xls <2 mm. MT: 1-2% anhedral xls <0.6 mm. G'MASS: qtz>kfs-bt>plag	Sillitoe and Neumann, 1972; Hollister, 1975; ‡Maksaev, 1990; ^Boric et al., 1990; ˜Hammerschmidt et al., 1992; this study.
Quartz monzonite. TE.pcq. 36.1 Ma.‡^˜ [d]. Fine to medium-grained plagioclase-orthoclase-quartz phyric quartz monzonite porphyry. Elongate irregular stocks and dykes >1.5 km^2.	PLAG: 12-20% subhedral <3 mm, zoned An_{5-30}; QTZ: 5% subhedral <3 mm; BT: 3% subhedral <0.8 mm; G'MASS: kfs>qtz	
Ujina Intrusive Complex		
Ujina Porphyry. TE.puj. 35.2 Ma.* Fine to medium grained light grey intensely plagioclase phyric quartz monzonite. Irregular dumbbell-shaped stock, ~1.5 km^2.	PLAG: 45-50% subhedral <6 mm; BT: 2-5% subhedral <0.7 mm; G'MASS: qtz>kfs>>mt.	Vergara, 1978; DeBeer and Dick, 1994; Bisso et al., 1998; *Masterman et al., 2004, 2005; **this study.
Inca Porphyry. TE.pic 34.7 Ma.** Fine to coarse grained grey-green intensely plagioclase phyric monzodiorite. Irregular short dykes and elongate stocks <500 m long.	PLAG: 26% euhedral blocky <4 mm, An_{4-10}; KFS: 4% anhedral xls <2 mm; QTZ: 2% anhedral <3 mm; HBL: 1% subhedral <1 mm, chloritised; G'MASS: plag-qtz.	
Rosario Porphyry		
Rosario Porphyry. TE.pro. 34.4 Ma.* Fine to medium grained, light grey, strongly plagioclase phyric quartz monzonite stock with numerous ?irregular roof dykes.	PLAG: 20% subhedral <3.5 mm, An_{20-36}, and 5-10%, An_{2-8}; QTZ: 7-10%, <4 mm round, resorbed; BT: 3-5%, <2 mm; G'MASS: qtz-plag>kfs-bt (description of Masterman, 2003)	Munchmeyer et al., 1984; Lee, 1994; *Masterman et al., 2004; 2005.

Footnotes a.), b.) and c.), and abbreviations are the same as Tables 3.1, 3.2 and 3.3.

d.) Ages given are the weighted averages of data compiled in Tomlinson et al. (2001a) for alteration related to the youngest, mineralised intrusive phase.

TABLE 3.5. *continued:* Petrological characteristics of the Late Eocene - Oligocene intrusive rocks of the Collahuasi district.

Lithofacies[a] / Age[a] / Geometry	Crystal Characteristics[b,c]	References
Eocene unmineralised stocks		
Cerro Sallihuinca Stock. TEmnzq. 41.9 Ma.* Medium grained, light pink to cream, seriate plagioclase phyric quartz monzonite. Multiple lobate stocks together ~3 km^2.	PLAG: 40% subhedral blocky <4 mm, zoned An_{0-8}. TM: 1-12% subhedral integrowths with granophyric qtz. G'MASS: kfs-qtz>bt>mt.	Barrilla Cortez, 1986; *Tomlinson et al., 2001a; this study.
Pitoguallaca Stock. TEmzdq. 37.8 Ma.* Medium grained equigranular tan-grey biotite-bearing quartz monzodiorite. Elongate polygonal stock >8 km^2.	PLAG: 68% subhedral <4 mm, An_{37}; BT: 6% subhedral <2 mm; QTZ: 14% anhedral <1 mm; KFS: 8% anhedral <1 mm; HBL: 4% subhedral prismatic <4 mm, accessory oxides.	*Tomlinson et al., 2001a; Amilibia and Skarmeta, 2003; this study.
Quebrada Blanca Intrusive Complex		
Q.B. Quartz Monzonite. TE.pqm. ≥36.7 Ma.†[d]. Medium grained weakly seriate light pink-grey quartz monzonite. Rhombic stock >8 km^2 and numerous lateral dykes.	PLAG: 30-40% subhedral <3.5 mm, An_{31}; KFS: 30-40% anhedral <2 mm; QTZ: 20-30% anhedral <3.5 mm; BT: 1-3% subhedral <0.5 mm. MT: 1% euhedral equant xls <0.4 mm. G'MASS: qtz-kfs.	Fam, 1974; Lehmann, 1980; Ware et al., 1981; †Hunt et al., 1983; Martini Vargas, 1984; Hunt, 1985; ‡Maksaev, 1990, ^Boric et al., 1990; Rowland, 1998; Dserochers et al., 2001; this study.
Q.B. Feldspar Porphyry 1. TE.qbfp. ≥36.7 Ma.‡^[d]. Dark grey fine to coarse grained, intensely plagioclase-biotite phyric "crowded" monzodiorite. Systematically oriented dykes <50m wide and <500 m long.	PLAG: 60% euhedral <4 mm, calcic cores with thin irregular albitic rims; BT: 5% subhedral <2.5 mm; QTZ: 8% subhedral <3 mm; MT: 1% subhedral <0.7 mm. G'MASS: qtz-kfs-bt.	
Q.B. Feldspar Porphyry 2. TE.qbfp. 36.7 Ma.‡^[d]. Mid grey fine to coarse grained, plagioclase-biotite phyric quartz monzodiorite. Systematically oriented dykes <10m wide and <250 m long.	PLAG: 26% subhedral <4 mm, An_{12}, with calcic cores and irregular ?albitic rims; QTZ: 6% anhedral rounded xls <3 mm; BT: 2% euhedral <3 mm. MT: 1% subhedral aggregates <0.4 mm; G'MASS: kfs>qtz-bt-mt.	

Footnotes a.), b.) and c.), and abbreviations are the same as Tables 3.1, 3.2 and 3.3.

d.) Ages given are the weighted averages of data compiled in Tomlinson et al. (2001a) for alteration related to the youngest, mineralised intrusive phase.

steep walls of Quebrada Guatacondo and Quebrada Sulfato and defines an irregular body that is elongate NNE-SSW and includes numerous roof pendants (Fig 3.25). The northwestern part of the complex is fine to medium-grained plagioclase-quartz-biotite phyric tonalite porphyry, whereas the southeastern part is fine to medium-grained plagioclase-orthoclase-quartz-(biotite)-phyric quartz monzonite porphyry. Pervasive alteration and widespread cover obscure the contact relationships between these two phases, but local dyke-like morphology of the quartz monzonite (Chapter 4; Sillitoe and Neumann, 1972) suggests that it is the younger of the two.

3.15.7 Ujina intrusive complex (TEpuj and TEpic, 34.4 ± 0.7 Ma)

The mineralised Ujina intrusive complex has an irregular N-S oriented dumbbell-shape in plan view (Fig. 3.25). It has subvertical walls defined from extensive exploration drilling (CMDIC mine database). The earliest and most voluminous phase, the Ujina Porphyry (TEpuj), is a medium-grained plagioclase-biotite phyric monzonite (Vergara, 1978; Dick et al., 1994; Bisso et al., 1998; Masterman et al., 2004). The Ujina Porphyry and the main mineralisation stages are cut by numerous irregular and discontinuous E to ENE-trending dykes and elongate stocks of a coarse-grained densely plagioclase-phyric monzodiorite, known as the Inca Porphyry (Dick et al., 1994; Bisso et al., 1998). Small bodies of porphyritic intrusive rocks visually similar to the Ujina Porphyry occur commonly in the area immediately west of Ujina, but are generally not associated with hydrothermal alteration (Fig. 3.25, Chapter 4).

3.15.8 Rosario Porphyry (TEpro, 34.2 ± 0.8 Ma)

The mineralised Rosario Porphyry did not crop out at surface, but is known from exploration drilling at the Rosario porphyry copper deposit (Fig. 3.25; Munchmeyer et al., 1984; Lee, 1994; Masterman et al., 2005) and has subsequently been exposed by mining. At shallow levels it is weakly elongate NW-SE (Munchmeyer et al., 1984) but recent deep drilling suggests that it becomes almost equant in plan view below ~4000 m elevation (Fig. 3.25; CMDIC mine database). Multiple intrusive phases have not been reported from Rosario, perhaps because of widespread pervasive advanced argillic alteration that is associated with late stage epithermal mineralisation (Dick et al., 1994; Lee, 1994; Bisso et al., 1998; Masterman et al.,

2005). In late 2005, drilling in the southwestern part of the deposit revealed lithic inclusions of a strongly potassically altered quartz-phyric porphyry within the Rosario Porphyry, suggesting that at least one older intrusive phase exists at depth (Chapter 4).

3.16 U-Pb Geochronology

3.16.1 Introduction

The quantity and quality of geochronological data for the Collahuasi district and for much of northern Chile is biased toward the mineralised systems of Paleocene and Eocene-Oligocene age (Vergara, 1978; Cornejo et al., 1997; Marsh et al., 1997; Clark et al., 1998; Reynolds et al., 1998; Ballard et al., 2001; Richards et al., 2001a; Rowland and Clark, 2001; Bouzari and Clark, 2002; Masterman et al., 2004). Tomlinson et al. (2001a) list 377 radiometric ages in their SERNAGEOMIN compilation volume for the Domeyko Cordillera between Chuquicamata and Quebrada Blanca, of which more than 80% are younger than Late Cretaceous. A

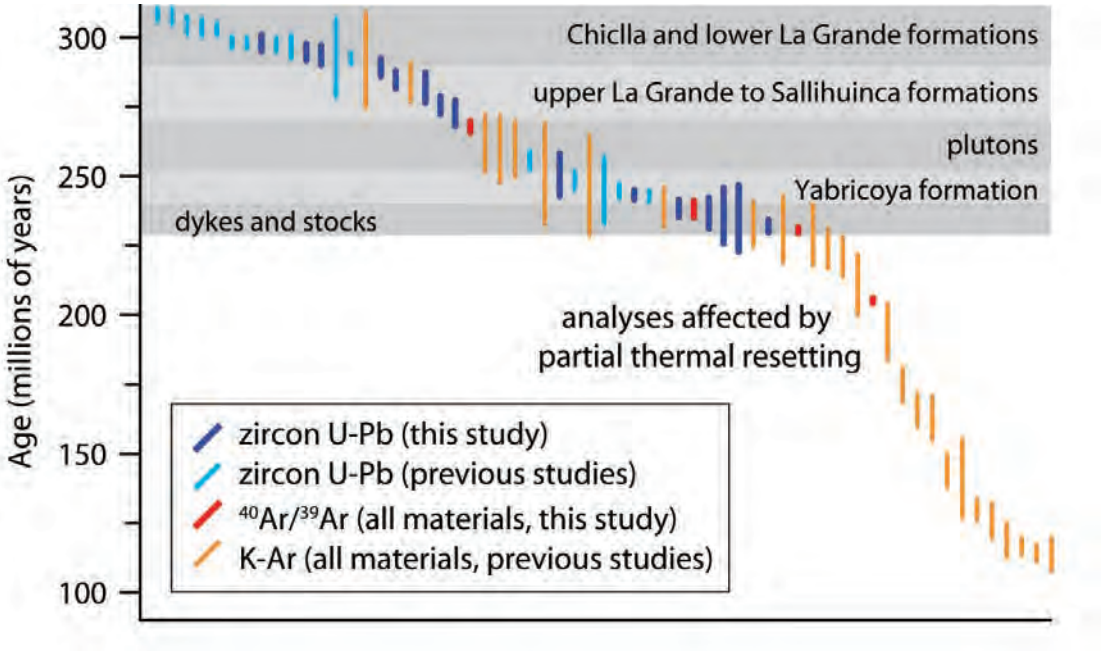

Figure 3.26. Summary of available geochronological data for Late Paleozoic rocks in the four map sheets that cover the Collahuasi district and surrounding area. Data compiled from Huete et al., 1977; Baker and Francis, 1978; Vergara, 1978; Damm et al., 1986; Maksaev, 1990; Tomlinson et al., 2001; Masterman, 2003; Munizaga et al., 2008; and this study. Grey bars are schematic and represent the temporal range of the principal magmatic events recorded by the Peine Group and related intrusions

major aim of this study was to resolve the chronostratigraphy of the Peine Group and apply that information to constrain the interpretation of the structural history of the district. Other studies of the district Peine Group geochronology have either been limited in scope (e.g., Masterman, 2003), or are of restricted use on their own as the samples were not stratigraphically constrained (Munizaga et al., 2008). A subsidiary aim was to confirm using zircon U-Pb geochronology the age of intrusions for which only lower temperature $^{40}Ar/^{39}Ar$ or K-Ar radiometric ages had been reported.

3.16.2 Previous and subsequent work – Middle Paleozoic to Triassic

Previous geochronological studies of the Peine Group in the Collahuasi district (Figs. 3.4, 3.26) reported ages of 292 ± 17 Ma southeast of Quebrada Blanca (K-Ar whole rock (?): Vergara, 1978) and 293 ± 14 Ma at Rosario (6-point LA-ICP-MS zircon U-Pb: Masterman, 2003). In a concurrent study, Munizaga et al. (2008) reported 10 stratigraphically unconstrained SHRIMP zircon U-Pb ages between 308 and 292 Ma (with precision of ± ~1%). These data accord with similar data elsewhere in northern Chile that describe an overall Late Pennsylvanian – Early Triassic age for the Peine Group (Huete et al., 1977; Breitkreuz and Zeil, 1994; Smoje and Marinovic, 1994; Bahlburg and Herve, 1997; Lucassen et al., 1999a; Richards et al., 1999; Tomlinson et al., 2001a; Busquets et al., 2005). The widespread sedimentary intercalation in the Peine Group (the Miembro Medio basin) is constrained below an ignimbrite emplaced at 268 ± 6 Ma in the section east of the Salar de Atacama (Gardeweg, 1988), consistent with a late Carboniferous paleontological age for the sedimentary section further to the south (Osorio and Rivano, 1985; Breitkreuz, 1992).

Pluton emplacement in the Collahuasi district occurred in the Late Permian. A zircon U-Pb age for the Chara Granite records crystallisation at 256.0 ± 3.4 Ma (Damm et al., 1986). Numerous K-Ar age determinations have been made on feldspar and biotite separates from the Escorial Granodiorite (Huete et al., 1977; Ware et al., 1981). Although these authors concede that many of their samples have been affected by hydrothermal alteration, a pair of analyses on hornblende-biotite returned concordant ages of 260 ± 10 Ma. Late Permian plutonism is at the younger end of the ~260 to ~340 Ma range for similar intermediate to felsic plutons from elsewhere in the Domeyko Cordillera (Huete et al., 1977; Tomlinson et al., 2001a).

Considerable scatter to younger ages among almost 30 other K-Ar dates reported for large plutons of the Collahuasi district is generally attributed to partial resetting (Figs. 3.26, 3.27: Vergara, 1978; Ware et al., 1981; Munchmeyer et al., 1984). These include a discrete cluster from 244 to 235 Ma (Fig, 3.26), consistent with a regional thermal event and widespread intrusive and extrusive activity around and to the immediate north of Chuquicamata dated by biotite K-Ar and zircon U-Pb in the range 229-238 Ma (Tomlinson et al., 2001). Masterman (2003) reports an imprecise six-grain zircon U-Pb age of 245 ± 12 Ma for the Collahuasi Porphyry at Rosario, suggesting that it relates to this event. More precise zircon U-Pb ages between 243 and 248 Ma have subsequently been reported from the blind La Profunda intrusion and from the Characolla prospect (Munizaga et al., 2008). $^{40}Ar/^{39}Ar$ analyses of illite from Characolla indicate that the hydrothermal system there cooled at the same time (within analytical uncertainty) of the youngest intrusive phases (A. Clark, written commun. 2006). Alteration at the El Loa porphyry prospect, located about 10 km SSE of the Collahuasi district is also Triassic in age, but is somewhat younger, and formed around 223 Ma (Ware et al., 1981; Tomlinson et al., 2001a).

3.16.3 Previous Work – Late Cretaceous to Oligocene

There are four principal Late Cretaceous to Oligocene magmatic events revealed by the body of geochronological research in the Collahuasi district (Fig. 3.27).

The Late Cretaceous event was the least well constrained by existing work, and was known primarily from samples of the Cerro Empexa Formation west of the Domeyko fault system (Tomlinson et al., 2001a). The only known Cretaceous rocks further east belonged to the northeastern part of the Tolaun intrusive complex. Baker et al. (1977) reported a K-Ar age of 71.1 ± 2.7 Ma from a chloritised biotite separate from a diorite, and Tomlinson et al. (2001a) reported a biotite K-Ar age of 72 ± 2 Ma for a monzodiorite in approximately the same location. Mafic to intermediate intrusions of late Cretaceous age occur sporadically throughout the Domeyko Cordillera. These include a large polyphase complex that makes up the Cerros de Montecristo, northwest of Chuquicamata (69 to 63 Ma: Maksaev et al., 1988; Ladino, 1998; Tomlinson et al., 2001a) and the Cerros Macata and Querone, southwest of Quebrada Blanca (Tomlinson et al., 2001a, and references therein). The

mineralised Cerro Colorado intrusive complex, 100 km NNW of Collahuasi, formed at 72-63 Ma (Huete et al., 1977; Rogers, 1985; Tomlinson et al., 2001a). Further south, Cretaceous intrusive complexes are extensively developed in the Escondida porphyry-Cu camp, where three distinct intrusive compelxes were emplaced between ~80 and 66 Ma (Urzua, 2009).

The age of Eocene-Oligocene intrusions of the Collahuasi district has been the subject of numerous studies (Vergara, 1978; Ware et al., 1981; Damm et al., 1986; Maksaev, 1990; Hammerschmidt et al., 1992; Clark et al., 1998; Tomlinson et al., 2001a; Masterman et al., 2004). Some 52 reported ages demonstrate magmatic and hydrothermal activity along the Domeyko Cordillera between ~46 and ~34 Ma.

Most of the older intrusions are unmineralised. Tomlinson et al. (2001a) reported a biotite K-Ar age of 41.9 ± 1.2 Ma from the Cerro Sallihuinca monzonite (Fig. 3.25). The stock immediately to the north on Cerro Cuno yielded a zircon U-Pb age of 42.7 ± 0.6 Ma (Damm et al., 1986) and another to the NW on Cerro Remedios yielded

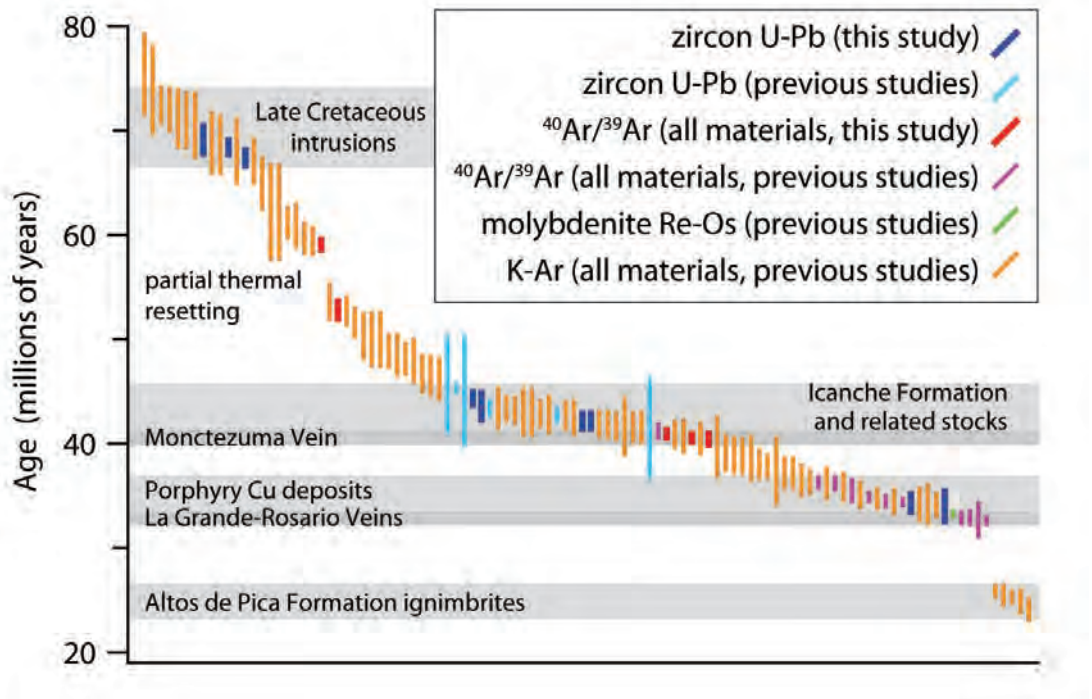

Figure 3.27. Summary of available geochronological data for Cretaceous to Oligocene rocks in the four map sheets that cover the Collahuasi district and surrounding area. Data compiled from Huete et al., 1977; Baker and Francis, 1978; Vergara, 1978; Damm et al., 1986; Maksaev, 1990; Hammerschmidt et al., 1992; Tomlinson et al., 2001; Masterman et al., 2004; and this study. Grey bars are schematic and represent the temporal range of the four principal magmatic events and two exclusively hydrothermal events recognised in the district. At this scale of presentation, the relative timing of the porphyry Cu deposits cannot easily be resolved.

a zircon U-Pb age of 41.5 ± 4.7 Ma (Damm et al., 1986). In the western Collahuasi district, Damm et al. (1986) reported a zircon U-Pb age of 45.0 ± 5.2 Ma the Picos de Majala diorite (Fig. 3.25), and Tomlinson et al. (2001a) reported a biotite K-Ar age of 37.8 ± 1.0 Ma for the Pitoguallaca Stock.

Intrusions related to porphyry mineralisation were emplaced primarily from 37-36 Ma (Quebrada Blanca and Copaquire) and 35-34 Ma (Ujina and Rosario). There are four reported whole rock and biotite K-Ar ages for the QB intrusive complex considered to reflect the emplacement age (Tomlinson et al., 2001a). Ages for the early quartz monzonite are indistinguishable from ages for the cross-cutting monzodiorite dykes (Section 3.15.5), such that the weighted average of 36.7 ± 1.3 Ma (recalculated from Ware et al., 1981; Hunt et al., 1983; Maksaev, 1990) represents a best estimate of the approximate emplacement age of the complex as a whole. This age is consistent with recent zircon U-Pb and molybdenite Re-Os geochronology for the intrusions and hydrothermal mineralisation at Quebrada Blanca (M. LaPointe, Aur Resources, pers. commun., 2005). Further biotite K-Ar and $^{40}Ar/^{39}Ar$ ages (Maksaev, 1990) reveals a second discrete thermal event at 34.9 ± 0.4 Ma.

There are five reported biotite K-Ar and $^{40}Ar/^{39}Ar$ ages for the Copaquire intrusive complex (Maksaev, 1990; Hammerschmidt et al., 1992). The weighted average of these dates is 36.1 ± 0.7 Ma, which is generally interpreted to be a minimum age for intrusion and the related hydrothermal system (Tomlinson et al., 2001a).

At Ujina, Masterman et al. (2004) report a biotite $^{40}Ar/^{39}Ar$ plateau age for the Ujina Porphyry of 35.2 ± 0.3 Ma, which they consider to be the minimum age of the intrusion. Intrusion of the post-mineral Inca Porphyry at 34.7 ± 0.3 Ma (Masterman et al., 2004) therefore brackets porphyry mineralisation at Ujina.

The Rosario porphyry Cu-Mo deposit is the largest and the youngest in the Collahuasi district. Masterman et al. (2004) report indistinguishable $^{40}Ar/^{39}Ar$ plateau ages for magmatic biotite from the Rosario Porphyry and hydrothermal illite from mineralisation at Rosario, of 34.4 ± 0.3 Ma and 34.5 ± 0.5, respectively.

Sampling Strategy

U-Pb geochronology is used here to constrain the complex volcano-sedimentary stratigraphy and also to confirm the previous results of radiometric chronometers with blocking temperatures in the hydrothermal regime. Stratigraphic samples were chosen that belong to dominant, easily recognised mappable units. Where possible, these were collected toward the upper- and/or lower limits of stratigraphic sequences that are separated by mapped unconformities.

3.16.4 Summary of Analytical Methods

Laser ablation inductively-coupled mass spectrometry (LA-ICPMS) zircon U-Pb geochronology has been widely applied in the last 10 years (e.g., Machado and Gauthier, 1996; Fernandez-Suarez et al., 1998; Ballard et al., 2001; Berry et al., 2001; Luo et al., 2004; Murphy et al., 2004; Kesler et al., 2005). The fundamentals of the technique are well described, although subtly different between laboratories (Belousova et al., 2001; Harris et al., 2004; Jackson et al., 2004; Simonetti et al., 2005; Chang et al., 2006; Paton et al., 2010). For brevity, a summary is provided here and the details of the methods used in this study are presented in Appendix III.

Geochronology samples were crushed, milled and sieved to –300 μm, and zircons were concentrated by panning. Colourless to pale pink and brown idiomorphic crystals >30μm on the short axis (Fig 3.28a) were picked under a petrographic microscope, then mounted in epoxy blocks, ground and polished. Transmitted and reflected light optical microscopy, and SEM cathodiluminescence (Fig. 3.28b) were used to identify crystal zoning and avoid crystals with prominent flaws and/or inclusions. LA-ICP-MS zircon U-Pb analyses conducted in this study include grain populations per rock sample of $n \leq 26$ grains. This is small compared to n = 30-80 results reported for some similar geochronological techniques (Ballard et al., 2001; Harris et al., 2004; Kesler et al., 2005). However, n=4 grains can be shown to be sufficient to identify up to 47% whole grain inheritance, and n=12 is sufficient to identify up to 78% whole grain inheritance at 95% confidence (Appendix III).

In this study, isotopic compositions of ablated material were measured using an Agilent HP4500 ICPMS coupled with a Merchantek 266 nm Nd:YAG laser at the Centre of Excellence in Ore Deposits, University of Tasmania. Analyses were performed with a 50μm diameter beam, a laser repetition rate of 5 Hz, and a power

setting of 0.88 mJ, which ablates a pit the width of the beam to ~30 µm depth. The ICP-MS was operated in time-resolved mode, collecting one point per mass per sweep of the mass range with a dwell time of 10 msec/mass. Spots to be analysed were cleaned with four single laser pulses at 1 Hz prior to the commencement of mass detection. After cleaning, background count rates on each mass were taken for 30 seconds prior to each ablation. Each analysis was followed by a 2 minute washout period during which the signal intensities returned to background levels.

Analyses were performed as runs of 12 unknowns bracketed by two sets of six standards, using the same analytical conditions. Curves describing both internal down-pit isotopic fractionation (Fryer et al., 1993; Hirata and Nesbitt, 1995) within each 30-second analysis, and instrumental drift over the 6-12 hour analysis periods were defined from results for the primary standards. The measured $^{206}Pb/^{238}U$, $^{207}Pb/^{235}U$, and $^{207}Pb/^{206}Pb$ ratios of the unknowns were corrected for drift based on

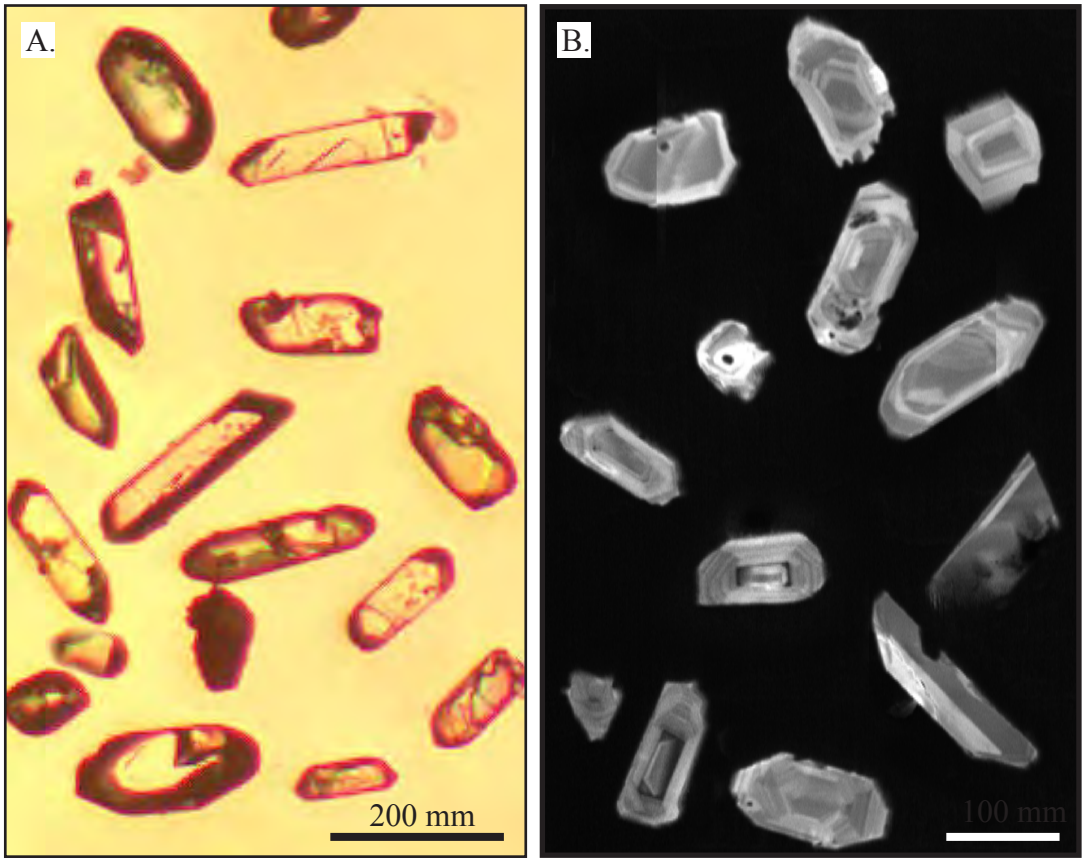

Figure 3.28. Images of typical zircons analysed by LA-ICP-MS in this study. A) plane light view showing largely inclusion-free euhedral prismatic and stubby crystals in the Ornajuno Rhyolite Breccia (TRy4), sample 271004_03. B) cathodiluminescence image of stubby euhedral crystals with weak oscillatory zonation common to zircons in Peine Group rocks, sample 180304_01, uppermost Chiclla formation (Pzpc1).

segment-wise linear regression of deviation from expected values for the internal standard, incorporating a drift correction error specific to the time of each analysis. Measured ratios for each sweep were automatically matched with- and corrected for down-pit fractionation by comparison with identical time intervals for the standards. Data were then reduced and plotted as time-resolved spectra using the LAMTRACE program (van Achterbergh et al., 2001).

Data reduction included common Pb correction and trimming of ablation intervals that exhibited anomalous compositions. Criteria for interval trimming were low-Zr non-zircon inclusions, elevated common Pb, elevated Nd, elevated U associated with apparent Pb loss (Appendix III), apparent mixing between crystal zones of different concordant U-Pb isotopic ratios, and/or rare unstable instrumental recording. Corrections for common Pb were applied using the single step ^{208}Pb method (Cumming and Richards, 1975). The Isoplot add-in for Excel (Ludwig, 2001) was then used to calculate weighted means and 2σ internal errors of the zircon grain populations from each rock sample.

Primary and secondary standards analysed in conjunction with unknowns yielded results within error of the accepted ages for those standards. Errors associated with the analytical uncertainty of the primary standards (Temora-1: 1.1%, and NIST91500: 0.33%; Appendix III) were propagated through error calculations of unknowns using an established algorithm (e.g. Meffre et al., 2007; 2008). Two secondary standards were also analysed and yielded results within error of their expected values. Twenty analyses of the Los Picos 98-521 zircon (42.6 ± 0.2 Ma.: C.Allen pers. commun.), and nine of the Mud Tank zircon (732 ± 5 Ma.: Black and Gulson, 1978), returned mean ages (2σ) of 41.7 ± 0.7, and 733 ± 34, respectively. The final precision reported on unknowns in this study is comparable with precision reported from technically similar studies (Black et al, 2003; Harris et al., 2004; Solari et al, 2009; Paton et al, 2010).

3.16.5 U/Pb Age Data

New LA-ICP-MS geochronology analytical results and grain population statistics are listed in Table 3.6 and presented as inverse concordia plots in Figures 3.29 to 3.31. Individual grain analyses are presented in Appendix III. All samples analysed were

euhedral crystals with weak to moderate oscillatory zoning (Fig. 3.28). In samples 190404_08, 180304_01, 200404_02, and 180504_10, crystals >200 µm were analysed in core and rim positions. At the relatively coarse 50 µm resolution of the technique (laser beam diameter), no chronological zonation was recognised.

Chiclla Formation. The subaerial volcanic Chiclla Formation is dated here by four samples that span the entire section in the Monctezuma-La Grande area. A rhyolite from the Monctezuma area (Pzpc.9; Sample 170504_13) is dated at 295.1 ± 3.1 Ma (n = 13). The bulk of the analyses extend from concordia toward common lead (Fig. 3.29a). Two grains with large $^{238}U/^{206}Pb$ errors relate to a short session marred by large instrumental drifts. A single grain dated at ~280 Ma is the most uraniferous in the group (1633 ppm U) and has probably suffered minor lead loss. Subtle lead loss may have also affected two further grains, and the calculated weighted average age should be considered a minimum age. A grain dated at ~315 Ma is distinct from the main cluster and is likely to be inherited. A further grain with strong common lead contamination was rejected from calculations and is not plotted on Figure 3.29a.

The Chiclla rhyolitic ignimbrite (Pzpc.5; Sample 190404_08) is dated at 298.5 ± 2.1 Ma (n = 16). The data form a tight cluster on concordia with some scatter toward common lead. No analyses were rejected (Fig. 3.29b).

The QB airstrip rhyolite (Pzpc.2; Sample 241005_02) is dated at 288.6 ± 3.3 Ma (n = 13), which is indistinguishable from a SHRIMP zircon U-Pb age for a rhyolite dome complex at El Colorado in the southwestern map area (Munizaga et al., 2008). The data form a cluster on concordia with some scatter to common lead (Fig. 3.29c). One grain was rejected on the basis of strong common lead contamination, and another, dated at ~305 Ma is likely to be inherited from the lower parts of the Peine Group.

A dacitic ignimbrite sample taken from the Quebrada Copaquire in the northwestern map area (Pzpc.1; Sample 180304_01) is petrologically similar to the uppermost Chiclla Formation dacitic ignimbrite that overlies the QB airstrip rhyolite in the central southern map area. This sample is dated at 289.7 ± 3.3 Ma (n = 12), in agreement with this stratigraphic correlation. The data cluster around concordia with no rejected grains (Fig. 3.29d).

data point error crosses are 2σ in all diagrams

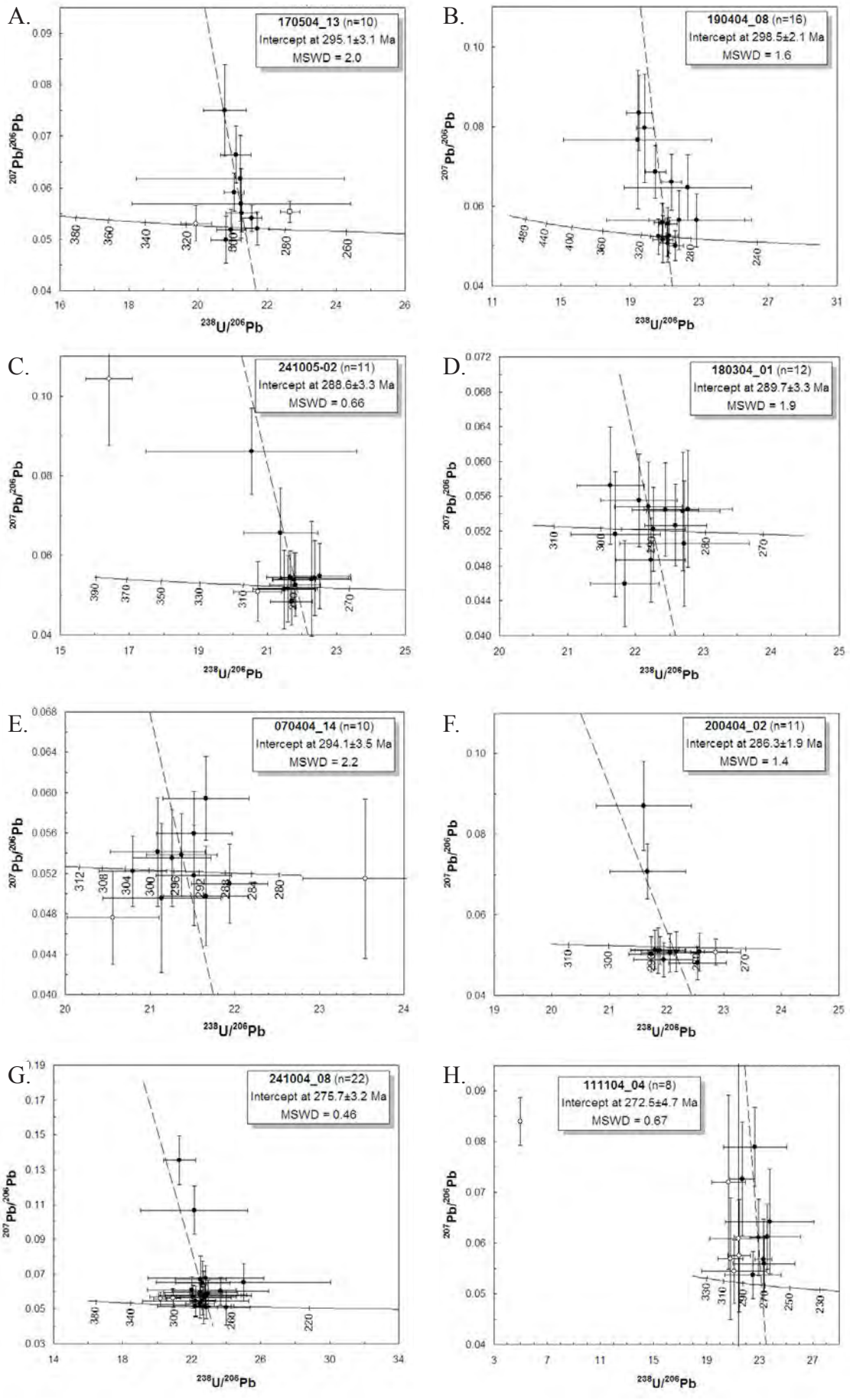

La Grande Formation. The subaqueous andesitic lower La Grande Formation is dated by one sample of a small dioritic dyke at La Grande, and is bracketed between the Chiclla and Cascasca Members. Sample 070404_14 is one of a number of isolated narrow dykes of dacitic composition that cut the Chiclla Formation in drilling at Cerro La Grande. This sample is dated at 294.1 ± 3.5 Ma (n = 12), by a cluster of analyses on concordia (Fig. 3.29e). One grain that yielded an age >300 Ma is interpreted to have been inherited. Another grain that yielded an age <265 Ma contained highly variable trace element contents including HFSE concentrations several orders of magnitude greater than those measured in other zircons analysed in this study for most of the ablation interval. This grain is interpreted to contain abundant microscopic inclusions was rejected on this basis.

Cascasca Formation. The Cascasca rhyolitic ignimbrite (Pzpa1; Sample 200404_02) is dated at 286.3 ± 1.9 Ma (n = 12). The data cluster on concordia with two analyses shifted toward common lead and three that yield younger ages than the main group (Fig. 3.29f). The youngest of these has anomalously high uranium content, may have suffered lead loss (appendix III), and was rejected. The other two appear to be good analyses, are within error of the main group, and have been retained. It is possible that the principal cluster of data are inherited and the two younger points more closely represent the crystallisation age of this unit at ~280 Ma. Lithic fragments are rare in this unit, so inheritance of >75% zircon grains seems unlikely. Regardless, the chronostratigraphic position of the Cascasca Formation is not affected by the ~5 m.y. difference between the two possible interpretations.

Huinquintipa Formation. The Huinquintipa dacite (Pzpg5) occurs throughout the middle and upper Peine Group in the central map area. Sample 241004_08 is

Figure 3.29. Inverse concordia plots for samples from the lower and middle Peine Group. Open points were excluded from regression fitting (for intercept ages) and weighted average calculations (preferred ^{207}Pb-corrected ages). Exclusions are discussed in the text. Dashed line is a best-fit regression pinned at $^{207}Pb/^{206}Pb$ = 0.85 of average late Paleozoic central Andean common lead (e.g., Tosdal and Munizaga, 2003). Numbers on the reference concordia traces are millions of years. A) Lower Chiclla Formation, Pzpc.9, sample 170504_13. B) Chiclla rhyolitic ignimbrite, Pzpc.5, sample 190404_08. C) QB Airstrip Rhyolite, Pzpc.1, sample 241005_02. D) Upper Chiclla Formation, Pzpc.1, sample 180304_01. E) Andesitic dykelet associated with the lower La Grande Formation, Pzpg12, sample 070404_14. F) Cascasca Rhyolitic Ignimbrite Pzpa1, sample 200404_04. G) Huinquintipa Dacite, Pzpg.5, sample 241004_08. H.) Rhyolite of the Sallihuinca Formation, Pzps2, sample 111104_04.

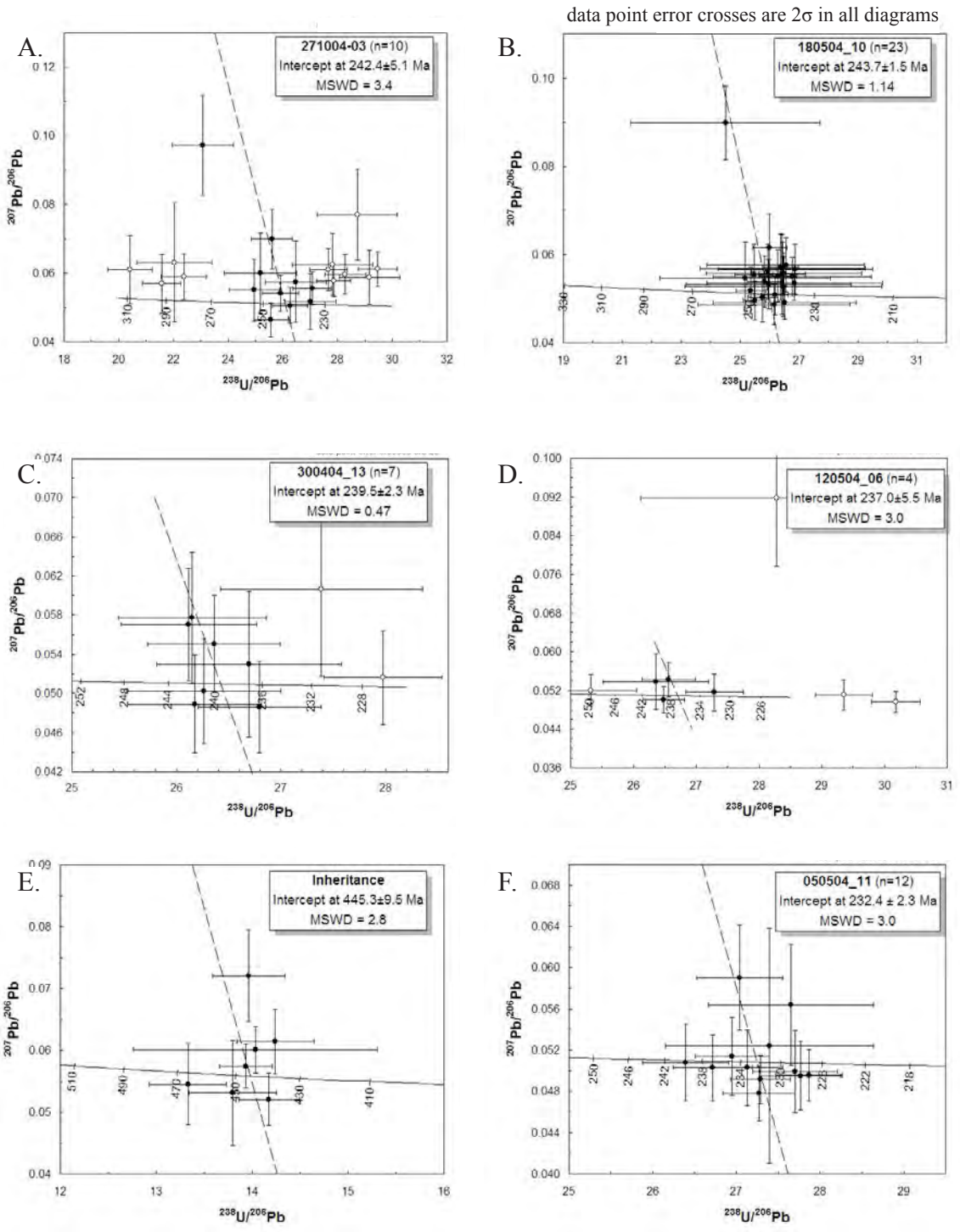

Figure 3.30. Inverse concordia plots for samples from the upper Peine Group and related intrusions. Open points were excluded from weighted average calculations. Dashed line is a best-fit regression pinned at $^{207}Pb/^{206}Pb = 0.85$ of average late Paleozoic central Andean common lead (e.g., Tosdal and Munizaga, 2003). Numbers on the reference concordia traces are Ma. A) Ornajuno Rhyolite Breccia, TRy4, sample 271004_03. B) Yabricoya Dacite, TRy3, sample 180504_10. C-D) Cascasca Dyke Swarm, TRmdd, samples 300404_03 and 120504_06. E) compilation of similar inherited ~440 Ma ages from several Cascasca Dyke Swarm samples. F) Cerro Silvar Porphyry, TR.pcs, sample 050504_11.

taken from an exploration drillhole near Casa de Lata, where it correlates with the lower part of the Huinquintipa Formation. This sample is dated at 275.7 ± 3.2 Ma (*n* = 24), and shows a tight cluster of analyses on concordia with minor scatter toward common lead (Fig. 3.29g). No data were rejected.

Sallihuinca Formation. The prominent flow banded rhyolite that comprises the southern knoll of Cerro Vega (Pzps2; sample 11104_04) is dated at 272.5 ± 4.7 Ma (*n* = 14). The data scatter away from concordia toward common lead, as do five ~300 Ma grains that are likely to have been inherited from the lower Peine Group stratigraphy.

Yabricoya Formation. The strongly lithic polymictic Ornajuno rhyolite breccia (TRy4) is not an ideal material for geochronology, however it was sampled as it is the uppermost felsic lithofacies unit with significant lateral extent in the western map area. Sample 271004_03 is dated at 242.4 ± 5.1 Ma (*n* = 26), and shows both pronounced high U-related lead loss and significant inheritance of lower Peine Group age material (Fig. 3.30a). The preferred age is calculated from a loose cluster of zircons on concordia with minor scatter toward common lead. These have <1000 ppm U (Fig. 3.16C), and are clearly distinct from four older, inherited, zircon grains.

The Yabricoya dacite (TRy3) is petrologically similar to coarsely plagioclase-phyric dacite (leuco-andesite) among the Huinquintipa Formation. However, sample 180504_10 is dated at 243.7 ± 1.5 Ma (*n* = 24) by a tight cluster of analyses on concordia. One grain shows common lead contamination (Fig. 3.30b). This unit is therefore considerably younger than the Huinquintipa Formation.

Triassic Intrusions. The andesitic Cascasca dyke swarm (TRmdd, SiO_2 = 49-62%, Zr = 91-148 ppm) contains very few zircons, but would theoretically have reached Zr saturation (using equations of Watson and Harrison, 1983) at a temperature above the wet solidus for tonalite (Ellis and Thompson, 1986; Schmidt and Thompson, 1996). These rocks are therefore expected to contain indigenous zircon. Samples 300404_13, 120504_06 yielded 9 and 10 zircon crystals larger than 50 μm, respectively, from >2 kg of sample each. Some of these contain > 1000 ppm U and show likely lead loss-related bias to inaccurate young ages (Fig. 3.30c, d; Appendix III). Nonetheless, loose clusters of data from grains with lower U contents allow

data point error crosses are 2σ in all diagrams

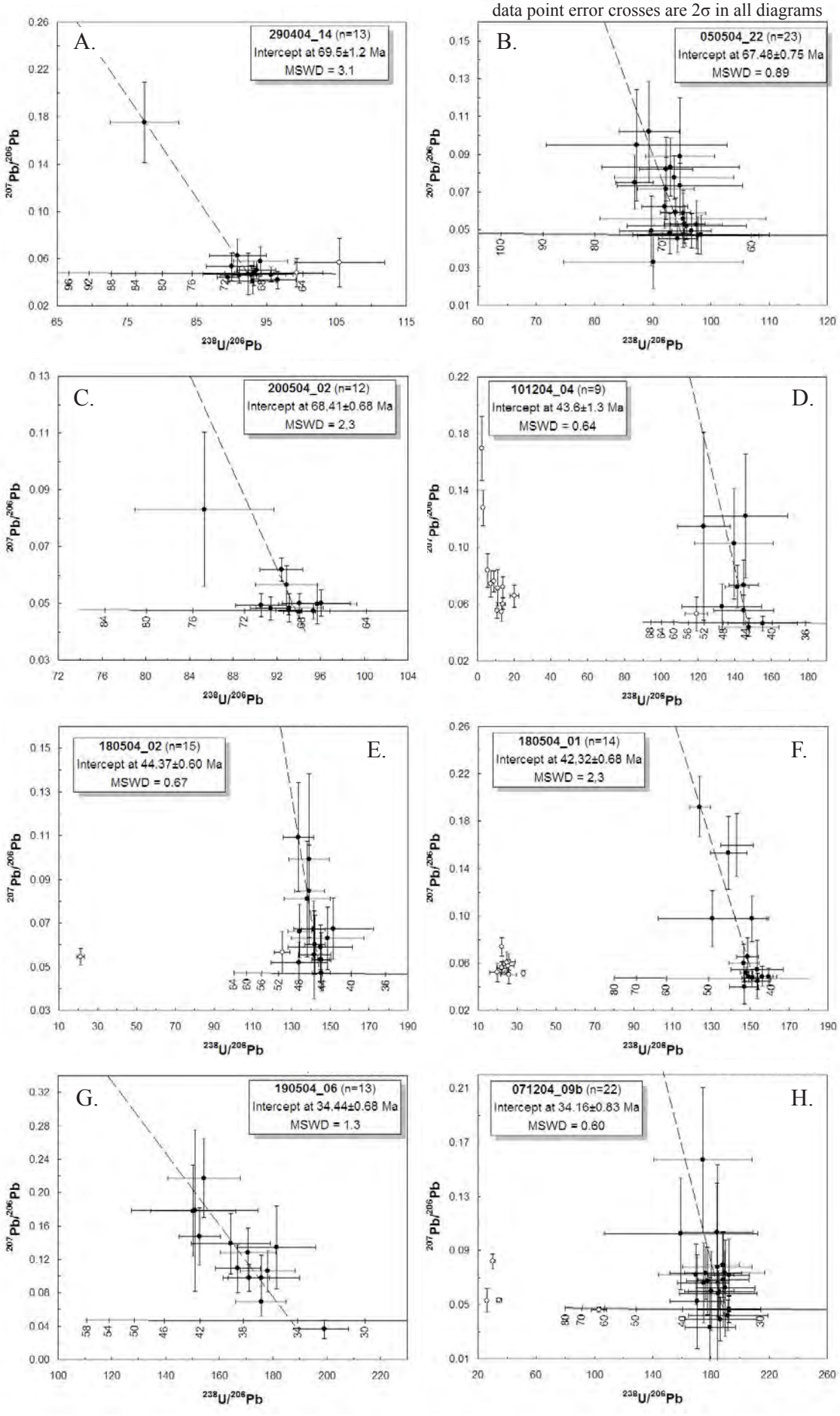

calculation of lower Triassic ages 239.5 ± 2.3 Ma (*n* = 9) and 237.0 ± 5.5 Ma (*n* = 10) for samples from the Coposa-Rosario Road and the Ujina-Rosario conveyor cutting, respectively. Inheritance of Peine Group zircons is evident in sample 120504_06. In contrast, 80% of the zircons analysed from microdiorite dyke sample 120504_05 appear to inherited from an Early Silurian source. Inherited zircons of this age also occur sporadically among the Peine Group samples and together yield a coherent population (Fig. 3.30e) with average age 445 ± 10 Ma (*n* = 7). This overlaps with previous geochronology on a peraluminous granite in basement inlier just outside the map area (431 ± 10 Ma, K-Ar muscovite: Vergara, 1978) and indicates the presence of magmatic rocks of the continental Puneño Arc (Damm et al., 1990) or its terminal Ocloyic tectonic event (Coira et al., 1982) in the basement to the Collahuasi district.

The felsic Cerro Silvar porphyry (TR.pcs; sample 050504_11) is dated at 232.4 ± 2.3 Ma (n = 12) by a cluster of data points on concordia with minor scatter toward common Pb (Fig. 3.30f). No data were rejected. It was therefore intruded at the same time as the youngest Peine Group volcanic rocks in the Chuquicamata area and is the youngest pre-Maastrichian magmatic rock in the Collahuasi district.

Tolaun Intrusive Complex. Three samples of the most felsic, late phases of the Tolaun intrusive complex and related dykes were analysed and all yield Late Cretaceous ages (Table 3.6) within the range for polyphase alkalic mafic to intermediate complexes throughout the Domeyko Cordillera (Tomlinson et al., 2001a, and references therein). A beige microsyenite dyke adjacent to the syenite stock in the southern part of the complex (sample 290404_14) yielded an age of 69.5 ± 1.2 Ma (*n* = 15). The data cluster on concordia (Fig. 3.31a) with one grain that contains significant common lead and two grains that yield young ages that may

Figure 3.31 (following page). Inverse concordia plots for samples of the Icanche Formation and Laramide-Oligocene intrusions. Open points were excluded from weighted average calculations. Dashed line is a best-fit regression pinned at $^{207}Pb/^{206}Pb = 0.85$ of average late Paleozoic central Andean common lead (e.g., Tosdal and Munizaga, 2003). Numbers on the reference concordia traces are millions of years (Ma.). A) Microsyenite dyke, Camino Rosario, KLmsy, sample 290404_14. B) Syenite stock, KLsyn, northern flank of Cerro Cascasa, sample 050504_22. C) Aplite dyke, KLmsy, Rosario Mirador, sample 200504_02. D) Icanche Formation polymictic rhyolite breccia, TEi7, sample 101204_04. E) Icanche Formation monomictic dacite breccia, TEi2, sample 180504_02. F) Icanche Formation rhyolitic ignimbrite, TEi1, sample 180504_01. G) Inca Porphyry dyke, TE.pic, Ujina mine, sample 190504_06. H) Rosario Porphyry, TE.pro, drillhole C293, sample 071204_09b.

TABLE 3.6. Summary of new U-Pb geochronology for the Collahuasi district (*continues on next page*).

Stratigraphic Unit	Sample Number[a]	UTM E[b]	UTM N[b]	n total	n inh.	n rej.	n[c]	Mean $^{206}Pb/^{238}U$ Age ± 2σ error[d]	MSWD	Prob.
Unknowns										
Rosario Porphyry (TE.pro)	071204_09b	530951	7681350	26	4	0	22	34.2 ± 0.8 Ma.	0.60	0.94
Inca Porphyry (TE.pic)	190504_06	537820	7679320	13	0	0	13	34.4 ± 0.7 Ma.	1.30	0.21
Vega Rhyolite Ignimbrite (TEi1)	180504_01	527314	7675003	24	8	1	15	42.3 ± 0.7 Ma.	2.30	0.00
Sallihuinca Breccia (TEi7)	101204_04	523555	7684848	21	12	0	9	43.6 ± 1.3 Ma.	0.64	0.72
Vega Dacite Breccia (TEi2)	180504_02	528430	7685829	17	2	0	15	44.4 ± 0.6 Ma.	0.67	0.84
Cerro Cascasca syenite (KLsyn)	050504_22	536650	7684109	23	0	0	23	67.5 ± 0.8 Ma.	0.89	0.66
Condor aplite dyke (KLmsy)	200504_02	532089	7682279	12	0	0	12	68.4 ± 0.7 Ma.	2.30	0.01
Camino Rosario monzonite (KLmsy)	290404_14	535513	7684664	15	0	2	13	69.5 ± 1.2 Ma.	3.10	0.00
Vega Rhyolite Ignimbrite (inh.)	180504_01	527314	7675003	4	-	-	4	250.7 ± 7.6 Ma.	0.22	0.88
Vega Rhyolite Ignimbrite (inh.)	180504_01	527314	7675003	4	-	-	4	282.1 ± 5.4 Ma.	0.95	0.42
Sallihuinca Rhyolite Breccia (inh.)	101204_04	523555	7684848	3	-	-	3	450 ± 43 Ma.	5.00	0.01
External Standards										
Fish Canyon Titanite: 28.3 + 0.5 (Daze et al. 2003)				6	-	0	6	23.4 ± 2.8 Ma.	1.00	0.41
Los Picos 98_521: 42.6 + 0.2 Ma (C.Allen pers. commun. 2003)				20	-	2	18	41.4 ± 0.7 Ma.	1.90	0.01
Mud Tank: 732 + 2 Ma (Black and Gulson, 1978)				9	-	1	8	733 ± 34 Ma.	2.70	0.01

a.) The original "TJI" prefix has been omitted. The Rosario Porphyry sample is equivalent to R200221 of Masterman (2003)

b.) The population of grains used to calculate the weighted mean $^{206}Pb/^{238}U$ age.

c.) ^{207}Pb-corrected for common Pb, 95% confidence interval.

Abbreviations: inh. = inherited; rej. = rejected; corr.= corrected; prob. = probability. Instrumental parameters: 213 nm laser @ 5 Hz, 72-88% power, 0.37mJ, 30 µm spot size, HP4500 quadrupole ICPMS. Absolute element concentration assumed stoichiometric zirconium in the zircons and used NIST 612 to calculate mass bias.

TABLE 3.6. *(continued)* Summary of new U-Pb geochronology for the Collahuasi district

Stratigraphic Unit	Sample Number[a]	UTM E	UTM N	n total	n inh.	n rej.	n[b]	Mean $^{206}Pb/^{238}U$ Age ± 2σ error[c]	MSWD	Prob.
Unknowns										
Cerro Silvar porphyry (TR.pcs)	050504_11	533991	7687192	12	0	0	12	232.4 ± 2.3 Ma.	3.00	0.00
Cascasca Dyke Swarm (TRmdd)	120504_06	536649	7680439	10	1	5	4	237.0 ± 5.5 Ma.	3.00	0.03
Cascasca Dyke Swarm (TRmdd)	300404_13	533002	7684445	9	0	2	7	239.5 ± 2.3 Ma.	0.47	0.83
Ornajuno Rhyolite Breccia (TRy4)	271004_03	515104	7681796	26	6	10	10	242.4 ± 5.1 Ma.	3.40	0.00
Yabricoya Dacite (TRy3)	180504_10	530323	7684616	24	0	1	23	243.7 ± 1.5 Ma.	1.14	0.29
rhyolite (Pzps2)	111104_04	528424	7684353	14	6	0	8	272.5 ± 4.7 Ma.	0.67	0.62
Huinquintipa Dacite (Pzpg.5)	241004_08	524899	7681593	24	2	0	22	275.7 ± 3.2 Ma.	0.46	0.99
Cascasca Rhyolite Ignimbrite (Pzpa1)	200404_02	537945	7682408	12	0	1	11	286.3 ± 1.9 Ma.	1.40	0.01
QB Airstrip Rhyolite (Pzpc.2)	241005_02	525285	7680223	13	2	0	11	288.6 ± 3.3 Ma.	0.66	0.74
dacite ignimbrite (Pzpc.1)	180304_01	514274	7690032	12	0	0	12	289.7 ± 3.3 Ma.	1.90	0.03
diorite dyke (Pzpg)	070404_14	529753	7679739	12	1	1	10	294.1 ± 3.5 Ma.	2.20	0.02
rhyolite (Pzpc.9)	170504_13	527317	7674959	13	1	2	10	295.1 ± 3.1 Ma.	2.00	0.04
Chiclla Rhyolite Ignimbrite (Pzpc.5)	190404_08	531740	7678985	16	0	0	16	298.5 ± 2.1 Ma.	1.60	0.06
inheritance	various	-	-	7	-	1	6	445.3 ± 9.5 Ma.	2.80	0.45
External Standards										
Los Picos 98_521: 42.6 + 0.2 Ma (C.Allen pers. commun. 2003)				20	-	2	18	41.4 ± 0.7 Ma.	1.90	0.01
Mud Tank: 732 + 2 Ma (Black and Gulson, 1978)				9	-	1	8	733 ± 34 Ma.	2.70	0.01

a.) The original "TJI" prefix has been omitted.

b.) The population of grains used to calculate the weighted mean $^{206}Pb/^{238}U$ age.

c.) ^{207}Pb-corrected for common Pb, 95% confidence interval.

Abbreviations: inh. = inherited; rej. = rejected; corr.= corrected; prob. = probability. Instrumental parameters: 213 nm laser @ 5 Hz, 72-88% power, 0.37mJ, 30 μm spot size, HP4500 quadrupole ICPMS. Absolute element concentration assumed stoichiometric zirconium in the zircons and used NIST 612 to calculate mass bias.

relate to Pb loss. The main body of syenite (sample 050504_22) is dated at 67.5 ± 0.8 Ma (n = 23). The data define a trend from concordia toward common Pb (Fig. 3.31b). No inheritance from the basement is recognised among the dated Late Cretaceous intrusions.

A white saccharoidal aplite dyke sampled immediately east of the Rosario pit viewing platform (sample 200504_04) yielded an age of 68.4 ± 0.7 Ma. These data also cluster on concordia as a unimodal group (Fig. 3.31c) with elevated common lead in three grains. On the basis of this result, widespread aplitic and microsyenitic dykes across the district are interpreted to be of a similar age.

Icanche Formation. The lowermost part of the Icanche Formation stratigraphy in the central-northern map area, the Sallihuinca rhyolite breccia (sample 101204_04; Fig. 3.14a), is dated at 43.6 ± 1.3 Ma by a loose spread of data (n = 21) between concordia and common Pb (Fig. 3.31d). Approximately half the grains analysed are inherited, consistent with the strongly polymictic nature of this unit. These xenocrysts range in age from Neoproterozoic to Ordovician, with a loose cluster at around 450 Ma, and suggest considerable involvement of the deeper basement levels during petrogenesis. One grain interpreted as a xenocryst yielded an Ypresian (Early Eocene) age, in accordance with the broader duration of Icanche Formation magmatism elsewhere in northern Chile (e.g., Tomlinson et al., 2001a).

The Vega dacite breccia (sample 180504_02) yielded a 15-point age of 44.4 ± 0.6 Ma (n = 17) that is also defined by a spread of data from concordia toward common Pb (Fig. 3.31e). Two grains are interpreted as inherited xenocrysts: a Lutetian age (Middle Eocene) grain was possibly sourced from an early Icanche-time magmatism, and an early Permian grain suggests some recycling of the Chiclla Formation.

The Vega rhyolitic ignimbrite (sample 180504_01; Fig. 3.31f) is dated here at 42.3 ± 0.7 Ma (n = 24), 2.2 ± 0.9 million years younger than the Vega dacite breccia from which it is separated by an angular unconformity (Fig. 3.20). The data cluster on concordia, with four grains that trend toward common Pb. Strong inheritance of Peine Group rocks is revealed by secondary data clusters around 251 and 282 Ma (Table 3.6), corresponding to the Yabricoya and Huinquintipa formations, respectively.

Mineralised intrusions. The Ujina, Inca and Rosario Porphyries were dated by Masterman et al. (2004) who used $^{40}Ar/^{39}Ar$ step-heating methods on biotite. Despite their careful petrography and selection of euhedral biotites that showed no evidence of alteration, the ~300ºC blocking temperature of this technique (McDougall and Harrison, 1999) is well within the thermal range of hydrothermal processes and suspicion commonly surrounds the inference that such dates record magmatic emplacement ages.

The Inca Porphyry at Ujina and the Rosario porphyry were dated as part of the present study at the explicit request of the Compañia Minera Doña Inés de Collahuasi (CMDIC). The largely post-mineral Inca Porphyry returned an age of 34.4 ± 0.7 Ma (sample 190504_06, n = 13). All but one of the data trend off concordia toward common Pb (Fig. 3.31g) and no inheritance was recognised. Likewise, the Rosario Porphyry (sample 070404_09b) yielded data that cluster close to concordia with a moderate trend toward common Pb and returned an age of 34.2 ± 0.8 Ma (Fig. 3.31h). Four xenocrysts record Late Cretaceous, Jurassic and Triassic crustal contributions. These results are less precise than, but are within error of existing data and support the interpretation of Masterman et al. (2004) that their $^{40}Ar/^{39}Ar$ analyses (Rosario: 34.40 ± 0.30 Ma, Ujina: 35.2 ± 0.3 Ma) date magmatic cooling of intrusions directly related to mineralisation.

3.17 Geochronology $^{40}Ar/^{39}Ar$

3.17.1 Sample Selection and Preparation

Samples of fresh, unaltered amphibole from microdiorite dykes of the Cascasca dyke swarm (TRmdd) were analysed using the $^{40}Ar/^{39}Ar$ step-heating technique during the current study to support the zircon U-Pb results from samples with few zircons. Samples were crushed to sand size, sieved to +120/-80 or +80/-60 mesh, and washed in de-ionised water. Single crystals of amphibole without attached material visible at 20x were hand picked and then washed again in an ultrasonic bath.

3.17.2 Analytical Method

The method described here is used at the Queens University argon geochronology

laboratory (e.g., Bouzari and Clark, 2002; Masterman et al., 2004). Description of the analytical method is presented in Chapter 4.

3.17.3 Age Data $^{40}Ar/^{39}Ar$

New $^{40}Ar/^{39}Ar$ geochronology results are presented as plateau plots and inverse isochron correlation diagrams in Figure 3.32. Details of samples analysed and the step heating analysis results are provided in Appendix IV.

Hornblende from the freshest examples of the Cascasca Dyke swarm were dated by $^{40}Ar/^{39}Ar$ to test the validity of the limited zircon U-Pb results. Hornblende phenocrysts in the three samples were analysed by electron microprobe and all contain ~0.47 weight % K_2O (Appendix 3). Step heating of sample 011104_03 yielded a pseudoplateau at 230.7 ± 1.1 Ma. The low Ar-volume, lower power steps record ages of between 50 and 70 Ma (Fig. 3.32a) and may reflect partial resetting associated with the Late Cretaceous intrusive event. These steps plot to the right of the isochron and are interpreted to have suffered some degree of Ar loss. Excluding these two steps, the data define an isochron that yields a correlation age of 235.9 ± 3.5 Ma (Fig. 3.32b). This age has smaller errors associated with it than the pseudoplateau age, and is within error of the zircon U-Pb ages for the Cascasca dyke swarm.

Step heating of the other samples returned disturbed spectra. Sample 120504_02 has an irregular staircase spectrum (Fig. 3.32c) indicative of argon loss (e.g., Lo et al., 2000). Argon loss is also suggested by the distribution of many of the steps to the right of an isochron that is controlled by the two oldest and largest volume steps. Large errors are associated with this analysis, but it remains within uncertainty of other data for the Cascasca dykes. Sample 150404_01 is marred by apparent excess argon in all the lower power steps (e.g., Kelley, 2002). The final fusion step that accounts for ~88% of the ^{39}Ar released is taken as a pseudoplateau akin to a conventional K-Ar analysis (Fig. 3.32c). This fusion step yields an age of 238.3 ± 3.1 Ma, which is also in agreement with the zircon U-Pb data. Excess argon among the lower power steps cause large errors and push the correlation age for this sample to a slightly younger result (Fig. 3.32d).

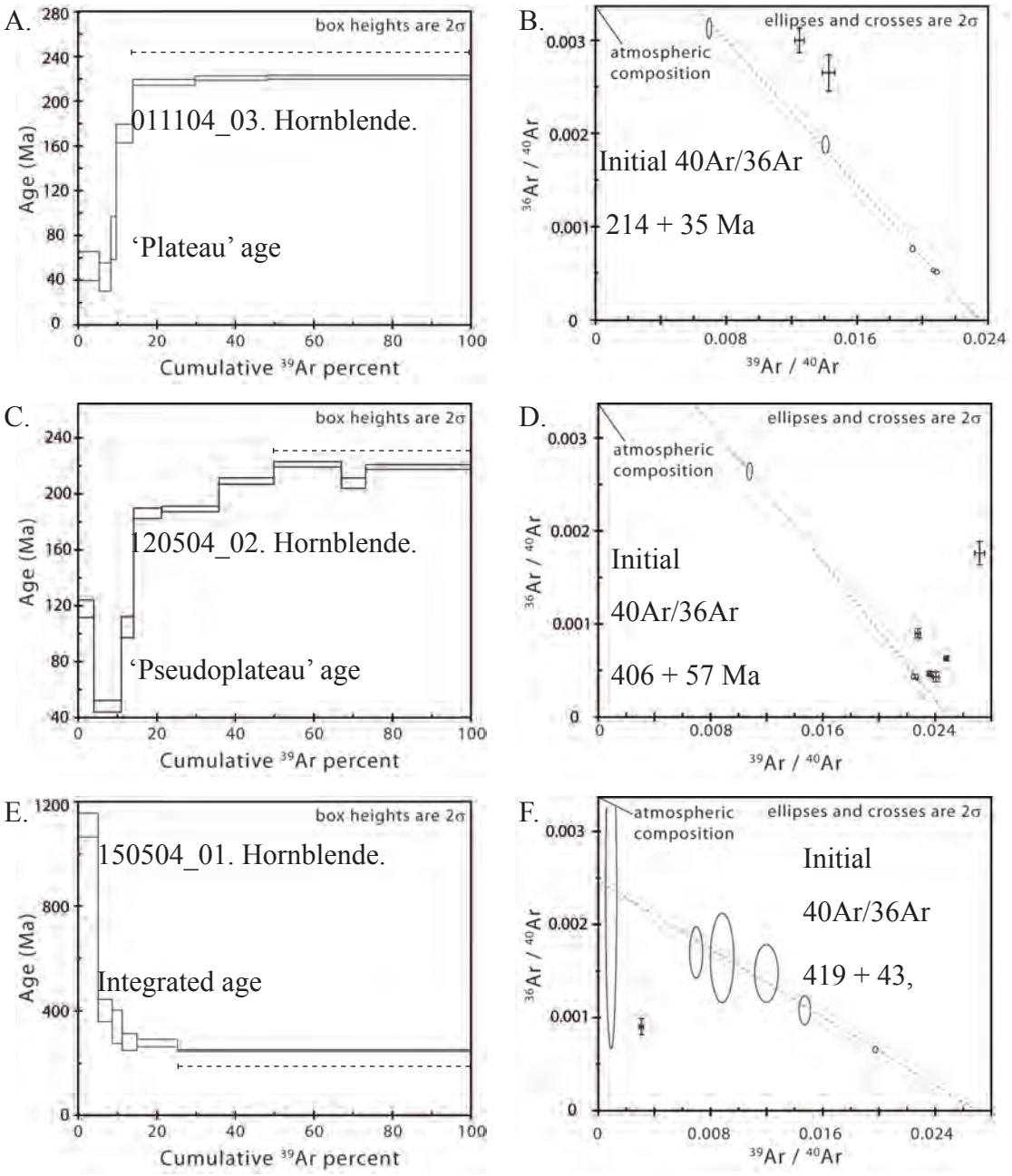

Figure 3. 32. Laser-heated $^{40}Ar/^{39}Ar$ age spectra and inverse isochron correlation diagrams for unaltered hornblende samples from microdiorite dykes (TRmdd) from west, and southeast of Rosario None of these analyses satisfy the plateau criteria recommended by Ludwig (2001), partly due to difficulties encountered in achieving good Ar release during step heating of hornblende samples. The final, large ^{39}Ar fraction steps for all samples approach sample fusion. "Pseudoplateau" refers to the weighted average of the heating steps interpreted to be least disturbed. Dashed horizpontal line indicated the steps included in these calculations. Lines on the inverse isochron plots are the least squares regressions calculated using the method of York (1969). Steps were excluded from correlation calculations if they appear to have been affected by argon loss or gain following the criteria of Kuiper (2002). These are shown with x-y error bars and are indicated in Appendix IV.

The results of zircon U-Pb and $^{40}Ar/^{39}Ar$ geochronology for the Cascasca dykes establish the intrusion of these dykes during the Middle Triassic. The dykes therefore postdate deposition of the dacitic lower Yabricoya Formation, but could be related to the uppermost andesitic members.

3.18 Chemistry of the Peine Group and Related Intrusive Rocks

3.18.1 Previous Work and Sampling Rationale

There are 98 published whole rock chemical analyses of Peine Group or related intrusive rocks from northern Chile. Of these, 37 are samples that correlate with the middle and lower Peine Group (Chiclla to Sallihuinca formations; Breitkreuz et al., 1989; Richards et al., 2001a; Masterman, 2003), among which only three are mafic. There are a further 37 published analyses of the major Permian plutons (Lopez-Escobar et al., 1979; Rogers et al., 1989; Brown, 1991; Lucassen et al., 1999a), and Mpodozis and Cornejo (1994) plot another 41 analyses from Permian plutons but did not publish their data. There are 12 analyses of rocks of the uppermost Peine Group, i.e. correlates of the Yabricoya formation (Rogers et al., 1989; Richards et al., 2001a), and six repeat analyses of the contemporaneous Collahuasi porphyry (Masterman, 2003). There are five analyses of Triassic lamprophyric dykes (Parada et al., 1991) and Rowland (1998) reports an average composition for andesitic dykes near Quebrada Blanca.

There has been some debate over the tectonic setting in which the Peine Group magmas formed. Breitkreuz and Zeil (1994) argue for a supra-subduction zone setting with highly oblique subduction leading to transtensional rifting along the magmatic front. In line with this argument, Mpodozis and Cornejo (1994) interpreted both supra-subduction and intracrustal melt contributions to the Upper Paleozoic basement at El Salvador, and concluded that subduction-related magmas had ascended through hot, thinned continental lithosphere. In contrast, Lucassen et al. (1999a, 2000) proposed magma formation for the Permian plutons by crustal anatexis in a marginal continental rift. These authors note, however, that subduction cannot be explicitly ruled out and suggest the bimodal Peine Group volcanic rocks may yield more distinctive characteristics. The eruption of primitive alkalic magmas

in Peru during the same period suggests that to the north of the study area, the margin was under pronounced extenstion (Kontak et al., 1985). Whatever the setting, Breitkreuz et al., (1990) and Parada et al., (1991) recognise a pronounced change in the chemistry of magmatic products during the late Triassic, and on that basis infer a change in the nature of the convergent margin.

In this study, samples were collected from throughout the Peine Group stratigraphy and associated Permo-Triassic intrusions. The new data are compiled with existing data and are used to constrain the tectonic settting in which Peine Group magmatism occurred, and then waned. Analytical procedures and data tables are provided in Appendix VI. Urqueta et al. (2009) reported no observable whole rock chemical changes associated with propylitic alteration at Collahuasi, but nonetheless the data presented have been screened for the effects of moderate to strong weathering and hydrothermal alteration. In summary, samples were excluded is if they contain Na_2O < 1 wt%, interpreted to reflect plagioclase destruction; >6.5 % K_2O, interpreted to reflect potassic alteration; Ca/Sr > 150, interpreted to reflect epidote replacement of calcic plagioclase; Al-alkali ratios that drive Nesbitt and Young's (1982) clay index of alteration above 73; and LOI >5 %, these latter two criteria interpreted to reflect the presence of Al-rich clay alteration minerals. Common methods for identifying mobility or immobility of elements during hydrothermal alteration relies on multiple analyses of samples from the same unit (e.g., Barrett and MacLean, 1994). Sampling in this study sought, instead, to cover as broad a stratigraphic range as possible, and so such methods are inappropriate. The screening described above (and in more detail in Appendix VI) and petrology tabulated in Appendix II serve as the basis for interpretation of chemical trends as primary features of the magmatic chemistry of these rocks. Anomalies among high field strength elements (HFSE), including the rare earth elements (REE) have been calculated using the exponential method of McCuaig et al. (1994).

3.18.2 Lower and Middle Peine Group

Rocks of the lower to middle Peine Group comprise a bimodal suite of magma compositions that is distinct from the Triassic volcanics and related intrusions that overlie, or cut the San Rafael unconformity (Fig. 3.12). They include a basaltic

andesite to andesite subset dominated by the lower La Grande formation (50-64% SiO_2) and a more voluminous dacite to rhyolite subset (67-78% SiO_2; Figs. 3.12 and 3.33a). Almost all lower and middle Peine Group rocks are subalkaline and peraluminous.

Mafic Suite. The least silicic members have very low potassium and tholeiitic iron contents (average Mg# 0.27; Fig. 3.33a, b). They generally plot within the range of values for oceanic magmatic arcs in FeO^T-MgO space (Figs. 3.33c). They contain higher Ti, Mn, V, and Y than any other group of rocks in the Collahuasi district, consistent with the very abundant opaque (?Fe-Ti oxide) phases evident in thin section (Fig. 3.8d, e). Like the mafic xenoliths in the Permian batholiths in central Chile (Parada, 1990), the mafic middle to lower Peine Group rocks are tholeiites.

The andesitic samples define a trend that crosses the K_2O-SiO_2 series boundaries at high angle, such that the most silicic samples have high-K calc-alkaline and even shoshonitic composition (Fig. 3.33a). The steep trend to more potassic composition means that fractional crystallisation (FC) of "gabbro", i.e. olivine ± clinopyroxene ± plagioclase, can be ruled out as the principal mechanism by which the 'mafic' magmas evolved. Nonetheless, normalised REE compositions of these samples show a mild negative Eu anomaly (average Eu/Eu* = 0.85), suggesting that FC of plagioclase played some role in their evolution.

The mafic Peine Group have several REE and HFSE characteristics in common with normal Andean subduction-related arc magmas such as those reported by Feeley et al. (1993) and Hollings et al. (2005). They have pronounced negative Nb and Ta anomalies (Fig. 3.35; average Nb/Nb* = 0.22) interpreted to characterise arc magmas because of sequestration of these elements in a rutile-bearing residue in the sub-arc melting column (Brenan et al., 1994; Foley et al., 1999; Xiong et al., 2005). They also have weak to moderate LREE enrichment (La/Sm_N = 3.76 - 0.61), and low Nb/U and Ce/Pb relative to rift-related magmas (Fig. 3.34), inferred to reflect contributions from fluids and melts, and hence as evidence of subduction processes (Hoffman et al., 1986). In contrast to younger Andean volcanic products, they are also strongly peraluminous (average molar Al/[Ca+Na+K] = 1.91, compare 0.71 - 0.94 for Volcán Ollagüe, adjacent to the Collahuasi district, or 0.86 - 1.14 the South Central Andes

at ~32ºS; references as above). The relative abundance of aluminium in fresh to weakly propylitised samples of the mafic Peine Group implies a significant role for assimilation of upper crustal materials. However, they are more potassic than local metamorphic basement at a given silica content (Fig. 3.33a), so wholesale incorporation of upper crustal wallrocks is unlikely. Rather, the range of alkali-silica compositions matches a mixing line between an arc-related tholeiitic basaltic andesite and an alkali rhyolite end-member such as Peine Group rhyolite.

Felsic suite. The felsic subset of middle and lower Peine Group rocks comprises rocks of mid-K calc-alkaline to shoshonitic composition, among which potassium (and sodium) do not correlate with silica (Fig. 3.33a). Na and K are generally antivariant in this suite, suggesting either that orthoclase replaced sodic plagioclase during magmatic evolution, or that weathering-related potassium metasomatism

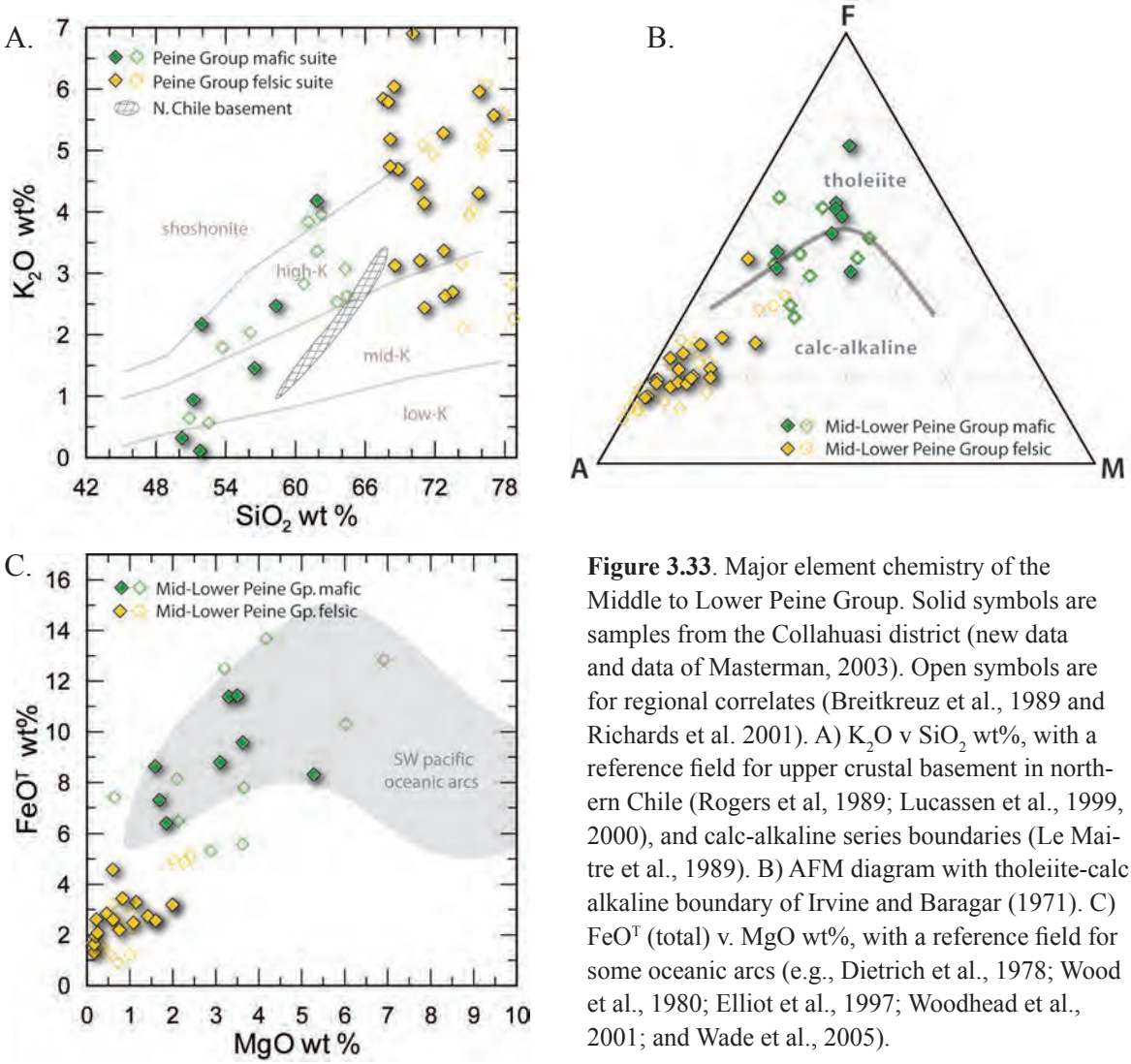

Figure 3.33. Major element chemistry of the Middle to Lower Peine Group. Solid symbols are samples from the Collahuasi district (new data and data of Masterman, 2003). Open symbols are for regional correlates (Breitkreuz et al., 1989 and Richards et al. 2001). A) K_2O v SiO_2 wt%, with a reference field for upper crustal basement in northern Chile (Rogers et al, 1989; Lucassen et al., 1999, 2000), and calc-alkaline series boundaries (Le Maitre et al., 1989). B) AFM diagram with tholeiite-calc alkaline boundary of Irvine and Baragar (1971). C) FeO^T (total) v. MgO wt%, with a reference field for some oceanic arcs (e.g., Dietrich et al., 1978; Wood et al., 1980; Elliot et al., 1997; Woodhead et al., 2001; and Wade et al., 2005).

effects many samples, or both. Ca and Al are both strongly compatible throughout the suite, suggesting that post-emplacment feldspar destruction is minimal. Strong negative Eu anomalies (average Eu/Eu* = 0.66) also characterise the suite, and indicates that FC of plagioclase occurred. However, like the mafic suite, the range of compositions crosses the K_2O-SiO_2 series boundaries and cannot be explained by FC alone. There is considerable overlap between the potassium content of the 'felsic' and 'mafic' subsets, but not between their respective silica contents (Fig. 3.33a). They can therefore not be derived directly from one another. Instead, the felsic rocks are more silicic than, and locally much more potassic than local gneissic basement rocks. They are extremely peraluminous (average molar Al/[Ca+Na+K] = 2.25) and have very strong LREE enrichment (La/Sm_N = 8.3 - 2.3). The suite spans a broad spread of Ce/Pb among the felsic Peine Group rocks (Fig. 3.34, arrow) that is uncommon among subduction-related suites, and instead characterises rift-related magmas (Fig. 3.34). Overall, the "felsic" suite and bulk upper continental crust (Fig. 3.35) are similar, and almost indisinguishable from the average of lower Paleozoic crustal rocks in northern Chile (Breitkreuz et al., 1989; Rogers et al., 1989; Lucassen et al., 1999a).

Felsic and intermediate Permian plutonic rocks share the evolved Nd-Sr isotopic composition of high grade metamorphic basement (Fig. 3.36: Rogers, 1985; Lucassen et al., 1999a). Three samples of upper La Grande formation felsic ignimbrites reported by Masterman (2003), and four samples of lower La Grande formation rhyolite and dacite reported by Munizaga et al. (2008) have Sr and Nd

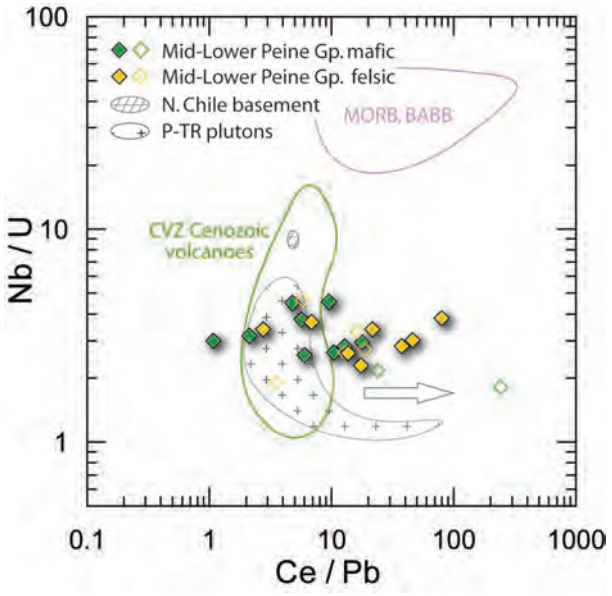

Figure 3.34. Nb/U v. Ce/Pb for the Middle to Lower Peine Group, with reference fields for Permian-Triassic (P-TR) plutons (Parada et al., 1990; Lucassen et al., 1999a; 2000) and basement (see Fig. 3.35a) in northern Chile, as well as for the Neogene Andean Central Volcanic Zone between 19º and 26ºS (CVZ; Baker et al., 1977; Hawkesworth et al., 1982; Wörner et al., 1992a; Matteini et al., 2002; Hollings et al., 2005), and for generic mid-ocean ridge and back-arc basin basalts (RidgePetDB, Lehnert et al., 2000, primarily including data of Dietrich et al., 1978; Mattey et al., 1980; Christie and Sinton, 1981; Briggs et al., 1990; Thompson et al., 1997).

isotope compositions at the primitive edge of the range known from the plutons and upper crustal gneissic basement (Fig. 3.36). The felsic Peine Group could therefore have been derived by partial melting of the northern Chilean middle-upper crust, as proposed by Lucassen et al. (1999a, 2000) for the Permian plutons. However, their isotopic composition at the primitive extreme of the range for related crustal magmas might imply, but doesn't explicitly demand some degree of hybridisation with mantle-derived magmas such as the mafic members of the lower Peine Group. The Chiclla rhyolitic ignimbrite, emplaced immediately before the onset of La Grande Formation basastic andesite volcanism, contains distinctly bimodal plagioclase populations including abundant andesine (Table 3.1), and hence supports the notion of magma mixing during Peine Group felsic magmatism.

3.18.3 Upper Peine Group and Related Intrusions

The uppermost Peine Group rocks; the Triassic Yabricoya formation, the Cascasca basaltic-andesitic dykes (section 3.9), and intermediate to felsic intrusions such as the Collahuasi and La Profunda porphyries (sections 3.14.2 - 3.14.5) comprise a

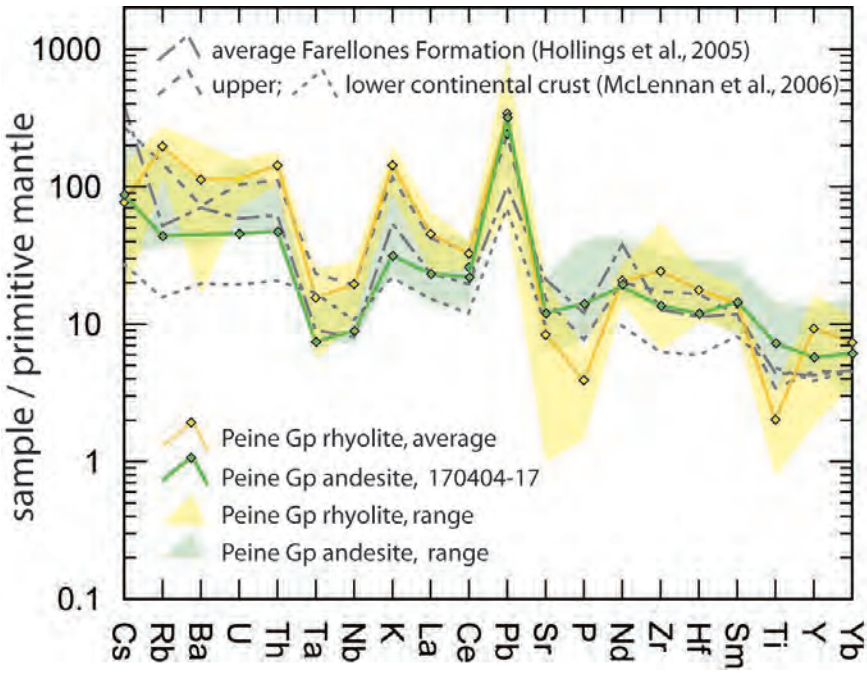

Figure 3.35. Chemistry of the Peine Group shown as a spider diagram showing trace elements normalised to primitive mantle (Sun and McDonough, 1989). Reference lines are shown for the central Chilean, Miocene, Farellones Formation (Hollings et al., 2005), and for average upper and lower continental crust (McLennan et al, 2006).

continuous suite of high-K calc-alkaline rocks that range from basaltic andesite to rhyolite in silica content (Fig. 3.37; four andesitic samples that plot at higher K_2O content have correspondingly low CaO and appear to have undergone selective alteration. With the exception of sample 300404_13, these rocks share the other chemical features of unaltered samples, and so have been retained in figures 3.37-3.40). The Agua Dulce and Cerro Crespo formations that erupted at about the same time further south along the arc (Rogers et al., 1989; Richards et al., 2001a) are mostly mid-K calc-alkaline rocks (Fig. 3.37; open symbols). Compared to the lower and middle Peine Group, the felsic Triassic units are less strongly peraluminous (molar Al/[Ca+Na+K] = 1.00 - 1.16), and the most felsic examples are subalkaline rather than shoshonitic (Fig. 3.37a).

The upper Peine Group suite shows major element trajectories consistent with "gabbro" fractional crystallisation; overall compatible Mg, Ti (Fig. 3.38a,b), Fe, Al, and Ca. Flat to weakly compatible differentiation trends among the REE and Y (Fig. 3.38c,d), and progressive M-HREE fractionation (Fig. 3.38 e) suggest a major role for amphibole in the differentiation of these magmas (e.g., Davidson et al., 2007;

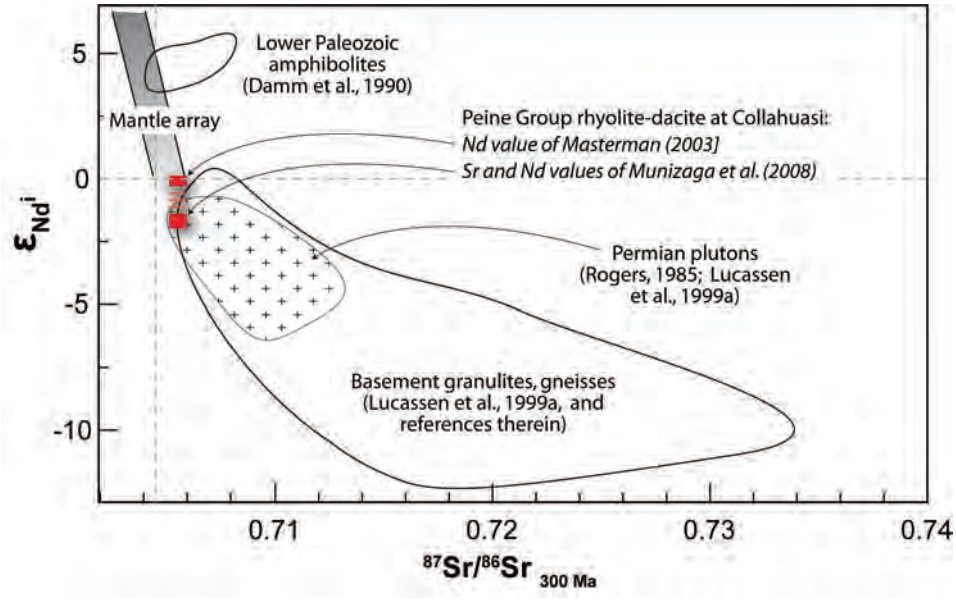

Figure 3.36. Summary of radiogenic Nd and Sr isotopic compositions of Andean Permo-Triassic rocks and outcropping basement units, recalculated to initial values (adapted from Lucassen et al., 1999a). Felsic* rocks of the Peine Group analysed by Masterman (2003) and Munizaga et al. (2008) are apparently transitional between Permian plutons of crustal derivation, and magmatic rocks sourced from the mantle. The 'mantle array' field is defined by analyses of abundant Jurassic to Cretaceous La Negra and Quebrada Mala arc rocks. *Munizaga et al. (2008) list three of their four samples as 'andesite', when the locations of their samples and bulk Rb content instead suggest that they are dacites.

Brophy, 2008). The onset of crystallisation of amphibole +/- iron oxides at ~55% SiO_2 is marked by inflexions in the Harker trends for Ti, Y, Zr, Th and many other trace elements. Compatible behaviour of Al, Zr (Fig. 3.38 f,g), Ba, Th and U among samples with >64% SiO_2 appears to record fractional crystallisation of plagioclase and zircon among the felsic members of the suite. These rocks also have weak to moderate negative Eu anomalies (Eu/Eu* = 0.63 - 0.82), whereas the mafic members have weak or no anomaly (Eu/Eu* = 0.83 - 1.00). The Cascasca dykes and mafic Yabricoya formation are the most magnesian (average Mg# 0.42; compared to 0.27) and Ni-rich Peine Group rocks (Fig. 3.38h). However, the intermediate and felsic members share the low-Ni composition of the lower and middle Peine Group. Olivine may therefore have crystallised during the early stages of differentiation of the Triassic magmas.

All the upper Peine Group units share chemical characteristics of supra-subduction zone magmas. They have prononunced negative Ta-Nb anomalies (average Nb/

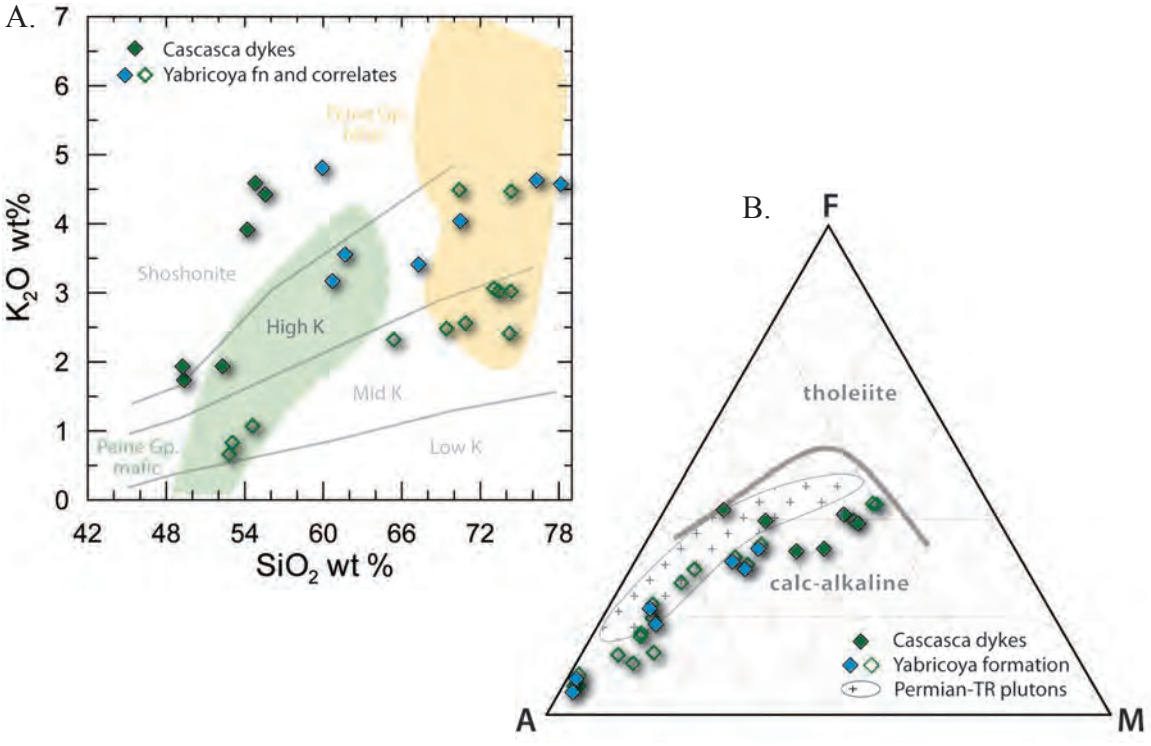

Figure 3.37. Major element chemistry of the Yabricoya formation and Cascasca dykes. A) K_2O v SiO_2 with reference fields for the middle and lower Peine Group. B) AFM diagram showing calc-alkaline character. Solid symbols are samples from the Collahuasi district, including an average of analyses of the Collahuasi Porphyry (Masterman, 2003), and an average of several analyses of dolerite dykes at Quebrada Blanca (Rowland, 1998). Open symbols are for regional correlates (Rogers et al., 1989, and Richards et al. 2001).

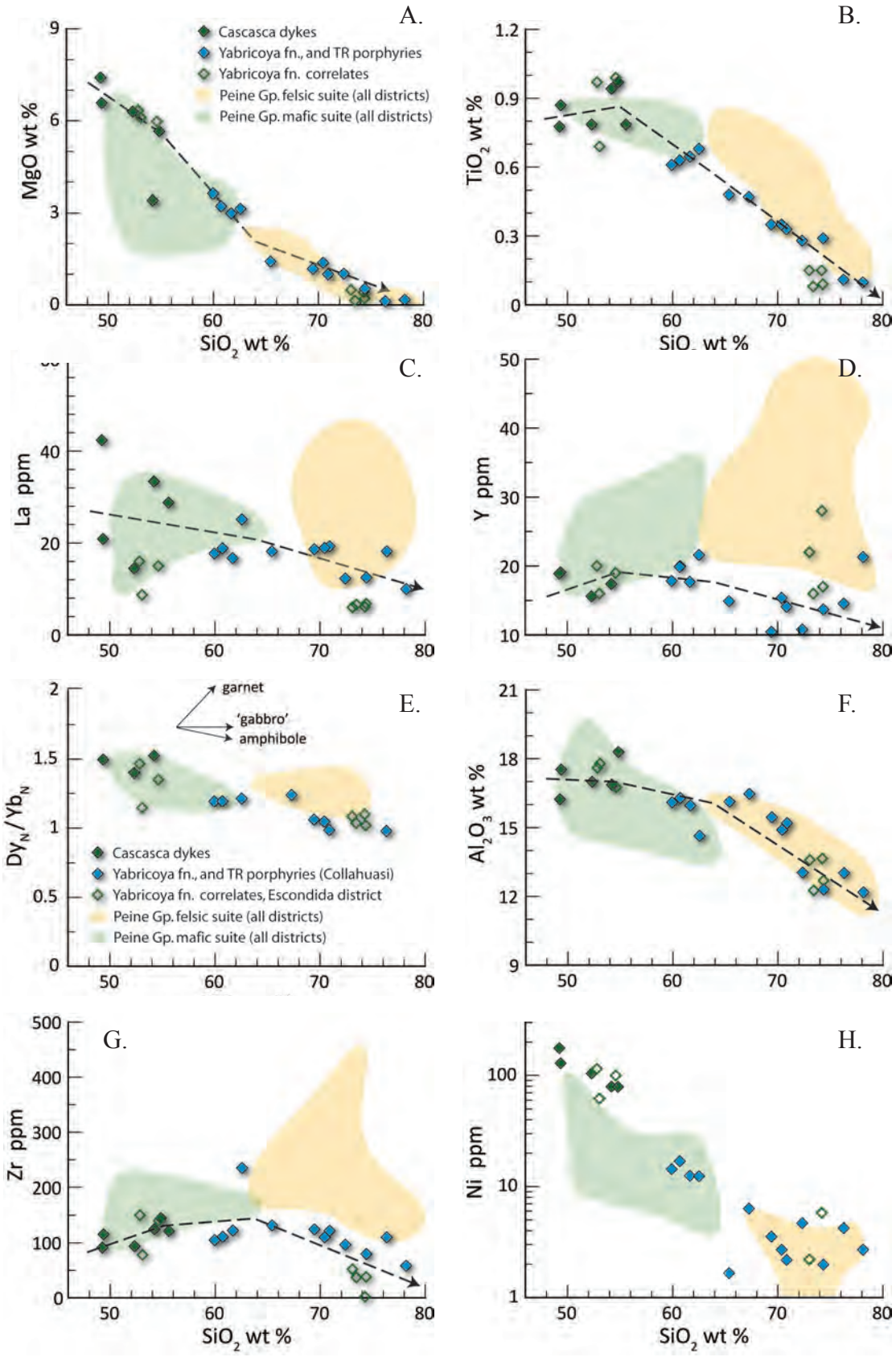

Figure 3.38. Harker diagrams for the Peine Group showing selected elements and element ratios indicative of fractional crystallisation processes. A) MgO, B) TiO2, C) La, D) Y, E) Dy/Yb normalised to chondrite, F) Al_2O_3, G) Zr, H) Ni. Data shown for the Yabricoya formation includes multiple analyses of the Collahuasi porphyry (Masterman, 2003), and data shown as regional correlates thereof are the uppermost Peine Group reported from the Esciondida district (Richards et al., 2001a). Dashed lines indicate interpreted differentiation trajectories.

Nb* = 0.23), strong LILE enrichment (Fig. 3.39), and moderate LREE enrichment (Cascasca dykes La/Sm_N = 2.05 - 2.95; Yabricoya formation La/Sm_N = 2.60 - 4.21). Consequently, they have low Nb/U and Ce/Pb ratios (Fig. 3.40a). The relative concentration of V to Sc has been used as a proxy for magma oxidation state (Aeolus-Lee et al., 2003; 2005) because of the particular sensitivity to redox conditions of V mineral-melt partitioning behavior (Toplis and Corgne, 2002). The Yabricoya formation and related intrusions have V/Sc that does not change with differentiation and plots mostly within the range of normal arc magmas defined by global on-line databases (Fig. 3.40b; Aeolus-Lee et al., 2005). These rocks are therefore likely to have been oxidised relative to mantle sources, as is inferred to result from the metasomatism of the mantle wedge by slab-related fluids (e.g., McGuire et al., 1991). They were possibly also hydrous, given the apparently significant role for amphibole during differentiation.

Upper crustal assimilation is implied by the presence of accessory lithic clasts (Table 3.1) and of Carboniferous, Silurian, and Proterozoic zircon xenocrysts (Appendix III) in some of the Triassic units. However, fractional crystallisation adequately explains the range of compositions observed among the Triassic magmatic rocks in the Collahuasi district. Likewise, the trace element composition of these rocks is consistent with normal arc magmas worldwide, and hence it appears that assimilation of upper crustal materials was much less significant at Collahuasi in the Triassic than it had been during lower and middle Peine Group time.

3.18.4 Tectonic setting of the Permo-Triassic Andean margin

The mafic Peine Group and related Triassic intrusions share most of the chemical characterics of suprasubduction zone magmas, such as pronounced negative Nb and Ta anomalies and enriched LREE (Figs. 3.35 and 3.39) and low ratios of Nb/U and Ce/Pb (Figs. 3.34 and 3.40a). These characteristics also persist in the continental crust (e.g., Arculus, 1981; Brenan et al., 1995), but to a lesser extent than in primary arc magmatic rocks (e.g., Nb/Nb* = 0.54 [lower crust]; 0.37 [upper crust]; McLennan et al., 2006; compared to Nb/Nb* mode = 0.28, and 70% < 0.37 for magmatic arcs [*n*=5447; GEOROC online database).

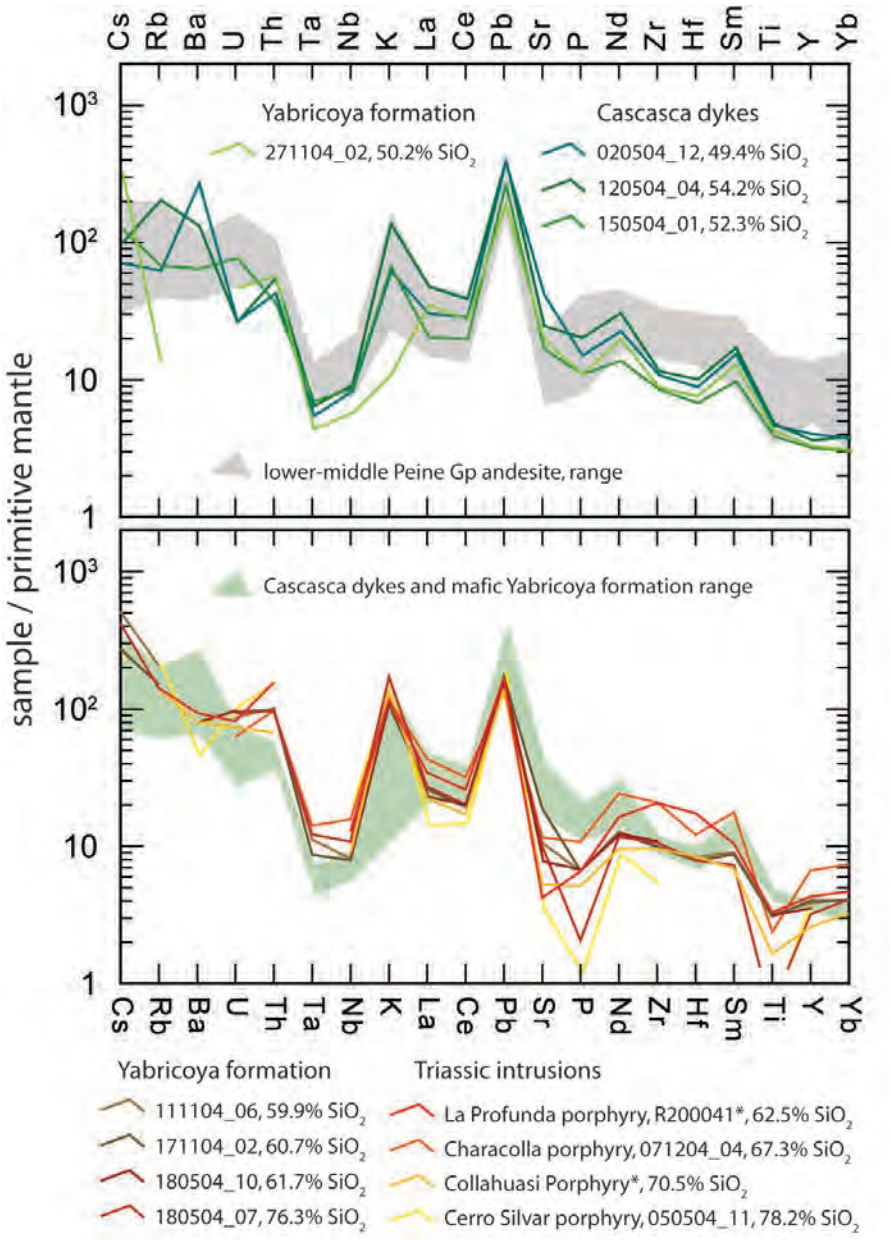

Figure 3.39. Chemistry of the upper Peine Group and related intrusions shown as a spider diagrams normalised to primitive mantle (Sun and McDonough, 1989). A) Basaltic rocks of the Cascasca dykes and lower Yabricoya formation. B) Intermediate to felsic Yabricoya formation and lower Triassic porphyritic intrusive rocks. Reference fields are shown for the range of lower to middle Peine Group andesites (from Fig. 3.37) and Triassic basalts (from A). Data marked with ansterisk (*) are from Masterman (2003), from which the Collahuasi Porphyry is represented as the average of six analyses.

The observed subduction-like character could record active subduction-related magmatism, recycling of fossilised metasomatised mantle belonging to an older subduction zone, or crustal melt extraction (under certain conditions). Permian sub-crustal lithosphere may have preserved domains of arc-related volatile- and LREE-enriched, rutile-bearing metasomatised mantle that had formed during early

Paleozoic arc magmatism (Famatina Arc, section 2.2.1). The Choiyoi Arc at least locally overlaps the inferred distribution of these older arc rocks (e.g., Damm et al., 1990), and hence this scenario is broadly permitted by the relative positions of the Lower and Upper Paleozoic arcs. However, where melting 'fossilised' metasomatised mantle has been demonstrated, such as in eastern Anatolia, the distribution of inherited subduction-like characteristics is highly variable in space (e.g., Keskin, 2003). There are not substantial differences between the mafic Peine Group rocks from the four locations in northern Chile for which data are available, so this scenario is unlikely, though it cannot be explicitly ruled out.

Reworking of the crust is an attractive explanation because of the peraluminous composition of the mafic Peine Group. Similar magma compositions could be uniquely be derived by partial melting of the mafic lower crust if the residual mineralogy contained rutile and/or garnet to cause the relative Nb-Ta depletion and REE fractionation. However, that too is unlikely since the western Andean margin crust did not achieve thicknesses sufficient to stabilise those minerals during the Paleozoic (Omarini et al., 1999; Xiong et al., 2005; Alvarado et al., 2007). Several other mineralogical criteria could be placed on a hypothetical gneissic or granulite residue to drive the other arc-like characteristics, but the coincidence of these

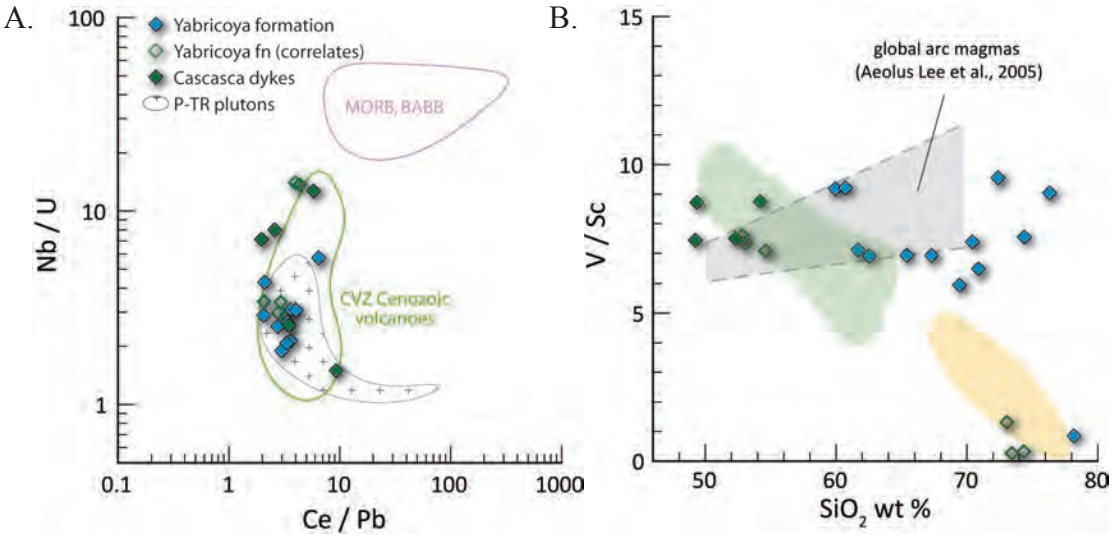

Figure 3.40. Trace element ratios indicating a supra-subduction zone origin for the Yabricoya formation and related rocks. A) Nb/U v. Ce/Pb, with reference fields as shown in Figure 3.37. B) V/Sc v. SiO_2 wt%, with a reference field for global arc magmas, adapted from Aeolus-Lee et al. (2005).

becomes increasingly improbable. Instead, the observed Ta-Nb-(U), Pb/Ce, and LREE anomalies are best explained if a component of the parental Peine Group magma formed in the metasomatised mantle wedge above an active subduction zone.

In contrast to the mafic rocks, the felsic lower Peine Group are interpreted to be largely the products of intracrustal melting, consistent with the previous interpretations drawn for the Peine Group and/or north Chilean Permian plutons (Kay et al., 1989; Brown, 1991; Parada et al., 1991; Lucassen et al., 1999a; Depine et al., 2005; Munizaga et al., 2008). Partial melting of the crust may have been mediated by the ascent of the basaltic arc magma, and mixing between these and intracrustal felsic melts adequately accounts for the aluminosity of all lower Peine Group rocks, the unusual alkali Harker trends (Fig. 3.33a), and the Sr-Nd radiogenic isotope composition of the felsic Peine Group at Collahuasi (Fig. 3.36).

Breitkreuz and Zeil (1994) inferred that the wide distribution of contemporaneous sedimentary strata across northern Chile marked incipient arc-parallel rifting along strike of a magmatic rift basin in southern Peru (e.g., Kontak et al., 1985). Indeed some aspects of the Peine Group chemistry support this hypothesis. Half the lower and middle Peine group mafic rocks have V > 290 ppm (n= 6) and Ti/V in the range 17-42 (average 30), and several samples have Zr/Y ~4. These values lie at the edge of, or just outside of the ranges for typical subduction-related basalts and within the ranges of rift-related basalts (e.g., Pearce, 1976, 1982). Similar HFSE compositions are recorded among Cretaceous to Miocene basaltic rocks of the South Central Andes (Nyström et al., 2003; Hollings et al., 2005) and Quaternary andesites of the Taupo Volcanic Zone, New Zealand (Price et al., 2005). These are appropriate comparators to the Peine Group in terms of the thickness of the continental column through which magmas must have ascended to erupt at the surface. In both cases magmatism occurred above an active subduction zone where continental extension encroached into the magmatic arc front (Yañez et al., 2002; Nyström et al., 2003; Price et al., 2005). The consequent upwelling of athenosphere would have driven anomalous heat flow and provided an environment that favoured intracrustal melting during arc magma ascent and storage.

New geochemical analyses of the middle and lower Peine Group therefore support the idea that the Choiyoi Arc was built above an active subduction zone that

underwent contemporaneous extension; the 'arc-graben' of Breitkreuz and Zeil (1994). The lower and middle Peine Group mafic magmas are inferred to be two component hybrids of tholeiitic arc basaltic magma, and a crustal alkali rhyolite melt. The voluminous felsic lower Peine Group reflects the products of largely undiluted variations of this intracrustal melt. Following the San Rafael tectonic event, the relative significance of intracrustal melting decreased, as is evidenced by the more primitive and less peraluminous (partly metaluminous) Yabricoya formation and related intrusions. The primary arc basalt composition changed to high-K calc-alkaline at the same time, plausibly by way of mineralogical changes related to higher pressures (greater depths) of volatile expuslion from the subducting slab (Schmidt, 1996), or of melt generation in the mantle wedge (Wyllie and Sekine, 1982). The implied deeper subduction processes during the terminal stages of Peine Group magmatism may therefore record the magmatic response to the onset of slab rollback along the Choiyoi Arc. Mafic dykes also cut the lower Triassic Este Granodiorite at Chuquicamata (Tomlinson et al., 2001a), and therefore emplacement of relatively primitive magmas at this time appears to have been at a regional phenomenon. However, Choiyoi Arc rocks locally became more anatectic in character at approximately the same time (Kay et al., 1989; Brown, 1991; Depine et al., 2005). The arc may therefore have been substantially segmented, and rollback may have been diachronous as a result.

3.19 Facies Associations and Tectono-Stratigraphic Evolution

The Peine Group stratigraphy is tilted generally northward in the Collahuasi district, such that the district itself appears as a section, albeit deformed, through the Peine Group stratigraphy (Fig. 3.4). This geometry emphasises cross-arc segmentation of depositional environments, and E-W lateral attenuation is a characteristic of most of the formations of the Peine Group described here. The new geochronology (Table 3.6) and 17 stratigraphic sections (Fig. 3.12) drawn from new mapping and drill logging (Fig. 3.2) permit chronological constraint of lithostratigraphic correlations made across the Collahuasi district. In Figure 3.12, the relationships between episodes of deposition are evident as truncation of certain lithofacies units against the bases of overlying formations. The mapped lithofacies units are grouped into

broader, more manageable lithofacies associations, each of which encompasses the facies variability among rocks deposited during related or broadly similar volcanic and sedimentary environments (Table 3.1, Figure 3.41).

3.19.1 Grey subaerial felsic volcanic and volcaniclastic facies association

The lowermost Peine Group stratigraphy are grey felsic and dacitic subaerial volcanics of the Chiclla Formation. Elsewhere in northern Chile, the lower part of the Peine Group is also dominated by felsic volcanics (e.g., Breikreuz and Zeil, 1994). Although the basal contact is unknown in the Collahuasi district, it appears that the north Chilean part of the Choyoi Arc was dominated by felsic volcanism from its inception. A marginal continental rift basin that had developed during the Devonian (Estratos de Quebrada Atahualpa: Niemeyer et al, 1985, in Tomlinson et al., 2001a) was inverted during the lower Carboniferous (Breitkreuz et al., 1990; Damm et al., 1990; Bahlburg and Breitkreuz, 1993; Diaz-Martinez, 1996; Busquets et al., 2005) such that the Choyoi Arc was initially subaerial and built on a basement high bound on the east and west by marine carbonate platforms (Donato and Vergani, 1985; Niemeyer et al., 1985). The principal rocktypes in the Chiclla Formation are thick welded ash-crystal-rich ignimbrites (Pzpc10, 5, and 1; Table 3.1). These likely formed from hot, energetic pyroclastic flows associated with the collapse of Plinian eruption columns (e.g., Wilson and Sparks, 1976; Sparks et al., 1978). Pyroclastic flow deposits of this type typically infill existing topography (Cas and Wright, 1987; McPhie et al., 1993), and continuity of the Chiclla Formation across the Collahuasi district might suggest that this Carboniferous substrate had experienced significant peneplanation prior to the onset of Choyoi Arc magmatism.

There is an apparent thickening of the Chiclla Formation in the central-eastern part of its exposure, and the Chiclla stratigraphy is thin-bedded in the western El Colorado sector. Associated coherent felsic volcanic facies (Pzpc9, 6, 4, and 2) appear to be concentrated about the NNE-trending Monctezuma Fault (Figs. 3.4, 3.5) and a subparallel fault three kilometres to the west. Likewise, coherent rhyolite (Pzpc2) occurs adjacent to the Domeyko Fault Zone in the El Colorado sector. Plinian eruptions and the subsequent association of lava domes and voluminous shard and pumice-rich ignimbrites are typically associated with silicic caldera eruptions such

as those of the Taupo Volcanic Zone in northern New Zealand (Brown et al., 1998; Milner et al., 2003), and the Miocene to Recent Central Volcanic Zone of the Andes (Francis and Baker, 1978; Hildyard et al., 2001; Ramelow et al., 2006). This style of volcanism has been suggested previously for the Peine Group (Davidson et al., 1985; Tomlinson et al., 2001a). Minor intercalated terrestrial sedimentary facies (Pzpc3) suggest fluvial valley incision and/or limited subsidence, consistent with the incipient rifting inferred from magmatic chemistry. The concentration of coherent lavas near major N-S and NNE-trending faults suggests that these faults may have served as conduits for magmas.

3.19.2 Subaqueous bimodal volcano-sedimentary facies association

The boundary between the Chiclla and La Grande formations is defined by a conformable lithological change to andesite as the dominant magmatic rock type and a change from subaerial to subaqueous depositional environments (Fig. 3.12). The absence of transitional shallow water sedimentary facies, and abundant gravity-

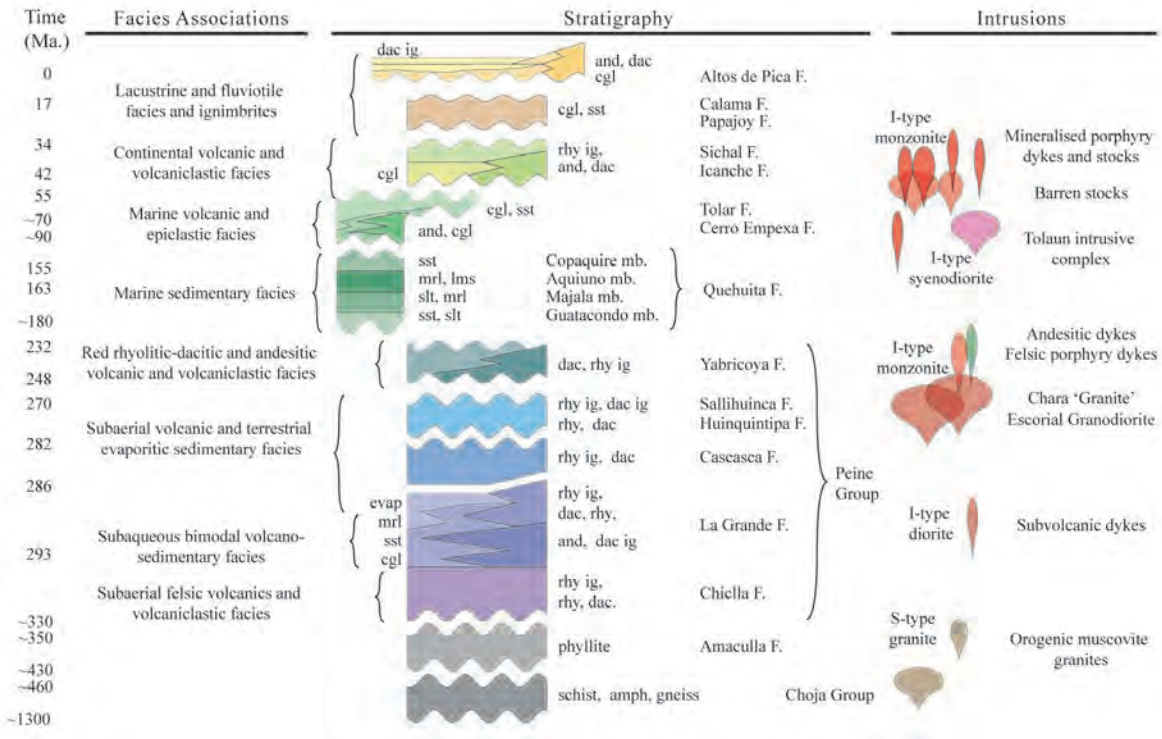

Figure 3.41. Schematic summary of the stratigraphic and intrusive history of the Collahuasi district. Sinusoidal margins indicate unconformities. Abbreviations: and = andesite, dac = dacite, rhy = rhyolite, rhy ig = rhyolitic ignimbrite, dac ig = dacitic ignimbrite, cgl = conglomerate, sst = sandstone, slt = siltstone, mrl = marl, lms = limestone, evap = evaporites, amph = amphibolite.

driven mass flow depositional style are interpreted as evidence of rapid transgression associated with tectonic subsidence. Eruption of the uppermost lithofacies units in the Chiclla Formation at ~ 289 Ma (Table 3.6) may have coincided with the onset of subsidence in the Collahuasi district. Debris flow and turbidite deposition are commonly associated with sub-wave base deposition (e.g., Sohn, 2000; Felix and Peakall, 2006). Likewise, rare laminated carbonaceous siltstones that occur among the pebble conglomerates of Pzpg12 indicate a low energy depositional environment during times of mass flow quiescence. With few exceptions (e.g White and McPhie, 1997), pyroclastic deposits are generally unable to undergo depositional welding if they are emplaced into water deep enough to resist complete displacement by the pyroclastic materials (i.e. welding is prevented because of cooling related to mixing of water and hot pyroclastic debris; McPhie et al., 1993; Keating, 2005). Felsic pyroclastic intercalations in the La Grande Formation are typically unwelded and commonly exceed 50 m in thickness (locally exceeding 100 m; Figs. 3.4, 3.12), suggesting water depths of at least this magnitude.

A transgressional event associated with andesitic volcanism is recognised as a segmented basin throughout the north Chilean Peine Group (Miembro Medio basin: Bahlburg and Breitkreuz, 1991; Breitkreuz and Zeil, 1994). These authors point out that except for the Miembro Medio basin, the Peine Group is predominantly subaerial between latitude 20ºS and 25ºS (Fig. 3.42). To the north of ~20ºN, the basin deepens and the materials deposited within it are largely sedimentary. South of ~25ºN the sedimentary intercalation is largely absent. These northern and southern limits to the Miembro Medio basin coincide approximately with the intersections of the Permian arc front with the NW-trending continental Lipez-Coranzuli and Archibarca lineaments, respectively (Fig. 3.42; Salfity, 1985; Richards, 2000). Although local subsidence may have been partly articulated along cross-arc faults such as these, the greater Miembro Medio Basin is interpreted to have been subparallel to the arc front and contiguous with a deeper marginal basin in Peru (e.g., Sempere et al., 2002).

3.19.3 Subaerial volcanic and terrestrial sedimentary facies association

Accommodation space in the La Grande area appears to have been filled with the andesite and clastic sediments of the upper La Grande formation within

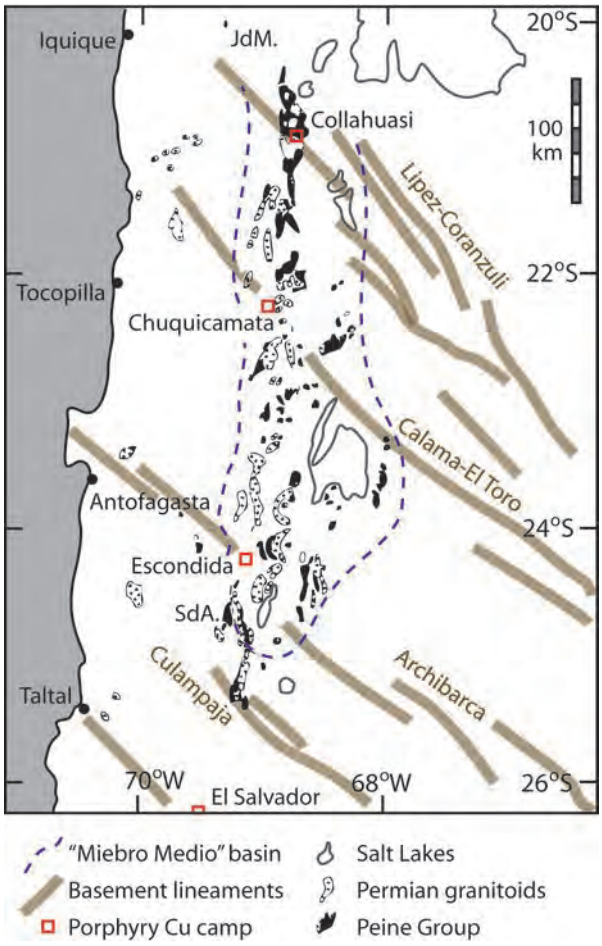

Figure 3.42. Permian Paleogeography of the Miembro Medio Basin. Simplified map of western South America from 20º-26ºS showing the distribution of Late Paleozoic intrusive rocks and volcano-sedimentary correlates of the Peine Group (modified from Breitkreuz and Zeil, 1994). Also shown are major porphyry copper camps, modern salt lakes, and crustal-scale NW-trending lineaments, after Salfity (1985) and Richards (2000). Sedimentary facies of the middle part of the Peine Group record transient subsidence within the Choiyoi arc during the Early Permian. Outcrops of entirely marine strata at Juan de Morales (JdM) and an entirely subaerial rock package in the Sierra de Argomedo (SdA) indicate the northern- and southern limits, respectively, of the Late Permian intra-arc basin. The locations of the lineaments appears to coincide with major changes in the architecture of the Miembro Medio basin. These positions also coincide spatially with salt lakes that mark depocentres within the Preandean Depression.

five million years (Table 3.6), and subsidence was not renewed in that location. During this period, the style of sedimentation changed as the basin filled; mass flows became finer grained and less common, and the deepest parts accumulated laminated calcareous siltstones (Pzpg8). Benthic bacterial communities inhabited the lacustrine sediment-water interface (Wood et al., 2002). Ultimately the basins became hypersaline and abiogenic cherts (e.g., Eugster, 1969; Krainer and Spoetl, 1998) and nodular evaporites were precipitated in shallow lacustrine environments that experienced periodic exposure (Pspg2; e.g., Warren, 1986; Kendall and Warren, 1988). Changes to water depth in the basin were synchronous with a worldwide regression at this time that also caused evaporite deposition in the contemporary marine basin of southern Peru (Kontak et al., 1985; Sempere et al., 2002; Rosas et al., 2003) and globally (Zharkov, 1984).

Volcanism persisted and became increasingly dacitic (Pzpg5), initially constructing edifices that may have restricted and infilled the basin in the San Nicolas and Casa de Piedra areas. In both locations, major NNE-trending faults may have served as

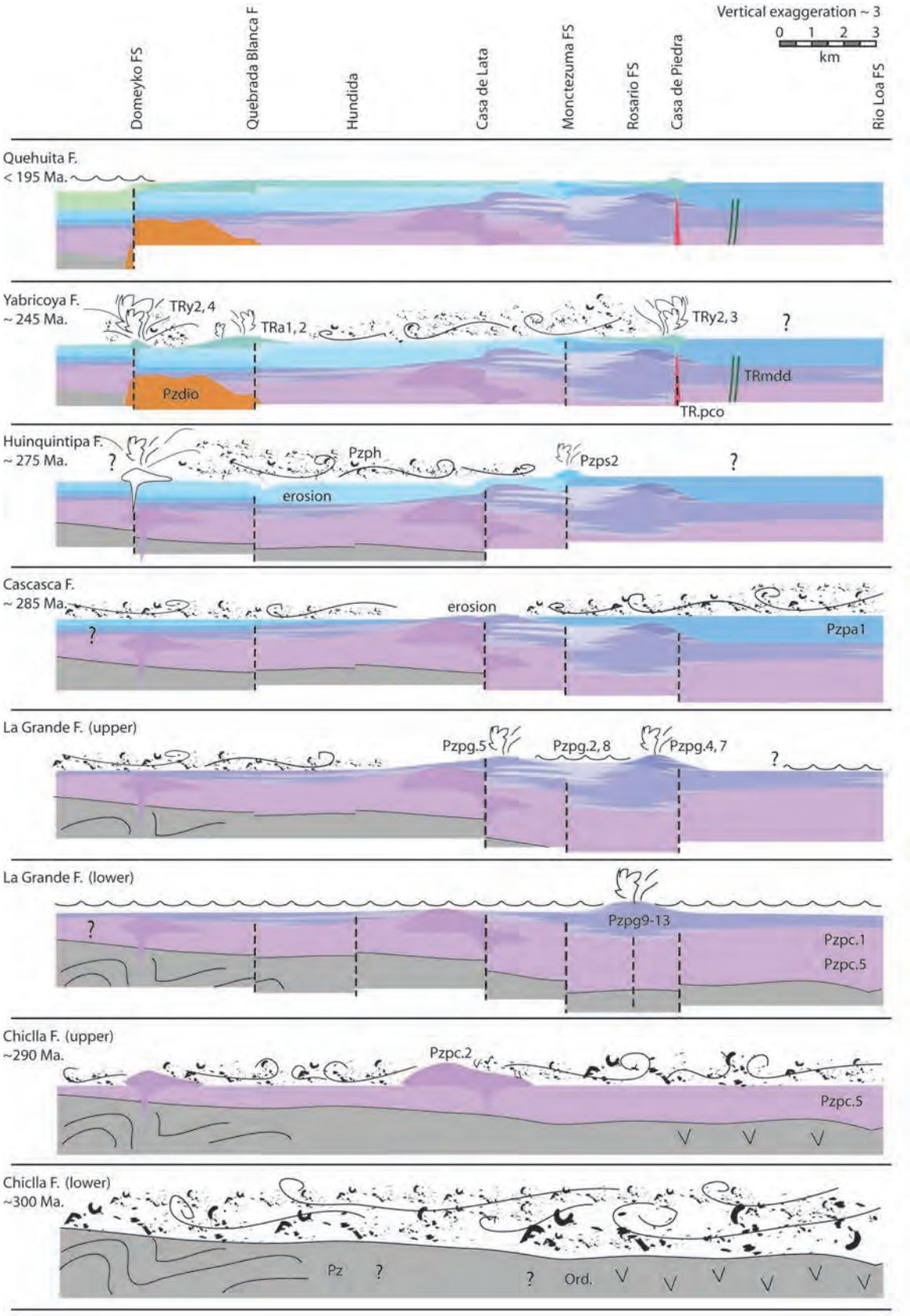

Figure 3.43. Schematic west to east sections showing the evolution of volcanosedimentary environments through the Late Carboniferous to Jurassic packages exposed in the Collahuasi District section. Colours are similar to those in Fig. 3.4 and selected lithology codes are shown for clarity. Steeply dipping meridional faults are named at the top of the diagram, and shown as vertical for simplicity. Faults active during each stage are marked by dashed lines and dip-slip displacement is indicated by offset of the basal surface of the blocks. During lower La Grande Formation time, the Rosario Fault System (oblique to the section) may have acted as a conduit for the main andesitic volcanic centre. Abbreviations F = Fault; FS = Fault System.

conduits for magma ascent (Fig. 3.43, Chapter 4). Dacitic magmatism at this time produced distinctive red extrusive rocks in which hornblende phenocrysts show strong hematitic reaction rims (Fig. 3.17c,d) indicative of prolonged low pressure crustal storage (Rutherford and Hill, 1993; Buckley et al., 2006). This shallow crustal storage may have developed in association with pronounced wallrock melting and assimilation of crustal materials (section 3.18.2). A series of increasingly larger explosive eruptions that filled the basin with welded pyroclastic material (Pzpg1, Pzpg3) mark the terminal stages of the La Grande Formation deposition.

A period of erosion and landform modification followed, apparently associated with uplift of an arc-parallel basement sliver in the central and eastern part of the district. The section in the area between the Monctezuma and subparallel faults to the west does not include the voluminous dacitic and rhyolitic explosive eruption products that comprise the Cascasca Formation (Figs. 3.4, 3.13, 3.43). It may therefore have been a topographic high at the time, where pyroclastic deposition was minimal and was subsequently removed by erosion. A local disconformity separates the Cascasca ignimbrite from the La Grande Formation in the eastern map area, but the two are concordant in the west (Fig. 3.4; 3.12) where the district was tectonically quiescent. Ongoing erosion and local valley incision exposed some parts of the La Grande formation along the western flank of the basement high, leading to a disconformity at the base of the Huinquintipa Formation (Fig. 3.12).

The basal Huinquintipa Formation comprises coherent red subaerial dacitic volcanics. These are overlain by a thick grey dacitic to rhyolitic ignimbrite (Table 3.1) that was deposited in a broad basin that may have been limited by the Monctezuma Fault on its eastern margin (Fig. 3.46). Valley incision appears to have been ongoing during magmatic lulls, such that these ignimbrites typically have poor lateral continuity and are locally associated with channelised fluvial conglomerates (Fig. 3.12). Petrographically the Huinquintipa Formation ignimbrites share aspects of both the grey and red subaerial facies lower in the stratigraphy. They are grey in colour but the amphibole phenocrysts commonly have oxide reaction rims. This hybrid character may indicate that explosive volcanism of the Huinquintipa Formation was prompted by voluminous recharge of an upper crustal magma chamber. Renewed tectonic activity and subsequent erosion caused a weak angular

unconformity to develop between these units and further pyroclastic deposits of the Sallihuinca Formation (Figs. 3.4, 3.32).

3.19.4 Intermediate-felsic plutonism and folding

A 25-30 million year period of volcanic quiescence between eruption of the Sallihuinca and Yabricoya (Agua Dulce) formations coincides with the emplacement of large, medium-grained, equigranular diorite and granodiorite plutons in the Collahuasi district (Fig. 3.26; geochronology of Ware et al., 1981; Damm et al., 1986). Emplacement of these plutons appears to have been associated with crumpling of the Peine Group stratigraphy that occurred before emplacement of the Cascasca dykes (section 4.33). Deformation in the late Permian (San Rafael tectonic event, Chapter 2) may therefore have accompanied plutonism and concommittant attenuation of volcanism, as it did in the southern Choiyoi Arc (e.g., Mpodozis and Kay, 1992; Fernandez Seveso et al., 1993; Creixall et al., 2006). The plutons intruded only the lowermost Peine Group stratigraphy (Fig. 3.4), and must have been emplaced under at least three kilometres of stratigraphy; the combined thickness of the upper La Grande, Cascasca, Huinquintipa and Sallihuinca formatios (Fig. 3.12).

Red rhyolitic-dacitic and andesitic volcanic and volcaniclastic facies association

Renewed arc magmatism occurred between 248 and 242 Ma, recorded by the Yabricoya Formation. Explosive volcanism and ignimbrite deposition spanned the Collahuasi district, but is only preserved in two structurally bound arc-parallel domains (Fig. 3.4). The absence of the Early Triassic volcanic stratigraphy to the west of the Monctezuma Fault cannot be explained by the sinistral net horizontal offset on this structure (Chapter 4). This implies that there was no deposition in this location, or that it was completely removed by erosion. In turn this suggests that the central Collahuasi district may have been a structural high during Yabricoya Formation time (Fig. 3.46). Associated coherent volcanic facies (andesitic in the west and dacitic in the east) are concentrated along major arc-parallel structures. These may have served as conduits for magma ascent.

3.19.5 Dykes, stocks and death of the Choyoi Arc

Subduction-related magmatism continued after the San Rafael tectonic event, without

the pronounced rift-related upper- and lower crustal anatexis that dominated the petrogenesis of the Carboniferous and Permian magmas. The Collahuasi Porphyry, La Profunda intrusion, and the mineralised Characolla Porphyry are geochemically similar to the Yabricoya Formation (Fig. 3.39) and were emplaced at around the same time as eruption of that unit (Masterman, 2003; Munizaga et al., 2008). At ~238 Ma, the more primitive magmas of the Cascasca dyke swarm were emplaced into an ~8 km-long NNW-trending structural zone (Figs. 3.4, 3.23). The NNW-trending dyke morphologies of most of these intrusions (the geometry of the La Profunda intrusion is unknown) implies a distinct strain environment from that which prevailed throughout the Permian. The composition of these intrusions and the Yabricoya formation at Collahuasi point to a more alkaline arc-related magma than the mafic components of the Permian Peine Group. These magmas also assimilated lesser amounts of evolved crustal materials during storage and ascent in into the upper crust, consistent with development of structural permeability implied by the dykes.

Minor Choyoi Arc intrusive magmatism continued shortly after emplacement of the Cascasca dykes. In the Collahuasi district this was represented by the 232 Ma NW-trending Cerro Silvar porphyry dyke. Ten kilometres to the south, another quartz porphyry stock intruded at this time was associated with minor porphyry style mineralisation (El Loa Porphyry: Huete et al., 1977; Baeza and Alfaro, 1994; Tomlinson et al., 2001a). Volcanic rocks of this age are widespread in the Domeyko Cordillera at the latitude of Chuquicamata, where they rest non-conformably on San Rafael-age plutonic rocks. In a number of locations between Chuquicamata and Collahuasi ignimbrites dated at ~233 Ma overlie an angular unconformity with the rest of the Peine Group (Ramirez and Gardeweg, 1982; Marinovic and Lahsen, 1984; Naranjo and Puig, 1984; Tomlinson et al., 2001a). These ignimbrites represent the terminal magmatic event in the north Chilean segment of the Choyoi Arc, after which the magmatic arc stepped trenchward some 150 kms to the position of the modern Coastal Cordillera (e.g., Scheuber et al., 1994). Taking account of the thickness of the lower Peine Group stratigraphy, relationships between the terminal ignimbrites and plutons suggest that local exhumation of some of the San Rafael-age plutons exceeded 100 m/m.y. during the period from ~260 to 230 Ma. It seems likely therefore, that the San Rafael tectonic event was caused by a tectonic reorganisation

which saw cessation of rifting along the Choiyoi Arc and set in train the demise of subduction-related magma generation therein.

Decline of the Choiyoi Arc in the early Triassic and trenchward stepping of the arc magmatic axis in the middle Triassic has been attributed to accretion of an unknown terrane into the subduction zone (Parada et al., 1991; Mpodozis and Kay, 1992), or to slab rollback and increased westward "push"of the continent (Breitkreuz et al., 1990). The case for a little-known collisional event is not supported by the extensional morphology and more arc-like character of the Triassic dykes. Instead, absolute upper plate drift is likely to have changed in the Early Triassic as a response to closure of Paleotethys (e.g., Stamplfli and Borel, 2002). Calculated rates of subduction hinge retreat along the Phanerozoic Andean margin (Oncken et al., 2006) show that this process could account for the ~130 kms of westward movement of the arc front over ~10 m.y., i.e. fast enough to not be recorded by sparse magmatic rocks that yield radiometric ages between 230 and 195 Ma (data compilation of Scheuber et al., 1994; Tomlinson et al., 2001a; Haschke et al., 2002a). Thus Breitkreuz et al. (1990)'s hypothesis of global tectonic causes for the decline of the Choiyoi Arc has a plausible explanation in terms of plate motion rates and histories.

3.19.6 Quehuita Formation

Subduction roll-back was associated with pronounced subsidence and creation of sedimentary accommodation space occurred in the back-arc Tarapacá Basin (e.g., Prinz et al., 1994). The Quehuita Formation records the middle and later stages of sedimentation in this basin in the Collahuasi area. In the Chuquicamata district, minor terrestrial and marginal marine facies of the Sama Formation (Orrego, 1992) record a relatively rapid Middle to Late Triassic transgression in the Tarapacá Basin. Shales, limestone and minor sandstones then accumulated in the basin through the Jurassic. Maximum flooding in this basin adjacent to the Collahuasi district is recorded by the predominance of carbonaceous shales in the Aquiuno Member during the Dogger epoch (Smoje, 1989). After this time the basin gradually shoaled and the latest Jurassic stratigraphy is dominated by fine grained redbeds (Galli, 1957; Smoje, 1989; Moreno et al., 2000).

3.19.7 Cerro Empexa Formation

The Cerro Empexa Formation is commonly subdivided into a lower terrestrial clastic sedimentary facies association and an upper subaerial andesitic volcanic facies association. The former are interpreted as amalgamated alluvial fan deposits shedding eastward from a mid-late Cretaceous volcanic axis immediately west of the position of the Domeyko Cordillera (Maksaev, 1978; Tomlinson et al., 2001a). The upper subdivision records the eastward growth of the magmatic front during the late Cretaceous (Scheuber et al., 1994; Tomlinson et al., 2001a). The youngest volcanism of the Cerro Empexa Formation coincides in time with the emplacement of the oldest porphryry Cu-Mo deposits of the Paleocene mineral belt (e.g., Williams, 1992; Camus, 2002). Barren alkaline intrusions were emplaced toward the back arc at the same time, and are conspicuous elements of the geology in all the major Eocene-Oligocene porphyry camps (Richards et al., 2001a; Tomlinson et al., 2001a; Campbell et al., 2006; Urzua, 2009; the Tolaun intrusive complex, this study).

3.19.8 Eocene-Oligocene subaerial volcanic facies association

The volcanic Icanche Formation occurs in the Collahuasi district as a complex package of small lava flows and abundant welded block and ash flow deposits suggestive of a subaerial vent-proximal environment (Table 3.2). The package is intruded by late Eocene stocks at Cerro Sallihuinca and Cerro Cuno and together comprise a volcano-plutonic complex that is interpreted to represent the eroded remnants of a Middle Eocene volcanic centre. The lowermost member, the Sallihuinca rhyolite breccia, contains abundant Neoproterozoic to Ordovician zircon xenocrysts (Appendix III). This implies assimilation of crustal materials at crustal levels deeper than the supracrustal Peine Group and related plutons.

An angular unconformity separates the main Icanche Formation occurrence from the uppermost member, the Vega rhyolitic ignimbrite. This ignimbrite is petrologically distinct and implies the presence of another active volcanic centre in the vicinity during the Middle Eocene. The occurrence of volcanics belonging to the Icanche Formation in the southwestern part of the district (Fig. 3.4; Maksaev, 1978) is consistent with this interpretation. Contemporaneous terrestrial sedimentary facies of the Sichal and Calama Formations (Maksaev, 1978; Marinovic and Lahsen, 1984;

Blanco et al., 2003) are widespread in the greater Chuquicamata area but are not recognised at Collahuasi. Sediments of this age are likely to have been eroded from most of the Collahuasi district structural high, but may occur in the basal levels of terrestrial basins (such as the Quebrada Caya) that accommodate younger sediments (Fig. 3.21).

3.19.9 Terrestrial sedimentary facies association

Consolidated Oligocene to Miocene conglomerates and lesser lacustrine sands and siltstones occur widely in the Collahuasi district. They record terrestrial sedimentation that occurred during a period of warm, humid climatic conditions that prevailed from at least the Eocene (Simpson, 1983; Gayo et al., 2005; Shellito and Sloan, 2006) until the establishment of the Humboldt Current along western South America at ~14 Ma (Alpers and Brimhall, 1988). These deposits are typically confined to highly localised structurally controlled basins, especially along the Domeyko fault system. This major arc-parallel structural corridor was transtensional throughout the Oligocene (Chapter 4) and sedimentary accommodation space developed on releasing bends during sinistral displacement (Tomlinson et al., 2001a). Thick basin fill of this type accumulated in one such basin adjacent to the El Colorado alteration system, and in Quebrada Caya in the northeastern part of the district (Figs. 3.4, 3.21). Local basins formed on NW-trending half grabens Quebrada Blanca and on NW and ENE-trending grabens at Huinquintipa (Chapter 4).

3.20 Conclusions

The Peine Group volcanic and sedimentary rocks exposed in the Collahuasi district were deposited over a period of ~55 million years from the late Permian to the earliest Triassic. Extension along the magmatic arc drove the creation of sedimentary accommodation space that led to a transgressional event at ~290 Ma, here correlated with subsidence in the regional Miembro Medio basin.

The lower part of the Peine Group; the Chiclla, La Grande, and Cascasca Formations, was deposited over 12 ± 4 m.y. and comprise the hybrid products of subduction-related arc that was undergoing active extension and crustal anatexis. Transgression and accumulation of sedimentary rocks that defines the La Grande Formation

occurred over a period of no more than 5 million years, prior to infilling of the basin and a return to subaerial volcanism. Voluminous, generally fine to medium-grained fragmental volcanic products of the Cascasca, Huinquintipa and Sallihuinca Formations formed from repeated highly explosive volcanic eruptions. These took place over ~15 million years, probably as a series of discrete pulses associated with the establishment of large upper crustal chambers in which upper crustal anatectic melts may have mixed with subordinate volumes of subduction-related magmas.

The San Rafael tectonic event, bracketed here between 272 and 244 Ma, coincided roughly with local open upright folding, a hiatus in extension-related volcanism, and emplacement of large epizonal intrusions. An approximately 10 m.y.-long episode of post-kinematic magmatism included andesitic to felsic subduction-related volcanism (the Yabricoya Formation), and emplacement of weakly mineralised quartz porphyry dykes and stocks and the Cascasca dyke swarm.

The Icanche Formation had not been recognised in the vicinity of the porphyry deposits of the Collahuasi district prior to this study. It records effusive and lesser explosive subaerial magmatism, the youngest of which occurred four to five million years before the emplacement of high level stocks related to porphyry mineralisation. Disparate xenocryst populations and internal unconformities between members of the Icanche Formation at Cerro Sallihuinca suggest dramatic changes in the location of magmatic crustal assimilation concommittant with active tectonism and erosion during the Middle to Late Eocene.

Chapter 4.

STRUCTURAL GEOLOGY AND RELATIONSHIPS WITH HYDROTHERMAL ALTERATION AND MINERALISATION

4.1 Introduction

Porphyry and related epithermal mineral deposits are shallow crustal phenomena by virtue of the physical constraints on magmatic fluid exsolution (e.g., White and Hedenquist, 1990; Hedenquist and Lowenstern, 1994; Shinohara and Hedenquist, 1997). They form primarily within the brittle structural regime of the upper crust, although thermal conditions associated with magmatism permit local and transient ductile behaviour (e.g., Fournier, 1999). These deposit styles form preferentially during periods of unusually dynamic tectonism (e.g., Barley et al., 2002; Blundell et al., 2005; Cooke et al., 2005). Since porphyry copper, and related styles of mineralisation are fundamentally derived from various fluids: magmas, liquids and gases (e.g., Shinohara and Hedenquist 1997), this relationship is likely to be due (at least in part) to coupling between seismicity and fluid flow in the seismogenic crust (e.g., Sibson, 2001; Cox, 2005).

Regional scale associations between the location of mineralisation and major mapped or inferred fault zones are a common feature of major mineralised terranes (e.g., O'Driscoll, 1981; Richards, 2000; Richards et al., 2001b, Gow and Walshe, 2005; Palacios et al., 2006). However, the relationships between intrusion-related mineralisation and brittle structures are not statistically robust, and have been suggested to be caused by subjective bias (Paterson and Schmidt, 1999). Most porphyry copper deposits are generally considered to have formed during the latter stages of compressional deformation through to incipient extension in magmatic arcs above oblique subduction zones (e.g., Heidrick and Titley, 1982; Tosdal and Richards, 2001; Gow and Walshe, 2005). Partly due to scale-dependencies that are rarely considered, there are conflicting hypotheses about the relative importance of contractional, extensional and strike slip strain accommodation during porphyry

emplacement. This debate is particularly acute in northern Chile, where the kinematic history and significance for mineralisation of the Domeyko Fault is the subject of ongoing research and discussion (e.g., Lindsay et al., 1995; Tomlinson and Blanco, 1997a, 1997b; McClay et al., 2002; Amilibia and Skármeta, 2003; Campbell et al., 2006). Understanding the relationship, if any, between stress environment and mineralisation is especially relevant to mineral exploration because it directly affects our notions of what constitutes a favourable structural trap, and therefore affects the definition and prioritisation of exploration targets. As Tosdal and Richards (2001) point out, there are few detailed studies of the interrelationships between structures and hydrothermal mineralisation at deposit, or smaller scales. The debate is therefore hampered by a lack of data. The research presented in this chapter seeks to partly redress that lack of smaller scale structural-hydrothermal information. To put this detailed information in context, the district scale structural architecture is first addressed.

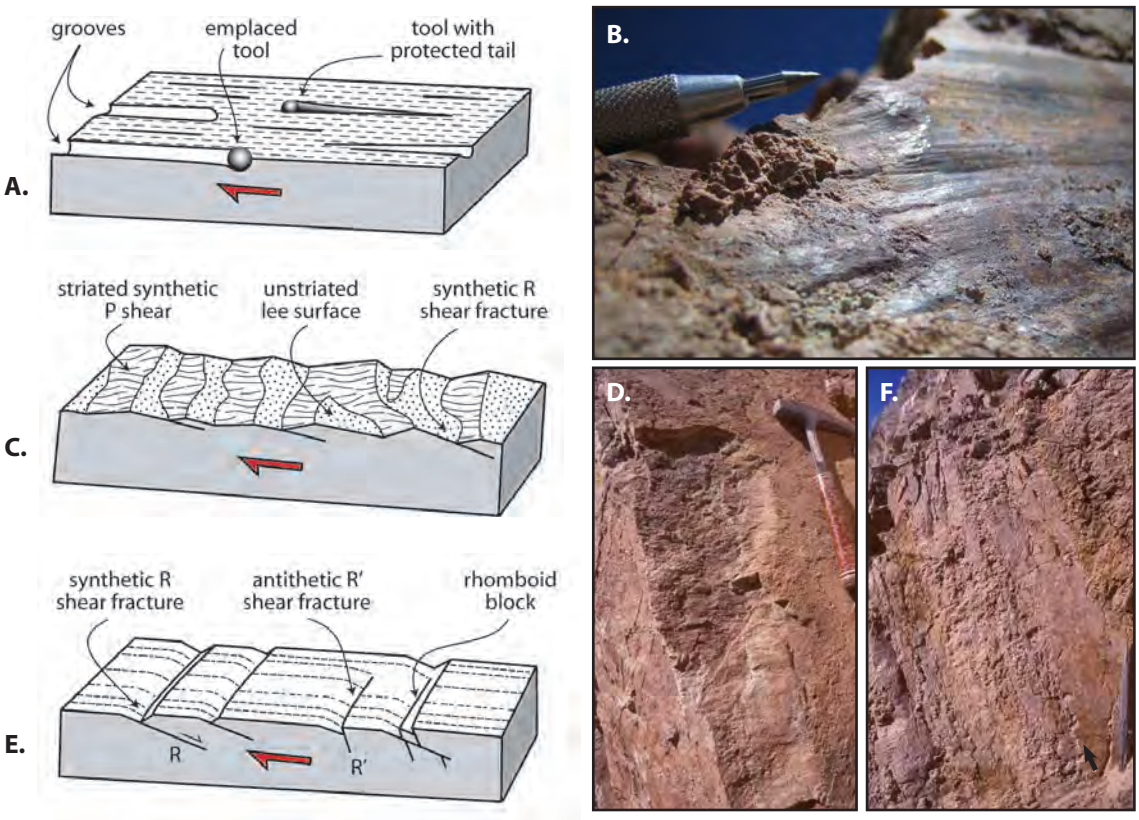

Figure 4.1. Schematic sketches and examples of common kinematic indicators. A-B) tools and grooves. Ridge of resistant tools near scribe tip in photo protected material in their lee, right, side. C-D) Fabric characterised by preferetial striation of synthetic P-shear fractures, as per the portion of the fault surface pictured to the left of the hammer. E-F) synthetic and lesser antithetic shear fractures on Riedel orientations relative to the main fault surface. Riedel shears are subvertical in photo, and are most strongly developed around an incipient fault surface, black arrow.

4.1.1 Mapping Methods and Contributory Information

Structural measurements were collected during this study from outcrops, road and conveyor cuttings, open pit mines and oriented drill core. Sense of movement on faults was determined following the criteria of Hancock (1985) and Petit (1987). Tensional shear fracture arrays on Reidel orientations, tools and groove marks, and preferential striation of P-fracture surfaces are by far the most common type of kinematic indicator observed (Fig. 4.1). Faults and shear zones showing ductile features such as S-C fabrics and porphyroclasts are extremely rare in the Collahuasi district. A subjective record was kept of the reliability of kinematic indicators. The structural maps and interpretation presented here integrate the new data with all the available existing data. A summary of the data volumes presented in Table 4.1 indicates the scope and style of structural data collected and compiled in this study. Appendix II contains explanations of the methods used for data weighting and geometric corrections.

Table 4.1. Populations of structural data collected and compiled for the Collahuasi district.

structural element, data source	Σ data points	% of total	Σ kin. sense	Σ kin. striae	% with kin. sense
Faults					
this study	1386	80.9%	784	142	56.6%
Fedorovic, 2001	160	9.3%	125	0	78.1%
Masterman, 2003	95	5.5%	95	95	100.0%
Desrochers et al., 2001	44	2.6%	0	0	0.0%
Munchmeyer et al., 1984	28	1.6%	0	0	0.0%
Joints					
this study	1278	74.1%	25	0	2.0%
Desrochers et al., 2001	446	25.9%	0	0	0.0%
Dykes					
this study	245	95.0%	50	0	20.4%
Desrochers et al., 2001	13	5.0%	0	0	0.0%
Veins					
this study	2127	~48%	33	0	1.6%
Lehmann, 1980	101	~2%	0	0	0.0%
Martini, 1984	only averages reported	~50%	0	0	0.0%
Depositional fabrics (bedding, pumice compaction etc.)					
this study	644	72.6%	-	-	-
Munchmeyer et al., 1984	219	24.7%	-	-	-
Masterman, 2003	24	2.7%	-	-	-

4.2 Previous Work

This study draws heavily on the body of previous work in the Collahuasi district (Tables 4.2 - 4.4). Appropriately, much of this previous research has been directed toward the timing and magmatic-hydrothermal evolution of the major mineral deposits. The relevant details are cited where they are reproduced and much of the analysis presented in this chapter rests on the compilation of new and existing data. In many cases, data presented in map form by previous workers has been captured digitally here to permit compilation and stereographic projection. As the more significant earlier studies were described in Chapter 1, only tabulated summaries are presented here (Tables 4.2 - 4.4). Literature that did not contribute new data or interpretation relevant to the structure of the district and its deposits, or add to the understanding of the hydrothermal paragenesis of the mineral deposits has not been included in the tables.

Table 4.2. Summary of previous structural and hydrothermal research at Copaquire.

Researchers	Study Type	Scope	Alteration and Vein Paragenesis	Structure and Geochronology
Villemur, 1963	Independent report	District mapping, evaluation of economic potential.	Identifies alteration zones and secondary Cu minerals at Copaquire, Quebrada Blanca and at Cerro Campana, N of Copaquire.	Maps orientation of small polymetallic vein deposits to the NE of QB
Camus and Fam Romero, 1971	Independent report	Prospect scale lithological and alteration mapping.	Presented simple maps of lithology and alteration distribution. Identify tourmaline in medial lateral positions around surface whole rock Mo-Cu anomaly.	–
Sillitoe and Neumann, 1972	Independent report	Prospect scale lithological and alteration mapping.	Presented maps and simple sections of alteration distribution	–
Hollister and Bernstein, 1975	peer-reviewed paper	Prospect scale lithological, alteration and structural mapping.	Described four intrusive phases, one breccia stage and three vein stages. Maps the distribution of alteration facies over a small area.	Suggested that porphyry intruded a dextral dilational jog adjacent to the Domeyko FS. Maps primarily NE-trending, subvertical veins.

TABLE 4.3. Summary of previous structural and hydrothermal research at Quebrada Blanca.

Researchers	Study Type	Scope	Alteration and Vein Paragenesis	Structure and Geochronology
Fam, 1974	Maestría (Honours)	1:10,000 mapping of the main QB alteration zone.	Commented on the extent of kfs-bt and ep-tm-spec-amph-calcite alteration around the QB deposit	Observed cross cutting relationships between magmatism, alteration and faults. Recognised that alteration is continuous from the stockwork SSW along the QB fault.
Lehmann, 1980	Maestría (Honours)	Mineralogy, geometry of molybdenite.	Identified very late-stage mo-rich and pyrite-kaolinite hydrothermal stages.	Mapped the NW-trending Moly Breccia and showed that it cross-cut earlier strockwork mineralisation.
Martini, 1984	Maestría (Honours)	Mineralogy, geometry and relative timing of late stage veins and associated alteration	Integrated vein and breccia parageneses. Identified tourmaline is intermineral, and records very late qtz-mo and py hydrothermal stages	Mapped orientation of thousands of late stage veins and investigated host rock and breccia controls on vein frequency. Showed that the Vuggy Breccia and the main pyrite-kaolinite stage were contemporaneous.
Hunt et al., 1985	peer-reviewed paper	Geological overview and resource assement	Described breccia facies and presents small scale maps and sections.	Mapped multiple overprinting ENE breccia bodies. Observed cross cutting relationships between faults, breccias and veins - faults active during late veining.
Rowland, 1998; Rowland and Wilkinson, 1999	PhD and reviewed paper	Magmatic chemistry, vein paragenesis, fluid inclusions	Described seven vein stages: three early stages with potassic alteration; one early stage with sericitic alteration; two intermediate qtz-mo-py stages; and a late py stage.	_
Desrochers et el., 2001	Company report	Lithological and structural mapping at 1:5,000.	_	Mapped the strike of faults and dykes in the QB deposit. Mapped bedding and folds at El Colorado.
LaPointe, 2003	Company report	Updated mine lithology mapping, and evaulation of hypogene resource.	Mapped distribution of dykes, breccias, grade and alteration that suggest a complex early alteration sequence.	Interpreted the QB intrusive complex to have intruded into a rhombic dextral dilational jog under ENE compression.
Sillitoe, 2005	Company report	Review of structural controls and economic potential.	Suggested that anhydrite was a hypogene phase during Vuggy Breccia formation. Interpreted El Colorado as the roots of a lithocap that originally extended over QB.	Considered the QB fault to have been under compression during porphyry emplacement, and all NW faults to be later "readjustment".

Abbreviations: QB = Quebrada Blanca, kfs = orthoclase, bt = biotite, ep = epidote, tm = tourmaline, spec = specularite, amph = amphibole, qtz = quartz, mo = molybdenite, py = pyrite.

TABLE 4.4. Summary of previous structural and hydrothermal research at Rosario-La Grande and Ujina.

Researchers	Study Type	Scope	Alteration and Vein Paragenesis	Structure and Geochronology
Ware et al., 1981; Munchmeyer et al., 1984	Company reports	District scale mapping	Mapped small regional mineral occurrences. Mapped the extent of hydrothermal alteration using electrical geophysics.	Mapped bedding orientations and veins across the La Grande area. Suggested a sinusoidal, en echelon vein array for La Grande.
Dick and DeBeer, 1994	peer-reviewed paper	Pre-feasibility review of deposit-scale data	_	Map geology and major structures in drill sections at Rosario and Ujina.
Lee, 1994	Masters thesis (N.Am.)	Deposit scale mapping, mineralisation and alteration paragenesis	Mapped early disseminated and stockwork mineralisation with potassic alteration and later fault-controlled vein stages with phyllic alteration.	Mapped veins in the vicinity of the Rosario Fault. Suggested that this structure is the principal control on porphyry emplacement.
Bisso et al., 1998	peer-reviewed paper	Summarised deposit scale geology, alteration and sulfide mapping	Described a generalised vein and alteration paragenesis for Rosario and Ujina. Recognised four conventional porphyry vein stages and three alteration facies at Ujina.	Mapped lithology, alteration and structures in section. Suggested Rosario prophyry formed during compression and that Ujina formed during extension.
Fedorowich, 2001	Company report	Sub-district scale structural mapping and sampling	Identified regional faults that host minor mineralisation.	Proposed that mineralisation accompanied compression and that NW- and NE-trending faults were active as strike slip conjugates.
Smoje, 2003	Company report	Deposit scale geotechnical mapping	_	Defined three NW-trending structural domains within shallow levels of the Rosario deposit. The central of these is dominated by the Rosario and Lulu faults and also shows stronger NE-trending faults.
Masterman, 2003; Masterman et al., 2004, 2005	PhD and reviewed papers	Deposit scale mapping and mineralisation and alteration paragenesis, fluid inclusions, geochronology, and geochemistry.	Described nine vein stages for the Rosario-La Grande system: four early stages with potassic alteration; one intermediate qtz-mo stage; two late pyritic stages with illite-muscovite alteration; and two very late polymetallic stages with qtz-alunite alteration.	Constrained the timing of mineralisation using $^{40}Ar/^{39}Ar$. Mapped structures in the Rosario deposit and inferred that the Rosario Fault controlled porphyry emplacement. Suggested porphyry mineralisation occurred during regional sinistral transtension and epithermal mineralisation during gravitiational collapse.

4.3 Structural Architecture of the Collahuasi District

At the latitude of Collahuasi the Domeyko Cordillera comprises an arc-parallel exhumed block (the "Collahuasi Block") of gently folded Permo-Triassic volcanosedimentary rocks. This is bound on its western margin with an east-vergent fold and thrust belt developed in Mesozoic sedimentary strata (Tomlinson et al., 2001a; Amilibia et al., 2008; Chapter 3). The bulk of the Eocene-Oligocene porphyry mineralisation in the district is hosted within, or very close to the Collahuasi Block. The principal structures in the vicinity of mineralisation were mapped to determine their kinematic history. This information, taken with the stratigraphic map pattern (Chapter 3) permits an interpretation of how, and when the district scale structural architecture developed.

The Collahuasi Block is bound on both sides by major, steeply-dipping, approximately N-trending regional faults; the Domeyko Fault and Rio Loa Fault (Fig 4.2). The primary internal structural divisions within the block are a series of NNE-trending, steeply dipping faults, including the Quebrada Blanca and Monctezuma faults. Short strike-length faults trending NW and NNW are common within the block, and generally link between younger faults. In the eastern half of the district, the Rosario Fault is the most prominent example of this group of structures (Fig. 4.2). Early Triassic dykes occupy NNW-trending fracture zones, notably the Collahuasi Porphyry near Rosario and the Cascasca andesitic dyke swarm exposed in the Ujina-Rosario conveyor cutting and the Rosario road. Moderately to steeply-dipping, arc-oblique ENE-trending faults comprise a fifth recognisable set within the Collahuasi Block. These commonly have very restricted displacement and occur as splays from, or links between NNE trending faults. The best-developed group of these extend from Quebrada Blanca to Huinquintipa and may extend right across the block as it aligns with the Tolaun Intrusive Complex and the Pabellón del Inca volcano in the east (Fig. 4.2).

4.3.1 The Domeyko Fault System and the Quebrada Blanca Fault.

The Domeyko Fault system is a continental scale fracture zone that stretches more than 1000 km along the Chilean Precordillera (Tomlinson and Blanco, 1997a). It coincides with a major Bouguer gravity anomaly boundary along its entire

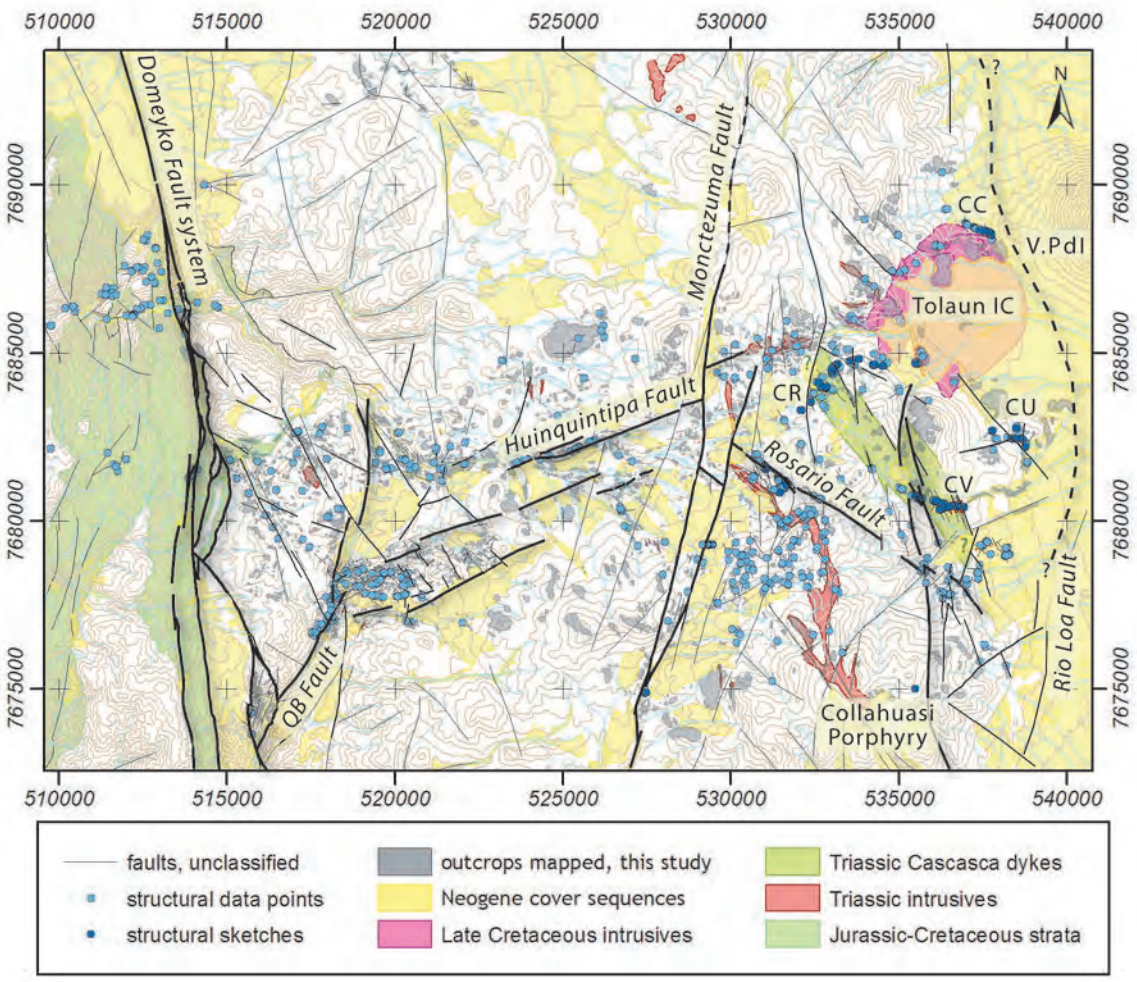

Figure 4.2. Map showing the principal structural elements of the Collahuasi district. Observation points of major structures and locations of detailed (1:~400) excavated wall structural sketches are also shown. Abbreviations: CC = Camino Coposa, CR = Camino Rosario, CU = Camino Ujina, CV = Conveyor cutting, IC = intrusive complex, V.PdI= Volcán Pabellón del Inca.

length (Rivera et al., 2006a). At depth it marks the trenchward limit of a shallowly W-dipping seismic reflector (Oncken et al., 1999) that becomes a seismogenic detachment at approximately 33ºS (Farias et al., 2006).

At Collahuasi the Domeyko Fault marks the eastern limit of the thick Jurassic marine succession (Chapter 4; Smoje, 1989; Tomlinson et al., 2001a) and is considered to be the master fault for an east-vergent series of reverse faults developed within that package of rocks (Smoje, 1989; Amilibia and Skármeta, 2003). Isopach maps of the Jurassic stratigraphy (Prinz et al., 1994) and regional compilations of sedimentary facies (Arcuri and Brimhall, 2002; Fig 2.5) show that depocentres of the Jurassic Tarapacá Basin align immediately west of the Domeyko fault. Jurassic volcanic rocks extend in a linear belt parallel to, and 100-200 kms west of the basin. The

basin is therefore interpreted as a regional half-graben developed inboard of the magmatic arc, in which subsidence was primarily articulated on a series of soft-liked extensional faults in the position of the modern Domeyko Fault system (e.g., Prinz et al., 1994; Tomlinson and Blanco, 1997a). The chemistry of the Jurassic magmatic rocks is transitional between typical suprasubduction magmas and back arc basin magmas, suggesting that extension prevailed in the Jurassic arc and back arc (Pichowiak et al., 1990; Pichowiak, 1994).

Extensional faults in the position of the Domeyko Fault system may have originated even earlier. The Permo-Triassic Choiyoi Arc in southern Peru was extensional and accumulated sedimentary rocks and rift-related primitive magmas (e.g., Noble et al., 1978). The time-equivalent Peine Group volcanic sequences of the Collahuasi district are associated with lacustrine or shallow marine sedimentary rocks (section 3.5) and to the north the sequence was entirely subaqueous (Breitkreuz and Zeil, 1994; Fig. 3.34). The basement beneath the Jurassic sequences to the west of the Domeyko Fault system does not include the Peine Group, and instead comprises Neoproterozoic to Silurian metamorphic rocks (Vergara and Thomas, 1984; Damm et al., 1986, 1990, 1991). The proto-Domeyko FS may therefore have originated as an east-side-down growth fault along the trenchward (western) margin of the Permo-Triassic arc-graben.

The Quebrada Blanca (QB) fault is a NNE-trending subvertical splay of the Domeyko Fault system (Fig. 4.2). Distinctive, coherent quartz-phyric rhyolites and monomictic dacitic volcanic breccias of the lower Chiclla Formation occur exclusively in the vicinity of the El Colorado sector (Figs. 3.12 and 3.21) where the Quebrada Blanca fault joins a strand of the Domeyko Fault. The QB fault extends from this location, at least eight kilometres to the northern limit of mapping. In that area it marks a pronounced change in the thickness and facies of the upper members of the Yabricoya Formation (Fig. 3.4). These andesites comprise a pile of interfingering flows a few tens of metres east of the Quebrada Blanca fault, whereas they are restricted to minor planar flow sheets immediately to the west of it. Among the Permian strata, the main Cascasca Formation rhyolitic ignimbrites are absent to the east of the QB Fault, but attain thickness of hundreds of metres to the west (Fig. 3.13). Similarly, the middle La Grande Fornation has a well developed sandstone-

rich intercalation to the east of the QB Fault, but a much-attenuated equivalent sedimentary section to the west (Figs. 3.4 and 3.12). This structure therefore appears to have influenced magma eruption throughout Peine Group time.

The Domeyko Fault system and the Quebrada Blanca fault have been inverted and multiply re-used during the post-Jurassic history of the region (e.g., Amilibia and Skármeta, 2003). This recent history is investigated in more detail in Chapter 5.

4.3.2 Rio Loa Fault Zone and the Preandean Depression.

The Preandean Depression is an irregular, orogen-parallel intermontane basin that contains numerous large salt lakes (Fig. 4.3). Faults that define its western margin (the eastern margin of the Domeyko Cordillera) are together referred to as the Rio Loa fault system, although these are generally concealed beneath Cretaceous to recent volcanic and sedimentary cover and are best known from seismic reflection surveys (e.g., Muñoz et al., 2002).

The oldest sedimentary rocks known from the Preandean Depression were deposited in half grabens that formed in the Cenomanian (Muñoz et al., 1997). This coincides with the late stages of a major regional extension event in southwestern Bolivia and northwestern Argentina (Salfity et al., 1985). In the Salar de Atacama sector,

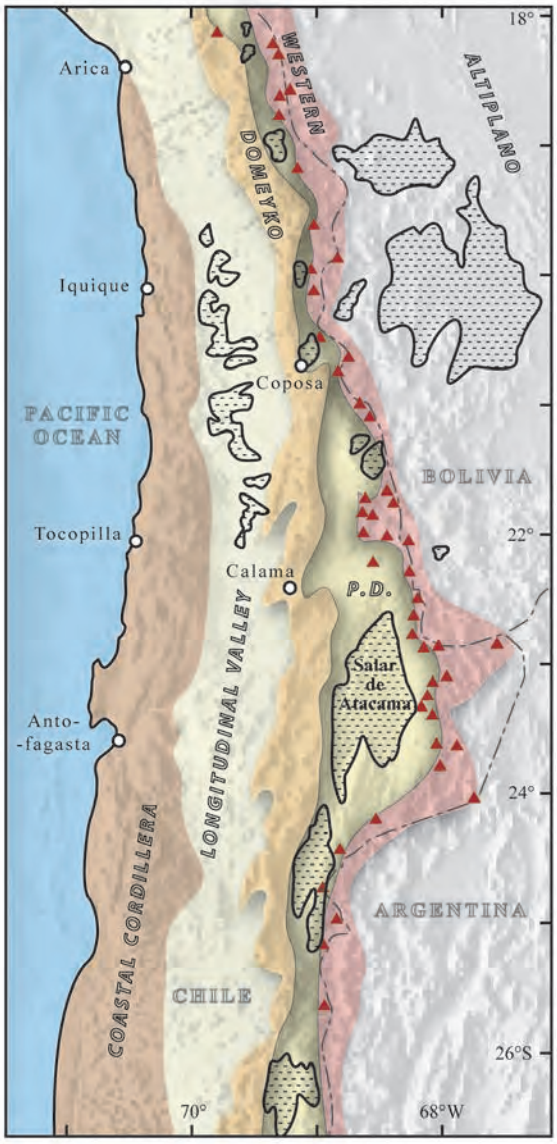

Figure 4.3. Simplified physiographic map of the Central Andes showing the major geomorphological subdivisions and the locations of major salt lakes (stippled). The Collahuasi district is located immediately south of Coposa. Although irregular, the Preandean Depression (P.D.) separates the Domeyko Cordillera from the Western Cordillera throughout the southern Central Andes.

the Rio Loa Fault system is interpreted as a major Cretaceous growth fault that was inverted during the latest Cretaceous or Paleogene (Muñoz et al., 2002). Although the basin is less well developed in the Collahuasi area (Fig. 4.3), a common Cenomanian extensional origin is inferred for approximately N-striking faults along the western margin of the Preandean Depression.

4.3.3 Folding and Plutonism.

The Peine Group stratigraphy in the Collahuasi Block dips broadly northward and includes several upright open folds (Munchmeyer et al., 1984; Chapter 3, Fig.4.4). Folding is disharmonic and fold wavelength is related to the rheology of the strata; sedimentary and thin-bedded pyroclastic units such as the Upper La Grande and Huinquintipa Formations exhibit shorter wavelength folding ($\lambda \sim 2$ km) than coherent volcanic parts ($\lambda \sim 5$ km; Figs. 3.4 and 4.5). Two sub-orthogonal sets of fold axes are evident, although both locally exhibit curved or possibly folded hinge lines (Fig. 4.5). To the west of the Domeyko Fault, the Jurassic and Cretaceous stratigraphy is folded into harmonic, open to tight, locally overturned folds with axes sub-parallel to the Domeyko Fault (Fig. 4.4; Smoje, 1989; Amilibia and Skármeta, 2003). These are interpreted as thrust-tip folds developed above blind east-vergent thrusts that splay from the Domeyko Fault (e.g., Maksaev and Zentilli, 1999; McClay et al., 2002; Amilibia and Skármeta, 2003; Amilibia et al., 2008).

Overall, the orientation of regional fold axes is similar for Mesozoic and Paleozoic strata (Fig. 4.6 a-b), although the style of folding is markedly different (Figs. 4.4, 4.5). The interference dome-and-basin fold pattern that is best developed to the north of Rosario (Fig. 4.6 c-d) could be interpreted as the result of overprinting of pre-Mesozoic E-W trending folds by Tertiary N-S trending folds. However, the Lower Triassic Cascasca dyke swarm (mean orientation 60º→250) has systematic and uniform orientation in the Camino Rosario and Conveyor Cutting sectors (Figs. 4.2 and 4.6), wherein fold axes in the host Peine Group trend E-W and N-S in the two sectors, respectively (Fig. 4.5). If the dykes are rotated so as to remove the effect of hypothetical post-Mesozoic folding event about N-S axes, then dykes in the two sectors have suborthogonal orientations. This is an unlikely emplacement geometry since NNW to NW is a common orientation for Triassic-Jurassic dykes and stocks

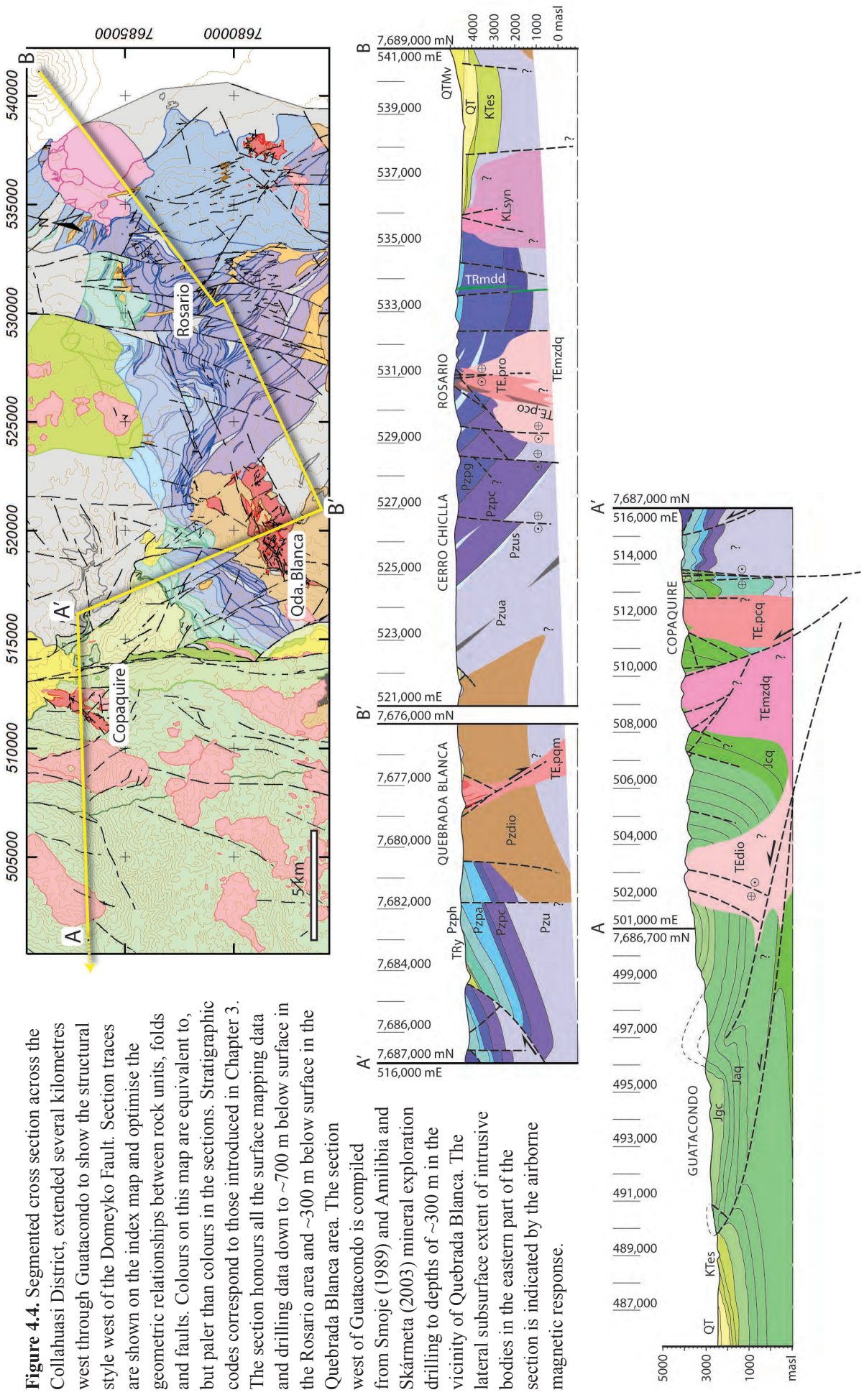

Figure 4.4. Segmented cross section across the Collahuasi District, extended several kilometres west through Guatacondo to show the structural style west of the Domeyko Fault. Section traces are shown on the index map and optimise the geometric relationships between rock units, folds and faults. Colours on this map are equivalent to, but paler than colours in the sections. Stratigraphic codes correspond to those introduced in Chapter 3. The section honours all the surface mapping data and drilling data down to ~700 m below surface in the Rosario area and ~300 m below surface in the Quebrada Blanca area. The section west of Guatacondo is compiled from Smoje (1989) and Amilibia and Skármeta (2003) mineral exploration drilling to depths of ~300 m in the vicinity of Quebrada Blanca. The lateral subsurface extent of intrusive bodies in the eastern part of the section is indicated by the airborne magnetic response.

throughout the Collahuasi district (chapter 3) and across northern Chile (Arévalo et al., 2003; Reyes and Cembrano, 2006). It therefore seems more likely that all the Peine Group folding occurred prior to emplacement of the NW-NNW trending dykes.

Three major granitoid plutons in the greater Collahuasi district occupy the anticlinal cores of regional domes (Fig. 3.4). In the western part of the district, the elongate body of the Escorial diorite forms an obvious core to a major N-plunging anticline ("Pzdio" in Fig. 4.4). Where they were mapped in this study, the Late Permian granitoids are medium grained and equigranular, and do not contain any macro- or microscopic mineral alignment or foliation. The characteristics of the Permian plutons are interpreted here to indicate shallow levels of emplacement and non-catastrophic ascent to the shallow crustal environment. The associated domal folding of the Peine group host package is consistent with intrusion accommodation via roof-uplift, and the plutons are anticipated to have tabular geometry, following Arévalo et al. (2002). Folding of the Peine group appears to have occurred primarily during emplacement of these plutons. The interference fold pattern reflects crumpling of rheologically weak strata rather than overprinting of two separate, suborthogonal folding events. However, tilting and gentle upright folding of the post-pluton Yabricoya Formation (Fig. 4.6f) requires that some fold tightening occurred after ~245 Ma (Chapter 3). At shallow crustal levels, shortening associated with Tertiary tectonism appears to have been predominantly accommodated by the Mesozoic stratigraphy and by faults related to the Domeyko Fault (Smoje, 1989; Tomlinson et al., 2001a; Amilibia and Skármeta, 2003; Amilibia et al., 2008).

All the mapped Lower Triassic intrusions in the Collahuasi district have elongate or dyke morphoplogy (Chapter 3), and all trend NW or NNW (Fig. 4.7). Stratigraphic offset accommodated on these structures is minimal (Fig. 3.4). The Cascasca dyke swarm and the Collahuasi Porphyry both occur over continuous strike of >8 kms, and therefore represent major elements of the structural architecture of the district (Fig. 4.2). The dyke orientation is interpreted here to reflect emplacement under WSW-directed extension (following the stress criteria of Pollard, 1987). The dyke orientation might alternatively reflect re-opening of an existing structural fabric under poorly constrained extensional conditions, but this seems unlikely given the general scarcity of NNW-trending faults in the district.

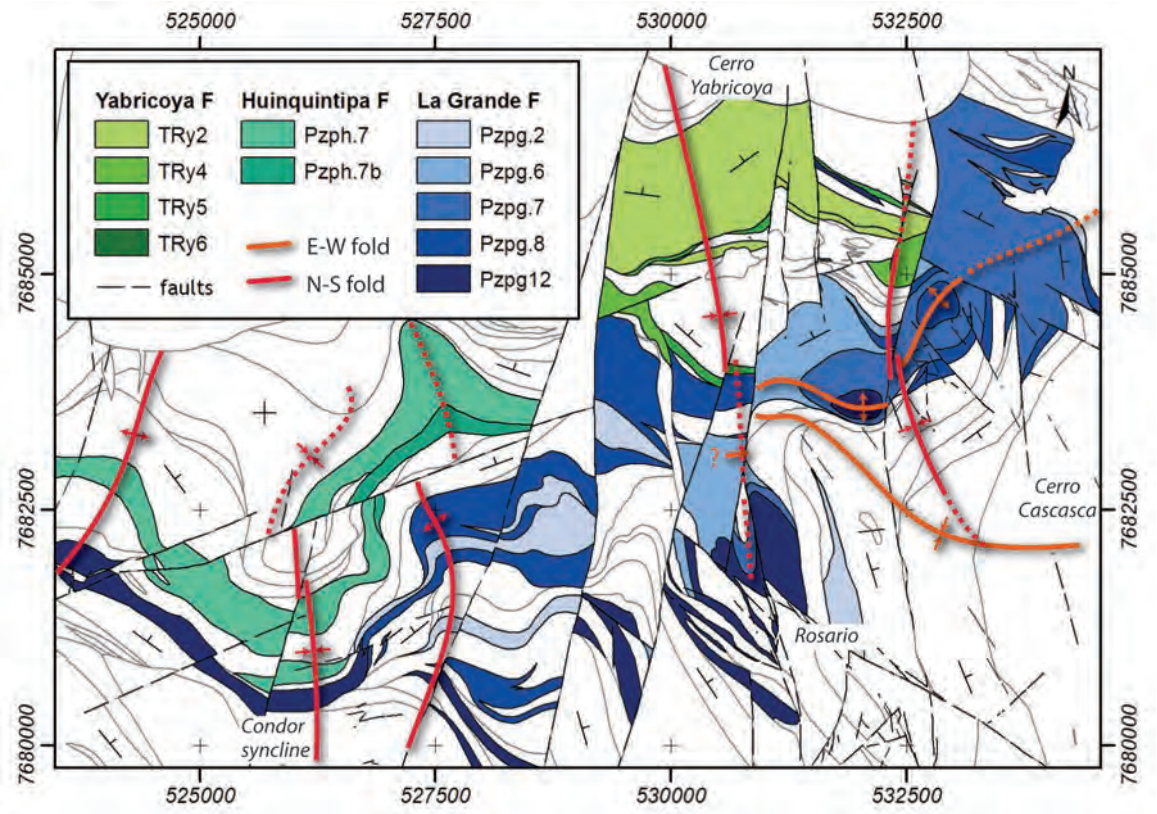

Figure 4.5. Map of the northeastern Collahuasi district in which overprinting dome-and-basin folding is developed in sedimentary and pyroclastic sequences of the middle Peine Group. Selected stratigraphic units are coloured to highlight the fold geometry and schematic strike and dip bedding symbols are shown.

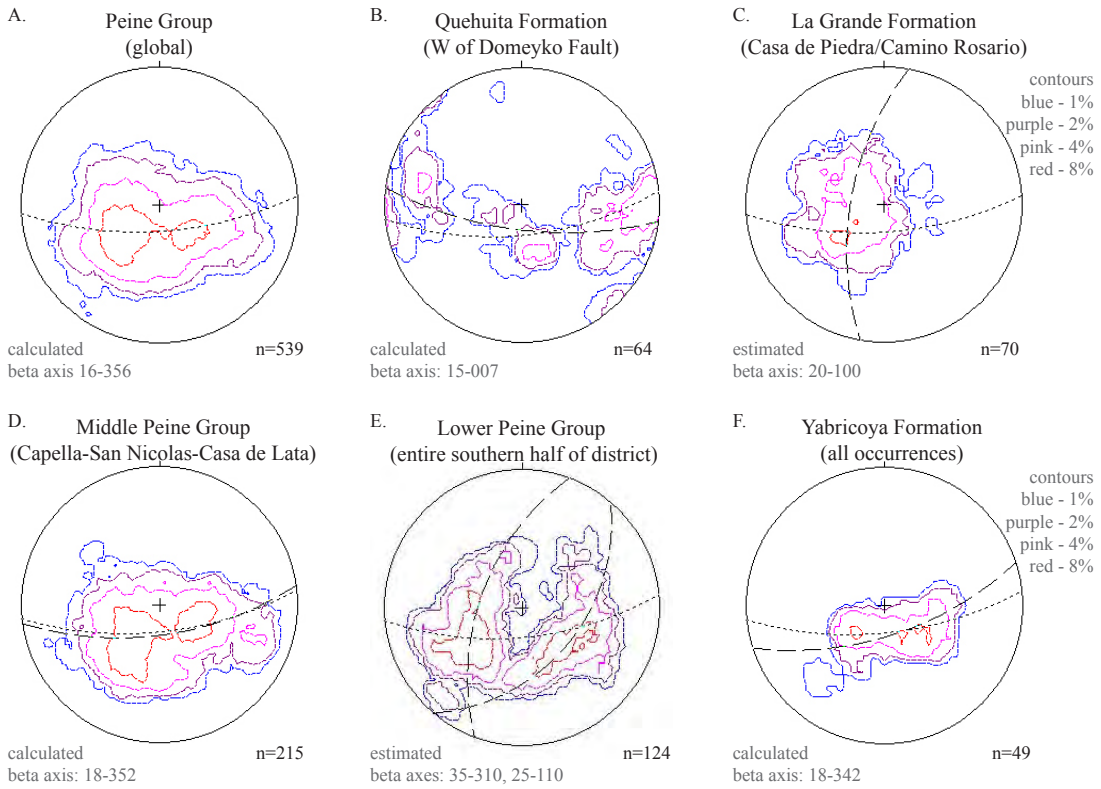

Figure 4.6. Equal area stereographic projections of bedding orientations (as contoured poles to planes) in selected sectors of the Collahuasi district (see Figs. 3.7 and 4.2 for locations). Light dashed great circles are the girdle to global Peine Group data, heavy dash are estimated girdles to local subsets.

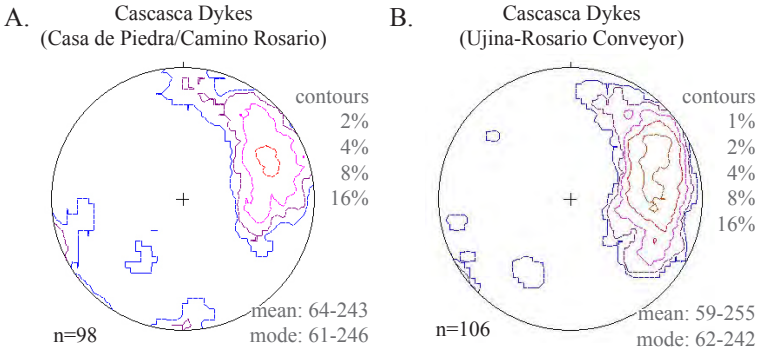

Figure 4.7. Equal area stereographic projections of the Cascasca dykes (as contoured poles to planes): A.) along the Camino Rosario, and B.) along the Ujina-Rosario conveyor cutting. Bedding in these two areas is shown in Figure 4.6.

4.3.4 Monctezuma, Rosario, and related faults.

The fault architecture of the eastern Collahuasi district is dominated by a series of NNE- and NNW-trending faults and fault zones that have hundreds of metres to kilometres of sinistral strike-slip displacement along part or all of their lengths (Fig. 4.8). From west to east, they are called the Monctezuma Fault (which has two principal strands that merge in the south), the Lulu Fault; the Collahuasi Fault, and the Cascasca Fault. To the immediate east of the Ujina porphyry, the N-trending Rio Loa Fault is inferred to be located under cover. These faults cut, link, or are cut by the NW-trending Rosario Fault (Figs. 3.4 and 4.8). The latter is a zone of anastamosing, moderately to steeply dipping fault strands that hosts Cu-Ag-rich massive sulfide veins and associated alteration at Rosario (DeBeer and Dick, 1994; Lee, 1994; Bisso et al., 1998; Masterman et al., 2005). The net displacement on these faults is summarised in Table 4.5, although this belies the complex kinematic histories of some of the faults. Changes in the lithofacies and/or the thickness of lithostratigraphic units across these faults suggests the major fault strands originated during deposition of the Peine Group (Fig. 3.35). However, dissection of the fold geometry evident in the overall map pattern suggests that the much of the displacement occurred after plutonism and folding.

The Rosario Fault is known to extend from its intersection with the Monctezuma Fault in the central part of the district, to the Cascasca Fault in the east. It is clearly truncated and offset by the eastern Monctezuma Fault (*cf.* Masterman et al., 2005; Fig. 4.8). The position west of the western Monctezuma Fault where the Rosario Fault might be expected to occur is marked by stratigraphic complexity but not by a through-going fault. The Rosario Fault may therefore have originated as a link fault

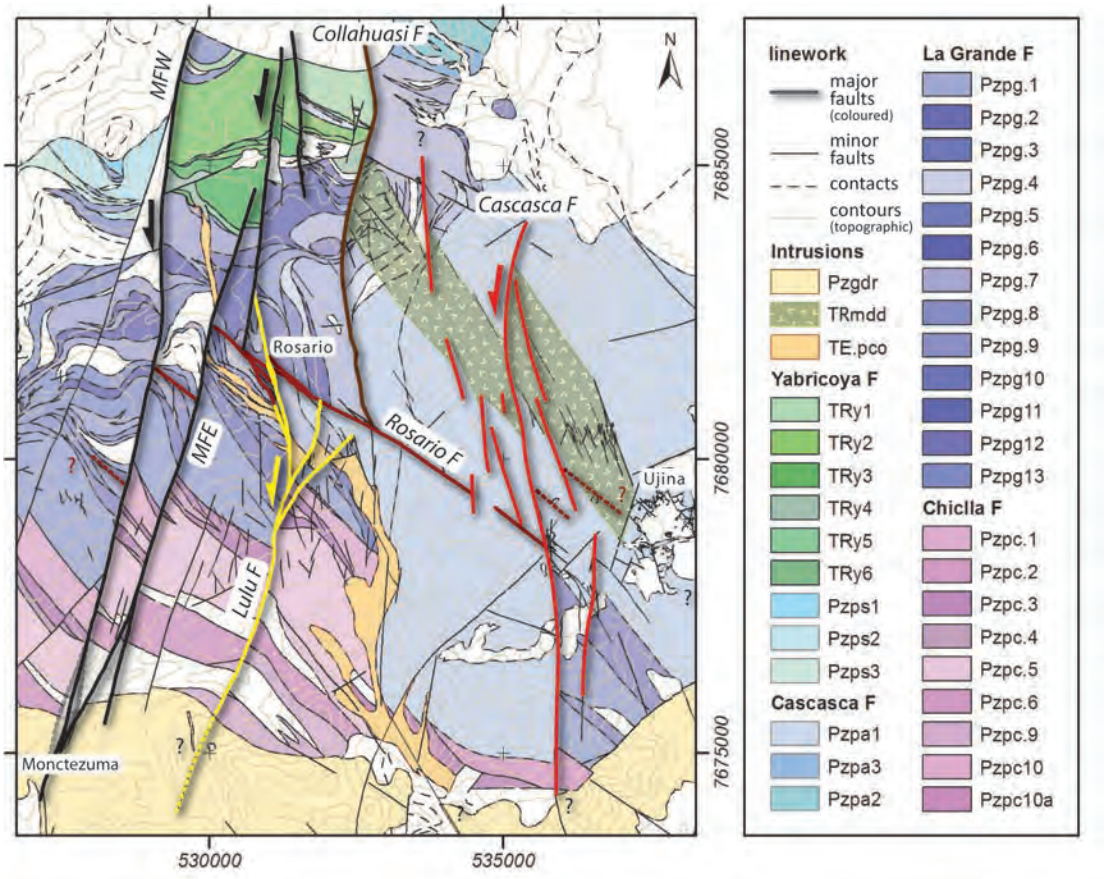

Figure 4.8. Geological map of the eastern Collahuasi district showing the principal fault systems and dykes that define the structural architecture. Linework colours serve only to identify related fault strands. MFE = eastern strand of the Monctezuma Fault, and MFW, the western strand. F = fault. Note that the margin of the Ceucis diorite (Pzgdr) in the south is largely covered by Neogene gravels and the absence of offsets along the marked boundary probably reflects limited map detail in that area, and does not constrain the timing of displacement on any of the faults.

that was active in concert with the Monctezuma Fault, rather than an older structure that has been subsequently displaced. Its relationship to the Cascasca Fault is similar. Restoring sinistral offset on the Cascasca Fault would place the SE extension of the Rosario Fault in the Ujina porphyry Cu deposit (Fig. 4.8). Northwest trending structures are known from Ujina (section 4.8), but there is not a single, dominant fault in this orientation.

In the Rosario porphyry Cu deposit, the Rosario Fault dips 45-65º toward the SW and cuts strata that dip ~50º to the ENE (Masterman et al., 2005). The fault plane steepens to 75º three km to the SE of the deposit (Fedorowich, 2001) where it cuts strata that dip ~15º to the NE. It therefore appears to be suborthogonal to the strata (as drawn in Fig. 4.4) and to have rotated into its present position during folding in the Late Permian. It is situated amid the thickest part of the conglomeratic and

andesitic Lower La Grande Formation section (Figs. 3.12 and 3.35). This part of the sequence is also characterised by abundant plagioclase megacrystic basaltic andesites ("*ocoita"*, Pzpg10). Upsection, the Cascasca Formation semi-conformably overlies the La Grande Formation north of the Rosario Fault, but the two units share an angular unconformity in the south (Fig. 4.8). Post-mineral straie mapped on the fault surface (section 4.9) indicate several stages of oblique slip, and this fault therefore seems to have not been optimally oriented for any of the younger tectonic events. On this basis, the Rosario Fault is interpreted to be at least as old as the lower La

Table 4.5. Net displacement (metres) on the major faults of the Collahuasi district.

Faults[a]	Key offset markers[b]	Sinistral[c]	Dextral[d]	Reverse[d]	Normal[d]
Domeyko	Stratigraphy, intrusive complexes, U-Th/He	~35,000	-	-	300 - 500
Quebrada Blanca	Stratigraphy, U-Th/He	-	1400 - 2400	400 - 1050	-
San Nicolas	Stratigraphy	200*	-	-	-
Monctezuma W	U-Th/He, intersection of bedding and Rosario Fault	2,200	-	300-800	-
Monctezuma E	as Monctezuma W	1,100	-	-	-
Cascasca	Cascasca dyke swarm	2500*	-	-	-
Rosario	Stratigraphy, striae	220	-	-	220
Lulu S	Intersection of Collahuasi porphyry and bedding	850	-	-	-
Lulu N	Rosario Fault, striae	50	-	-	250
Jack Rock	Intersection of Collahuasi porphyry and bedding	-	-	-	200

a.) The San Nicolas fault is sympathetic to the Monctezuma faults and is located immediately west of them. The Lulu Fault is subdivided into a northern part where it trends NNW and interacts with the Rosario Fault, and a southern part that comprises N- and NNE trending splays that each contribute to the larger net displacement. The Jack Rock fault is a SW-dipping normal fault in the hanging-wall of the Rosario Fault.

b.) Where possible, offsets were determined from the intersection of structural and stratigraphic elements that could be recognised on both sides. In some cases, the results of U-Th/He thermochronology (Chapter 5; McInnes et al., 1999; Tomlinson et al., 2001b) have been included. Offsets marked with an asterisk (*) are those for which only two-dimensional data are available.

c.) Sinistral net offset on the Domeyko fault is that suggested by Campbell et al. (2006), which is of the same order as that suggested by Dilles et al. (1997) and Tomlinson et al. (1997b)..

d.) Offsets with a range of values include interpretation based on new U-Th/He data (Chapter 5).

e.) Totals are for the Collahuasi district only and do not include the regional offset along the Domeyko Fault system.

Grande Formation and may have influenced Permian sedimentation and magmatism, although obvious post-Triassic displacement dominates the contact relationships mapped along the fault (Figs. 3.4 and 4.50).

Stratigraphic evidence also constrains the early history of the principal arc-parallel, approximately N-trending faults. The Monctezuma Fault is the most demonstrably long-lived ~N trending fault in the distict. The lower La Grande Formation thins markedly across the Monctezuma Fault and two subparallel NNE-trending faults to the west (Figs 3.4, 3.12 and 4.8). Likewise, the Huinquintipa and Sallihuinca Formations are known only on the west side of the Monctezuma fault (Fig. 3.15). On the eastern side of the fault, the equivalent stratigraphic position is occupied by a slight angular unconformity between the La Grande and Yabricoya Formations (Fig. 3.12). This implies the at least the western strand of the Monctezuma Fault was a normal fault during the Late Permian. In contrast, the Yabricoya Formation is absent from the western block (Figs. 3.16 and 4.8). Its stratigraphic position is occupied by an angular unconformity between the Sallihuinca and Icanche Formations (Fig. 3.12). In turn, this imples that the Monctezuma Fault was inverted during the San Rafael orogeny, broadly contemporaneous with folding and plutonism. Like the Rosario Fault, the Monctezuma Fault has a consistent angular relationship with the Peine Group stratigraphy. However, as it is approximately orthogonal to the hinge of the major regional fold, the plane of the Monctezuma Fault was not rotated more than 10º during folding. Similar stratigraphic arguments can be made for the existence and extensional or transtensional nature of the Collahuasi and Cascasca Faults during Peine group time.

The Aluk-South American plate convergence vector was oriented SE (modern coordinates) prior to the Middle Cretaceous, highly oblique to the western Gondwanan margin (Fig. 4.9. Pichowiak et al., 1990; Scheuber et al., 1994). This convergence geometry implies that the Choiyoi arc would have been broadly transtensional (e.g., Jarrard, 1986). This is well established for the Lower Jurassic arc, in which NW-trending dyke swarms occur between strands of the sinistral, arc-parallel Atacama Fault system (Scheuber and Gonzales, 1999; Reyes et al., 2006). At Collahuasi, the NW-trending Rosario Fault and subparallel structures may also have originated as link faults between regional arc-parallel strike slip faults such as

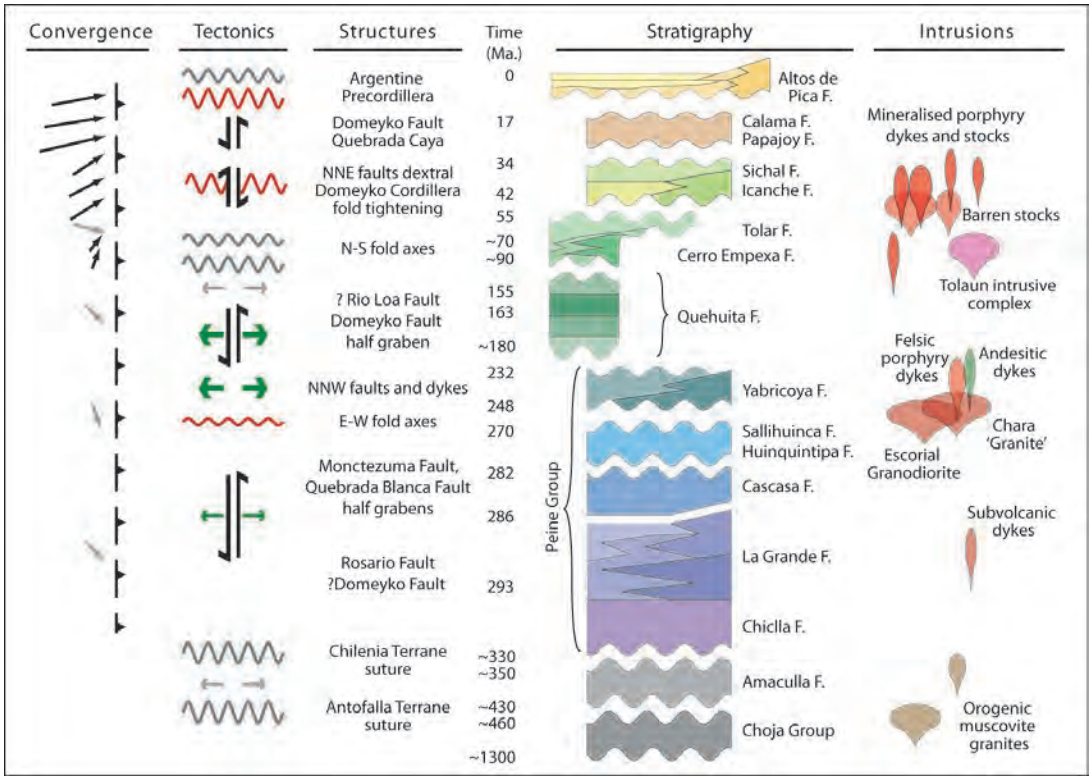

Figure 4.9. Simplified tectonostratigraphic scheme for the Collahuasi District. Most of the principal faults that define the district's structural architecture originated duriung extensional phases in the Permian and Triassic. "Convergence" is the Nazca/Aluk - South American plate Euler vector. Arrow lengths are proportional to convergence rate (1mm = 2 cm/yr). Cenozoic vectors after Somoza and Ghidella (2005), Mesozoic and Paleozoic vectors estimated by Pichowiak et al. (1990) and Scheuber et al. (1994). Grey vectors are poorly constrained. Tectonic events: sinusoids = compression and/or folding, black arriows = strike slip sense, green arrows = extension. Symbols in grey are poorly represented in the Collahuasi district (see Table 2.1 and Fig. 2.3 for more detail and sources of data).

the Monctezuma, Cascasca or Rio Loa faults. The subsequent sinistral shear couple would have favoured dilation on the NW-trending structures. The distribution of sedimentary and volcanic facies indicates that arc-parallel faults focussed local subsidence, creation of sedimentary accommodation space, and magma ascent. At their inception, these major elements of the structural architecture of the Collahuasi district were all extensional or transtensional faults.

4.3.5 Mesozoic Structural Evolution

Compressional deformation and magmatic attenuation ascribed to the Middle Cretaceous Peruvian tectonic event (Steinmann, 1929; Mégard, 1984; Tosdal et al., 1984) are not strongly developed in northern Chile. This event occurred in response to the southward migration of the Aluk-Farallón spreading ridge along the Andean

subduction zone. Subduction of the spreading ridge is recorded as a period of magmatic quiescence between 90 and 78 Ma (e.g., Osozawa, 1997), after which the arc magmatic front shifted westward and became much narrower (Fig. 4.10). Within the Collahuasi Block there is little evidence of significant structural development at this time, perhaps owing to the limited distribution of Cretaceous rocks. However, Tomlinson and Blanco (1997a), and Tomlinson et al. (2001a) describe stratigraphic evidence suggesting that this event saw the early stages of development of the E-vergent fold and thrust belt that is developed along the western part of the Collahuasi district. Following ridge subduction, the regional tectonic convergence vector changed from SSE-directed, to ENE-directed (e.g., Scheuber et al., 1994; Fig. 4.9). The corresponding change in the subduction obliquity, from ~35º, to >60º, dramatically changed the stress regime within the magmatic arc, from transtensional to transpressional (e.g., Jarrard, 1986). Constriction of the magmatic front at this time (Fig. 4.10) is interpreted to reflect this change in the tectonic geometry and concommitant increased compression within the arc.

Another compressional tectonic phase affected the southern Central Andes in the earliest Paleocene (65-63 Ma; Cornejo et al., 2003; Mpodozis et al., 2005). This event drove the inversion of the Preandean Depression (effectively the continental back arc) along the Rio Loa Fault (Muñoz et al., 2002). Sporadic alkalic magmatism in that back arc environment is represented at Collahuasi by the Tolaún intrusive

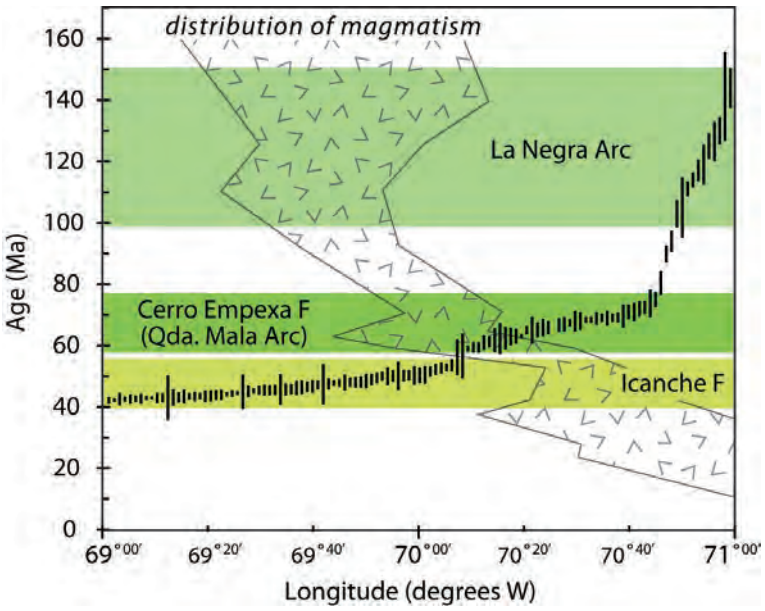

Figure 4.10. Graph showing the compilation of Late Jurassic to the Middle Eocene radiometric dates from the southern Central Andes, between the latitude of Chuquicamata and Collahuasi. The longitudinal distribution of magmatism is shown for comparison. The 10-15 m.y. magmatic gap in the Middle Cretaceous corresponds to the Peruvian Tectonic Event. Compiled largely from Scheuber et al. (1994) and Tomlinson et al. (2001a).

complex and a series of microsyenite dykes that occur across the district (Fig. 3.24, KLmsy). These dykes typically dip steeply and strike NW (Fig. 4.11). Emplaced at around 68.5 Ma (Chapter 3), they necessitate district-wide extension almost parallel with the direction of tectonic convergence, two to five million years before the

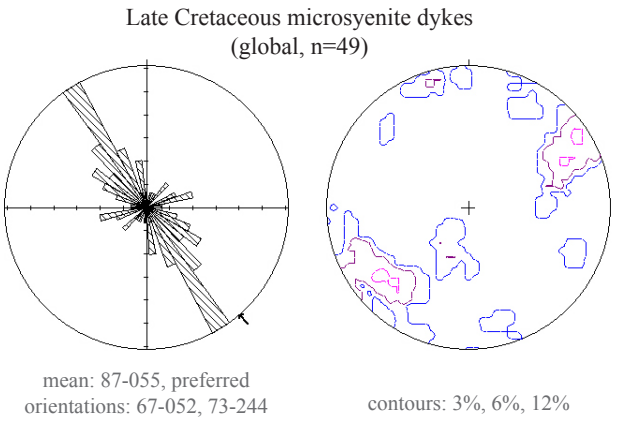

Figure 4.11. Rose diagram and equal area stereographic projection (contoured poles to planes) of Late Cretaceous microsyenite dykes (KLmsy) for the entire Collahuasi district. Latest Cretaceous dykes suggest local extension parallel to the regional tectonic convergence at that time.

K-T compressional event. However, neither compression or extension around this time seems to have been sufficiently intense to create new, penetrative faults in the Collahuasi district

4.3.6 Huinquintipa and Related Faults

The Huinquintipa Fault, and its extensions westward toward Quebrada Blanca (Fig. 4.2) are the only major ENE-trending faults in the Collahuasi district. Linear features defined by the collinear arangement of three or more topographic, magnetic or multispectral features (e.g., Landsat, GeoScan) clearly define the structural fabrics relating to faults trending NNE, NNW and NW. A further set of these linear features commonly trend ENE and is inferred to reflect a district-scale fracture array on this orientation (Fig. 4.12). This fracturing might conveniently reflect propogation into the shallow arc crust of the horizontal stresses related to tectonic convergence since the onset of ENE-directed subduction in the Late Cretaceous. The paucity of major faults with this trend suggests that subsequent shortening strain has either been accommodated by re-use of existing structures, in rheologically weak zones such as the fold and thrust belt to the west of the Domeyko Fault (e.g., Amilibia et al., 2008), and/or in lower parts of the crust.

Along the upper reaches of the Quebrada Huinquintipa (Fig. 3.15), preservation

of the Sallihuinca Formation on the south side infer that the Huinquintipa fault has accommodated 200 to 300 metres of net offset. Oligocene and younger conglomerates and sandstones have accumulated in small, steep-sided elongate half grabens along its length. Near Quebrada Blanca, faults that are mapped in the open pit are inferred to extend to the ENE and control Neogene subbasins that accumulated tens, and up to a hundred metres of poorly consolidated gravels and sands (Martin LaPointe, Aur Resources, pers. commun, 2005).

The Huinquintipa exotic copper deposit comprises Neogene gravels along the Quebrada Huinquintipa that have been cemented by exogenous supergene hydrous

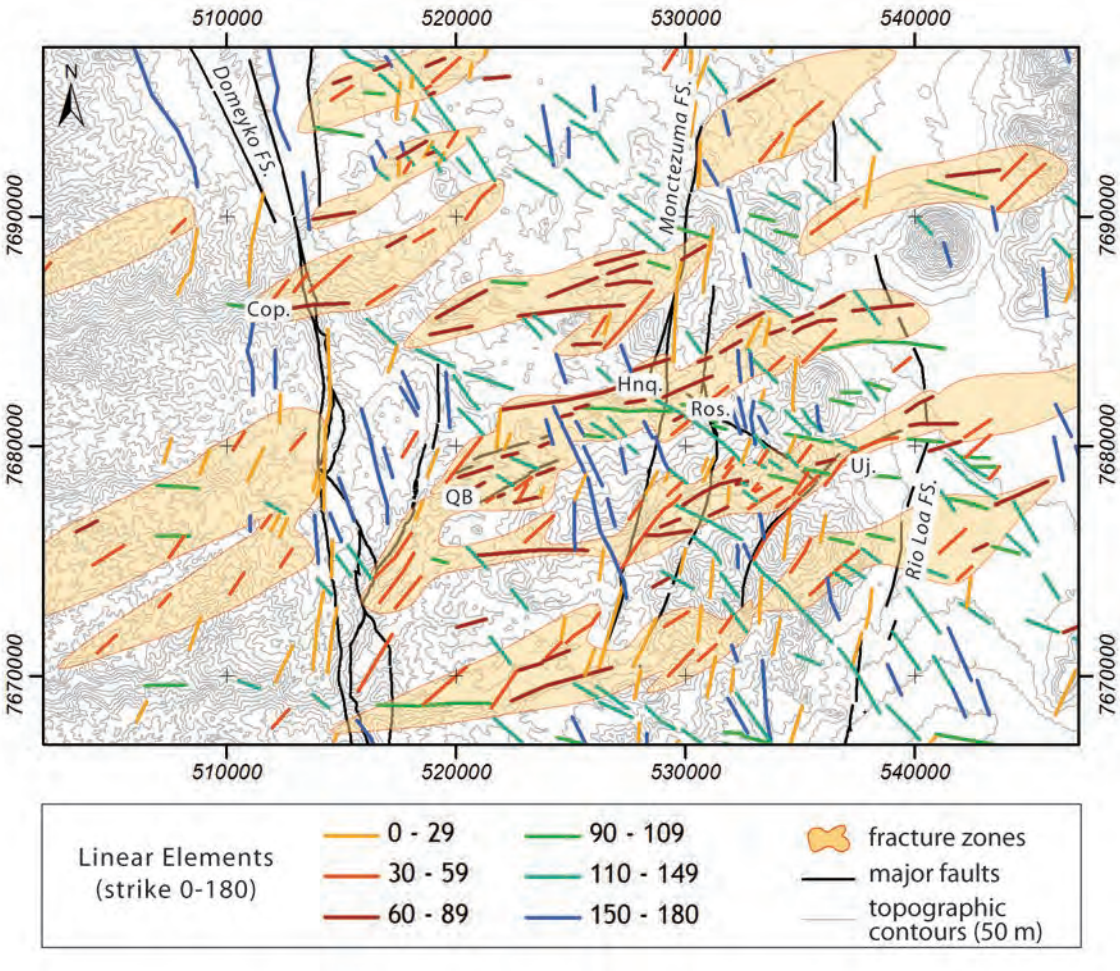

Figure 4.12. Interpreted linear elements map of the greater Collahuasi district, incorporating linework of Fedorowich (2001). Elements were defined by the linear arragement of topographic features (in a 90 m pixel SRTM image), a Landsat visible spectrum satellite image, and an airborne total magnetic intensity image reproduced in Behn et al. (2001). Linears drawn from all the datasets were compared, and only those features that appear in more than one dataset were retained. ENE-trending elements are approximately as abundant as elements that correspond to the preeminent regional fault sets. Groups of linear elements define broad ENE-trending zones interpreted as regional fractiure zones. Abbreviations: FS = fault system, Cop = Copaquire, QB = Quebrada Blanca, Hnq = Huinquintipa exotic Cu deposit, Ros = Rosario, Uj = Ujina.

copper-(manganese) silicate minerals (Munchmeyer et al., 1984). This style of mineralisation is thought to form at the same time as gravel deposition (Munchmeyer, 1994) and hence accommodation space was created along the Huinquintipa Fault during the Oligocene to Miocene deposition of the gravels and exhumation of the porphyry deposits (e.g., Maksaev, 1990). The fault also appears to be offset in by the western strand of the Monctezuma Fault (Fig. 4.2). Since this sinistral offset (Table 4.4) is thought to have occurred between the Late Eocene and Late Oligocene (e.g., Tomlinson et al., 1997b; Chapter 5), then the proto-Huinquintipa Fault must have originated earlier. The principal deformation that affected the Central Andean cordillera in the later Mesozoic and Paleogene is the Middle Eocene Incaic tectonic event (peak deformation at ~38.5 Ma: Perelló and Mueller, 1984; Clark et al., 1990a; Maksaev, 1990). Folding of the Mesozoic strata to the west of the Domeyko Fault is generally considered to have occurred during this event and this fold belt appears to have accommodated much of the related shortening strain (e.g., Tomlinson et al., 2001a). The ENE and NE trending fracture arrays are more strongly developed within the Collahuasi Block than outside it. Brittle fracturing on these orientations could therefore plausibly reflect a limited amount of strain accommodation within the Collahuasi Block during the Incaic tectonic event. Fracture formation during the K-T or latter stages of the Peruvian tectonic events cannot however be ruled out.

4.3.7 Is there a spatial relationship between porphyry and epithermal mineralisation and district-scale structural elements?

At deposit scale, the relationships between mineralisation and faults or fracture sets is commonly obvious. There is, for example, K-feldspar and muscovite alteration and related veining concentrated along the Quebrada Blanca Fault (Fam, 1974). The Monctezuma epithermal veins are hosted directly by the fault of the same name (Munchmeyer et al., 1984). Similarly, epithermal massive sulfide veins that are superimposed on the Rosario stockwork are hosted in the Rosario Fault (Munchmeyer et al., 1984; Lee, 1994; Bisso et al., 1998; Masterman et al., 2005). The detail of those relationships is investigated in the next section. However, it is the spatial relationships between mineral deposits and those structural elements that are mappable at district or regional scale that may be of most import to mineral

explorers. Working at this scale, mapping may involve only cursory field work, and instead be driven by the integration of existing geological survey maps with structural and lithostratigraphic interpretations based on aerial photography, various processed remote spectral images, and a digital elevation model.

There are three groups of principal structures that define the structural architecture of the Collahuasi district: NNE to NW-trending extensional and transtensional faults of lower Peine Group age, NNW-trending dykes and dyke swarms of upper Peine Group age, and ENE-trending fracture zones of likely Eocene age. Of these, the Eocene structures are defined by remote sensing data, the lower Peine age faults are partly revealed in remote sensing data but were originally recognised in 1:50,000 district scale mapping (e.g., Ware et al., 1981), and the dykes were only delineated by more detailed (1:10,000) mapping (Munchmeyer et al., 1984; this study).

Subjectively, it appears that the four Eocene-Oligocene porphyry deposits in the Collahuasi district are located at the intersection of these major structures (Figs. 4.12 and 4.13). The mapping presented in Chapter 3 confirmed that the principal faults shown on Figures 4.2 and 4.13 are the principal faults in the district, and are not an artefact of bias caused by more detailed investigation of the mineral deposits themselves. Three of the four porphyry copper deposits are located close to major extensional structures that were active during the Permian basin evolution (the stratigraphic setting of Copaquire is less clear because it is not hosted by the Peine Group). The two western deposits are located on splays of the continental-scale Domeyko Fault. Both fault splays are recognisable as pronounced topographic features in aerial photographs and as spectral anomalies in multispectral satellite imagery. The two largest deposits are situated inboard of the Domeyko Fault, and are each coincident with major Triassic dykes. These are not apparent in remote sensing imagery. The Rosario deposit also coincides spatially with the Rosario fault, which originated during the Permian as a growth fault for a local basin and possible magma conduit (section 4.3.4). Localisation of the Ujina deposit may also have been influenced by this fault, prior to sinistral offset along the Cascasca Fault. All of the deposits are located on the loosely-defined ENE-trend fracture zones, although these account for ~40% of the area under investigation.

For this small sample set, there is a repeated spatial relationship between major basement-penetrating structural intersections and mineralisation. Substantially pre-mineral extensional structures therefore appear to have been particularly good conduits for the ascent of small magma volumes into the shallow crust during the Middle and Late Eocene, generically because of coupling and reduced differential stress near structural intersections, and specifically because their extensional origin affords greater crustal penetration. Subsequent tectonism in the Cretaceous, Paleocene and Eocene does not appear to have generated abundant new, penetrative faults. Except for the ENE-trending faults through Quebrada Blanca and Huinquintipa, Tertiary structures manifest only as diffuse zones of fracturing that may have contributed to the bulk structural permeability. The majority of the long strike-length faults with offsets >200 m originated as extensional structures when the Andean crust was much thinner (Chapter 2). Along with the broader Domeyko

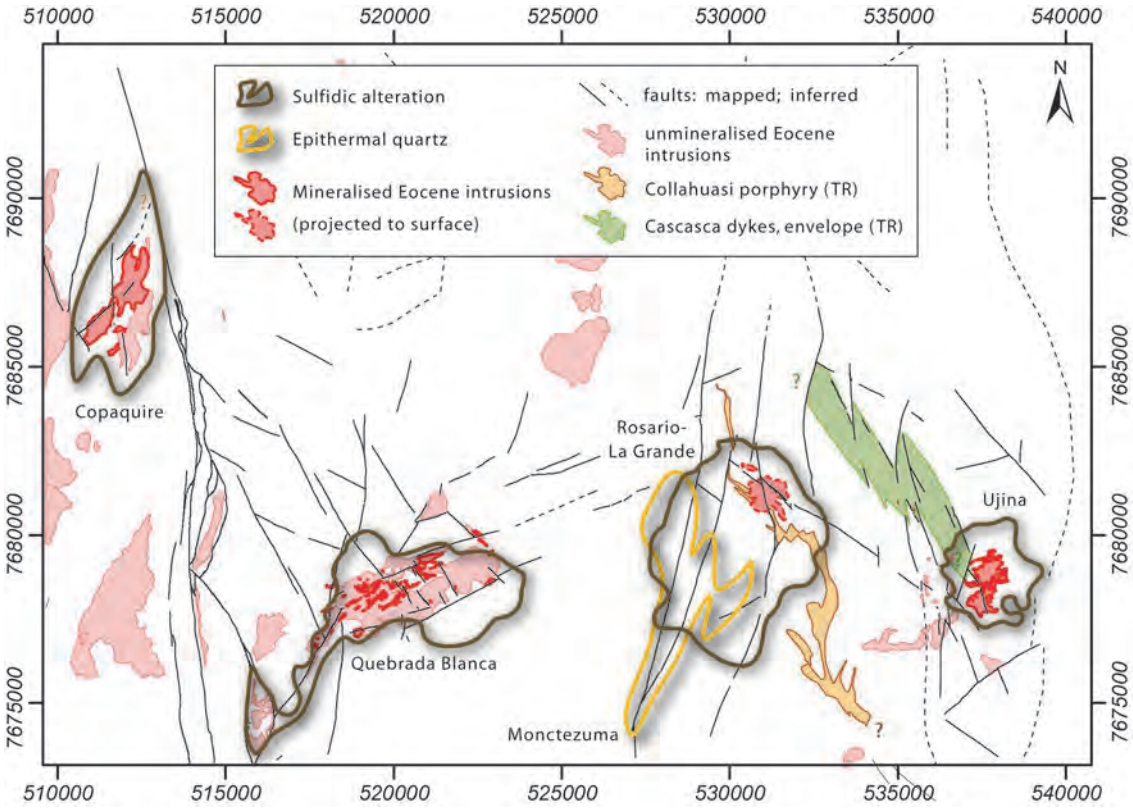

Figure 4.13. Simplified map showing the distribution of major alteration zones relative to major structural elements of the Collahuasi district. Porphyry and epithermal mineralisation is uniformly located on, or adjacent to faults and dykes that formed during extensional events that preceeded orogenesis, mineralisation and crustal thickening by more than 150 million years. Alteration zone boundaries are an approximation drawn using surface mapping and interpolated subsurface low resistivity zones (pole-dipole IP surveys: Quebrada Blanca, Rosario-La Grande, Ujina).

Cordillera, they were inverted during the Incaic tectonic event prior to-, and during mineralisation (e.g., Skármeta et al., 2003). This history gave rise the thick-skinned geometry of deeply penetrating multiply re-used faults that appears to have directly influence the localisation of younger magmatic-hydrothermal mineralisation. The ultimate source of magmas related to this mineralisation is in the sub-arc mantle (e.g., Mathur et al., 2000), and so one might anticipate a spatial coincidence between deposits and faults that penetrate to considerable depth in the crust. Thick-skinned tectonics preferentially occurs where previous extensional structures are subsequently contracted (Copper and Williams, 1989; Coward, 1994; McClay, 1995). Arc magmatic terranes where the basement has this extensional history prior to inversion are therefore likely to be favourable for shallow magma ascent during- and immediately after subsequent inversion. Given several other fortuitous coincident factors (e.g., Tosdal and Richards, 2001) terranes with this history can be considered as prospective for major porphyry mineralisation. Away from major continental-scale structural corridors such as the Domeyko Fault, some of the key district-scale sites of extension, such as the Triassic dykes at Collahuasi, might not be easily identified in regional mapping.

4.4 Structural Geology of Porphyry Copper Deposits

4.4.1 Introduction

Fractures form in the porphyry environment due to forces with three discrete origins: magmatic forces imparted during intrusion and crystallisation; hydrothermal forces related to fluid pressures; and tectonic forces referred into the upper crustal brittle domain from broader district or regional-scale processes (Tosdal and Richards, 2001). Intrusion-related forces tend to impart radial-concentric fracture arrays whereas tectonic forces impart linear or conjugate arrays. Hydrothermal processes may directly cause fracturing, as is common during phase separation, or may facilitate tectonic fracturing by lowering the failure stress of the host rocks. Pre-existing structures may contribute to the complexity of the fracture pattern, although reactivation or inversion will only occur under certain geometric relationships between existing fractures and the principal stresses (Nalpas et al., 1995; Sibson,

1995). Thermal energy carried into the shallow crust by ascending magmas causes transient changes in rock rheology about magmatic-hydrothermal systems (Fournier, 1999). This sensitivity to temperature underlies a relationship between the cooling and crystallization history of syn-mineral plutons and the relative importance of the different fracture-forming mechanisms. There is a general progression to stronger tectonic control among the later, cooler stages of typical porphyry paragenesis: A-veins show weaker linearity and shorter strike length than B-veins, themselves in turn less linear and shorter than D-veins (e.g., Gustafson and Hunt, 1975). The brittle, penetrative structural style of the latest veins in porphyry systems is commonly equivalent to that shown by many epithermal systems. However, rheological change associated with magma crystallisation shares an imperfect relationship with hydrothermal fluid evolution. Complexity arises from the interplay of physical conditions related to the depth of emplacement, the geothermal gradient, the volume of magma, and the timing of volatile exsolution (e.g., Cline and Bodnar, 1991; Fournier, 1999). In some cases, higher lithostatic loading in the deeper levels of the hydrothermal system correlates with more systematic vein orientations, whereas shallower zones may be more chaotic (e.g., Tosdal and Richards, 2001).

A range of stockwork arrays results from the relative importance or timing of radial-concentric fracturing driven by magmatic forces, and orthogonal or conjugate fracturing mediated by tectonic forces (Table 4.6). Extreme examples of tectonic control include syn-mineral dykes or dyke swarms associated with sheeted vein sets (e.g., Yerington, Cadia, and Elatsite; Table 4.6). Hybrid geometries develop when tectonically-controlled shallower, lower temperature vein system(s) are telescoped over a porphyry deposit due to rapid exhumation within the timeframe of the intrusion-related hydrothermal activity (e.g., Rosario, Chuquicamata and Batu Hijau: Table 4.6). In some cases, the intrusion and related hydrothermal system result in local stress fields where the maximum compressive stress is subvertical and cause radial fracture arrays. Stalling of intrusion and/or collapse of the hydrothermal system may then cause local implosion and the generation of concentric fracture and vein arrays (e.g., El Teniente, Cannell et al., 2005). Radial-concentric patterns are generally interpreted to reflect fracture formation under conditions of low differential

horizontal stresses (e.g., Tosdal and Richards, 2001). Whereas porphyry systems were once believed to form over tens to hundreds of thousands of years, i.e. time frames similar to that required for cooling of their source plutons (e.g., Arribas

Tectonic Influence	Structural Geometry	Examples
Minor	Concentric zonations with radial-orthogonal vein orientations	El Teniente, El Salvador, La Escondida, (Chile); Grasberg (Indonesia); Bajo de la Alumbrera (Argentina); San Juan district (USA).
	Concentric zonations with weakly anisotropic radial-conjugate vein orientations	Batu Hijau (Indonesia); Assarel, Medet (Bulgaria); Far Southeast (Philippines); Bagdad, Hillsboro (USA).
	Moderate concentric zonations with strongly anisotropic conjugate vein orientations	Chuquicamata, Radomiro Tomic, Rosario, Zaldivar (Chile); Bingham Canyon, Superior-Globe-Miami, Sierrita-Esperanza (USA).
Major	Weak-moderate concentricity, intrusions commonly dykes and some vein sets sheeted	Cadia, Cadia East (Australia); El Abra, (Chile); Elatsite (Bulgaria); Yerington, Ann Mason, Morenci (USA); Frieda River, Yandera (PNG).

Table 4.6. Examples of varying degrees of magmatic and tectonic influence on porphyry geometry. For further detail, see studies of **El Teniente** (Kay et al., 1999; Godoy et al., 1999; McKinnon and de la Barra, 2003; Cannell et al., 2005); **El Salvador** (Gustafson and Hunt, 1975; Mpodozis et al., 1994; Tomlinson et al., 1994; Cornejo et al., 1997; Watanabe and Hedenquist, 2001); **La Escondida** (Ojeda et al., 1990; Richards et al., 1999; Padilla-Garza et al., 2001; Richards et al., 2001a); **Grasberg** (Titley and Heidrick, 1978; Titley et al., 1990; Sapiie and Cloos, 1994), **SW USA porphyries** (Heidrick and Titley, 1982; Rehrig and Heidrick, 1972); **Bajo de la Alumbrera** (Sasso and Clark, 1998; Proffett, 2003; Harris et al., 2005), **Batu Hijau** (Clode et al., 1999; Garwin, 2000); **Assarel and Medet** (Ignatovski, 1979; Ignatovski, 1980; Bogdanov, 1983; Chobanova, 1984; Bogdanov and Boyle, 1990; Ignatovski et al., 1994; Strashimirov et al., 2002), **Far Southeast** (Sillitoe et al., 1985; Concepcion et al., 1989; Arribas et al., 1995; Hedenquist et al., 1995; Shinohara and Hedenquist, 1997; Hedenquist et al., 1998; Hedenquist, 1999), **Chuquicamata** (Sillitoe et al., 1994; Lindsay et al., 1995; Zentilli et al., 1995; Reutter et al., 1996; Sillitoe et al., 1996; Cuadra et al., 1997; Ossandon and Zentilli, 1997; Cuadra and Camus, 1998; Ossandon et al., 2001; Arnott and Zentilli, 2003), **Radomiro Tomic** (Leiva et al., 2000); Rosario (Munchmeyer et al., 1984; Dick et al., 1994; Lee, 1994; Bisso et al., 1998; Clark et al., 1998; Masterman, 2003), **Zaldivár** (Maturana and Saric, 1991; Richards et al., 2001a; Campos et al., 2002), **Bingham Canyon** (Bowman et al., 1987; Babcock et al., 1995; Harrison et al., 1997; Phillips et al., 1997; Maughan et al., 1999; Inan et al., 2000; Hattori and Keith, 2001; Redmond et al., 2002), **Sierrita-Esperanza** (Anthony et al., 1985; Titley et al., 1986; Anthony and Titley, 1994; Jensen et al., 1998), **Cadia** (Holliday et al., 2002; Squire and Miller, 2003; Wilson et al., 2003), **El Abra** (Ambrus, 1977; Dilles et al., 1997; Gerwe et al., 2003), **Elatsite** (Kalaydzhiev et al., 1984; Fanger et al., 2001; von Quadt et al., 2002), **Yerington and Ann Mason** (Carten, 1986; Dilles, 1987; Dilles and Einaudi, 1992), **Freida River** (Hall et al., 1990; Bainbridge et al., 1994; Crowhurst et al., 1997; Espi, 1999).

et al., 1995; Cathles et al., 1997; Clark et al., 1998), there is increasing evidence for hydrothermal lifespans of several million years, comprising multiple pulses of hydrothermal activity (Marsh et al., 1997; Masterman et al., 2004; Harris et al., 2005; Bertens et al., 2006). In cases where the dilational strain differs markedly between vein generations, there is potential therefore that these record changes in the local stress field related to either regional tectonic or local magmatic-hydrothermal effects.

4.4.2 Vein array mapping and interpretation at Collahuasi

The orientations of the principal generations of veins were mapped for each of the major porphyry and epithermal deposits of the Collahuasi District. The mineralisation, hydrothermal paragenesis and geochronology of each deposit are reviewed and/or amended in concert with presentation of the new structural data. The fractures that host veins in porphyry copper deposits are considered here to be analogous to joints in unmineralised rocks. Interpretation of the stress environment under which these small brittle structures form has been based on the geometric relationships between contemporaneous fracture populations following Dunne and Hancock (1994). Most critically, for conjugate arrays the maximum principal stress axis has been inferred to bisect the acute angle between subsets in the array. Likewise, the intermediate principal stress axis has been inferred as parallel to the intersection of the conjugates.

The subsequent sections of this chapter describe the structural architecture of each of the major porphyry and epithermal deposits at Collahuasi in the chronological order of their formation.

4.5 Structural and Hydrothermal Geology of the Monctezuma Epithermal Ag-Au-Mn deposit

The Monctezuma Fault hosts (and takes its name from) Au-Ag-Mn rich epithermal veins that occur in the southern part of the district where the two main fault strands converge and impinge on the Ceucis diorite (Fig. 4.14). The veins crop out as a subvertical NNE-trending rampart across the Quebrada Chiclla valley and are the apparent source of alluvial gold worked by artisan miners in that valley (Munchmeyer et al., 1984). Exploration drilling in the 1980s indicated that the principal Monctezuma Vein averages one to two metres in width and is semi

continuous over ~800 m of strike. Strongly elevated Au and Ag grades (up to ~40 and ~2000 ppm, respectively) are restricted to a 200 m-long zone where the veins intersect the margin of the Ceucis diorite. There are intermittent occurrences of similar quartz-rich, banded, sulfide-poor epithermal veins along the trace of the Monctezuma Fault, some of which were worked in the late 19th century (Fig 4.14; Moore and Masterman, 2002). Mullock from old underground workings of Anita and Don Eduardo veins on Cerro La Grande, and colluvium in that area (Fig. 4.14) also includes this style of vein material. In the Capella area, massive to weakly banded

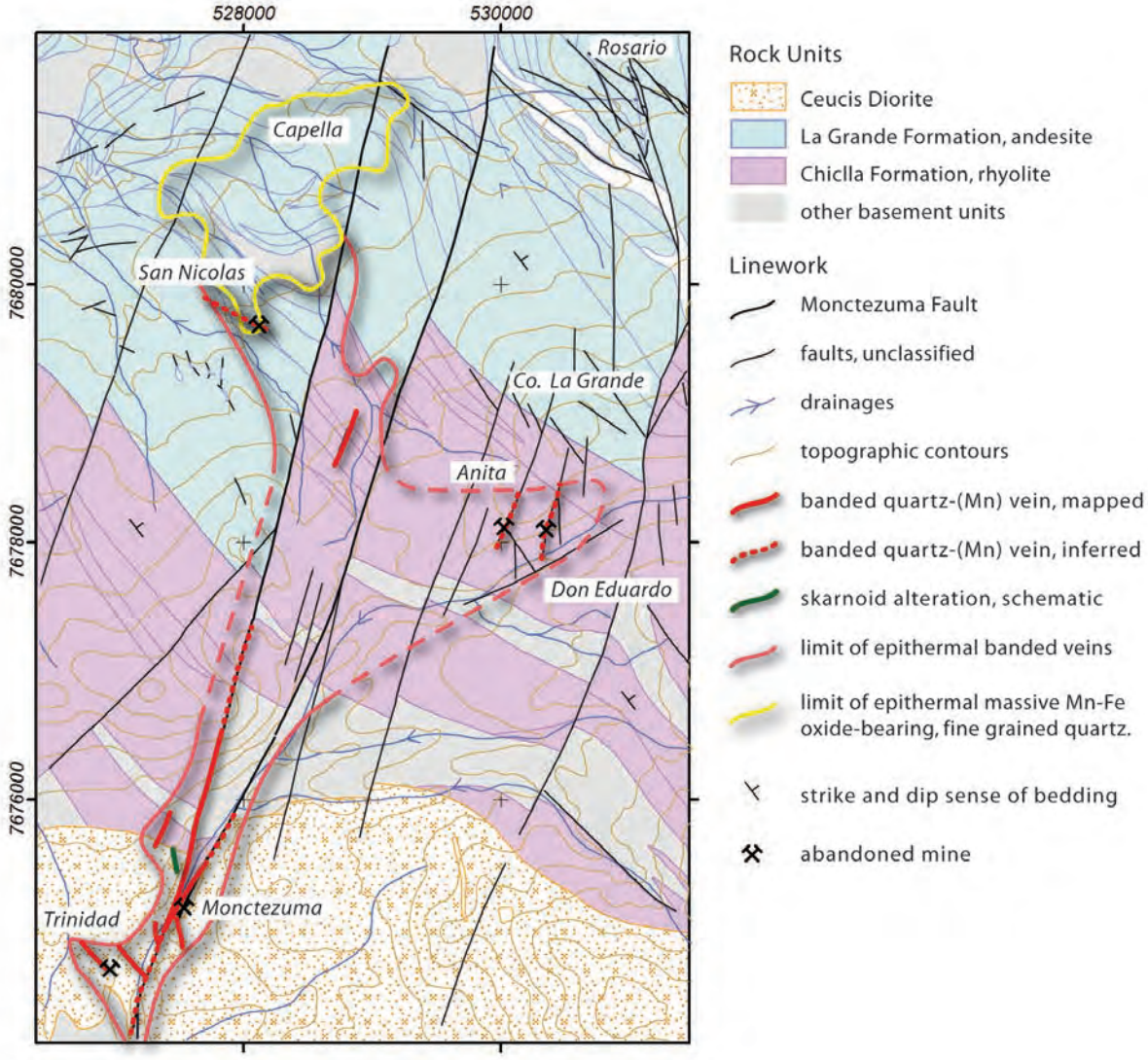

Figure 4.14. Simplified geological map of the south central Collahuasi district showing the distribution of banded epithermal quartz vein occurrences. Au and Ag were extracted historically from veins exploited in small shafts and pits at Monctezuma, Trinidad and San Nicolas. At Don Eduardo, veining of this type is generally metal-poor and workings targeted younger Cu-As-Ag bearing massive sulfide veins (not shown). Nonetheless, colloform banded quartz veins occur in the area, and one of the Don Eduardo adits appears to have yielded unusual epithermal quartz-wolframite veins.

very fine grained black manganiferous quartz occurs widely. Outboard of this, cockade-banded ferroan carbonate-quartz veins occur locally, perhaps suggesting a distal position in the system (by analogy with Simmons and Browne, 2000). Quartz-rich veins or alteration could not be traced further north, and this is interpreted as the northern limit of epithermal mineralisation related to the Monctezuma system.

4.5.1 Vein and Alteration Mineralogy and Textures

At surface the Monctezuma veins comprise massive to weakly cockade and colloform banded quartz veins and vein breccias with variable amounts of supergene manganese oxides (Fig. 4.15a; up to ~15%; Munchmeyer et al., 1984). Boxworks after minor disseminated pyrite occur locally. Quartz ranges from finely crystalline to coarsely crystalline and forms euhedral crystals around common open cavities. Alteration around the veins is indistinguishable from weathering, although the depth of oxidation is generally deeper in the vicinity of the veins and associated faults than elsewhere.

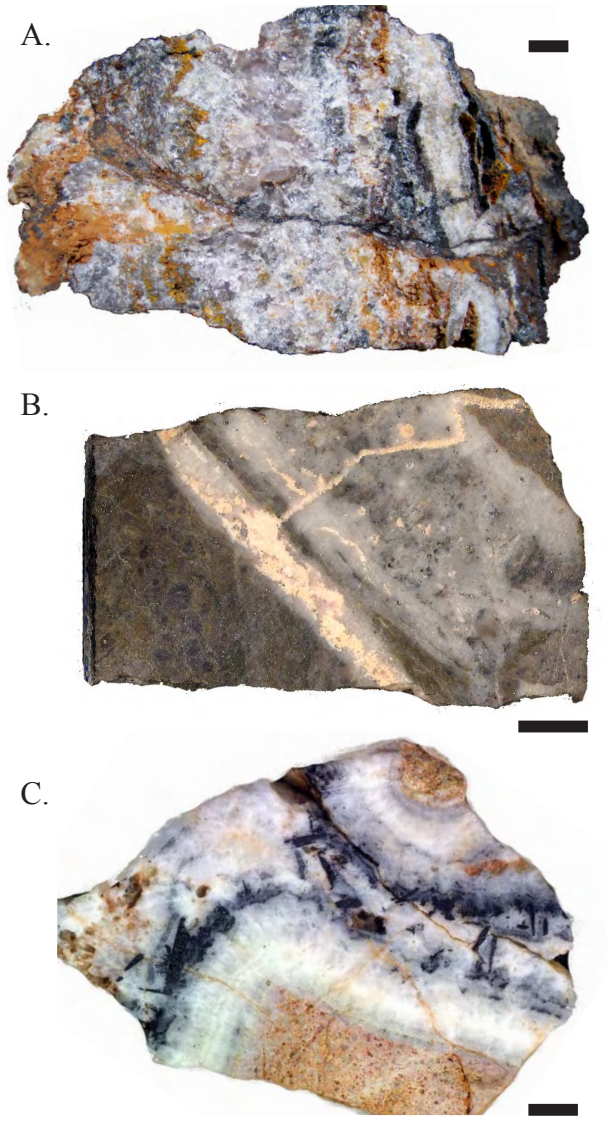

Figure 4.15 Photographs of the Monctezuma and related veins. A) Weakly cockade banded vein with coarse grained amethystine quartz (centre) and secondary Mn oxides (right) after rhodochrosite. Vicinity of 528,840 mE; 7,678,730 mN. B) Strongly mineralised vein sample (150404_06; >5 ppm Au, >100 ppm Ag) showing cross cutting relations between early quartz-sulfide veins and later quartz-rhodochrosite veins. Strong pervasive muscovite-pyrite alteration affected the host dacite. C) Hand specimen of cockade banded quartz vein breccia with wolframite crystals. This occurrence is unique to the Don Eduardo adit on the south flank of Cerro La Grande (530,430 mE; 7,678,325 mN), although metal-poor banded quartz veins are widespread in the area. Black bars are 1 cm. Locations for all rock samples are contained in Appendix II unless specified in the relevant figure caption.

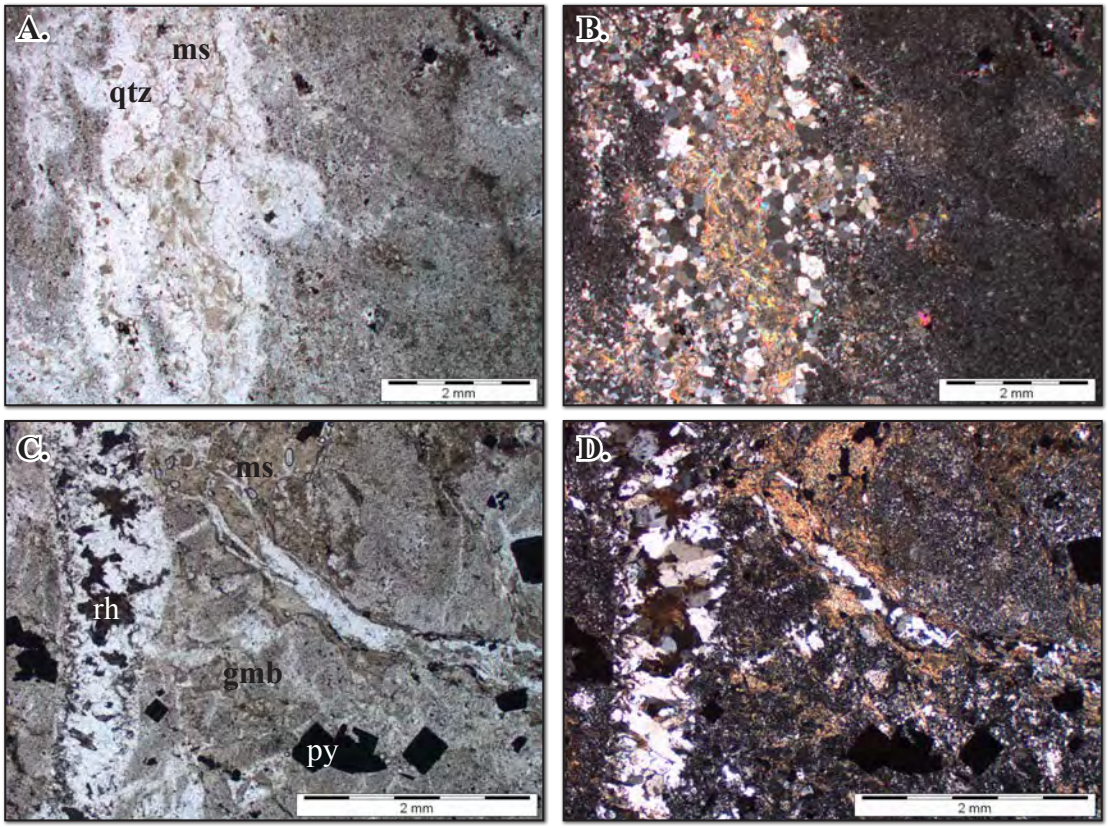

Figure 4.16. Photomicrographs of veins and alteration at Monctezuma (the same samples used in $^{40}Ar/^{39}Ar$ geochronology, section 4.5.3). A) Muscovite crystals (ms) and recrystallised quartz (qtz) define a flow band in the Monctezuma Dacite (150404_12). B) The same view as A under crossed polars. The muscovite crystals have high order birefringence colours. C) Epithermal quartz-rhodochrosite (rh) veinlet (150404_06) cuts a finer quartz veinlet with a fine-grained crystalline muscovite selvedge (ms - brown). Euhedral pyrite crystals (black) are disseminated in the groundmass, which itself comprises a microbreccia of angular muscovite-altered dacite clasts with hydrothermal quartz-muscovite cement (gmb). D) The same view as C under crossed polars.

Unweathered examples show irregularly distributed pyrite, galena and chalcopyrite associated with poorly banded fine grained quartz. This vein stage is anticipated to be the principal location of gold residence. Intergrown fine grained quartz and rhodochrosite commonly accompanies quartz-sulfide veins, but locally cut the latter (Fig. 4.15b). Most of the veins intersected in drilling are dominated by weakly banded cockade quartz and are only weakly mineralised. Veins that are visually similar to those along the Monctezuma Fault also occur on the southern flank of Cerro La Grande (Fig. 4.14). In this location they are cut by, and rarely re-opened by veinlets of iron oxides interpreted to be weathered pyrite. In the mullock heap of one shaft on the Don Eduardo vein, cockade banded quartz veins and breccias contain abundant coarsely crystalline prismatic wolframite (Fig. 4.15c). Import of this material to such a remote site seems unlikely, and texturally similarity of these veins

to the Monctezuma veins is taken as evidence for a genetic relationship between the two.

Multiple overprinting stages of alteration occur in the vicinity of the Monctezuma veins. In the south, flow banding in the Monctezuma dacite (Pzpc.6) is highlighted by distinctive pink alteration (Fig 3.6a, b). This alteration comprises discrete bands of crystalline muscovite with granophyric quartz selvedges (Fig. 4.16a, b). It occurs throughout the dacite encountered in exploration drilling and does not appear to increase in intensity toward the veins. To the immediate west of the main vein zone, the Ceucis diorite hosts numerous fracture-controlled zones of zoned clinopyroxene-(garnet-epidote)-albite alteration. These range up to several metres in width and have strike lengths of up to 15 metres. Alteration of this style was not encountered in drilling of the vein zone.

The Monctezuma fault zone is characterised by multiple overprinting clast-supported breccias that are typically <2 metres wide (true thickness) and have narrow gradational margins. The earliest have hydrothermal cement composed of chlorite, hematite and pyrite, and are associated with disseminated pyrite alteration in the clasts. These are overpinted by zones of pervasive, texture-destructive grey-brown illite-(pyrite) alteration (Fig. 4.16 c and d). Alteration directly associated with the epithermal veins comprises veinlets of crystalline quartz and phengitic illite and fine grained microbreccias cemented by the same minerals (Fig. 4.16 c-d). In turn, this alteration is cut by the younger rhodochrosite-bearing vein stage that has negligible associated wallrock alteration.

4.5.2 Structure of the Monctezuma Veins

The earliest alteration at Monctezuma comprises fracture controlled endoskarn within the Ceucis diorite. This alteration is tightly restricted to short strike-length NNW- and lesser NW-trending fractures (Fig. 4.17a, b) suborthogonal to the intrusion margins, in the vicinity of, but not within the Monctezuma Fault. Specific alteration of the NNW-NW fracture set, and absence of this alteration from the main Monctezuma Fault could be interpreted to imply that the fault had not propogated through the intrusion prior to alteration, or that this episode of alteration manifests differently outboard of the intrusion (as is perhaps implied by intrusion-age muscovite alteration

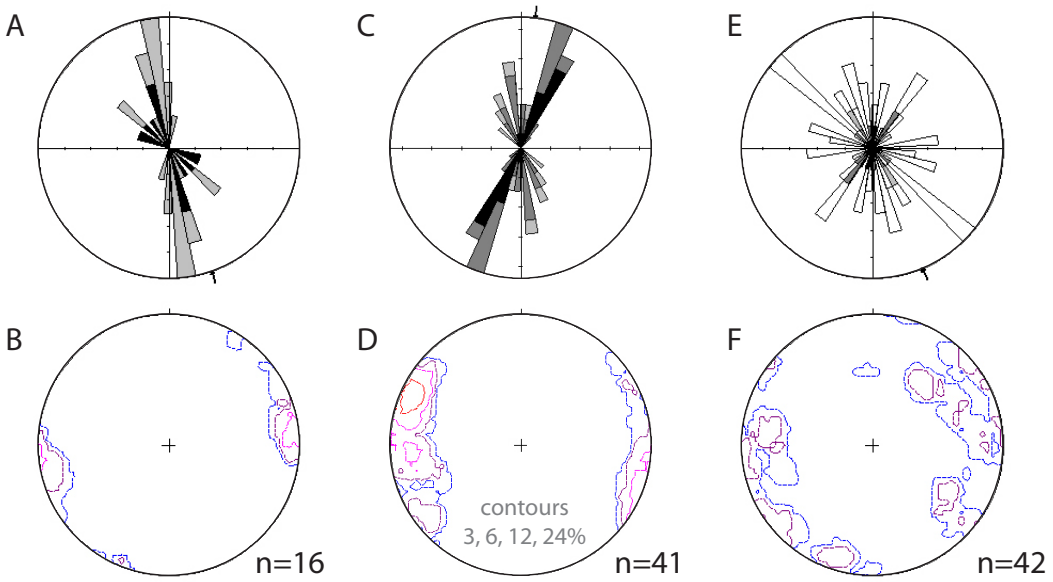

Figure 4.17. Structural data for the Monctezuma deposit area. Darker colours on rose diagrams depict greater magnitude structures. Equal area stereograms show countoured poles to planes. A-B) Skarn-like alteration. C-D) Banded epithermal veins. E-F) Unmineralised fractures and faults.

near the fault; section 4.5.3). The geometry of the fracturing compares favorably with the broadly SW-directed oblique tectonic convergence during the Permian (Scheuber et al., 1994). The skarnoid-altered fractures are subparallel to abundant splays and joint sets developed adjacent to the Monctezuma Fault, and could therefore have originated as the synthetic R' shears prior to hard-linking of this fault. Alternatively, their relationship to the pluton margin may simply record radial fracturing associated with pluton emplacement and hydrothermal fluid pressure.

Mineralisation at Monctezuma is dominated by thick (1-10 m) banded epithermal veins that trend NNE and are hosted within the single southern strand of the Monctezuma Fault. Detailed mapping in this area reveals vein and veinlet orientations that cluster in three groups, trending NNE, NNW and NW, in that order of frequency (Fig. 4.17c, d). A shaft and several stopes open at the surface were dug on the main NNE-trending vein at Monctezuma in the early history of the district (Moore and Masterman, 2002). Smaller pits were dug on NW-trending veins at Trinidad and San Nicolas (Munchmeyer et al., 1984), suggesting that significant dilation was locally accommodated on splays with this orientation. Faults and fractures on many orientations occur in the Monctezuma area, but the Monctezuma Fault is the single major penetrative structure (Fig. 4.17e, f).

Dilational strain imposed during mineralisation therefore appears to have been accommodated on the most significant pre-existing structures; the Monctezuma Fault and related splays. Concentration of dilation on these older structures suggests that fluid pressures likely exceeded the regional stress, and that correspondingly, the overall regional stress may have been weak at the time. Nonetheless, fractures on all but ENE orientations locally host minor epithermal mineralisation, implying some difference in the strength of tectonically-imparted horizontal stresses.

Post-folding stratigraphic offset on the Monctezuma Fault could either suggest sinistral, or normal, i.e. west-side down, displacement. Mapped straie are subhorizontal, but those fault surfaces cut the epithermal veins and therefore reflect younger movement. Nonetheless, the absence of ENE-trending veins corresponds to differential horizontal stress oriented NNW. The Monctezuma Fault was misaligned for pure dilation under this regime, and the vein array plausibly reflects re-use of this fault as a sinistral shear, with renewed tensional fracturing oriented NW-SE (Figs. 4.14 and 4.17). Some degree of strike slip throw during mineralisation is also inferred by concentration of veining adjacent to the Ceucis diorite. Under these conditions, the pluton might have served as a buttress that forced greater dilation of the Monctezuma Fault in the south near the intrusive margin than elsewhere. Epithermal vein mineralisation at Monctezuma is therefore interpreted to have formed during very weak WSW-directed extension, which drove minor sinistral shear along the Monctezuma Fault.

The textural and mineralogical zonation from S to N within the broader Monctezuma alteration system (Fig. 4.14) might suggest the entire block has been tilted northwards some time after mineralisation. There are no bedded Oligocene or younger strata that permit direct resolution of this possibility. However, the occurrence of the ~44-41 Ma Icanche Formation above an angular unconformity with the Peine Group (Figs. 3.4 and 3.12) suggests that the Peine Group at Monctezuma had been tilted and eroded prior to the Eocene, and hence prior to mineralisation. The orientation of the basal Icanche unconformity is not known, but the uppermost unit of the Icanche Formation dips ~15º to the north (Fig. 3.4). This small amount of northward tilting may have also affected Monctezuma area, but the mineral zonation is expected to primarily reflect lateral outflow.

Table 4.5. $^{39}Ar/^{40}Ar$ sample details and summary results from the Monctezuma Fault Zone

Sample No.	Location[a]	Lithology[b]	Alteration[c]	Separate[d]	Composition[e]	Plateau Age[f], 2σ error (Ma)	% $^{40}Ar^*$	MSWD	Correlation Age, 2σ error (Ma)	MSWD
150404-12	527,629 mE, 7,675,311 mN.	Grey, weakly plagioclase phyric, planar pink flow banded dacite	Flow bands replaced by granophyric qtz & crystalline muscovite (<400 mm)	gemmy muscovite crystals. 125-180 µm	10.75 % K_2O	267.98 ± 2.45	50.3	0.0	268.1 ± 2.2	0.0
150404-01	527,627 mE, 7,675,286 mN.	Grey to beige dacite breccia cut by multiple generations of quartz-py-rhodoch. veinlets	Pervasive fine-grained texture-destructive and illite with lesser disseminated pyrite	illite/ phengite, 2-5 µm	7.26 - 9.1 % K_2O	59.28 ± 0.57	40.3	0.36	60.1 ± 0.9	18.0
				illite/ phengite, 2-10 µm		52.80 ± 0.81	27.8	2.2	52.7 ± 3.4	6.9
150404-06	527,629 mE, 7,675,311 mN.	Pale pink-green altered, crackle-brecciated dacite cut by cocks-comb quartz-rhodoch.-pyrite veins	Intense pervasive feldspar- and groundmass-selective illite-pyrite, cut by crystalline illite veinlets	illite (+qtz) 2-10 µm		40.42 ± 0.45	93.9	1.5	39.9 ± 0.4	1.2
				illite (+qtz) <2 µm	10.16 % K_2O	40.85 ± 0.69	85.2	9.1	41.1 ± 2.1	12
				combined		40.54 ± 0.29	78.1	2.9	40.4 ± 1.0	10.8

a) Coordinates refer to the PSAD 56 datum. b) All samples are hosted in the Monctezuma dacite, Pzpc6. c) Observed in hand specimen and by transmitted light microscopy. d) Determined by XRD (at Queens University) for size fractions <10 µm. The XRD spectrum of sample 150404-06 suggested that this sample is illite, but microprobe analysis instead requires that muscovite is the principal alteration mineral in this sample. e) Determined by electron microprobe (at the UTas CSL; Appendix V) except for illite-phengite sample 150404-01, for which the normal stoichiometric range is given. f) "Plateau Age" is used in this table to denote an age identified from a step heating age spectrum. In some cases these do not satisy the plateau criteria of Ludwig (2001). Abbreviations: rhodoch = rhodochrosite; py = pyrite; qtz = quartz.

4.5.3 Geochronology of Alteration along the Monctezuma Fault.

Laser step-heating $^{40}Ar/^{39}Ar$ geochronology was applied to muscovite and illite from the wallrocks and from the immediate alteration halo to the veins (Figs. 3.6 and 4.15-16). The results reveal three stages of hydrothermal alteration; in the Permian, Paleocene and Eocene (Table 4.5).

Samples for geochronological analysis were crushed, liberated by ultrasonic bath and centrifuge, and then washed in 10% hydrochloric and 10% nitric acid. Several size fractions were separated and the mineralogy of these was determined by X-ray diffraction (XRD). Geochronological analyses were performed only on those separates in which illite, phengite or muscovite were the only potassic phase. The crystal aggregates of the target mineral in the same samples was analysed by electron microprobe to determine their composition (Appendix V). Definition of transitional illite and phengite is ambiguous by XRD because of their crystallographic similarity and compositional solid solution (Meunier and Velde, 2004). The samples identified as illite/phengite by XRD contain more potassium than stoichiometric illite (but less than muscovite, Table 4.5) and are interpreted to be a transitional species.

Distinctive mm-scale pink flow bands are ubiquitious in the Monctezuma dacite (Pzpc6) in the vicinity of the Monctezuma Fault. The flow bands are made up of a central crystalline muscovite zone and a granophyric quartz border (Fig. 4.9 a-b). Step heating $^{40}Ar/^{39}Ar$ analysis of this muscovite yielded a typical argon-loss "staircase" spectrum (Fig. 4.11a; e.g., Kirschner et al., 1996). The inverse isochron for this sample shows a pronounced Ar-loss pattern (e.g., Kuiper, 2002) and no geologically reasonable correlation age could be calculated. The final heating step and sample fusion caused release of half the ^{39}Ar in the sample and returned an age of 267.98 ± 2.45 Ma. This date is considered to be a minimum age for wallrock muscovite alteration. It is within error of the accepted K-Ar age of the Escorial Granodiorite (260 ± 10 Ma; Huete et al., 1977; Ware et al., 1981) near Quebrada Blanca. No precise geochronology exists for the Ceucis diorite, the equivalent Paleozoic intrusion that occurs 200 metres south of the Monctezuma veins. However, the Ceucis and Escorial plutons share similar petrography and structural relationships with the Peine Group and probably intruded at around the same time. It seems likely that the muscovite alteration dated here occurred during or shortly after plutonism

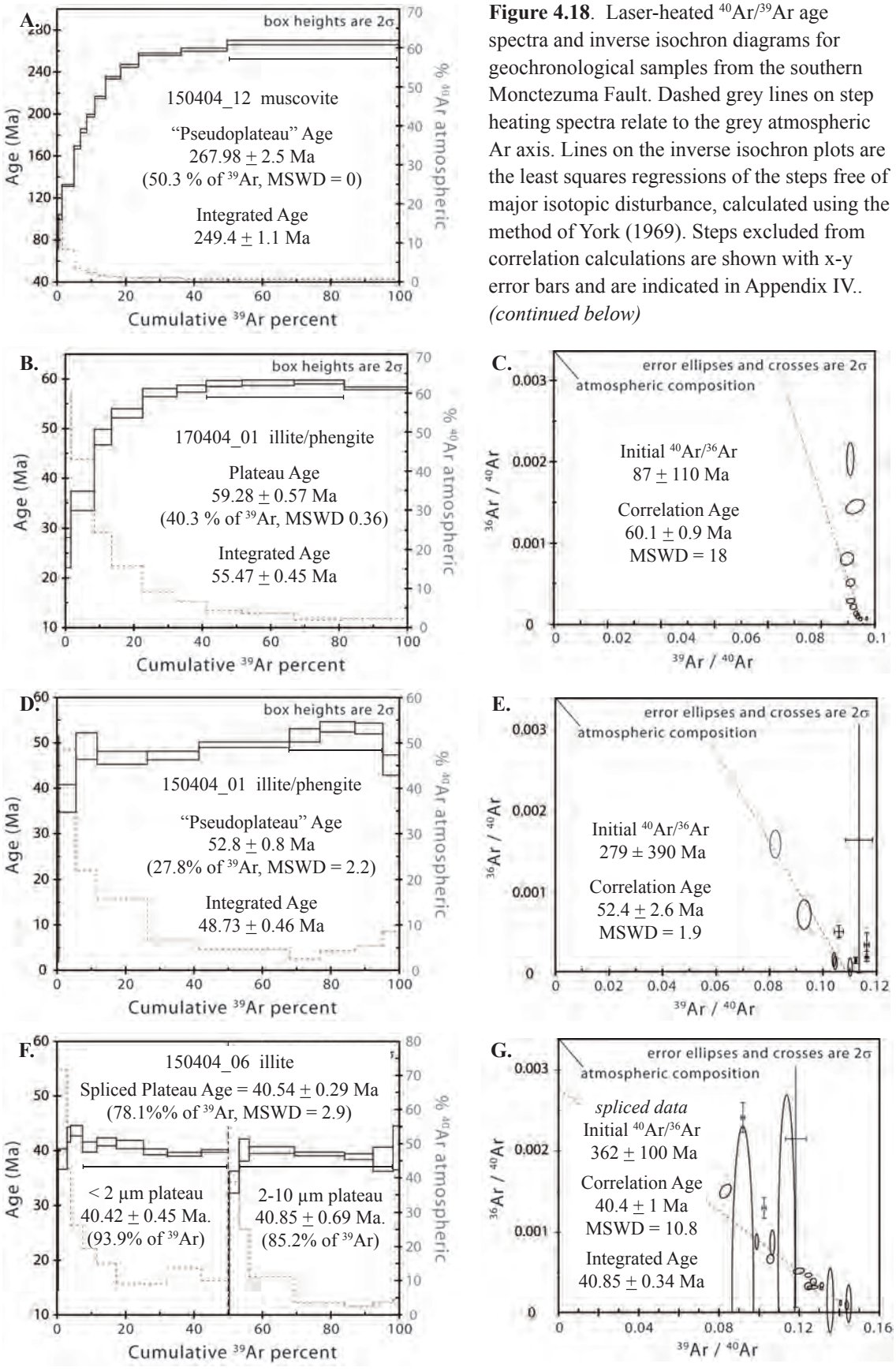

Figure 4.18. Laser-heated $^{40}Ar/^{39}Ar$ age spectra and inverse isochron diagrams for geochronological samples from the southern Monctezuma Fault. Dashed grey lines on step heating spectra relate to the grey atmospheric Ar axis. Lines on the inverse isochron plots are the least squares regressions of the steps free of major isotopic disturbance, calculated using the method of York (1969). Steps excluded from correlation calculations are shown with x-y error bars and are indicated in Appendix IV..
(continued below)

Figure. 4.18 *(continued)* A) Crystalline muscovite defining a flow band in the Monctezuma dacite (Pzpc6). B-E) groundmass illite/phengite from the wallrocks to the Monctezuma veins. F-G) combined reuslts for analyses of two different size fractions of crystalline muscovite from the immediate vicinity of precious-metal rich quartz-rhodochrosite veins at Monctezuma.

and records cooling after crystallisation of the Ceucis diorite. This style of alteration is uncommon away from the Monctezuma Fault, and therefore the fault appears to have been an active conduit for hydrothermal fluids since at least the Permian.

Two samples of fine grained (<2 μm and 2-5 μm) illite/phengite from the groundmass of a dacite sample from Monctezuma yielded Paleocene ages. The coarser sample (17040401; Fig 4.10 b-c) is affected by Ar loss among the lower power steps but the higher power steps yielded a plateau age comprising ~40% of the ^{39}Ar. Approximately 80% of the ^{39}Ar released comprises steps yielding ages within 2 m.y. of the plateau. The inverse isochron age and the plateau age are well within error of each other. The finer grained sample (150404_01) has a disturbed spectrum that includes a pseudoplateau of ~27% of the ^{39}Ar released among the higher power steps. Like the coarser sample, the majority of the steps, and ~90% of the ^{39}Ar released yield ages in the vicinity of the shorter plateau. Both samples show limited Ar loss, but there is no suggestion among the spectra of mixing between Permian and younger Ar reservoirs (such as excess radiogenic Ar that may be held in relict muscovite; e.g., Kelley, 2002). Across the eastern part of the district, early K-Ar analyses of thermally reset wholerock samples from the Peine Group and the Collahuasi Porphyry cluster around 60 Ma (Ware et al., 1981; Tomlinson et al., 2001a). The new data are therefore interpreted as record of hydrothermal activity along the Monctezuma Fault at this time, contemporaneous with early Icanche Formation volcanism elsewhere in northern Chile (e.g., Tomlinson et al., 2001a, and references therein).

Two size fractions of illite/phengite from the immediate vicinity of an epithermal vein were analysed to date the related mineralisation (Table 4.4, Fig 4.10 f-g). These samples returned results that are indistinguishable from each other and have been treated together. They yield a plateau age (~78% of the ^{39}Ar), inverse isochron age and integrated age that are all consistent and within error at approximately 40 Ma (Fig. 4.17 f-g). Since the temperature at which epithermal quartz-rhodochrosite veins typically form (e.g., White and Hedenquist, 1990) is similar to the isotopic closure temperature of illite (e.g., Von Blanckenburg et al., 1989), these results are interpreted to record the time of formation of the Monctezuma veins. It is also the time of proposed weak WSW-directed extension in the Collahuasi district.

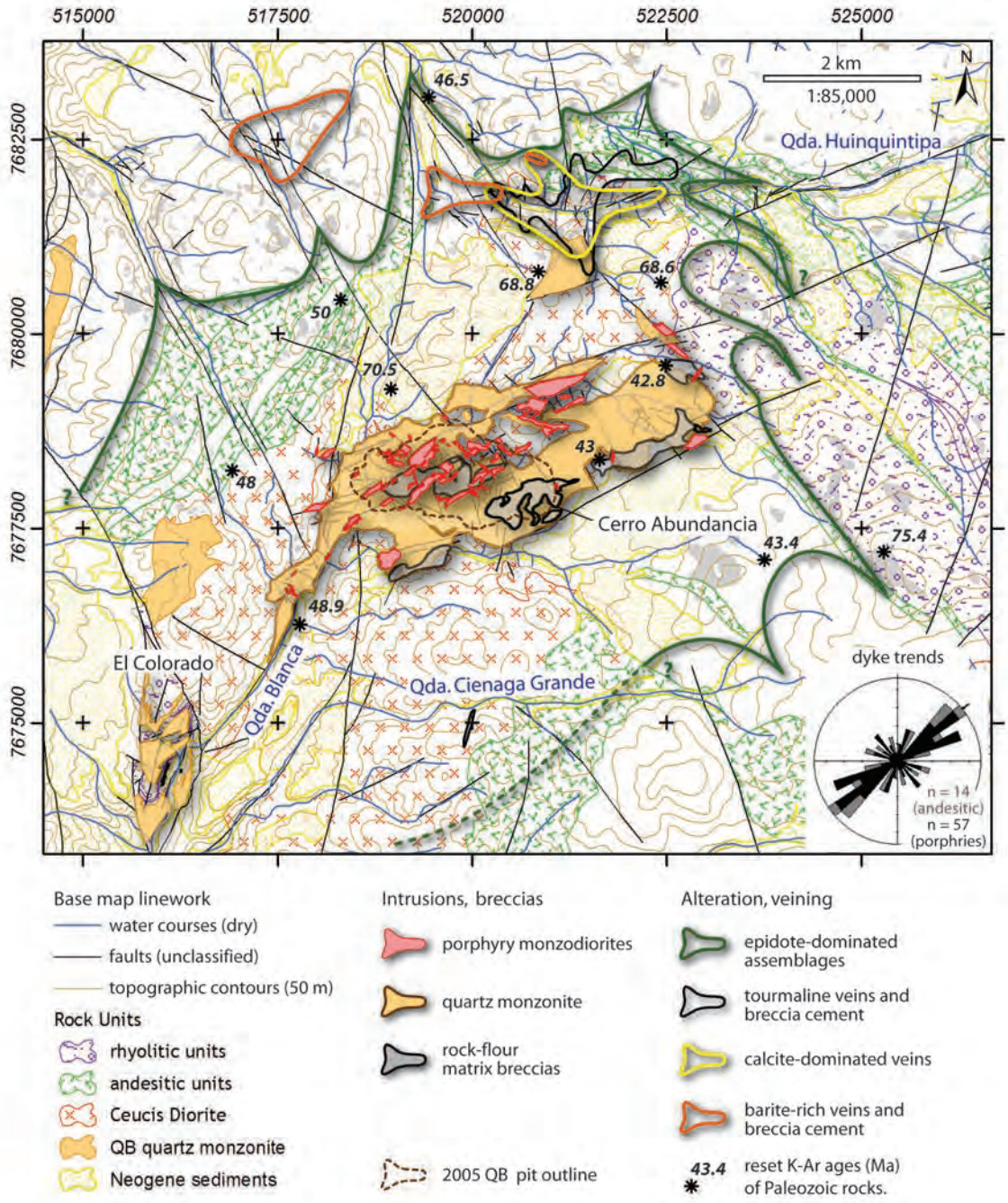

Figure 4.19. Selective geological map showing the distribution of intrusive and breccia bodies, and peripheral alteration zones around the Quebrada Blanca intrusive complex. Intrusive body and breccia outlines, and 80% of dyke orientations reproduced from Ware et al. (1981) and Desrochers et al. (2001). Geochronological data are biotite and whole rock K-Ar dates reported by Baker et al. (1977) and Ware et al. (1981). Alteration zones depict the interpreted outer limits of occurrence of each mineral, based on new mapping of outcrops (transparent grey). Potassic alteration is ubiquitous in the vicinity of the major breccias and porphyry quartz diorite and monzodiorite dykes, and selective biotitisation was also noted as far south as Qda. Cienaga Grande (Fam Romero, 1974). The abundance of epidote is strongly controlled by the host rock composition and permeability and may continue further to the E under cover. The extent of epidote in the south and west is poorly constrained, but is interpreted to extend beyond occurrences of tourmaline and biotite alteration. K-Ar radiometric ages within the epidote zone are ubiquitously reset to ages much younger than the Permian and earliest Triassic crystallisation ages (Chapter 3). Unreset ages outboard of the epidote zone are not shown.

4.6 Structural and Hydrothermal Geology of the Quebrada Blanca Porphyry Cu-Mo deposit

The structural controls on alteration and veining in the Quebrada Blanca (QB) deposit have been the subject of three detailed, unpublished, Maestría (Honours) theses (Fam Romero, 1974; Lehman,1980; Martini, 1984). A summary of the vein paragenesis was presented in the doctoral thesis of Rowland (1998) as the basis for a detailed fluid inclusion study. The definition and distribution of the numerous intrusions and breccia facies were described in the internal report of Ware et al. (1981) and a summary was published by Hunt et al. (1983). Updates to this mapping were done by the Compañía Minera Quebrada Blanca during 2000-2001 and are reproduced with permission of the company (Desrochers et al., 2001). The vein paragenesis of the deposit described by Martini (1984) is not entirely compatible with the summary presented by Rowland (1998). This section amends the vein and breccia paragenetic scheme based on new observations of mineralogy and cross cutting relations.

The principal aim of this work at Quebrada Blanca was to map the orientations of several generations of stockwork veinlets and faults, to permit recognition of temporal changes in strain accommodation, and hence the stress environment during mineralisation. Mapping was done on the 4150 level in six sectors around the perimeter of the 2005 open pit. This is the same level as the now-excavated Vizcachas exploration tunnels in which both Lehmann (1980) and Martini (1984) collected significant veinlet structural data. Veinlets were classed as major, moderate or minor, depending on their width and strike length relative to the overall population. On stereonets and rose diagrams, the larger veins are weighted to reflect the greater dilational strain accommodated on these fractures. Definitions and weighting detail are contained in Appendix VII.

4.6.1 Intrusive and Hydrothermal History

Quebrada Blanca (QB) has the most complex magmatic and hydrothermal history of the Collahuasi porphyry deposits. It comprises a polyphase intrusive complex, multiple cross-cutting breccia facies and at least two separate hydrothermal stages (Lehmann, 1980; Ware et al., 1981; Martini, 1984).

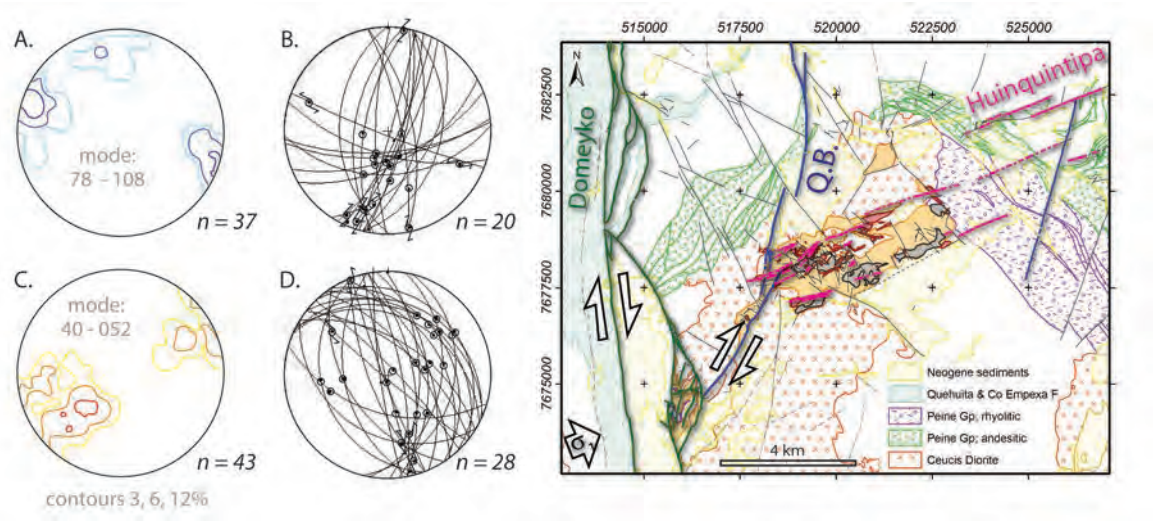

Figure 4.20. Fault orientation and slip sense data for the Quebrada Blanca mine and environs. A.) contoured poles to planes for early gouge, crush and fracture zones associated with intrusions and related breccia bodies. B.) Great circles and slip planes for those data in A for which striae could be identified. Note that ~40% of the data in A was extracted from Desrochers et al. (2001), who did not record slip data. C.-D.) The same two data types for late normal and sinistral faults. The map highlights the broader geometry of the Domeyko, Quebrada Blanca (QB) and Huinquintipa fault zones as they may have interacted as a dextral dilational jog during emplacement of the QB quartz monzonite.

Intrusive complex. The QB intrusive complex is made up of three recognised phases; an early, medium grained equigranular quartz monzonite, and late strongly porphyritic quartz monzodiorite and monzodiorite dykes (Hunt et al., 1983). The quartz monzonite occurs as a rhomb-shaped stock adjacent to the QB Fault, and as a series of dykes and sills that trend along this fault and into the structurally complex El Colorado sector (Figs. 3.4 and 4.19). It is a common host rock for mineralisation at QB, along the QB fault, and at El Colorado, but is not mineralised along its eastern and northern apophyses and to the north of El Colorado (Fam Romero, 1974). Plagioclase-biotite-phyric monzodiorite and quartz monzodiorite porphyries occur primarily in the central part of the intrusive complex, as a series of ENE-trending dykes. Quartz-bearing dykes with comparatively open phenocryst framework (<50% crystals >3 mm) are mineralised to similar intensity as the host stock (Lehmann, 1980), and occur as fragments in all the major breccia facies (Ware et al., 1981). Quartz-poor dykes with comparatively crowded (>60% crystals > 3 mm) phenocryst framework are only weakly altered and mineralised (Lehmann, 1980; Hunt et al., 1983). These dykes cut the early rock-flour matrix breccia facies (M. LaPointe, Aur Resources, written commun. 2005).

Fault Architecture. Two principal generations of brittle structures occur in the Quebrada Blanca deposit and environs (Fig. 4 20): early, steeply dipping NNE and ENE-trending gouge and crush zones that bound and merge with elongate breccia and dyke bodies; and late, moderately dipping faults with discrete fault planes that offset dykes and breccias and are locally occupied by late pyrite veins and attendant phyllosilicate alteration.

Striae and kinematic indicators mapped in faults of the early generation reveal a chaotic history that has included both principal senses of dip slip and strike slip movement on NNE-trending fault segments related to the Quebrada Blanca Fault (Fig. 4.20a, b). The QB quartz monzonite extends as a dyke-like body along this fault, which is therefore interpreted to have been active during emplacement of that intrusion. Faults trending ENE are generally inferred on the basis of elongate dyke and breccia distribution. They are commonly obscured by mineralisation, but where observed they have normal dip slip kinematics (Fig. 4.20b). Projected to the east there is negligible displacement of the Peine Group on these structures, although joint sets on this orientation are common in the area. The spatial coincidence of these faults with early and intermediate stage breccias, and their orientation subparallel to the porphyry dykes and the main quartz monzonite body are all taken to infer that ENE faults served as dilational sites during emplacement of the QB magmatic complex. Kilometre-scale post-Triassic absolute dextral throw on the QB fault is implied by the modern map pattern and thermochronology results (Fig. 3.4; Table 4.5; Chapter 5). Although the temporal constraint of this displacement is poor, the relationships are nonetheless permissive of dextral shear on the QB Fault during magmatic emplacement. That kinematic scenario permits ENE-trending structures to be dilational, and is consistent with the expected strike-slip displacement on this fault geometry under the influence of the far field tectonic stress regime (Fig. 4.20)

A series of moderately to steeply dipping, NW-trending faults with displacements of 1-20 m dissect the orebody. These faults typically offset older faults, dykes and breccias (Hunt et al., 1985). The NW-trending faults commonly host late pyritic veins and strong chalcocite enrichment, implying that they were dilational both during the latter stages of porphyry mineralisation and during subsequent supergene Cu mineralisation. The largest of these faults offsets the Peine Group stratigraphy

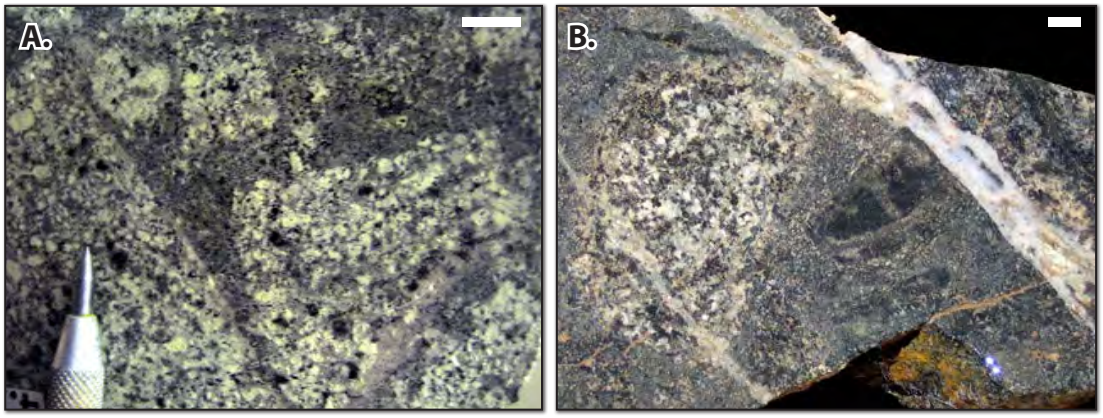

Figure 4.21. Early-stage breccia facies of the Quebrada Blanca porphyry system. A) Monomict angular clast framework-supported biotite-altered rock-flour matrix breccia in quartz monzonite (TE.qmz). Vicinity of 7,677,814 mN; 519,800 mE. B) Polymict strongly biotite-altered, rock flour matrix breccia including a fragment of fine grained equigranular andesitic dyke (TRmdd). Note the strong alteration rim around the microdiorite and absence of rimming alteration about quartz monzonite clasts. The sample is cut by early quartz-pyrite-chalcopyrite veinlets with muscovite haloes (Vqb) and transtional white quartz-(molybdenite) veinlets (Vqm). Sample 180706_01. Unmarked white bars are 1 cm.

to the north of QB and appears to have accommodated subsidence in a Neogene basin to the south (Fig. 4.20). The sense of displacement on these faults is generally normal dip slip (Fig. 4.20c, d). However, a subset of the mineralised NNW-trending faults with strong chalcocite enrichment have shallowly plunging striae and underwent sinistral shear. The similar pyrite veining shared by NW-trending normal faults and NNW-trending sinistral faults is interpreted to reflect a related dilation and kinematic history. Fracturing on these orientations occurred at least as early as the late-stage porphyry veining, under broadly west-directed extension. During supergene enrichment, NW and NNW-trending faults appear to have been active together during Oligocene along-arc sinistral shear. Later, subsidence and creation of sedimentary accommodation space on these faults, as well as faults on a variety of other orientations implies generalised extension during part of the Neogene.

Rock-flour matrix breccias and potassic alteration. Elongate bodies of clast-supported rock-flour matrix breccia dominate the central, strongly mineralised part of the Quebrada Blanca porphyry system (Fig 4.2) and the southern margin of the QB intrusive complex. The margins of the breccias are generally gradational over short distances (< 2 m) and are locally abrupt. The largest single breccia body is greater than 600 m long and 150 m wide in plan, and extends down to the limit of drilling at ~500 m below surface. Elongate dyke-like bodies of breccia extend along strike

of this principal breccia body and occur as isolated zones to the north and south (Hunt et al., 1983). With a few local exceptions, these bodies strike ENE and dip moderately to steeply to the SSE, parallel to the long sides of the quartz monzonite rhomb and to the prevailing porphyry dyke orientation (Fig. 4.19). They are cut by younger breccia bodies (below) and are cut and offset tens of metres by younger, commonly NW-trending normal faults (Hunt et al., 1983). These orientations may have been affected by ~15º of post-mineralisation tilting (section 4.6.3).

The breccias are composed of 2 - 50 cm diameter, approximately equant, subangular to subrounded clasts of the monzonite and lesser quartz monzodiorite porphyry, and diorite and microdiorite wallrocks. The matrices were described by Hunt et al. (1983) as fine grained phaneritic quartz monzonite. However, the matrices were observed during this study to be softer and less competent than the clasts. The have also been affected by stronger hydrothermal alteration that locally produced very coarse-grained rocks. Although the original texture has largely been obliterated by this alteration, the high fracture permeability of an original rock flour matrix to the breccia is more compatible with the present alteration pattern than a primary coherent igneous cement.

Selectively pervasive potassic alteration has affected the entire breccia complex and extends into the surrounding quartz monzonite and Escorial diorite. Alteration is crystal- and variably groundmass selective in the clasts, pervasive in the breccia matrix, and is locally associated with short, irregular-walled veinlets of the principal alteration minerals (vein types 1 and 3 of Rowland, 1998). Alteration rims are not observed around quartz monzonite clasts, but are strongly developed around wallrock clasts (Fig 4.21b). A central zone is dominated by matrix-selective and plagioclase-selective othoclase alteration. An irregular outer zone is dominated by matrix-selective and ferromagnesian mineral-selective biotite ± orthoclase-magnetite alteration (Hunt et al., 1983; Aur Resources pers comm. 2005). Breccia matrix biotitisation locally produced crystal sizes greater than 6 mm. In the wallrocks to the intrusive complex, hornblende in microdiorite dykes are uniformly biotitised in the vicinity of the quartz monzonite stock. Ware et al. (1981) report shreddy biotite overgrowths on hornblende in the Escorial diorite as far south as Quebrada Cienaga Grande (Fig. 4.19).

Quartz-(sulfide) veinlets with muscovite-biotite haloes (Vqmsb). The oldest field-mappable vein generation at Quebrada Blanca comprises subplanar veinlets of quartz, pyrite and lesser chalcopyrite that commonly occur as sheeted groups with strike lengths of 1-3 metres. The veinlet fill attains maximum thickness of 2 mm, and the veinlets have distinctive alteration haloes 4-10 times broader than the vein fill (Fig. 4.22). They are cut by all other vein generations that are easily recognised in hand specimen or pit wall exposure (Fig. 4.22a, b). In the quartz monzonite the alteration haloes comprise a single zone of grey to white muscovite, whereas in the early monzodiorites and biotite-altered breccias they have an outer biotite zone (Fig. 4.22c). In thin section these veinlets are characterised by highly irregular vein walls and alteration margins (Fig. 4.23). Biotite alteration that occurs on some fracture surfaces without vein fill has the same texture and appearance as the outer halo biotite and appears to a weak manifestation of the same alteration stage (Fig. 4.22c).

Rowland (1998) noted the presence of veinlets with sericitic haloes at Quebrada Blanca but did not establish

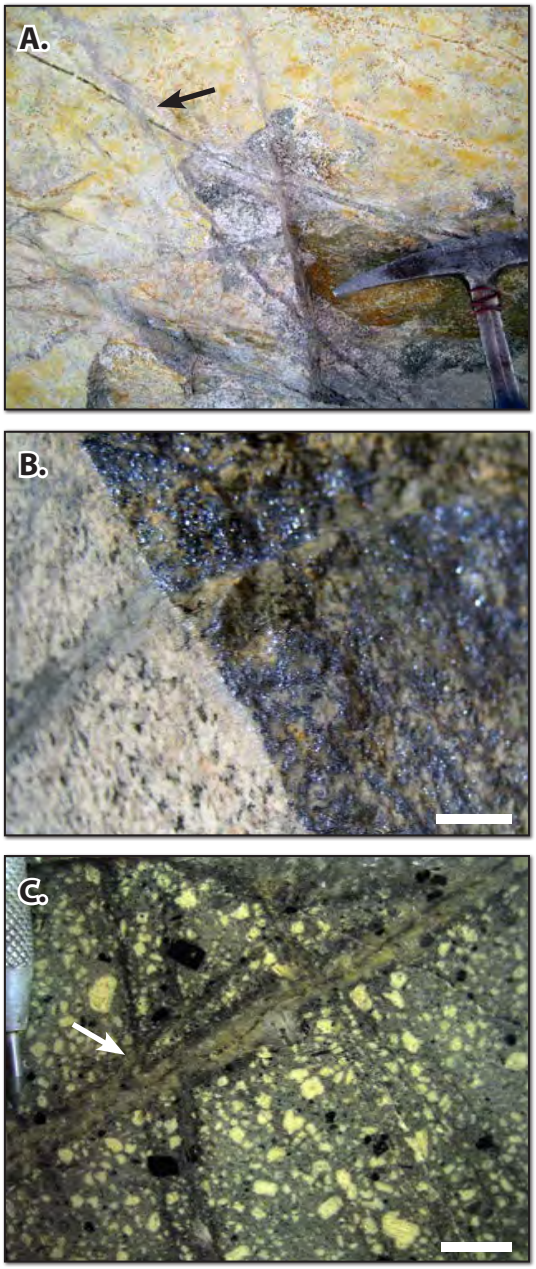

Figure 4.22 Early stage stockwork veining at Quebrada Blanca. A) Open pit exposure in the NC pit map sector (Fig. 4.24) showing typical open array of narrow sheeted Vqmsb veinlets with pronounced haloes, cut by a main stage Vqcp veinlet (arrow). Hammer for scale. B) Specimen of an early stage Vqmsb veinlet with typical grey sericite halo in quartz monzonite (TE.qmz). The fracture surface (right hand side of photo) is a transitional stage molybdenite veinlet that cuts the early veinlet. Sample 301104_02. C) Specimen of early stage Vqmsb veinlets with zoned sericite-biotite haloes in quartz monzodiorite (TE.qbfp). These veinlets cut texturally similar bioite-magnetite veinlets (white arrow). Sample 180706_02. Unmarked white bars are 1 cm.

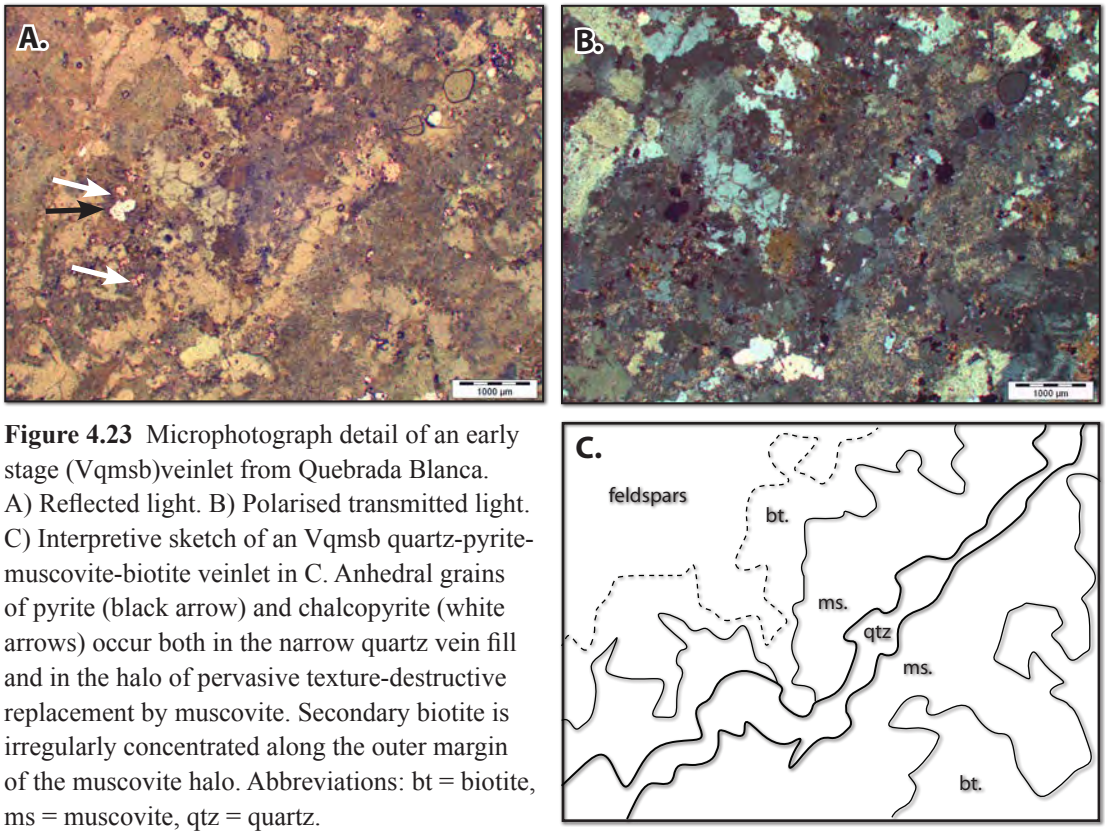

Figure 4.23 Microphotograph detail of an early stage (Vqmsb)veinlet from Quebrada Blanca. A) Reflected light. B) Polarised transmitted light. C) Interpretive sketch of an Vqmsb quartz-pyrite-muscovite-biotite veinlet in C. Anhedral grains of pyrite (black arrow) and chalcopyrite (white arrows) occur both in the narrow quartz vein fill and in the halo of pervasive texture-destructive replacement by muscovite. Secondary biotite is irregularly concentrated along the outer margin of the muscovite halo. Abbreviations: bt = biotite, ms = muscovite, qtz = quartz.

their timing relative to other early stage veinlets. He documented coexisting liquid-rich and vapour rich fluid inclusions and determined a minimum entrapment temperature of 360 - 410ºC. Veins with similar mineralogy occur in a few porphyry deposits elsewhere, and are typically accompanied by andalusite as an accessory alteration phase (Seedorff et al., 2005), although this has not been obseved at Quebrada Blanca. Veinlets with similar fill and alteration mineralogy also occur as an early stage at Butte ("early micaceous" veinlets of Brimhall, 1977) and as an intermediate stage at Los Pelambres ("type 4" veinlets of Atkinson et al., 1996) and at El Salvador ("C-veins" of Gustafson and Quiroga, 1995).

The orientation of early Vqmsb veinlets (Fig. 4.24) is strikingly different to the orientations of early breccias, dykes and faults (Figs. 4.19 and 4.20). In general, these veins dip either shallowly or moderately toward the NE (ranging from ESE to N), and less commonly toward the west. Veinlets on these orientations commonly comprise a conjugate array (Fig.4.22a). The moderately dipping veins, and less common steep veins also preferentially strike NW. Rare, early epidote-chlorite veins mapped in the northern and northwestern peripheries of the hydrothermal system

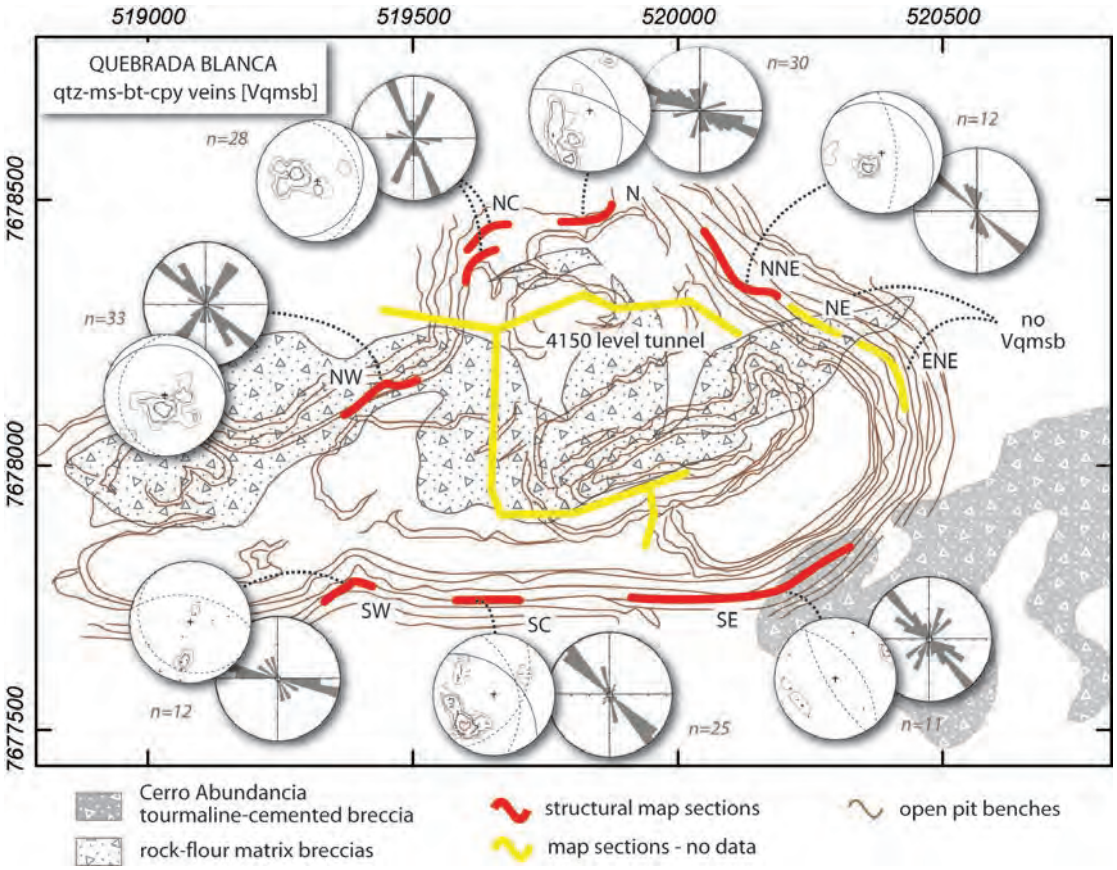

Figure 4.24. Orientations of early Vqmsb veinlets. Stereonets are equal area lower hemisphere projections of raw data, shown as contoured poles to planes with the corresponding great circles of apparent principal orientations (dashed great circles are secondary orientations). Rose diagrams are symmetrical and include only those veins dipping at >45º, weighted for vein width. 2D Terzaghi corrections have been applied using a 10º minimum divergence from the plane of mapping. Background image is a selective geological map of the Quebrada Blanca mine showing the 2005 interior pit benches, structural mapping points and the early-intermediate stage breccia bodies including the Cerro Abundancia tourmaline-cemented breccia (p. 207-8). Structural mapping in this study was done on the 4150 level around the periphery of the pit, in sectors denoted by the compass points: NW, N, NNE, NE, ENE SE, SW, SC (south central) and NC (north central). Data sections in yellow are locations for which Vqmsb do not occur or for which data are not available. The 4150 level Vizcachas exploration tunnel was the source of Vqmo and Vp1 orientations mapped by Lehmann (1980) and Martini (1984) but those authors did not map the Vqmsb vein stage. Breccia distribution adapted from Hunt et al. (1983) and Desrochers et al. (2001).

(n=12) also dip steeply and strike NW, consistent with the flaring of the epidote alteration zone along NW-trending faults (Fig. 4.19). The principal exception to this geometry is a subset of Vqmsb in the northwest and north central map sections that trend NNE (Fig. 4.24). These domains are interpreted to reflect inherited fracturing associated with the Quebrada Blanca fault zone. Given the current distribution of mapping, there is no evidence of a radial array around the Quebrada Blanca intrusive complex or the early breccia bodies or dykes. Vqmsb veinlets are more abundant in the northern half of the pit, and are completely absent from the easternmost map

segments. This distribution does not appear to relate systematically to other aspects of the geology such as the distribution of breccias (Fig. 4.24).

Quartz-sulfide-(othoclase) veinlets without haloes (Vqcp). The principal hypogene cupriferous vein stage at Quebrada Blanca comprises fine to medium grained semimassive to saccharoidal quartz-(orthoclase) veins with variable content of chalcopyrite > pyrite > bornite ("type 1 and 3 veinlets" of Rowland, 1998). These veins are subplanar over strike lengths of 1-5 metres and generally have subparallel vein walls. They attain maximum thickeness of 10 cm, but are generally less than one cm wide. Similar veins have been documented from most porphyry deposits related to calc-alkaline intrusions ("A-veins" of Gustafson and Hunt, 1975; Seedorff et al.,

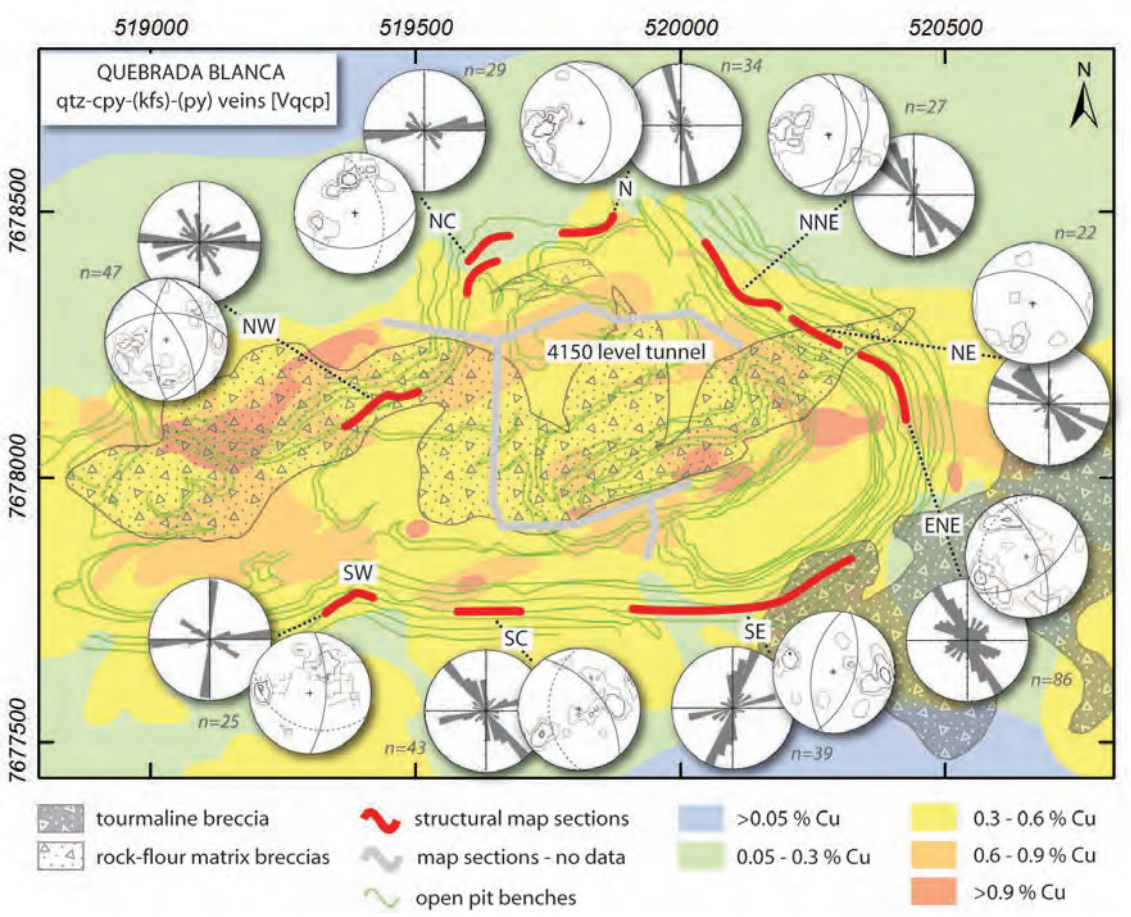

Figure 4.25. Orientations of early quartz-chalcopyrite-(orthoclase-bornite) [Vqcp] veinlets. Stereonets, rose diagram and mapping area details as per Figure 4.24. Background image is a selective geological-geochemical map of the Quebrada Blanca mine showing the 2005 interior pit benches, structural mapping areas and the early-intermediate stage breccia bodies (adapted from Hunt et al., 1983 and Desrochers et al., 2001) superimposed on the primarily hypogene 4105 level Cu contours (0.15%, 0.3%, 0.6%, 0.9% Cu: Aur Resources unpublished data, 2005). The 4150 level Vizcachas exploration tunnel was the source of Vqmo and Vp1 orientations mapped by Lehmann (1980) and Martini (1984) but those authors did not map the Vqcp vein stage. Note that apparent discordance between rose diagrams and the NW and NNE stereonets arises because of the bias correction (2D Terzaghi) for the orientation of the plane of mapping.

2005). Veins with this texture and mineralogy commonly accompany early, high temperature potassic alteration (Seedorff et al., 2005), but at Quebrada Blanca they cut the early muscovite-biotite bearing veins and clearly postdate pervasive potassic alteration. However, they do not exhibit any alteration halo and appear to have formed in chemical equilibrium with the earlier alteration minerals.

The orientations of Vqcp veins is strongly domainal but shows some transition between the orientations of earlier veins and breccias. Moderate to steeply E to NE-dipping veins dominate, and shallowly dipping veins are subordinate (Fig. 4.25). A subset of veins dips moderately to the SSE and S, subparallel to the major breccias. The coincidence of this strike (ENE) with the elongation of high hypogene Cu grades (Fig. 4.25) perhaps suggests that veins on this orientation are particularly abundant in those areas. Steeply dipping veins subparallel to the NNE-trending QB Fault occur prominantly in the southeastern and southwestern map areas, commonly in association with NE-trending veinlets. This array is similar to the overall array of early faults and fractures (Fig. 4.19). The pattern of major cupriferous veinlets is therefore neither radial nor concentric, but instead mimics the strong NW trending grain in the eastern parts of the deposit, and appears to variously mimic the breccia fabric and elements of the QB Fault system in west and south of the deposit.

Quartz-molybdenite veinlets without haloes (Vqmo). Planar veinlets consisting of grey to white crystalline quartz with either selvedges and/or centrelines of molybdenite and no alteration halo define the intermediate hydrothermal stage at Quebrada Blanca (Lehmann, 1980; “type 4 veins” of Rowland, 1998; equivalent generally to “B-veins” of Gustafson and Hunt, 1975). These veins attain thicknesses of several centimetres and reach strike lengths > 3 metres. Locally, fracture surfaces with coatings of pure molybdenite accompany the veins (Fig. 4.22b; Lehmann, 1980). Ambiguous cross cutting relations betwen these and quartz-molybdenite veins suggest the two are related, in which case the molybdenite-coated fractures could be a precursor event that preceeded quartz precipitation. This vein stage is distinguished from younger breccia-hosted molybdenite by its ubiquitous vein morphology, the absence of associated muscovite or illite alteration, and very high rhenium concentration (Re = 700-1400 ppm, avg. 943 ppm; Lehmann, 1980). In all observed cases these veins cut the Vqmsb and Vqcp stages, but are cut by later pyritic veinlets

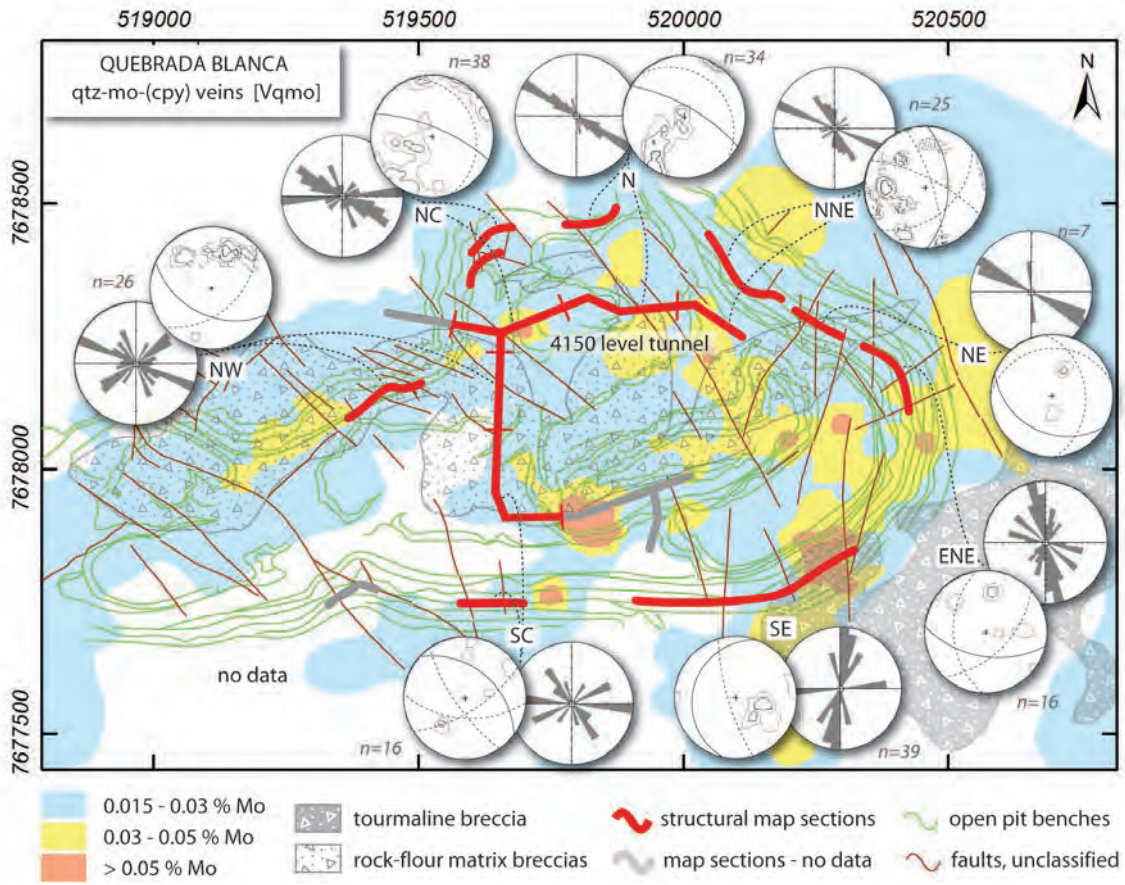

Figure 4.26. Orientations of intermediate quartz-molybdenite [Vqmo] veinlets. Stereonets, rose diagram and mapping area details as per Figure 4.24. Background image is a selective geological-geochemical map of the Quebrada Blanca mine showing similar line detail to Fig 4.25 as well as mapped faults and the hypogene 4105 level Mo contours (0.01%, 0.03%, 0.05% Cu: Aur Resources unpublished data, 2005). Data of Lehmann (1981) from the 4150 level exploration tunnel was incorporated with new data in the same radial segment of the deposit, as indicated by dashed lines.

(this study; Martini, 1984; Rowland, 1998). Fam Romero (1974) documents limited occurrence of these veinlets along a dyke-like body of quartz monzonite that occupies the Quebrada Blanca Fault to the SW of the main porphyry copper deposit (Fig 4.19).

The orientations of Vqmo veins at Quebrada Blanca is similar in many respects to the preceeding Vqcp stage. The eastern part of the deposit is dominated by NW and NNW-striking veins. The western areas have mixed ENE and WNW-striking veins and the southeastern sector has a strong NNE fabric. However, shallow vein orientations are comparatively common among Vqmo veins. In several sectors shallow and steep veinlets have approximately the same strike (sectors SE, NC, N and NNE). These arrays manifest as short, broad shallowly inclined segments that link narrower steeper veins of longer strike extent. The grade distribution of Mo is complex because of the influence of a late stage of NW to NNW-trending

molybdenite-cemented breccias. Nonetheless, distinct grade trends to the ENE and NE are evident (Fig. 4.26) and coincide with veins on these orientations in the higher grade map sectors.

"Vuggy Breccia" and pyrite-quartz veinlets with kaolinite-muscovite-(illite) haloes (Vp1). A discrete ENE-trending body of pyrite- and quartz-cemented hydrothermal breccia with 5-10 volume percent open space occurs in the central, eastern part of the Quebrada Blanca porphyry deposit (Figs. 4.27 and 4.28; Hunt et al., 1983; Martini, 1984). Clasts are generally subangular to angular, range up to ~1 m in size, and define a chaotic framework-supported fabric with abrupt margins. The open space was interpreted by Sillitoe (2001) as the result of supergene dissolution of hypogene anhydrite, though anhydrite is not recorded as a component of similar hydrothermal stages in any other deposits (Seedorff et al., 2005). Nonetheless, the high bulk permeability and pyrite content of the Vuggy Breccia are likely to have contributed to strong and coherent supergene chalcocite mineralisation therein (Aur Resources pers. comm., 2005). Clasts in the Vuggy Breccia are pervasively altered to a texturally-preserving quartz-illite-kaolinite; though much of the kaolinite is interpreted to be supergene (Hunt et al., 1983).

Veinlets dominated by massive to euhedral crystalline pyrite ± quartz and with broad haloes of similar bleaching alteration to that in the Vuggy Breccia occur widely in the Quebrada Blanca deposit (Fam Romero, 1974; Hunt et al., 1983; Martini, 1984). They are characteristically planar and may extend over strike lengths of 10 metres. Veins of this style consistently cut the three principal earlier vein stages and the main tourmaline breccia on Cerro Abundancia (Fig. 4.29a). Locally, these veins either occupy, or have been re-used as normal faults that focussed supergene chalcocite enrichment. They are also reported to be widely developed along the Quebrada Blanca Fault zone between the main porphyry deposit and the El Colorado prospect (Fig. 4.19; Fam Romero, 1974). In his detailed study of this vein stage, Martini (1984) described Vp1 veinlets in clasts within the vuggy breccia, and a small number that cut the breccia. Vein densities are generally low inside the Vuggy breccia and are highest immediately outboard of it (Figs. 4.27c and 4.28). Hypogene mineralisation in the vuggy breccia therefore appears to have formed within the time frame of formation of the Vp1 veins. The same author mapped the orientation of over five

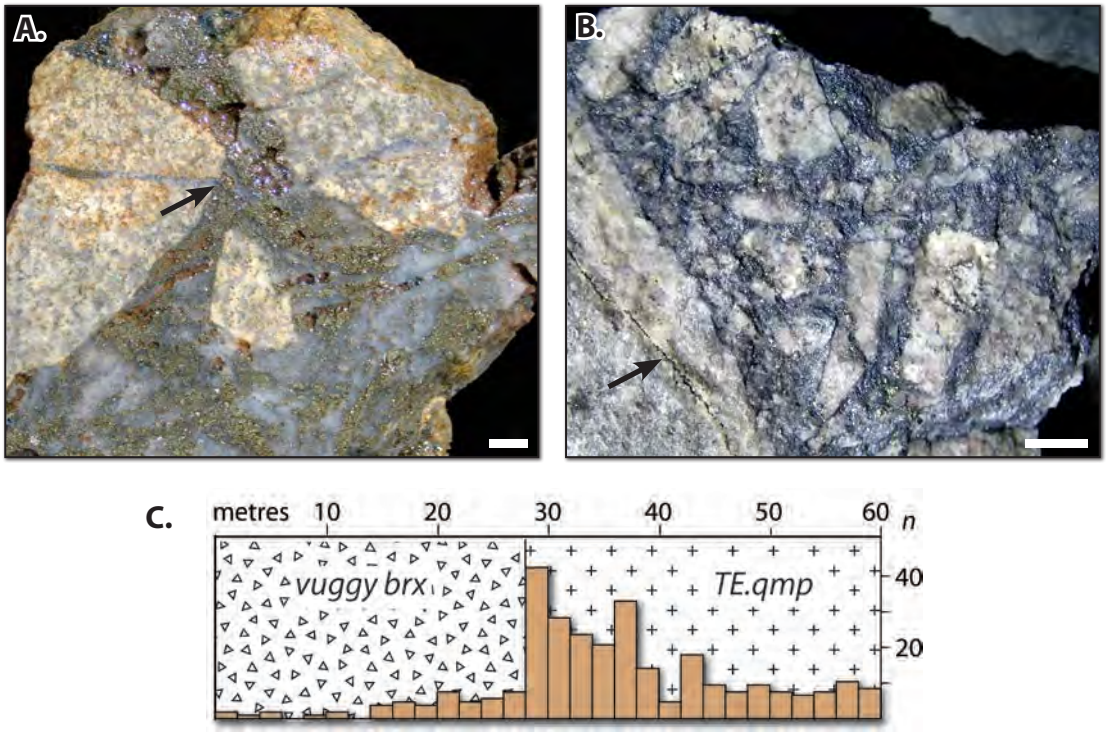

Figure 4.27. Late stage breccias at QB. A) Quartz-pyrite-(anhydrite) cemented "Vuggy Breccia" including angular clasts with transitional-stage quartz-molybdenite veinlets (arrow). Matrix-supported texture in this sample is non-representative. Sample 281105_01. B) Specimen of the "Moly Breccia" showing framework-supported internal geometry, molybdenite-cement, and angular elongate form of sericite-altered clasts. Arrow indicates Vp1 veinlet in a clast. Mapping by Lehmann (1980), Hunt et al. (1983) and Martini (1984) suggest the Moly Breccia trends NW and cuts the Vuggy Breccia. Sample 281105_03. C) Frequency of Vp1 veinlets (expressed as *n* veins/m) in a drive cutting the southern margin of the Vuggy Breccia (zone 29; Fig. 4.28: Martini, 1984). Veining is strongest in the unbrecciated wallrocks and decreases to background at a distance of 15 m outboard of the breccia. Few veins are mapped cutting the breccia, suggesting contemporaneous breccia cementation and vein formation.

thousand Vp1 veinlets in the Vizcachas 4150 level exploration tunnels. He did not distinguish the early Vqmsb vein stage that also has an alteration halo, so it is unclear how much "contamination" occurs within his Vp1 data. Nonetheless, mapping in this study generally avoided Vp1 veinlets and interpretation rests on the existing data (Fig. 4.28).

Pyrite-Cu sulfide vein infill with pyrophyllite-muscovite haloes (Vp2). The Vuggy Breccia and a small number of Vp1 veins were observed by Martini (1984) to contain a late-stage infill of chalcopyrite, bornite, digenite and covellite (Fig. 4.30). These veins and breccia zones are described as being associated with localised advanced argillic alteration haloes including quartz, diaspore and andalusite and appear to be analogous to the late stage infill of the La Grande vein system described by

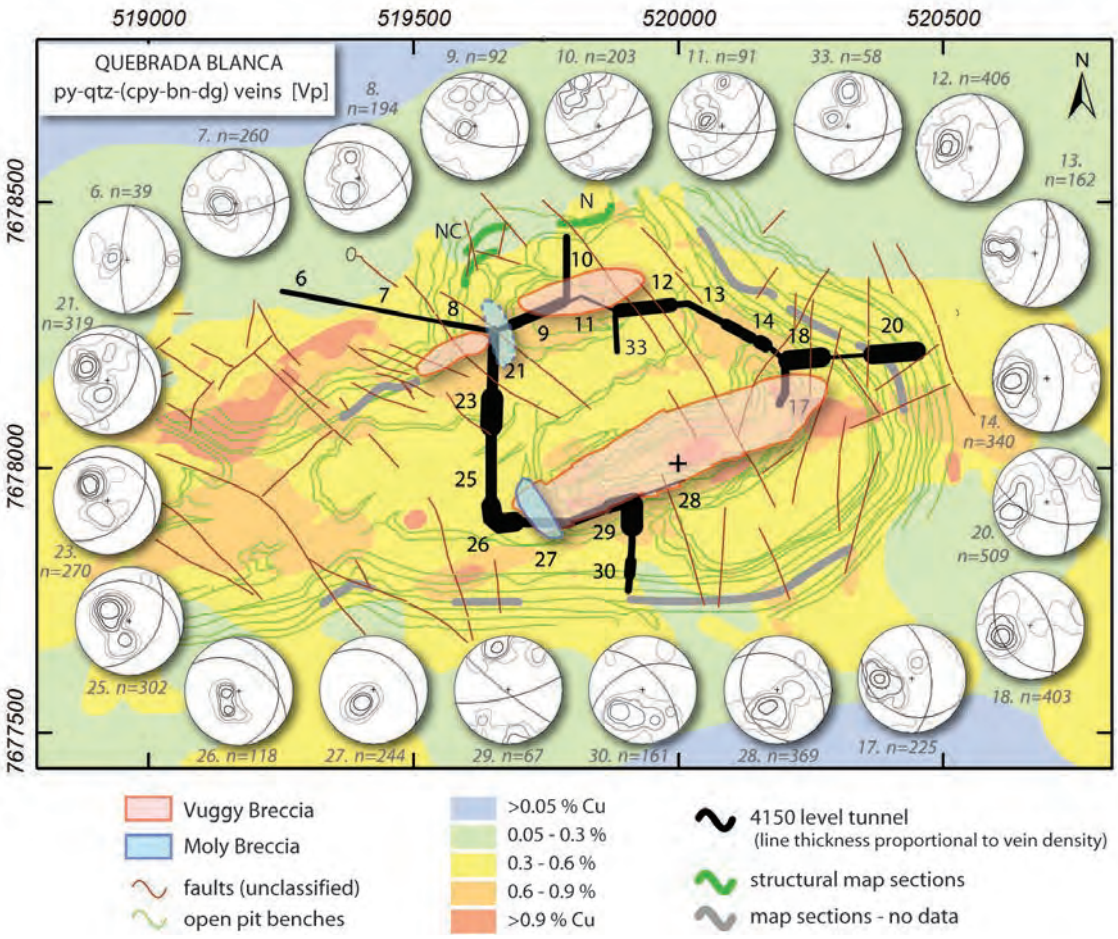

Figure 4.28. Orientations of late pyrite veins with muscovite-illite haloes (Vp1 and 2). Stereonets are equal area projections redrafted from Martini (1984) for veins mapped in the 4150 level exploration tunnel. The thickness of the tunnel lines indicate the mean vein density mapped in that study. Numbers adjacent to stereonets correspond to numbered tunnel segments. Background image is a selective geological-geochemical map of the Quebrada Blanca mine showing the 2005 interior pit benches, structural mapping areas and the late stage breccia bodies (adapted from Lehmann, 1980; Hunt et al., 1983, and Desrochers et al., 2001) superimposed on the primarily hypogene 4105 level Cu contours (0.15%, 0.3%, 0.6%, 0.9% Cu: Aur Resources unpublished data, 2005).

Masterman et al. (2005). This assemblage was not observed during this study and may have only ever developed at high levels that had been mined out prior to 2004.

Late pyritic veinlets (Vp1 and Vp2) occupy a wide range of orientations that vary dramatically between domains of the QB porphyry (Fig. 4.28). Overall, veinlets that strike NE to NW and are moderately inclined to the E are the most common. A discrete subset of veins are parallel to abundant short-displacement normal faults that strike NW and dip moderately to shallowly NE. Unlike early Vqmsb veinlets, these shallowly dipping late pyritic veinlets do not form well developed conjugate arrays with more steeply dipping examples in the same domain. The distribution of vein orientations does not show any systematic radial or concentric arrangement with

regard to the Eocene intrusions or grade distribution. However, pronounced domains of N to NW-trending veins, locally subparallel to, and associated with normal faults appear to mark the along-strike limits of the main Vuggy Breccia body (sectors 17, 18, 20 and 26, 27 in Fig. 4.28). The abundance of late pyritic veins is generally highest outboard of, and close to Vuggy Breccia, and many of the veinlets in the long walls of these breccia bodies have strikes subparallel to the breccia margins (sectors 10, 11 and 29, 30 in Fig 4.28).

Molybdenite-(quartz-pyrite)-cemented breccia with illite-quartz alteration. A 90 x ?50 m, NW-trending body of high grade (up to 1.0%) Mo mineralisation in the central southern part of the deposit corresponds to a breccia cemented primarily by molybdenite. This breccia was described by Lehmann (1980) and is called the Moly Breccia. Another such body in the central northern part of the deposit is shown on sections presented in Lehmann (1980). Molybdenite in these breccias contains an average of 340 ppm Re (range 240-400 ppm), and is compositionally distinct from Re-rich molybdenite in the intermediate stage veins. It has a chaotic clast-supported geometry in which angular to subrounded clasts are pervasively altered to illite and supergene kaolinite. The main molydenite-cemented breccia partly occurs within, and cuts the Vuggy Breccia. Clasts commonly contain Vqmo and Vp1 veinlets (Fig. 4.27b). However, the Moly Breccia body dips moderately to the SW, parallel to local Vp1 veins (sector 27 in Fig 4.28: Lehmann, 1980). The two occurrences of Mo-cemented breccias are not considered to be controlled by the same master structure, as they are not collinear along the NW strike of veinlets near the southern body or NW trend of elevated Mo grades in that area (Fig 4.27).

Tourmaline-cemented breccias and veins. The tall eastern wall of the Quebrada Blanca open pit exposes the Cerro Abundancia breccia (Figs. 4.24 - 4.26). This is the largest and most tourmaline-rich of several hydrothermal breccia bodies that extend ENE along the southern margin of the quartz monzonite stock (Fig. 4.19). Tourmaline in the breccia cement comprises massive intergrowths and local acicular black-green crystal sprays 10-30 microns long. The breccias are composed of angular fragments of all the major intrusive and wallrock lithologies, as well as some strongly quartz-phyric rhyolitic rocks of the Chiclla Formation. The breccia comprises large domains of chaotic, clast supported texture separated by zones

of irregularly stratified matrix-supported breccia in which elongate clasts are moderately aligned (Fig. 4.29a, b). The northern margin of the breccia body is a moderately SSE-dipping fault close to which the concentration of basement rhyolite clasts reachs a maximum (Aur Resources, pers. comm., 2005). Clasts include early Vqmsb, Vqcp and Vqmo veinlets, but the breccia is cut by later Vp1 veinlets (Fig. 4.29a). These relationships constrain the timing of tourmaline breccia formation to a late-intermediate stage within the development of the Quebrada Blanca stockwork (Fig. 4.30). Feldpars and biotite in breccia clasts are not pervasively altered to the phyllosilicate assemblages of later hydrothermal stages, except in the halo to later veins. The pervasive tourmaline-quartz cementation therefore appears to have closed the breccia porosity prior to formation of Vp1 veins, and was not directly related with any feldspar-destructive alteration.

Tourmaline occurs commonly in a zone to the north of Quebrada Blanca, most noticeably as arborescent spotting (Fig. 4.29c) and fracture controlled alteration associated with albite and hematite (Fig. 4.29d) in a small stock of monzonite immediately south of the Quebrada Huinquintipa (Fig. 4.19). In this vicinity, tourmaline also occurs with quartz as massive irregularly banded replacements of fault zones and permeable sandstone horizons. It it also occurs irregularly with various calcite-hematite veins, in which it forms strongly zoned, stubby euhedral crystals up to 1 cm long. Elsewhere, fault-fill and replacement tourmaline are recorded from a location south of Quebrada Blanca, and from the El Colorado prospect to the SW.

Tourmaline veins and tourmaline-cemented tectonic breccias across the broader Quebrada Blanca area (Fig. 4.19) generally occupy steeply dipping NNE-trending structures (Fig. 4.30). A subordinate group trend NE, and broad tourmaline alteration or vein zones exclusively take one of these two orientations. The tourmaline-cemented breccias at Cerro Abundancia have an overall ENE strike. The geometry of tourmaline-bearing structures is therefore similar to that of the early QB Fault and related structures (Fig. 4.20a, b).

Epidote-dominated veins and alteration. Epidote-rich alteration assemblages are much less common at Quebrada Blanca than at Rosario and Ujina, but more common than at Copaquire (subsequent sections). These minerals generally occur

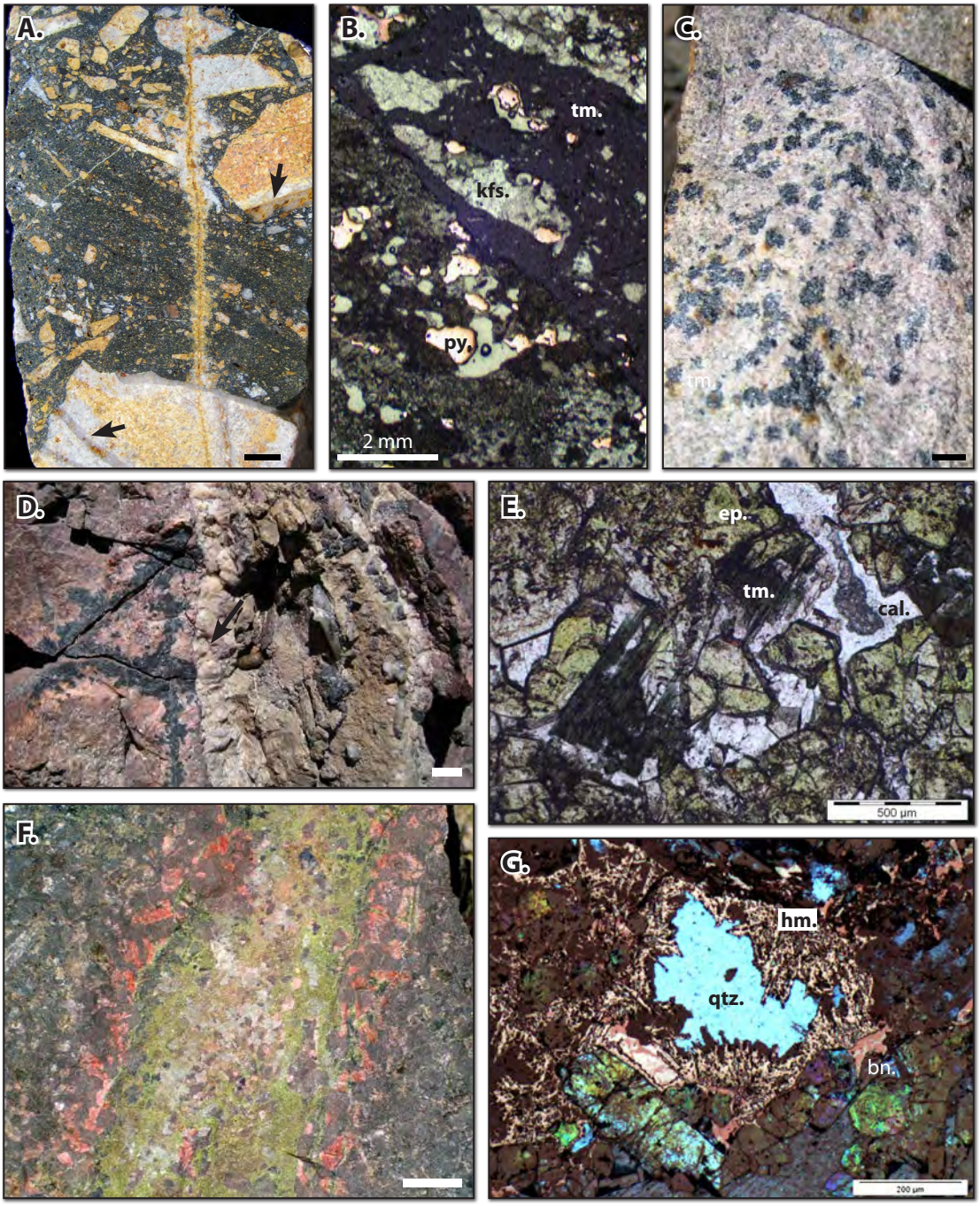

Figure 4.29. Tourmaline and epidote-bearing alteration at Quebrada Blanca. A) Cerro Abundancia tourmaline-cemented breccia. Early grey Vqs occur in breccia clasts (black arrows) whereas late stage Vp1 crosscut the breccia. Subparallel domains of matrix- and framework support and alignment of clasts define diffuse local stratification. Sample 221104_01. B) Detail of A showing fragmentation of early stage pyrite and the absence of alteration or sulfide addition related to tourmaline cementation of the breccia (reflected and transmitted light microphotograph [RT]). C) Spotty tourmalinisation of quartz monzonite near Quebrada Huinquintipa (Fig. 4.19; 7,684,932 mN; 525,250 mE). D) Calcite-hematite vein cutting fracture controlled tourmaline-albite-hematite alteration in quartz monzonite. Vicinity of 521,430 mE; 7.681.380 mN. E) Coexisting epidote, tourmaline, calcite and barite (not pictured) in a distal propylitic vein (plane light). Sample 241105_01. F) Epidote-dominated vein with narrow halo of strong selectively pervasive red albite-hematite alteration of plagioclase phenocrysts in ocoita andesite (Pzpg.10) and distal chlorite-dominated groundmass alteration. Sample 171005_02. G) Detail of F showing prismatic euhedral epidote crystals, acicular-dendritic hematite associated with minor bornite (RT). Abbreviations: tm = tourmaline, py =pyrite, kfs = orthoclase, cal = calcite, qtz = quartz, hm = hematite, bn = bornite. Unmarked black or white bars are 1 cm.

outboard of, and overlap the margins of, zones of potassic and tourmaline alteration. The bulk distribution of epidote coincides approximately with the zone in which K-Ar radiometric age determinations of the Permo-Triassic Peine Group and Escorial Diorite are reset to much younger ages (Fig 4.19). This is interpreted to correspond to the thermal halo related to peripheral parts of the QB hydrothermal system, since the minimum temperature of formation of epidote (250-280ºC: Browne, 1978; Reyes, 1990) is above the closure temperature for the potassium feldspar K-Ar chronometer and is in the vicinity of the closure temperature for the biotite chronometer (see

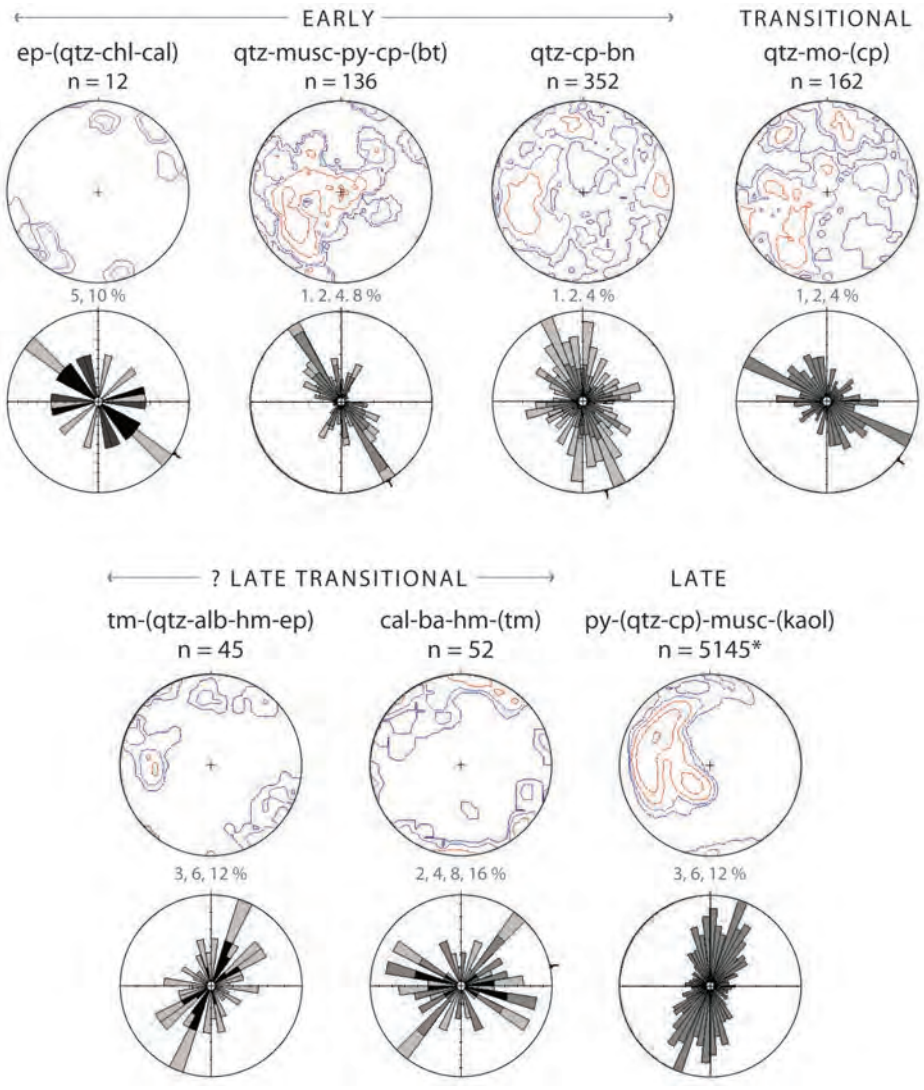

Figure 4.30. Lower hemisphere stereographic projections and rose diagrams of global vein populations for the Quebrada Blanca deposit and environs. Plots are arranged by the likely sequence of formation and have been restored to their likely original orientation by removal of 15º of northward post-mineralisation tilting. Rose diagrams exclude veins inclined < 45º and darker segments correspond to broader veins. Plots for transitional qtz-mo and late py-qtz veins include new data and the data presented by Lehmann (1980) and Martini (1984)*.

McDougall and Harrison, 1999, for a summary of closure temperatures). This hydrothermal regime therefore extended at least two, and locally more than three kilometres outboard of the Quebrada Blanca intrusive complex.

Vein-, fault-, and breccia-fill epidote-(chlorite) occurs widely in the zone N and E of Quebrada Blanca, and is locally very abundant in areas of high primary porosity such as the sedimentary breccias of the La Grande and Huinquintipa formations. Elsewhere, this alteration assemblage is only weakly and irregularly developed and is uniformly restricted to the most mafic and permeable lithologies. To the immediate north and northwest of Quebrada Blanca the assemblage epidote-chlorite-calcite occurs as weakly developed amgydule fillings in andesite beneath the Cascasca Formation - La Grande Formation disconformity. Actinolite is reported with this assemblage in the closest occurrences to the QB porphyry Cu deposit (Fam Romero, 1974), though these locations are now obscured by the mining operations. The zonation is nonetheless consistent with that described from other porphyry deposits, such as Tintic, Utah (Norman, 1991) and Batu Hijau, Sumbawa (Garwin, 2000). Veins of epidote attributed to this generation are rare. The orientations of a small number of mapped veins to the N of QB varies widely but appears to favour the NW-strike of pre-existing faults in that area (Figs. 4.19 and 4.30).

More complex assemblages and zonation are evident in the distal hydrothermal environment of the eastern parts of the system. In the southern periphery of tourmaline alteration zones and breccia at Cerro Abundancia, epidote occurs with tourmaline, hematite and calcite (Fam Romero, 1974). This spatial relationship between tourmaline and epidote is also observed to the NE of Quebrada Huinquintipa, where fracture intersections are altered to irregular clots of semimassive finely crystalline epidote with irregular cores of tourmaline and barite-calcite infill (Fig. 4.29e). Outboard of this, and also to the east of Quebrada Blanca, plagioclase-selective epidote alteration is variably associated with haloes of plagioclase-selective bleaching and reddening (hematite-albite alteration; Fig. 4.29f). This assemblage is consistent with increasing oxidation state of the fluid, as determined experimentally by Holdaway (1972). Several such examples have supergene chrysocolla on the fracture surfaces and contain small amounts of hypogene bornite and specular hematite (Fig. 4.29g). In one unusual fault-hosted

example in the same area, epidote is associated with crystalline red-brown garnet and beige albite. These oxidised assemblages are the most distal common manifestation of the QB hydrothermal system that is recognised in the field.

The timing of formation of epidote-rich assemblages is uncertain. In general, the volume of fluid expelled in each major hydrothermal pulse from a porphyry magmatic-hydrothermal centre is thought to decrease in time, i.e. that the broadest peripheral alteration facies is the distal manifestation of early (potassic) proximal alteration stages (e.g., Titley et al., 1986). That at least three km^3 of the QB intrusive complex has potassic alteration suggests that this event was associated with major hydrothermal fluid flow. On that basis it is anticipated that some of the epidote-

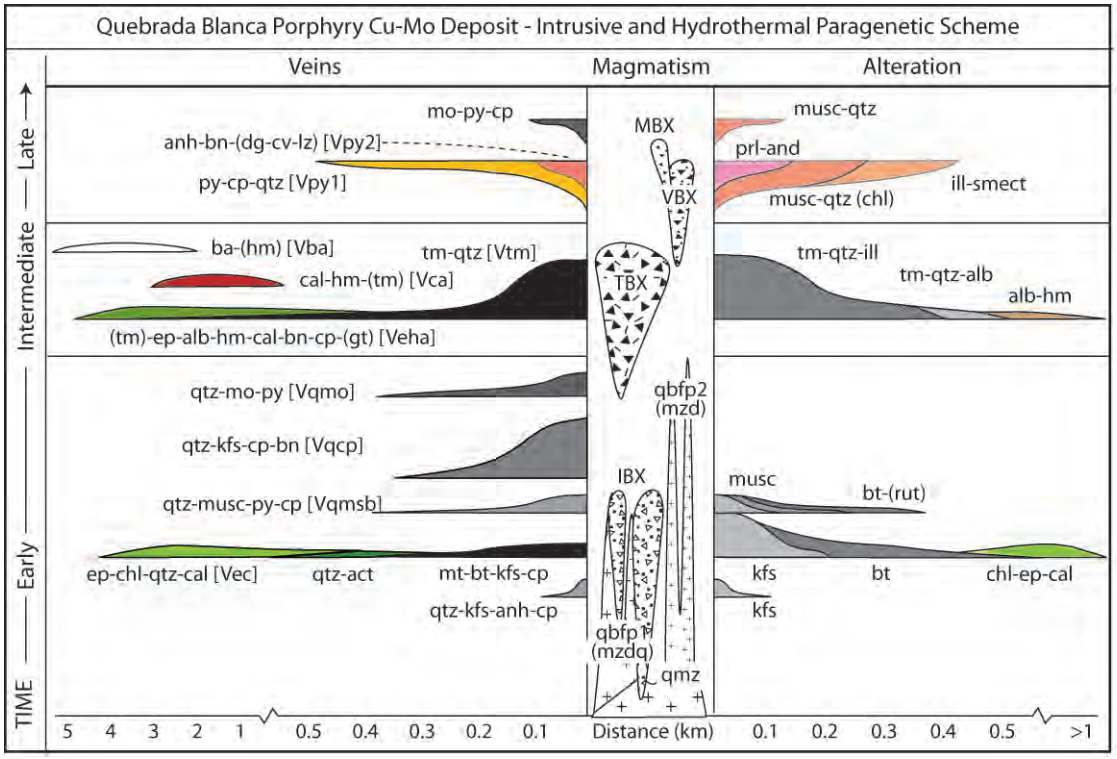

Figure 4.31. Schematic diagram of spatial and temporal relationships between intrusions, breccia formation, and vein and alteration assemblages at Quebrada Blanca. The mineralogy of proximal vein and alteration stages is compiled from Lehmann, (1980), Ware et al. (1981), and Martini (1984). The distribution and mineralogy of peripheral vein stages was determined in this study. The relative timing of vein and breccia events incorporates new data and cross cutting relationships documented in previous studies. Synchroneity of early and intermediate proximal and distal veins and alteration is inferred. Rock abbreviations: qmz = QB quartz monzonite; qbfp = QB feldspar porphyry; mndq = quartz monzodiorite; mzd = monzodiorite; IBX = rock flour-matrix 'intrusive' breccia; TBX = tourmaline-cemented breccia; VBX = Vuggy Breccia; MBX = Moly Breccia. Mineral abbreviations: anh = anhydrite; bn = bornite; dg = digenite; cv = covellite; lz = luzonite; mo = molybdenite; py = pyrite; cp = chalcopyrite; qtz = quartz; musc = muscovite; prl = pyrophyllite; and = andalusite; chl = chlorite; ill = illite; smect = smectite; ba = barite; hm = hematite; tm = tourmaline; alb = albite; kfs = potassium feldspar; ep = epidote; cal = calcite; act = actinolite; mt = magnetite.

bearing alteration occurred at this early stage. However, epidote-bearing assemblages are most abundant and well developed in the vicinity of the small commonly tourmaline-albite-hematite altered monzonite stock south of Quebrada Huinquintipa (Figs. 4.19; 4.29c, d). If this stock is contemporaneous with the tourmaline-cemented breccia at Cerro Abundancia, then the strongest epidote alteration, as well as related hematite, calcite and barite veins may have occurred during a late-intermediate stage within the porphyry paragenesis (as depicted on Fig. 4.31).

Calcite and Barite veins. Planar, fault-hosted and/or faulted veins of sparry calcite or calcite reddened by fine grained hematite occur in the area of tourmaline alteration around a monzonite stock south of the Quebrada Huinquintipa (Fig. 4.19). Calcite veins consistently cut tourmaline alteration (Fig. 4.29d) but locally include coarse zoned tourmaline crystals. They are re-opened or cut by sparry white barite or barite-hematite veins that occur in three areas outboard and to the N and W of the calcite zone (Fig. 4.19). Veins of these styles were not encountered anywhere else in the Collahuasi district. They are preferentially developed in extensional faults that trend broadly E-W and dip steeply to the S (Fig. 4.30).

4.6.2 Age of the Quebrada Blanca System

The Quebrada Blanca porphyry system formed in two stages; an early, main magmatic and hydrothermal stage at ~37 Ma; and a younger hydrothermal event represented by the Moly Breccia at ~35 Ma (Fig. 4.32). Taking the weighted

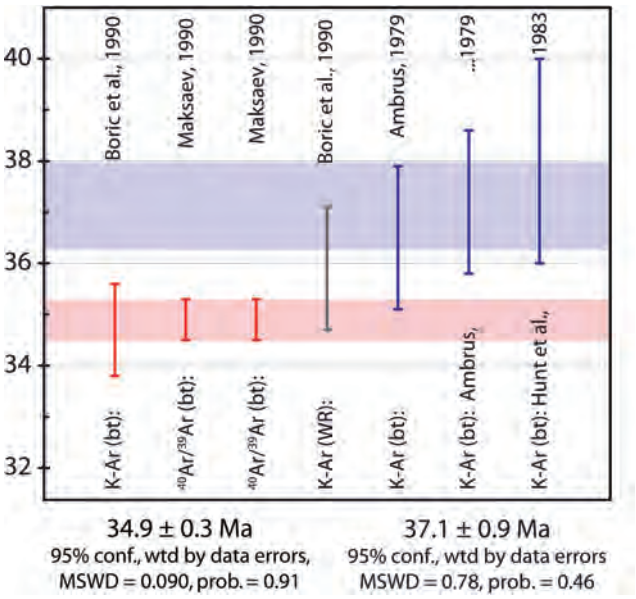

Figure 4.32. Compilation of open file radiometric ages for the Quebrada Blanca deposit (extracted from Tomlinson et al., 2001). Weighted averages of two distinct clusters of age results suggest an early ?magmatic-hydrothermal pulse between 38.0 and 36.2 Ma (light blue bar), and a later hydrothermal event between 34.6 and 35.2 Ma (pink bar). The one whole rock sample reported (grey error bars, centre) appears to reflect a mixture of isotopic reservoirs or partial resetting by the younger event.

average of open-source data, the two events were separated in time by a minimum of one million years. This conclusion is drawn from the compilation of five K-Ar and two $^{40}Ar/^{39}Ar$ ages reported in Tomlinson et al. (2001a). These averages are in clear agreement with, albeit at lower precision than unpublished zircon U-Pb and molybdenite Re-Os ages for the monzodiorite dykes and the molybdenite in the Moly Breccia, respectively (V. Maksaev, written commun 2006; Aur Resources, pers. commun., 2006).

With one exception the compiled results are analyses of biotite separates, denoted as secondary biotite in the case of two of the younger samples. Although the original information on the sampling context could not be retrieved, it appears that the hydrothermal renaissance of the system either caused further biotite alteration, or was sufficiently hot (≥300ºC) to cause resetting of the older hydrothermal biotite. There is no known textural evidence for biotite alteration overprinting the intermediate vein and alteration stages, and the resetting interpretation is therefore preferred.

4.6.3 Structural Evolution of Quebrada Blanca: Interpretation

At Quebrada Blanca, the major early breccia bodies and dykes dip consistently 45-65º to the SSE (Hunt et al., 1985; Desrochers et al., 2001). Magmatic-hydrothermal breccias associated with porphyry copper deposits are typically subvertical (see Sillitoe, 1973, for a review) and the inclination of the Quebrada Blanca breccias suggests tilting of the system. Twelve kilometres to the NW, the eroded upper surface of the Copaquire porphyry is inclined moderately to the NNE (section 4.7). A similar distance to the NE, the uppermost member of the Icanche Formation at Cerro Vega dips gently to the NNW (Fig. 3.4). There are no widespread Eocene or Oligocene units at Quebrada Blanca that can be used to constrain the syn-mineral reference frame. However if we accept that the tourmaline breccias at Cerro Abundancia are unlikely to have formed below the main porphyry-related stockwork, then their location to the south of, and partly underlain by the stockwork restricts the amount of tilting that may have occurred. The are no major structural breaks between Quebrada Blanca and the Icanche Formation at Cerro Vega. Therefore, approximately 15º of northward tilting that affected these bedded rocks could plausibly have also affected Quebrada Blanca. This is also approximately the

difference between the dip of Peine group rocks to the west of the Monctezuma Fault (~45º) and those on the east of the Monctezuma Fault (~30º; Fig. 3.4), suggesting that post-mineralisationisation tilting was accommodated on this structure. Some of the Neogene sandstones and shales that partly overlie the northwestern part of the intrusive complex dip gently southward, and hence tilting occurred between porphyry emplacement and development of the hyperarid modern climate in the Early to Middle Miocene (e.g., Alpers and Brimhall, 1988).

Dykes and pre-mineral breccias at Quebrada Blanca systematically trend NNE and ENE, and therefore record maximum dilational strain oriented NNW and subhorizontal. The same orientations are defined by widespread faults and fractures within the Quebrada Blanca porphyry copper deposit (Fig. 4.20a, b). The pre-mineral QB quartz monzonite also has a broadly rhombic plan geometry that is locally bound by short-displacement faults on these orientations (Fig. 4.20). As both NNE and ENE-trending structures host similar styles of intrusion and brecciation, faults on these orientations are inferred to have been active together during mineralisation, and may be considered as a conjugate array. Following the geometric rules of Hancock (1985) and Dunne and Hancock (1994), the intersection between the two conjugate planes corresponds to the intermediate principal stress axis (σ_2), which in this case would have been subvertical. The maximum principal stress axis bisects the acute angle between two conjugate planes, and hence would have been subhorizontal and oriented between NE and ENE. The minimum principal stress axis (σ_3) was therefore subhorizontal and directed between NW and NNW (Fig. 4.33), approximately parallel to the axis of maximum dilational strain that accompanied intrusion. Under this stress environment dextral strike slip strain would have been accommodated along the Domeyko Fault. The existing geometric relationship between the Domeyko and Quebrada Blanca (QB) faults implies that the latter was likely to have acted as a sympathetic dextral shear. It may have been linked to the Monctezuma Fault along an ENE-trending fracture array including the Huinquintipa fault, so that these structures articulated together as a dextral shear couple during intrusion.

In their present orientation, thin, early stage veins with muscovite-biotite haloes (Vqmsb) describe a conjugate array of shallowly and moderately dipping veins that strike NW. Restoration of tilting of the QB block suggests that the shallower set were

originally subhorizontal and the steeper conjugate was moderately inclined toward the NE (Fig. 4.30). This latter orientation corresponds the most widespread and well-developed fracture orientation in the western Collahuasi district (Desrochers et al., 2001; this study), and so may represent propogation of a regional fabric through the intrusive complex. In contrast, the subhorizontal set is almost unique to the immediate QB deposit environment. The shallowly-dipping conjugate array implies a NE-directed compressional regime if the maximum principal stress axis (σ_1) bisected the acute angle between the conjugate sets. This stress environment is consistent with the environment envisaged for magmatic emplacement, and only requires that the minimum principal stress axis rotated to subvertical (Fig. 4.33), which is the

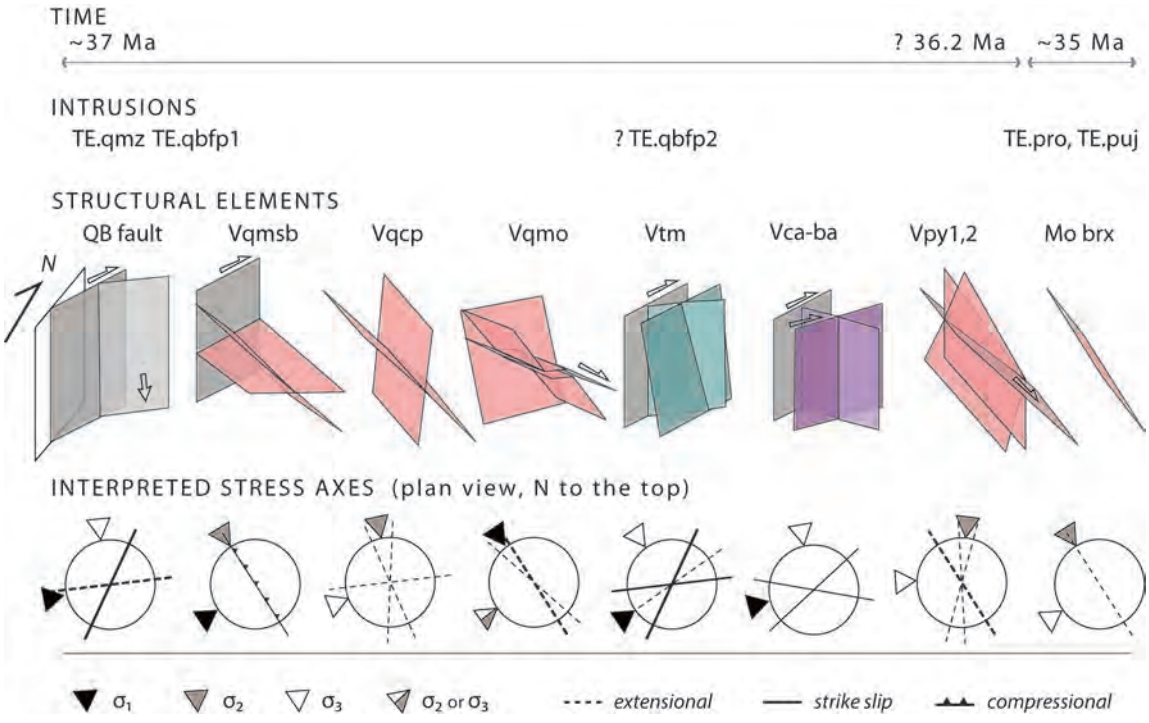

Figure 4.33. Schematic representation of the principal vein and fault orientations at Quebrada Blanca, and the interpreted orientations of local stress axes for the prevailing regime during formation of each generation. The effects of subtle northward tilting of the system have been removed. Interpretation of stress orientations is largely based on the simplified fracture geometry - stress orientation scenarios described by Hancock (1985) and Dunne and Hancock (1994). Similar results were obtained by treating the veins as small faults that underwent pure tension and using a basic stress tensor solution program based on the geometry of Etchecopar et al. (1981). This approach tended to yield imprecise results reflecting the inherent scatter in the stockwork vein geometries. For simplicity, the stress axes are here depicted in the horizontal and vertical planes, but absolute inaccuracy of <15° applies in most cases. Grey planes and heavy lines represent plan view fault orientations. Coloured planes and fine lines depict vein orientations in plan. Broadly, mineralisation appears to have spanned two cycles of dextral wrench deformation related to the Quebrada Blanca fault, each succeeded by a period of extension during which the bulk of the veins were formed. The first wrench event changed from transtensional during magma emplacement to transpressional during early Vqmsb veining.

expected response to development of a hydrothermal system under lithostatic load. Fluid inclusion data reported by Rowland (1998) support lithostatic conditions for these early veins.

The main cupriferous stage of veins (Vqcp) also occupies the regional NW-striking, moderate to steeply NE-dipping orientation, although shallowly-dipping veins are scarce. Subsets of the Vqcp population take steeply ESE- and SSE dipping orientations, parallel to the major pre-mineral fault geometry (Fig. 4.30). This vein generation therefore occupies all of the major pre-existing fracture sets in the QB deposit environment, except the subhorizontal planes. While a radial array is not evident from the mapping done in this study, it is likely that the array reflects fluid overpressure and widespread re-use or propogation of existing fractures. Dominance of hydraulic forces implies that differential horizontal stresses were likely to have been low, but the absence of shallow vein orientations suggests that the axis of maximum principal stress was subvertical (i.e. the environment was broadly tensional). The global array records an oblate strain wherein the axes of major and intermediate dilational strain are subhorizontal and oriented WSW and NNW, respectively, which might suggest that extension was weakly directed to the WSW (Fig. 4.33). Overall, the Vqcp vein array at Quebrada Blanca formed during tensional conditions that impliy a distinct relaxation of the tectonic stresses inferred for the earlier intrusion and vein events.

Molybdenum-bearing intermediate stage veins (Vqmo) take more varied orientations than the other vein generations. The most common strike is WNW (Fig. 4.30), within which there are abundant steep veins and a range of subordinate, moderately- and shallowly-dipping veins. These shallower orientations in many cases manifest as linking fractures between more steeply dipping veins (Fig. 4.33) and coincide approximately with the orientation of late normal faults (Figs. 4.20 and 4.30). Rowland and Wilkinson (1999) used detailed fluid inclusion data to argue that intermediate stage veins at QB record pronounced fluid overpressure (i.e. pressure > lithostatic load) in the system related to entrapment of a vapour-like fluid at close to its critical point. Dilation recorded by shallow veins and vein segments therefore appears to reflect hydrothermal inflation of the system. The diversity of orientations among Vqmo veins implies that horizontal differential stresses were

generally low during formation of this vein stage. However, the paucity of veins that strike NE-ENE implies that normal stress was greater on these orientations. The environment of formation of Vqmo veins was similar to that of the preceeding Vqcp stage, however, the presence of shallowly-inclined veins suggests that the maximum principal stress axis may not have been subvertical, and rather, might have been oriented NW-NNW (Fig. 4.33).

Tourmaline and calcite-hematite-(barite) veins north of the main Quebrada Blanca deposit have a different geometry to the main stockwork vein stages. Tourmaline is preferentially hosted by faults and fractures subparallel to the QB fault and related splays that would be dilational under a dextral wrench environment. Calcite and barite veins are hosted in subsidiary 3rd and higher order faults in the wallrocks and occupy a conjugate array of strike-slip fault-veins and breccias focussed at the intersections of conjugate NE and ESE-trending structures (Figs. 4.30). Tourmaline-rich veins and faults record NW-directed dilational strain, whereas calcite-hematite-(barite) record principal dilation toward the north (Fig. 4.33). In both cases, outcrop scale occurrences characteristically comprise a master structure with smaller veins developed in conjugate shear orientations. If the maximum principal stress axis during vein formation bisected the acute angle between the conjugate vein sets, then syn-vein stress regime would have been NE to ENE-directed compression. Alternatively, these fracture sets may have been well developed during the earlier NE-directed compressional history of the area, and the vein arrays are simply reflecting high fluid pressure and hydraulic re-opening of these fractures.

The timing of formation of these veins is ambiguous because they do not occur within the main stockwork. It is possible that the tourmaline-rich veins formed independent of the tourmaline-cemented breccias. In this case, the similar structural geometries might suggest regional tourmaline occurrences are contemporaneous with magmatism, brecciation and biotite alteration. However, this seems unlikely as there is no mineralogical continuity or transition between early biotite alteration and the principal occurrence of tourmaline veins to the north of QB (as there is within the Sur Sur Breccia at Rio Blanco; Frikken et al., 2006). A simpler geochemical scenario is one in which all tourmaline in the broader QB system relates to a single boron-rich hydrothermal pulse (as depicted in Figs. 4.30, 4.31 and 4.33). Throughout

the northern Chilean porphyry camps, tourmaline-cemented breccias are the single B-rich hydrothermal stage, and are regularly associated with minor barite and carbonate infill (Sillitoe and Sawkins, 1971). It is therefore most likely that all the tourmaline at QB formed at the same stage of evolution of the hydrothermal system. Considered together, tourmaline-bearing veins and breccias occupy an array of NNE, NE and ENE-trending steeply-dipping orientations similar to the array of pre-mineral faults interpreted to have affected magma emplacement (Figs. 4.20a, b). The intermineral tourmaline-bearing hydrothermal event was undoubtedly associated with exceptional fluid pressures related to development of the major Cerro Abundancia breccia. Therefore, hydraulic re-opening of existing fracture arrays is also expected to have occurred widely. However, the scarcity of NW-trending tourmaline, calcite and barite veins implies that the stronger horizontal stress was oriented approximately NE (Fig. 4.33). The intermineral tourmaline event therefore implies a re-establishment of the syn-intrusion stress regime.

Late stage pyritic Vpy1-2 veins are the most strongly polarised of any vein generation at QB, consistent with the general trend to cooler, more brittle and more tectonically mediated fracturing common to the later stages of many porphyry deposits (Tosdal and Richards, 2001). Fluid inclusions in late veins are interpreted to record the change from lithostatic to hydrostatic pressures (Rowland and Wilkinson, 1999). High fluid pressures are evidenced by formation of the Vuggy Breccia, which primarily hosts alteration and hydrothermal cement identical to the broader Vpy1-2 vein array (Fig. 4.27). In their present position Vpy1-2 primarily dip eastward and strike NNE to NNW. Restored to the pre-tilting orientation of the deposit, the principal orientations trend from N to NE and dip moderately to steeply to the east (Figs. 4.28 and 4.30). A subset of these veins occupies moderately NE-dipping faults that commonly have kinematic indicators that suggest a range of oblique-slip normal displacements, although recogniseable faulting was largely post-mineral (Fig. 4.20). Where Vpy1 veins occupy these faults, they also commonly occupy subvertical fractures in the hangingwall of the faults. This relationship is interpreted as evidence that the moderately-dipping faults were re-used by hydrothermal fluids during this stage. In contrast, the commonly high frequency steeply-dipping N to NE-trending veins do not correspond to a recognised pre-existing fracture pattern, and are

interpreted as the product of new fracturing that records principal dilational strain oriented W to WNW. The Vpy1-2 array is therefore likely to have formed under broadly arc-normal tensional conditions that may have been influenced by orogenic collapse following uplift of the cordillera along the Domeyko Fault.

Hydrothermal rejuvenation of the system is recorded by the molybdenite-cemented breccia that formed approximately 2 million years after the main QB stockwork (Fig.4.32). A SW-directed extensional environment is inferred for this event because of the NW-trending sheet-like geometry of the breccias, which cross-cut all other fabrics in the deposit. This is consistent with a sinistral wrench environment (Fig. 4.33) that is inferred to have affected the Monctezuma and Lulu faults at approximately the same time (Fig. 4.65; section 4.9).

Vein and fault arrays mapped at Quebrada Blanca are interpreted to document cyclical changes in the tectonic stress regime from dextral transpression driven by regional ENE-directed stress, through weakly extensional stress states (Fig. 4.33). If intermineral breccias and tourmaline-barite-calcite veins record a transient return to the dextral transpressional environment, then two such cycles occurred through the life of the hydrothermal system. Magmatism related to early-stage mineralisation commenced about 37 Ma, and was complete by some time before 36.2 Ma; the younger limit of the weighted average of interpreted main stage potassic alteration (Fig. 4.32). The last stage of hydrothermal mineralisation, during which molybdenite-cemented breccias formed, occurred at ~35 Ma under broadly SW-directed extension or sinistral transtension.

4.7 Structural Geology of the Copaquire Mo-Cu deposit

The Copaquire porphyry Mo-(Cu) deposit was the first major large tonnage, low grade mineral deposit recognised in the Collahuasi District. It is located immediately W of the Domeyko Fault Zone and is dissected by two steep valleys (*quebradas*) draining westward off the Domeyko Cordillera (Figs. 4.4, 4.13). The weak vein stockwork and surrounding bleached, oxidised alteration crop out over approximately 7 km^2 along the Quebrada Sulfato (Villemur, 1963: Figs. 4.34, 4.35). Leachable supergene copper mineralisation was extracted from several adits near valley level during the l890s and early 1900s, but the secondary copper

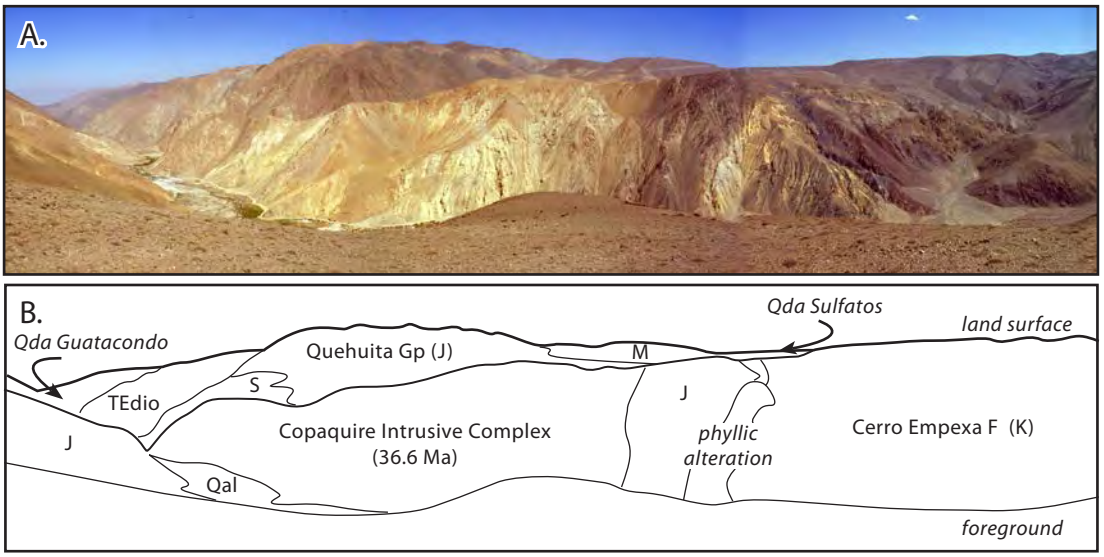

Figure 4.34. Surface expression of the Copaquire porphyry Mo-Cu deposit. A) Panoramic view to the northwest taken from the south side of Quebrada Copaquire, and B) corresponding interpretive sketch. Supergene kaolinite-rich alteration is exposed by valley incision into the central part of the porphyry.

development at Copaquire is patchy and rarely exceeds 0.4% Cu (Villemur, 1963). The hypogene mineralisation is copper-poor by comparison with the other deposits of the Collahuasi district. The economic potential as a molybdenum deposit has been investigated on numerous occasions, including renewed interest and exploration since 2005 that has significantly increased the global resource (Table 1.1: Camus and Fam Romero, 1971; Munchmeyer, 1972, www.tbxinternational.com). However, the principal record of the geology stems from two field based studies in the early 1970s (Table 4.2: Sillitoe and Neumann, 1972; Hollister and Bernstein, 1975). There is considerable disagreement between the alteration maps presented in these studies. The aim of the current study was to compile and amend a coherent intrusive and hydrothermal paragenesis, and a district-scale alteration map, and to collect structural data from veins and faults within the deposit.

4.7.1 Intrusive and Hydrothermal History

Copaquire intrusive complex (CIC). The CIC belongs to a cluster of two dozen small (0.1 - 10 km^2) medium to fine grained stocks that intruded the Mesozoic stratigraphy west of the Domeyko Fault. These intrusions were not emplaced in their present position relative to the main Collahuasi block. Instead, they formed some ~37 kilometres further north, and were juxtaposed with the Collahuasi block after sinistral

strike-slip offset along the Domeyko Fault zone (e.g., Tomlinson and Blanco, 1997b; Campbell et al., 2006; *cf*. Amilibia and Skármeta, 2003). The mineralised intrusive complex is comprised of at least three discrete, cross-cutting porphyritic intrusive phases and a related breccia body (Sillitoe and Neumann, 1972). These intrusions are a pre-mineral, variably quartz-bearing diorite, an approximately syn-mineral quartz monzonite, and a late- to post-mineralisationisation tonalite (Hollister and Bernstein, 1975, who refer to the tonalite as "dacite" because of its very fine grained groundmass). Together, these comprise a polyphase stock that is elongate NNE and has dimensions of ~3 x 1 km (Figs. 4.13, 4.35a). Polyphase stocks, and porphyritic lithogies are uncommon in the cluster of small intrusions. The vast majority are composed of single-phase, equigranular rocks. The Copaquire intrusive complex is therefore distinctive among the Tertiary intrusive rocks of the western Collahuasi district, and it is the only such stock that is known to host porphyry mineralisation. A petrographically similar polyphase stock is known from the area north of the Picos de Majala mountain (Fig. 4.35a) and irregular zones of argillic alteration were mapped in this area by Villemur (1963).

Hydrothermal Alteration and Mineralisation. Alteration related to the Copaquire deposit is clearly visible in the walls of the valleys that incise into it, where it manifests as a broad zone of intensely bleached rock (Fig. 4.34, 4.35b) with variable goethite-jarosite-hematite staining (in that order of abundance). The hydrothermal paragenesis comprises four principal stages (Fig. 4.36) interpreted by Hollister and Bernstein (1975) to relate spatially and temporally to intrusion of the quartz monzonite stock. The earliest stage comprises short, fine, irregular grey veinlets of intergrown quartz and orthoclase (Fig. 4.36). In contrast to many porphyry deposits (e.g., Seedorff et al., 2005), these are scarce and are spatially restricted to the zone

Figure 4.35 Geology and field relations at Copaquire. A) Selective geological map showing the distribution of intrusive and breccia bodies, and major alteration zones around the Copaquire intrusive complex (CIC). CIC intrusion and breccia outlines, and inner alteration zones reproduced from Sillitoe and Neumann (1972). Pitoguallaca Stock and background lithology mapping from Tomlinson et al. (2001). Outer alteration zones and bedding data for the Quehuita Formation (inset) were mapped in this study. Alteration lines depict the interpreted outer limits of occurrence of each mineral, based on several traverses in the area. B) View to the south at the northeastern edge of the Copaqurie alteration system showing bleached illite-kaolinite altered rocks (right, centre) and tilting of the erosional upper surface of the porphyry and stratified Papajoy Formation gravels that overlie it (arrow). Vicinity of 512,200 mE; 7,688,600 mN.

A.

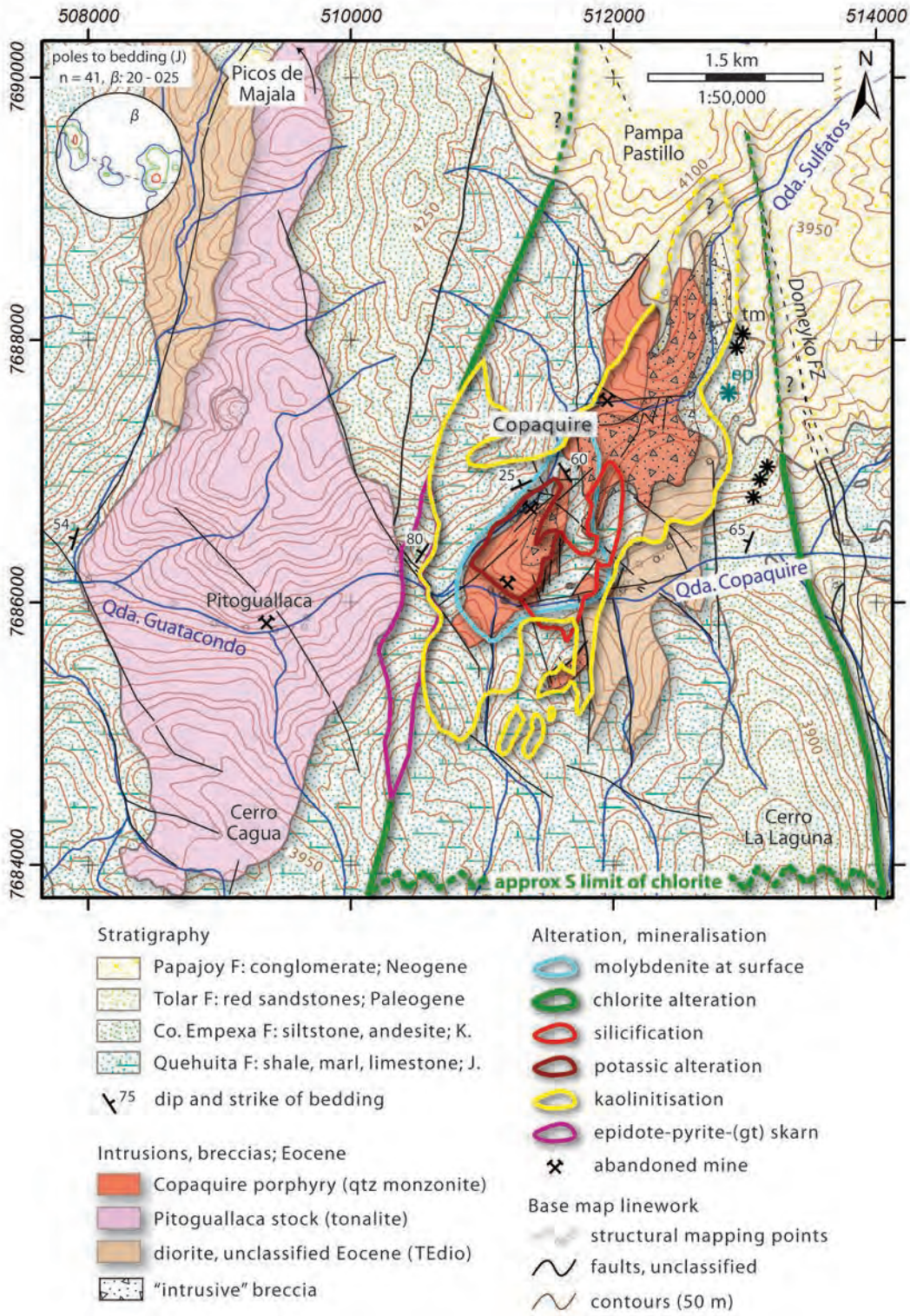
508000
510000
512000
514000
7690000
7688000
7686000
7684000
poles to bedding (J)
n = 41, β: 20 - 025
β
Picos de Majala
1.5 km
1:50,000
N
Pampa Pastillo
Qda. Sulfatos
Domeyko FZ
tm
ep
Copaquire
Qda. Copaquire
Pitoguallaca
Qda. Guatacondo
Cerro Cagua
Cerro La Laguna
4250
4100
3950
3900
approx S limit of chlorite
Stratigraphy
Papajoy F: conglomerate; Neogene
Tolar F: red sandstones; Paleogene
Co. Empexa F: siltstone, andesite; K.
Quehuita F: shale, marl, limestone; J.
75 dip and strike of bedding
Intrusions, breccias; Eocene
Copaquire porphyry (qtz monzonite)
Pitoguallaca stock (tonalite)
diorite, unclassified Eocene (TEdio)
"intrusive" breccia
Alteration, mineralisation
molybdenite at surface
chlorite alteration
silicification
potassic alteration
kaolinitisation
epidote-pyrite-(gt) skarn
abandoned mine
Base map linework
structural mapping points
faults, unclassified
contours (50 m)

B.

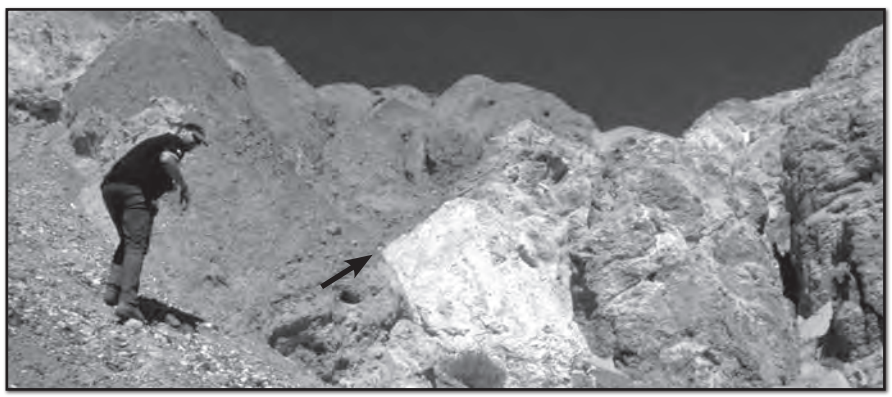

of potassic alteration centred on the southern lobe of the quartz monzonite (Figs. 4.35a). The irregular morphology of these veins suggests formation prior to complete solidification of the host intrusion (e.g., Gustafson and Hunt, 1975).

The principal metalliferous vein stage at Copaquire is a series of grey to white quartz veins that commonly contain molybdenite and pyrite ± chalcopyrite. These veins comprise fine to medium grained, locally semi-granular quartz that may show vein wall-parallel grain size or sulfide banding (Fig. 4.37). They are variably accompanied by haloes of texture-preserving white mica alteration. Outboard of the main vein zone, irregular selectively pervasive chloritisation affects the volcanic rocks, chlorite-calcite veins adjacent to major structures, and minor epidote-garnet-(pyrite) skarn occurs in calcareous lithologies (Fig. 4.36). This alteration is inferred to be the distal manifestation of the early hydrothermal pulse that formed the main-stage veins (e.g., Titley et al., 1986; Cathles and Shannon, 2007). However, chlorite-dominated alteration occurs in an elongate zone parallel to the Domeyko Fault (Fig. 4.35a) and it is unclear how much of it relates fault-controlled hydrothermal activity independent of the Copaquire porphyry.

The late hydrothermal stages are dominated by planar quartz-pyrite-chalcopyrite veins associated with widespread pervasive muscovite and/or illite alteration. The younger variations of this stage have more pyrite than quartz and are associated

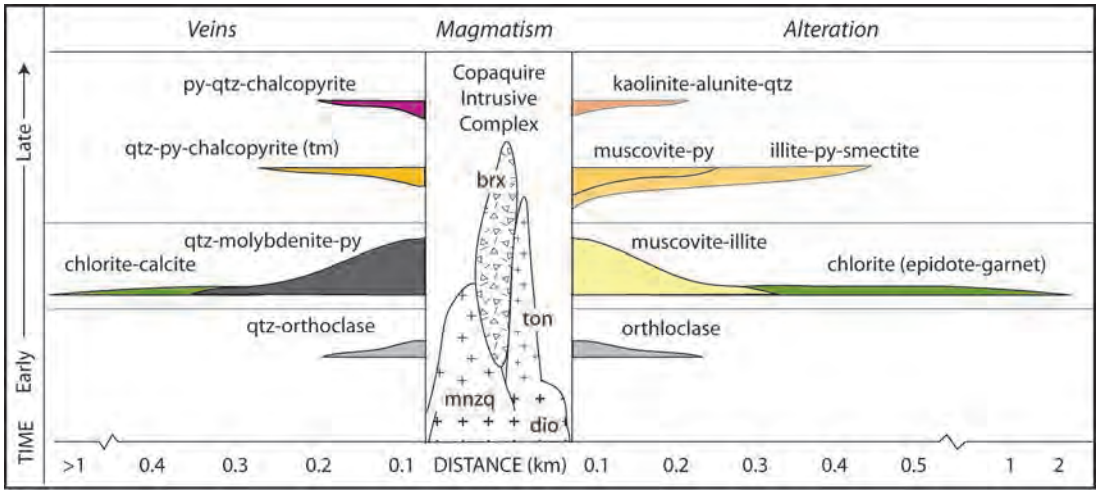

Figure 4.36. Schematic diagram of spatial and temporal relationships between intrusions, breccia, and vein and alteration assemblages at Copaquire. Compiled from Sillitoe and Lehmann (1972), Hollister and Bernstein (1975) and new data, primarily for the earlier stages. Synchroneity of intermediate proximal and distal veins and alteration is inferred. Abbreviations: dio = diorite; mnzq = quartz monzonite; ton = tonalite; brx = breccia; qtz = quartz; py = pyrite; tm = tourmaline.

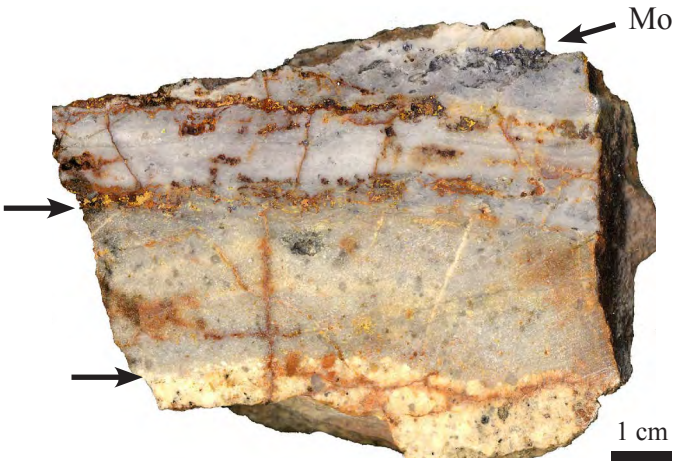

Figure 4.37. Hand specimen of a typical weakly banded quartz-molybdenite-pyrite vein with a strong alteration halo in the host quartz monzonite (lower left arrow indicates margin of halo). Oxidation of these veins commonly produces minor ferrimolybdite (upper left arrow) associated with jarosite. Vicinity of 511,635 mE; 7,686,140 mN.

with more acidic alteration assemblages in the vein halos (Fig. 4.36; Hollister and Bernstein, 1975). These veins are the primary host of Cu in the deposit, and irregular but decreasing Cu grade with depth (www.pbxinternational.com) might indicate that they are most strongly developed in the upper parts of the deposit. A hydrothermal breccia body that extends along the eastern side of the Copaquire intrusive complex (Sillitoe and Neumann, 1972) is locally cemented by the same mineral assemblage, plus minor tourmaline (Hollister and Bernstein, 1975). This breccia is therefore considered to have formed late in the magmatic-hydrothermal evolution of the system. It formed at approximately the same time as emplacement of the sparsely and irregularly altered late tonalite ("dacite": Hollister and Bernstein, 1975) and appears to mark the end of hydrothermal mineralisation at Copaquire.

Overall, pyrite is the dominant sulfide mineral at Copaquire and the exposed porphyry has undergone extensive supergene kaolinite alteration that manifests as broad zones of crumbling, bleached rock. Supergene kaolinitsation overprints and extends beyond the proximal hypogene alteration facies, locally associated with gypsum and minor azurite and malachite. The distribution of kaolinite-altered rocks shown in Fig. 4.35 depicts this supergene overprint rather than the more restricted hypogene phyllosilicate-rich alteration facies. Discrimination of the hypogene alteration styles in the field is difficult, as there are major inconsistencies between the distribution of these minerals as presented by Camus and Fam (1971), Sillitoe and Neumann (1972), and Hollister and Bernstein (1975). Nonetheless, the zone of occurrence of molybdenite at surface (Fig. 4.35) identifies the area of strongest

hypogene mineralisation. Recent exploration drilling has shown that hypogene Mo mineralisation occurs in the subsurface over at least the spatial extent of the exposed Copaquire intrusive complex, and extends a few hundred metres beneath cover to the south (www.pbxinternational.com). However, the high Mo:Cu ratio, and dominance of shallowly inclined veins may be interpreted as evidence of exposure of the deeper parts of the hydrothermal system (e.g., Haynes and Titley, 1980), and the depth extent of hypogene mineralisation may be restricted.

4.7.2 Structural History

Original orientation of the Copaquire block. The northernmost exposures of the alteration related to the Copaquire deposit are overlain by poorly consolidated, planar bedded gravels attributed to the Late Eocene to Oligocene Papajoy Formation (Tomlinson et al., 2001). The unconformity between the intrusive complex and the gravels dips moderately to the NNE (Fig. 4.35b: orientation 39º-030). The intrusive complex intruded an upright open antiform within the Jurassic host sequence, and the axis of this fold also plunges to the NNE (Fig. 4.35a; orientation 20º-025). It appears therefore that the intrusive complex and the immediate package of host rocks has been tilted 20-39º to the NNE during the Neogene. All the pre-Neogene structural data presented in this section has therefore been restored to an approximate original geometry by removal of 30º of inclination toward bearing 028. Tilting affected at least the block between the Domeyko Fault and a N-NNE trending fault separating the Copaquire and Pitoguallaca intrusions (Fig. 4.35a).

Pre- and syn-mineral faults. Faults and fractures that host mineralisation or related alteration, or show any form of ductile deformation, have been interpreted to precede tilting of the block hosting the Copaquire deposit. Steep, NE-trending faults that show either normal or dextral kinematic indicators are the most discrete population of these faults (Fig. 4.38 a). Another group of pre-tilting faults take a range of shallowly dipping orientations, most commonly to the WSW. In the main zone of mineralisation, all pre- and syn-mineral faults and fractures are overprinted by supergene oxidation and weathering and it is unclear which faults make have directly influenced mineralisation. However, the skarn on the western margin of the deposit (Fig. 4.35) is intimately associated with a shallowly ENE-dipping fault and

an array of subparallel joints. A weakly altered, possibly pre-mineral dyke in the same area also has this orientation.

Post-mineral faults. The supergene profile is subhorizontal and appears to have not been tilted significantly. Faults that offset the either the supergene profile or the hypogene hydrothermal alteration patterns are therefore interpreted to have been active after tilting of the Copaquire block. The most obvious structural element at Copaquire belongs to this group and comprises subvertical short-displacement faults and zones of >10 fractures per metre without mappable displacement. The most abundant of these fracture sets trend NNE to NNW, although orientations vary widely. Of these, a series of WNW-trending faults that underwent normal dip slip displacement (Fig. 4.38 b) occur in the central part of the intrusive complex and might partly account for the segmentation of the mapped distribution of the intrusions (Fig. 4.35). A discrete group of subvertical NE-trending post-tilting faults

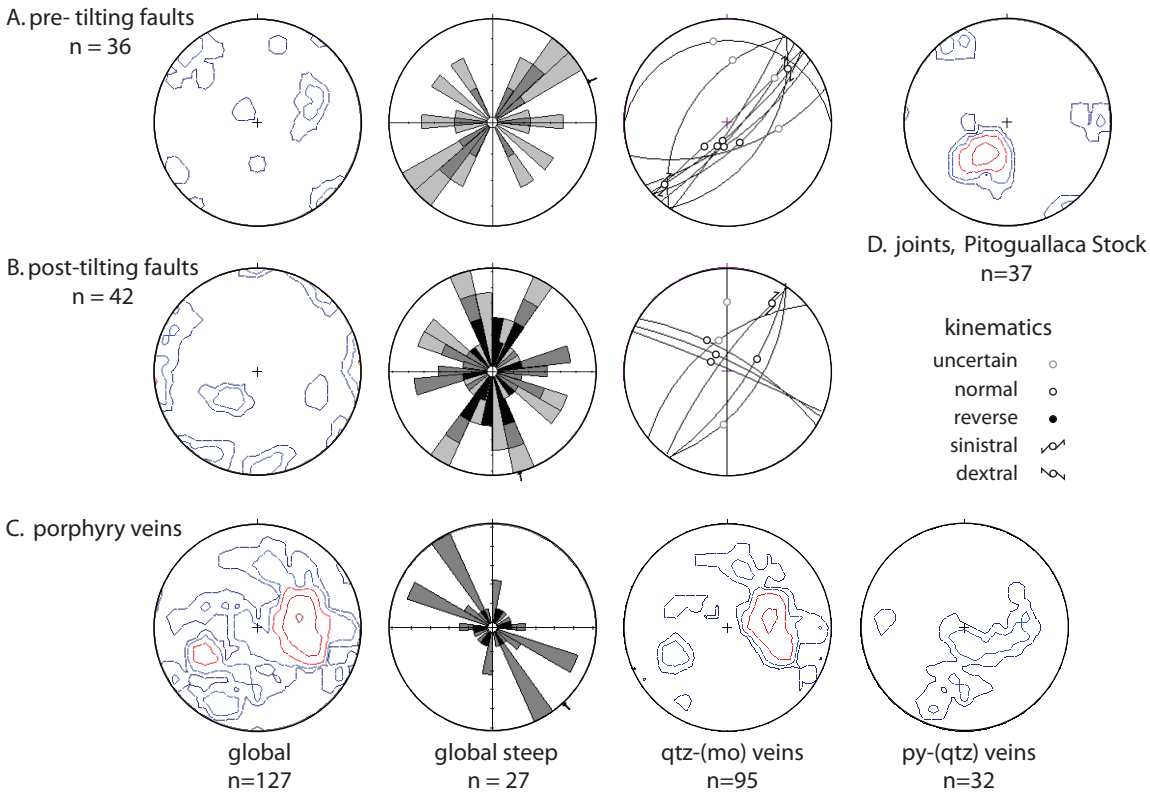

Figure 4.38. Equal area stereonets and rose diagrams for structural data from the Copaquire porphryy and environs. Darker tones on rose diagrams reflect larger magnitude structures. All porphyry veins and faults deemed to precede or be associated with mineralisation have been restored to their original orientation by removing ~30º tilting to the NNE. The principal vein stages have shallow inclinations, similar to systematic unmineralised joints in the slightly older Pitoguallaca Stock.

is well developed along the northwestern margin of the intrusive complex, parallel to Quebrada Sulfato. These are geometrically indistinguishable from a similar set of faults that host hypogene alteration. The mapped kinematic indicators could therefore have been imparted in response to similar displacement during and after mineralisation. An alternative explanation is that all the mapped displacement on faults of this orientation is a post-mineralisationisation feature that has commonly re-used fractures that had been present during mineralisation. The timing relationship between normal and dextral motion could not however be established because the two sets of straie were not encountered on the same slip plane.

Veins and related structures. The veins that comprise the main porphyry stockwork mapped in this study at Copaquire are overwhelmingly shallowly inclined. Removal of the interpreted tilting yields a conjugate array of gently ENE and W-dipping veins, among which the latter is orientation is dominant (Fig. 4.38 c). There are subtle differences between the main quartz-molybdenite stage and the younger pyritic veins, but the overall tendency to shallowly inclined orientations is unchanged between the two vein generations. This is in contrast to the upright N- to NE-trending veins described by Hollister and Bernstein (1975). The structures mapped by those authors could not be located in the present study, and instead, shallowly dipping veins were encountered in transects through the deposit on three sides of the main surface Mo-anomalous area (there is limited exposure on the eastern side). To the west of Copaquire, the 37.8 Ma Pitoguallaca Stock also contains systematic shallowly inclined fractures that are developed throughout the exposure in Quebrada Guatacondo (Fig. 4.35; geochronology of Tomlinson et al., 2001a). In this case the dominant orientation dips toward the NE and the fractures manifest as locally penetrative joint sets without hydrothermal alteration (Fig. 4.38 d). Systematic fracturing parallel to the subvertical intrusion walls or a simple inferred flat or domed intrusion ceiling is not evident in either the Pitoguallaca Stock or the Copaquire intrusive complex.

The three-dimensional geometry of the late-mineral breccia body is unconstrained by the present mapping nor by earlier studies. However, in constrast to the veins, it is expected to dip steeply like other intrusion-related breccias in northern Chile (Sillitoe and Sawkins, 1977).

4.7.3 Age of the Copaquire Porphyry System

Five radiometric ages for the Copaquire intrusive complex were compiled by Tomlinson et al. (2001a), and no further geochronology has been published subsequently (Fig. 4.39). Three samples are described as belonging to the Copaquire intrusive (Boric et al., 1990; Maksaev, 1990), and two samples (Hammerschmidt et al., 1992) are re-interpreted by Tomlinson et al. (2001a) to belong to the basal gravel overlying Copaquire. Together they yield an aggregate average age of 36.1 ± 0.7 Ma. The resedimented samples are included here as they occur toward the head of the valley and could not have been transported from any of the other known Eocene intrusions in the catchment. By virtue of the resedimented sampling location and the absence of alteration among the samples of Hammerschmidt et al. (1992), the younger ages probably date post-mineralisationisation intrusive phases such as the late tonalite and the average should be taken as a minimum age. Other intrusions dated from this area west of the Domeyko Fault consistently yield ages in the range 45 - 38 Ma (Tomlinson et al., 2001a), and the imprecise age of Boric et al. (1990) is permissive of commencement of magmatism at Copaquire toward the end of this period.

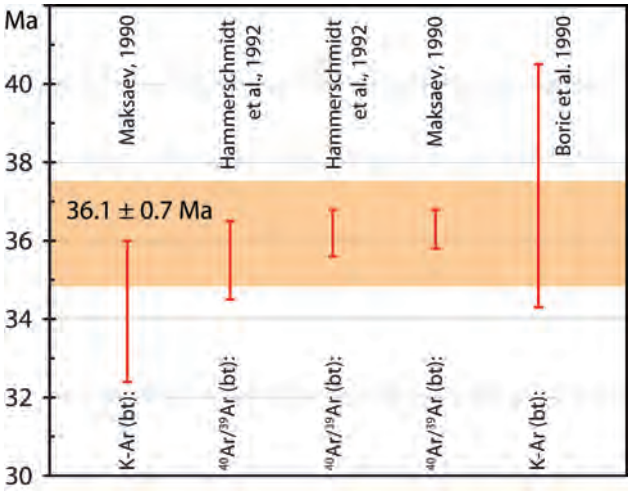

Figure 4.39. Weighted average plot of open file radiometric ages for intrusive rocks from the Copaquire deposit area (data from Tomlinson et al., 2001). The samples are not described in terms of the intrusive history at Copaquire, and the weighted average is therefore an aggregate age for the intrusive complex. Samples analysed by Hammerschmidt et al. (1992) are euhedral magmatic biotite sampled in the basal gravel overlying Copaquire. The calculated aggregate age is reported at 95% confidence, with MSWD = 1.8 and probability = 0.12.

4.7.4 Structural Evolution of Copaquire: Interpretation

The structural evolution of the Copaquire porphyry system was dominated by transtensional and transpressional dextral wrench environments. Dextral wrench displacement occurred along the Domeyko Fault zone in the Chuquicamata and

El Salvador districts during the Early and Middle Eocene (Tomlinson et al., 1994; Reutter et al., 1996; Tomlinson et al., 1997a). At Copaquire, the triangular NE-elongate shape of the intrusive complex is unusual among the Eocene intrusions in the Collahuasi district (Fig. 3.25); just one other intrusion shares this geometry and occurs in a similar location relative to the Domeyko Fault. The prevailing NE-trending hypogene-altered fault set therefore appears to have influenced intrusion in this location. Although the northern extensions of these faults are covered by Neogene sedimentary rocks of the Pampa Pastillo (Fig. 4.35), the NE-trending structures are anticipated to have been active as splays from the Domeyko Fault (Fig. 4.40). Under the influence of the ENE-directed regional tectonic convergence (Fig. 4.9) these faults would have acted as synthetic shears during dextral strike-slip displacement on the Domeyko Fault. The dextral kinematic indicators observed on some of these faults may therefore have developed around this time. Implicitly,

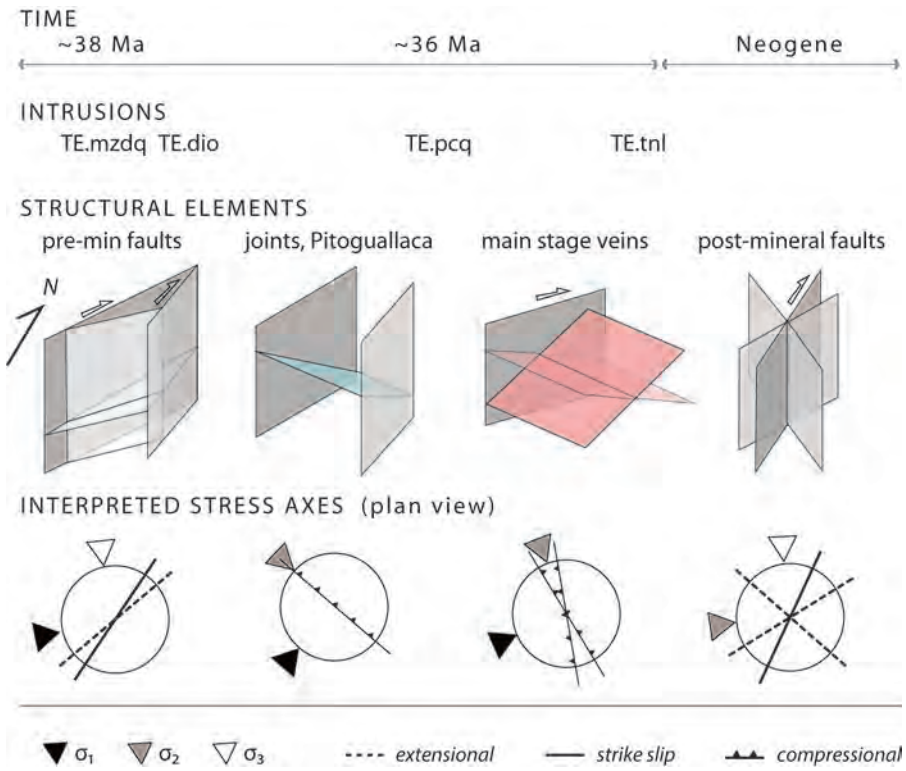

Figure 4.40. Schematic representation of the restored, pre-tilting principal vein and fault orientations at Copaquire, and the interpreted orientations of local stress axes for the prevailing regime during formation of each generation. Broadly, emplacement of the Copaquire intrusive complex appears to have occurred during dextral transtension on a splay of the Domeyko Fault. Shallow fractures that host veins at Copaquire, and unmineralised fractures at Pitoguallaca appear to have formed during ENE-directed compression. Post-mineral faulting likely records several stages of fracture development, the most significant of which appears to dextral transtension. Plane colours and precedent for interpretation of stress axes as per Figure 4.33.

ascent of magma into a shallow steep-walled conduit within this kinematic regime required that the local stress environment was trantensional at approximately 37 Ma.

The shallowly inclined veins at Copaquire and sheeted joints at Pitoguallaca (Fig. 4.35a) record a prolate strain with the elongation direction subvertical. These fractures are not geometrically related to the intrusion geometries and therefore appear to have formed in response to the tectonic stress environment. The unusual shallow vein and joint geometry suggests that the maximum principal stress axis was subhorizontal and directed NE to ENE shortly after intrusion (i.e. assuming σ_1 bisected the two shallowly-dipping sets; Fig. 4.40). The relationship between the steep NE-trending faults (and intrusions), and the shallow veins and joints is unclear as veins are rare in the immediate walls of the faults (as occurs commonly in strike slip systems; Cembrano et al., 2003, 2005). However, this geometric relationship is the expected response if the intermediate and minimum principal stresses were on the same order of magnitude, and fluctuating hydrothermal fluid pressures caused them to "flip" during main-stage hydrothermal activity.

Based on the gross intrusion form and vein geometry, the N- and NE-oriented subvertical faults of the Domeyko system and related splays are interpreted to have been under dextral transpression during mineralization. This kinematic regime and the associated generation of shallowly inclined fractures within the Eocene intrusions may have prevailed contempraneously at Copaquire and Quebrada Blanca. Intrusion during compression at both deposits may have been facilitated by differential stress reduction in the vicinity of fault intersections along the Domeyko Fault System. As at Quebrada Blanca, a relaxation of compression may have also occurred following early hydrothermal stages at Copaquire, to permit the implied subvertical emplacement of the late-mineral breccia body. Alternatively, the fluid pressure and explosivity associated with this style of hydrothermal(?) brecciation may have overcome the regional stress regime.

Some time after tilting of these western mineralised blocks, a series of subvertical brittle fractures and faults developed at Copaquire. The faults that trend N - NE most likely reflect re-establishment of the dextral wrench environment. However, a series of steeply dipping NNW and WNW trending faults also occurs, the latter with normal displacement (Fig. 4.38). These two fault sets commonly occur together (Fig. 4.35)

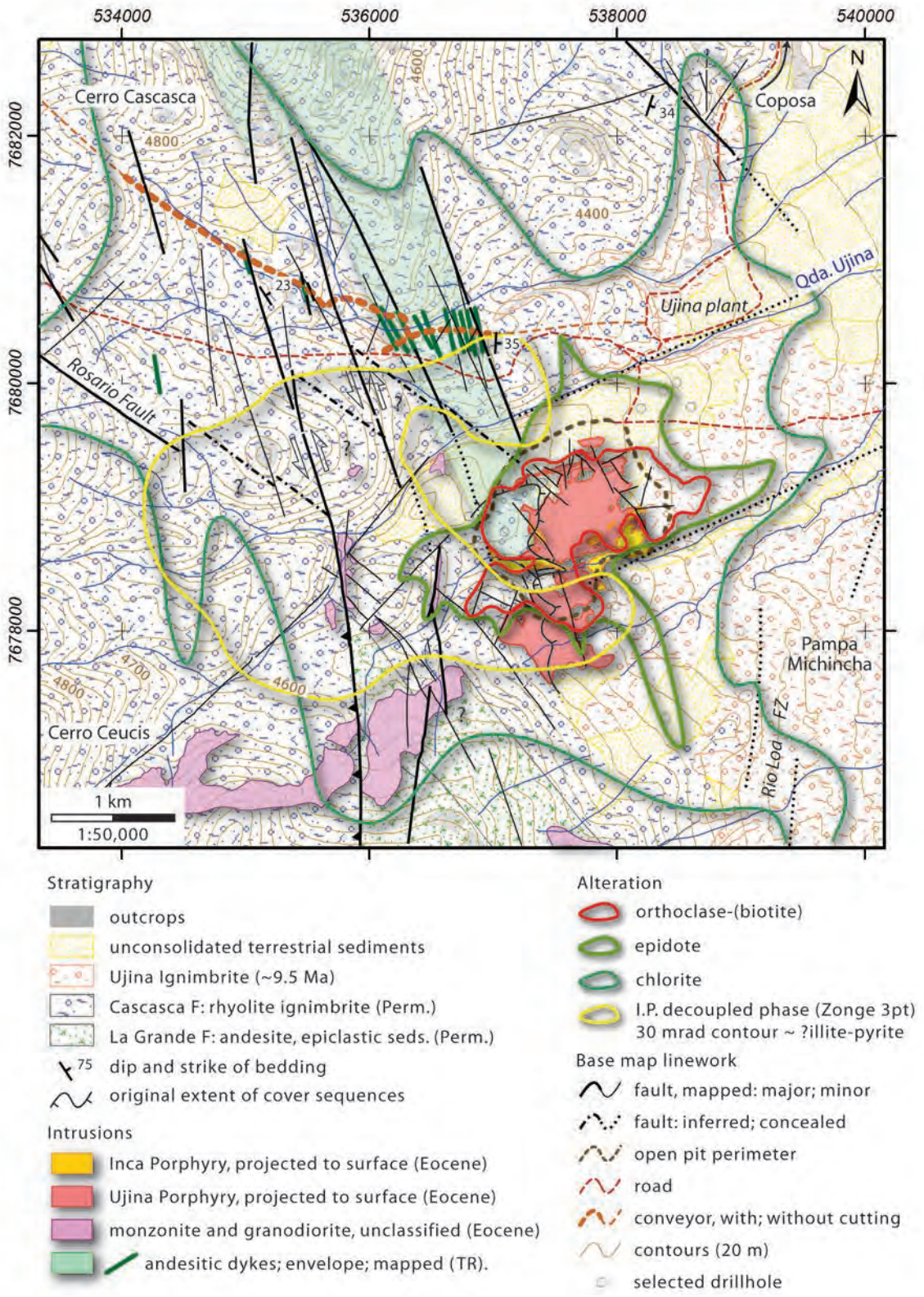

Figure 4.41. Selective geological map showing the distribution of intrusions and major alteration zones around the mineralised polyphase Ujina intrusive complex. Ujina centre intrusion outlines are projected to surface and reproduced from CMDIC in-house data (constrained by resource definition drilling). Unmineralised stocks and faults in the southern map area reproduced from Fedorowich (2001). Alteration zones, faults, dykes and bedding mapped in this study. Detail of faults within the intrusive complex has been removed for clarity. Inner alteration zones incorporate subsurface occurrences logged in resource definition drilling (CMDIC data). Alteration lines are depict the interpreted outer limits of occurrence of each mineral, irrespective of depth below surface within the 0 to ~400 m depth interval of widespread drilling. Structurally controlled alteration zones have been artifically broadened in the diagram to permit presentation at this scale.

and possibly formed during Oligocene sinistral wrench along the Domeyko Fault zone (e.g., Tomlinson and Blanco, 1997b).

4.8 Structural Geology of the Ujina Porphyry Cu-Mo deposit

The Ujina porphyry Cu-Mo deposit was the first mineral deposit to be exploited in the Collahuasi district since renewal of exploration in the 1970s. Both Ujina and Rosario are held by the Compañia Minera Doña Inés de Collahuasi (CMDIC). Although Rosario was discovered earlier and has a much larger total resource (Chapter 1), the geometrically simple, high grade supergene Cu enrichment blanket at Ujina (originally 168 million tonnes @ 1.6% Cu: DeBeer and Dick, 1994) was instrumental in the economics of the joint operations (Moore and Masterman, 2002). The papers of DeBeer and Dick (1994); Bisso et al. (1998) and Masterman et al. (2004), as well as the PhD thesis of Masterman (2003) each deal in part with the Ujina deposit. The geology of Ujina has not been the principal subject of a major study to date, and previous work contains little information regarding hydrothermal alteration and structural geology. In this study, an alteration map was drawn from surface mapping and compilation of CMDIC drill log data, and the orientations of faults and veins were mapped in detail in nine locations around the perimeter of the mine. Detailed 1:~400 scale structural mapping along the Ujina-Rosario conveyor cutting (Figs. 4.2 and 4.41) serves to provide further constrain on the fault history of the immediate deposit environment.

Overview of mineralisation and alteration. Mineralisation at Ujina comprises a classical porphyry Cu vein stockwork that developed during and after intrusion of the Ujina porphyry quartz monzonite stock and before intrusion of several dyke-like bodies of the Inca porphyry monzodiorite (Bisso et al., 1998; Masterman et al., 2004). The stockwork is made up of three principal macroscopic vein stages; early granophyric grey quartz-Cu sulfide; intermediate banded quartz-molybdenite-(pyrite); and late pyrite-quartz-(chalcopyrite-bornite-enargite). The early veins are associated with pervasive orthoclase-(biotite) alteration, which is the central alteration facies in the deposit, proximal to the Ujina intrusive complex (Fig. 4.41). An inner peripheral zone of epidote-bearing alteration and an outer zone of chlorite-bearing alteration (Fig. 4.41) are irregularly developed outboard of the potassic

zone. These are inferred to have formed at the same time as potassic alteration. A transitional zone of actinolite-bearing alteration such as occurs around the potassic zone at Tintic (Norman et al., 1991) and Batu Hijau (Garwin, 2000) has not been identified at Ujina. Intermediate stage veins are not associated with a distinct alteration facies, and late stage pyritic veins have strong bleached alteration haloes dominated by white phyllosilicate minerals. Alteration associated with these late veins is uncommon outside the immediate stockwork, but a broad zone of strong induced polarisation response at shallow levels (300 m pole-dipole, N=1) to the west of the deposit apparently coincides with the gross distribution of structurally controlled kaolinite-illite-pyrite alteration (Fig. 4.41). At deeper levels this geophysical anomaly migrates eastward and narrows over the main stockwork body suggesting that phyllosilicate alteration flares upward and outward away from the stockwork.

4.8.1 Intrusive and Structural History

Ujina Intrusive Complex. The Ujina intrusive complex is the largest stock among a cluster of small (<1 km^2) intrusions of Late Eocene age in the southeastern Collahuasi district (Fig. 4.9). The other intrusions in the cluster are unaltered except for within major fault and fracture zones (Fedorowich, 2001). The main Ujina porphyry stock has steep walls and an irregular dumbbell shaped outline in plan (Figs. 4.9, 4.41: CMDIC data). Numerous dyke-like apophyses of Ujina porphyry intruded outward and upward from the walls of the main body on all sides, as depicted in the simplified section of Bisso et al. (1998). Porphyry mineralisation

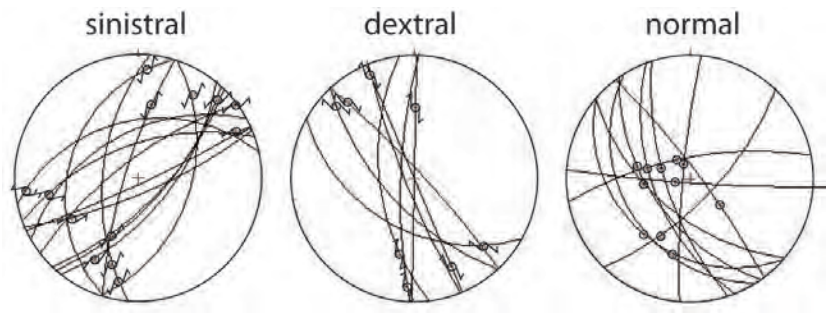

Figure 4.42. Global populations of faults mapped in the Ujina open pit, shown as great circles with slip vectors. Grouping is purely by kinematic history as cross cutting relationships are commonly contradictory (next Figure) and all groups have similar internal texture and mineralogy.

and related hypogene potassic alteration is centred on the northern lobe of the Ujina porphyry (Fig. 4.41), and it is possible that the southern lobe is a separate pre-mineral intrusive phase of similar modal mineralogy. Main stage mineralisation and all quartz monzonites attributed to the Ujina porphyry are cut by a series of strongly porphyritic monzodiorite dykes collectively termed the Inca porphyry. The two main bodies of this rock comprise E- and ENE trending dykes that follow the southern margin of the main mineralised lobe of the Ujina porphyry (Fig. 4.41). Smaller dykes of Inca porphyry trend WNW to NNW and dip moderately to the SW. Minor magmatic breccias are developed along the margins of the major bodies of Inca porphyry. These breccias locally contain high grade hypogene bornite mineralisation that must have post-dated emplacement of the dykes (Bisso et al., 1998).

Masterman et al. (2004) constrained the timing of intrusion and mineralisation at Ujina with $^{40}Ar/^{39}Ar$ analyses on euhedral magmatic biotite. Their results suggest cooling of the mineralised Ujina porphyry at 35.2 ± 0.3 Ma and of the main Inca porphyry body at 34.7 ± 0.3 Ma, and hence bracket main stage hydrothermal mineralisation between these two ages. A zircon U-Pb age of 34.4 ± 0.7 Ma for the Inca porphyry generated during this study (Chapter 3) confirms that the ages reported by Masterman et al. (2004) record the ages of igneous cooling in the Ujina intrusive complex.

Structural Architecture of the Ujina porphyry deposit. The Ujina Cu-Mo deposit is undisrupted by major through-going faults, and both the supergene and hypogene orebodies are geometrically simple (DeBeer and Dick, 1994; Bisso et al., 1998; CMDIC data). Routine bench mapping in the open pit mine and a small amount of detailed pit mapping conducted in this study reveal an array of steeply dipping faults that trend NW, NE and N. Faults on all orientations and with disparate displacement histories contain blocky to fine grained poorly consolidated gouge zones with weak to strong kaolinite alteration ± supergene chalcocite mineralisation. The overall fault density is low throughout most of the deposit and unambiguous examples of cross cutting relationships were not found during this study. Few of these faults appear to have had displacement of greater than a few metres since development of the supergene profile.

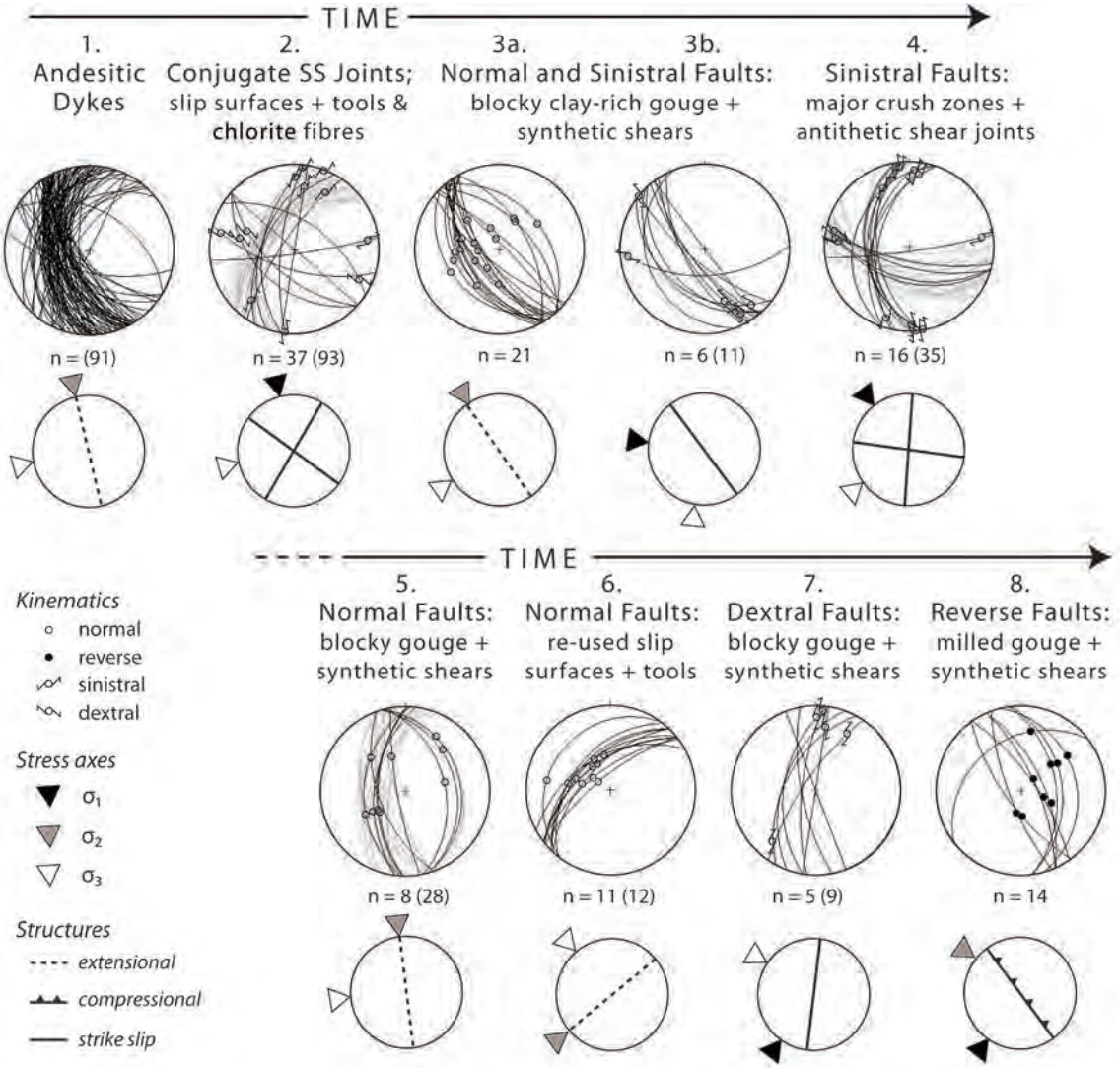

Crosscut Frequency

STAGE	1	2	3a	3b	4	5	6	7	8
1									
2	RRXXX XXXX					*X = cross cuts (faults) or abuts (joints)*			
3a	RRRRRR XXXXX	XXXXX							
3b	RRX	RXX				*R = re-uses*			
4	RXXXX XXXX	XXXXX XXXXX	X	RXX					
5	RRRXX XXX			R	RRXXX				
6	X	RRR			X				
7	RRRXX	X		RR	XXXXX XXX				
8	XXXXX	XXXX XX	XX		XXXXX XXXXX	XXXXX XXX	X	XXXXX	

Figure 4.43. Structural elements mapped along the Ujina conveyor cutting, presented as great circles with kinematic indicators on equal area stereonets, in the sequence of formation and/or displacement. "n" values in parenthesis are global populations of structures including those without mappable slip lineations. Generalised descriptions of characteristics of each generation of structures are given. Events 2 and ?3 appear to have accompanied porphyry mineralisation at Ujina... *(next page)*

The three principal fault orientations coincide broadly to fault populations with three distinct kinematic histories (Fig. 4.42). Faults trending NE typically have sinistral kinematic indicators, those that trend N and NNW were commonly dextral, and those that trend NW often underwent oblique normal slip. Among all groups, tool marks, fibres and minor SC fabrics developed in supergene kaolinite and chalcocite are the most common indicator of the sense of shear. The movement recorded by these indicators is therefore taken to represent displacement during or after supergene oxidation and enrichment. However, faults on all of these orientations could be related to older structural elements of the immediate surrounding district; SW-dipping faults to the Rosario Fault, subvertical N-trending faults to the Rio Loa fault system, and steeply WSW-dipping, faults to the Cascasca dyke swarm (Fig. 4.41).

The fault history of the area immediately northwest of Ujina is evident in four newly-exposed line-kilometres of excavation mapped along the Rosario-Ujina conveyor cutting during this study (Figs. 4.41 and 4.43). This area is within the peripheral chlorite alteration halo that encompasses both the Rosario and Ujina deposits.

The oldest group of structures in the cutting are the ~237 Ma Cascasca dykes that consistently dip steeply to the WSW (Chapter 3; Fig.4.43-1). Hornblende in these dykes is variably chloritised depending on their proximity to major structures. The walls of many dykes have been re-used as later fault surfaces. Faulted dyke margin that are chloritised have shallowly plunging striae that indicate dextral slip on NW-striking margins and sinistral slip on NNE-striking margins. Joints and centimetric slip faults in the host rhyolitic ignimbrite take similar orientations and have similar kinematics indicated by chlorite fibres and PT fabrics (Fig. 4.43 - 2). This style of irregular, tightly fracture-controlled occurrence is the most common manifestation of chlorite in the peripheral alteration zone (Fig. 4.41).

More commonly, the dykes are re-used by normal and sinistral faults characterised by blocky, beige clay-rich gouge (Fig. 4.43 - 3). Similar faults also occur commonly

Fig. 4.43, *(continued)* ... and events 4-8 record post-mineralisation faulting. Small Figures beneath each stereonet present simplified results of modelling of the stress axis orientations, following the method of Etchecopar (1981). More than 80% of the mapped faults and slip lineations fit the calculated stress axes with an average angular error of <10 degrees. Resolution of the sequence of brittle structural development follows the field methods of Hancock (1985) and McClay (1991), and the theory of Angelier (1991) and Potts and Reddy (1999).

within the ignimbrite and cut the chloritised structures. Clay in the gouge zones is not accompanied by pyrite and/or quartz veinlets, or any secondary copper minerals. These faults pre-date movement on major meridional sinistral faults (Fig. 4.43-4) that manifest as steeply dipping, broad clay-rich unconsolidated breccia zones and lesser gouge. Common, steeply SSW-dipping joints that locally underwent dextral slip formed during the same time bracket (between the preceding and subsequent fault events). The major sinistral faults comprise the Cascasca fault system and are interpreted to have together caused approximately 2.5 kilometres of sinistral displacement of the Cascasca dyke swarm between the Ujina Conveyor and the Camino Rosario, and of the unconformity between the La Grande and Cascasca Formations south of Ujina (Figs. 4.8and 4.41, Table 4.5). Restoration of this offset brings the southeastern end of the Rosario Fault into line with two major NW-trending faults mapped in the west wall of the Ujina open pit (Fig. 4.44).

The NW-trending normal faults in the Ujina pit appear to have formed during post-intrusion reactivation of the Rosario Fault. Their development might relate to the stage 3a faults mapped in the conveyor cutting. In the pit they cause minor disruption to the grade distribution and the geometry of dykes near the margin of the Ujina porphyry stock, but do not control either vein or intrusive geometry (Figs. 4.44 and 4.45). Their most recent movement therefore post-dates mineralisation. Within the Ujina pit, they are in turn truncated by north-trending faults (Fig. 4.44) that most recently underwent dextral slip (Fig. 4.42). These share the orientation and sense of shear with the late dextral faults (Fig. 4.43, stage 7) mapped in the conveyor cutting. Northeast-trending sinistral faults mapped in the pit do not clearly relate to any faults mapped in the conveyor cutting. They cut the early normal faults and abut the late dextral faults, with which they might have articulated as a conjugate array.

Structural elements that strike east-northeast are notably absent from the Ujina conveyor cutting, despite that structures with this orientation are common in the Ujina deposit. Dykes in the perimeter of the Ujina porphyry stock typically have this strike, most notably in the northern part of the deposit (Figs. 4.44 and 4.45). Likewise, this is also the most common orientation of major dykes of the post-mineralisation Inca porphyry, and both early and late stage veins locally occupy east-northeast trending fractures (Figs. 4.44 and 4.47; section 4.8.2). Penetrative

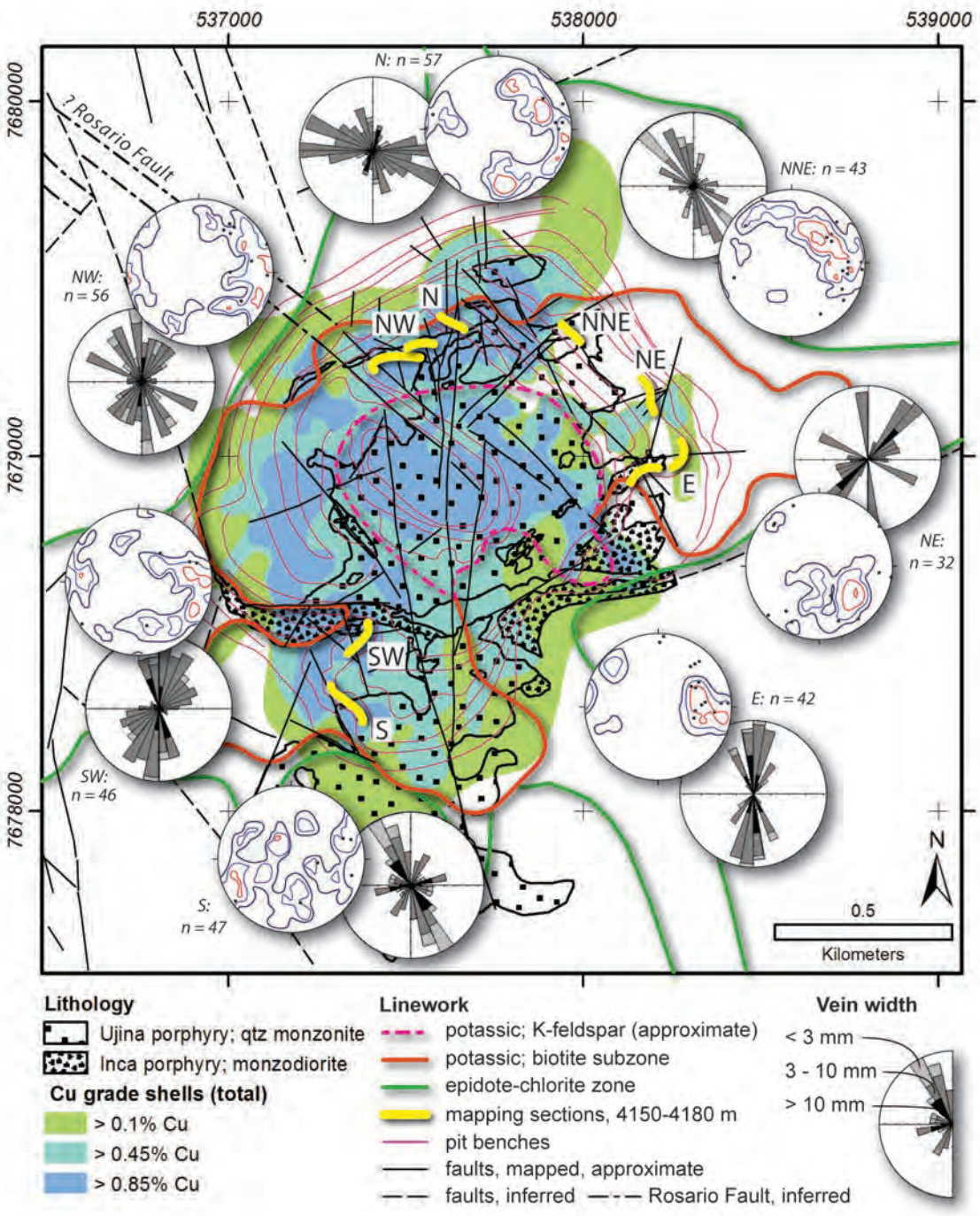

Figure 4.44. Map of the Ujina Mine showing new 4150-4180 level structural data for early quartz-Cu sulfide veins and the Cu grade distribution for the 4180 level of the mine (CMDIC grade data). The central high grade zone is dominated by supergene mineralisation whereas the outer high grade zones are primarily hypogene mineralisation. Minor overlap of hypogene alteration and grade shells with the Inca porphyry is an artefact of projection to surface. Early hypogene alteration zone boundaries are shown for reference. Fault linework is the approximate surface projection of faults described by CMDIC pit mapping and contrained by new mapping within the areas of new detailed mapping. The distribution of these areas were restricted as the mine was being actively infilled at the time of mapping. Stereonets are equal area projections of poles to planes, weighted for vein width, and contoured at 2, 4, 8, and 16% in most cases. Black points are poles to planes of faults with gouge with >5 cm mapped in the same section. Rose diagrams were constructed using only orientations with inclination >45º, weighted for vein width and Terzaghi corrected using a minimum angle of divergence from the mapping section of 20º in most cases. Plots for non-linear bench segments were constructed with greater allowance for the angular difference.

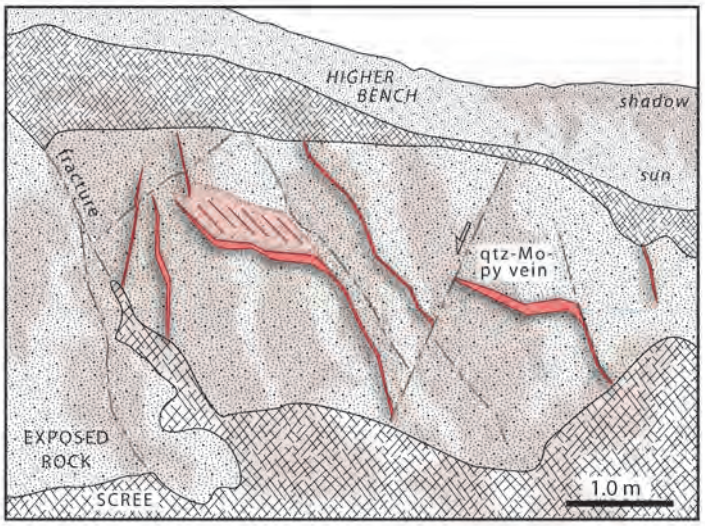

Figure 4.46. Sketch of a 4150 level bench in the S part of the Ujina open pit, looking southwest, showing the geometric relationship between shallow and steeply inclined segments of quartz-molybdenite veins. Continuous, narrow, steep are linked by shorter, shallowly inclined vein segments. Scale is appropriate for the foreground only. Cross hatching depicts broken or transported material. Mauve-brown hue depicts areas in shadow.

fracturing or faults on this orientation therefore appear to have existed in the location of the Ujina deposit prior to mineralization but not further west, and appear to have played a role in localisation of the mineralised intrusion.

4.8.2 Hydrothermal History

Quartz-chalcopyrite-(bornite) veins and early alteration stages. Veins of grey fine grained anhedral quartz ± potassium feldspar and 2-10 percent anhedral disseminated copper sulfides are the principal cupriferous hydrothermal stage at Ujina. These veins typically have strike lengths of less than two metres and have locally asymmetric wall morphologies. They are equivalent to the "A" veins documented at El Salvador (Gustafson and Hunt, 1975), and to the "A3" veins at Rosario (Masterman et al., 2005). They are spatially associated with potassic alteration that is zoned from a central potassium feldspar-dominant zone to a biotite-dominant zone around the margins of the Ujina porphyry stock (Fig. 4.44). The sulfide mineralogy of these veins is zoned from chalcopyrite-bornite in the central feldspar-rich alteration subzone, out to chalcopyrite-dominant in the biotite subzone, and pyrite becomes the dominant sulfide in the immediate margins of the system (Bisso et al., 1998).

The orientation of early quartz-Cu sulfide veins is strongly domainal across the Ujina deposit. Very broadly, they dip steeply to moderately westward, but strikes commonly vary from southeast, through south, to southwest. Local vein populations also exist that dip steeply eastward, north-northwest, and that are shallowly inclined (Fig. 4.44). In the E, NW and S mapping segments, populations of early veins are

subparallel to major faults mapped in the same sectors of the deposit and suggest some interrelationship between activity along approximately meridional faults and early veining. In contrast, early veins in the NW map segment appear unrelated to NW-trending faults in that area. Across the deposit, a few northeast-trending veins

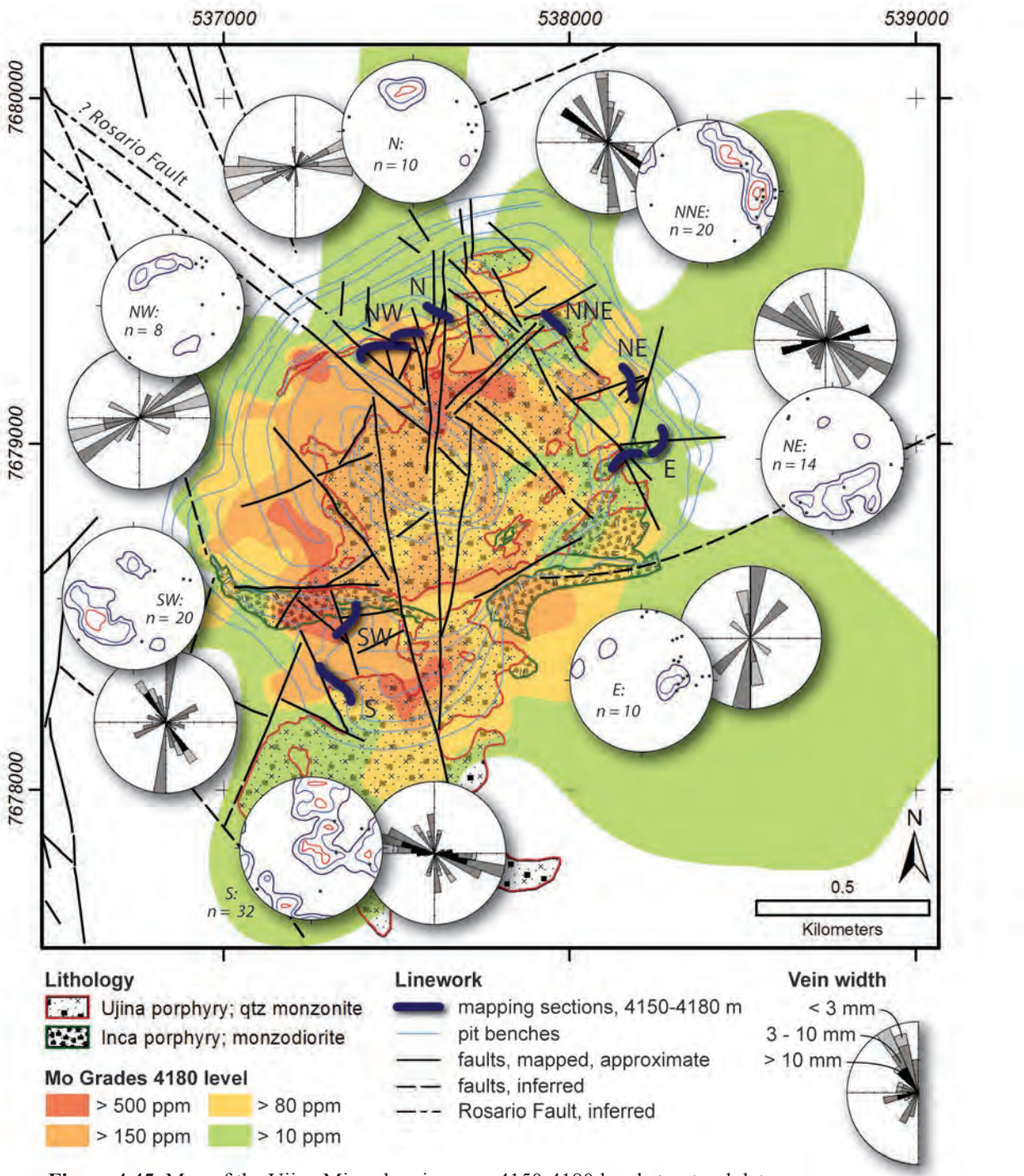

Figure 4.45. Map of the Ujina Mine showing new 4150-4180 level structural data for intermediate quartz-molybdenite veins and the distribution of major lithologies on the Oligocene paleosurface (CMDIC polygons for the porphyry intrusions). Early hypogene alteration zone boundaries are shown for reference. Fault linework is the approximate surface projection of faults described by CMDIC pit mapping and contrained by new mapping within the areas of new detailed mapping. Stereonet details as per Figure. 4.44.

show opening under dextral shear. In the southern part of the deposit, shallowly inclined veins and vein segments occur, locally as linking structures between steeper veins (Fig.4.44). Major populations of veins in the eastern and southern part of the deposit dip in toward the northern lobe of the Ujina porphyry stock, suggesting an overall loose concentric array that is commonly dominated by pre-existing tectonically imparted fracture patterns.

Quartz-molybdenite veins. The intermediate hydrothermal stage at Ujina comprises veins of grey to white anhedral quartz with coarse symmetrical banding parallel to the vein-walls, that contain 1-15% euhedral molybdenite, and minor pyrite. Banding in these veins is defined by changes in quartz grain size and molybdenite is concentrated along the vein selvedges and between quartz bands. The veins have straight and symmetrical walls and may extend over strike lengths of five metres or more. They are therefore analogous to the "B" veins at El Salvador or Rosario (Gustafson and Hunt, 1975; Masterman et al., 2005).

These intermediate stage veins take distinctive, moderately inclined orientations that are systematically inclined toward the central part of the northern lobe of the Ujina porphyry stock (Fig. 4.45). Variations from this pattern are few, and correspond to fracture sets parallel to local faults in the E and S pit map segments. In the S map segment, short, broad, subhorizontal vein segments are common and typically link more extensive, narrow subvertical veins (Figs. 4.45 and 4.46). Overall, the inward-dipping concentric array dominates the geometry of intermediate stage veins at Ujina.

Pyrite-quartz-(chalcopyrite-bornite) veins and phyllosilicate alteration. Veins of subhedral to euhedral pyrite and quartz with variable amounts of chalcopyrite comprise the prominent late vein stage at Ujina. These veins are laterally continuous up to tens of metres, have straight, symmetrical walls and locally contain primary open spaces. They are associated with strong white phyllosilicate alteration that is dominated by kaolinite ± pyrophyllite with disseminated pyrite in the immediate vein walls. This style of alteration is best developed as an overprint on the early biotitic potassium-rich alteration (Bisso et al., 1998) and apparently contributes to the high hypogene copper grades about the margins of the Ujina porphyry stock (Fig. 4.44).

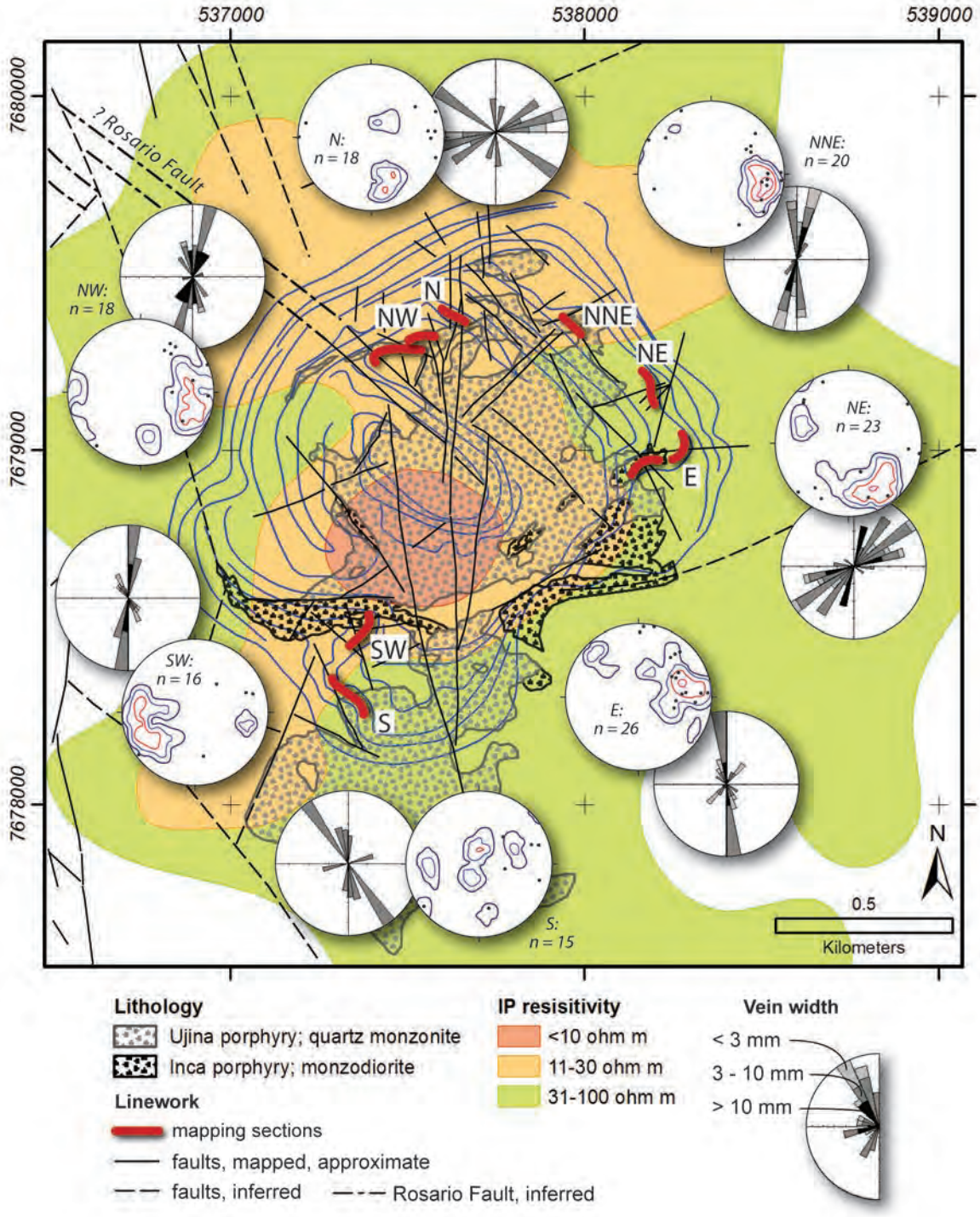

Figure 4.47. Map of the Ujina Mine showing new 4150-4180 level structural data for late stage pyritic veins, the distribution of major intrusions on the Oligocene paleosurface, and resistivity recorded by an exploration pole-dipole induced polarisation survey (N=4, ~350 m below surface; CMDIC lithology and geophysical data). The 100 ohm metre contour approximates the outer limit of structurally controlled white phyllosilicate alteration related to late stage veins. This area is somewhat broader than most of the inner propylitic epidote-chlorite alteration zone (compare Fig. 4.46). Fault linework is the approximate surface projection of faults described by CMDIC pit mapping and constrained by new mapping within the areas of new detailed mapping. Stereonet details as per Figure 4.44.

Based on the comparison of copper grades across the hypogene stockwork as a whole (0.66% Cu) and within the biotite zone overprinted by late stage veins (0.8-1.0% Cu; Bisso et al., 1998), these late veins are estimated to host approximately 20% of the hypogene Cu budget of the deposit. Most of these veins formed prior to intrusion of the Inca porphyry, but local vein reopening and bornite infill might coincide with mineralisation of breccias in the margins of that intrusion (Bisso et al., 1998).

Late stage veins at Ujina tend to have consistent orientations within a given domain and across the deposit they typically dip steeply and strike either north or east-northeast (Fig. 4.47). In the NNE, NE, E and NW map segments these orientation correspond to major faults mapped in the same areas. Late veins in all sectors are commonly re-used by younger faults and the contain significant secondary copper sulfides. However, late veins that cement or metasomatise pre-existing fragmental fault rocks have not been observed. The N map segment is distinct and is dominated by NNE-dipping early and late stage veins that apparently do not coincide with a major fault in that location (Figs. 4.44 and 4.47). As for the other vein types, late stage veins in the southern pit map segment include abundant subhorizontal and shallowly inclined orientations. The persistence of these fractures as vein hosts throughout the stockwork evolution is unique to this map segment, which is the only one located in the southern lobe of the Ujina stock.

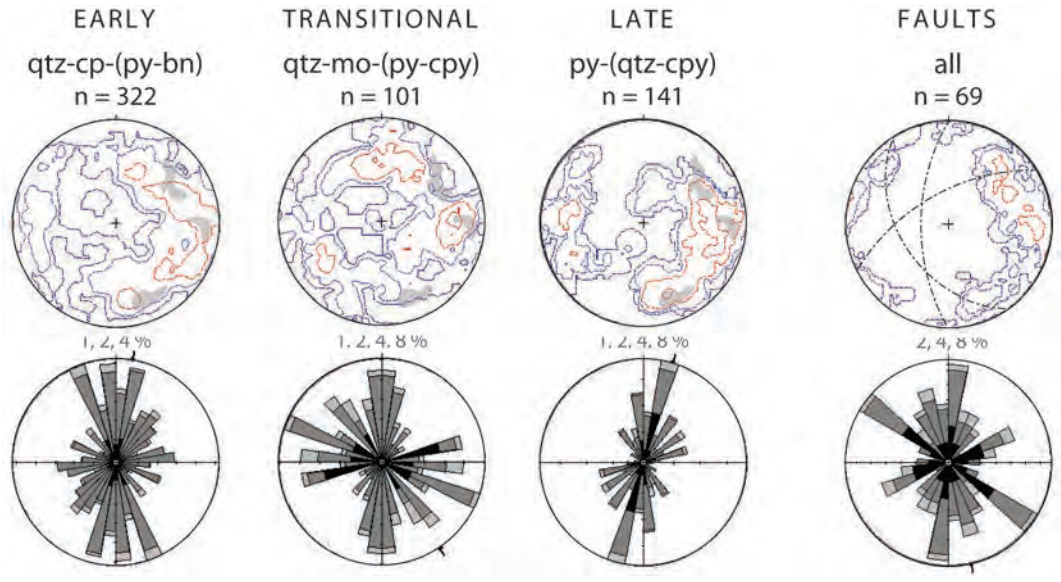

Figure 4.48. Equal area stereographic projections and rose diagrams for global vein populations and faults mapped in the Ujina open pit. Transparent grey areas indicate the loci of fault orientations for comparison with to veins. Dashed great circles correspond to the three principal fault orientations.

4.8.3 Structural History of the Ujina porphyry Cu-Mo deposit: Interpretation.

The Ujina intrusive complex occupies the location where three major district scale structures intersect; the Cascasca dyke swarm, the Rosario Fault, and an ENE-trending fracture zone that spans the Collahuasi block (Figs. 4.12 and 4.13). It occurs within a 3 km-wide arc-parallel sliver of rock bound on the west by the Cascasca fault and on the east by the Rio Loa Fault zone (Figs. 4.8 and 4.41). The site of the mineralised intrusion was therefore a small, highly fractured body of rock prior to emplacement of the intrusive complex.

Of these 'basement' structural elements, it is the ENE-trending fracture zone that experienced the greatest dilational strain during intrusion of both the early Ujina porphyry and late Inca porphyries. The dyke array is interpreted as evidence that pre- and post-mineral magma emplacement occurred under a stress regime in which the

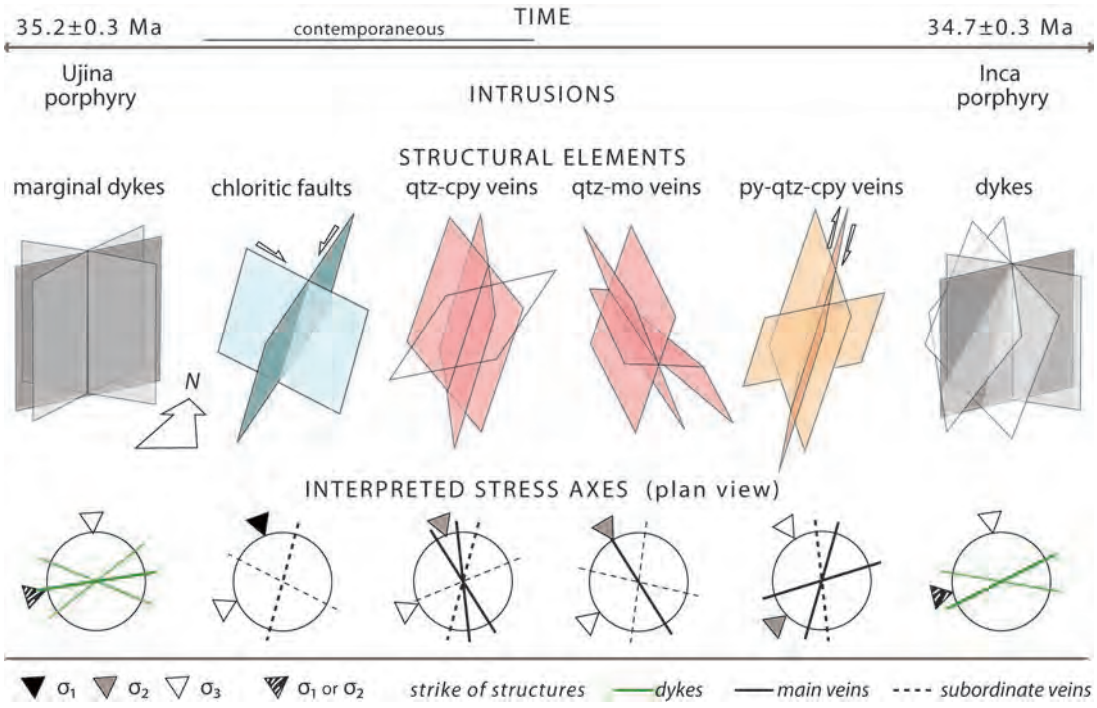

Figure 4.49. Schematic representation of the principal dyke and vein arrays at Ujina, and the interpreted orientations of local stress axes during formation of each generation. Broadly, emplacement of the Ujina intrusive complex appears to have occurred during weak dextral transtension that caused dilation of ENE-trending fractures along to an established arc-parallel structural corridor. The main metal-bearing vein arrays appear to record transient reversal of the tectonic stress and increasing dominance of hydrothermally mediated subvertical hydrothermal stresses. Late veins and dykes record decline of the hydrothermally imparted stress field and fracturing dominated by the regional far-field stress field. Pink and orange planes are stockwork vein generations, grey are dykes, and green planes are chlorite-altered fractures outside the main porphyry. Precedent for interpretation of stress axes as per Figure 4.33.

maximum principal horizontal stress axis was oriented ENE (Fig. 4.49). However, the gross distribution of peripheral early epidote alteration defines a rough cross with the arms oriented ENE and NNW (Fig. 4.41). Epidote and chlorite characteristically form together in the marginal alteration around porphyry copper deposits (e.g., Norman et al., 1991), and so chlorite-altered faults in the Ujina conveyor cutting most plausibly formed at around the same time as the epidote. These imply an unambiguous subhorizontal NNW-directed maximum principal stress orientation during formation or propylitic alteration. As this alteration generally reflects the outer manifestation of voluminous early potassic alteration (e.g., Haynes and Titley, 1980; Titley, 1982; Seedorff et al., 2005), the same stress field might be expected to have affected early Vqcp vein formation. Shallowly inclined link-veins, widespread re-use of fault-parallel fractures, and the weak concentric array shown by these veins all suggest that subvertical hydraulic forces strongly affected fracture dilation during Vqcp vein formation. Although this also implies that differential horizontal stresses were likely to have been low, the gross dominance of N- and NNW-trending orientations is consistent with the NNW-oriented maximum principal stress axis determined from chlorite-altered faults.

The relative significance of the hydrothermal fluid pressure is reflected in the degree to which vein arrays assume a concentric, inward-dipping geometry about the main mineralised stock (e.g., Park, 1983; Tosdal and Richards, 2001). Therefore, the concentric, inward-dipping vein array occupied by intermediate veins (Fig. 4.45), as well as the thick, shallowly-inclined link veins common to this generation are interpreted as evidence of prononced fluid overpressure and hydrothermally mediated fracturing. Differential horizontal stresses were most likely very low during intermediate stage vein formation, to permit fluid dominance of the local stress field. However, a weak preference of steeply inclined intermediate veins to strike approximately NW (Figs. 4.45 and 4.48) is also broadly consistent with the relative differential horizontal stress geometry implied by earlier Vqcp veins and chlorite-bearing faults. In contrast, later stage veins show effectively no concentric arrangement, have more consistent orientations than earlier vein sets across the deposit, and are dominated by N- to ENE-trending orientations. They are therefore interpreted to reflect a return to tectonically-driven fracturing. In that case, the

maximum principal stress axis would have bisected the dominant N- and ENE-trending sets, and therefore been subhorizintal and oriented to the NE (Fig. 4.49). The post-mineralisation Inca porphyry dykes mark the decline of the hydrothermal system and appears also to have formed in a stress regime in which the normal stress on ENE-trending fractures was minimal.

In summary, the Ujina porphyry intrusions (early and late) and late stage veins formed during conditions in which shear strain on the arc-parallel faults such as the Collahuasi and Rio Loa faults would have been dextral, albeit mild, as significant displacements in this sense are not observed. Fracturing on orientations between ENE and NE may have developed as part of an incipient dextral shear couple between these two faults, with dilation localised at a pre-existing structural intersection between the Rosario Fault and the Cascasca dyke swarm. Main and intermediate stage veins formed during low overall differential horizontal stress conditions. Nonetheless, the preferred orientations of these veins, as well as propylitic-altered faults outboard of the deposit imply a relaxation and reversal of the differential horizontal stress at the time of main stage mineralisation. In contrast with the principally tectonic fracturing at Quebrada Blanca and Copaquire, local stresses related to development of the hydrothermal system at Ujina dominated tectonic forces during main and intermediate stage vein formation (Fig. 4.49). The differences might indicate that tectonically imposed forces weakened between 36 and 35 Ma, and/or that the referral of regional stress into the shallow crust was partitioned into the vicinity of the Domeyko Fault zone. Away from this principal arc-parallel fault system, regional stresses were probably weaker most of the time.

4.9 Structural and Hydrothermal Geology of the Rosario Porphyry Cu-Mo deposit and the La Grande Cu-Ag epithermal veins

The Rosario porphyry Cu-Mo deposit and adjacent, younger La Grande high sulfidation Cu-Ag veins represent the largest concentration of these metals in the Collahuasi district by a wide margin (Table 1.1). This composite mineralised body is unique among the porphyry-style deposits in the district because of the juxtaposition of one of the major epithermal veins (the Rosario Vein) into the central part of the main porphyry stockwork (Munchmeyer et al., 1984; Bisso et al., 1998; Masterman

et al., 2005). This contributed as much as 50% of the Cu budget within the better-known upper 500m of the deposit (Masterman et al., 2005). Previous studies of the structural geology of the Rosario deposit have uniformly focussed on the Rosario Fault and associated veins, and all have concluded that this fault was the principal control on emplacement of the Rosario porphyry and the related porphyry stockwork (Lee, 1994; Bisso et al., 1998; Masterman et al., 2005). On the basis of fault kinematic mapping in pre-mining exploration trenches at Rosario, Masterman et al. (2005) suggested that emplacement of the porphyry accompanied dilational re-use of the Rosario fault during sinistral shear along the Monctezuma fault system. This interpretation relies on the assumption that the strain environment recorded by dilation and mineralisation of the Rosario Fault and vein at ~32.6 Ma had also prevailed at ~34.4 Ma when the Rosario porphyry was emplaced (geochronology of Masterman et al., 2004). In this study, structural measurements were taken along extensive road cuts northeast of Rosario on the main access; the Camino Rosario, around the well-exposed southeastern walls of the Rosario phase 1 open pit, and in the best-exposed exploration trench on Cerro La Grande, southwest of Rosario (Fig. 4.50). The new mapping permits the distinction of multiple brittle deformation events that have affected the broader Rosario area from the Triassic to the Neogene (Fig. 4.51). The evident structural history therefore provides a broader context in which to interpret the stress environment in which mineralisation occurred.

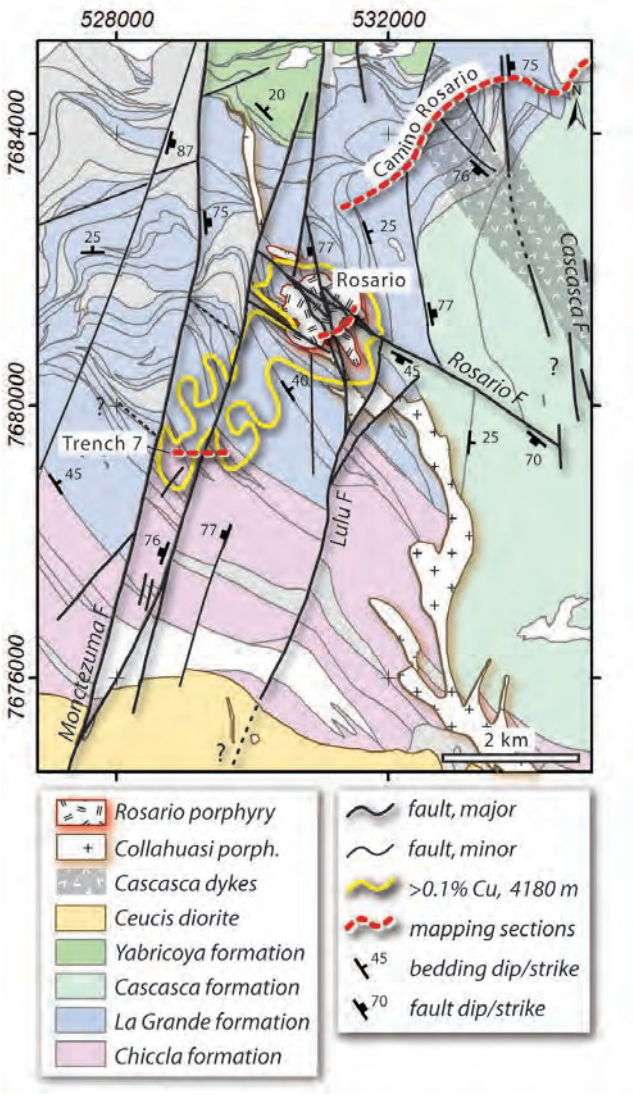

Figure 4.50. Summary map showing the location of structural mapping sections in the Rosario area relative to major faults, intrusions, and Cu mineralisation. F = fault.

4.9.1 Fault Geometry and Evolution

The principal structural elements in the central Collahuasi district are multiply re-used Peine Group-age features (section 4.3.4): the NW-trending Rosario fault, a series of NNE-trending structures including the Monctezuma faults, the NNW-trending Collahuasi porphyry, and the Cascasca dyke swarm (Figs. 4.8 and 4.50). Both of the major fault systems have well developed conjugate arrays with similar dip to their master faults (Fig. 4.51). It therefore appears that the block to the east of the Monctezuma fault has not been rotated significantly since the post-folding development of these structures. This contrasts with the mild northward tilting of the western part of the district (sections 4.6 and 4.7).

Four, and possibly five episodes of deformation can be distinguished at both Rosario and along the Camino Rosario section (Fig. 4.51A-B), and two (possibly three) of these are recognised at La Grande (Fig. 4.51C). Structures that controlled and host hydrothermal alteration related to the Rosario system occur in all the mapped areas and are interpreted to have been active during mineralisation. More broadly, episodes of deformation are interpreted to have been contemporaneous if, within the constraints of the mapped cross-cutting relationships, they record strain indicative of similar local stress conditions. By this approach, the data from the three mapping sections can be grouped neatly into episodes of deformation that affected all, or large parts of the central Collahuasi district (Fig. 4.51).

Pre-Maastrictian faulting. The earliest recognisable group of structures in the investigated sections are numerous steeply WSW-dipping narrow andesitic dykes along the Camino Rosario. These define the northern extent of the Cascasca dyke swarm that is also exposed in the Ujina conveyor cutting (Figs. 4.7, 4.41 and 4.51; CR1). The dykes in both locations are petrologically and morphologically similar. A few such dykes also occur at Rosario but have been intensely dismembered by subsequent faulting. At Rosario, a series of moderately dipping normal faults with striae indicating near-pure dip slip defines the first stage of post-folding displacement on the Rosario Fault (Fig. 4.51; R1). The relative timing of the earliest faulting at Rosario and dyke emplacement along the Camino Rosario cannot be unequivocally established. The emplacement of the dykes occured in the Lower Triassic (sections

Figure 4.51. Compiled structural data for the greater Rosario - La Grande area.

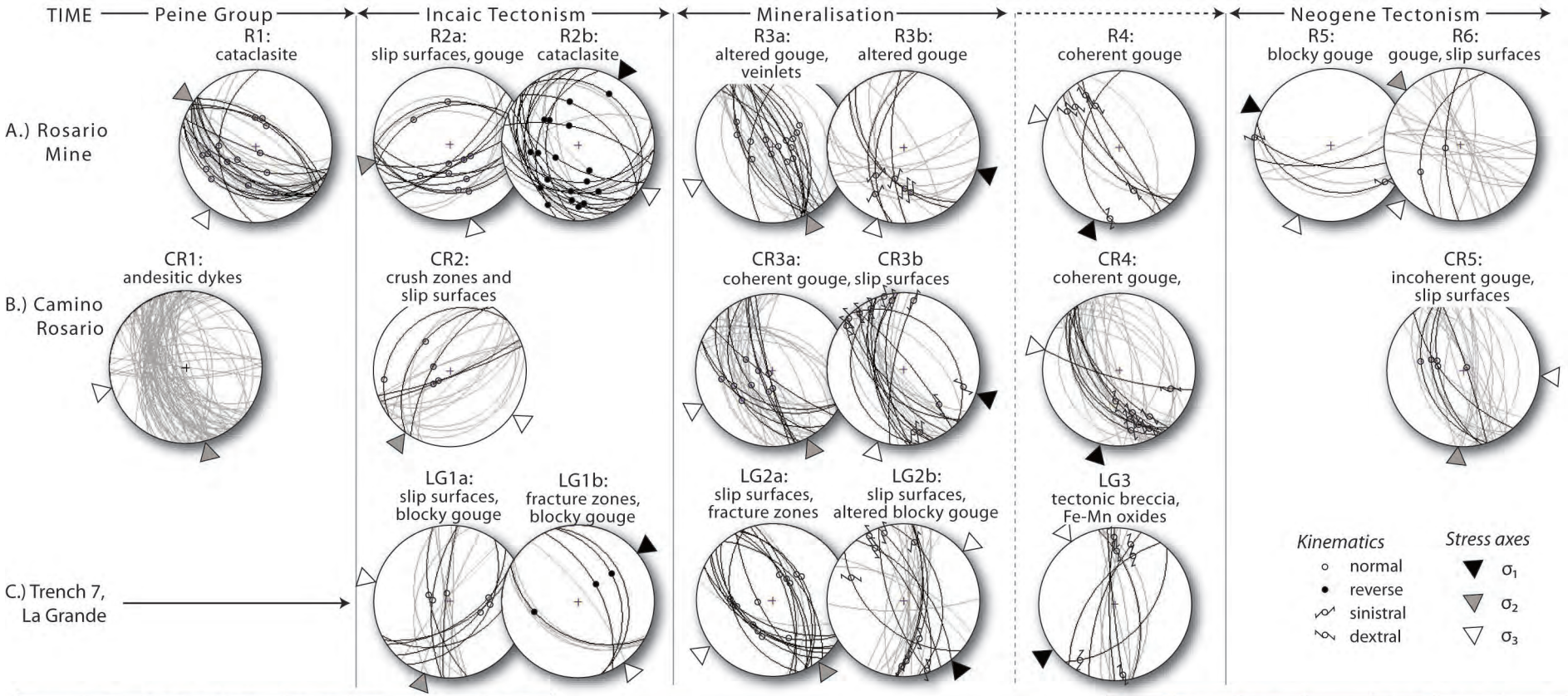

	R1	R2a	R2b	R3a-b	R4	R5	R6
R1		XXX			A.) Rosario Pit		
R2a	XXX						
R2b	XXXXXX XXX	XX					
R3a-b	XXXXXX XXX	XXX	XXXXX				
R4	-	X	-	XXXXXX X			
R5	XXXXXX	XX	XX	XXXXXX	-		
R6	XXXXXXX XXXXXXX	XXX	XXXXXX XX	XXXXXXX XXXXXXX	XXXXX	XXXXXX X	

	CR1	CR2	CR3a-b	CR4	CR5
CR1			B.) Camino Rosario		
CR2	XXXXXX				
CR3a-b	XXXXXX	X			
CR4	XX	XX	XXX		
CR5	XXX	-	XX	X	

	LG1a	LG1b	Vmctz*	LG2a	LG2b	LG3
LG1a	XX		C.) Trench 7, La Grande			
LG1b	X				X	
Vmctz*	-	-				
LG2a	X	X	-			
LG2b	-	-	XX	X	X	
LG3	-	-	-	XX	X	

3.16 and 3.17) and marks a transient stage of arc-othogonal extension that characterises the decline of the Choiyoi Arc. In contrast, the early dip slip in the Rosario Fault might have occurred intermittently under the along-arc sinistral wrench environment that prevailed from the Permian to the Middle Cretaceous (Chapter 2).

Incaic tectonism-associated faulting. The second major group of brittle structures include broadly NE-trending normal faults and joints, and NW-trending reverse faults. The earlier normal faults are characterised by narrow gouge zones and slip surfaces (Fig. 4.51) and are not typically associated with large stratigraphic offsets. They did not accommodate more than a few decimetres of displacement on any given fault. The orientation of these faults varies from ENE at Rosario, to NE on the Camino Rosario, to N and NE at La Grande (Fig. 4.51; R2a, CR2 and LG1a). Together these faults record minor, broadly NW-directed dilation that is anticipated to have occurred during along arc dextral transtension. The differences in the strike of the faults could reflect bedding-parallel slip along the Camino Rosario or deviations in the local stress field in proximity to either the Rosario and/or Monctezuma Faults.

At Rosario and La Grande, the NE-trending faults are cut by a series of moderately inclined reverse faults defined by cataclasite and/or blocky gouge zones (Fig. 4.51; R2b, LG1b). These are not present along the Camino Rosario section, and are perhaps concentrated near the major district-scale fault systems (Fig. 4.50). At Rosario these faults strike between N, NW and W, and commonly record inversion of strands of the Rosario Fault. Some of the reverse faults in the Rosario deposit cause at least mesoscopic displacement of other structural elements. These fault generations record NE-directed compression that is most easily explained by a change from

Figure 4.51. (previous page) Compiled structural data for the greater Rosario - La Grande area shown as equal area stereographic projections: A) SE wall of the Rosario open pit, 4415 to 4480 m levels, B) Camino Rosario within 5 kms of Rosario, and C) Trench #7 at La Grande. Brief descriptions of the character of structures in each generation and crosscut frequency matrices indicate the basis for distinction of fault generations in each location. Note that at La Grande, the banded quartz-Mn epithermal Monctezuma veins are included as an important time marker. Dark great circles are faults with measured striae, grey great circles are structures attributed to a given generation on the basis of morphology, mineralogy and/or sense of shear. Greyscale triangles indicate the likely trend of the two principal stress axes closest to horizontal during each generation of faulting, calculated after Etchecopar (1981). Resolution of the sequence of brittle structural development follows the field methods of Hancock (1985) and McClay (1991), and the theory of Angelier (1991) and Potts and Reddy (1999).

transtension to transpression within the along-arc dextral wrench environment that had prevailed along the Central Andean margin since the Middle Cretaceous (Chapter 2 and Fig. 4.9). This implies a switch between the intermediate and maximum principal stress axes which might be the expected response of the regional stress field to increased compression related to either the Lower Paleocene "K-T" or Middle Eocene "Incaic" tectonic phases (Table 2.1). Dextral wrench with fluctuating transpression and transtension is also the environment in which mineralisation is interpreted to have occurred at Quebrada Blanca and Copaquire. Inversion of the Rosario Fault may therefore have been contemporaneous with mineralisation in the western Collahuasi district.

Syn-mineralisation faulting. Steeply dipping faults that strike NNW and have a close spatial association with hydrothermal alteration are a prominent feature of all three mapping sections (Fig. 4.51). At Rosario and on the Camino Rosario, these faults underwent either normal dip-slip and/or sinistral strike slip displacement. The relative timing of the two displacement senses is ambiguous as cross-cutting relationships are scarce. However, on two such fault surfaces at Rosario, strike slip striae have overprinted earlier dip slip straie. At La Grande there is a slight angular discordance between normal and sinistral faults (Fig. 4.51; LG2a-b) and one altered sinistral fault was mapped that cut and offset an altered normal fault. These sparse

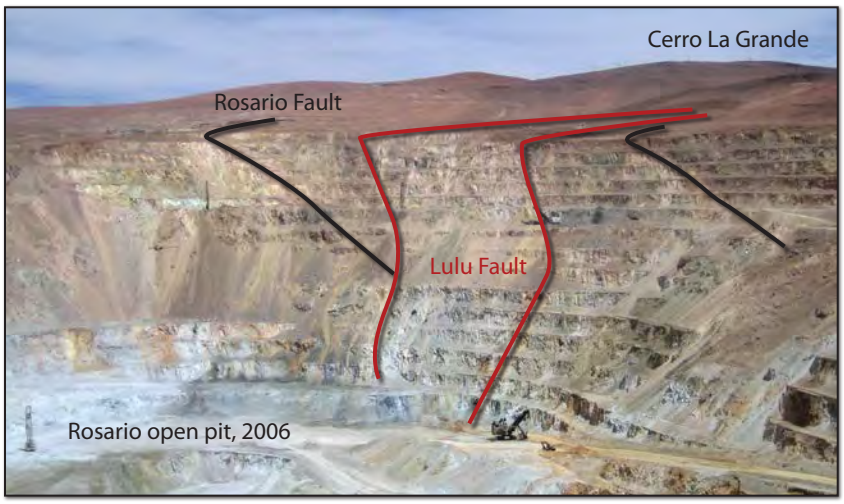

Figure 4.52. Photograph of the SE wall of the Rosario open pit, annotated to highlight the cross-cutting relationship between the Lulu Fault and the Rosario Fault. Bleaching supergene kaolinite alteration accompanies both structures. Bench height is 15m

data lead to the interpretation that WSW-oriented dilation recorded by the dip-slip faults preceeded sinistral wrench strain accommodated by subparallel strike slip faults. The hypogene alteration assemblages that may have accompanied specific structures are difficult to determine because supergene kaolinite-illite-(dickite) alteration affects most shallow permeable zones that were originally sulfidic. Nonetheless, it appears that the earlier stages of mineralisation accompanied WSW-directed extension. Later stages of mineralisation apparently occurred during sinistral wrench that was most plausibly articulated along the Monctezuma are related faults.

Relationships between the Rosario and Lulu faults imply a more complex syn-mineral kinematic history at Rosario. Epithermal Cu-Ag mineralisation that characterises the moderately dipping fracture zone associated with the Rosario fault occurred late in the hydrothermal paragenesis (Masterman et al., 2005). However, that structure is offset approximately 200 metres by the steeply-dipping Lulu Fault that is also strongly altered but does not host major late-stage veins (Fig. 4.52). This contradicts the inference from the measured fault surfaces that displacement on NNW-trending normal faults (such as the Lulu Fault) was the earlier of two broadly syn-mineral faulting stages. The net displacement on the Lulu Fault can be determined from the relative positions in the footwall and hangingwall of the point of intersection between the Rosario fault and major stratigraphic boundaries. These reveal approximately 200 metres

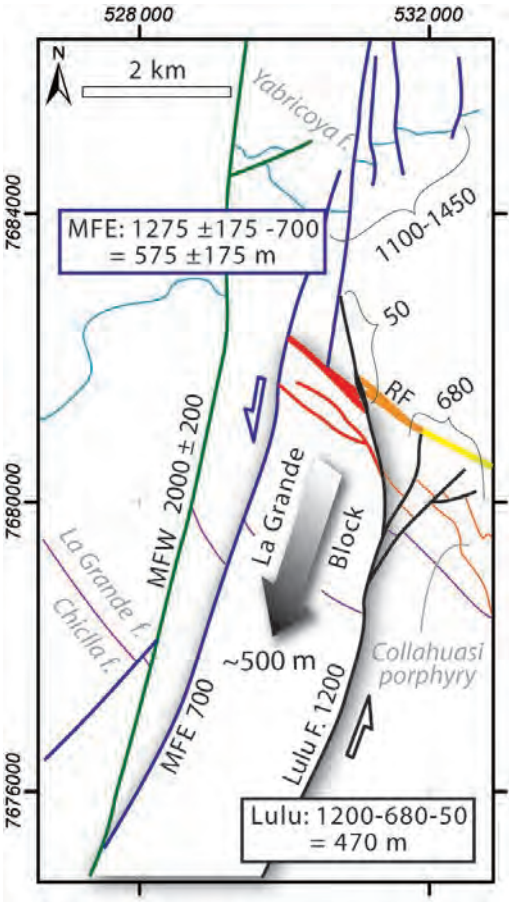

Figure 4.53. Simplified structural map of the central Collahuasi district showing the bulk sinistral offsets on faults of the Monctezuma and Lulu fault systems. The differences in bulk offsets on these faults imply a southward translation of ~500 m of the La Grande block. Narrow coloured lines depict major lithological contacts that affect the interpretation of bulk offsets. Warmer colours used for the Rosario and related faults reflect greater dip-slip displacement related to escape of the La Grande block. MFW, MFE = West and East Monctezuma Fault, respectively. RF = Rosario Fault, F = fault, f = formation.

of west side-down normal, and 50 metres of sinistral displacement on the strand of the Lulu Fault that transects the Rosario deposit (Table 4.5). Throughout the central Collahuasi district, sinistral wrench displacements of hundreds of metres are common among NNE-trending faults such as the Monctezuma Fault. Bulk displacements vary significantly either side of the Rosario Fault (Fig. 4.53) suggesting that NNE and NW-trending faults articulated together. The discrepancy between sinistral offset along a) the northern and southern parts of the East Monctezuma Fault, and b) between the Lulu Fault at Rosario and south of amalgamation of its horsetail further SE, is uniquely explained by southward escape of the intervening block (Fig. 4.53). This block, bound by the southern Lulu Fault, western Rosario Fault, and eastern Monctezuma Fault is here informally called the La Grande block. Masterman et al. (2005) recognised approximately 15º of northeastward tilting of the hangingwall of the Rosario Fault at Rosario, which they attributed to extensional faulting along this structure. Escape of the La Grande block provides a mechanism by which this may have occurred. Fluid inclusion evidence was used by Masterman et al. (2005) to conclude that the late stage mineralisation at Rosario formed at much shallower depth than the early paragenetic stages. Unroofing of the Rosario porphyry by southward translation of the La Grande block therefore appears to have occurred during late stage mineralisation and this kind of catastrophic failure may account for the fluctuation between lithostatic and hydrostatic fluid inclusion trapping pressures calculated by Masterman et al. (2005) for the youngest generation of veins. The latter mineralisation stages therefore appear to be related to development of a major hard-linked sinistral shear couple articulated between the eastern Monctezuma and Lulu faults (Fig. 4.53). Northwest-trending fault segments such as the Rosario fault underwent pronounced extension at this time. This proposed scenario also conveniently accounts for the sub-district scale change in the nature of the Rosario fault (Fig. 4.53); from a major 10-100 m-wide damage zone at Rosario (e.g., Lee, 1994; Masterman et al., 2005), to a discrete, <5 m-wide fault zone three kms along strike to the SE (Fedorowich, 2001).

Post-mineral faulting. Two principal groups of post-mineralisationisation faults can be distinguished across the central Collahuasi district; a series of moderately to steeply dipping, N- to NW-trending dextral faults that typically have coherent gouge

(Fig. 4.51; R4, CR4, LG3), and a group of steeply dipping N- to NNW-trending normal faults characterised by unconsolidated gouge stained by transported goethite (Fig. 4.51; R6, CR5). Both groups of faults are associated with displacements of a few centimetres to a few metres at most. The dextral faults characteristically re-use older fault and alteration zones, and are associated with locally well-developed tectonic brecciation. Differences in the orientation of late dextral faults between the La Grande and Rosario areas are consistent with differences between the orientations of their respective older fault sets (Fig. 4.51).

New observations of late dextral faults support the interpretation of Masterman et al. (2005), that these faults record re-use of pre-existing structures. In outcrops to the southeast of La Grande, faults belonging to this generation are cemented by intergrown fine grained quartz and massive iron and manganese oxides. This is interpreted as a discrete hydrothermal episode, as there are none of the banded and sulfidic vein textures characteristic of the surface exposures of the older Mn-rich Monctezuma epithermal system. In general, the gouge and breccia zones associated with these late dextral faults are coherent fault rocks. Minor hydrothermal cementation of the faults by quartz may therefore have occurred more widely during dextral faulting. The timing of this faulting is not well-constrained, as cross cutting relationships are rare because of the multiple re-use history. However, the associated mild hydrothermal activity might suggest that it marks the final decline of the Rosario-La Grande hydrothermal system. Alternatively, the limited dextral wrench could have occurred at some later time, although that demands the development of a previously unrecognised hydrothermal system. The only known Neogene hydrothermal activity; associated with oxidation and supergene enrichment, was most likely accompanied by sinistral wrench (section 5.4.2). If cementation of these faults does indeed record the death of the La Grande hydrothermal system, then it requires that strain accommodation through the central part of the district changed from sinistral to dextral wrench (Fig. 4.51) within the time frame of the hydrothermal system, i.e. over a few hundred thousand years (e.g., Arribas et al., 1995; Cathles et al., 1997).

The youngest faults recognised in the Rosario area are primarily discrete, narrow, steeply dipping short-displacement faults with oxide staining. These are best

developed in the Rosario deposit, but also occur along the Camino Rosario. They have not been observed at La Grande. At Rosario they define a conjugate array of faults that strike N and WNW. The WNW-striking subset locally underwent dextral shear (Fig. 4.51; R5) whereas the N-striking faults have normal dip slip to oblique normal-sinistral slip (Fig. 4.51; R6). Along the Camino Rosario, late faults with similar morphology to those at Rosario strike NNW and underwent normal dip-slip or oblique normal-dextral slip (Fig. 4.51; CR5). The late faults at Rosario record minor WSW-directed dilation whereas those along the Camino Rosario record WNW-directed dilation. The difference might imply either diachronous faulting, strain partitioning relative to the positions of the major district-scale faults, or both. Generally they record approximately orogen-orthogonal extension which is most likely to relate to gravitiational collapse (e.g., Stuewe and Barr, 2000) following the main period of Miocene orogenesis in the Central Andes (e.g., Sandeman et al., 1995; Chapter 1).

4.9.2 Intrusive and Hydrothermal History

The hydrothermal paragenesis of the Rosario porphyry Cu deposit and adjacent La Grande veins were investigated in detail in the research theses of Lee (1994) and Masterman (2003), and published by Masterman et al. (2005), a simplified, adapted version of which is presented in Figure 4.54. Overall, the veins and related alteration mineralogy and spatio-temporal distribution are very similar to the pattern reported form the other major Eocene-Oligocene porphyry copper deposits of the central Andes (e.g., Gustafson and Hunt, 1975; Ambrus, 1977; Lindsay et al., 1995; Ossandon et al., 2001). The similarities to other examples are such that Masterman et al. (2005) applied the sequential alphabetic nomenclature developed elsewhere (Gustafson and Hunt, 1975; Dilles and Einaudi, 1992; Arancibia and Clark, 1996). That nomenclature has been retained here and descriptions are provided here only for those veins identified macroscopically and systematically mapped in the field.

Intrusive history. The intrusive history that might relate to mineralisation at Rosario and La Grande comprises at least two, and possibly four stages. The main body of early to intermediate stage stockwork mineralisation is centred on, and formed at approximately the same time as the Rosario porphyry, within analytical

error (Masterman et al., 2004, 2005; this study). This intrusion is the massively predominant Eocene age intrusive rock known from Rosario and sets it apart from the markedly polyphase intrusive complexes to which large porphyry copper deposits are commonly related (e.g., Cornejo et al., 1997; Gustafson et al., 2001; Ossandon et al., 2001; Padilla Garza et al., 2001; Seedorrf et al., 2005).

Three other intrusive stages are inferred to be genetically associated with the Rosario porphyry. An exploration drillhole immediately SW of Rosario contains xenoliths of a medium grained porphyritic rock with strong, pervasive pink K-feldspar alteration (Fig. 4.55a). These are overgrown by the beige K-feldspar alteration that is common in the Rosaro porphyry, and imply the presence, at depth, of an earlier intrusive phase that underwent potassic alteration distinct from that associated with the Rosario porphyry. These are most likely fragments of a pre-mineral intrusion related to the

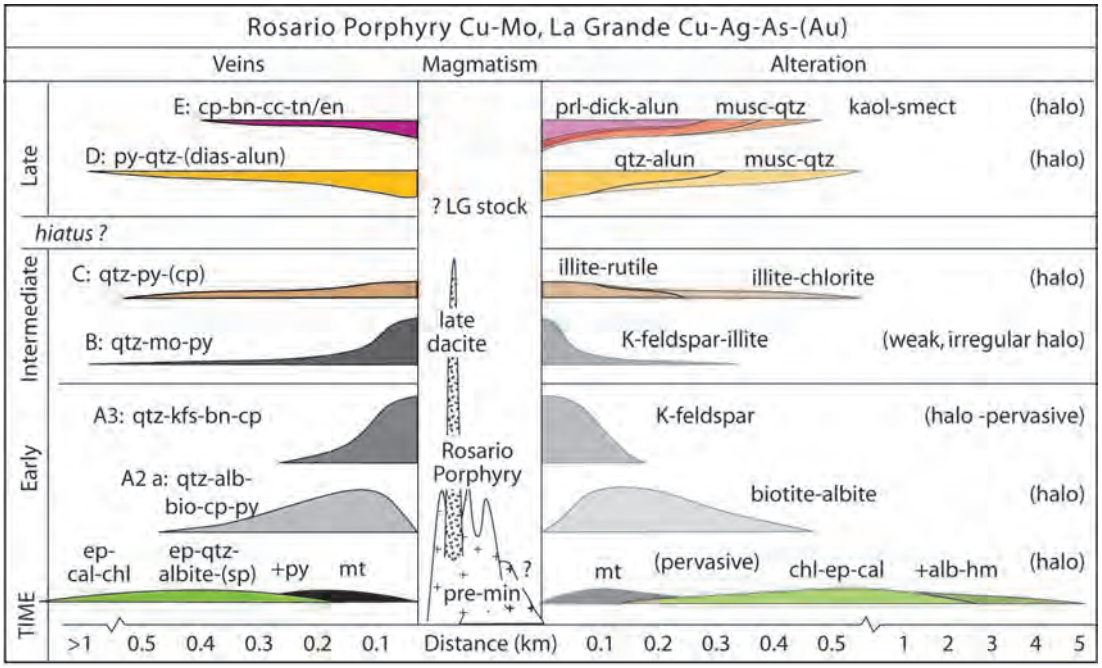

Figure 4.54. Schematic diagram of spatial and temporal relationships between intrusions, veins and alteration assemblages at Rosario-La Grande. The mineralogy of proximal vein and alteration stages is compiled from Lee (1994) and Masterman et al. (2005). The relative timing and distribution of vein stages is taken primarily from the mapping and documentation of cross-cutting relationships of Masterman et al. (2005). The distribution and mineralogy of A2 veins and all epidote-bearing assemblages are adaptations of the original scheme based on new data collected in this study. Synchroneity of early proximal and distal veins and alteration is inferred, as discussed in the text. Abbreviations: premin = possible pre-mineral porphyritic intrusion at Rosario; LG stock = proposed blind stock beneath the La Grande veins; alb = Na-feldspar; alun = alunite; bio = biotite; bn = bornite; cal = calcite; cc = chalcocite/covellite/digenite; chl = chlorite; cp = chalcopyrite; en = enargite; ep = epidote; hm = hematite; mt = magnetite; musc = muscovite; py = pyrite; qtz = quartz; sp = sphalerite; tn = tennantite.

Rosario porphyry (Fig. 4.54, bottom), though a significantly older intrusion and alteration event in the same location cannot be yet ruled out.

During excavation of the early stages of the Rosario open pit, several small, subvertical fine grained “dacitic” dykes were encountered cutting the volcano-sedimentary Peine Group host sequences (I. Smoje, CMDIC, written commun, 2004). These were interpreted by CMDIC as a minor post-mineralisationisation intrusive phase (Fig 4.54), although they could belong to the Cretaceous alkaline intrusive event. They have not been encountered cutting the Rosario porphyry and were described from an area where supergene alteration had destroyed the early hypogene alteration assemblages.

A younger intrusion was proposed by Masterman et al. (2005) to have intruded at depth two to three kilometres SW of Rosario, contemporaneous with formation of late-stage epithermal veins (Fig. 4.54). The presence of an intrusion in this locality has not been confirmed, although there are several lines of mineralogical evidence that this location was the thermal centre of the La Grande epithermal system (Masterman et al., 2005; C. Deyell, unpublished data). In this scenario, intrusion may have been contemporaneous with southward escape of the La Grande block (Fig.

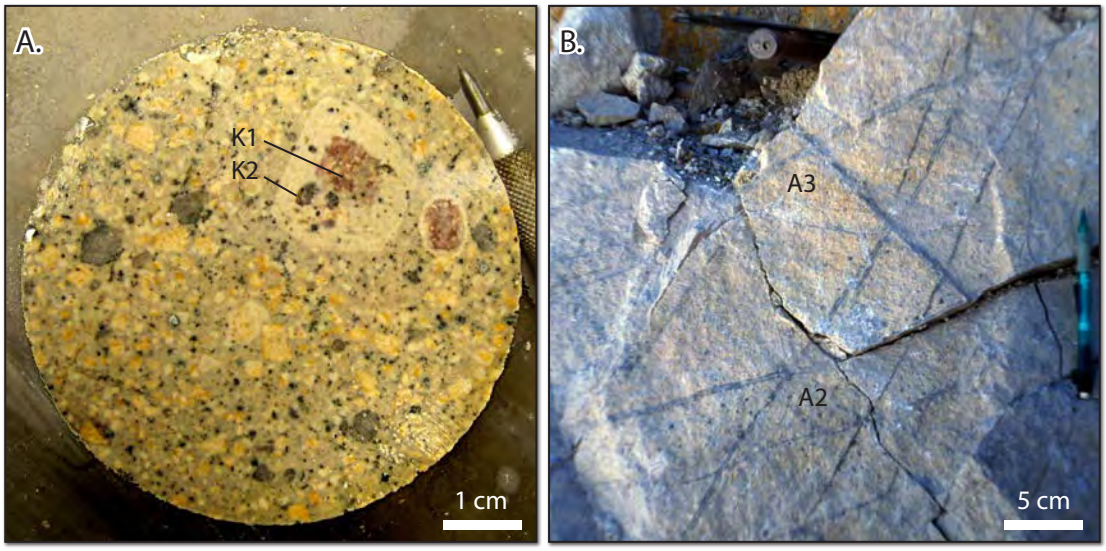

Figure 4.55. Intrusive and cross cutting vein relations at Rosario. A) Xenoliths of pink pervasively orthoclase-altered rock (K1) with strong beige orthoclase overgrowths in the Rosario Porphyry (K2). Sample was unique at the time of deep exploration drilling in the Rosario-La Grande transition area, GC243. B) Early stage veinlet stockwork comprising a conjugate array of narrow A2 veinlets with distinct alteration haloes cut by a thicker grey quartz-sulfide (A3) veinlet (SE inner pit mapping segment; Fig. 4.56).

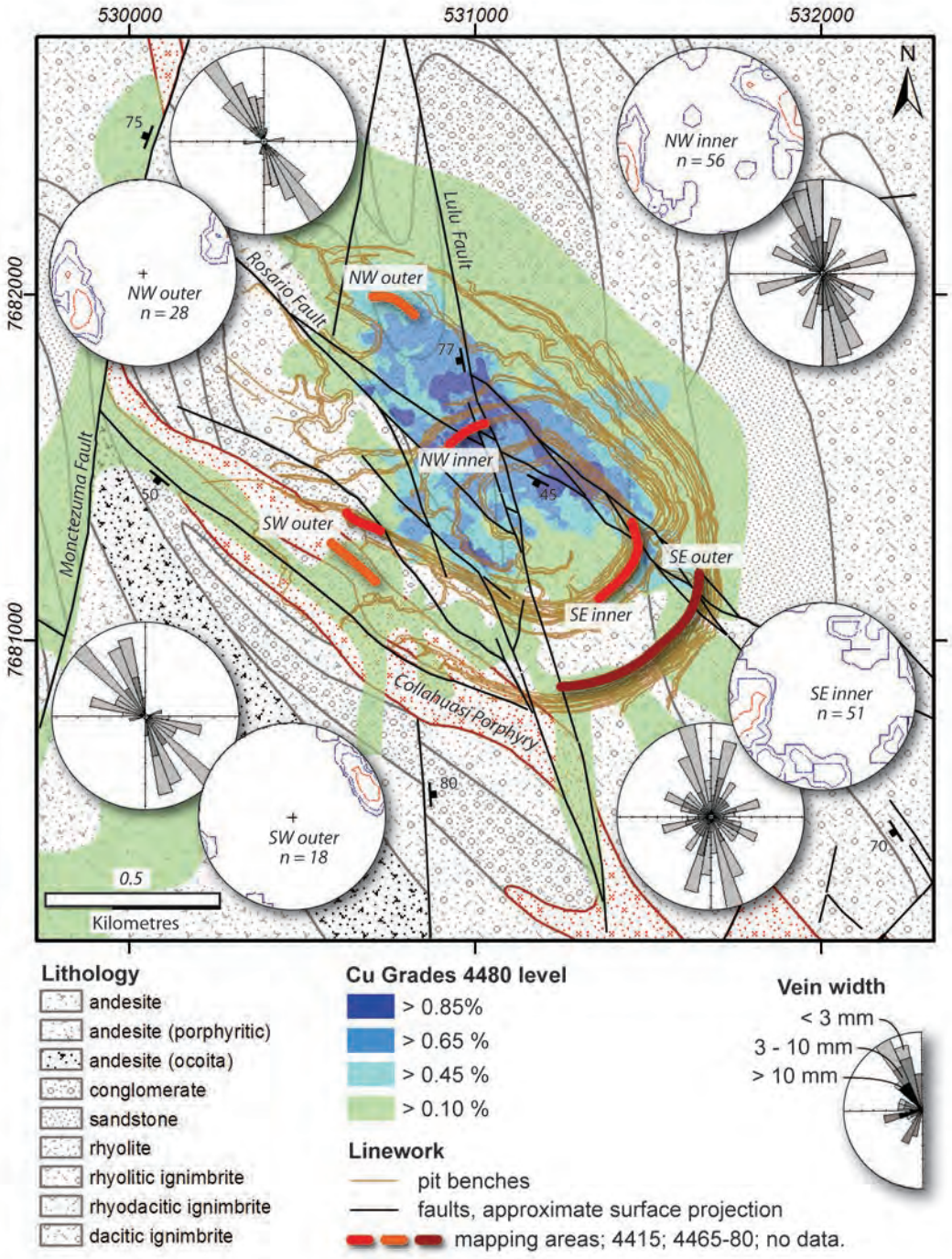

Figure 4.56. Map of the Rosario open pit showing new 4415-4480 level structural data for early quartz-Cu sulfide veins and the Cu grade distribution for the 4480 level of the mine (CMDIC grade data). The grade distribution at this level is strongly affected by supergene processes and primarily reflects Neogene structural permeability in the intersection zone between the Rosario and Lulu faults. Lithological boundaries and fault linework is based primarily on pre-mining 1:2,000 mapping of Masterman et al. (2005). The distribution of the mapping areas was restricted as the phase 1 cut back of the SW wall was in progress at the time of mapping. Stereonets are equal area projections of poles to planes, weighted for vein width, and contoured at 2, 4, 8, and 16% in most cases. Rose diagrams were constructed using only orientations with inclination >45º, weighted for vein width and Terzaghi corrected using a minimum angle of divergence from the mapping section of 20º in most cases. Plots for non-linear bench segments were constructed with greater allowance for the angular difference.

4.53).

Potassic alteration and early stage veinlets (A2, A3 veins). A series of early quartz-rich veinlets accompany secondary biotite and K-feldspar alteration that affects the Rosario porphyry and surrounding wallrocks to a maximum distance of ~500 m outboard of the intrusive margins (Fig. 4.54). These veins and the associated alteration contain hypogene chalcopyrite and lesser bornite that account for 40-50% of the Cu budget of the Rosario deposit (Masterman et al., 2005). In the upper levels of the open pit mine, above the carapace of the Rosario porphyry, the A2 and A3 vein generations are well developed. They are easily distinguished because A3 veins are dominated by sub-saccharoidal grey quartz and K-feldspar, whereas A2 veins are narrow, and have more complex fill mineralogy surrounded by pronounced biotite-bearing haloes (Fig 4.55b).

The orientations of early stage veins were mapped in four sections of the phase 1 open pit. Although locally discordant (e.g., Fig 4.55b), the global populations of A2 and A3 veins are indistinguishable and both types of veins most commonly strike NNW and dip steeply eastward (Fig. 4.56). In the SE inner map section a subset of these veins strikes NNE, and in the inner NW sector a subset strikes ENE. Moderately SW dipping veins sympathetic to the Rosario fault and associated late stage veins are rare and were only observed in the immediate area of this structure. The small number of data collected in an exploration drive by Lee (1994) and published in Masterman et al. (2005) therefore appear to record this local sub-population. Sparse early veins in the outer SW map sections also strike NNW, and appear to rule out a radial array centred on the Rosario porphyry (Fig. 4.56). Overall, the early vein stages mapped in the upper parts of the Rosario deposit record WSW-directed dilation.

Epidote-rich veins and alteration assemblages. Epidote-rich alteration assemblages occur intermittently over an area of ~15km^2 outboard of the main stockwork mineralisation at Rosario (Fig. 4.57). Epidote is principally restricted to zones of high fracture density or framework permeability among fragmental or strongly vesicular lithologies. Alteration dominated by chlorite and minor calcite, and lacking epidote, occurs commonly in less permeable domains within the epidote zone. Epidote-poor chlorite alteration also occurs and as a narrow peripheral zone outboard

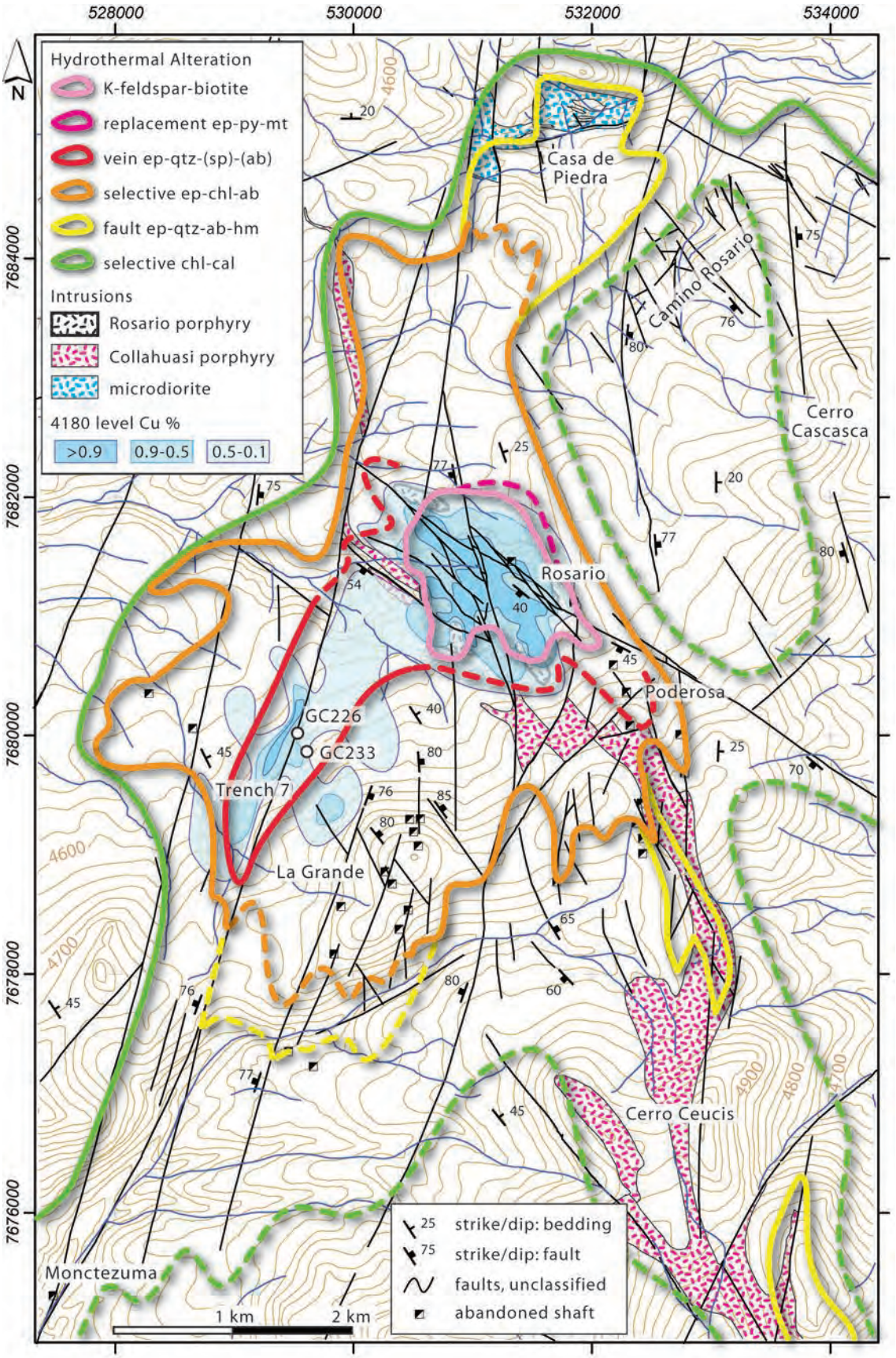

Figure 4.57. Map of the central Collahuasi district showing the lateral distribution of early hydrothermal alteration. Dashed lines indicate approximate positions. Alteration domains depict a combination of surface occurrences mapped in this study and alteration occurrences recorded in the CMDIC exploration drilling database (typically <350 m below surface). At the scale of mapping, the effective Z-axis compression is assumed to not grossly affect the map pattern. Abbreviations as Fig 4.57, and sp=sphalerite, ab = Na-feldspar, chl = chlorite, cal = calcite.

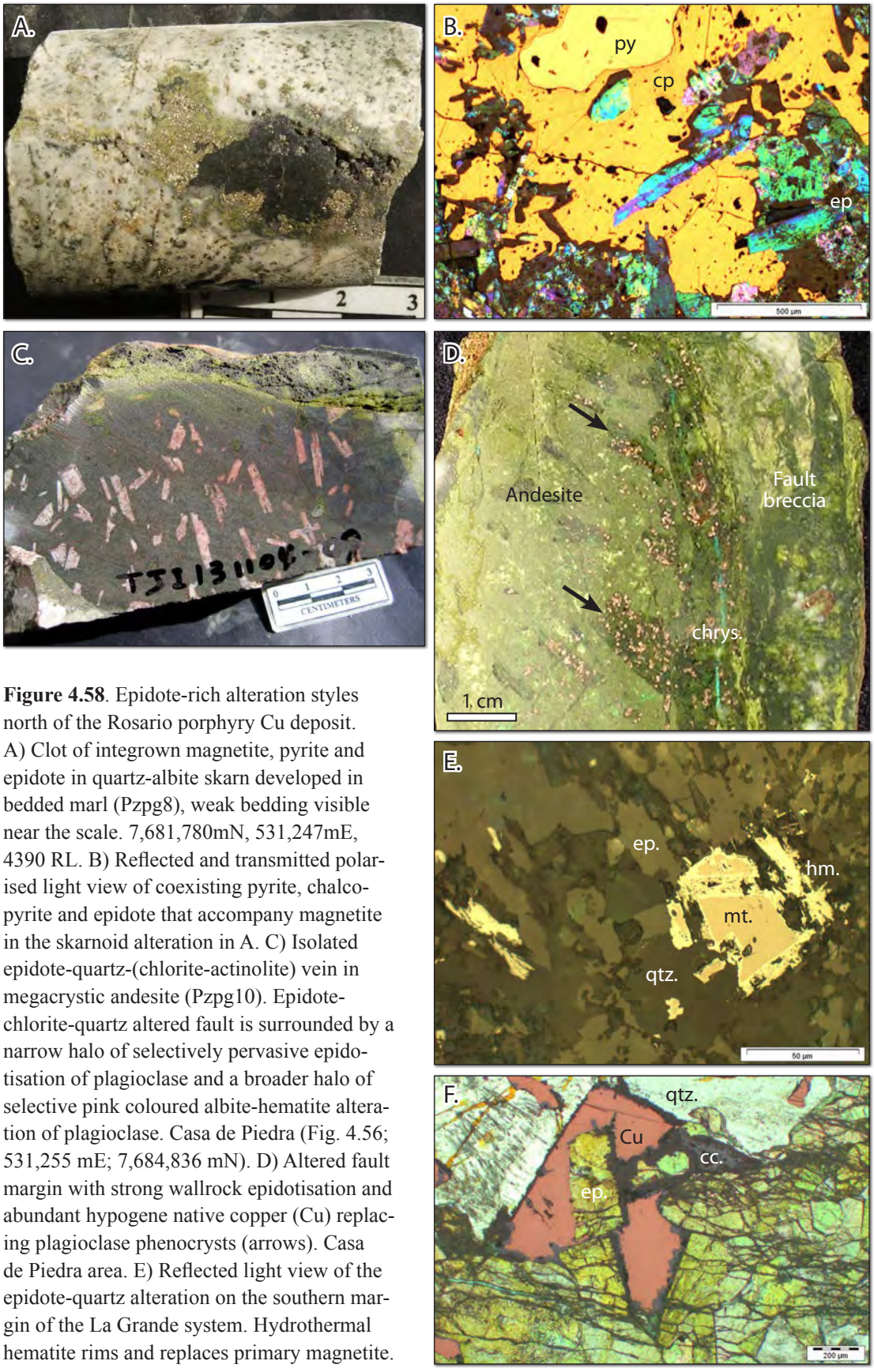

Figure 4.58. Epidote-rich alteration styles north of the Rosario porphyry Cu deposit. A) Clot of integrown magnetite, pyrite and epidote in quartz-albite skarn developed in bedded marl (Pzpg8), weak bedding visible near the scale. 7,681,780mN, 531,247mE, 4390 RL. B) Reflected and transmitted polarised light view of coexisting pyrite, chalcopyrite and epidote that accompany magnetite in the skarnoid alteration in A. C) Isolated epidote-quartz-(chlorite-actinolite) vein in megacrystic andesite (Pzpg10). Epidote-chlorite-quartz altered fault is surrounded by a narrow halo of selectively pervasive epidotisation of plagioclase and a broader halo of selective pink coloured albite-hematite alteration of plagioclase. Casa de Piedra (Fig. 4.56; 531,255 mE; 7,684,836 mN). D) Altered fault margin with strong wallrock epidotisation and abundant hypogene native copper (Cu) replacing plagioclase phenocrysts (arrows). Casa de Piedra area. E) Reflected light view of the epidote-quartz alteration on the southern margin of the La Grande system. Hydrothermal hematite rims and replaces primary magnetite. DDH CC211, 122.0 m. F) Reflected-transmitted light microscopic view of sample in D. Native copper fills interstices between quartz (qtz) and epidote (ep) crystals and is partly altered to chalcocite (cc) along grain boundaries. Chlorite occurs as very fine crystal inclusions in quartz. Supergene chrysocolla fills late fractures in the fault zone.

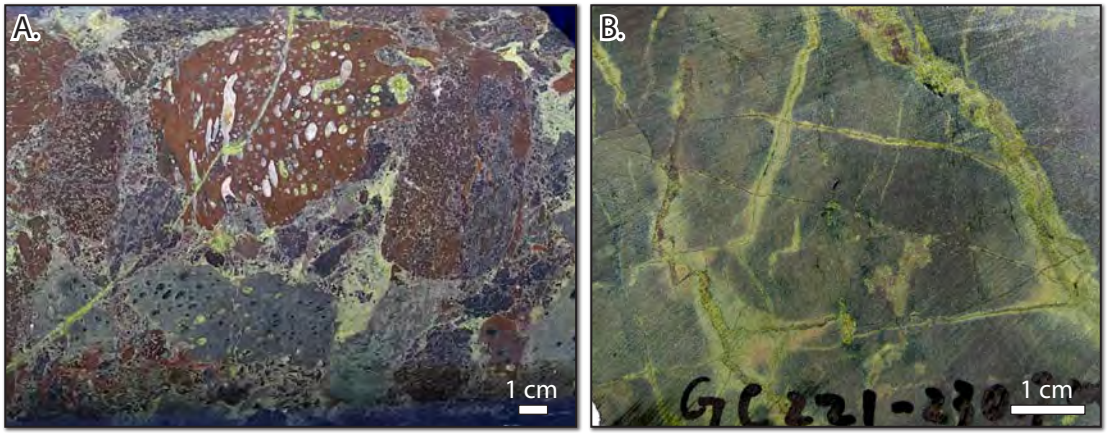

Figure 4.59. Epidote-rich alteration and veining from the main La Grande vein zone. A) Epidote-altered andesite breccia from La Grande showing the principle modes of epidote occurrence in the La Grande andesites (Pzpg13): fragmental rock cement; vesicle fill; and fracture fill. DDH GC217, 270 m. B) Stockwork of epidote veinlets in weakly amphibole-phyric andesite, GC221, 230 m. Brown sphalerite accompanies epidote in the veins, and there are irregular bleached Na-feldspar alteration halos and amphibole-selective chloritisation in the andesite.

of the epidote zone (Fig. 4.57) The overall epidote zone is wedge-shaped, extending along the eastern side of the Monctezuma Fault and flaring to encompass Rosario and Cerro La Grande. The outermost occurrences of epidote are approximately four kilometres outboard of the potassic alteration related to the Rosario stockwork.

The style of occurrence and mineral assemblages that accompany epidote are coarsely zoned around the Rosario porphyry and La Grande epithermal veins. The innermost style comprises skarnoid alteration developed in calcareous siltstone immediately adjacent to potassic alteration on the northeastern side of Rosario (Fig. 4.57). This alteration occurs as grey-white quartz and calc-silicate replacement of the sedimentary rocks, cut by epidote-magnetite-pyrite-(chalcopyrite) veins, clots and irregular replacements (Fig. 4.58 A and B). Carbonate-poor host rocks in this vicinity are cut by veinlet stockworks with the same mineralogy but surrounded by haloes of biotite-chlorite alteration. This is interpreted to reflect continuity between the potassic and skarnoid alteration assemblages.

The outermost style of epidote alteration comprises discrete fault-fill and wallrock alteration and occurs principally in the Casa de Piedra area north of Rosario (Fig. 4.57). Similar occurrences were mapped by Fedorowich (2001) along faults intersecting the Collahuasi porphyry SSE of Rosario. These peripheral occurrences are characterised by massive pervasive quartz-epidote-(chlorite) replacement and

cementation of fault breccias, with narrow haloes of selectively pervasive epidotisation of wallrock plagioclase (Fig. 4.58c, d). These are surrounded by broader haloes of plagioclase-selective albitisation that commonly has pink, orange or red colouration caused by fine grained hematite (Fig. 4.58c). Coarse grained crystalline hematite also occurs as a wallrock alteration phase in this zone, typically as replacements of magnetite (Fig. 4.58e). Rarely, this outer epidote-rich assemblage includes native copper. No relicts of earlier copper minerals were observed, and native copper is altered to chalcocite and chrysocolla along grain boundaries and fractures (Fig. 4.58f). It appears therefore that native copper is a rare primary component of this most distal, oxidised epidote-rich assemblage.

Medial positions within the epidote zone include fracture- and amydule-fillings, and breccia-cementation by epidote, quartz and chlorite (Fig. 4.59b). There is a rough increase in fracture-hosted epidote toward both the Rosario and La Grande mineralisation, analogous to that described in detail by Haynes and Titley (1980) for fracturing about the Sierrita porphyry copper deposit, Arizona. At La Grande, the abundance of epidote increases irregularly both with depth and with proximity to major fault zones over distances of up to a kilometre. Within 100-200 metres of some major faults, epidote occurs as irregular stockworks and conjugate vein arrays in which it is associated with irregular haloes of pervasive wallrock Na-plagioclase alteration, and minor crystalline sphalerite (Fig. 4.59 B). Although many fault zones in the area host polymetallic sulfide-rich veins, these do not systematically have epidote stockworks in their immediate wallrocks. Likewise, some epidote-albite-sphalerite stockwork zones are not adjacent to major epithermal veins.

The zonation of epidote alteration facies about the Rosario porphyry centre and the La Grande veins can be interpreted to reflect either one, or two stages of epidote formation. The skarnoid and distal oxidised assemblages are unequivocally interpreted to have formed during main stage porphyry mineralisation at Rosario (Fig. 4.54). The timing of the stockwork-style epidote-quartz-Na plagioclase-(sphalerite) assemblage is less clear. Fluid inclusions suggest that the temperature of formation of the late epithermal veins were permissive of epidote formation (Masterman et al., 2005). During this study, this assemblage was observed only in the central-northern La Grande area, although this may in part reflect more detailed investigation and

greater drill coverage in this area. The assemblage is anticipated to occur along other major faults that are inferred to have controlled hydrothermal alteration, as depicted in Figure 4.57. Importantly, epidote veins have not been observed cutting early or intermediate stage veins anywhere in the system during this study, nor reported in any previous study. The apparent, approximate spatial association between epidote-Na

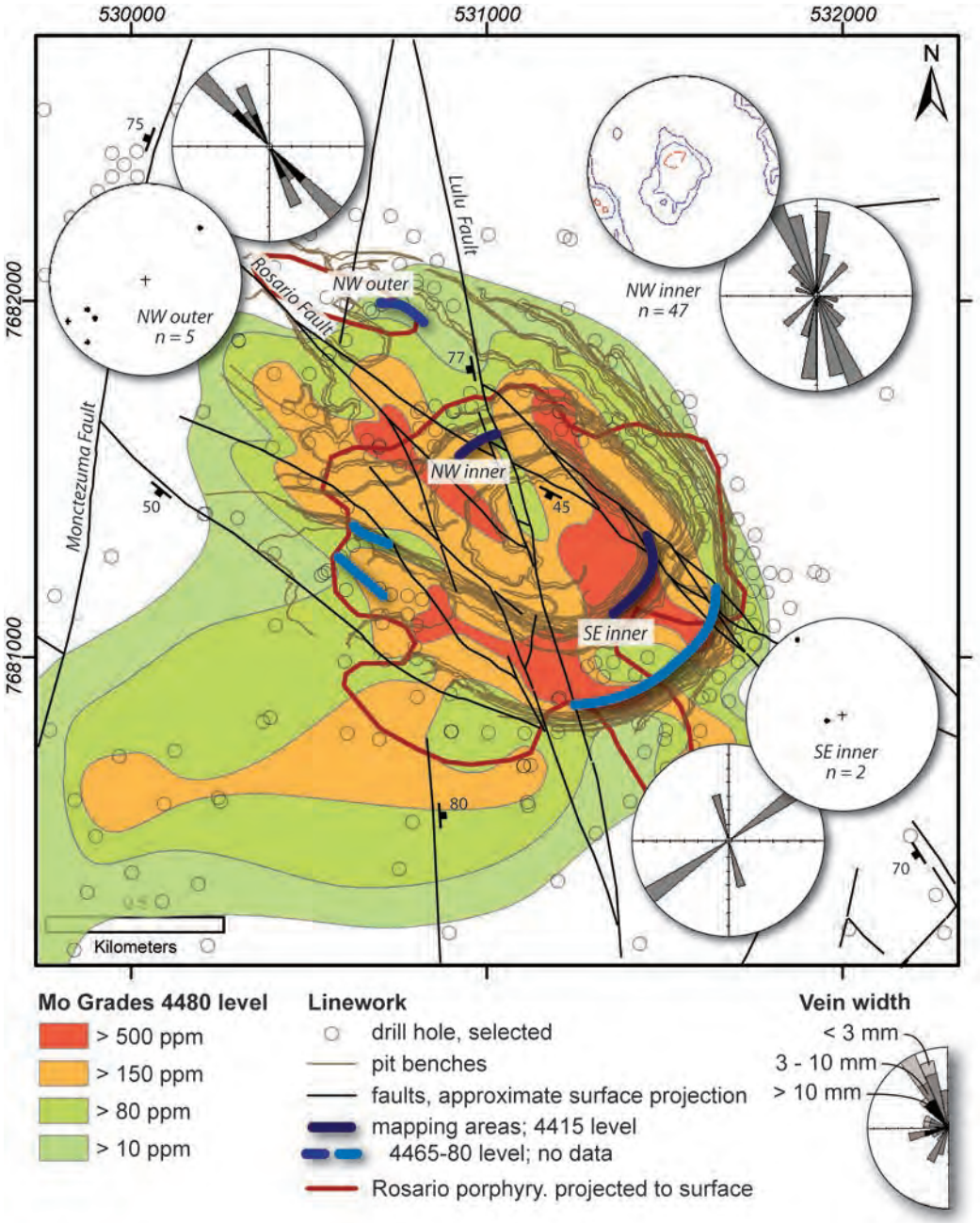

Figure 4.59. Map of the Rosario open pit showing new 4415-4480 level structural data for intermediate stage quartz-Mo veins and the Mo grade distribution for the 4180 level of the mine (CMDIC grade data). The grade distribution shown depicts a level ~300 m below the mapped benches as shallower data were not available. Structural linework, distribution of the mapping areas, and method of rose diagram construction are as per Figure 4.56. Stereonets are equal area projections of poles to planes, weighted for vein width, and contoured at 2, 4 and 8 %.

feldspar stockworks and late polymetallic veins is therefore interpreted as an over-printing, rather than genetic relationship that reflects re-use of the same permeable zones. This interpretation implies that the Na-feldspar-rich, sphalerite-bearing epidote facies might also have formed in medial positions relative to the Rosario porphyry, in other high strain, high fluid-flow zones during early stage mineralisation.

Intermediate stage veins (B- and C- veins). Continuous, planar veins composed primarily of grey-white quartz and molybdenite-rich bands and/or selvedges represent a discrete episode of hydrothermal precipitation at Rosario. These veins, referred to as B-veins (Lee, 1994; Bisso et al., 1998; Masterman et al., 2005) account for most of the molybdenum budget of the deposit. They occur primarily in the Rosario porphyry and in the immediate 100-200 m of wallrock (Fig. 4.54), as is reflected in the paucity of these veins in the outer mapping sections investigated in this study. However, similar veins are observed at depth in several drillholes between Rosario and Cerro La Grande (notably C526A), perhaps inferring that hydrothermal continuity betwen the two was established during intermediate stage vein formation.

A second, paragenetically later group of intermediate stage veins was described by Masterman et al. (2005) and termed C veins (Fig. 4.54). Like B-veins, these are also quartz rich and have some internal banding. They lack molybdenite, but have a central infill of pyrite and chalcopyrite. They have alteration haloes of chlorite and minor illite that are best developed in biotitic host rocks (Masterman et al., 2005). A small number of B veins also have a central pyritic seam and weak haloes of muscovite developed in the Rosario porphyry. This is interpreted to reflect some degree of transition between the formation of B and C veins. C veins are extremely rare in the Rosario open pit at the levels mapped here, but the small number identified have been treated together with populations of B veins.

At the levels of active mining during field work for this study, intermediate stage veins were principally encountered in the inner NW map segment (Fig. 4.59). These veins, and a handful mapped in the outer NW segment, occupy an orthogonal array composed of subvertical NNW-striking fractures, and subhorizontal fractures. A small number of moderately SW-dipping intermediate veins mapped by Lee (1994) have not been observed elsewhere in the deposit and appear to record the localised

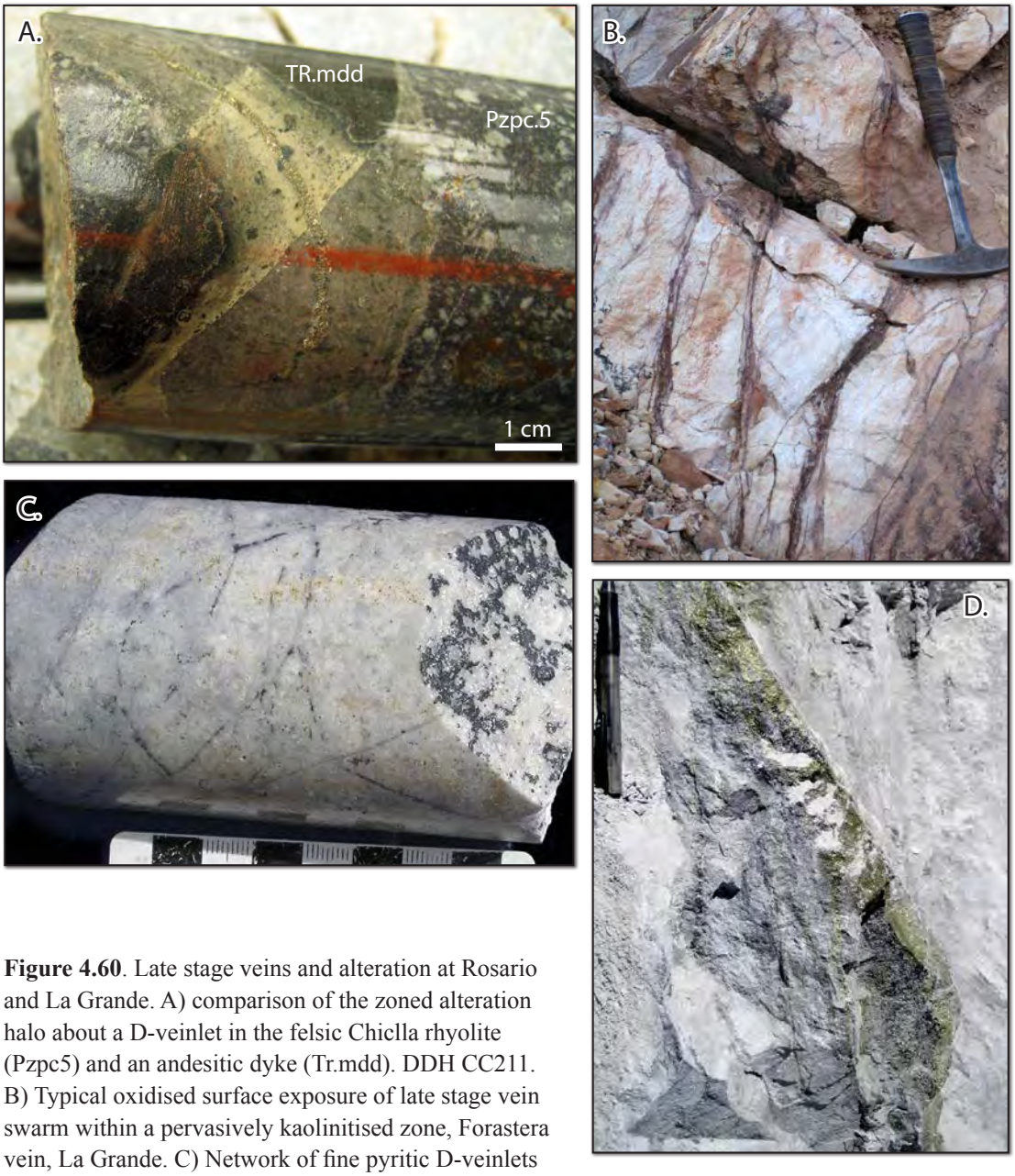

Figure 4.60. Late stage veins and alteration at Rosario and La Grande. A) comparison of the zoned alteration halo about a D-veinlet in the felsic Chiclla rhyolite (Pzpc5) and an andesitic dyke (Tr.mdd). DDH CC211. B) Typical oxidised surface exposure of late stage vein swarm within a pervasively kaolinitised zone, Forastera vein, La Grande. C) Network of fine pyritic D-veinlets with strong supergene chalcocite development, Rosario-La Grande transition zone; DDH C526A, 348 m. D) moderately inclined dilational jog on a subvertical pyrite-chalcopyrite vein with multiple fine subsidiary veinlets in the footwall of the jog, Rosario open pit, approx. 531,150 mE; 7,681,500 mN.

influence of the Rosario Fault. However, at deeper levels in the deposit the distribution of Mo tends to show elongation along strike of the Rosario Fault and associated structures (Fig. 4.59). Post-intermediate stage displacement along the Lulu Fault is inferred by dislocation of the Mo distribution coincident with the position of this structure.

Late stage epithermal veins (D and E veins). Planar and laterally continuous veins of pyrite, with subordinate quartz and chalcopyrite, and prominent muscovite altera-

tion haloes (D veins) dominate the late hydrothermal stages at Rosario and comprise the main stage of veining at La Grande (Masterman et al., 2005). In host rocks with appreciable iron and magnesium, the alteration haloes are zoned from texture-destructive muscovite, through texture-preserving muscovite-chlorite, to marginal chlorite (Fig. 4.60a). Among felsic host rocks the alteration halos are broader and

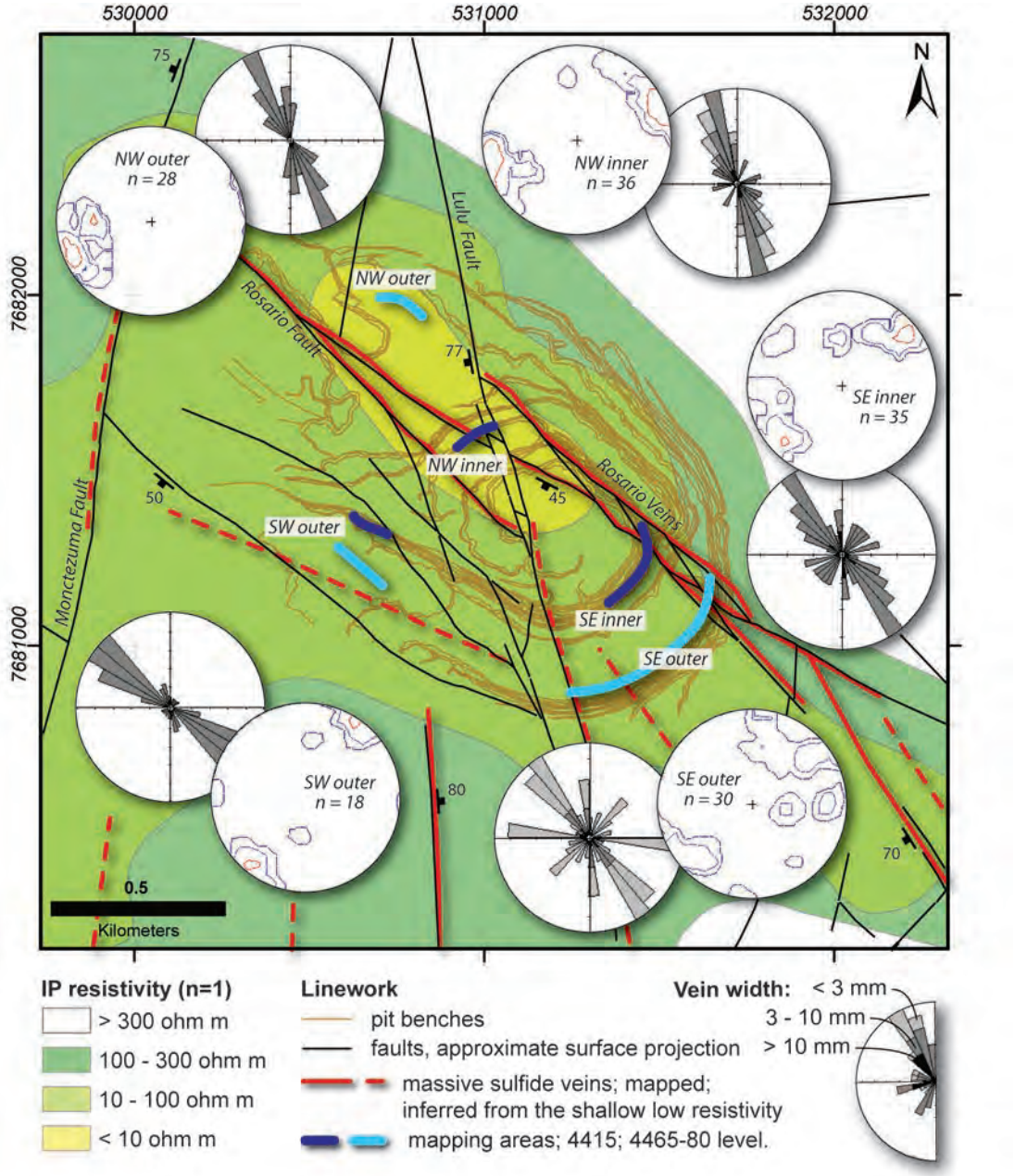

Figure 4.61. Map of the Rosario open pit showing new 4415-4480 level structural data for late stage pyrite-chalcopyrite veins. Background image is N=1 resistivity and the Mo grade distribution for the 4180 level of the mine (CMDIC grade data). The grade distribution shown depicts a level ~300 m below the mapped benches as shallower data were not available. Structural linework, distribution of the mapping areas, and method of rose diagram construction are as per Figure 4.56. Stereonets are equal area projections of poles to planes, weighted for vein width, and contoured at 2, 4 and 8 %.

comprise texture-preserving pervasive muscovite with a narrow peripheral illite zone. At surface, D-veins manifest as swarms of gossanous iron oxide veinlets hosted in pervasively kaolinitised rock (Fig. 4.60b). Kaolinite is much more abundant at oxidised shallow levels than at unweathered deeper levels suggesting that much of it is supergene in origin. Around 4200 m elevation, secondary chalcocite mineralisation is strongly developed at both Rosario and La Grande, wherein D veins served as the principal site of chalcocite precipitation (Fig. 4.60c). Nonetheless, kaolinite crystallinity increases toward the veins exposed in trenches at La Grande (C. Deyell, unpublished data), implying that some kaolinite is likely to be part of the high level hypogene assemblage.

Pyritic late stage veins are widespread in the upper levels of the Rosario deposit and were mapped in all of the pit wall segments investigated (Fig. 4.61). Oxidised veins interpreted to have originally contained more sulfides than gangue were mapped as late stage veins. The broadest vein segments are characteristically short dilational segments that have shallow dips compared to the longer adjacent vein segments (Fig. 4.60d). In the inner and outer NW map segments, D-veins tend to strike NNW and are either subvertical or steeply E-dipping (Fig. 5.60). In contrast, in the other three map segments they tend to strike NW and occupy a steeply and subordinate moderately dipping orientations toward both NE and SW (Fig. 5.60). These orientations are similar with those measured by Lee (1994) and presented in Masterman et al. (2005), except that those authors report a slightly greater proportion of moderately dipping orientations consistent with the focus of their mapping near the Rosario Fault. In general, late stage veins at Rosario show a strong degree of structural inheritance, preferentially occupying orientations sympathetic or conjugate to faults in the same sections. However, veins inclined as shallowly as the Rosario Fault (~45º) are rare. Instead, the commonest inclination of late stage veins at Rosario is ~72º. On the 4415 level (inner pit map segments), veins measured during this study within the deformation zone related to the Rosario Fault primarily dip steeply and are laterally discontinuous. The Rosario “Vein” therefore may instead be an en echelon series of steeply inclined vein segments developed within the broader Rosario fault zone.

Polymetallic massive sulfide veins composed largely of pyrite, chalcopyrite, bornite,

tennantite and enargite (E veins) overprint and commonly re-open earlier D veins. These veins include variable amounts of gangue, up to 40 volume percent quartz, as well as lesser alunite, diaspore and zunyite (mineralogy of Masterman et al., 2005). The veins occur infrequently as infill of major structures and associated splays. They pinch and swell, locally attaining widths of up to 15 metres, and in some cases disappear completely over vertical intervals of less than 150 of metres. They occupy the Rosario Fault zone and transect the main body of stockwork mineralisation (Munchmeyer et al., 1984; Lee, 1994; Bisso et al., 1998; Masterman et al., 2005). Structures hosting polymetallic veins have strong texturally destructive alteration envelopes up to 15 metres wide, dominated by pyrophyllite, dickite and alunite. This assemblage is zoned outward through muscovite to a marginal illite-smectite assemblage (mineralogy of Masterman et al., 2005). Together, late stage D and E veins contribute 40-50% of the Cu budget of the upper levels of the Rosario porphyry (Masterman et al., 2005). They are inferred to have contributed almost all the copper concentrated in the main supergene enrichment at La Grande ("Rosario Oeste" ~248 mT @ 1.48% Cu: www.xstrata.com), as no other high level mineralisation is known in this area. Assuming the line-kilometre extent of eroded late polymetallic veins (Fig. 4.62) was comparable to the remaining extent, this equates to ~300 metres vertical extent of mineralisation above the present land surface, and therefore total pre-erosion vertical extent of ~700 metres.

At surface, polymetallic veins typically manifest as structurally disrupted alteration zones containing gossans rich in iron oxides, and which locally carry secondary copper-arsenic minerals (Fig. 4.63a). Chenevixite, the copper analogue of scorodite, is common in the major vein zones and occurs as arborescent yellow-green boxworks interpreted to have replaced primary enargite (Fig. 4.63b). Olivenite occurs as grey-green bladed crystals lining vughs (Fig. 4.63c) in which it overgrows chenevixite. A late stage of very fine, hair-like olivenite also occurs locally. Rarely, the immediate wallrocks to the veins contain fracture-fillings of radiating dark blue-green clinoclase and globular dark green cornwallite (Figs. 4.63d, e). These overgrow early coarse grained olivenite. Chryscolla locally pseudomorphs the copper arsenates (Fig. 4.63f). The oxide paragenesis suggests initial neutralisation of an acidic groundwater, followed by depletion of the dissolved Cu budget (Fig. 4.64). In the presence of

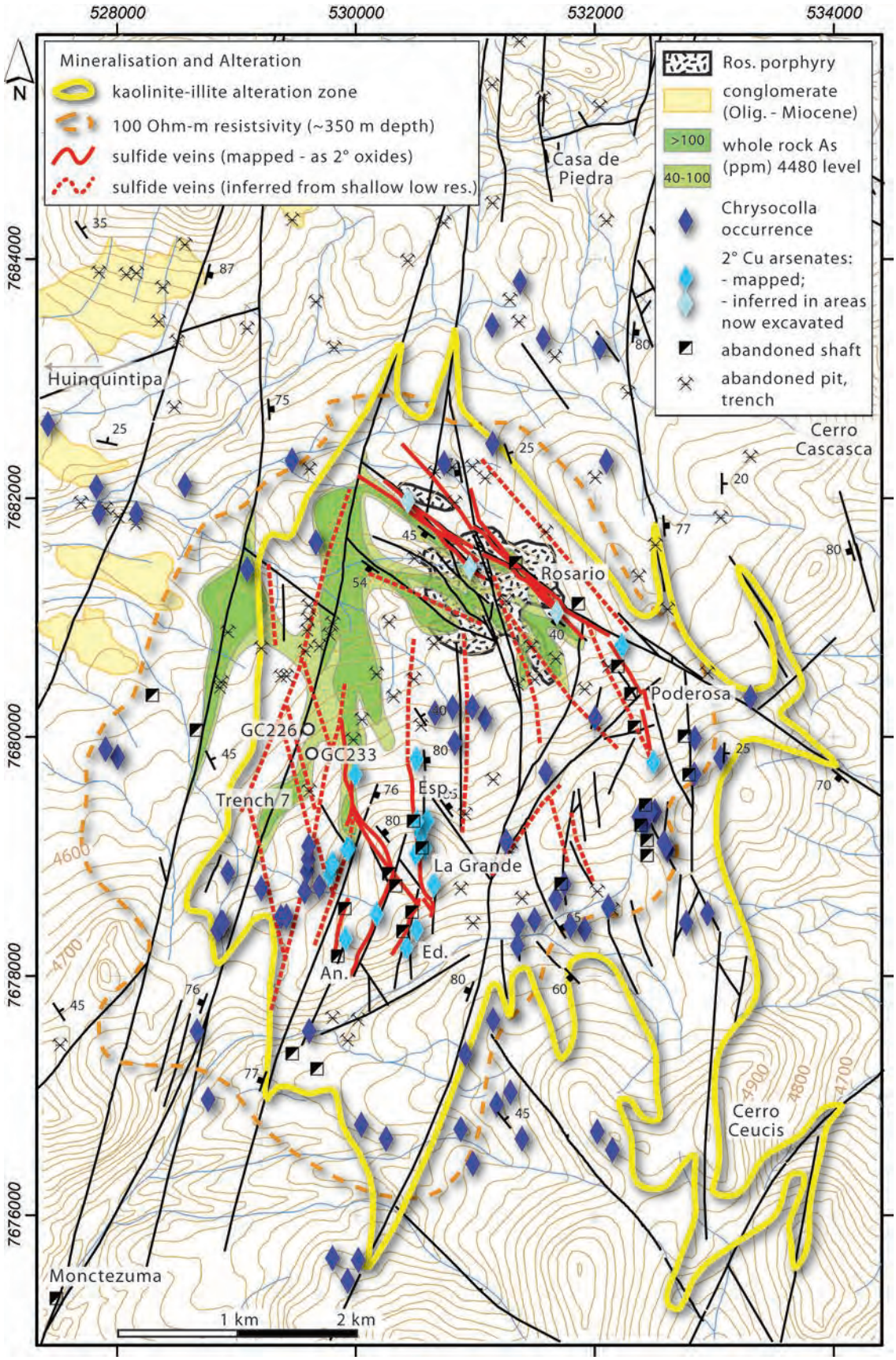

Figure 4.62 Distribution of elements of the late stage pyritic-polymetallic vein mineralisation at Rosario-La Grande; mapped and interpreted vein positions; white phyllosilicate alteration; surface occurrences of secondary Cu minerals; 4180 level As distribution based on exploration drilling; and shallow low resistivity anomaly. Neogene conglomerates in the northwestern map area are the easternmost Huinquintipa gravels that host significant chrysocolla-rich exotic Cu mineralisation.

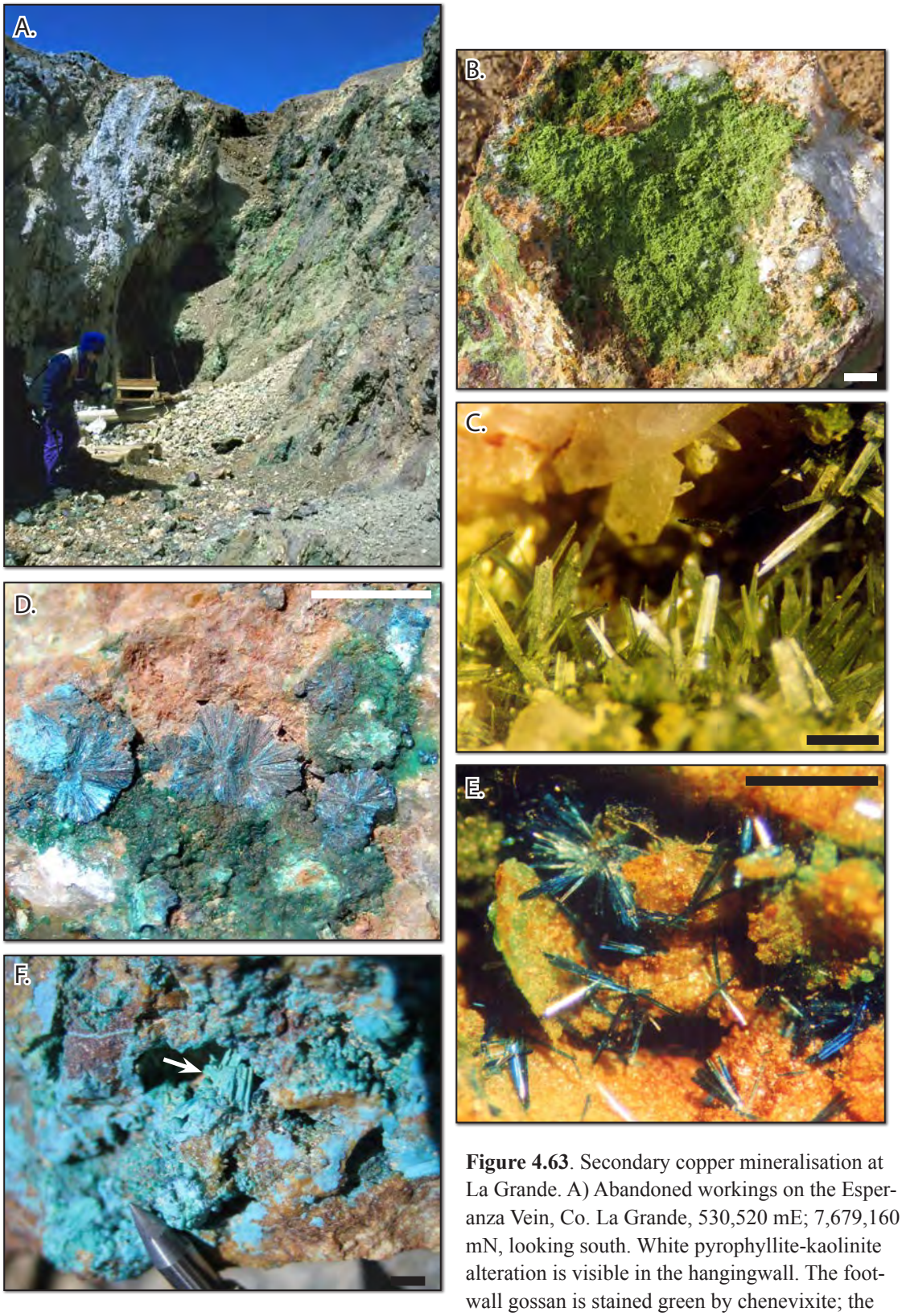

Figure 4.63. Secondary copper mineralisation at La Grande. A) Abandoned workings on the Esperanza Vein, Co. La Grande, 530,520 mE; 7,679,160 mN, looking south. White pyrophyllite-kaolinite alteration is visible in the hangingwall. The footwall gossan is stained green by chenevixite; the Cu-analogue of scorodite. B) Chenevixite boxwork lining a cavity after pyrite and enargite; Don Eduardo workings. C) Characteristic sword-shaped crystals of olivenite in a quartz-dominated vein from the Anita Vein workings. D-E) Hand specimen and microscopic detail of coexisting radiating and acicular bladed dark aqua-blue clinoclase, and globular green cornwallite occurring as fracture fillings in gossanous wallrocks to the Don Eduardo vein. F) Gossan sample with abundant botryoidal chrysocolla and a well preserved pseudomorph after clinoclase (arrow). All close-up photos are from the vicinity of 530,380 mE; 7678030 mN. Black bars are 1 mm, white bars are 1 cm. Mineral formulae are given in Figure 4.64.

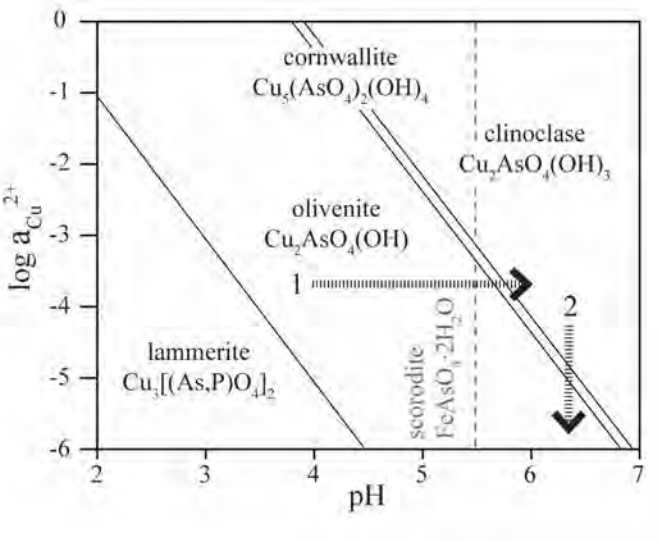

Figure 4.64. Phase diagram for the system Cu-As-O-H at atmospheric conditions (Magalhaes et al., 1988). The limit of the stability field for scorodite in the system Fe-As-O-H-S at 25ºC, ρ = 1 atmosphere and ΣAs = ΣFe = ΣS = 10^{-6} *m* is shown as a dashed line (Vink, 1995). At moderate to high Fe activity this stability field is anticipated to approximate the stability of the Cu analog chenevixite. Dashed lines indicate the likely reaction paths (1, 2) followed by oxide-zone groundwaters at La Grande.

phosphorus or calcium, an equally distinctive suite of largely endogenous secondary minerals (P: libethenite, pseudomalachite, cornetite; Ca: conichalcite) would have been stable under similar physical conditions (Magalhaes et al. 1988).

The distribution of these uncommon copper arsenates is closely related to the distribution of polymetallic veins at surface. Their occurrence was used in the field to distinguish D and E veins mapped at surface. At 4180 metres elevation, ~350 m lower than the surface at Rosario and ~650 m lower than outcropping veins at La Grande, arsenic is concentrated along the Monctezuma Fault, near the intersection with the Rosario Fault (Fig. 4.62). In contrast, chrysocolla, a hydrous copper silicate, occurs very commonly as an exogenous fracture coatings and clastic rock cement over an area of ~40 km^2. Its distribution is roughly coincident with the zones of mapped kaolinite-illite alteration and the distribution of this alteration inferred from anomalously low resistivity (Fig. 4.62). Neither the Rosario porphyry nor the main La Grande vein mineralisation is centred within this broad, hybrid hypogene-supergene phyllosilicate alteration zone.

Orientations of polymetallic veins were mapped in the Rosario open pit, and at surface and in oriented drillholes GC223 and 226 at La Grande (Fig. 4.62). These veins tend to strike approximately N, or NW, and dip steeply (Figs. 4.62 and 4.65). A similar array is described by D-veins mapped in the La Grande area (Fig. 4.65). Late stage veins at both La Grande and Rosario record WSW-directed dilation. However, the array of major veins or alteration zones inferred from the positions of narrow, shallow low resistivity zones (T.Whenlan, Falconbridge Ltd, unpublished

data) reveal that NW striking veins are typically linking structures between laterally continuous meridional veins (Fig. 4.62). This relationship is interpreted to suggest vein formation during accommodation of sinistral wrench strain through the central Collahuasi district (Fig. 4.65).

4.9.3 Structural Controls on the Rosario-La Grande deposits: Interpretation.

The syn-mineralisation kinematic scenario indicated by fault measurements across the central Collahuasi district indicate a progression from syn-early stage WSW-directed extension to syn-late stage sinistral wrench deformation along a shear couple involving the eastern Monctezuma, southern Lulu and western Rosario faults (Fig. 4.53). The geometry of vein stages that comprise both the Rosario porphyry-related stockwork and the La Grande epithermal vein arrays are consistent with this interpretation. Veins of all generations show a strong tendency for NNW or NW-trending orientations. This, and the persistence of the similar deformation history on syn-mineralisation fault arrays throughout the central part of the district, imply a strong contribution of regional tectonic stresses to the mineralisation environment. There is no sense of radial or concentric arrays that might indicate dominance of intrusion-related or hydrothermal forces among any of the vein generations (Figs. 4.56, 4.59, 4.61, and 4.62).

Uniquely at Rosario, early epidote-rich veins describe a suborthogonal array of NNW and ENE-trending, steeply-dipping veins. Late dykes at Ujina also trend ENE, and apparently intruded during a period in which stresses related to the tectonic convergence were transmitted into the shallow levels of the crust in the eastern Collahuasi district. This regime may have been in its waning stages during the formation of the earliest epidote-bearing veins at Rosario. Overall, the oblate strain recorded by epidote veins, and the similarity between the orientations of these vein and existing fracture sets (e.g., Fig. 4.51 R2a) is interpreted as evidence of hydraulic dominance of the local stress environment at that time. The Rosario porphyry intruded into the intersection zone between the Triassic Collahuasi porphyry, the Rosario Fault and a strand of the Monctezuma Fault. This location is interpreted to have been a deeply penetrating zone of repeated brittle deformation. Intrusion was likely to have been localised here because of high bulk structural permeability rather

than because of dilation on any individual structure.

The early quartz-Cu sulfide and intermediate vein sets are dominated by steep to subvertical fractures that strike NW. The A2 and A3 veins that introduce at least half the Cu in the system, record prolate WSW-directed dilational strain. Dip-slip movement on faults with the same orientation is anticipated to have occurred at this time. These veins formed from a hypersaline brine under lithostatic pressure (Masterman et al., 2005). If weak ENE-directed horizontal compressive stress persisted following late-stage dyke intrusion at Ujina, then fracturing, faulting and A2-A3 vein formation suggest relaxation of the tectonic stresses, and extension collinear with the generalised tectonic convergence. Intermediate stage veins take similar orientations but include a discrete subset that is subhorizontal. Masterman et

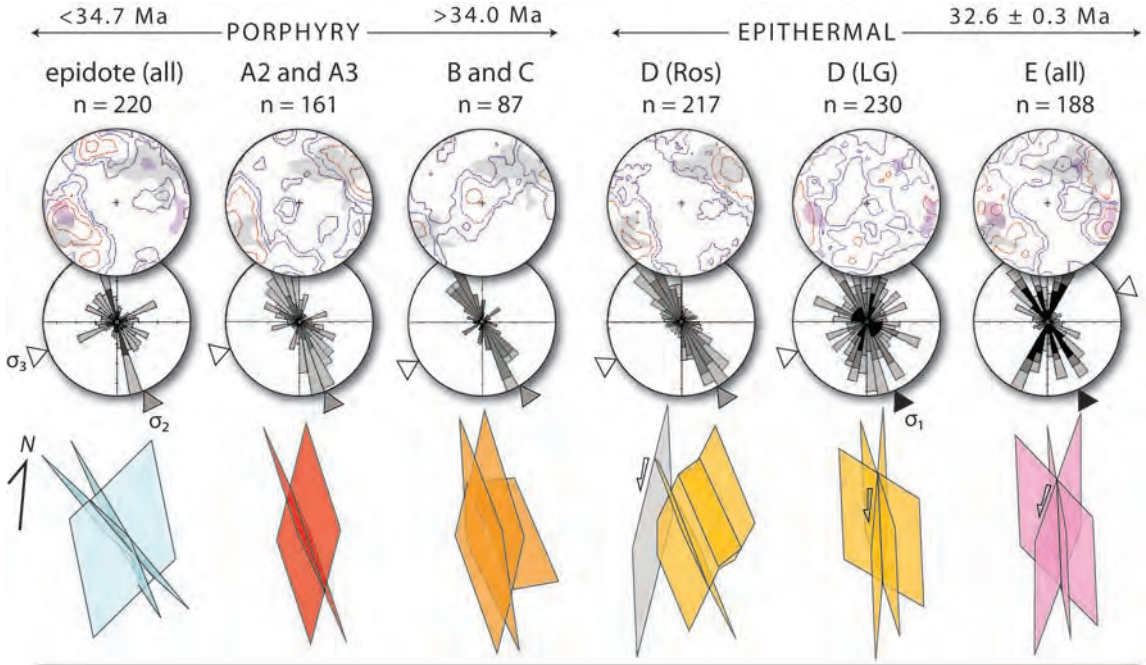

Figure 4.65. Summary of vein orientations at Rosario and La Grande. Lower hemisphere equal area stereographic projections and rose diagrams for global vein populations, arranged in sequence of formation, and showing absolute age limits from Masterman et al. (2004). Structural data includes surface and pit mapping, and measurements made in oriented drillholes GC223 and 226 at La Grande. Compilations incorporate data of Munchmeyer et al. (1984) and Lee (1994). Darker rose segments record structures or comparatively greater width. Coloured schematic diagrams show the principal vein orientations and greyscale traingles indicate the trend of the principal two local stress axes interpreted to be closest to horizontal during formation of stage. Variations in the relative magnitude of the principal stresses can account for differences in vein arrays among the early and intermediate vein arrays. Broadly, emplacement of the Rosario porphyry appears to have occurred during WSW-directed extension. Late stage epithermal mineralisation appears to have accompanied sinistral wrench along the Monctezuma and Lulu Faults, the transition to which might have included hard-linking of the Lulu and Rosario faults and escape of the La Grande block. Method used for interpretation of stress axes as per Figure 4.33.

al. (2005) interpreted boiling of these fluids under hydrostatic pressure based one the coexistence of vapor- and liquid-rich fluid inclusions. The transition to hydrostatic pressure appears to have prompted boiling by depressurisation and permitted hydraulic opening of subhorizontal fractures. Hydraulic forces dominated the tectonic regime at this time.

Late stage D and E veins mineralised major pre-existing NNE- and NW-trending structures related to the Monctezuma and Rosario faults (Fig. 4.65). The intersection between these faults hosts the deepest parts of the late stage vein system, as inferred from whole rock As anomalism (Fig. 4.62). These veins formed under fluctuating hydrostatic and lithostatic pressures at considerably shallower depth than the Rosario porphyry (Masterman et al., 2005). Locally, dilation of shallowly dipping segments implies hydraulic forces that exceeded the lithostatic load. Overall, the veins record WSW-directed dilation, most clearly reflected by the strong preferred NW-NNW orientation of late veins at Rosario. Tectonic unroofing of the Rosario porphyry is proposed to account for the difference in depth of formation between intermediate and late stage veins (Masterman et al., 2005). A scenario is envisaged in which a sinistral shear couple developed by linkage of the southern Lulu Fault with the Rosario and Monctezuma faults. This enabled southward escape of the La Grande block (Fig. 4.53), within which the bulk of the late stage mineralisation and alteration are contained (Fig. 4.62). The D and E vein arrays at La Grande are therefore interpreted to comprise NNE-trending master structures with significant veining along NNW-trending synthetic- and NW-trending antithetic shear fractures. The change from dip-slip to strike slip faulting between the intermediate and late stage stages of mineralisation implies switching of the maximum and intermediate principal stress axes during this time (Fig. 4.65).

4.10 Discussion and Conclusions

4.10.1 Faulting, mineralisation and evolving stress conditions; 45-32 Ma.

The detailed structural mapping presented in this chapter, including investigation of each of the mineral deposits of the Collahuasi district, reveals a complex kinematic history during the period of prolific intrusion-related mineralisation in the Central

Andes. Structural mapping of three well exposed reference localities shows that, especially at Rosario, the deformation recorded in the deposits also affected parts of the district outboard of the hydrothermal systems and away from major district scale faults. The sequence of major brittle deformation stages and contemporaneous hydrothermal activity is depicted in Figure 4.66.

Tectonic convergence between the Nazca and South American plates during the Middle Eocene (Lutetian) was oriented NE (Pardo-Casas and Molnar, 1987; Somoza and Ghidella, 2005). Under this regime, dextral transpressional wrench strain was partitioned along arc-parallel structures, as recorded by the early dextral history of the Domeyko Fault near Chuquicamata (Lindsay et al., 1995; Reutter et al., 1996; Tomlinson and Blanco, 1997a; Amilibia and Skarmeta, 2003). Broadly, the two older porphyry copper deposits in the Collahuasi district formed under tectonically-imparted stress regimes consistent with this tectonic environment. In contrast, Ujina appears to have formed during an environment of very low differential stress, and Rosario formed during WSW-directed extension that evolved into sinistral transtension by the time of formation of the La Grande epithermal system. The geometry of the mineral deposits therefore maps a gross transition from dextral transpression prior to 35.5 Ma, to sinistral transtension after 34 Ma. This change in the sense of along-arc shear is consistent with the results of thermochronology presented in Chapter 5.

In detail, there may have been substantially more dynamism in the regional stress history. The Central Andean margin was compressional at least as early as 45 Ma, the age at which the earliest Incaic unconformities are recorded (Tomlinson et al., 2001a, and references therein). However, at 40 Ma at Collahuasi, the Monctezuma epithermal veins record weak extension and probable minor sinistral shear along the Monctezuma Fault (Fig. 4.66a). The local stress conditions that accompanied vein formation imply a significant reversal of both the sense of arc-parallel wrench shear and the direction of the principal subhorizontal compressive stress. This could not have occurred simply by local dominance of the hydraulic forces related to the hydrothermal system, and instead is interpreted to reflect an episode of relaxation of the tectonically imposed stress field. Across the Collahuasi district the period 44-40 Ma is characteristed by increased magmatic activity; approximately 40% of the

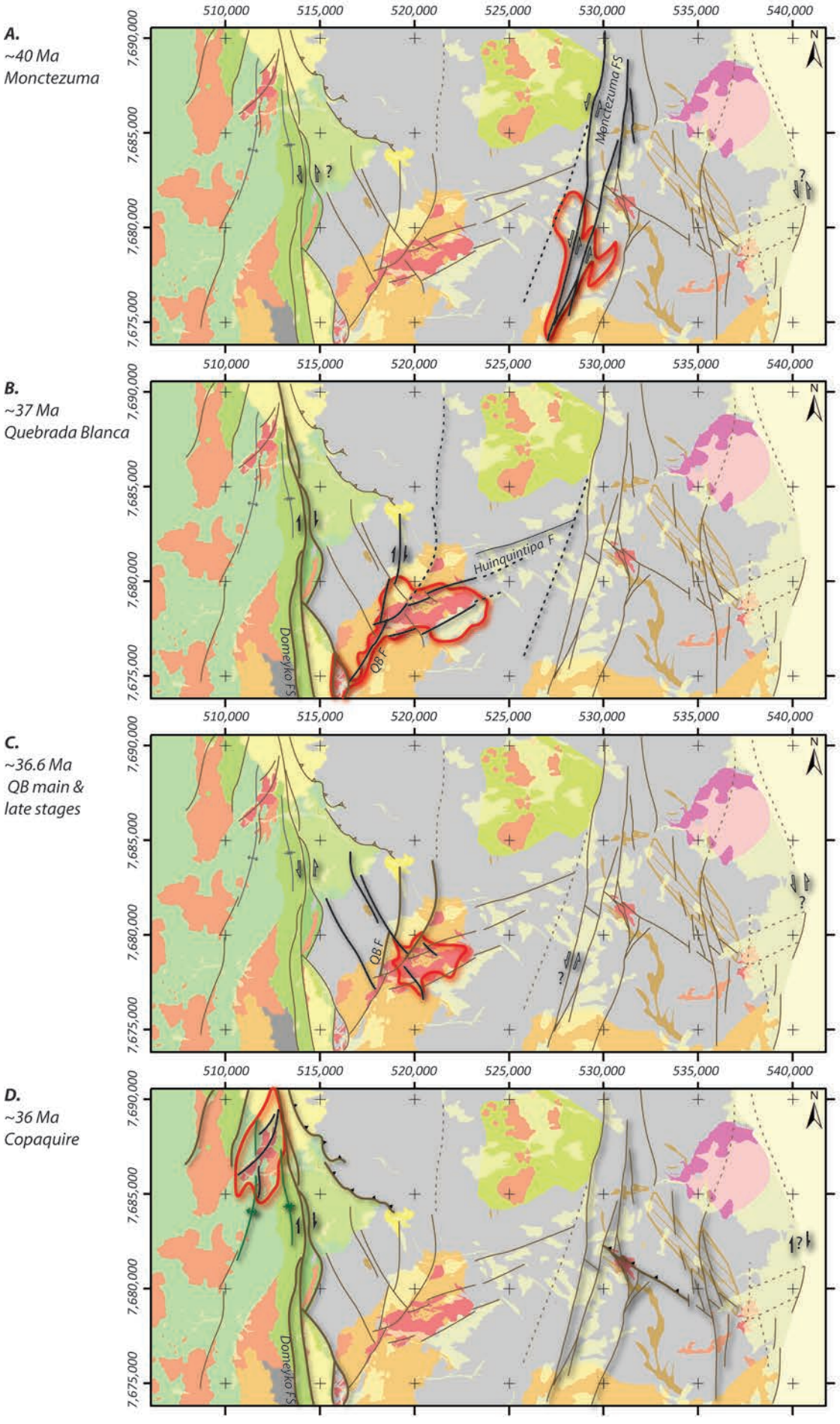
A.
~40 Ma
Monctezuma
B.
~37 Ma
Quebrada Blanca
C.
~36.6 Ma
QB main &
late stages
D.
~36 Ma
Copaquire
510,000
515,000
520,000
525,000
530,000
535,000
540,000
7,690,000
7,685,000
7,680,000
7,675,000
N
Monctezuma FS
Huinquintipa F
QB F
Domeyko FS

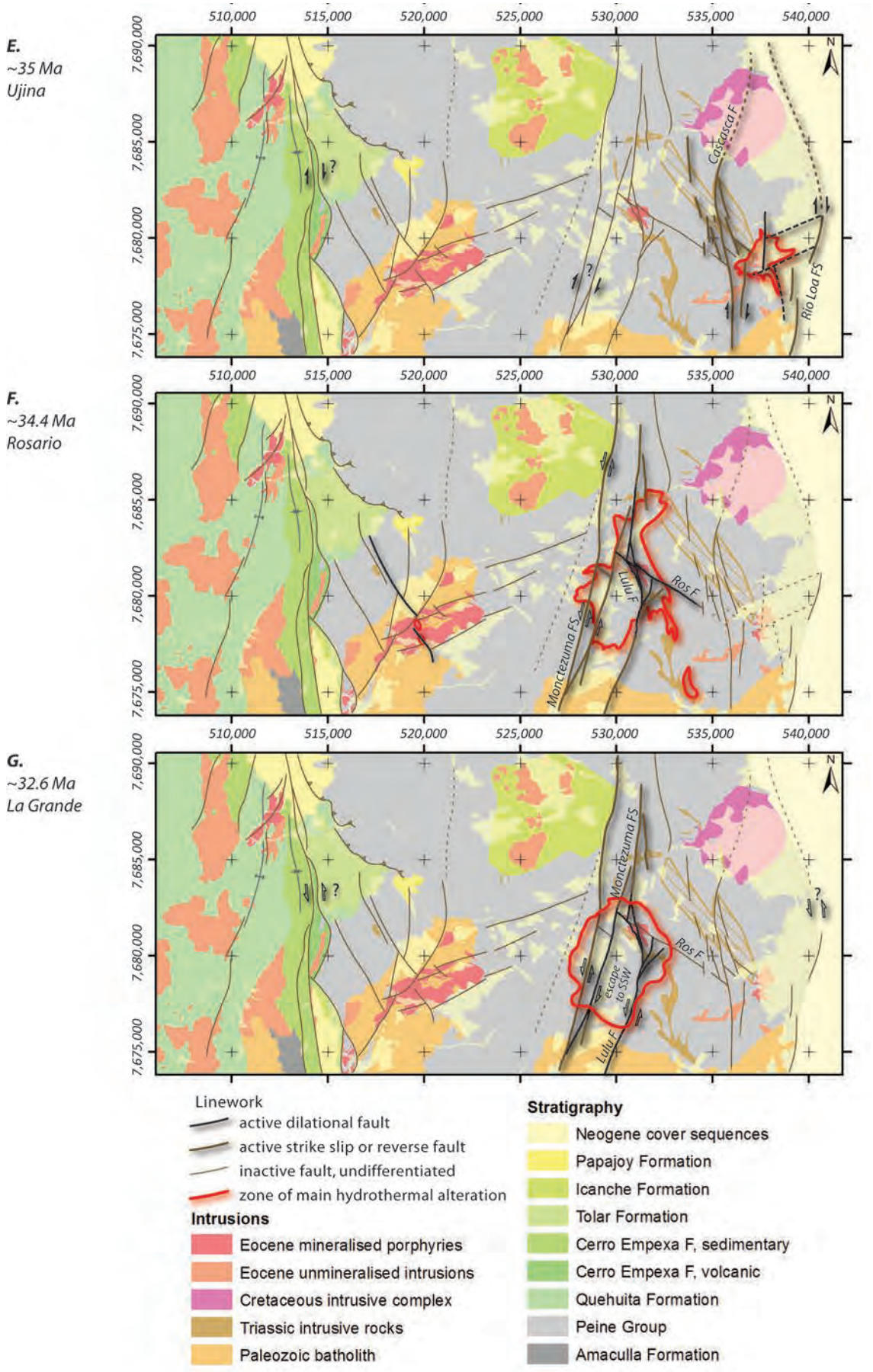

Figure 4.66. Sequential geological maps A-G showing the interpreted distribution and kinematics of active faulting and hydrothermal activity during the main 41 - 32 Ma metallogenic event in the Collahuasi district.

reliable radiometric age data for Paleogene units yield ages in this range (based on 68 ages compiled from Tomlinson et al., 2001; Masterman et al., 2004; this study). The Icanche Formation volcanic complex at Cerro Vega (Fig. 3.19), and related intrusions at Cerro Sallihuinca (Fig. 3.25) also formed at this time (U-Pb geochronology of Tomlinson et al., 2001a; see also Chapter 3). Widespread shallow crustal magmatism and the situation of the Sallihuinca volcano-plutonic complex adjacent to the northern Monctezuma Fault support the interpretation that extension occurred through the Collahuasi district immediately prior to the main compressive phase of the Incaic tectonic event.

Peak compression related to the Incaic tectonic event is accepted to have occurred at around 38.5 Ma and was associated with dextral transpression (e.g., Maksaev and Zentilli, 1990; Tomlinson and Blanco, 1997a). By ~37 Ma dextral wrench occurred along the Domeyko Fault and related splays at Collahuasi (Fig. 4.66b). Intrusions were emplaced into dilational strike-slip shear couples such as that defined by the Quebrada Blanca and Huinquintipa Faults. Shallow vein arrays formed during the earliest stages of mineralisation also imply an overall compressional environment at this time. However, main stage mineralisation accompanied low differential horizontal stresses and possibly even weak WSW-directed extension (Fig. 4.66c). Late stage veining at at Quebrada Blanca also occurred under a broadly extensional environment, speculatively related to gravitational collapse of the Domeyko Cordillera.

Dextral wrench strain was again accommodated along the Domeyko Fault at ~36 Ma during emplacement of the Copaquire intrusive complex. As at Quebrada Blanca, a strike-slip shear couple is interpreted to have permitted intrusion of steep-walled stocks into a generally compressional environment evidenced by abundant subhorizontal fracturing and veining (Fig. 4.66d). Thrusting on a number of NW-trending faults across the district, including the Rosario Fault, may also have occurred at this time, or during peak Incaic deformation (Fig. 4.66d). The dextral wrench environment persisted at least until ~35 Ma, when intrusion and mineralisation stepped inboard into the easternmost Collahuasi district (Fig. 4.66e). The intersection zone between the Cascasca dyke swarm, the Rosario Fault and an ENE-trending fracture zone is interpreted to have localised intrusion at Ujina. Syn- and post-mineralisation dykes occupy the ENE-trending fracture set at Ujina, and are the last evidence of

the far field tectonic stress regime during the fertile epoch in the Collahuasi district. Early and intermediate stages of alteration and veining show pronounced hydraulic dominance of the local stress environment, indicative of overall low differential horizontal stresses. However, there is some suggestion of NNW-directed horizontal stress among chlorite-altered faults and the main stage veins at Ujina (Figs. 4.43 and 4.46).

The NNW-directed horizontal stress stabilised and strengthened, such that at ~34.4 Ma, the youngest and largest mineralised system in the district, Rosario, formed during WSW-directed extension. This environment is recorded by vein and fault arrays in the Rosario deposit and throughout the central part of the district. Early alteration is elongate along the eastern Monctezuma Fault, and implies that this structure was active at the time of mineralisation, implicitly as a sinistral shear (Fig. 4.66f). Renewal of the hydrothermal system at Quebrada Blanca occurred at the same time and also records WSW-directed extension. Emplacement of the mineralised Rosario porphyry was localised in a structurally complex zone at the intersection of the Collahuasi porphyry dyke, the Rosario Fault and the Lulu Fault. At, or prior to ~32.6 Ma, extensional conditions gave way to a pronounced wrench environment indicated by sinistral fault displacement and NW-trending dilational stepovers. The shear couple caused removal of the hangingwall above the Rosario Fault by southward translation of the La Grande block and probably accompanied development of the La Grande epithermal mineralisation (Fig. 4.66g).

4.10.2 Stress conditions during porphyry Cu mineralisation at Collahuasi

At regional scales and at a frequency of 5 - 20 million years, there is commonly a temporal relationship between accelerated tectonic plate convergence, orogenesis and porphyry metallogeny (Nielsen, 1979; Sillitoe, 1988; McKee and Noble, 1989; Maksaev and Zentilli, 1990; Ward, 1991; Kay et al., 1995; Sillitoe, 1998). The above description of the structural geology of each of the main hydrothermal mineral deposits of the Collahuasi district provides some insight into the interplay between tectonics, upper crustal stress conditions, and porphyry mineralisation. Mineralisation took place during the latter stages of, and extending ~5 million years after cessation of the compressive Incaic tectonic phase (44-37 Ma: Perelló and Muller 1984; Clark et al. 1990a; Hammerschmidt et al. 1992; Breitkreuz and Zeil,

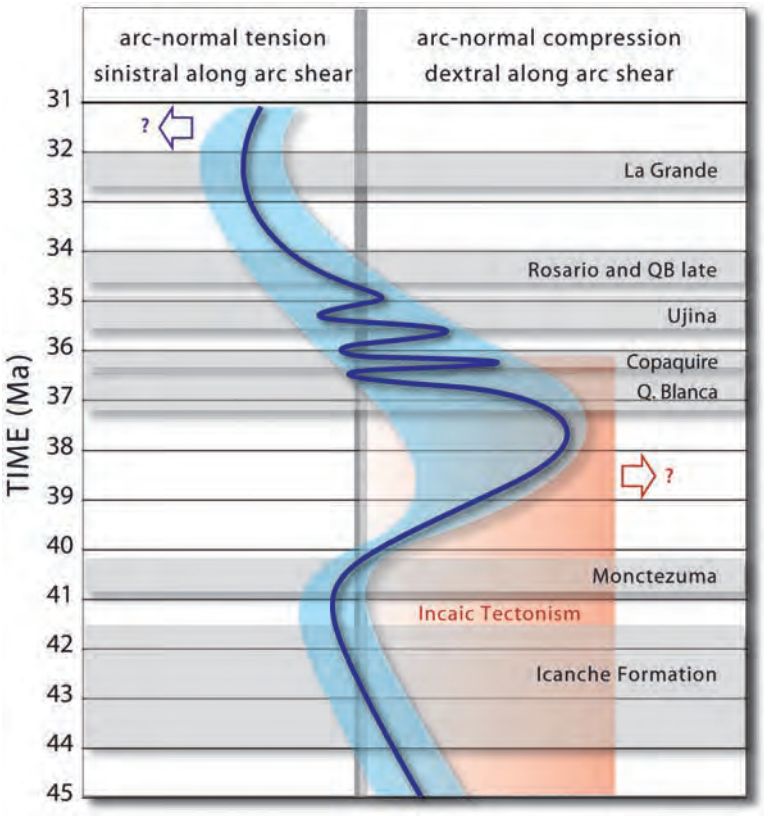

Figure 4.67. Schematic depiction of the temporal variation in the interpreted relative magnitude of subhorizontal stress oriented ENE and NNW, parallel and orthogonal to tectonic convergence, respectively. The time intervals over which mineralisation and magmatism occured are shown at the resolution of current geochronology. Vertical orange bar indicates the period generally referred to as the Incaic tectonic event.

1994; Tomlinson et al. 1994; Cornejo et al. 1997; Tomlinson and Blanco 1997a). A significant magmatic event with only minor associated mineralisation preceeded the main stage of tectonism. Following Incaic tectonism there was an overall reversal in the intra-arc stress environment, from dextral compressional, to sinistral and extensional (Fig. 4.67). The low differential horizontal stresses considered by Tosdal and Richards (2001) to favour porphyry copper mineralisation must have prevailed at Collahuasi during the regional change in the stress environment.

A more aggressive interpretation of the data suggests that the major brittle faults in the district underwent repeated shear reversals during the period from ~45 Ma to ~32 Ma, driven by an apparent oscillation between ENE-directed compression and extension. There was moderate obliquity between the tectonic convergence and the arc front at the time, so this oscillation would also have been associated with reversals of the sense of shear strain partitioned into arc-parallel faults. Negligible differential horizontal stresses may have transiently characterised the local stress environment during formation of each of the major mineral deposits in the district. If this interpreation is correct, then it demands kinematic changes to the tectonic

environment that occurred over frequencies of one million (Ujina - Rosario), to less than a few hundred thousand years (Quebrada Blanca). The implied frequency of stress field oscillation at Collahuasi is therefore five to ten times more rapid than that modelled for changes in the physical parameters affecting plate boundary forces (Iaffaldano and Bunge, 2008). Such changes in boundary forces are the mechanism by which subduction geometries change (e.g., Oncken et al., 2006), and hence they control the rate at which specialised settings associated with metallogeny (e.g., Cooke et al., 2005; Rosenbaum et al., 2005) may be established. Instead, the inferred Late Eocene stress field variability at Collahuasi occurred at a frequency similar to that reported for local episodicity of orogenic processes elsewhere (Lister et al., 2001; Lister, 2006). This perhaps reflects the impact of local mechanical coupling and multiple lock up - release events superimposed on the tectonic stress regime.

4.10.3 Structural localisation of mineralised intrusions

Within the broader stress regime, the emplacement of small volumes of hydrous magma into the shallow crust is widely accepted to occur at sites at which stress field is perturbed, and implicitly, weakened (Sillitoe, 1990; Tosdal and Richards, 2001; Amilibia and Skármeta, 2003; Richards, 2003). Transcurrent release has been proposed as an efficient mechanism for creating dilational sites with high vertical structural permeability (e.g., Sibson, 2001). Many porphyry and epithermal deposits worldwide are interpreted to have formed at bends or on splays on strike-slip faults, including those in the Batu Hijau District, Sumbawa (e.g., Garwin, 2000), the Mankayan and Baguio districts, Luzon (e.g., Garcia, 1991; Cooke and Berry, 1996; Disini et al., 1998), the Boyongan district, Surigao (Braxton et al., 2009), the Miocene deposits of Papua New Guinea (e.g., Titley and Heidrick, 1978), districts in the Balkan Peninsula (e.g., Jankovic et al., 1998; Strashimirov et al., 2002) and in western Canada (McIntyre and Villeneuve, 2000). A significant number of deposits are also interpreted to have been emplaced into reverse fault systems or during active compression (Mpodozis et al., 1994; Tomlinson, 1994; Skármeta et al., 2003; McClay, 2004; Perelló et al., 2004; Bertens et al., 2006). In some cases, strike slip faults host mineralised plutons in the hangingwall of major thrusts and these faults appear to have articulated against the thrust (Hill et al., 2002; Gow and Walshe,

2005). That scenario is envisaged for the Copaquire deposit, where the intrusions and controlling faults must interact at depth with thrust faults related to folding of the Mesozoic sequence (Fig. 4.4). The other mineralised intrusions in the Collahuasi district were emplaced at major, long-lived structural intersections that at QB and Rosario were subsequently re-used as dilational splays and stepovers during wrench faulting. At Ujina, emplacement appears to have been affected most strongly by the high degree of pre-existing penetrative fracturing. Critically, the deposits are located in structural positions that underwent dilation during either dextral or sinistral wrench, depending on whether emplacement occurred before, or after the regional change in along arc shear that followed Incaic tectonism.

Chapter 5.

THERMOCHRONOLOGY AND IMPLICATIONS FOR REGIONAL STRUCTURAL EVOLUTION

5.1 Introduction

New U-Th/He thermochronological data were gathered to constrain the denudation history across the Collahuasi district. Other low temperature chronological studies have been done elsewhere in northern Chile with similar aims of resolving uplift and denudation histories during mineralisation (e.g., Maksaev, 1990; Maksaev and Zentilli, 1999). By comparing the denudation histories across major structures, the timing, quantity and gross sense of displacement can be inferred, as has been attempted previously for the Domeyko Fault system (McInnes et al., 2001; Olivares, 2001; Tomlinson et al., 2001a). The kinematic behaviour, and in particular the strike slip strain accommodation along major arc-parallel faults such as the Domeyko Fault are used here to infer aspects of the tectonic environment.

5.2 Thermochronology and the Cenozoic History of Major Faults

The structural architecture of the Collahuasi district was discussed from a stratigraphic standpoint in Chapter 4, based on mapping presented in Chapter 3. The district can be considered to comprise a series of fault-bound blocks that are essentially internally coherent (Fig. 5.1). Folding was primarily associated with late Permo-Triassic plutonism (section 4.3.3) such that the bulk of Mesozoic and Tertiary deformation was brittle and manifested as displacement along these major faults.

(U-Th)/He thermochrometry is based on measurement of the amount of U, Th (and, rarely, Sm), and their alpha decay product, He, in a manner analogous to other radiometric dating techniques (e.g., Reiners, 2005). Radiogenic ^{4}He diffuses out of the mineral at a rate that is sensitive to temperature, the He diffusivity of the mineral, and the proportion of the grain volume sufficiently close to the surface that beta particles can be ejected from the grain. The concentrations of ^{4}He and the parent

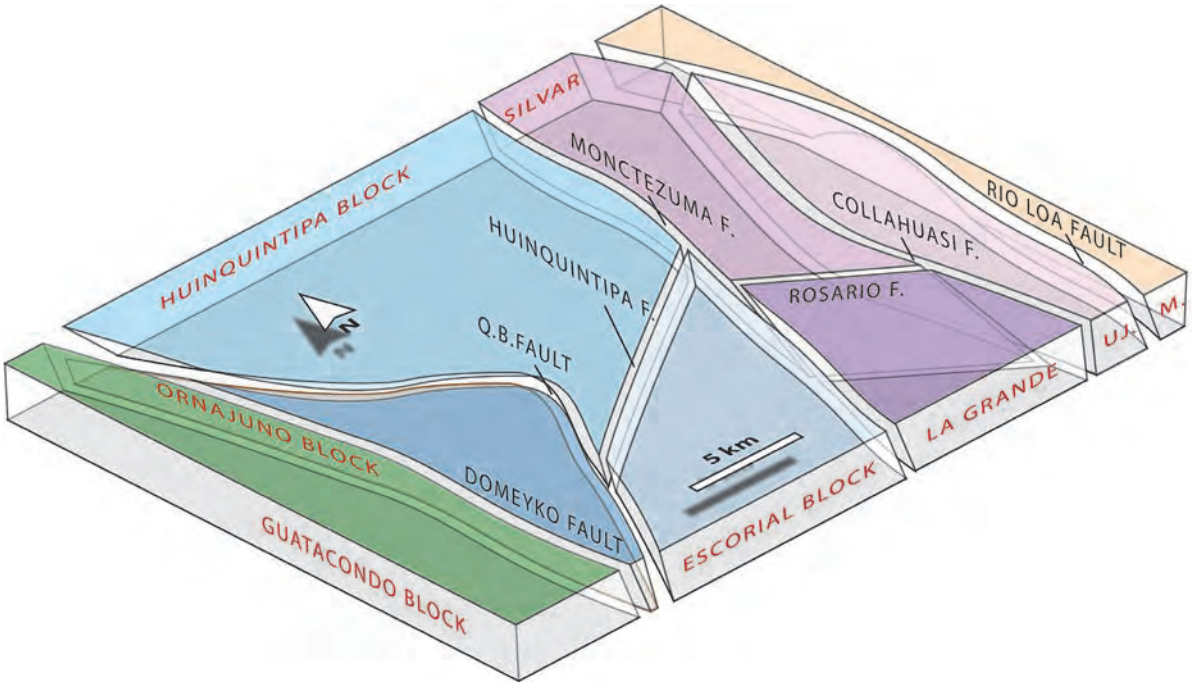

Figure 5.1. Simplified 3D model of the principal coherent blocks that comprise the Collahuasi district. Major bounding faults are named in black, generally above the model; blocks are named in red on their sides. Colours are arbitrary. Abbreviations: UJ. = Ujina Block; M. = Michincha Block; F. = Fault.

isotopes can therefore be used to calculate a He cooling age (Zeitler et al., 1987; Zeitler, 1999; Harrison and Zeitler, 2005).

The technique is applied here to constrain the amount and timing of bulk displacment on several of the block-bounding faults, following the methods and interpretation outlined by McInnes et al., (1999), Farley, (2002), Ehlers (2005), and Reiners (2005). The data may be also be used to infer the rate of cooling of temperature of a given rock mass, and therefore to make some inferences about the exhumation rate and the geothermal gradient. In this regard it is partly analogous in its utility to apatite fission track dating (AFT). The (U-Th)/He method is applied to constrain shallow crustal phenomena because the blocking temnperature for He retention is sufficiently low that the results primarily reflect the passage of a sample through the ambient geothermal gradient (50-75°C for apatite [referred to as AHe], 160-210°C for zircon [ZHe], the range arising from a weak covariation with cooling rate [Wolf et al., 1996, 1998; Reiners, 2005]). Over short time scales, exhumation-related convective cooling cannot unequivocally be separated from hydrothermally mediated advective cooling (i.e. a moving geotherm) in the immediate enviroment of intrusions and hydrothermal systems (Moore and England, 2001; Ehlers, 2005; Dempster and Persano, 2006). The

interpretation of thermochrometry data in hydrothermal environments therefore relies on estimates and modelling of cooling rates for intrusions and hydrothermal systems (e.g., Ehlers, 2005; McInnes et al., 2005).

5.2.1 Previous work.

Prior to this study, there were 33 published apatite fission track ages (Maksaev and Zentilli, 1999), and nine published and 13 unpublished AHe ages for samples from the southern Central Andes (McInnes et al., 1999; Olivares, 2001). All but three of the published ages relate to samples collected in the vicinity of Chuquicamata (Fig. 1.3), south of the Collahuasi district. These data were collected for the purpose of constraining interpretation of the uplift history of the Domeyko Cordillera and the kinematic history of the Domeyko Fault (Maksaev and Zentilli, 1999; McInnes et al., 1999). In contrast, approximately half of the data presented in the maestría (honours) thesis of Olivares (2001) pertain directly to the Collahuasi district, and constrain movement on the Quebrada Blanca Fault (Fig. 5.2). With Olivares' explicit written permission, these data are treated together with new data for the Collahuasi district (B. Olivares, written commun. 2006).

5.3 Sampling and Analysis

5.3.1 Sampling

Samples were collected from across the district such that they complement the data of Olivares (2001) to cover the bulk of the district, east of the Collahuasi Fault (Fig. 5.2). Intrusive rocks were sampled exclusively to negate the possibility that some of the sedimentary and volcanic units may have never been buried deep enough for the crustal geotherm to have reset the chronometer. Sample locations were chosen to span as broad a range of elevations as possible within each block. A total of 42 samples were collected, of which 16 were chosen for analysis based on their location and presence of suitable zircon crystals. The final suite of samples provides vertical elevation ranges of between 540 and 970 metres for each block, except the Silvar block (200 m range). Apatite (AHe), zircon (ZHe) and AFT data can all be treated together by using a pseudoelevation determined from the difference in blocking

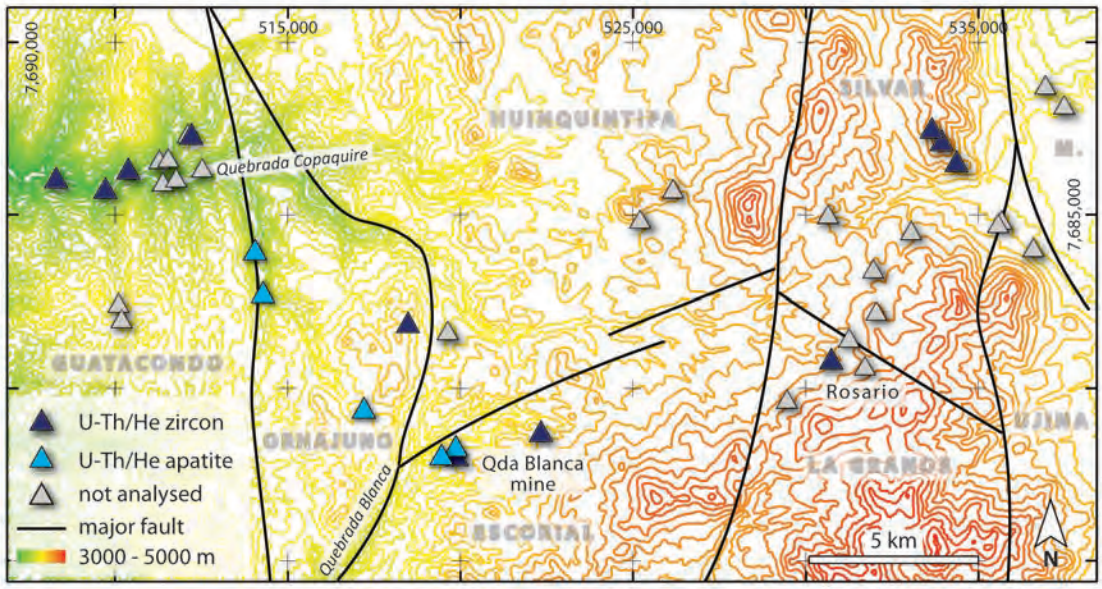

Figure 5.2. Map of the Collahuasi district showing the locations of samples analysed by zircon U-Th/He methods in this study (navy), apatite U-Th/He sample sites from a previously study (Olivares, 2001; light blue), as well as samples collected for thermochronometry, but which were not analysed. In general, sampling in any one block spans ~500 m vertical spread. At Quebrada Blanca and Rosario, samples were collected from deep drillholes and the vertical extent of sampling is not evident in plan view. Topographic relief with 50 m contour intervals is shown in the background, such that hotter colours are higher elevations. Italicised names indicate drainages mentioned in the text.

temperature and the thermal gradient (Reiners et al., 2003). The combination of Olivares' apatite data and the new zircon data therefore yield an effective vertical range of pseudoelevation of ~2000 m for the Escorial and Ornajuno blocks (Appendix VII).

5.3.2 Methodology

Samples were crushed and gently pulverised to 75% passing 500 microns, and then zircons were concentrated by traditional gravitation and magnetic methods at the University of Tasmania. (U-Th)/He analyses were done by Peter Reiners and Stefan Nicolescu, then at Yale University (now University of Arizona). The largest, most complete, inclusion-free, euhedral, doubly terminated single crystals were hand picked under transmitted polarised light at 160 times magnification using the method described by Reiners et al. (2002).

The selected crystals were measured, packed individually in platinum capsules, and heated using a Nd:YAG laser to liberate helium. The resultant gas was extracted, diluted with ^{3}He, the helium concentrated, cryogenically purified and then measured

using a quadrupole mass spectrometer. Reheating and iterative gas extractions were performed on several samples, yielding negligible amounts (<0.5% of the previous degassing) of ^{4}He. The grains were then retrieved and uranium and thorium were measured by ^{229}Th and ^{233}U isotope dilution using a Finnigan Element2 inductively coupled plasma mass spectrometer. Corrections were made for alpha ejection following the zircon method detailed in Farley (2002).

In this study, 25 new analyses are reported. In most cases, two grains were analysed from each sample. Six analyses were done of the Fish Canyon Tuff zircon standard and one of the Durango apatite standard. Calculated internal 2σ uncertainty for all unknowns and standards is 1.68%. However, the replicate analyses are commonly not within error of each other (although they are similar; Table 5.1), suggesting that external errors affect the data. Gross 2σ uncertainty of ~5% is generally estimated for ZHe analyses from the same laboratory (e.g., Reiners et al., 2004). However, Farley and Clark (2006) consider that implicit uncertainties in several aspects of the technique limit the precision to ~8%. A fuller description of the analytical method is provided in Appendix VII.

5.4 (U-Th)/He Results

The principal analytical results of new (U-Th)/He data for the Collahuasi district are presented in Table 5.1. In general, the samples yield Eocene to Oligocene cooling ages that are several million years younger than the nearest high level intrusions (range 62 - 26 Ma, mode 32 Ma; Table 5.1; Figs. 5.3 and 5.4). Unpublished AHe ages for the western Collahuasi district are Oligocene to Middle Miocene (16 - 31 Ma; Olivares, 2001).

A small number of analyses are outliers from these general patterns. Single grains from three samples (Silvar: 161104_02, 161104_07, and La Grande: 200504_02) returned ages that are younger than the patterns defined by the other analyses from the same blocks. Single grains from two other sample yielded ages older than the trends defined by the other samples for the corresponding blocks (Fig. 5.4). The younger ages might reflect incomplete He degassing or partial hydrothermal resetting, whereas older ages are typically attributed to in-situ α-injection from

TABLE 5.1. (U-Th)/He samples and analytical results. A more comprehensive table is contained in Appendix X.

Sample ID[a]	Block	Sample Elevation	Material	Crystal Morphology	Mass (μg)	U (ppm)[b]	Th (ppm)[b]	^{4}He (nmol/g)	Raw Age (Ma)	F_T[c]	Corrected Age 2σ (Ma)
050504_11a	Silvar	4670	zircon	euhedral unblemished	1.434	243.19	170.20	52.300	34.15	0.67	51.30 ± 2.17
050504_11b	Silvar	4670	zircon	euhedral unblemished	2.260	392.28	323.61	84.925	33.53	0.70	48.06 ± 1.89
161104-02c	Silvar	4520	zircon	euhedral unblemished	3.607	716.15	478.90	203.796	45.43	0.73	62.50 ± 1.31
161104_02a	Silvar	4520	zircon	one tip is chipped	5.817	543.74	386.76	147.235	42.87	0.74	57.65 ± 2.31
161104_02b	Silvar	4520	zircon	one pyramid missing	2.808	755.95	433.99	141.493	30.51	0.69	44.30 ± 1.81
161104_07a	Silvar	4720	zircon	one tip is missing	5.090	883.00	551.10	223.632	40.82	0.74	55.13 ± 2.52
161104_07b	Silvar	4720	zircon	euhedral unblemished	2.933	465.86	353.78	88.062	29.67	0.71	41.74 ± 1.65
291104_05a	Huinquintipa	4270	zircon	euhedral unblemished	4.323	360.30	261.52	71.123	31.19	0.74	41.98 ± 1.77
291104_05b	Huinquintipa	4270	zircon	euhedral unblemished	2.697	195.10	194.26	36.644	28.15	0.72	39.29 ± 1.61
301104_06a	Escorial	3538	zircon	one tip is chipped	7.412	684.17	677.57	114.248	25.06	0.80	31.39 ± 1.26
301104_06b	Escorial	3538	zircon	euhedral unblemished	1.221	495.48	220.16	54.555	18.47	0.66	27.99 ± 1.14
301104_03a	Escorial	4050	zircon	one pyramid missing	2.416	562.12	311.56	84.984	24.76	0.70	35.13 ± 1.44
301104_03b	Escorial	4050	zircon	one pyramid missing	2.026	624.63	388.74	84.682	21.90	0.70	31.49 ± 1.34
301204_01a	Escorial	4375	zircon	euhedral unblemished	7.757	304.20	169.89	51.020	27.44	0.79	34.62 ± 1.37
301204_01b	Escorial	4375	zircon	one tip is chipped	3.630	478.14	473.39	120.869	37.89	0.72	52.91 ± 2.04
301204_01c	Escorial	4375	zircon	euhedral unblemished	3.692	327.08	241.84	60.972	29.38	0.74	39.90 ± 0.84
071204_10a	La Grande	3964	zircon	euhedral unblemished	2.738	390.81	294.55	53.697	21.60	0.71	30.55 ± 1.16
071204_10b	La Grande	3964	zircon	one tip is missing	5.738	325.89	209.99	44.622	22.01	0.76	29.05 ± 1.09
200504_2a	La Grande	4690	zircon	euhedral unblemished	1.616	640.10	503.21	71.615	17.48	0.67	26.01 ± 0.96
200504_2b	La Grande	4690	zircon	one tip is missing	1.320	1194.16	692.11	145.847	19.90	0.64	31.13 ± 1.21
200504_2c	La Grande	4690	zircon	one tip is missing	0.861	1164.41	968.85	145.979	19.41	0.57	33.77 ± 1.29
071204_08a	La Grande	4139	zircon	one tip is missing	6.155	242.08	226.78	39.855	24.96	0.77	32.53 ± 1.25
071204_08b	La Grande	4139	zircon	one edge chipped	1.828	368.64	170.50	43.612	19.76	0.68	29.12 ± 1.19
281204_06	Guatacondo	4220	zircon	subhedral crystal	10.804	1658.67	2078.64	346.213	29.80	0.82	36.26 ± 1.30
201204_20	Guatacondo	3700	zircon	one large crack	8.502	997.40	406.88	154.045	26.09	0.79	33.10 ± 1.30
291204_11	Guatacondo	3515	zircon	euhedral unblemished	6.296	346.90	154.70	59.924	28.94	0.76	37.93 ± 1.48
291204_06	Guatacondo	3250	zircon	euhedral unblemished	5.656	584.86	232.05	81.758	23.68	0.77	30.71 ± 1.19

a) Lower case alphabetic (a, b, c) suffixes reflects repeat analyses of grains from the same sample.

b) In all samples, Sm concentrations are low and Sm contributed negligible ^{4}He relative to the contributions from U and Th.

c) F_T is the geometric correction factor as described by Farley (2002). The corrected age is the quotient of the raw age and F_T.

adjacent grains of other U-Th-rich accessory minerals (e.g., Farley and Clark, 2006). Both types of anomalous ages might result from errors associated with the geometric corrections for α-ejection, especially among partial crystals (Farley, 2002). The interpretations presented here exclude these outlying analyses, although the "outlier" assumption could be more rigorously tested by larger analytical populations.

5.4.1 Cooling Histories, Thermal Gradients and Exhumation

Constraints on thermochronological data interpretation. The significance of thermochronometry results can only be determined if the background thermal state of the upper crust can be constrained, or at least shown be consistent for two adjacent blocks. In his review, Ehlers (2005) considered the phenomena that most affect simple geothermal models (and hence the interpretation of thermochronometry results) to be 1) tectonic erosion or loading; 2) prolonged erosion or sedimentation; and 3) intrusion and hydrothermal advective heat transfer. Dempster and Persano (2005) also show that convective groundwater flow is likely also important.
The Phanerozoic Collahuasi district has not experienced catastrophic extension nor tectonic loading (emplacement of thrust sheets). Neither have any of the faults at Collahuasi experienced the multi-kilometre vertical offsets required to noticeably affect the thermal gradient at the resolution of the technique. Net vertical displacement on the Domeyko Fault, the most significant in the district, might have reached a little over 1 km (section 5.4.3), and apparently achieved this in several stages. The present constraints of the paleogeothermal environment are insufficient to rule out hydrological thermal effects that tend to lead to over-estimation of exhmation rates (Dempster and Persano, 2005). However, these effects are unlikely to have been dramatic prior to 32 Ma since paleontological studies suggest that the elevation of the Domeyko Cordillera was probably less than 1 km above sea level during the Eocene (Simpson et al, 1983). Erosion and advective heat transfer are therefore taken to be the primary phenomena that might have caused deviation from a steady-state geothermal gradient, although convective heat transfer may have influenced the Oligo-Miocene conditions.

Cooling rates and advective heat transfer. Cooling histories presented as time-temperature (Tt) plots may be determined by combining data from multiple chronometers (e.g., McInnes et al., 2005; Fig. 5.3). The slope of the Tt curve is the cooling rate. Typically, in the vicinity of high level intrusions, the history defines a J-shaped curve wherein early, rapid cooling of the intrusion or related hydrothermal system is followed by much slower cooling related to exhumation and evolution of the regional geotherm (Fig. 5.3a). For example, the abundant data available for the Chuquicamata intrusive complex show that it cooled rapidly until ~31 Ma, then was reheated by a second hydrothermal pulse, cooled rapidly again to 100°C by ~29 Ma, and then cooled slowly thereafter. Generic thermal models built with parameters for emplacement of an intrusion at one to two kilometres depth, imply that the thermal effect of the intrusion (ignoring exceptional hydrothermal flow) will only affect the ZHe chronometer within a radius equal to the width of the intrusion (Ehlers, 2005). However, taking the epidote alteration zone as evidence of hydrothermal temperatures above 280°C (e.g., Reyes, 1990), the hydrothermally mediated regime about the Quebrada Blanda porphyry system extended laterally at least twice the breadth of the intrusive complex (Fig. 4.19). Inside an intrusion, the model thermal regime falls to below the ZHe blocking temperature after a period related to the volume of the intrusion: ~10^5 years for a columnar stock 1 km in diameter, and 10^6 years for a columnar stock 5 km in diameter (Hanson, 1995; Ehlers, 2005).

At Collahuasi, the Silvar Block is unique in that it hosts Late Cretaceous, rather than Eocene intrusions (Chapter 3). ZHe data in the block record Middle Paleocene to Middle Eocene cooling temperatures (Fig. 5.3b). The ZHe data are at a minimum

→

Figure 5.3. (next page) Age - Temperature plots showing data from multiple chronometers. A) an example dataset from Chuquicamata. B) the Silvar block near Collahuasi, and a comparison suite from the Cerros de Montecristo. C) the Guatacondo block, including the Copaquire porphyry complex, and a comparison suite from the Los Picos stock. D) the Ornajuno block and a comparison suite from the Sierra Limon Verde. E) the Escorial block, including the Quebrada Blanca porphyry complex. F) the La Grande block, including the Rosario porphyry complex. Curves were fitted manually, and below 300°C pass through analyses from samples collected at approximately the same altitude. All comparator datasets are from locations in the Chuquicamata district. Other geochronological data from data from Tomlinson et al., 2001a and references therein; Olivares, 2001; and Chapter 3 of this study. Closure temperatures above 150ºC are the mid-point of experimentally-determined ranges (Lee et al., 1997; McDougall and Harrison, 1999; Barra et al., 2003). For the lower temoerature chronometers, data are plotted at closure temperatures that reflect geologically reasonable cooling rates in the Neogene Andes (Ketcham et al., 1999; Farley, 2000; Reiners et al., 2002).

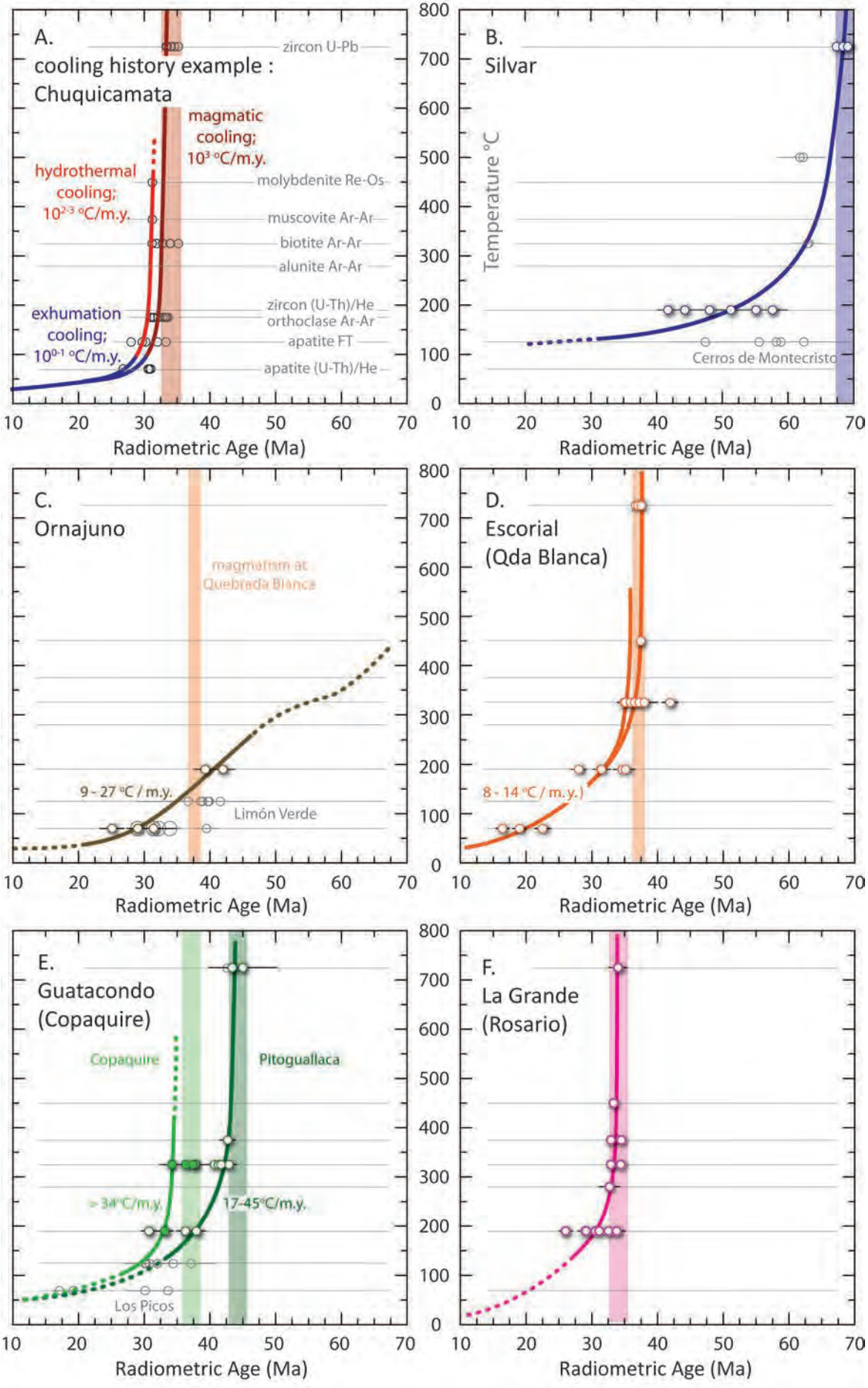
A.
cooling history example :
Chuquicamata
zircon U-Pb
magmatic cooling; 10³ °C/m.y.
hydrothermal cooling; 10²⁻³ °C/m.y.
molybdenite Re-Os
muscovite Ar-Ar
biotite Ar-Ar
alunite Ar-Ar
exhumation cooling; 10⁰⁻¹ °C/m.y.
zircon (U-Th)/He
orthoclase Ar-Ar
apatite FT
apatite (U-Th)/He
B.
Silvar
Temperature °C
Cerros de Montecristo
C.
Ornajuno
magmatism at Quebrada Blanca
9 - 27 °C / m.y.
Limón Verde
D.
Escorial
(Qda Blanca)
8 - 14 °C / m.y.)
E.
Guatacondo
(Copaquire)
Copaquire
Pitoguallaca
> 34°C/m.y.
17-45°C/m.y.
Los Picos
F.
La Grande
(Rosario)
Radiometric Age (Ma)
0
100
200
300
400
500
600
700
800
10
20
30
40
50
60
70

TABLE 5.2. Calculated rates of cooling, exhumation and shallow crustal geothermal gradients.

Block	Age (Ma) (2_σ)[a]	Cooling rate (°C/m.y.)	Geotherm (°C/km)[b]	Exhumation Rate (m/m.y.)[c]	Derivation and Calculation[d]
Escorial (Quebrada Blanca)	36.3 ± 0.6	130 - ∞			slope of T-*t* regression through youngest intrusion zU-Pb and early event biotite ArAr ages
	33.4 ± 1.2	130 - ∞			slope of T-*t* regression through late event biotite ArAr and Zhe cooling ages
	27.8 ± 6.5	9 - 14			slope of T-*t* regression through ZHe and AHe at ~3950m
	22.9 ± 7.5	8 - 11			slope of T-*t* regression through ZHe and AHe at ~3500m
	36.5 ± 0.8		170 - 340		calculation based on paleosurface elevation relative to Vpy1 fluid inclusion samples; age from biotite ArAr
	Late Eocene-Oligocene			380 - 1600	calculation based on cooling rate and geotherm at main stage D-vein (Vpy1) formation
	Oligocene		< 37		back calculation using mid-Oligocene cooling rates, assuming Eocene exhumation rate persisted for ~ 10 m.y.
	19.6 ± 4.1			47 - 87 (59)	slope of the best fit age-elevation regression through AHe data
La Grande (Rosario)	34.8 ± 0.6	290 - ∞			slope of T-*t* regression through zircon U-Pb and biotite ArAr
	33.5 ± 1.2	29 - 58			slope of T-*t* regression through biotite ArAr and alunite ArAr at ~4150 m
	31.4 ± 1.5	30 - 130			slope of T-*t* regression through alunite ArAr and ZHe at ~4150 m
	32.6 ± 0.3		290 - 730		calculation based on paleosurface elevation from E-vein fluid inclusions; time from alunite ArAr
	Late Eocene-Oligocene			54 - 420	calculation based on cooling rate and geotherm results during E vein formation
	Oligocene		19 - 260		back calculation using mid-Oligocene cooling rates (Escorial) and assuming persistent exhumation of Rosario
Ornajuno	34.9 ± 6.9	9 - 27			slope of T-*t* regression through AHe and ZHe at ~4300 m
	29.0 ± 5.8			58 - 180 (80)	slope of the best fit age-elevation regression through AHe data

a) Determined from the average of the ages used for regressions. Where multiple analyses exist for a given event, the average, weighted by internal errors, was used for regression.

b) Determined from the spatial relationships between samples and the paleosurface implied by fluid inclusion pressures. Also back calculated if the exhumation and cooling rates.

c) Calculated from as the cooling rate divided by the contenporaneous geothermal gradient.

d) Abbreviations: T = temperature; *t* = time; zU-Pb = zircon U-Pb age; ArAr = $^{39}Ar/^{40}Ar$, AHe = apatite (U-Th)/He, ZHe = zircon (U-Th)/He, Vpy1 = pyritic, stage 5-6 veins (Rowland, 1998; section 4.6.1, Fig. 4.33); E = tennantite-enargite veins (Masterman et al., 2005; section 4.9.2, Fig. 4.65).

of seven million years younger than the intrusions, beyond the span of magmatism-related thermal regimes (e.g., Ehlers, 2005). The data therefore do not record the cooling of the nearby Tolaun intrusive complex. In contrast, similar alkaline intrusions near Chuquicamata (Cerros de Montecristo) cooled rapidly from magamatic temperatures to below the ZHe blocking temperature. The difference may reflect comparatively deep emplacement of the Tolaun complex, consistent with the generally coarse grained equigranular nature of these rocks (Table 3.4).

The only intrusive rocks known from the Ornajuno block are Triassic, and the results from this block therefore indicate of the background thermal regime away from major Paleogene intrusive centres. The ZHe data are older than the Quebrada Blanca porphyry, ruling out any possible influence of this system. Using these data with the AHe data of Olivares (2001), cooling rates in the range 9-27°C/km are calculated for this block during the Late Eocene to Middle Oligocene (Fig. 5.3c; Table 5.2). These are similar to rates calculated from data collected from basement blocks on either side of the Calama Basin near Chuquicamata (Fig. 5.3c); AHe data for the Sierra Limón Verde (Olivares, 2001), and AFT data from the Cerros de Paqui (Maksaev and Zentilli, 1999). It appears therefore that cooling rates of this magnitude were a regional phenomenon in the Domeyko Cordillera during the Late Eocene and Oligocene, and were probably unrelated to magmatism.

Multiple chronometer data from the Quebrada Blanca porphyry copper deposit (Escorial Block) show rapid cooling of at least 126°C/m.y. between 37 and 34 Ma (Table 5.2, Fig. 5.3d; V. Maksaev, unpublished data). This is a minimum rate, and the transient cooling rate was probably much faster given trapping temperatures of fluid inclusions at Quebrada Blanca (Rowland, 1998) and the 10^4-10^5 year lifespans of most porphyry hydrothermal events (e.g., Seedorff et al., 2005). In detail, there were at least two hydrothermal pulses at Quebrada Blanca (section 4.6.2), but after 34 Ma the thermochronometry data show a similar range of Oligocene cooling rates to blocks without magmatism (Fig. 5.3d). This leads to the interpretation that these data reflect broader crustal processes, and that they were not overwhelmed by the transient thermal regime related to magma emplacement and cooling. The corresponding interpretation is that the wallrocks into which the intrusions were emplaced were already warmer than the ZHe blocking isotherm (~190°C; Reiners et

al., 2002; Reiners, 2005).

Cooling rates cannot be calculated below 190°C for the Guatacondo block (Copaquire, Pitoguallaca stocks) or for the La Grande block (Rosario porphyry) as the new ZHe data are the only low temperature geochronometer data available (Fig. 5.3e, f). For both Copaquire and Rosario, the ZHe data are within error of ages determined from higher temperature chronometers. Magmatic-hydrothermal cooling cannot therefore be ruled out as the principal phenomenon recorded by these data. Likewise, it follows that the host rocks to these intrusions were at, or near, the ZHe blocking isotherm at the time of intrusion. However, new ZHe ages from the Pitoguallaca stock are distinctly younger than the intrusive age. A history of magmatic cooling to ~300°C at ~ 41 Ma, followed by slower cooling dictated by regional processes, is therefore inferred.

Geothermal gradients. Interpretations of exhumation rates and of relative block displacement using thermochronology requires constraint of the geothermal gradient. The present day geothermal gradient in the Central Andes has been measured at 22.4°C/km (Springer and Forster, 1998), although at ~70 km thick (e.g., James, 1971), the Central Andean crust is much thicker now than it would have been prior to the Middle Miocene (e.g., Allmendinger et al., 1997). By extrapolation based on estimates of cumulative shortening through the Cenozoic (e.g., Oncken et al., 2006), crustal thickness for the middle Oligocene (e.g., Kay et al., 1994a), and the chemistry of post-tectonic granitoids (e.g., Haschke et al., 2002a) the crust appears likely to have been between 35 and 45 km thick at the beginning of the Incaic tectonic phase (Chapter 2). Modern convergent margins with a continental upper plate and

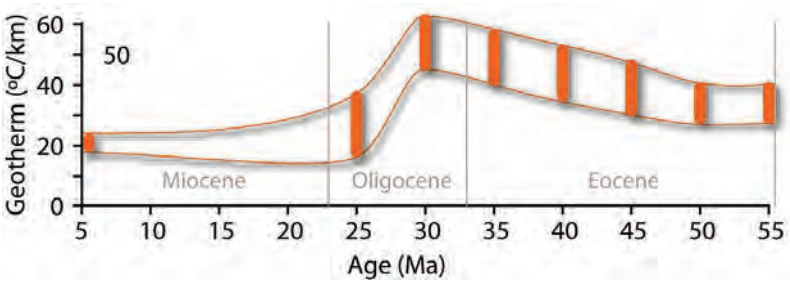

Figure 5.4. Secular variation in the geotherm in the Central Andes, based on an initial Paleocene estimate (see text), followed by pronounced Eocene increase related to erosion during the Incaic tectonic phase, and subsequent Oligocene calculations based on thermchronometry data.

equivalent crustal thickness may therefore be better analogues, such as in the South Island of New Zealand (37°C/km; Shi et al., 1996), West Sumatra (48-53°C/km; Koning, 1996), and southern Alaska (30-66°C/km; Magoon et al., 1997; Berger et al., 2008). Based on these examples, the background geotherm in the Eocene Central Andes might have been in the range 30-65°C/km. Transient hydrothermally-mediated thermal gradients are known to be much higher, and exceed 150°C/km (e.g., Fuentes et al., 2004).

Sustained and rapid erosion can impact markedly on the thermal gradient. Ehlers (2005) calculated that 10 m.y. of erosion at 200 m/m.y. would cause an increase of ~20°C/km in the geothermal gradient. The blocks under investigation here are small relative to the geometry of the Domeyko Cordillera, such that erosion is assumed to have affected them all at similar rates. Erosion of the Domeyko Cordillera during the period 50-30 Ma is estimated at 150–250 m/m.y (Maksaev and Zentilli, 1999; Kober et al., 2002), such that the regional thermal gradient may have been as much as 40°C/km higher at 30 Ma than it had been prior to the Incaic tectonic event (Fig. 5.4). The La Grande block may be an exception, insofar as that tectonic escape during late stage mineralisation (Masterman et al., 2005; Chapter 4) appears to have facilitated even faster erosion, and hence an even higher background geotherm might be anticipated in that block during the earliest Oligocene.

The geothermal gradient was calculated here using the relative elevation of samples for which different chronometers (implicitly with different blocking temperatures) recorded indistinguishable ages in approximately the same location (Table 5.2). Late hydrothermal stages were associated with transient thermal gradients of 170-340°C/km at Quebrada Blanca during the Late Eocene, and 290-730°C/km at Rosario during the Early Oligocene. Back-calculations based on exhumation and cooling rates (Table 5.2) lead to an estimation of the Middle to Late Oligocene geothermal gradient of no more than 37°C/km in the Escorial block, and of no less than 19°C/km in the La Grande block (Table 5.2; Fig. 5.4).

Exhumation. Thermochronometry data can be used, under stable geothermal conditions, to calculate the exhumation rate as the slope of the age-elevation curve (e.g., Ehlers, 2005). This approach is of restricted use here because of the apparent

secular variation in the thermal structure of the Central Andean crust during the Paleogene, and the prevalence of transient hydrothermal and magmatic thermal regimes in the Collahuasi district. It is applied, with caution, to the AHe data of Olivares (2001) and the ZHe data from the Silvar block, as these record ages that coincide with periods of apparently stable geothermal gradient before and after the Incaic tectonic phase (Fig. 5.4). Best fit lines through the AHe age-elevation plots yield estimated exhumation of 80 m/m.y. in the Ornajuno block during the Late Oligocene, and 59 m/m.y. in the Escorial block during the Early Miocene (Table 5.2). Prior to the Incaic tectonism, exhumation in the Slivar block appears to have been ~18 m/m.y.

Rates of exhumation may also be calculated as the quotient of the cooling rate and the geothermal gradient (e.g., Hurford, 1991). This method was used here for the Late Eocene and Early Oligocene, and the same data were used for the calculation of cooling rates. Consequently, the resulting estimates account for high, hydrothermally mediated, geothermal gradients and are independent of the decline of these thermal regimes. These calculations yield estimates of exhumation of 380 to 1600 m/m.y. for the Escorial block and 54 to 420 m/m.y. for the La Grande block, at the time of late stage vein formation at Quebrada Blanca, and Rosario, respectively (Table 5.2). Mineralisation therefore accompanied rapid unroofing, consistent with the independent conclusions of Maksaev and Zentilli (1999) and Masterman et al. (2005).

5.4.2 Net Fault Displacements

The relative net displacement across a major fault may be estimated using age-elevation curves defined by thermochronometry data collected on either side of the fault (e.g., McInnes et al., 1999, 2005). The effect of short wavelength topography on the form of the isotherms above 50°C is effectively nil ($\lambda < 5$ km; Reiners et al., 2003). As the topography in the Collahuasi district satisfies this criterion, no correction to the age-elevation plots (Fig. 5.5) is necessary. Pseudoelevations have been calculated for the AHe data to permit these to be plotted alongside the ZHe data. The calculation is based on the estimated geotherm at the time of cooling through the blocking temperature (Fig. 5.4, Appendix VIII). The determination of relative offset rests on the assumption that blocks on both sides of the fault investigated

had a common thermal history prior to displacement. There is an approximate covariation between the average ZHe age and the magmatic ages of the nearest intrusive complex, which could be interpreted as evidence the the ZHe data record late magmatic cooling that is not contemporaneous in all blocks. However, since most of the ZHe ages, and all the AHe ages are several million years younger the most recent nearby magmatism or hydrothermal activity (Fig. 5.3), most of the data are considered to record regional phenomena that are common to all blocks in the district.

Monctezuma Fault. The La Grande and Escorial Blocks are separated by the Monctezuma Fault (Fig. 5.1), which was active during two distinct epithermal miner-

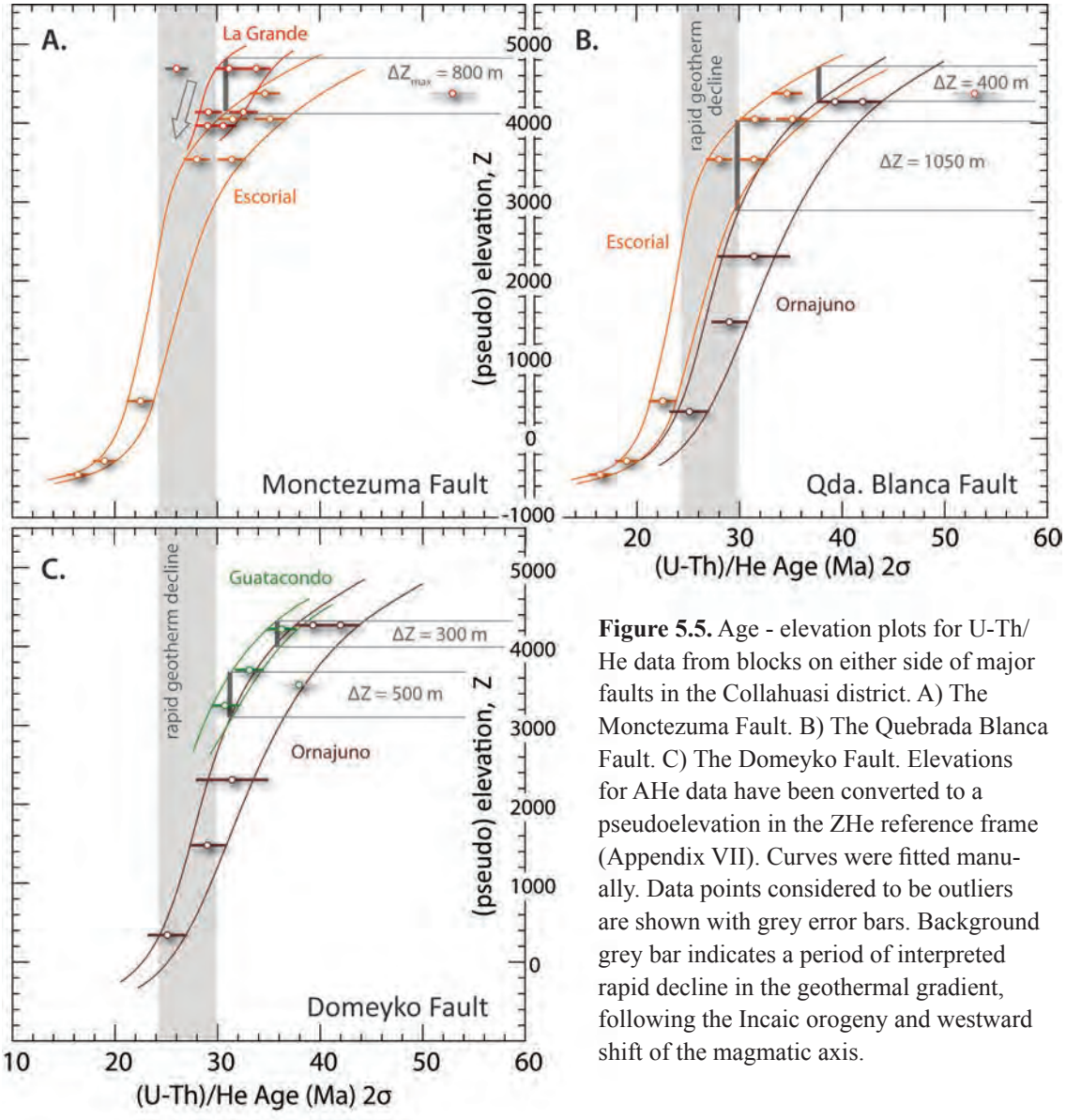

Figure 5.5. Age - elevation plots for U-Th/He data from blocks on either side of major faults in the Collahuasi district. A) The Monctezuma Fault. B) The Quebrada Blanca Fault. C) The Domeyko Fault. Elevations for AHe data have been converted to a pseudoelevation in the ZHe reference frame (Appendix VII). Curves were fitted manually. Data points considered to be outliers are shown with grey error bars. Background grey bar indicates a period of interpreted rapid decline in the geothermal gradient, following the Incaic orogeny and westward shift of the magmatic axis.

alisation events (Chapter 4, sections 4.5 and 4.9). Samples in the eastern (La Grande) block cooled more recently than those at the same elevations to the west of the fault (Fig. 5.5a). This relationship could imply that the La Grande block has been uplifted relative to the Escorial block, by as much as 800 m, since ~25 Ma. However, this should be considered a maximum, as the difference between the two blocks becomes less at younger ages (Fig. 5.5a, arrow), perhaps implying that the older ZHe ages at Rosario record the waning stages of the hydrothermal system (Fig. 5.3). Nonetheless, striae mapped on minor strands of the Monctezuma Fault tend to plunge shallowly to the south. The sense and magnitude of uplift is therefore consistent with the ~3 km of net sinistral offset on this structure. A smaller amount of E-side up displacement is inferred from the relative position of the intersection of the Rosario Fault with the contact between the Chiclla and La Grande Formations (Table 4.5).

The Quebrada Blanca Fault. The Ornajuno block and the Escorial block, which hosts the Quebrada Blanca porphyry Cu deposit, are separated by the Quebrada Blanca Fault (Fig. 5.1). This fault hosts mineralised intrusives that were emplaced at ~37 Ma (Fig. 4.20), and causes ~2 kms of dextral separation of the outcrop pattern of Peine Group stratigraphy in the Ancho de Huinquintipa valley (Figs. 3.4 and 3.16, Table 4.5). The strata dip to the north (Figs. 3.4 and 4.4), such that the same pattern could be generated by displacement in a dextral, or normal, or oblique sense.

AHe and ZHe ages are at least two million years younger in the Escorial block than samples at the same elevations in the Ornajuno block (Fig. 5.5b). These imply relative uplift of 400 - 1050 m since 22 Ma. Olivares (2001) determined a relative uplift of 385 m based on modelling of the AHe data only, and assuming a fixed thermal gradient. No straie were evident on mapped fault surfaces, but post-mineral dextral offset seems unlikely as there is no apparent sideways dismemberment of the porphyry system (Fig. 4.19). The sense and magnitude of displacement implied by the thermochronology is consistent with difference in the inferred depth of exhumation of mineralised systems on either side of the fault, i.e. porphyry levels are exposed at Quebrada Blanca whereas shallower hydrothermal levels are exposed at the El Colorado prospect in the southernmost Ornajuno block (Fig. 3.1; Sillitoe, 2005). However, the implied displacement is contrary to that suggested by the stratigraphic offset. The discrepancy requires an explanation in two stages. Possibly, the

Quebrada Blanca fault underwent major dextral (or normal) displacement during the Eocene, and was later re-used as a reverse fault during Miocene tectonic events. This is consistent with the independent interpretation of a dextral strike slip regime during emplacement of, and mineralistaion in the Quebrada Blanca porphyry (Chapter 4), and might also explain the rapid lateral changes in alteration facies on the northern margin of the porphyry system (Fig. 4.19).

Domeyko Fault. The Ornajuno and Guatacondo blocks are separated by the Domeyko Fault system (DFS); an arc-parallel high strain corridor that extends semi-continuously for 1400 kilometres from 18° to 31°S (section 4.3.1). ZHe data for samples from the Guatacondo block are younger than for samples from the same elevation in the Ornajuno block (Fig. 5.5c). The difference implies 300 - 500 metres of relative upthrow of the western, Guatacondo, block since 30 Ma. McInnes et al. (1999) reported similar results from AHe and AFT analyses on both sides of the DFS at Chuquicamata, for which they calculated relative west-side up separation of 600 ± 100 metres. In the Collahuasi district, these results are qualitatively consistent with the much greater abundance, and generally larger size of Eocene intrusions exposed at equivalent elevations on the western side of the DFS (Fig. 3.25).

The implied displacement is contrary to the observation that morphologically the DFS (and the Rio Loa Fault) together comprise a basement-involved thrust belt that gives rise to an orogen-parallel pop-up; the Domeyko Cordillera (e.g., Fig. 4.4; Skarmeta, 1993; McClay et al., 2002; Amilibia et al., 2003; 2008). Across the segment of the fault between the Chuquicamata and El Abra porphyry Cu deposits, Maksaev et al. (1994), Tomlinson and Blanco (1997b), and Dilles et al. (1997) mapped unique geological pierce points that demonstrate primarily strike-slip displacement on the DFS, associated with 500 - 600 m of west-side *down* displacement. Absolute downthrow of the Guatacondo block is implicit since Mesozoic stratigraphy dominate in that block, whereas Paleozoic stratigraphy dominates the Collahuasi district to the east of the DFS (Chapters 3 and 4, Fig. 3.4). The magnitude of this downthrow is likely to be on the order of the local topographic amplitude (<1000 m), and therefore similar to that mapped near Chuquicamata, since the Paleozoic unconformity at the base of the Quehuita Group is exposed along the western margin of the Domeyko Cordillera (e.g., Damm et al., 1986; 1990),

including in the southern part of the Guatacondo block on Cerro Amaculla (Fig. 3.4).

There has been controversy over the displacement history of the DFS. Amilibia et al. (2008) showed detailed structural sections that reveal principally compressional strain, and Amilibia et al. (2003) suggested that the DFS accommodated little or no strike-slip strain. In line with this argument, major lateral offsets are generally not evident in the magnetic data presented by Behn et al. (2001). In contrast, structural and paleomagmetic data suggestive of major strike slip displacement have long been documented in the fault segments near Chuquicamata (e.g., Reutter et al., 1991, 1996; Astudillo et al., 2008). Stratigraphic and structural correlations indicating ~35 kilometres of net sinistral displacement along the DFS were provided by Baker et al. (1987), Dilles et al. (1997), Tomlinson and Blanco (1997b), Maksaev et al. (1994), Arnott and Zentilli (2003), and Campbell et al. (2006). Of particular note, Maksaev et al. (1994) and Tomlinson et al. (2001a) restored the sinistral offset and presented the resulting paleogeographic reconstructions. Occurrences of the Tolar and Sichal Formations that are scattered and have incoherent paleocurrent orientations in their present positions, appear in the reconstructions to have been deposited in coherent, discrete, intermontane basins that were subsequently dismembered. Arnott and Zentilli (2003), and Campbell et al. (2006) documented detailed chronology and petrological characterisation of the Los Picos - Fortuna, and the Pajonal - El Abra intrusive complexes, on the west and east sides of the DFS, respectively, and separated by ~35 kms. The two complexes are effectively indistinguishable from each other. When restored, the combined original complex had a rhombic geometry with N and NE-trending margins (Maksaev and Tomlinson, 1995), consistent with

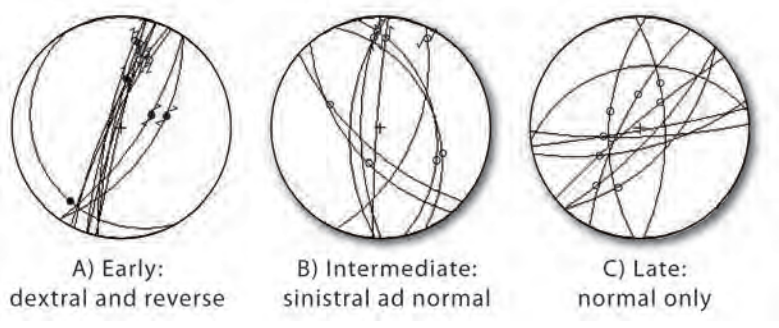

Figure 5.6. Structural data from the Domeyko fault system in the Qda Copaquire and Qda Blanca drainages shown as great cirlcles with slip lineations. Solid symbols are reverse faults. Lineations on some early shears were calculated as the orthogonal to the intersection of the S and C foliations.

emplacement into the intersection of the proto-DFS with the San Cristobal fault (also referred to as the Calama-Antofagasta Lineament: Palacios et al., 2007), a dextral splay of regional extent. The evidence in favour of major sinistral displacement on the DFS since the latest Eocene seems unassailable.

Strands of the DFS exposed in the Quebrada Copaquire and Quebrada Blanca drainages (Figs. 4.19, 4.35 & 5.2) were mapped during this study. Three types of structural elements characterise the zone: submylonite and cataclasite, faults with major gouge development, and faults without gouge development. Structures with ductile fabrics are associated with folding of the Mesozoic stratigraphy, whereas the largest sinistral faults are located in the margins of high aspect ratio Paleogene basins and have truncated subhorizontal conglomerates of the Tolar and Papajoy formations (Fig. 3.4). The ductile shears must therefore be older than the brittle faults, such that these represent an approximate transition in time from ductile to brittle modes of strain accommodation. Early shear zones have either dextral, or reverse kinematic indicators (porphyroclasts, S-C fabrics; Fig. 5.6a) whereas later faults tend to have striae indicative of sinistral or normal slip (Figs. 4.1b and 5.6b). Because of limited exposure, no crosscutting relations between early reverse and dextral shears were observed. Very late short-displacement faults that cut the broader shear zones tend to have strikes oblique to the main zone, and steeply plunging striae that indicate normal slip (Fig. 5.6c).

Tomlinson et al. (2001b) reconciled the difference between the apparent offsets implied by thermochronology and stratigraphy in terms of the post-Eocene sinistral displacement and the slope of the Eocene land surface (and hence geotherm). This may indeed be correct, but their precise solution is very sensitive to the interpretation of the paleogeotherm. Instead, observations made here imply a stage-wise kinematic history (Fig. 5.7) in which differences in either the cumulative exhumation or a decline in the geothermal gradient (Fig. 5.4) account for the ductile nature of early structures and the brittle nature of younger ones. The data are permissive of an early (i.e. Incaic) stage of oblique reverse dextral displacement on the DFS, during which the overall pop-up architecture of the Domeyko Cordillera (e.g., Hammerschmidt et al., 1992; Amilibia et al., 2003; 2008) is envisaged to have formed (Fig. 5.7a). This regime appears to have evolved such that by 37 Ma dextral strike-slip strain was

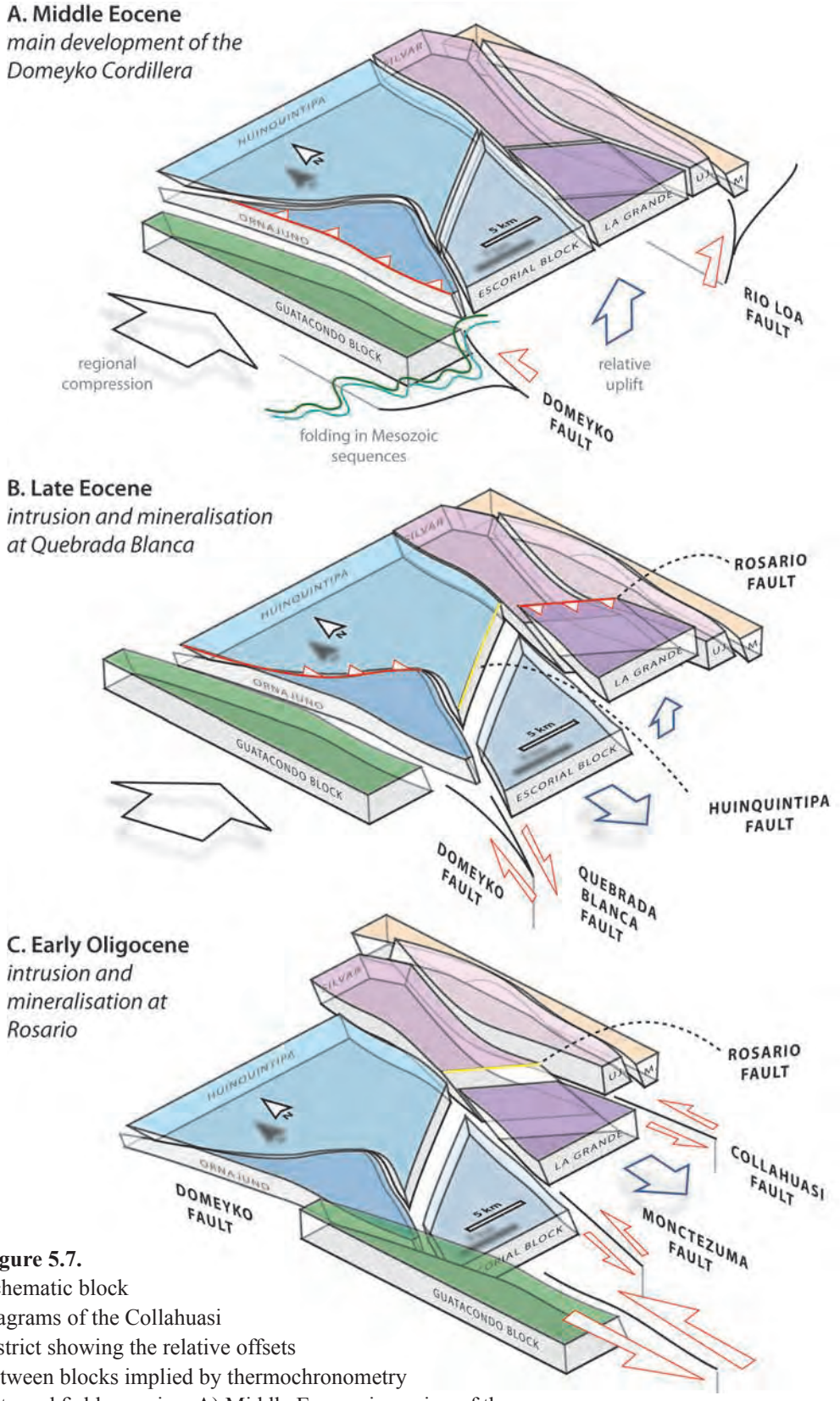

Figure 5.7.
Schematic block diagrams of the Collahuasi district showing the relative offsets between blocks implied by thermochronometry data and field mapping. A) Middle Eocene inversion of the Domeyko and Rio Loa faults that caused pop-up of the Paleozoic basement to the Domeyko Cordillera. B) Late Eocene dextral transpression along the Domeyko and related faults, transitional from A. C) Early Oligocene major sinistral transtension along arc-parallel structures. Surface trace of thrusts (red) and extensional faults (yellow). Relative Oligocene or younger uplift of the La Grande and Guatacondo blocks were caused by obliquity of strike slip faults.

partitioned into the DFS (Fig. 5.7b; Chapter 4). The kinematic environment then changed dramatically and ~35 km of sinistral slip occurred. This manifests at surface as brittle strike slip faults associated with terrestrial basins such as the Quebrada Caya (Fig. 3.21). Most sinistral striae mapped on the DFS plunge very shallowly to the north (Fig. 5.6), such that tens of kilometres of sinistral displacement would also have caused W-side up offset of 10^2-10^3 metres, thereby satisfying the counter-intuitive post-Eocene offsets implied by thermochronology (Fig. 5.7c).

5.4.3 Significance of the Incaic tectonism and variable strain along the DFS.

The above interpretation means that the gross upthrow of the Paleozoic core of the Domeyko Cordillera during the Incaic tectonic event was 1000-1200 m, approximately double that implied by the present day map pattern (e.g., Maksaev et al. 1994). The Incaic event was therefore a more significant contractional event than is generally envisaged, and estimates of Incaic shortening based on the net stratigraphic separation are likely to have significantly underestimated the total (e.g., Amilibia and Skarmeta, 2003, Haschke and Gunther, 2003).

The change in kinematic strain accommodation on the DFS that followed shortening; first to dextral transpression and then to sinistral transtension, implies dramatic changes to the regional stress environment in the late Eocene and/or early Oligocene. In particular, the approximate timing of the switch in the sense of strike slip strain along the DFS permits a relationship to the Late Eocene metallogenic epoch in the Central Andes. Deposits that formed prior to 36 Ma in the Collahuasi district were emplaced under dextral strain whereas those formed subsequently were emplaced into negligible or sinistral strain environments (Chapter 4). The changing style of deformation also coincides broadly in time with the cessation of volcanism in the Domeyko Arc (e.g., Sandeman et al., 1995; Trumbull et al., 2006), as well as a pronounced westward shift in the locus of shortnening in the Central Andes (e.g., Oncken et al., 2006). In the next chapter, the magmatic response to these phenomena is investigated.

Chapter 6.

MAGMATIC CHEMISTRY AND THE TECTONIC EVOLUTION OF THE NORTH CHILEAN ANDES FROM 70-25 Ma.

6.1 Introduction

The magmatic rocks directly associated with many porphyry copper deposits are chemically distinctive (e.g., Mason and MacDonald, 1978; Kay et al., 1994b; Maksaev and Zentilli, 1999; Richards et al., 2001a), which implies that their petrogenesis was unique. Numerous attempts have been made to connect the distinctive chemistry of syn-mineral magmatic suites to certain physical conditions, tectonic settings and/or deformation environments (Kay and Mpodozis, 1999; Richards et al., 2001; Campos, 2002; Hollings et al., 2005; Rohrlach and Loucks, 2005). However, an integrated, widely applicable petrogenetic-tectonic-metallogenic model has remained elusive. Richards (2003, p.1515), suggested that "no unique processes appear to be required for [porphyry copper] formation, although additive combinations of common tectono-magmatic processes...can affect the grade and size as well as the location of the resulting deposits". In apparent contrast, Cooke et al. (2005, p.801) observed that "...the formation of [Neogene] giant porphyry copper...deposits in the circum-Pacific region has been closely associated with subduction of aseismic ridges, seamount chains, and oceanic plateaus...". The aim of investigating magmatic chemistry here is to help identify what was unusual about the petrogenesis of the Eocene suites in the south Central Andes. Comparisons with a compilation of data from other porphyry copper camps in the Central Andes and in the southwest Pacific permit an evaluation of the inter-arc, and inter-regional persistence of distinctive geochemical trends. A hypothesis is proposed for a more broadly applicable petrogenetic model for porphyry copper deposits.

Whole rock geochemical analyses were performed on a suite of samples that spans all the major Paleogene rock units mapped in the Collahuasi district. Attention was

paid to all the low-volume intrusive suites because macroscopically they are easily confused in the field. Without the benefit of an established geochronological and petrographic framework (e.g., Chapter 3), each of the suites might potentially be related to mineralisation.

6.1.1 Previous work

The magmatic chemistry of intrusions related to Tertiary porphyry copper deposits of central and northern Chile has been the subject of considerable research; 209 published and open file whole rock geochemical analyses for magmatic suites related in time and/or space to porphyry copper and high sulfidation mineralisation in the Central Andes were compiled in this study (Table. 6.1). However, just 15 are from the Collahuasi District, and all of those remain unpublished. A further 90 analyses of Late Cretaceous rocks belonging to the Quebrada Mala Formation and contemporaneous intrusions were also compiled (Lopez-Escobar et al., 1979; Rogers and Hawkesworth, 1989; Williams, 1992; Cornejo et al., 1997; Lucassen et al., 1999a; Haschke et al., 2002a).

6.1.2 Sampling and Analytical Methods

Twenty-five new analyses are presented here that provide data for unmineralised Maastrichtian to Late Eocene volcanics and stocks. These extend geochemical coverage to all four mineralised intrusive complexes and two suites of barren intrusions in the Collahuasi district. Samples were selected to specifically augment existing data for each of these major units.

The least altered samples were selected, although proximity to mineralisation made it necessary in some cases to analyse samples that had undergone weak alteration. Samples were cut to remove oxidised exterior or fracture surfaces, crushed and pulverised. All samples were analysed for major elements by x-ray fluorescence (XRF, n_{total}=46) and a subset of these were analysed for trace and rare earth elements by inductively-coupled plasma mass spectrometry using standard multi-acid digestions (ICP-MS, n=23). This study presents 12 new analyses of rocks related to the Eocene-Oligocene metallogenic event, 12 of the Cretaceous intrusive rocks, and 22 analyses of Permo-Triassic rocks. Analyses were performed at UTas and at Ontario

Geoscience Laboratories (OGS), Thunder Bay, Ontario, following methods outlined by Tomlinson et al. (1998), Robinson et al. (1999), Yu et al. (2001), Burnham et al. (2002), and Burnham and Schweyer (2004). In general, good agreement was obtained between the ICP-MS and XRF analytical methods although samples analysed at OGS by ICP-MS variably under-report vanadium, and to a lesser extent zirconium (Appendix VI). If V resides primarily in spinel group minerals, then this might imply that Ti, Ta, Sc and Cr are also under-reported. Incomplete digestion of zircon further suggests that the REE might be under-reported in some of the OGS samples.

Table 6.1. Summary of compiled geochemical data for Andean mineralised porphyries and related rocks

Area	Sample Material	*n* [a]	*n* rej.	Elemental Suite	Source
Collahuasi	Icanche Formation	5	-	major & trace	this study
	Pre-mineral stocks	1	-	major & trace	this study
	Syn-min: Copaquire	3	-	major & trace	this study
	Syn-min: QB	2	-	major & trace	this study
		2	-	major & trace	Rowland, 1998
		7	-	major only	Rowland, 1998
	Syn-min: Rosario	6	3	major & trace	Masterman, 2003
	Syn-min: Ujina	2	-	major & trace	Masterman, 2003
		1	-	major & trace	this study
Chuquicamata	Icanche Formation	26	3	major & trace	Haschke et al., 2002a
	Syn-min: Chuquicamata	10	4	major & trace	Pemberton, 1997
El Abra	Syn-min: El Abra	2	-	major & trace	Haschke et al., 2002a
		5	-	major & few trace	Rogers et al., 1989
El Salvador	Icanche Formation	7	-	few trace	Cornejo et al., 1997
	Syn-min: El Salvador	4	-	few trace	Cornejo et al., 1997
		11	-	major only	Gustafson and Hunt, 1975
El Teniente	Syn-min: El Teniente	12	2	major & trace	Cannell et al., 2005
		2	-	major & trace	Hollings et al., 2005
Escondida	Icanche Formation	1	-	major & trace	Richards et al., 2001
	Pre-mineral stocks	27	-	major & trace	Richards et al., 2001
	Syn-min: Escondida	3	1	major & trace	Richards et al., 2001
	Syn-min: Zaldivar	29[b]	1	major & trace	Campos et al., 2002
Maricunga Belt	Syn-min: Maricunga	7	-	major & trace	Kay et al., 1994
	Maricunga pre-mineral	34	-	major & trace	Kay et al., 1994

a.) *n* = number of samples, inclusive of those rejected (rej.) because of evident hydrothermal alteration.

b.) Campos et al (2002) present 29 melt inclusion analyses. These data were excluded during construction of fields for Chilean mineralised porphyries shown on geochemical plots later in this chapter.

Abbreviations: syn-min = intrusions spatially and temporally related to mineralisation; QB = Quebrada Blanca.

Measurement accuracy was determined by replicate analyses of international standards and is better than 5% for all elements except Ba, Ni, Zn, Cu, and Cr for which accuracy is better than 10% from both laboratories. Lithological classifications are applied following the IUGS scheme of Le Maitre (1989). Chondrite- and primitive mantle-normalized values were calculated using the values of Sun and McDonough (1989), supplemented for primitive mantle Y and Sr from Nakamura (1974) and chondrite Y and Sr from Taylor and McLennan (1986). Ratios that indicate spider diagram anomalies (i.e. Eu/Eu*) are calculated following the logarithmic method of McCuaig et al. (1994). Tabulated data and a more detailed analytical methodology is presented in Appendix VI.

Element mobility during hydrothermal alteration. Hydrothermal alteration has the potential to cause significant changes to whole rock chemistry, as is evident from the non-isochemical mineralogical changes that characterise some alteration facies. Immobility of a given pair of elements can be demonstrated if multiple repeat analyses are available for the same rock unit and these retain the original ratio of the chosen pair of elements, i.e. such that regression of a bivariate plot of the two passes through the origin (Winchester and Floyd, 1977; Barrett and Maclean, 1994). This approach is not appropriate for databases such as that compiled here, which instead contain few data from each of a larger number of rock units. The exception is six analyses of the Rosario Porphyry reported by Masterman (2003) from the same UTas laboratory and using the same methods as those presented here. However, as these samples were collected in drillcore, the sampled volumes (of this coarsely porphyritic rock) were unlikely to have captured a representative population of accessory mineral grains that host much of the trace element budget. Scatter among these repeat samples cannot therefore be confidently attributed to either alteration or statistical integrity. Urqueta et al. (2009) collected whole rock data for a widespread suite of samples across the district with the specific aim of quantifying the chemical changes associated with of hydrothermal alteration. These authors conclude that "[Pearce element ratio] analysis documents no mass transfer during propylitic alteration besides a minimal increase in the carbon content", and therefore implies that the samples of unaltered to weakly propylitised rocks analysed in this study are likely to represent original magma compositions.

Analyses (new and existing) were screened for alteration effects. Those passing the following criteria were retained in subsequent plots and interpretation: $Na_2O > 1$ wt%, $K_2O < 6.5$ wt%, clay index of alteration (CIA: Nesbitt and Young, 1982) < 73, ignition losses < 5%, or Ca/Sr < 150. Samples with CIA between 66-73 and ignition losses of 3-5 % have been retained but are treated with caution as these values imply some degree of alteration of the primary mineralogy. For the suite of mineralised plutons, samples with molar K/Na > 3 were also screened out, as these consistently plot off the trends defined by other samples and are considered likely to have been affected by K-silicate alteration. Other aspects of alteration effects, or lack thereof, are discussed in the relevant sections below. Plots showing the screened populations are presented in Appendix VI.

Mineralogical arguments can also be made that suggest the effects of alteration are minimal in the samples retained after screening. Hydrothermal alteration associated with the inner zones of porphyry copper deposits is dominated by potassium-feldspar replacement of the groundmass and plagioclase crystals, and/or biotite replacement and overgrowth of hornblende and pyroxene (e.g., Seedorff et al., 2005). Unaltered plagioclase and euhedral coarse grained biotite are typically preserved in the Rosario and Quebrada Blanca samples compiled here (Rowland, 1998; Masterman et al., 2005; this study, Appendix II). Nor are these samples depleted in Na or Ca as would be expected if hydrothermal orthoclase or biotite replaced plagioclase.

6.2 Late Cretaceous to Paleogene Magmatic Rocks

6.2.1 Petrology and Stratigraphic Setting; summary

The stratigraphic setting, age and petrology of the rock suites investigated here is described in detail in Chapter 3, and in Masterman et al. (2004, 2005). A short review that includes some regional data, is provided here.

Quebrada Mala Formation. Late Cretaceous to Paleocene (~76-63 Ma) volcanic and intrusive rocks occur along the North Chilean Valle Central (Chapter 2) wherein they are typically exposed in the lower western flanks of the Domeyko Cordillera (Scheuber and Reutter, 1992; Charrier and Munoz, 1994; Tomlinson et al., 2001a). These are typically subalkaline andesitic to dacitic rocks that host slightly younger

porphyry Cu-Mo and epithermal polymetallic deposits (e.g., Williams, 1992; Bouzari and Clark, 2006). The Quebrada Mala Formation post-dates the Cerro Empexa Formation and is not represented *sensu stricto* in the Collahuasi district (Fig. 3.3). Unmineralised alkalic magmatic rocks of the same age occur as isolated intrusive complexes inboard of the main arc along the eastern Domeyko Cordillera and intercalated with sediments of the Preandean Depression, 20-100 kms inboard of the main arc front (Charrier and Reutter, 1994; Scheuber et al., 1994; Tomlinson et al., 2001a; Urzua, 2009). The Tolaún intrusive complex at Collahuasi (Fig. 6.1) is one such complex, which was emplaced in the latest Cretaceous (Chapter 3). Rocks of this approximate age and position relative to the arc from throughout northern Chile are collectively referred to here as the "Tolaún suite".

Icanche Formation. The Icanche Formation (Maksaev, 1978) comprises subaerial volcanics and related stocks that erupted from 55 to 42 Ma along a narrow arc located along, and generally west of the Domeyko Fault (Tomlinson et al., 2001a; Urzua, 2009). This distribution pattern about the Domeyko Fault is evident in the abundance of syn-Icanche stocks in the western Collahuasi district (Fig. 6.1) and in the distribution of the Icanche Formation volcanics more regionally (e.g., Tomlinson et al., 2001a). Extrusive and shallow intrusive levels are preserved on both sides of the Domeyko Fault, such that the distribution is not an artefact of differential erosion.

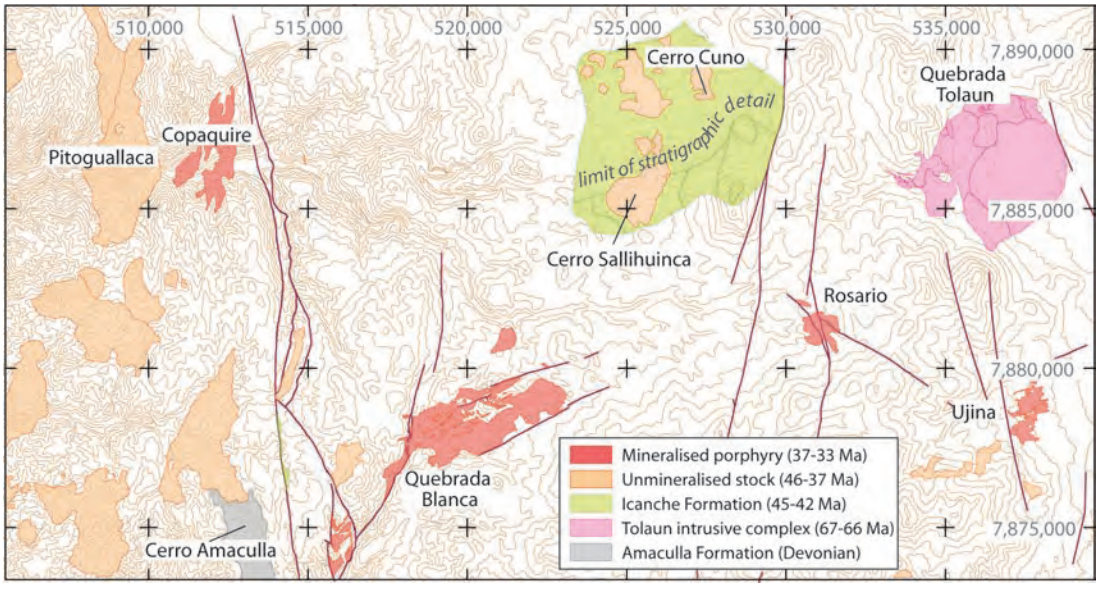

Figure 6.1. Location map showing distribution of Late Cretaceous to Paleogene magmatic suites and upper crustal basement units in the Collahuasi district. Pale linework are topographic contours, dark lines are simplified interpreted major faults.

These rocks therefore represent the last magmatic products of the Central Andean margin before the onset of Incaic tectonism and the formation of major porphyry copper deposits. At Collahuasi, the Icanche Formation comprises a single volcanic complex in the central-northern part of the district near Cerro Sallihuinca (Figs. 3.19 and 6.1). It includes hornblende- and biotite-phyric dacites to rhyolites, and common brecciated and pyroclastic equivalents (section 3.11, Appendix II). Contemporaneous intrusions such as the Sallihuinca and Pitoguallaca stocks (Fig. 6.1) are primarily hornblende- and less commonly biotite-monzonites, monzodiorites and tonalites, with lesser granodiorites (section 3.15, Appendix II). Geochemical data for the volcanic and intrusive facies are here treated together and are referred to as the "Icanche suite".

Mineralised Intrusions. Stockwork and disseminated Cu-Mo deposits in the Collahuasi district are related in time and space to small, high level porphyritic intrusions (Fig. 6.1; Ware et al., 1981; Rowland, 1998; Masterman et al., 2005). These are typically quartz monzonite to quartz monzodiorite in mineralogy and have phenocryst assemblages dominated by plagioclase with lesser biotite and/or hornblende. In contrast to the numerous intrusive phases recognised at other major porphyry copper centres (e.g., El Salvador; Gustafson and Hunt, 1975; El Teniente; Cannell et al., 2005), the Collahuasi porphyritic complexes are paragenetically simple (at least at the present level of exposure and drilling), and comprise three-phase (QB, Copaquire), and two-phase (Rosario, Ujina) composite stocks (Chapter 4). The data from any one centre are therefore insufficient to describe the evolution of a comagmatic suite, and rather, all samples from the district are presented together. Richards et al. (2001a) argued that abundant unmineralised dioritic stocks in the Escondida district represented less evolved equivalents of the mineralised intrusions in that camp. In the absence of such intrusions in the Collahuasi district, and similar composition of mineralised intrusions in the two camps (compare data of Masterman, 2003 and Richards et al., 2001a), the barren Escondida district data serves as a useful comparator.

6.2.2 Classification by Major Element Chemistry

Of the Paleogene magmatic suites in the Collahuasi district, the Late Cretaceous

Tolaun suite includes a broad compositional range from basalt through rhyolite, whereas the two Eocene suites are restricted to dacitic and rhyolitic compositions. However, elsewhere in northern Chile the Icanche suite ranges from basaltic andesite to rhyolite. The Escondida district (Richards et al., 2001a) is the only major Eocene-Oligocene porphyry camp in Chile in which syn-mineral (albeit barren) intermediate to mafic rocks are well known. The suites have been classified here on the basis of their relative alkali, iron, magnesium and silica content (Fig. 6.2) using the

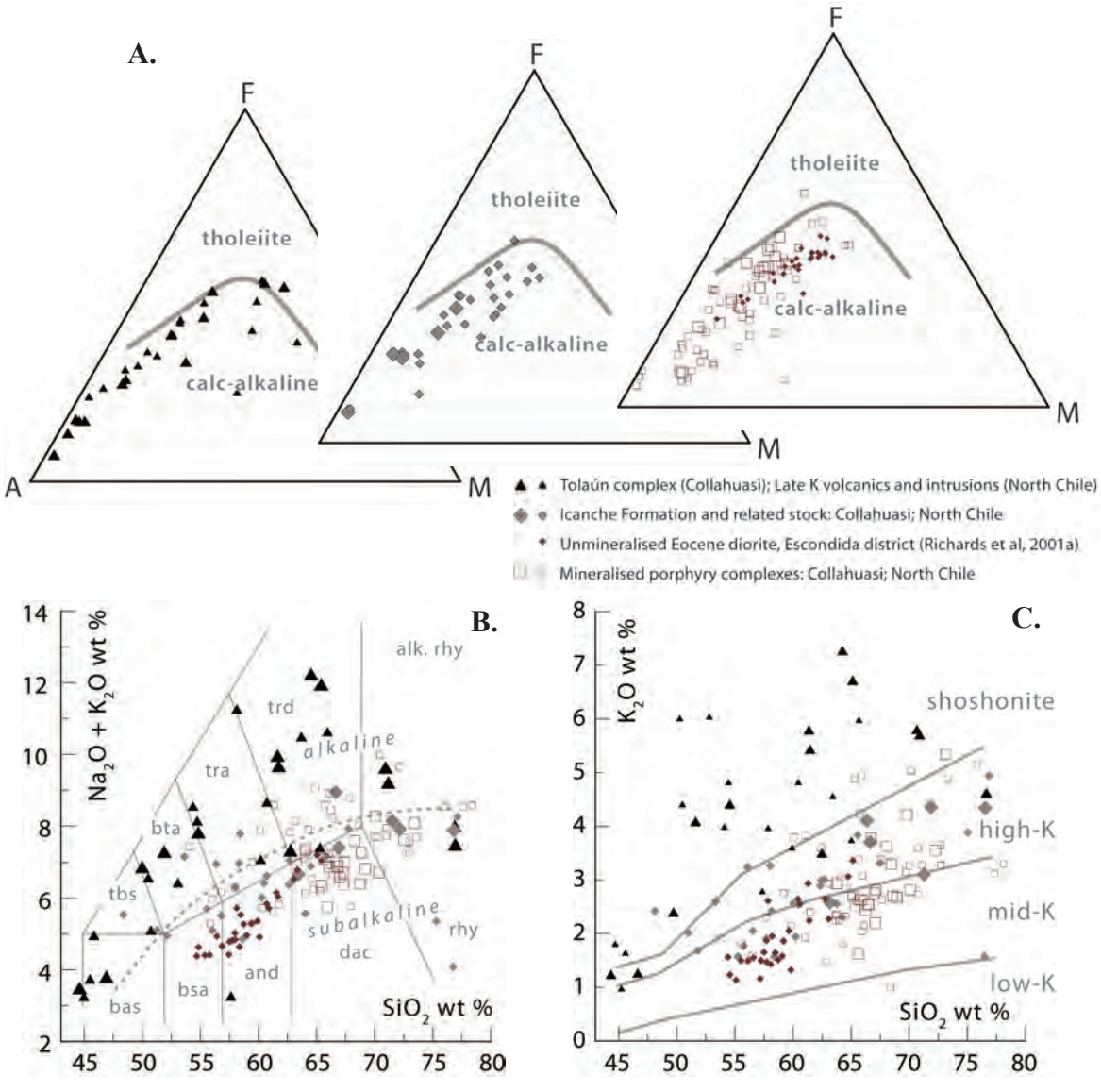

Figure 6.2. Magma series classification of Paleogene magmatic suites in the Collahuasi district. A.) AFM diagram with tholeiite/calc-alkaline boundary of Irvine and Baragar (1971); B.) $Na_2O + K_2O$ v. SiO_2 with volcanic rock nomenclature from Le Bas et al. (1986) and alkaline/subalkaline boundary (dashed: Miyashiro, 1978); C) K_2O v. SiO_2 with calc-alkaline series boundaries of Le Maitre et al. (1989). Abbreviations: tbs = trachybasalt; bta = basaltic trachyandesite; tra = trachyandesite; trd = trachydacite; alk. rhy = alkaline rhyolite; bas = basalt; bsa = basaltic andesite; and = andesite; dac = dacite; rhy = rhyolite. Note that in these, and all subsequent bivariate plots, larger symbols represent samples from the Collahuasi district and these are dominated by new analyses. References to the sources of additional data are given in section 6.1.1. and Table 6.1.

classification schemes of Irvine and Baragar (1971), Peccerillo and Taylor (1976), and Le Bas et al. (1986).

The Collahuasi suites are chemically similar to compositional trends defined from contemporaneous magmatic rocks studied elsewhere in northern Chile. None of the suites show the iron-enrichment trend that defines the tholeiite magma series, and they therefore all belong to either the calc-alkaline or alkaline series (Fig. 6.2a). The Tolaun suite have high total alkali contents (Fig. 6.2b) and low $CaO/(Na_2O+K_2O)$ (~0.4 at 60 wt % SiO_2) that classify them as alkaline magmas. They plot well into the shoshonite field in terms of potassium oxide (Fig. 6.2c) such that their alkalinity is driven by elevated potassium. They evolved along an alkaline trend from trachybasalt to trachydacite composition, after which the more felsic members record quartz-saturated evolution to subalkaline rhyolite compositions. In contrast, the Icanche suite and mineralised intrusions are mostly subalkaline (Fig. 6.2b), though there is some scatter to alkaline compositions among mineralised rocks from other north Chilean porphyry copper districts. Both suites evolved through the calc-alkaline basaltic andesite - andesite - dacite - rhyolite sequence. The most mafic members of both groups are mid-K calc-alkaline, and both evolved to high-K calc-alkaline compositions. However, dacitic mineralised rocks are generally less potassic than the Icanche formation; they typically contain ~2 wt% K_2O at 67% SiO_2, compared to ~2 wt% K_2O at 62% SiO_2 for the Icanche suite (Fig. 6.2c). The mineralised suite at Collahuasi is also peraluminous (average molar Al/[Ca+Na+K] = 1.27), whereas the Icanche suite is typically metaluminous (average molar Al/[Ca+Na+K] = 0.93). In terms of both alkali and alumina contents, the unmineralised syn-mineral diorites at Escondida resemble the Icanche suite rather than the mineralised suites (Fig. 6.2c).

6.2.3 Evidence for the Tectonic Setting of Magmatism

All three Paleogene magmatic suites in the Collahuasi district are characterized by overall LILE and LREE enrichment and relative depletion of Nb, Ta and Ti in primitive mantle- and chondrite-normalised plots (Figs. 6.3 and 6.4). Excluding the most silicic samples, all the suites have La/Ta > 30; Ba/La > 20, Ce/Pb < 7 and Nb/U < 7 (including new and compiled data). These features are characteristics of magmas generated above a subduction zone, wherein the distinctive chemistry relates to the

metasomatism of the athenospheric mantle by a slab-related silicic or hydrous melt (e.g., Perfit et al., 1980; Hickey et al., 1986; Pearce and Peate, 1995; Hacker et al., 2003; Davidson and Arculus, 2006). Six samples of the Rosario Porphyry reported by Masterman (2003) permit limited evaluation of the effects of potassic alteration that might have affected the syn-mineral intrusive rocks, and hence the integrity of these results. With the exception of one sample in which sodium has largely been replaced by potassium (K/Na = 90, Na_2O = 0.08%), the other samples show a narrow range of Na/K, and consistent trace element patterns (Fig. 6.4d). The characteristics recorded by the "immobile" or weakly mobile trace elements are therefore taken to be primary magmatic features. The distinctive chemical characteristics of supra-subduction zone magmas are generally present, but are variably less pronounced among Tolaun and Icanche suite samples with >70% SiO_2. These samples are generally very rich in the LILE, U and Th (Fig. 6.3) and are interpreted to reflect mixing between sub-arc and intracrustal melts.

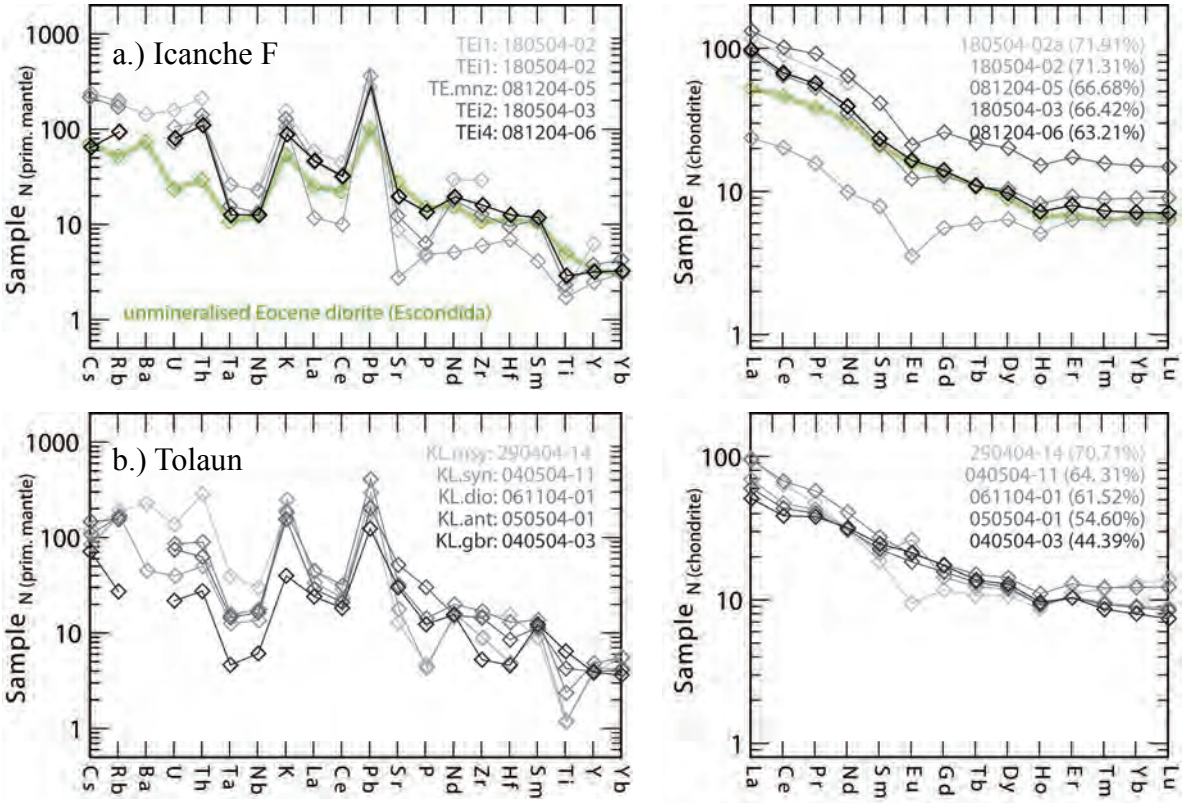

Figure 6.3. Trace element spider diagrams and REE plots for unmineralised Late Cretaceous and Eocene magmatic rocks of the Collahuasi district. Linework corresponds to the sample numbers in the same shade. Darker lines relate to less silicic samples, with the SiO_2 content in parentheses in the REE plots. The broad green line in a) and in the next figure is an average of the 12 most mafic Middle Eocene diorite stocks in the Escondida district (data of Richards et al., 2001a). Incomplete traces reflect different analysis suites. Lithology codes on the spider plots correspond to those used in maps and sections in Chapter 3. Normalisation values used are those of Sun and McDonough (1989).

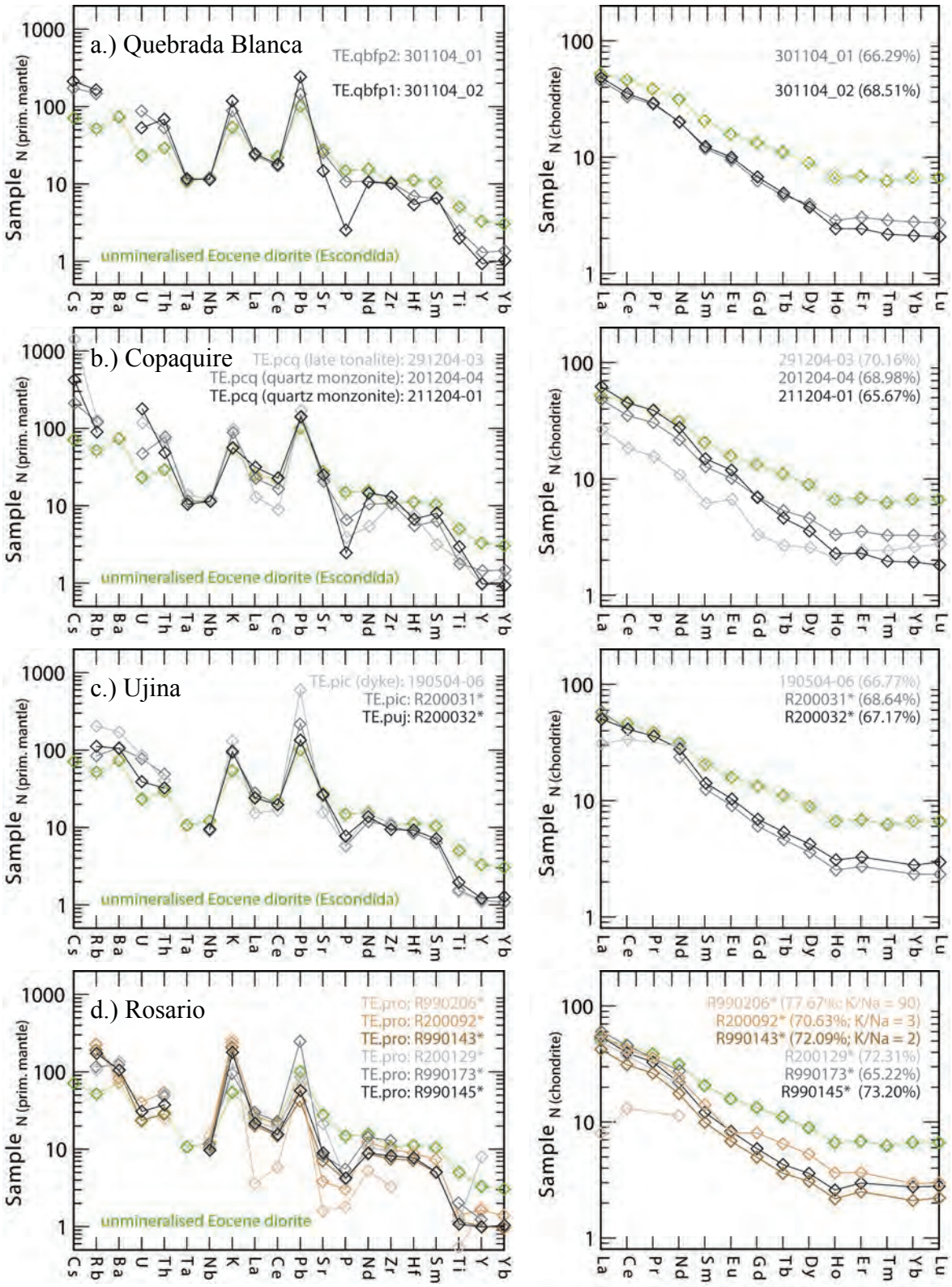

Figure 6.4. Trace element spider diagrams and REE plots for mineralised intrusive complexes of the Collahuasi district. Linework corresponds to the sample numbers in the same shade. Brown lines in d) are samples from Rosario with high molar K/Na indicative of plagioclase destruction during potassic alteriation. Darker lines relate to less silicic, or paragenetically earlier rocks, with the SiO_2 content in parentheses in the REE plots. Green lines on all plots are an average mafic Icanche formation composition calculated from data of Richards et al. (2001) and Haschke et al. (2002a). Incomplete traces reflect different analysis suites for some samples. Normalisation values used are those of Sun and McDonough (1989).

The potassic alkaline character of the Tolaun suite at Collahuasi (and throughout the Domeyko Cordillera: Richards et al., 2001a; Tomlinson et al., 2001a; Urzua, 2009) is typical of magmas formed inboard of the main arc front (e.g., Dickinson, 1975; Ryan et al., 1995). Potassic melt compositions are predicted to characterise this environment because of the persistence of K-rich phases (notably phengite) at depths beyond that of normal subduction zone melting regimes (Schmidt, 1996). However, the Tolaún suite have normal arc-like abundances of the non-conservative elements (i.e those such as La and Ba that are dominated by the slab-related flux: Pearce and Peate, 1995; Fig. 6.3). Ratios of these to conservative elements with similar partitioning behaviour reflect the strength of the subduction signal. On these grounds, the Tolaún suite appears arc-like (average mafic-intermediate La/Nb = 3.16, range 2.02 - 5.83 [arcs: 3-5; backarcs: <1.6]) and does not represent continental back arc magmatism. During the Late Cretaceous, the Preandean Depression was under active extension (e.g., Wilkes and Görler, 1994). It seems likely therefore that the Tolaun suite, 20-50 kms inboard of the Quebrada Mala Arc and concentrated about the basin-bounding Rio Loa Fault (Chapter 4), records the ascent of small volumes of potassic arc magma into extensional sites in retro-arc position.

The tectonic setting of the Icanche and mineralised suites is of particular interest since the two suites partly overlap in space and arguably in time (depending on whether one attributes to the Icanche Suite unmineralised stocks such as the Escondida district diorites). In considering the Icanche suite, it is informative to also consider the Neogene Central Volcanic Zone (CVZ). Figures 6.6 - 6.12 include a field for Volcán Ollagüe, a Quaternary basaltic andesite to dacite stratovolcano adjacent to the Collahuasi district (Wörner et al., 1992a; Feeley et al., 1993). This volcano is considered typical of the Neogene CVZ (Feeley and Davidson, 1994), and indeed broadly similar magmatic suites have been reported from other volcanoes along the Neogene Western Cordillera arc (Baker et al., 1977; Lopez-Escobar et al., 1977; Hawkesworth et al., 1982; Matteini et al., 2002; Richards and Villeneuve, 2002). The Icanche suite is, on average, similar to CVZ lavas (Figs. 6.6-6.12) except that it scatters more than the Volcán Ollagüe reference suite. This scatter is inferred to result from both the grouping of data from a number of volcanic centres, and to differences in crustal contributions related to local heterogeneities and the post-Eo-

cene evolution of the Andean crust (e.g., Hildreth and Moorbath, 1988; McMillan et al., 1993). Nonetheless, the general similarity between the two is taken to imply that the tectonic setting of the Icanche suite resembles the setting of the Neogene Andean margin (e.g., Angermann et al., 1999; Oncken et al., 1999). Given the longevity of intermediate arc volcanism in the CVZ (e.g., Trumbull et al., 2006), this is taken to approximate "normal" Central Andean arc magmatism.

Much of the remainder of this chapter focusses on distinguishing the process(es) that separate the arc petrogenesis of the fertile suites from this "normal" magmatism. Fertile magmatism began as a transient phenomenon during the Incaic Tectonic Phase, between ~41 and 37 Ma (the period in which North Chilean porphyry copper deposits and barren stocks overlap (e.g., Richards et al., 2001a; Tomlinson et al., 2001a; Camus, 2003). Subsequently, in the Collahuasi district, as elsewhere in North Chile, mineralised suites became the predominant type of magmatic product until ~32 Ma (Chapter 3). A wholesale change in the dynamic setting and petrogenesis is therefore permissible after ~37 Ma (Chapter 4).

6.2.4 Major and Large-Ion Lithophile Elements

The Icanche Formation. Icanche suite rocks show compatible behaviour of alkali earth and transition metals, P, and Sr, and incompatible behaviour of the alkalis (Figs. 6.6, 6.7). The bulk abundances and trajectories described by the compiled data for the Icanche suite are coincident with those for Volcán Ollagüe (Figs. 6.6, 6.7).

At Collahuasi, the Icanche suite is dominated by felsic volcanic facies that include numerous accessory lithic fragments (section 3.11, Appendix II). These samples have correspondingly diverse compositions. Nonetheless, their Harker trajectories for Al and Ca steepen at ~65% SiO_2 (Fig. 6.6a, b), and negative Eu anomalies are typical (Fig. 6.3a; Eu/Eu* = 0.53 - 0.91). As Eu is principally partitioned by plagioclase during magma crystallisation (Drake and Weill, 1975), these characteristics imply a role for plagioclase, either by fractional crystallisation or as a residue, late in the evolution of the Icanche suite. Compatible Ca, Mg, Fe, and Ti (Fig. 6.6) are permissive of either fractional crystallisation of clinopyroxene ± amphibole, and/or assimilation of evolved crustal materials throughout the evolution of the Icanche Formation.

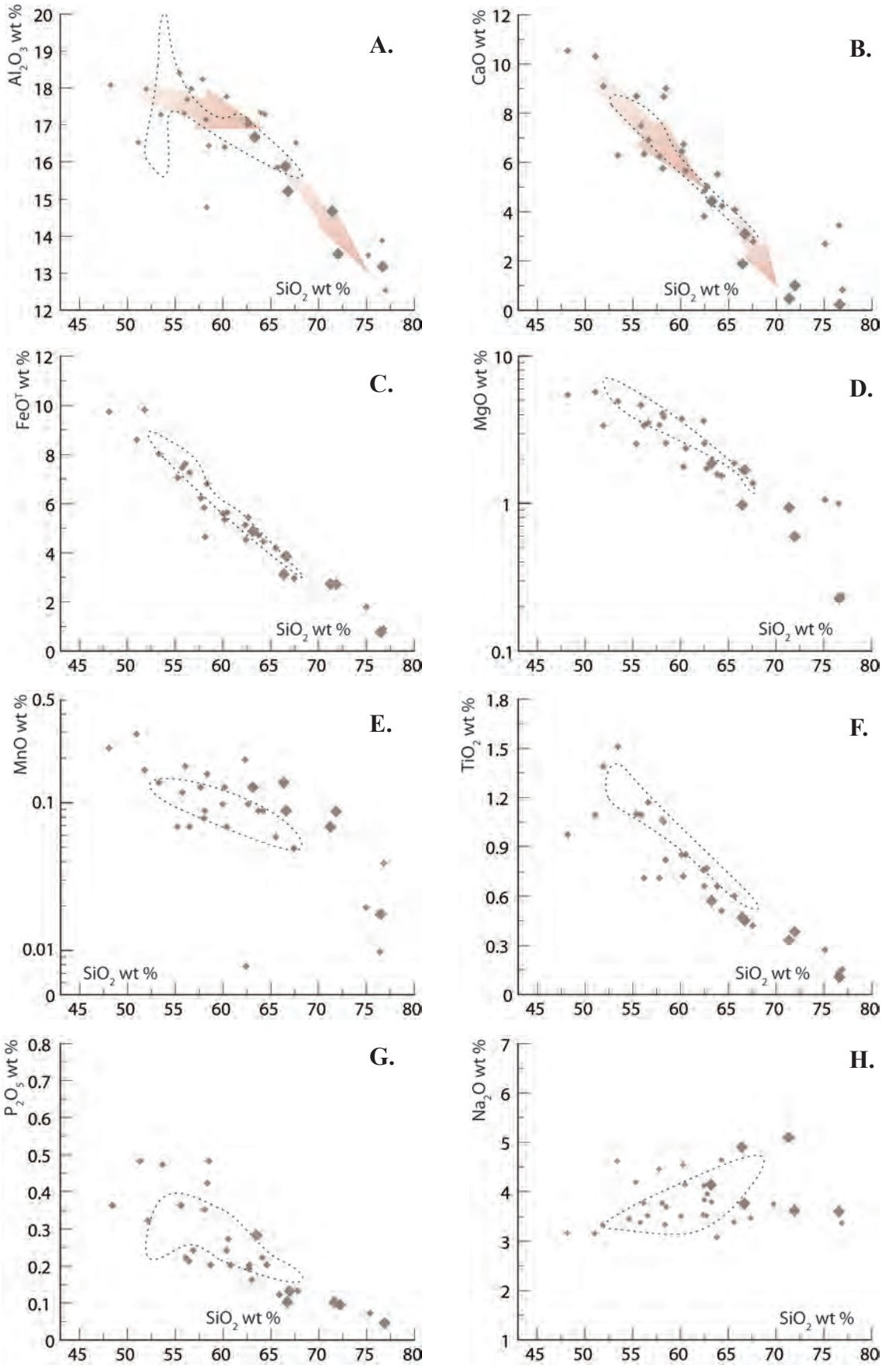

Figure 6.6. Harker diagrams showing the behaviour of major elements with increasing silica in the Icanche suite at Collahuasi (large symbols) and elsewhere in northern Chile (small symbols; Table 6.1). Light dashed field encompasses 95% of Volcán Ollaguë volcanic rocks (Wörner et al., 1992a; Feeley et al., 1993). Arrows indicate trends and inflexions discussed in the text.

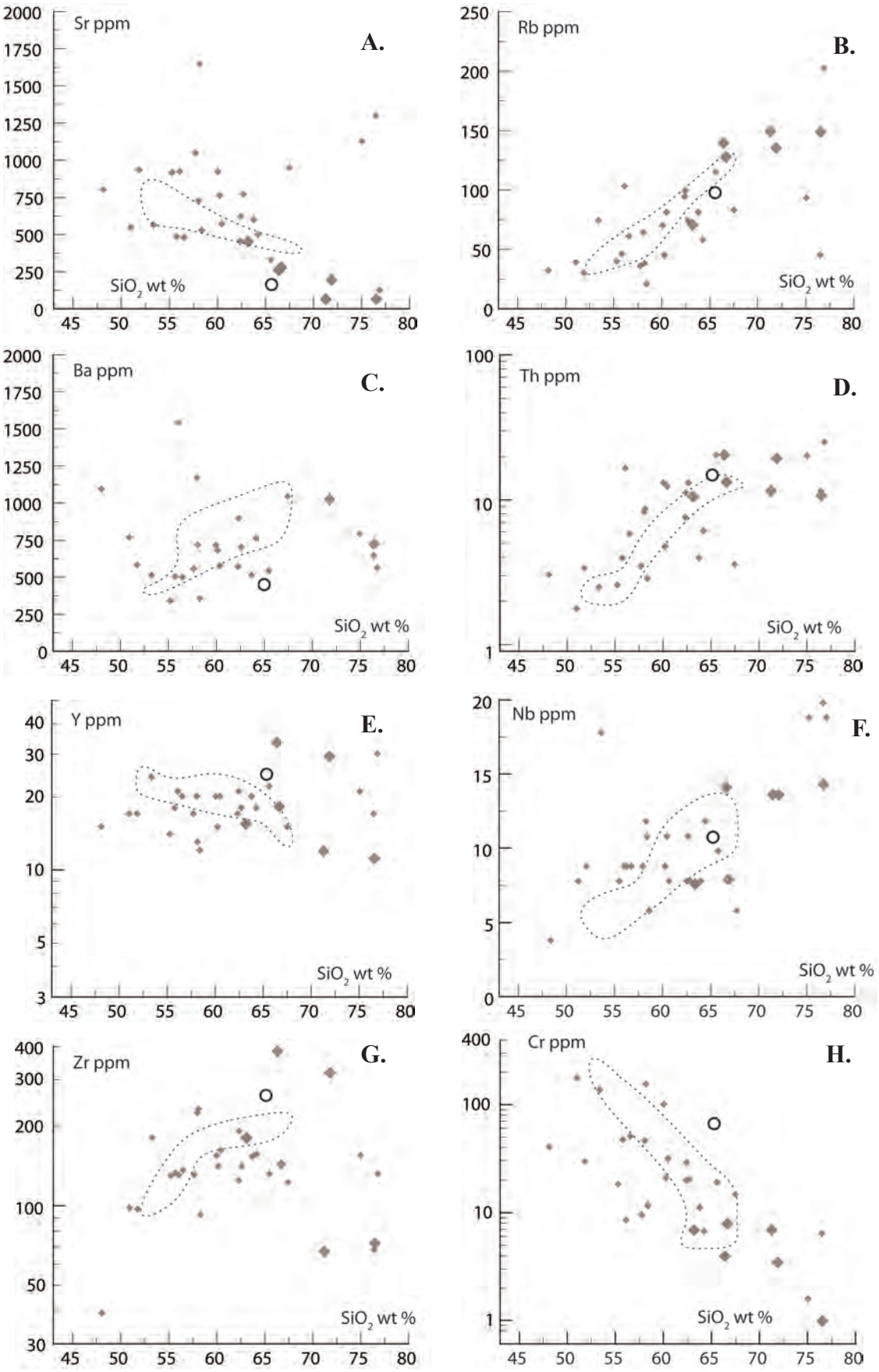

Figure 6.7. Harker diagrams showing the behaviour of trace elements with increasing silica in the Icanche suite at Collahuasi (large symbols) and elsewhere in northern Chile (small symbols; Table 6.1). Dashed field is for Volcán Ollaguë (Wörner et al., 1992a; Feeley et al., 1993). The circle is average N Chile gneissic basement (Lucassen et al., 1999a). Arrows indicate trends discussed in the text.

The Tolaun Suite. Compared to the Icanche-Ollagüe "normal" magmatism, the Tolaun suite is poorer in Mg, Ca, Ti, and its mafic members are richer in the nonconservative elements (Rb, Ba, Sr; Figs. 6.8 and 6.9). These are characteristics generally consistent with its overall alkaline chemistry, and inferred deeper source and lower degrees of partial melting in a retro-arc position. Clinopyroxene is the most abundant ferromagnesian phase among the mafic members of the Tolaun suite (Appendix II). Calcium, FeO and MgO are all compatible, permissive of differentiation by removal of any calcic ferromagnesian phase. Aluminium is incompatible, and Mn is less strongly compatible than among the other suites. Clinopyroxene generally excludes Al and accepts less Mn than other major ferromagnesian phases (Arth, 1976; Pearce and Norry, 1979). These relationships are interpreted to reflect fractional crystallisation of calcic clinopyroxene. Inflexions in the Harker diagrams for Al_2O_3, CaO, P_2O_5, Sr and Ba at ~52% SiO_2 (Figs. 6.8 and 6.9) are interpreted to record the onset of plagioclase + minor apatite crystallisation. Gravimetric separations performed on Tolaun suite samples used for geochronology yielded abundant, large (>100μm), euhedral apatite crystals, in line with this interpretation. One intermediate sample from the main Tolaun intrusive complex has a positive Eu anomaly that implies plagioclase accumulation (Fig. 6.5b: Eu/Eu* = 1.49), whereas Eu anomalies are generally absent from the more mafic members. A second apparent inflexion of Al_2O_3 in the Tolaun suite data occurs at ~65% SiO_2 (Figs. 6.8 and 6.9) and separates two Ca-poor microsyenite samples from the more voluminous stocks (Chapter 3). These felsic (microsyenite dyke) members have distinct negative Eu anomalies (Fig. 6.5b: Eu/Eu* = 0.63) that permits them to be the products of the residual liquid after plagioclase accumulation among other parts of the suite. At near exhaustion of Ca in this residual liquid, coincident inflexions in the Harker trajectories of K_2O, Na_2O, Rb, Zr and Y imply a role for late stage fractional crystallisation of alkali feldspar and zircon.

Syn-mineral suites. Presented collectively, the mineralised intrusions from across Northern Chile appear to show differentiation trends that are grossly similar to those for the Icanche Formation and CVZ, albeit less well-defined (Figs 6.6 and 6.7). In detail there are important differences.

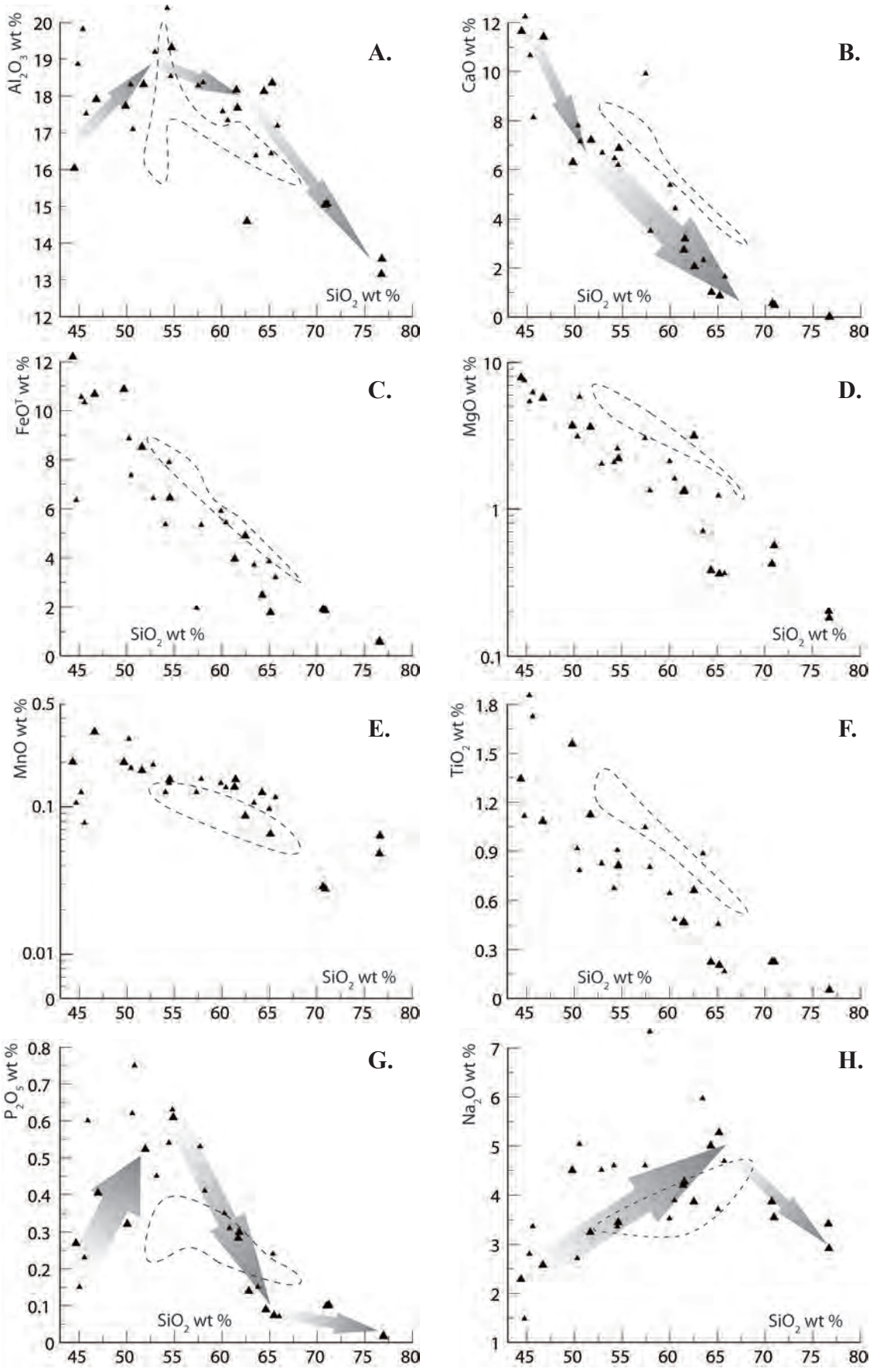

Figure 6.8. Harker diagrams showing the behaviour of major elements with increasing silica in the Tolaun complex (larger symbols) and contemporaneous magmatic rocks elsewhere in northern Chile (references in section 6.11). Light dashed field encompasses 95% of Volcán Ollaguë volcanic rocks (Wörner et al., 1992a; Feeley et al., 1993). Arrows indicate trends and inflexions discussed in the text.

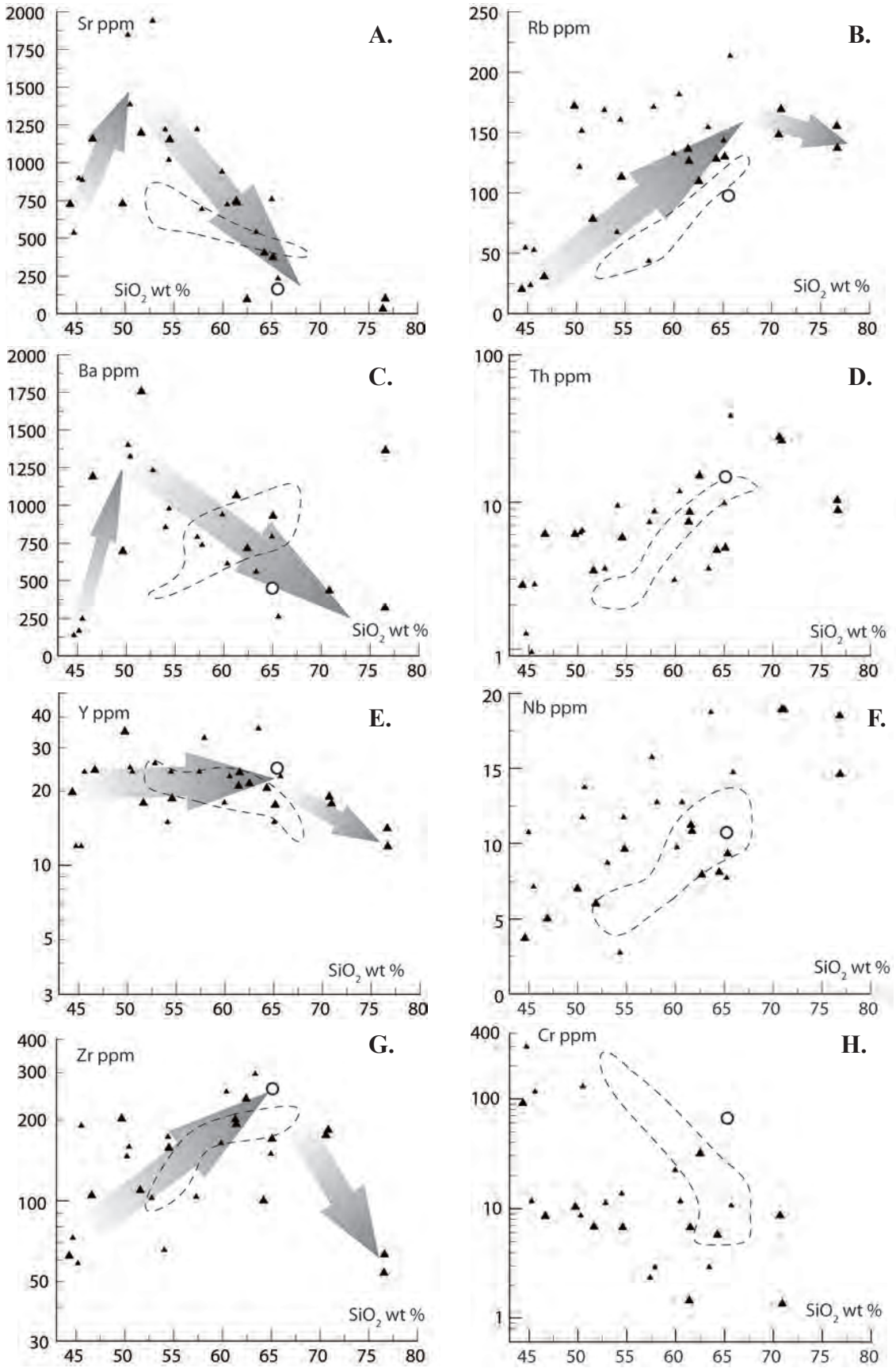

Figure 6.9. Harker diagrams showing the behaviour of trace elements with increasing silica in the Tolaun complex (larger symbols) and contemporaneous magmatic rocks elsewhere in northern Chile. Dashed field is for Volcán Ollaguë (Wörner et al., 1992a; Feeley et al., 1993).White circle is average N Chile gneissic basement (Lucassen et al., 1999a). Arrows indicate trends discussed in the text.

Aluminium, Ca and Sr are all generally compatible among the intrusions related to mineralisation, however Al and Sr are slightly enriched at dacitic bulk compositions, relative to the Icanche suite and CVZ (Figs. 6.10a, b; 6.11a and 6.12a; note that "compatible" and "incompatible" are used here to refer to Harker trends, without any inference that these describe liquid lines of descent). These elements also define Harker trajectories that are steeper than those described by the Icanche and CVZ. The compatible behaviour of this suite of elements suggests a role for plagioclase crystallisation, and the steepness of the Al_2O_3 - SiO_2 trajectory further implies an almost exclusive role for it in the dacite-rhyolite evolution of the syn-mineral suites (Fig. 6.12a). However, Al, Ca, Sr and Na all range from greater than-, to less than the ranges of composition defined by the other suites. Likewise, Eu anomalies among the syn-mineral rocks may be positive or negative, and are generally weak (Fig. 6.4; Eu/Eu* = 0.76 - 1.17). These suites are characteristically strongly porphyritic and contain substantial plagioclase crystal populations (Table 3.5; Appendix II). Therefore, the textural and chemical relationships are interpreted as evidence that plagioclase removal by crystallisation was variably balanced or by crystal accumulation during the evolution of these magmas.

Potassium and Rb are incompatible among all the mineralised suites, but increase with silica more rapidly than among unmineralised suites (e.g., Figs. 6.2c; 6.11b; 6.12b). Syn-mineral intrusions of dacitic bulk composition are slightly poorer in K and Rb than unmineralised rocks. This pattern could be generated by crystallisation of oligoclase or andesine, i.e. a comparatively sodic and silicic plagioclase (Fig. 6.12b). Masterman (2003) presents electron microprobe analyses of unaltered plagioclase phenocrysts in the Rosario porphyry, which average An_{20} - An_{36}, which are consistent with this notion. The alkali-aluminium trends could also be satisfied by mixing between a mid-K calc-alkaline magma with a shoshonitic peraluminous intracrustal melt. However, local gneissic crustal materials in the vicinity contain abundant HFSE and Y, and these elements are distinctively un-enriched among the syn-mineral suites (Fig. 6.11d-g). Potassium metasomatism related to the porphyry systems is ruled out because the trend is not toward the composition of orthoclase or biotite, and nor are the K/Na systematics of these samples upset (Fig.

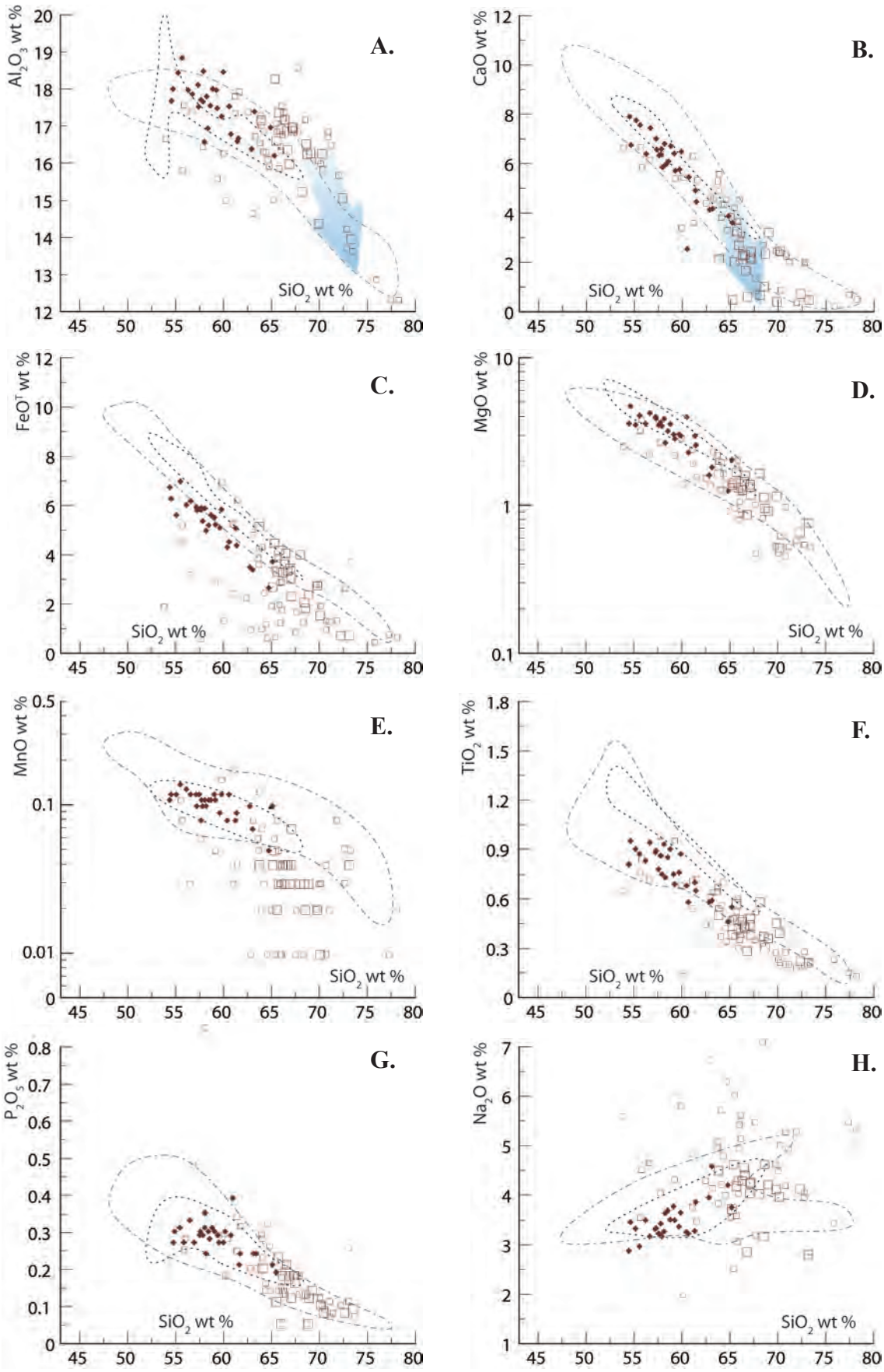

Figure 6.10. Harker diagrams showing the behaviour of major elements among syn-mineral suites at Collahuasi (large symbols) and elsewhere in northern Chile (small symbols; Table 6.1). Solid symbols are diorites unrelated to mineralisation at Escondida (Richards et al., 2001a). Light dashed field as per figures 6.6-6.9; grey dashed field indicates the compositional range of most Icanche suite rocks.

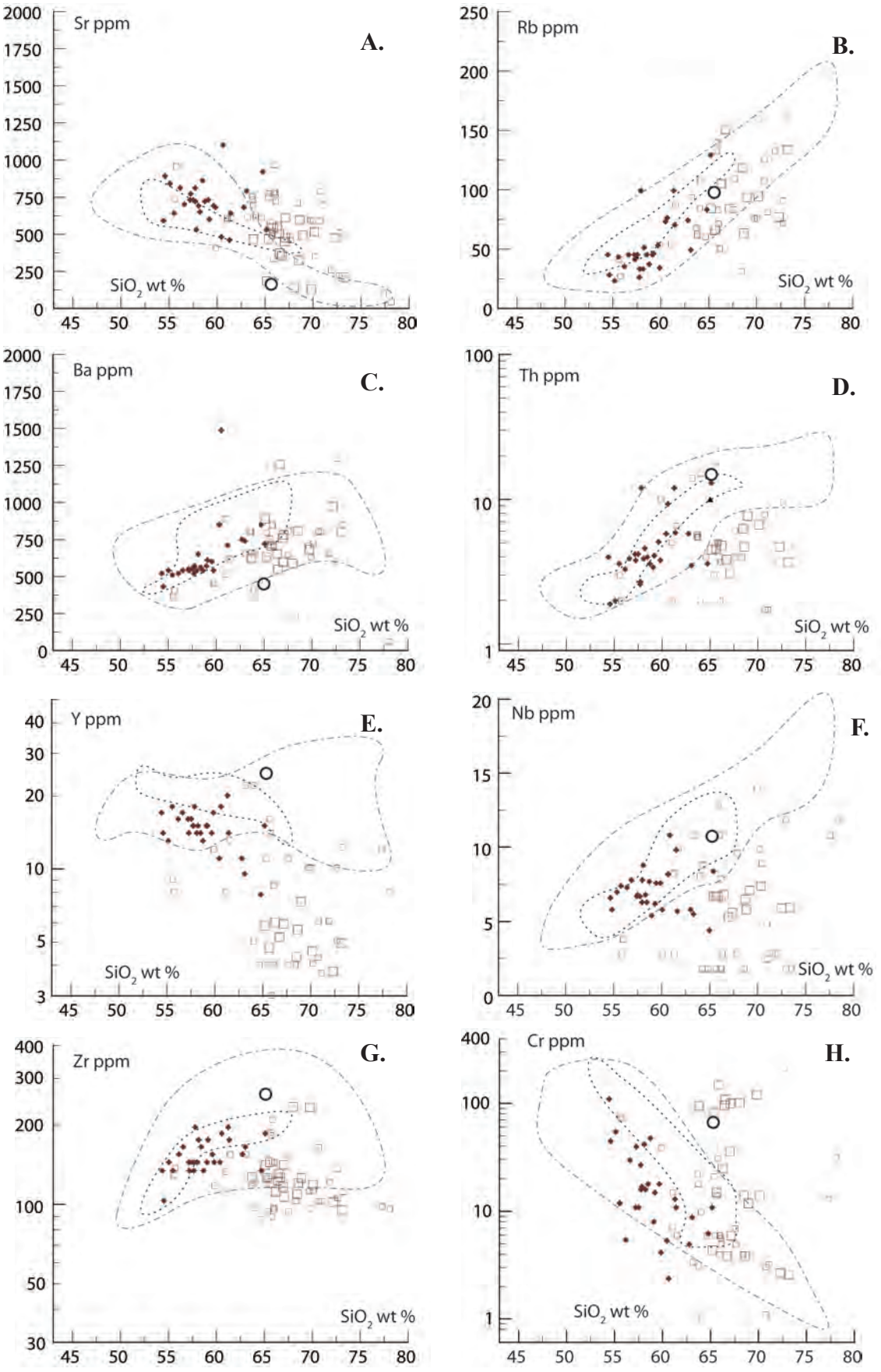

Figure 6.11. Harker diagrams showing the behaviour of minor elements among syn-mineral intrusive suites at Collahuasi (large symbols) and elsewhere in northern Chile (small symbols; Table 6.1). Symbology, data sources and reference fields as per figures 6.9 and 6.10.

6.4). Rather, the unusual alkali-alumina-silica relationships appear to be primary characteristics of the mineralised suites that resulted from fractional crystallisation and/or accumulation of oligoclase. The same weak enrichment in Al, Ca, and Sr relative to unmineralised background (and depletion in K, and Rb), as well as steep Harker trajectories for these elements, are recogniseable among datasets for several prolifically mineralised terranes in the SW Pacific (Fig. 6.12a, b). The involvement of sodic plagioclase, as opposed to more calcic, less silicic varieties, appears to be common to fertile intrusive suites in both continental and oceanic terranes.

The Andean mineralised suites also have compatible MgO, FeO^t, TiO_2 and P_2O_5 (Fig. 6.10). These demand a role for a ferromagnesian phase and apatite in their evolution. Notably, the mineralised rocks are variably less ferruginous, less calcic and less titanian than normal Andean magmas (Fig. 6.10b, c, f). They also have strikingly lower MnO content, that locally approaches the detection limit of the analytical method (Fig. 6.10e). In contrast, they have normal content and trajectories of MgO and P_2O_5. These differences and similarities to other suites are interpreted to reflect a distinctive role for an Fe-Ti-(Mn)-bearing phase (likely an oxide), and to preclude unusual behaviour of apatite in the evolution of these magmas. The barren syn-mineral suite from Escondida shares the low-Fe, low-Ti trend defined by the mineralised suites (Fig. 6.10c, f), whereas it is similar to the Icanche suite in terms of CaO, MgO and the LILE (Figs. 6.10; 6.11). This also suggests that Fe and Ti were affected by a process distinct from that which controlled the Ca-Mg and LILE composition. This extra process was common to barren and mineralised Late Eocene suites, but did not affect the pre-mineral magmas. It therefore demands a

→

Figure 6.12. (next page) Harker diagrams for HFSE from individual Andean porphyry copper camps, and a comparative suite compiled from three major SW Pacific porphyry Cu-Au camps. Arrows indicate the principal trends defined by Cenozoic volcanic products of Volcán Ollagüe, which is used as a proxy for the similar, but less well constrained Icanche Formation (Blue), and for unmineralised syn-mineral stocks at Escondida (Red). Andes data sources: Collahuasi district (Colla: Rowland, 1998; Masterman, 2003; this study); Escondida district (Esc: Richards et al., 2001a; Campos et al., 2002); Chuquicamata district (Chuq: Pemberton, 1997); El Abra district (Abra: Rogers et al., 1989; Haschke et al., 2002a); Volcán Ollagüe (Wörner et al., 1992a; Feeley et al., 1993). Numbers of data are indicated in the legend, although for Collahuasi, Escondida and El Abra, only ~75% of the data were analysed for Nb and Zr. Southwest Pacific data are a compilation of suites from Pliocene porphyry copper-gold camps at Batu Hijau, Indonesia (Garwin, 2000), Tampakan, Philippines (Rohrlach, 2002) and Baguio, Philippines (Hollings, 2006), with background data for the same arc segments from the online GEOROC database.

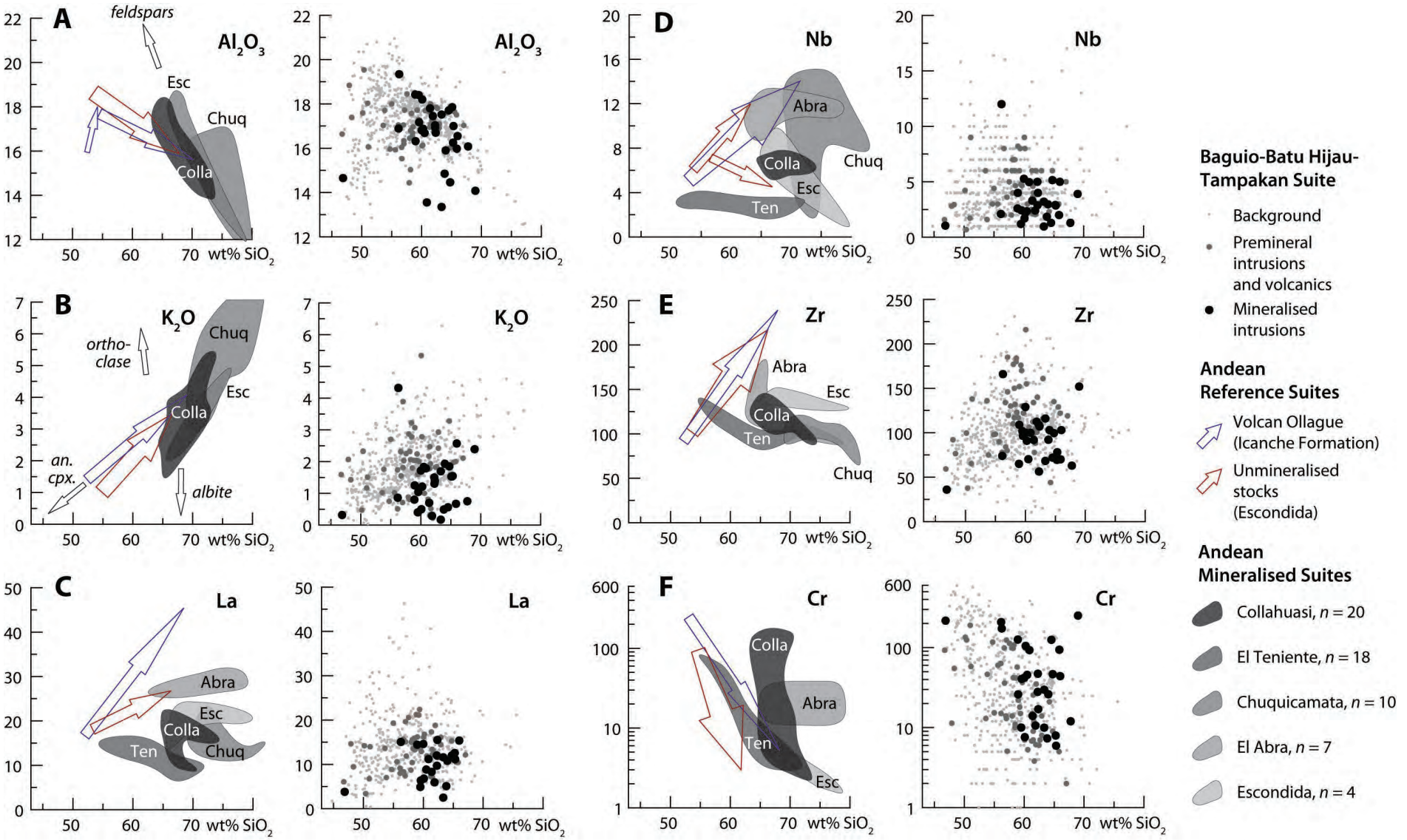
A
feldspars
Al2O3
Esc
Chuq
Colla
B
K2O
ortho-
clase
an.
cpx.
albite
C
La
Abra
Esc
Colla
Ten
Chuq
D
Nb
Abra
Colla
Esc
Chuq
Ten
E
Zr
Abra
Esc
Colla
Ten
Chuq
F
Cr
Colla
Abra
Ten
Esc
wt% SiO2
Baguio-Batu Hijau-Tampakan Suite
Background
Premineral intrusions and volcanics
Mineralised intrusions
Andean Reference Suites
Volcan Ollague (Icanche Formation)
Unmineralised stocks (Escondida)
Andean Mineralised Suites
Collahuasi, n = 20
El Teniente, n = 18
Chuquicamata, n = 10
El Abra, n = 7
Escondida, n = 4

more complex solution than the high degrees of amphibole fractional crystallisation to which Rohrlach (2002) attributed relatively depleted Fe, Ca and Ti among mineralised rocks at Tampakan, Philippines. Trace element evidence suggests that fractional crystallisation of amphibole is common in arc petrogenesis (e.g., Davidson et al., 2007; Richards and Kerrich, 2007), and therefore unlikely to be distinctive of the infrequent and localised generation of mineralised suites.

6.2.5 Rare Earth and High Field Strength Elements

The HFSE and REE content and Harker trajectories of all the Eocene suites distinguish them from the Cretaceous and Quaternary rocks. The distinctive characteristics can be classified into two groups showing similar behaviour; the LREE and HFSE, and the M-HREE and Y.

Light to Middle Rare Earth and High Field Strength Elements. Among the mineralised suites, the LREE, Zr, Nb, and Th all characteristically show invariant, or weakly compatible behaviour relative to SiO_2 (Figs. 6.12 and 6.13). Mid- to low-pressure fractional crystallisation of olivine-clinopyroxene-plagioclase ± amphibole) from a mafic parental magma should cause incompatible behaviour of the REE until at least 70% SiO_2 (Brophy, 2008). This pattern of strong and systematic increase in the concentration of the LREE-HFSE with increasing silica is shown by CVZ suites such as Ollagüe and by a subset of the Icanche suite (Figs. 6.8; 6.9; 6.12c-e). It is not evident among syn-mineral suites (Fig. 6.12c-e), and so at felsic bulk compositions, these contain less LREE-HFSE than unmineralised suites. Bulk relative depletion of Th in Andean mineralised suites was identified by both Baldwin and Pearce (1982) and López (1982), but recognition of distinctive patterns among the LREE and other HFSE has not been published elsewhere.

A valid hypothesis for the genesis of magmas that are fertile for porphyry copper mineralisation must account for the occurrence of this deposit style in oceanic and continental terranes. The HFSE-LREE composition of mineralised intrusions in oceanic arcs is similar to the composition of Andean mineralised rocks (Fig. 6.12c-e). However, in the SW Pacific suites there is no distinction of mineralised and unmineralised intrusions in terms of these elements. The background magmatic products in continental and oceanic terranes differ from each other substantially

more than do their respective mineralised magmatic rocks (Figs. 6.12 and 6.13). This observation supports a well-established hypothesis for the petrogenesis of 'normal' Andean magmas that invokes a major role for assimilation crustal materials (e.g., Hawkesworth et al., 1982; Hildreth and Moorbath, 1988; Rogers and Hawkesworth, 1989). It follows that part of the distinctiveness of the mineralised Andean suites arises from lesser (or negligible) crustal assimilation *en route* to the shallow crustal environment. This is consistent with their radiogenic isotopic compositions that suggest little crustal assimilation (Maksaev, 1990; Masterman, 2003), although Proterozoic zircon xenocrysts in some mineralised intrusions demand at least a

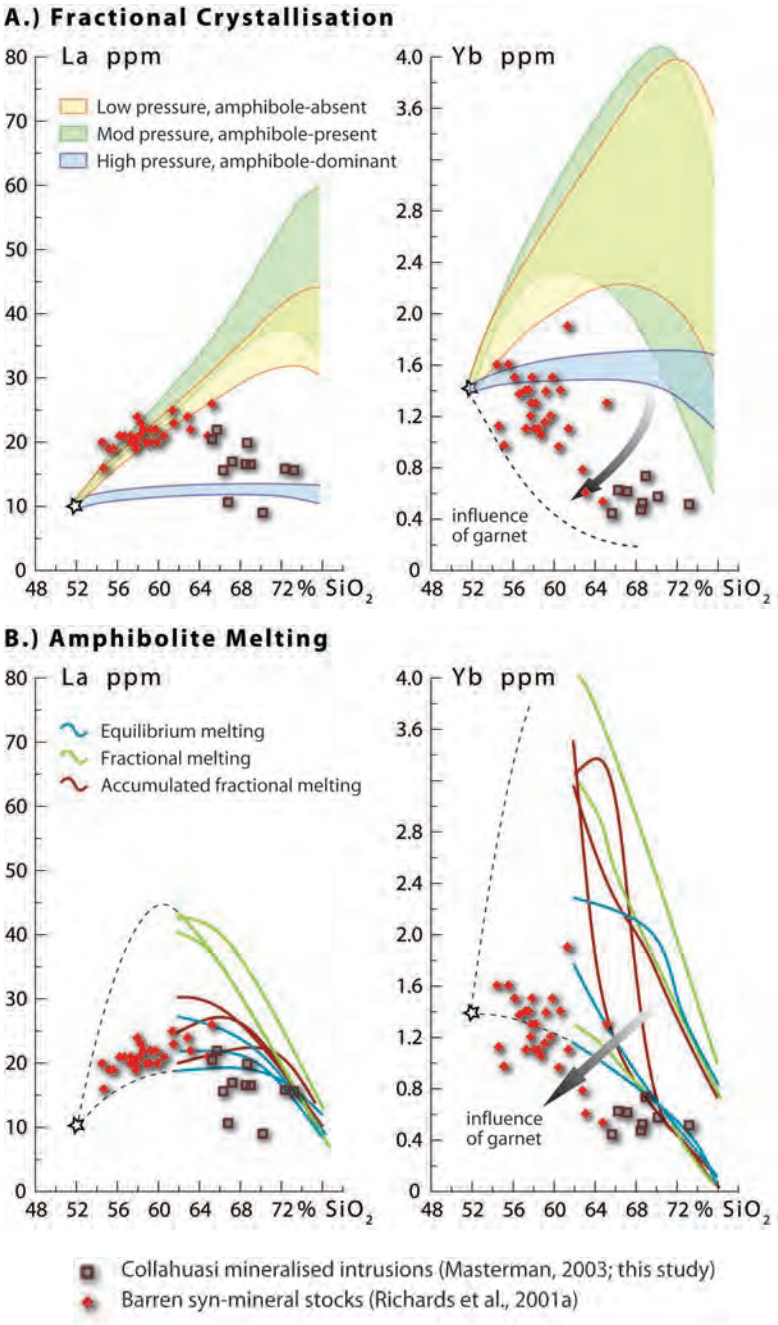

Figure 6.13. Comparison of observed La and Yb Harker diagrams for barren and mineralised Middle-Late Eocene Andean rocks, and model trajectories for various fractional crystallisation and amphibolite melting scenarios. Model ranges and trajectories recalculated from Brophy (2008) for a starting composition with 10 ppm La and 1.4 ppm Yb at 52% SiO_2. A.) Model ranges incorporating the known range of partition variability for three fractional crystallisation histories in which pressure dictates the stage of onset of amphibole as a fractionating phase; B.) Mean model trajectories for three natural arc-related ortho-amphibolite starting compositions, generated by melting according to batch (equilibrium)-, fractional-, and accumulated fractional melting equations (Brophy, 2008). Dashed lines are schematic and indicate the necessary convergence of melt and source compositions at high melt fractions. Arrow indicates the sense of translation of the models in the presence of garnet residue (e.g., Arth and Hanson, 1975).

small degree of assimilation (e.g. Tosdal and Munizaga, 1996; Urzua, 2009). The mineralised Andean suites also contain variable, but commonly high Cr and Ni relative to their unmineralised equivalents. The same is true of several SW Pacific mineralised suites (Fig. 6.12f). These compositions demand either assimilation of mantle peridotites or mixing with primitive arc basalts (e.g., Kay, 1978). The fertile suites therefore form beneath, or at the base of the crust and ascend effectively uninterrupted into the shallow crust in both oceanic and continental terranes.

The highly unusual differentiation-invariant to compatible behaviour of the some of the HFSE and LREE demands an additional explanation. Equilibration of the melt with the high pressure assemblage lawsonite-omphacite ± rutile-zircon would sequester the requisite group of elements (e.g., Usui et al., 2007). However, this possibility seems unlikely to be involved in the petrogenesis of fertile magmas, since the lawsonite is unstable at temperatures and pressures implied by the shallow dip of the subducting Nazca plate (e.g., Pilger, 1981).

Amphiboles partition the LREE more strongly than other major silicate phases, although they only contain higher concentration of LREE than coexisting magma at felsic bulk compositions (e.g., Dalpé and Baker, 2000). Low Mg# amphiboles also strongly partition Ti, Nb, Th, Zr (Ionov and Hoffmann, 1995; Tiepolo et al., 2000a; 2000b; Moine et al., 2001). Amphiboles are unique in that their partition coefficients for the REE (and by inference for the HFSE) increase logarithmically with the silica content of the magma. Amphibole Mg# mimics the coexisting liquid composition (Alonso-Perez et al., 2009), and so amphiboles probably accommodate the HFSE in a similar manner to the LREE. The compositional dependency of amphibole partitioning behaviour means that monomineralic fractional crystallisation of amphibole leads to flat Harker trends for all REE. In contrast, melting of amphibolites leads to convex patterns that inflect at ~63% SiO_2 for the LREE (Fig. 6.13a; Brophy, 2008). Richards et al. (2001a) argued that barren syn-mineral stocks at Escondida were cogenetic with the mineralised rocks suite there. Taking these to be representative of the less evolved equivalents of mineralised Eocene Andean suites, then combined with the data for syn-mineral suites at Collahuasi they show precisely this convex Harker pattern (Fig. 6.13b). A subset of the least enriched Icanche suite rocks define the same trend, except that they show much greater scatter (Fig. 6.14a). The SW Pacific

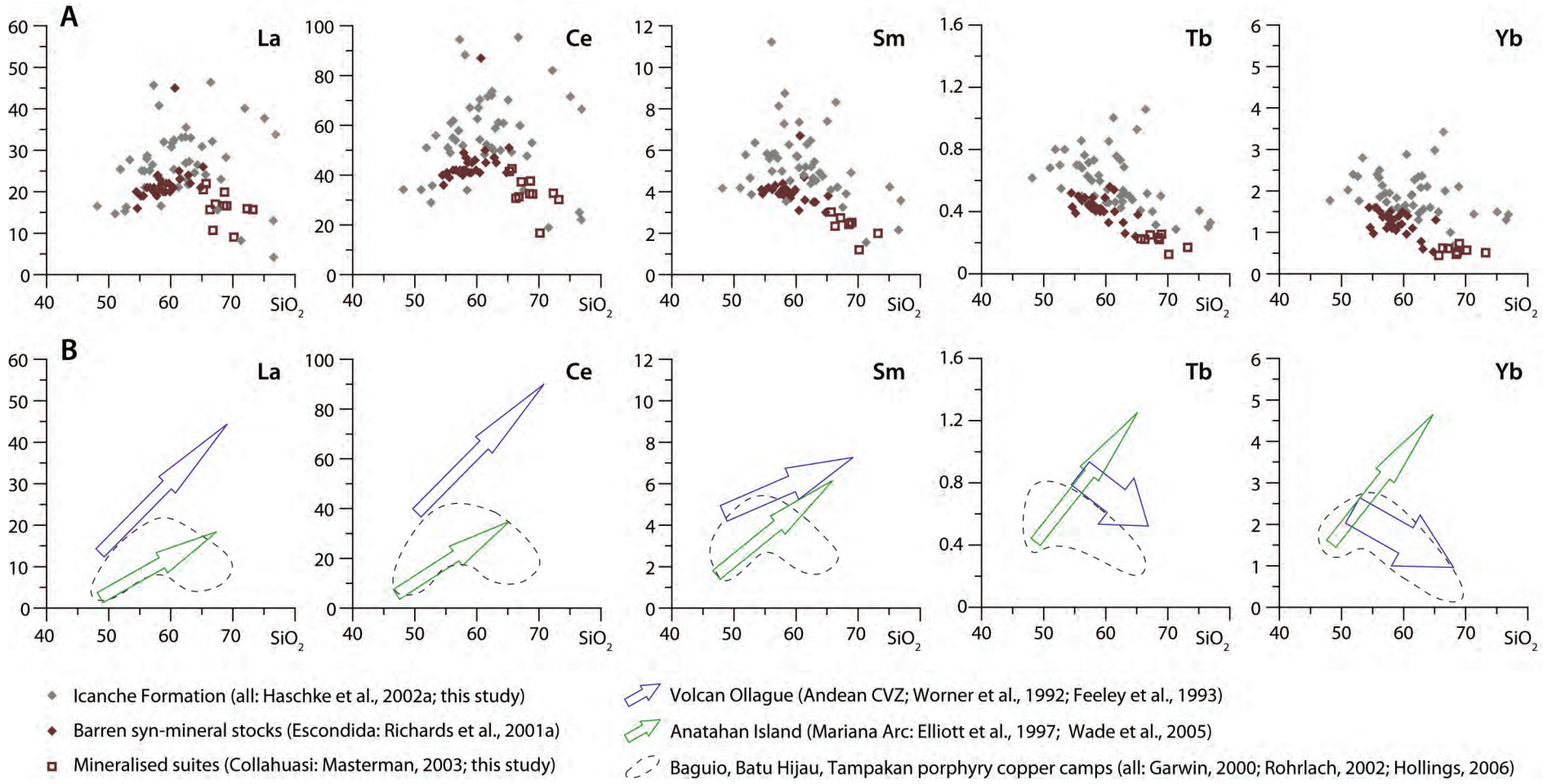

Figure 6.14. Harker diagrams showing the comparative behaviour of the rare earth elements among Andean and SW Pacific arc magmatic suites; A) Eocene to Oligocene North Chilean Suites including Collahuasi district mineralised intrusions; B) Reference suites from the Cenozoic Andes, Mariana oceanic arc, and three well-endowed porphyry copper-gold camps from the SW Pacific; Bagiuo and Tampakan, Philippines; and Batu Hijau, Indonesia (GEOROC online database and references in legend). All REE values are in ppm, silica in weight %.

suites also exhibit these convex patterns, for the LREE (Fig. 6.14b) as well as for the HFSE (Fig. 6.12c-e). Convex Harker patterns are therefore a feature of pre- syn- and post-mineral magmatic rocks in mineralised districts in both continental and oceanic settings. It is not a feature of unmineralised arcs in either setting (Fig. 6.14b).

However, the LREE and HFSE differentiation trends are not uniformly convex, nor uniformly flat among Andean porphyry copper mineralised suites. In addition to Collahuasi, La is also compatible at El Teniente and Chuquicamata, but has flat patterns at El Abra and Escondida (Fig. 6.12c). Niobium has flat patterns at Collahuasi, El Teniente and El Abra, but is compatible in the Escondida suite, and scatters widely between depleted and normal Andean values at Chuquicamata (Fig. 6.12d). Similar variablity among Harker patterns are observed for Th and Zr (Fig. 6.12e). Some of this camp-to-camp variability could be controlled by variable degrees of both amphibole melting and subsequent fractional crystallisation. However, some of the mineralised rocks at Collahuasi, as well as some at Escondida, and most of the El Teniente suite show greater depletion of LREE than can be explained by amphibolite melting or crystallisation alone (Figs. 6.12 and 6.13).

To explain the variability shown by HFSE and LREE among Andean mineralised suites it is necessary to appeal to involvement of minor phases that sequester some or all of these elements (Fig. 6.15). Apatite was ruled out previously because the mineralised suites do not show unusual phosphorus differentiation patterns. Brophy (2008) also shows that mass balance restrictions imposed by the phosphorus budget preclude significant REE control of arc magmas by apatite. Richards and Kerrich (2007) appealed to titanite as one of a number of minerals that may affect the REE content of subduction-related magmas. However, titanite does not sequester Th, and accepts relatively little Zr (Fig. 10), so if titanite plays a role, then it must be accompanied by a Th-Zr-rich phase, such as zircon. Zircon has the highest partition coefficient for U among common magmatic minerals (Fig. 6.15). Therefore, an exceptional role for zircon in the petrogenesis of fertile magmatic rocks should be reflected in strongly depleted U and low U/Th; neither is observed in either Andean or SW Pacific mineralised suites. Allanite also sequesters some of the HFSE and REE, but an important role for allanite should cause elevated U/Th, which is not observed either ($U/Th_{mineralised}$ = 0.2-0.35; U/Th_{CVZ} = 0.2-0.5). Allanite may be an

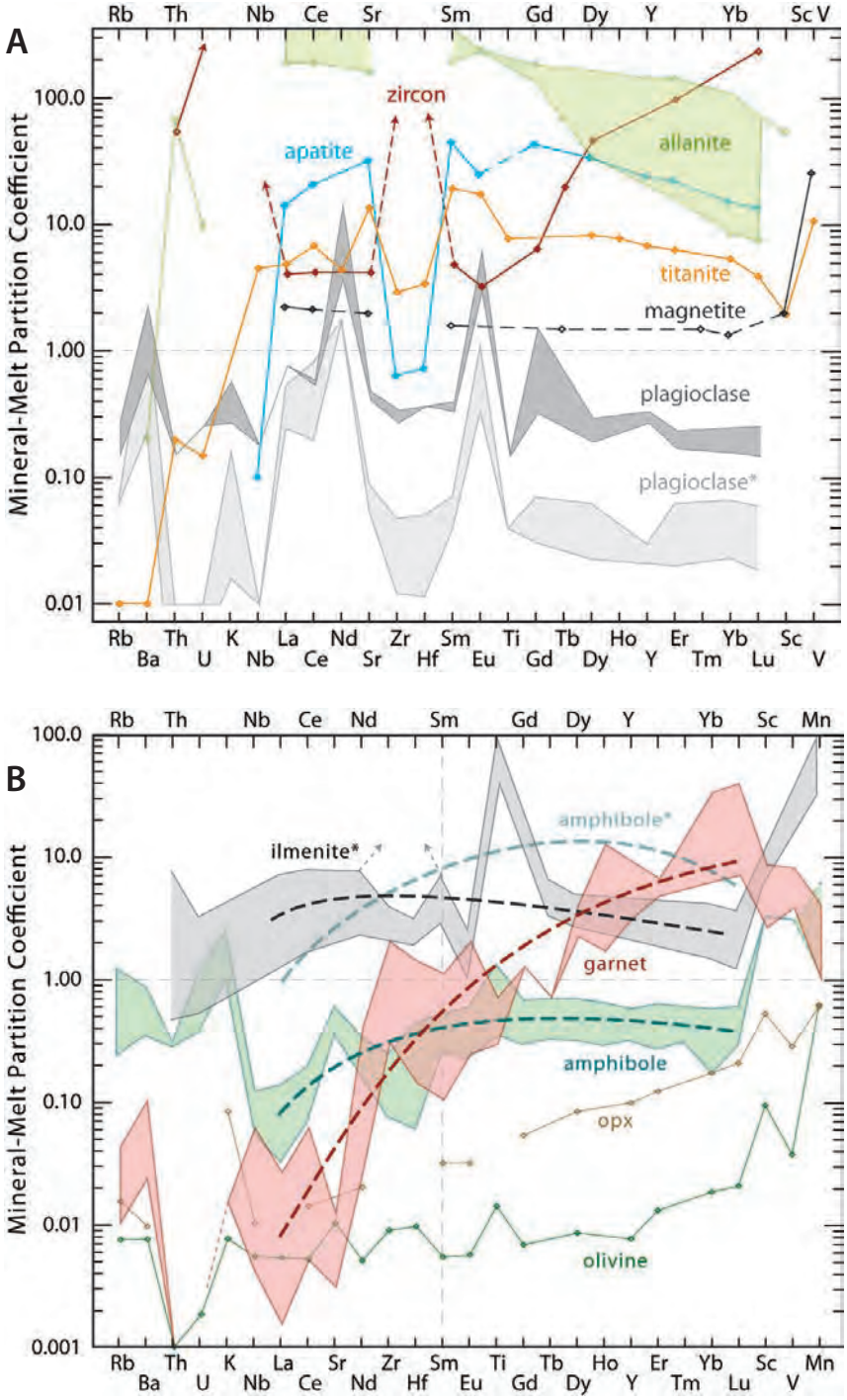

Figure 6.15. Compilations of mineral- melt partition coefficients. A) Coefficients for selected minor phases and anorthitic plagioclase in felsic liquids (* indicates mafic liquids). Values are averages of published data for volcanic rocks or for experiments conducted at crustal pressures; B) Coefficients for major minerals in the sub-arc mantle and lower crust in equilibrium with mafic liquids (* indicates values for felsic liquids). Values are shown as averages or ranges determined experimentally at upper mantle or lower crustal conditions ~1000°C and 2-3 GPa. Heavy dashed curves indicate the trajectory of coefficients for the REE and do not imply a lattice strain solution. Clinopyroxene has been omitted for clarity but its partitioning behaviour among mafic melts is comparable with amphibole for the REE and comparable with olivine-orthopyroxene for the HFSE and LILE. (Arth, 1976; Irving and Frey, 1978; Pearce and Norry, 1979; Nash and Crecraft, 1985; Nielsen et al., 1992; Johnson, 1998; Dalpe and Baker, 2000; Hermann, 2002; Tiepolo et al., 2002; Toplis and Corgne, 2002; and other compilations cited in Rollinson, 1993). Dashed arrows for ilmenite Zr and Hf are implied from zircon exsolution from ilmenite during granulite facies metamorphism (Bingen et al., 2001).

important metamorphic phase in the subducted lithosphere, but it has not been recorded as a crystallising phase in experiments on mafic or intermediate rocks at upper mantle or lower crystal pressures (e.g., Hermann, 2002). Rather, ilmenite crystallises early along with common silicate phases in crystallisation experiments on hydrous, oxidised, i.e. arc magmas (Beard and Lofgren, 1991; Rapp and Watson, 1995; Berndt, 2005; Brophy, 2008; Alonso-Perez et al., 2009). Uniquely, ilmenite appears to have HFSE partitioning behaviour that coincides with the entire suite of elements for which mineralised suites show unusual behaviour. Although limited mineral-melt partitioning data are available, at least among felsic liquids ilmenite accepts considerable, and comparable amounts of the LREE, Nb, Zr and Th, and does not strongly fractionate U from Th (Fig. 6.15; Nash and Crecraft, 1985). A role for ilmenite in the petrogenesis of mineralised magmatic suites is particularly attractive because it might explain the observed patterns of the HFSE, LREE as well as those for Fe and Ti.

The melting and fractional crystallisation scenarios modelled by Brophy (2008) suggest that for La (and by inference the LREE and HFSE generally), most of the Eocene suites could be generated by variable degrees of melting of arc-related amphibole-rich cumulates (Fig. 6.13b). Scatter among the Icanche suite would be expected to arise from crustal assimilation suggested by the polylithic fragmental components of these rocks. Dehydration melting studies on natural arc amphibolites (Beard and Lofgren, 1991; Rapp and Watson, 1995) show that ilmenite is a residual phase during incongruent melting of amphibole at low melt fractions (<30% melting), but may be involved in melting at higher melt fractions following amphibole exhaustion. The ‘normal’ HFSE and LREE chemistry of most of the unmineralised Eocene rocks (Fig. 6.12) could therefore arise if these rocks represent higher degrees of partial melting at which ilmenite (and/or other minor phases) were partially consumed. The most silicic barren stocks at Escondida have compositions that are transitional between their more mafic equivalents and the Collahuasi (and Escondida) mineralised suites, consistent with this hypothesis.

Middle to Heavy Rare Earth Elements and Yttrium. Depletion of the M-HREE and Y has been noted almost ubiquitously among the Andean mineralised suites for which data are available (Baldwin and Pearce, 1982; López, 1982; and

references in Table 6.1). At Collahuasi, the mineralised suites systematically contain less than half the M-HREE and Y content of the most mafic barren syn-mineral rocks (Fig. 6.7 e, Y; and Fig. 6.14 a, Tb and Yb). The Icanche Formation, unmineralised syn-mineral stocks, and Volcán Ollagüe rocks all show systematic compatible trends at intermediate to felsic compositions with a possible inflexion to incompatible behaviour among the most mafic samples (<55% SiO_2; Fig. 6.14 a). The unmineralised Eocene stocks at Escondida are equivalent to the least-enriched Icanche suite (Figs. 6.7 e and 6.14 a). Mineralised suites at both Collahuasi and Escondida coincide with the projection of this trend to higher silica. A valid petrogenetic model must account for both the unusual Harker trajectories (and relative bulk depletions they cause) as well as any fractionation of the MREE from the HREE.

Depletion of the M-HREE and Y in magmatic rocks is typically attributed to sequestration in garnet, as it accommodates one to two orders of magnitude more HREE and Y than other major silicates in equilibrium with basaltic liquids (Fig. 6.15; e.g., Nicholls and Harris, 1980; van Westerenen et al., 2000). Garnet may crystallise as a liquidus phase at 1.2 GPa, and even at 0.8 GPa from hydrous melts (Alonso-Perez et al. 2009). Simple Rayleigh crystallisation models (Fig. 6.16) suggest

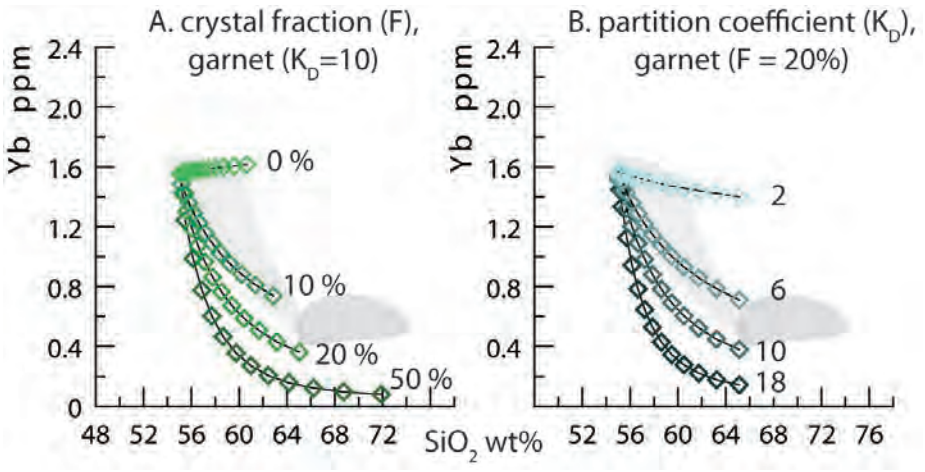

Figure 6.16. Rayleigh fractional crystallisation models for a hypothetical arc magma with 55% SiO_2 and 1.6 ppm Yb, shown as the composition of the residual magma after incremental 5% removal of an assemblage of amphibole-clinopyroxene-garnet up to 60% crystallisation. Grey fields are ranges of values for barren syn-mineral Escondida stocks (paler) and mineralised stocks at Collahuasi (darker). A.) Variability imposed by the amount of garnet in the crystallising assemblage, at fixed garnet-melt Yb partitioning behaviour; B.) Sensitivity of the models to the partition coefficient of garnet, at fixed mineral proportions (amph:cpx:gt = 5:3:2). Note that the models do not take account of the compositional dependency of the garnet-melt partition coefficients, so the curvature of the models is accentuated and the Yb content at high degrees of crystallisation is overestimated.

that the compatible trends and bulk depletion of Yb shown by the unmineralised Eocene rocks and CVZ volcanos such as Ollagüe could be generated by fractional crystallisation in which garnet comprises 10-20% of the crystal fraction. If garnet is a more significant fractionating phase, the slope of the HREE-SiO_2 trend steepens beyond that observed among the Eocene and Quaternary Andean suites, and the opposite applies if garnet is a less significant phase (Fig. 6.16a). The uniformity of observed patterns among both the Eocene and Quaternary rocks (Fig. 6.14) is at odds with the sensitivity of the modeled silica-REE trend to the amount of crystallising garnet. Likewise, in both the Andean suites and those form the SW Pacific, the Harker trajectories for all of the REE from Yb to Tb are similar (Fig. 6.14). If garnet exclusively controlled the MREE, they should yield almost flat Harker trajectories (e.g., the K_D=2 example in 6.16b), and garnet can not have been an common or widespread fractionating phase during genesis of these magmas.

Among Neogene volcanic rocks of the Central Andes, garnet is more commonly interpreted to be a residual phase with which magmas equilibrate in their source or storage regions in the lower crust or mantle lithosphere (e.g., Kay et al., 1994; Matteini et al., 2002; Richards and Villeneuve, 2002). The CVZ suites such as Ollagüe are characterised by depletion of the HREE relative to the MREE, perhaps most clearly observed in the ratio Tb/Yb (6.17a). This REE fractionation occurs independent of the differentiation trends (Fig. 6.14b), and therefore supports the interpretation of a garnet-stable melt residue. In contrast, chemically indistinguishable suites of rocks from the Cretaceous-Paleocene Central Andes and Cretaceous-Lower Miocene Southern Central Andes shows weak systematic REE fractionation in the opposing sense (Fig. 6.17a). This is the predicted outcome for evolution via fractional crystallisation of amphibole (e.g., Davidson et al., 2007), but residual amphibole should also yield similar compositions.

Most samples from mineralised suites at Collahuasi (and at most other North Chilean camps for which data have been compiled) have Tb/Yb that indicates melt equilibration with a garnet-bearing residue (Fig. 6.17b). A small number of samples show no sign of garnet involvement. At Collahuasi and Chuquicamata, the two camps for which most data are available, the mineralised suites span a wide range between moderate to strong fractionation of the M-HREE in both senses. This is

tentatively interpreted to reflect variable involvement of both amphibole and garnet in the petrogenesis of these mineralised suites. For the older porphyry metallogenic events known in Chile (e.g., Camus, 2002; Chapter 2), there is no indication of garnet involvement (Williams, 1992; Haschke et al., 2002a). Nor is melting of a garnetiferous source suggested by the M-HREE composition of magmatic rocks in several mineralised SW Pacific arc suites (Fig. 6.17c). These relationships explicitly rule out metamorphic reactions involving garnet as a critical ingredient (though they may serve as a contributory ingredient) in porphyry copper metallogeny (*cf.* Kay et al., 1999). Rather, the involvement of garnet in arc petrogenesis may be the coincidental response to tectonism in arcs that have sufficiently thick upper plate lithosphere.

Returning to the Harker trajectories for the M-HREE and Y, compatible patterns

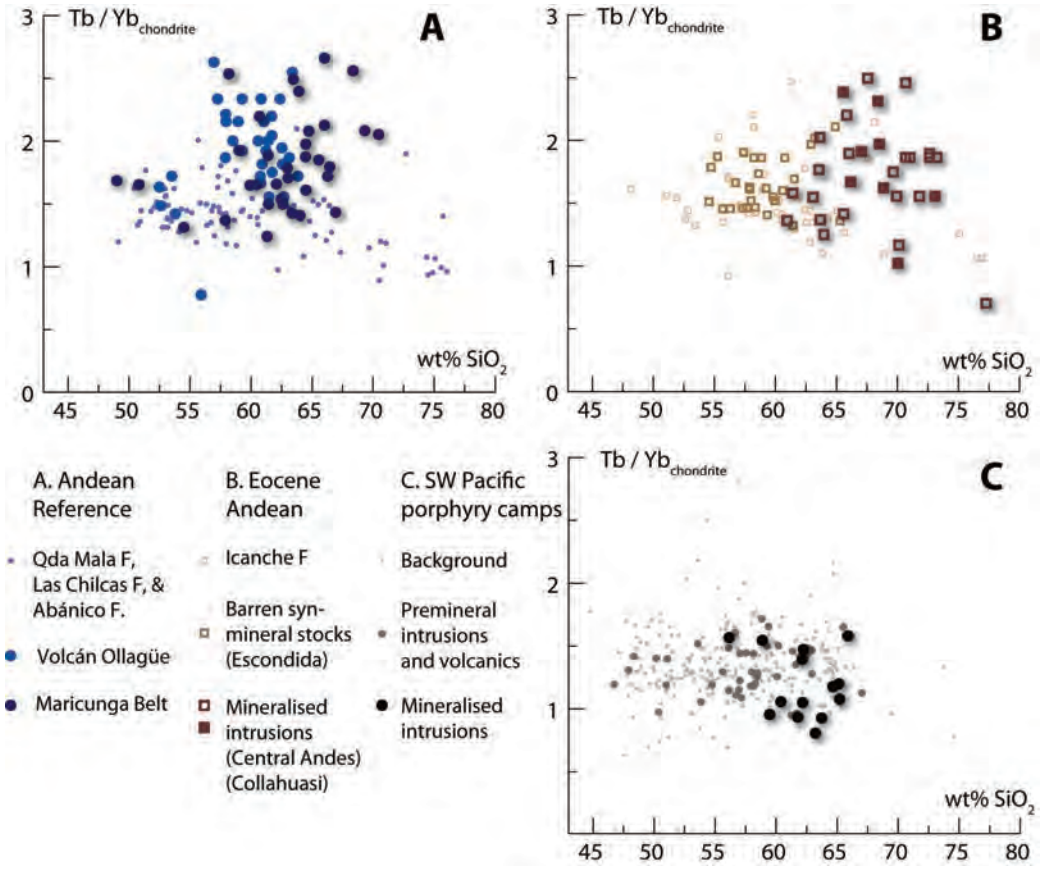

Figure 6.17. Tb/Yb normalised to chondrite values of Sun and McDonough (1989), showing the influence of garnet on M-HREE fractionation. A) Neogene magmatic rocks with unusually high Tb/Yb from Volcan Ollagüe (Wörner et al., 1992a) and the Maricunga Belt (Kay et al., 1994), and a reference compilation of Cretaceous-Miocene rocks from the Southern Central Andes (Hollings et al., 2005) and Cretaceous-Paleocene rocks from the North Chilean Longitudinal Valley (Williams, 1992); B) Eocene rocks from Northern Chile including mineralised suites from Collahuasi (solid symbols); C) Neogene rocks from mineralised camps in the SW Pacific (as Figs. 6.12 and 6.14).

such as those in the post-Paleocene North Chilean suites are not common among arc rocks. Most arc-related suites have incompatible M-HREE (e.g., Fig. 6.12: Anatahan Island, Mariana Arc: Elliott et al., 1997; Wade et al., 2005). Incompatible patterns also characterise the Scotia, Aleutian, Izu Bonin, North Honshu, New Britain and Sunda-Banda oceanic arcs (data compiled by Brophy, 2008; GEOROC database). More scattered, but generally incompatible patterns also characterise Jurassic and Cretaceous suites in the Central Andes (Rogers and Hawkesworth, 1989; Pichowiak et al., 1994; Haschke et al., 2002a) and Cretaceous to Lower Miocene suites in the

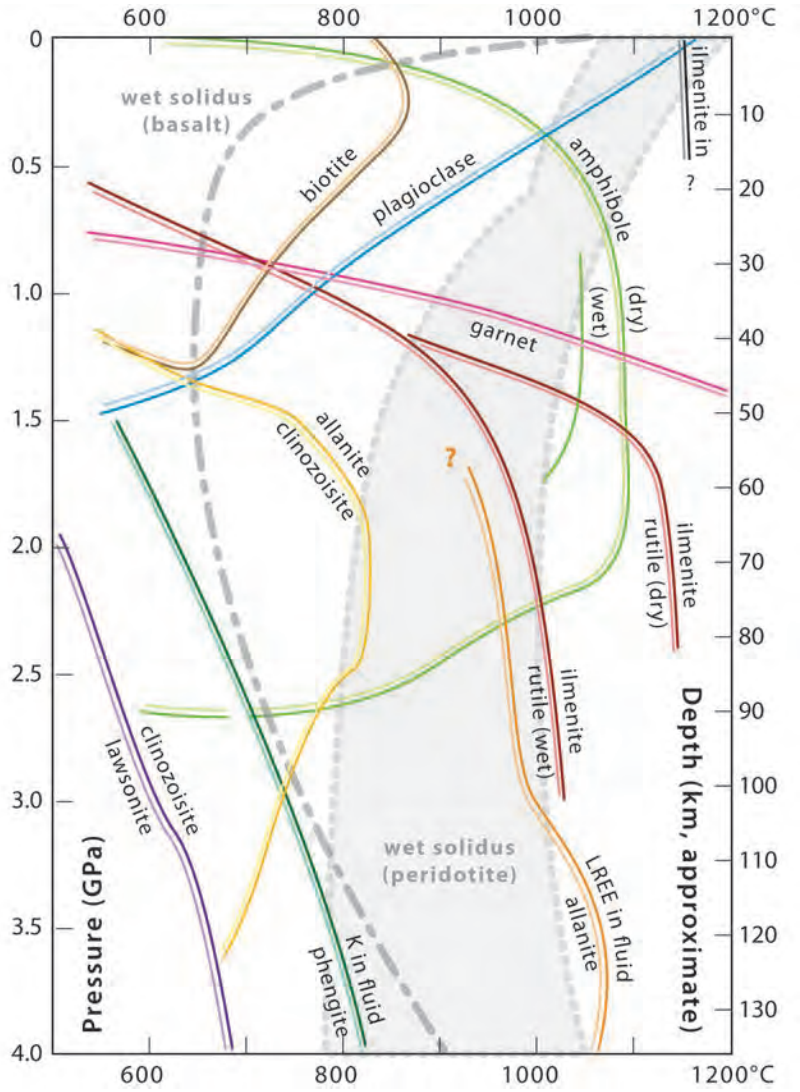

Figure 6.18. P-T stability field diagram for the selected minerals involved in metamorphism and melting in the immediate sub-arc environment (Compiled from experiments and/or models of Yoder and Tilley, 1962; Green, 1972; Holloway and Burnham, 1972; Spulber and Rutherford, 1983; Bohlen and Liotta, 1986; Poli, 1993; Schmidt, 1993; Pawley, 1994; Schmidt, 1996; Arisikin and Barmina, 1999; Okamoto and Maruyama, 1999; Frost et al., 2000; Hermann, 2002; Hacker et al., 2003; Kessel et al., 2005; Xiong et al., 2005; and Grove et al., 2006). Heavy dashed lines depict fields for hydrous fluids (Mungall et al., 2002).

southern Central Andes (e.g., Hollings et al., 2005). However, compatible HREE patterns among andesitic and felsic compositions are common to arc magmatic rocks from Mindanao and Luzon, Philippines, and Sumbawa, Indonesia (e.g., Fig. 6.14b). The abundant mafic rocks in these oceanic arc suites show pronounced inflexions in the differentiation patterns. Dreher et al. (2005) and Macpherson et al. (2006) interpreted this inflexion, in suites from Mindanao, as the point at which amphibole crystallisation began. However, the silica content at which each of the rare earth patterns inflects, varies systematically for the different REE. The silica content at which inflexion occurs varies in concert with the amphibole-melt partition coefficients for these elements (Fig. 6.19). Further, for amphibole fractional crystallisation to generate the observed patterns, the amphibole-melt partition coefficients for the M-HREE must be substantially greater (e.g., $K_D \geq 5$) than has been indicated by a large number of experimental studies ($K_D \leq 1$; Fig. 6.15b; e.g., Dalpé and Baker, 2000).

Therefore, these convex REE-silica patterns are interpreted here to be produced among magma suites generated by different amounts of partial melting of

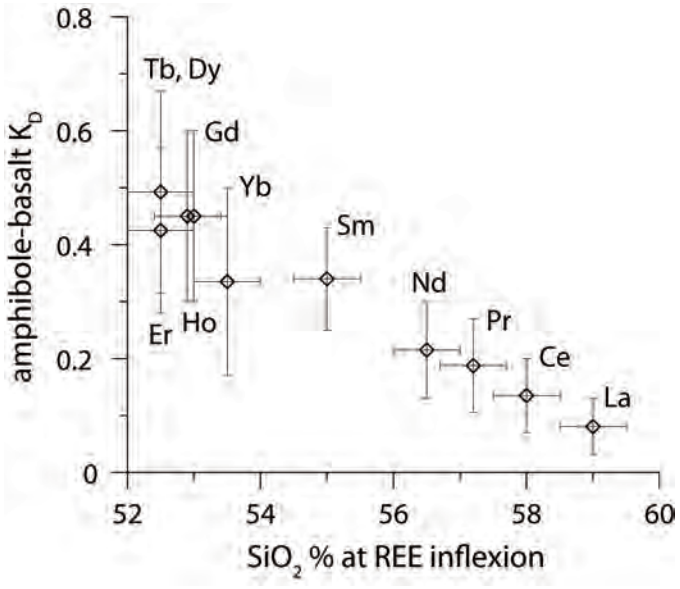

Figure 6.19. Relationship between amphibole-basalt partition coefficients (K_D) and the whole rock silica content at which Harker plots for the REE strongly inflect between compatible and incompatible behaviour. Drawn from data for SW Pacific porphyry copper camps (Fig. 6.14b; Garwin, 2000; Rohrlach, 2002; Hollings, 2006; GEOROC database). K_D values and errors taken as the average and range of experimental data compiled by Dalpé and Baker, (2000). The SiO_2 content at inflexion was determined graphically from the Harker plots, to which a fixed ± 0.5% error has been ascribed.

amphibolite (i.e. not the product of amphibole fractional crystallisation, *cf*. Dreher et al., 2005; Macpherson et al., 2006; Richards and Kerrich, 2007). Accepting that syn-mineral barren stocks at Escondida are reasonably interpreted as mafic equivalents of the mineralised suites there, as well as at Collahuasi, then together they map a convex trajectory that, as for their LREE and HFSE composition, is most plausibly created by partial melting of amphibolite (Fig. 6.13b; Brophy, 2008). Additionally, the central Andean syn-mineral suites (but not all of the Icanche suite) show such strong HREE depletion that, having previously ruled out titanite and zircon (*cf*. Kerrich and Richards, 2007) garnet must have been present as a residuum. The source rock for these fertile magmas was a garnet-ilmenite amphibolite.

6.3 Summary and Dynamic Implications

All of the Paleogene suites recognised in the Collahuasi district; the latest Cretaceous Tolaun intrusive complex (TIC), the Icanche Formation, and the syn-mineral intrusions, are unambiguous subduction-related magmatic rocks. In primitive mantle-normalised spider diagrams, they have pronounced negative anomalies in Nb, Ta and Ti, and enrichment in alkalis, alkali earths, Pb and the LREE (Figs. 6.3-6.4). The three suites are nonetheless distinct in terms of their bulk contents and differentiation trajectories of many elements. In terms of standard whole rock classifications, the TIC is alkaline, whereas the two younger suites both span the mid-K and high-K calc-alkaline ranges (Fig. 6.2). Of those, the mineralised suites are distinctly less alkaline and more aluminous at a given silica content.

6.3.1 Late Cretaceous - Paleocene Magmatism.

The 68-66 Ma TIC is contemporaneous with Middle Cretaceous to Paleocene volcanics attributed to the Quebrada Mala Formation (e.g., Maksaev, 1978). These are primarily distributed along the Longitudinal Valley (e.g., Marinovic and Garcia, 1999; Tomlinson et al., 2001a), such that the TIC intruded in a position ~50 kms further inboard of the main arc axis at the time. The TIC is chemically similar to other feldspathic, alkalic intrusions that occur sporadically along the eastern Domeyko Cordillera at least as far south as Escondida (e.g., Richards et al., 2001a; Tomlinson et al., 2001a). They represent a regional phenomenon that occurred

between ~80 and 66 Ma along an arc segment of at least 400 kms length (geochronology of Richards et al., 2001a; Tomlinson et al., 2003; Cornejo et al., 2003; Masterman, 2003; Urzua, 2009, and this study). The TIC and correlated magmas formed above the Quebrada Mala subduction zone, and show little or no chemical evidence to suggest back-arc rifting and decompression-related melting. Instead, they carry an alkalic signature consistent with pressure-mediated breakdown of phengite in the subducted lithosphere (e.g., Schmidt, 1996) or of phlogopite in the deeper parts of the metasomatised mantle wedge (e.g., Wyllie and Sekine, 1982). Differentiation among the TIC suite occurred via fractional crystallisation of clinopyroxene, and later, of plagioclase and apatite. Several mafic-intermediate examples are plagioclase cumulates, whereas the most felsic examples are plausibly the cogenetic residual liquids.

A compressional tectonic event that peaked at 65-62 Ma (Andriessen and Reutter, 1994; Cornejo et al., 2003) appears to terminate the retro-arc TIC-suite intrusive activity. However, syn- to post-tectonic mineralised intrusions occur along the main axis of the Quebrada Mala arc, including the 51.8 Ma Cerro Colorado and 56 Ma Mocha porphyry copper deposits ~100 kms north-northwest of Collahuasi (Sillitoe, 1988; Williams, 1992; Bouzari and Clark, 2002, 2006). The TIC and correlates therefore represent unexceptional retro-arc magmatism that largely preceded tectonism and intrusion-related mineralisation in the Paleocene arc. That retro-arc magmatism ceased, and fertile magmatism began either side of the terminal Cretaceous tectonism implies a fundamental change in the intra-arc strain regime and petrogenetic process at that time.

6.3.2 Late Paleocene -Middle Eocene Magmatism (Icanche Formation).

The Icanche Formation (Maksaev, 1978) includes a diverse group of arc volcanic rocks that generally preceded, and were emplaced during the earlier stages of the Incaic tectonic phase (Chapter 2). Occurrences of the Icanche formation and related stocks at Collahuasi are commonly dacitic to rhyolitic in bulk composition. The volcanic units are characteristically strongly fragmental with polymicitic lithic components. Both the new Collahuasi district samples and the regional dataset of Hascke et al. (2002a) show marked compositional diversity, interpreted to principally reflect

variable crustal assimilation, consistent with their polylithic petrography.

Overall, chemical data for the Icanche suite define trends that are indistinguishable from Quaternary volcanic products of nearby Volcán Ollagüe (Figs. 6.6, 6.7, 6.12, 6.14; Wörner et al., 1992a; Feeley et al., 1993), and from other Quaternary volcanoes in the CVZ between 20º and 27ºS (references in Table 6.3). Therefore, the petrogenesis of these rocks is interpreted, generally, to follow accepted continental 'subduction factory' processes (e.g., Hacker et al., 2003), i.e. whereby hydrous slab related fluids caused metasomatism of the mantle wedge, from which moderate degree partial melts (~15-25%, e.g., Pearce and Peate, 1995) rose buoyantly to the base of the crust. Substantial modification of the magma composition occurred by way of melting, assimilation and homogenization during storage in a partially molten zone at the mantle-crust transition (MASH: Hildreth and Moorbath 1988). Further modification by low pressure fractional crystallisation (e.g., Crawford et al., 1987) and upper crustal assimilation (e.g., Hawkesworth et al., 1982) likely occurred during ascent and mid- to upper crustal storage.

The principal difference between the Icanche suite and the Quaternary CVZ is observed in the behaviour of the REE (Fig. 6.14). The M- and HREE are generally compatible in andesitic-dacitic Icanche Formation, whereas only the HREE are compatible in the andesitic-dacitic Neogene CVZ, which therefore have M-HREE fractionation (Fig. 6.17a, b). Therefore amphibole was abundant, and garnet was scarce in the Icanche-time MASH zone, whereas the opposite appears to characterise the Neogene MASH zone (e.g., Matteini et al., 2002; Richards and Villeneuve, 2002). The more recent abundance of garnet is explicable in terms of tectonism and crustal thickening that have occurred since the Middle Eocene, and hence forced the sub-arc MASH zone into the garnet stability field. However, the apparent dominance of amphibole in this zone, rather than olivine, plagioclase and clinopyroxene, requires an additional explanation that is common to the Icanche Formation, and both barren and productive syn-mineral suites.

6.3.3 Late Eocene - Early Oligocene (syn-mineral) Magmatism.

The syn-mineral suites at Collahuasi, all of them related to hydrothermal mineralisation, are mid-K to high-K calc-alkaline, unambiguously subduction-related

TABLE 6.2. Average Chemical Characteristics at 1.5% MgO of Magmatic Suites in the Collahuasi District.

Magma Suite[1]	Age (Ma)	$Al_2O_{3,1.5}$	$Sr_{1.5}$	$TiO_{2,1.5}$	$FeO^t_{1.5}$	$MnO_{1.5}$	$CaO_{1.5}$	$Mg\#_{1.5}$	$Nb_{1.5}$	$La_{1.5}$	$Ce_{1.5}$	$Sm_{1.5}$	$Dy_{1.5}$	$Yb_{1.5}$	$Y_{1.5}$	$K_2O_{1.5}$	$Rb_{1.5}$	$Ba_{1.5}$	$Pb_{1.5}$	$Th_{1.5}$	$Cr_{1.5}$	$Ni_{1.5}$
	Absolute average values at 1.5% MgO																					
Volcan Ollague	<2	15.7	440	0.61	3.6	0.06	3.6	0.295	11.5	38.5	75	6.6	3.5*	1.4	16.25	3.65	124	900	17.7	13.5	7	5.5
Mineralised stocks	37-34	17.1	500	0.48	3.25	0.035	3	0.32	7.4	21.5	43	3.05	1.3	0.45	6.9	2.2	72	600	11.5	4.5	65*	24
Escondida unmineralised	~38	16.7	740	0.53	3.25	0.0782	3.7	0.32	6.3	22	44.5	3.3	1.45	0.65	9.2	2.85	68	790	11	5	4	6
Icanche Formation	55-37	16.6	390	0.55	4	0.08*	3.7	0.26	11	31	66	4.2	2.6	1.7	17.5	3.15	113	700	16	12*	7.5	4.5
Tolaun Complex	68-66	18.1	750	0.6	4.5	0.15	3.8	0.225	11	28	51	5.5	4.1	2.5	25*	4.8	132	890	9	7*	6	11.5
Yabri F-Cascasca dykes	245-232	19	280	0.8	7.2	0.19	1.15	0.5	7.3	24	42	4.8	3.5	1.9*	20	4.6	265	1130	14	7.4	60	26.5
Chiclla F-Sallihuinca F	300-265	15.3	200	0.6	4.1	0.085	2.2	0.235	13*	24*	62	3.15	5.5*	2.7	32.5	3.5	120	650	12	16	6	5
	Percentile difference (between mineralised suites and others) [2]																					
Neogene CVZ	<2	8.9	13.6	-21.3	-9.7	-41.7	-16.7	8.5	-35.7	-44.2	-42.7	-53.8	-61.4	-70.4	-57.5	-39.7	-41.9	-33.3	-35.0	-66.7	829	336
Escondida unmineralised	~38	2.4	-32.4	-9.4	0.0	-55.2	-18.9	0.0	17.5	-2.3	-3.4	-7.6	-10.3	-30.8	-25.0	-22.8	5.9	-24.1	4.5	-10.0	1525	300
Icanche Formation	55-37	3.0	28.2	-12.7	-18.8	-53.6	-18.9	23.1	-32.7	-30.6	-34.8	-27.4	-50.0	-73.5	-60.6	-30.2	-36.3	-14.3	-28.1	-62.5	767	433
Tolaun Complex	68-66	-5.5	-33.3	-20.0	-27.8	-76.7	-21.1	42.2	-32.7	-23.2	-15.7	-44.5	-68.3	-82.0	-62.0	-54.2	-45.5	-32.6	27.8	-35.7	983	109
Yabri F-Cascasca dykes	245-232	-10.0	78.6	-40.0	-54.9	-81.6	161	-36.0	1.4	-10.4	2.4	-36.5	-62.9	-57.9	-65.5	-52.2	-72.8	-46.9	-17.9	-39.2	8.3	-9.4
Chiclla F-Sallihuinca F	300-265	11.8	150	-20.0	-20.7	-58.8	36.4	36.2	-43.1	-10.4	-30.6	-3.2	-75.5	-83.3	-78.8	-37.1	-40.0	-7.7	-4.2	-71.9	983	380

* denotes elements that do not define a coherent bivariate array with MgO at the present sampling frequency. CVZ = Central Volcanic Zone (see text for references); Yabri F = Yabricoya Formation.

1. "Mineralised Stocks" here refers to just those from the Collahuasi district (Rowland, 1998; Masterman, 2003; this study) to reduce scatter and permit calculation of a meaningful average. While the absolute values will change if calculations were made for other camps, the relative sense of enrichment/depletion is persistent across districts. Data for the Icanche and Tolaun suites were determined from a broader North Chilean data set (Richards et al., 2001a; Haschke et al., 2002; this study). The "Escondida unmineralised" category refers to the barren syn-mineral dioritic stocks reported by Richards et al. (2001a).

2. The lower part of this table should be read, for example, such that at 1.5% MgO, the Nb content of the average mineralised sample represents a depletion of 35.7% relative to Volcán Ollagüe.

rocks (Figs. 6.2 & 6.4). However, they are distinct both in terms of bulk abundances (Table 6.2) and differentiation trajectories (Figs. 6.12 & 6.14) from all other Central Andean arc magmas that share no such relationship with mineral deposits. Compared to the Icanche Formation and Cenozoic CVZ at a given silica content, they are commonly richer in Al, Sr, Cr and Ni, and poorer in the alkalis and LILE, Mn, Fe, Ti, Ca and almost all the HFSE and REE. They share these relationships with many other productive Andean porphyritic intrusions emplaced during the Eocene-Oligocene and Miocene-Pliocene. The bulk abundances and differentiation trajectories that characterise the Andean mineralised suites are also common to several mineralised suites from the SW Pacific, which were emplaced through a thinner crustal column. However, the differences between mineralised suites and background arc magmatic products are more pronounced in the Andes. Radiogenic isotope evidence (e.g., Hildreth and Moorbath, 1988; Rogers and Hawkesworth, 1989; Maksaev, 1990; Masterman, 2003) suggests that this reflects a greater role for intracrustal modification of 'normal' magmas during ascent through the thicker Andean crust. Two important corollaries of this are that the processes that control fertile magma generation are common to continental and oceanic arcs, and that magma ascent from source to emplacement depth is strikingly efficient in all cases.

In the absence of equivalent syn-mineral barren rocks at Collahuasi, a suite of unmineralised diorites at Escondida (Richards et al., 2001a) provides the best approximation of contemporaneous magmas that did not form hydrothermal mineral deposits. These are more mafic than most Andean mineralised suites and have chemistry that is transitional between the mineralised suites and the Icanche Formation, consistent with Richards et al's (2001a) interpretation that they are less evolved equivalents. However, the HFSE and REE trajectories defined by syn-mineral suites, both at Collahuasi and elsewhere, and among both mineralised and barren examples, is inconsistent with models of pronounced amphibole fractional crystallisation (*cf.* Richards et al., 2001a; Rohrlach, 2002). Rather, the HFSE and REE chemistry of the barren and productive syn-mineral suites is more consistent with a range of compositions derived by different degrees of partial melting of an ilmenite-amphibole bearing source rock (Figs. 6.12, 6.13, 6.14 & 6.19). The barren Escondida suites are interpreted to have been produced by higher degree partial

melting, which at its extreme caused total consumption of amphibole and ilmenite in the source and produced magmas with unexceptional HFSE and REE characteristics (Figs. 6.12 and 6.14). In contrast, contemporaneous mineralised suites represent low degree partial melts that leave residual ilmenite and amphibole. The mineralised Andean suites (but not the oceanic suites) have particularly strong HREE-Y depletion that implies an additional, but variable role for residual garnet (Figs. 6.7, 6.14 & 6.17). The Icanche Formation is envisaged to originate in the same way as the barren syn-mineral suites, but to then assimilate substantial amounts of crustal materials that cause the observed chemical scatter and polylithic petrography.

6.3.4 A Mechanism for Fertile Petrogenesis and Emplacement

The above interpretation represents a refinement of well established models of the petrogenesis of productive porphyry intrusive suites (e.g., Kay and Mpodozis, 1999; Tosdal and Richards, 2001; Rohrlach, 2002; Richards, 2003). Nonetheless, the difference between fractional crystallisation of amphibole, and melting of amphibole, might advance our understanding of the mechanisms that underlie porphyry metallogeny. A causative relationship between porphyry metallogeny and the latter stages of compressional tectonism has been widely proposed (e.g., Burnham, 1979; Maksaev and Zentilli, 1988; Kay et al., 1994a, 1999; Tosdal and Richards, 2001; Garrido et al., 2002; Rohrlach, 2002; Hollings et al., 2005; Braxton, 2007). An empirical relationship between tectonism and short bursts of metallogenic activity has been established independently for southern Peru (Clark et al., 1990); New Guinea (Titley and Heidrick, 1975; 1978; Sillitoe, 1997), the western Tethyan (Lips, 2002; Neubauer, 2002) and the Laramide western North American margin (Nielsen, 1979; McCandless and Ruiz, 1993; Keith and Swan, 1995; Keith et al., 2000). Tosdal and Richards (2001), observe that in most of these cases the periods of prolific porphyry copper deposit formation occurred near the end of periods of arc magma productivity in a given location. In line with this observation, at the latitude of the Collahuasi district, Trumbull et al. (2006) observe that accentuated shortening rates during the early Oligocene correspond to a pronounced regional decline in volcanic productivity. Tosdal and Richards (2001) explain this coincidence in terms of a net distillation of metals and ligands in long-lived MASH zones. The results of this study

suggest some adjustment of that interpretation is warranted.

There is empirical and theoretical evidence for the presence, in the lowermost crust and/or mantle lithosphere, of amphibole-rich primary arc cumulates, and/or related orthoamphibolites (e.g., Ducea and Saleeby, 1998; Claeson and Meurer, 2004; Davidson and Arculus, 2006; Müntener and Ulmer, 2006; Davidson et al., 2007). Unlike subducted oceanic crust, this mafic cumulate material would be plagioclase poor, owing to suppression of this mineral both in hydrous magmas (Baker and Eggler, 1983; Moore and Carmichael, 1998), and at crystallisation pressures above 11-14 kbar (i.e. depths of 30-40 kms; Green, 1972; Lambert and Wyllie, 1972, 1974; and see Peacock, 1990, and Richards and Kerrich, 2007, for further evidence against a role for melting of subducted lithosphere). The sub-arc cumulates would also be sufficiently dense that they would be located beneath the seismic Moho (i.e in the lithospheric mantle; Griffin and O'Reilly, 1987; Griffin et al., 1998; Müntener and Ulmer, 2006). They would preserve arc-like trace element characteristics such as Nb-Ta-Ti depletion relative to MORB and primitive mantle, but they could be expected to lack some of the incompatible components, the alkalis and LILE (e.g., Pearce and Parkinson, 1993), which in this case would have been concentrated in the complementary residual liquids that ascended into the arc crust proper. Claeson and Meurer (2004) point out that in at least one case, partial melts from garnet-poor sub-arc amphibolites have their REE budgets dominated by amphibole, even when amphibole comprises only a few percent of the source rock. Amphibolitic arc cumulates appear therefore to satisfy each of the major criteria required to yield magmas with the composition of those related to porphyry copper deposits. However, if they play a fundamental role in porphyry copper metallogeny, then the sporadic and domainal distribution of such deposits and related magmatic suites in space and time (e.g., Sillitoe, 1988) demands either that they are not a ubiquitous component of sub-arc lithospheric mantle. The emerging hypothesis demands an explanation of (at least) four central questions that appear key to fertile petrogenesis: 1) what drives regional development of amphibolitic arc cumulates? 2) why are the resulting partial melts so productive? 3) what causes the lithospheric mantle to melt? and 4) how and under what conditions do these melts reach the shallow crustal environment effectively unmodified?

Amphibole in Sub-Arc Cumulates. Convergent margin arc magmas are distinctively hydrous, in contrast to magmas formed in other settings (e.g., Wilson, 1989; Candela and Piccoli, 2005). Their hydrous nature promotes crystallisation of amphibole, rather than plagioclase (Burnham, 1979; Naney, 1983), but this in itself is not unique to mineralised arc segments, rather it occurs throughout the mid-late stage differentiation of magmas in many arc terranes (Davidson et al., 2007). However, under certain conditions amphibole has been found to crystallise at the expense of olivine and plagioclase in paragenetically early arc cumulates (Meurer and Claeson, 2002). Experimental work suggests that this may occur above a threshold magma water content (9 wt% at 950ºC) at which amphibole replaces clinopyroxene as the principal ferromagnesian liquidus phase in basaltic compositions. At lower temperatures the same occurs over a broader range of water contents (Alonso-Perez et al., 2009). Stress conditions in the upper plate impact on the location of magma storage (e.g., Charvet and Ogawa, 1994) and therefore indirectly on magma evolution. Rohrlach (2002) calculates that the 'orogenic deformation rate' (i.e. the shortening strain rate) in the overriding plate correlates with the height of the accumulated magma column (i.e. the MASH zone or similar in the lithospheric mantle) required to exceed confining pressure and ascend by dyke propogation. The shortening strain rate also correlates inversely with the density (and hence degree of differentiation) required for ascent of a magma given a constant height of the magma column (Rohrlach, 2002). These calculations imply that active compression favours prolonged deep magma storage, which would in turn favour development of sub-arc mafic cumulates. Positive feedback loops between depth of storage and plagioclase inhibition, and between prolonged storage-crystallisation and hydrous inhibition of clinopyroxene might be expected to operate. Voluminous amphibole-bearing cumulates are therefore interpreted to form during active compression, which promotes sub-crustal magma storage at pressures that inhibit plagioclase, and also permits the development of high levels of hydration that inhibit clinopyroxene.

Why should arc amphibolites yield fertile magmas? Cline and Bodnar (1991) argued that regular calc-alkaline magmas flux sufficient metals and volatiles to make porphyry copper deposits of the magnitude commonly observed. Evidently, normal arc magmas do not make these mineral deposits, as they are irregularly distributed in

space and time among a much broader and continuous history of arc magma productivity. Likewise, the magmas related to mineralised suites are strikingly distinct in terms of bulk composition (Table 6.2), isotopic composition (e.g., Maksaev, 1990), and oxidiation state (e.g., Garrido et al., 2002). Partial melting of amphibolitic cumulates to yield productive magmas is partly consistent with Tosdal and Richards' (2001) concept of distillation of the critical components. Adjustments to their model are necessary because a simple distillation should drive levels of concentration related directly to the compatibility behaviour of each element. Instead, a cumulate source model is consistent with relative depletion of the alkalis and LILE in productive suites, and several independent lines evidence suggest it may also permit unusual pre-concentration of metals, sulfur and oxygen.

High oxidation states are required by productive magmatic systems because the chalcophile metals are compatible in magmas in which reduced sulfur predominates (Bornhorst and Rose, 1986; Richards et al., 1991; Spooner, 1993). Aeolus Lee et al. (2005) argue on the basis of global arc V/Sc systematics that the high oxidation state achieved by the mantle wedge and some arc magmas (e.g., Parkinson and Arculus, 1999) may only be achieved by repetition of the slab-related metasomatism that characterises the subduction zone melting environment. The presence of magmatic anhydrite in ore-age volcanics at Yanacocha, Peru (Chambefort et al., 2008), and veins of native sulfur in the propylitic zones of the Grasberg porphyry deposit, Indonesia (Pollard and Taylor, 2002), imply that sulfur is the key limiting ingredient to deposit size at the upper end of the range. Sulfur is concentrated in porphyry copper deposits by the greatest enrichment factor of any element (Hattori, 2007). Likewise, Takagi and Tsukimura (1997) calculate that the redox state of a magma can only achieve magnetite stability (common and perhaps critical to mineralised systems, e.g., Sun et al., 2004) when there is a high proportion of sulfur to other volatiles. I therefore speculate that voluminous sub-moho storage and crystallisation of arc magmas leads, initially, to retention of S (relative to other volatiles) and of chalcophile metals in the resulting amphibolitic cumulates. Subsequent influx of new batches of oxidising slab-related fluids (e.g., McGuire et al., 1991) would cause repeated metasomatism and eventually drive the bulk oxidation state above

a threshold that controls S speciation and chalcophile metal release. Partial melts of this metasomatised cumulate material would be loaded with metals and oxidised sulfur, as is suggested by analyses of melt inclusions in porphyry copper deposits (e.g., Kamenetsky et al., 1999; Campos et al., 2002; Davidson et al., 2006; *cf*. Cline and Bodnar, 1991). As Hattori (2007) points out, among primitive arc magmas in a given terrane, Cu correlates most systematically with V, the behaviour of which is strikingly sensitive to redox conditions (e.g., Toplis and Corgne, 2002).

Dynamic scenarios for arc cumulate melting. Any tectonic setting that causes either heating of the mantle lithosphere in situ, or moves parts of it to greater depth (and hence temperature and/or pressure) might reasonably be expected to prompt partial melting and therefore yield fertile magmas. The principal mechanisms by which lithospheric mantle may be moved deeper are delamination (Fig. 6.19; Kay and Kay, 1993) and subduction erosion (Scholl et al., 1970; Rutland, 1971). Delamination is thought to occur in response to density contrasts generated by metamorphic reactions during crustal thickening (Kay and Mahlburg-Kay, 1991;

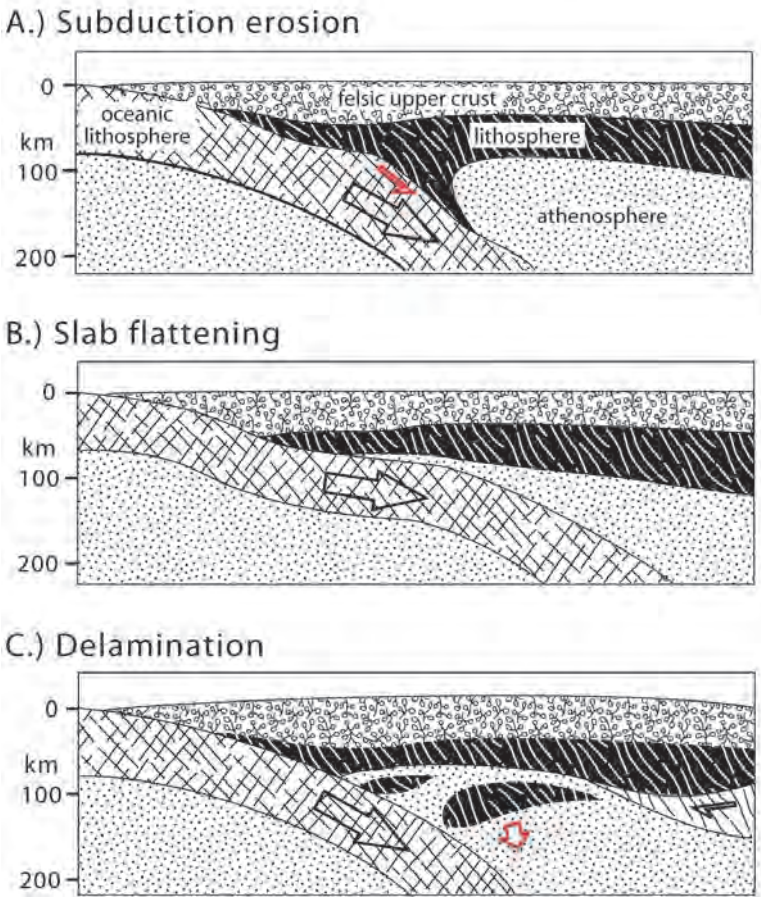

Figure 6.19. Scaled tectonic sketch sections showing subduction-related scenarios in which the sub-crustal lithosphere could melt. A.) During subduction erosion, with entrainment of the lithosphere along the subduction interface; B.) During flattening of the slab geometry. Both these scenarios may be enhanced by the subduction of anomalously thick or hot oceanic lithosphere; and C.) in response to lithospheric delamination, in response to crustal thickening and metamorphically imparted density contrasts. Delamination may also be prompted by undertrusting of the continental hinterland (e.g., the Brazilian shield example), or by accretion or collision (not shown). Modified from Kay and Mpodozis (1999).

Elkins-Tanton, 2005), and has also been attributed to continental collision/accretion events (e.g., Pearce et al., 1990; Keskin, 2003). Subduction erosion is principally a function of the shear strength of the interplate boundary (and therefore of plate coupling), which is inversely related to sediment supply to the trench, and may be more than doubled by aseismic ridge subduction (Kukowski and Oncken, 2006). However, subduction of ridges does not singularly drive mineralisation, as shown by the passage of the Juan Fernandez Ridge under the effectively barren Late Oligocene to Early Miocene CVZ (Yañez et al., 2001; Trumbull et al., 2006).

Another mechanism is plausible if slab-related fluids were able to cross the athenospheric mantle wedge. There they may react with anhydrous phases in the lithospheric mantle to create more amphibole, and upon continued volatile addition, cause its partial melting (e.g., Peacock, 1990). Therefore, shallow or flat subduction geometries in which the mantle wedge is effectively occluded might also cause melting of the lithospheric mantle by volatile addition (e.g., Fig. 6.19; James and Sacks, 1999; Kay and Mpodozis, 1999). Perturbation of athenospheric flow along the margins of a flat subduction regime (e.g., Wagner et al., 2006) provides a related mechanism by which the mantle lithosphere might melt in response to higher athenospheric heat flux. However, whereas subduction of active spreading ridges may drive orogeny (e.g., the Cretaceous Peruvian event; Steinmann, 1929), flat subduction (e.g., Martinod et al., 2005) and unusual magmatism (e.g., Guivel et al., 2006), this tectonic environment does not appear to cause major metallogeny. Mineral deposits are scarce in the 90-80 Ma Central Andean belt or in Quaternary southernmost Chile-Patagonia. Rather, there is a space-time coincidence between major porphyry copper camps and subduction of aseismic ridges (Rosenbaum et al., 2005; Cooke et al., 2005). Although models of aseismic ridge subduction are generally unable to yield flat subduction geometries (e.g., Van Hunen et al., 2002, 2004), the modern subduction geometry around the Juan Fernandez Ridge in central Chile is clear evidence of at least a contributory role for aseismic ridge subduction in slab flattening (e.g., Martinod et al., 2005). Subduction of thickened oceanic lithosphere also drives changes to the upper plate strain regime (e.g., Espurt et al., 2006) that may promote mineralisation by facilitating efficient magma ascent into the shallow crust.

It may also be possible to for the lithospheric mantle to melt without major changes to the geometry of the subduction zone if the MASH zone deepened to incorporate parts of the mantle lithosphere, or that a MASH-like zone developed at mantle depths. Transient deepening of the MASH zone was suggested by Richards and Villeneuve (2002) to explain intercalated Miocene lava flows with distinctly different trace element behaviour from the Cerro Llullaillaco volcano in the CVZ. This phenomenon may also explain the cyclical increase and then resetting of La/Yb associated with regional compressive tectonic events (Fig. 6.20; e.g., Hollings et al., 2005), as opposed to cumulative crustal thickening, which is more likely to correspond to a gradual secular increases in background and syn-tectonic maximum La/Yb (Fig. 6.20, *c.f.* Haschke et al., 2002a). Physical modelling (Rohrlach, 2002) independently suggested that deepening of the MASH zone is only physically plausible during compressive tectonism. However, an alternative explanation is that

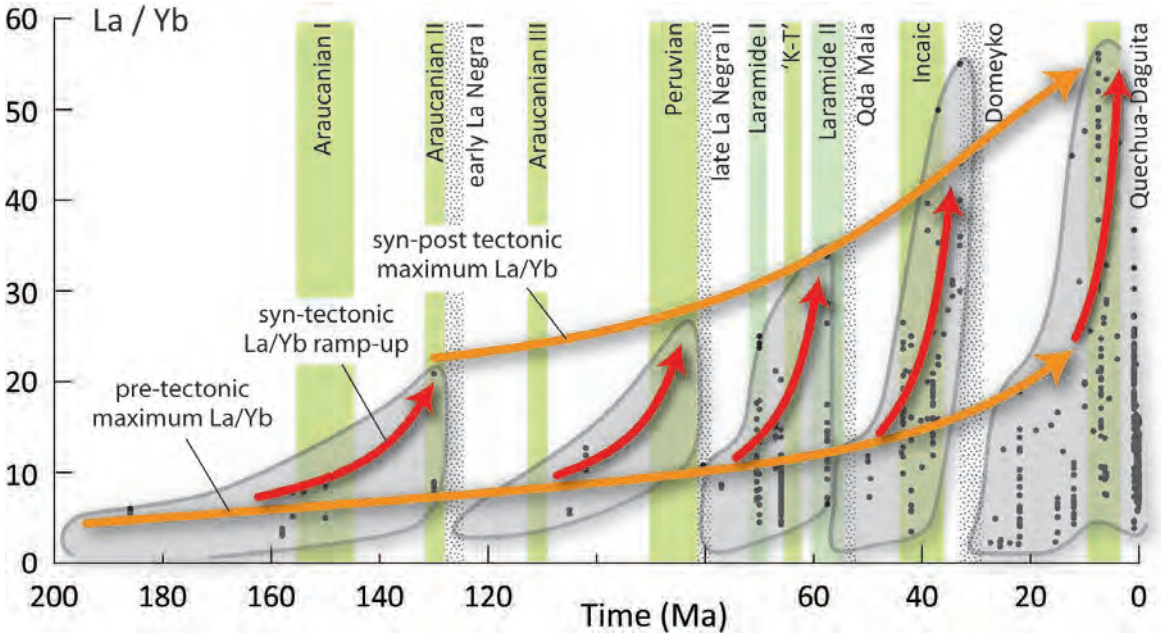

Fig. 6.20. La/Yb versus time (inverted scale) for Central Andean magmatic rocks from the Jurassic to the present. Grey areas are fields defined by global geochemistry-geochronological datasets adapted from Haschke et al. (2002a) to accommodate a more comprehensive dataset compiled and produced in this study (Table 6.1; Hawkesworth et al., 1982; Hickey et al., 1986; Baker et al., 1987; Gerlach et al., 1988; Fierstein et al., 1989; Wörner et al., 1992a; Feeley et al., 1993; Dungan et al., 2001; Matteini et al., 2002; Richards and Villeneuve, 2002; Hollings et al., 2005; GEOROC database; and references cited in Chapter 3). Arrows indicate secular changes to crustal thickness (orange) and transient changes apparently related to tectonism (red). Green background fields indicate the main local tectonic events, blue-green fields are selected regional tectonic events, and stippled fields indicate amagmatic periods at the decline of magmatism in each of the Andean Cycle belts (McCandless and Ruiz, 1993; references cited in Table 2.1).

cyclical ramp-up of La/Yb during and after each tectonic phase may also reflect increasingly efficient tapping of the middle to lower crust. Cumulative increases in structural permeability are expected to occur during progessive deformation along major strike-slip fault zones (Kelly et al., 1998; Sibson, 2001).

A combination of the three major tectonic processes mentioned above each contribute the time-integrated 'ablative subduction' (Pope and Willett, 1998; Davidson and Arculus, 2006) required to account for the felsic bulk composition of the continental crust by recycling mafic arc products back into the athenosphere. Although transient, they are therefore likely to be recurring processes along continental margin arcs. Subduction erosion and flat slab subduction occur during strong interplate coupling (e.g., Van Hunen et al., 2002, 2004; Sobolev et al., 2006), which typically drives deformation in the upper plate (e.g., Yañez and Cembrano, 2004; Lallemand et al., 2005; Oncken et al., 2006). In turn, upper plate deformation and thickening are considered major precursors to lithospheric delamination (Kay and Mahlburg-Kay, 1991; Elkins-Tanton, 2005). Therefore compressive tectonism provides the general environment in which amphibolitic cumulates are envisaged to form in the sub-arc lithospheric mantle, and four mechanisms that could cause them to melt them are transient manifestations of the changing sub-arc physical environment during, or following tectonism. This appears therefore to provide a first order link between compressive tectonism and porphyry metallogeny.

Conditions for efficient mantle-shallow crust magma migration. Mantle-like Sr, Nd, Pb isotopic composition (Maksaev, 1990; Masterman, 2003) and elevated Cr and Ni (Fig. 6.12f) imply that productive Andean syn-mineral suites were not substantially modified during their ascent into the shallow crust. Preliminary Os isotope evidence even suggests that there may even be a coarse secular relationship between deposit size, age, and the efficiency of magma ascent, since the largest deposits show the least crustal contamination, and are typically the youngest (e.g., Mathur et al., 2000; Camus, 2002; 2003). This lends support to the concept of secular increases in crustal permeability related to progressive deformation along major strike slip fault zones within the arc (previous page).

In this chapter I have argued that the chemistry of the Collahuasi district productive

intrusive suites requires that they formed from low degree partial melts of specialised amphibole-ilmenite-garnet bearing sources in the lowermost crust or lithospheric mantle. These relatively low-volume melts formed at depths of more than 30 kms. They evidently traversed the crustal column without freezing, and without assimilating much wallrock. Although the thermodynamics of this process are beyond my scope, the mantle-like isotopic chemistry and increasingly pronounced trace element composition of these rocks is consistent with rapid magma ascent that involved minimal interaction with the wallrocks, and therefore reduced the opportunity for thermal equilibration. Such a phenomenon clearly demands highly specialised, deeply penetrative structural permeability.

In the Central Andes, Trumbull et al.'s (2006) compilation of volcanic centres shows little or no Late Eocene-Early Oligocene magmatism outside the latitudinal range of the contemporaneous porphyry belt (between 14º and 28ºS; Fig 2.7). It is unlikely that the distribution of these rocks is an artefact of greater uplift and exposure in the Central Andes, because both pre- and post-Eocene units are well exposed outboard of the belt of Eocene-Oligocene mineral deposits. Rather, this distribution must be a primary feature of late Eocene-Oligocene arc and demands either that a) magma productivity was negligible outside these latitudes, or b) magma ascent pathways were anomalously efficient within the mineralised belt. Subduction was persistent along the greater Andean margin throughout this period (e.g., Scheuber et al., 1994), and so variations in arc magma productivity seem unlikely. Instead, the latitudinal range of this porphyry belt coincides closely with the extent of the modern Altiplano-Puna Plateau. This major physiographic block is considered to have maintained its approximate outline since initiation of uplift in the Middle Eocene Incaic tectonic event (Haschke and Günther, 2003; Victor et al., 2004; Oncken et al., 2006). A relationship is therefore implied bewteen efficient magma ascent into the shallow crust and upper plate shortening strain.

Comparisons with regional shortening and tectonic parameters (Fig. 6.21; Oncken et al., 2006) permit the evaluation of several possible regional-scale controls. I have argued here that the magmatic chemistry of the productive suites imply a broad genetic relationship with compressive tectonism, in line with previous empirical

observations (e.g., Tosdal and Richards, 2001). In their comprehensive review of shortening estimates for the Central Andes, Oncken et al. (2006) show that neither net tectonic convergence rate nor obliquity (Fig. 6.21), nor climate-induced sediment starvation to the trench (e.g., Lamb and Davis, 2003) were first order controls on Central Andean shortening. Instead, the difference between the hinge/slab rollback and the westward drift of the South American plate is the critical variable affecting upper plate shortening (Russo and Silver, 1996; Heuret and Lallemand, 2005; Oncken et al., 2006). Yet the temporal relationship between shortening and mineralisation is inconsistent. Increases in the bulk shortening rate across the orogen coincided with mineralisation in the Domeyko Arc, and during the Middle Miocene. In contrast, Andean metallogenic events in the Early and Late Miocene were not

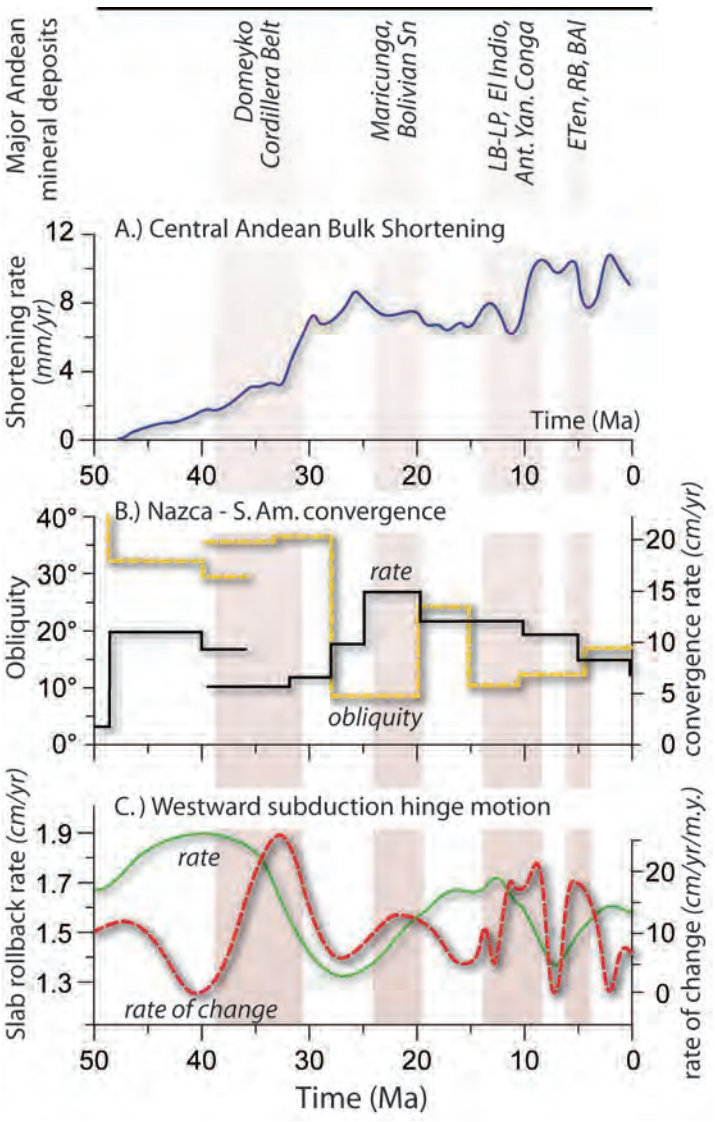

Figure 6.21. Time correlations between major epochs of intrusion-related metallogeny and tectonic parameters. A) bulk shortening in the Central Andes. B) Nazca-South American plate convergence. C) westward motion rate and rate-of-change of the subduction hinge. Adapted from Oncken et al., (2006). Abbreviations and geochronology sources: 'Domeyko Cordillera Belt' includes all major deposits in the El Salvador, La Escondida, Chuquicamata, and Collahuasi districts (Cornejo et al., 1997; Richards et al., 2001a; Masterman et al., 2004; Campbell et al., 2006). 'Maricunga' and 'Bolivian Sn' refer the earlier of two recognised events in these two belts (Sillitoe et al., 1998; Muntean and Einaudi, 2001). LB-LP = Los Bronces - Las Pelambres (Bertens et al., 2003, 2006). Ant = Antamina; Yan = Yanacocha; Conga = Minas Conga district; ETen = El Teniente; RB = Rio Blanco; BAl = Bajo de la Alumbrera.

associated with orogen-wide increases in shortening rate (Fig. 6.21a). Rather, it is the rate of change of subduction hinge motion (i.e. rollback acceleration or deceleration) that is the unique variable that accompanies all four major Central Andean metallogenic periods since the Eocene (Fig. 6.21c). Each of the four Cenozoic Andean metallogenic events (Fig. 6.21) is mirrored by a simultaneous event in the accreted Tethyan arc terranes of Eurasia (Lips, 2002; Richards et al., 2006b; Perelló et al., 2008). Dynamism of these major subduction zones is therefore plausibly linked across the Atlantic and is driven by global tectonic processes (e.g., Silver et al., 1998).

Convergence between two plates must be accommodated either by subduction of the downgoing slab, or by shortening of the upper plate. The subducting slab is much less able to adjust to variations in convergence than the upper plate (Oncken et al., 2006), and therefore changes in the rate of rollback equate to changes in the rate at which strain must be absorbed by shortening of the upper plate, i.e. to strain acceleration. The connection between upper plate deformation and magmatic-hydrothermal mineralisation may lie in how magmas ascend into the shallow crustal environment. Hydrothermal fluid flow is strongly dependent on structural permeability (and hence strain rate) in active fault zones (e.g., Miller et al., 2004), laboratory experiements (Tenthorey and Fitz Gerald, 2006), and is also implied by fault and vein arrays and fluid compositions in orogenic gold deposits (e.g., Cox et al., 2005). Espurt et al. (2006) conducted scaled model experiments in which they found that subduction of aseismic ridges created a deformation front that radiated away from the leading edge of the subducted ridge. In contrast, following subduction, the area above the ridge returned to a steadier strain environment. This observation matches the time-space radiation of Miocene mineralisation (mostly intrusion-related) away from the leading edge of the subducting Nazca Ridge in Peru (Rosenbaum et al., 2005). Magmas therefore appear to behave in a similar fashion to hydrous fluids, such that their movement (primarily ascent) in compressional arc terranes is favoured at high or changing strain rates. In this way, perturbation of the intra-arc strain environment should permit efficient migration of mantle-derived or lower crustal magmas into the shallow crust (e.g., Richards, 2003). However, the Eocene-Oligocene porphyry copper deposits of the Central Andes were emplaced

contemporaneously along an arc segment at least 1200 km long (e.g., Camus, 2002; 2003). Subduction of a hypothetical aseismic ridge could not, independently, have caused this geometry of upper plate strain acceleration and related low volume intrusion.

Two major tectonic phenomena affected the late Eocene-Oligocene Central Andean margin; slab flattening (Isacks 1988; Sandeman et al., 1995; Allmendinger et al. 1997; James and Sacks, 1999; Kay et al. 1999) and oroclinal bending (e.g., Beck, 1988; Roperch and Carlier, 1992). Creager et al. (1995) make geophysical arguments that suggest that flat subduction regimes facilitate oroclinal bending. Evidence for a flat slab at this time comes primarily from the space-time distribution of volcanism and shortening strain accommodation. The Early to Middle Oligocene marks the total decline of arc magmatic activity in the Domeyko Arc, and the establishment of a continental thrust belt well inboard of arc (in the central and eastern Altiplano of Argentina, Bolivia and Peru: Sandeman et al., 1995; Ege, 2004; Silva-González, 2004; Elger et al., 2005). During the latter part of the Oligocene, volcanism occurred along a broad arc that migrated westward and narrowed as the slab steepened during the Miocene (Scheuber et al., 1994; Trumbull et al., 2006). Late Eocene-Oligocene slab flattening may have had three contributory effects to metallogeny, as discussed above, by way of permitting metasomatism of the cumulates in the sub-moho lithospheric keel, by driving anomalous athenospheric flow that may have further promoted melting of this material, and by causing transient changes to the strain rate within the upper plate. It is interpreted to have been a consequence of the Incaic tectonic phase, which was driven by westward acceleration of the South American plate (Silver et al., 1998; Oncken et al., 2006), and was enhanced by progressive desiccation that resulted in sediment starvation of the trench (e.g., Davis and Lamb, 2003). However, shallow crustal magmatism and mineralisation persisted for 11 million years along this arc segment during establishment of the flat slab. A different mechanism is therefore required to explain the persistence of a strain environment that periodically allowed efficent magma ascent from the mantle to the upper crust.

Paleomagnetic data constrain an Eocene-Middle Oligocene age for accommodation of most of the roughly symmetrical finite bending strain of 25-40º on each side of the Bolivian Orocline (Fig. 6.22a; Arriagada et al., 2000; Roperch et al., 2000;

Somoza and Tomlinson, 2002, Arriagada et al., 2003c). Estimates of post-Paleocene bulk shortening are also roughly symmetrical about the axis of bending (Fig. 6.22b), which led Oncken at al. (2006) to deduce an interdependence between the shear strength of the plate interface, slab flattening, subduction erosion and bending of the Andean margin. That is, that because the axis of the orocline coincides with axis of greatest shortening, then the orocline as a whole may be envisaged as an indented margin, where the indentation arises not from collision but from accentuated interplate coupling.

The regional structure of the Chilean margin is dominated by a series of three arc-parallel high strain corridors; the Atacama, Domeyko and Rio Loa fault systems (Fig. 6.22a; sections 2.2.3 and 4.3.2). Throughout the Cenozoic the regional tectonic convergence should have partitioned a component of dextral along-arc shear into

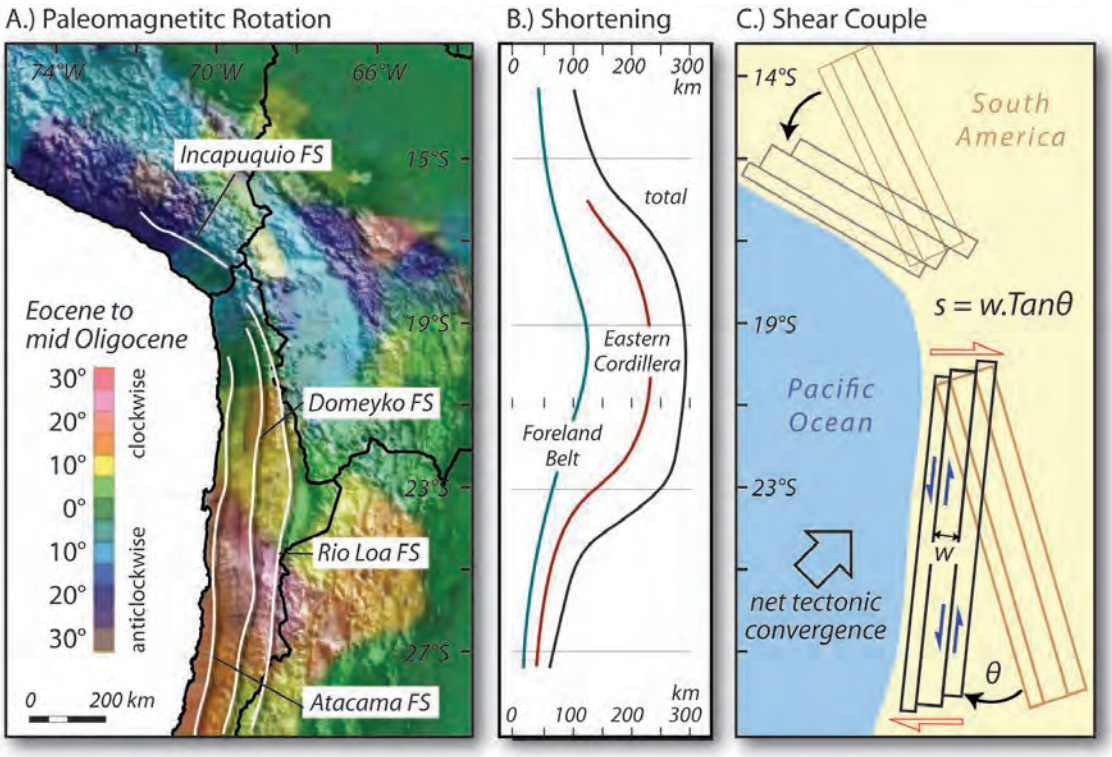

Figure 6.22. Evidence supporting a relationship between Andean oroclinal bending, continental shortening, and strike slip displacement on arc parallel faults such as the Domeyko fault system. A) Eocene-mid Oligocene finite rotation map calculated from a compilation of paleomagnetic data (colour scale; Arriagada et al., 2003), shown on SRTM topography (greyscale background). The position of major arc-parallel strike slip faults are indicated. B) Average bulk shortening v. latitude, at the same latitude scale as A and C, after the compilation of Oncken et al., (2006). Shortening is symmetrical about the Bolivian Orocline in the easternmost 'Foreland Belt', the Eastern Cordillera, and in total, across the orogen. C) Schematic diagram indicating the geometric relationships in a hypothetical shear couple (Tomlinson et al., 2001a) wherein bending drives sinistral strike slip on arc-parallel faults south of the Orocline.

these arc-parallel fault systems. This sense of displacement would cause clockwise rotations of sub-blocks within an along-arc shear system. While this effect likely contributes to the variability in net rotation across the Chilean Central Andes (Fig. 6.22a), clockwise rotations are ubiquitous south of 19ºS, and have been measured well beyond the immediate environment of the arc parallel fault systems (Roperch et al., 2000; Arriagada et al., 2003). To explain this discrepancy, Roperch et al. (2000) argued on the basis of widespread paleomagnetic measurements that oroclinal bending drove wholesale rotation of the southern Andean margin about a pivot in the central part of the Orocline. Tomlinson et al. (2001a) proposed that pivoting might have been achieved by establishment of a continent-scale dextral shear couple in Chile, in concert with an equivalent sinistral couple in Peru (Fig. 6.22c, red arrows). Shear strain on this scale amounts to flexural slip folding of the continent (Fail, 1969; Weiss, 1969), which is entirely consistent with Oncken et al.'s (2006) interpretation of the orocline as an indented margin. Folding of the Andean margin about a subvertical axis through the Orocline would have driven sinistral shear along the major arc-parallel faults (Fig. 6.22c, blue arrows). It also implies that the the arc-parallel shears penetrate to the base of the lithosphere.

The magnitude of the sinistral displacement is dependent upon the width (W) of the arc-parallel slivers that comprise the shear couple, and their absolute rotation (θ; Fig. 6.22c). The average width of the block between the Atacama and Domeyko fault systems is ~60 km, such that the observed 30-35º clockwise rotation of the Chilean margin corresponds to 34.6 - 42.0 km of sinistral displacement along the Domeyko fault system. This hypothesis therefore predicts accurately the ~37 kms of net sinistral displacement along the Domeyko fault system for which there is diverse geological evidence (Chapter 5, section 5.4.2; Dilles et al., 1997; Tomlinson and Blanco, 1997b). This order of magnitude of sinistral displacement is also implied by thermochronometry results from Chuquicamata (Tomlinson et al., 2001b) and Collahuasi (Chapter 5; Fig. 5.7).

Arc-parallel structures in the Chilean Andes therefore experienced opposing forces during the Eocene and earliest Oligocene; dextral shear partitioned from the tectonic convergence (Fig. 6.22c), and sinistral shear driven by the bending of the Bolivian Orocline. Both thermochronometry data (Chapter 5) and structural

mapping (Chapter 4) in the Collahuasi district record Middle Eocene dominance of the dextral shear that was surpassed by sinistral shear in the earliest Oligocene. Along the Andean margin, the late Eocene-Oligocene was the period of most rapidly changing upper plate strain environment since onset of Incaic shortening (Fig. 6.21c). This environment of protracted and possibly stuttering changeover in the sense of along-arc lateral shear coincides in time and space with the major Eocene-Oligocene porphyry copper deposits of northern Chile. This environment is therefore envisaged to have played a key role in the regional metallogeny by permitting the efficient ascent of low volume fertile magmas in the Domeyko Arc. No such conflict of shear sense occurred in the contemporaneous Peruvian margin, and perhaps explains the apparent paucity of magmatism (and mineralisation) in that section of the arc.

Concluding summary. The Eocene-Oligocene Andean margin was characterised by a series of partly coincident, complementary tectonic and structural phenomena that led directly to the formation of fertile magmas at, or below the base of the crust, and permitted their subsequent efficient ascent. The Incaic tectonic phase provided an environment in which amphibole-bearing arc magmatic cumulates formed in the sub-arc lithospheric mantle. This event led ultimately to the establishment of a flattened subduction geometry, that permitted metasomatism of the sub-arc cumulates by slab related fluids. Initially, magmas reaching the upper crust were related to the formation of the amphibolitic cumulates, and/or derived from moderate to high degrees of melting of this material. In the absence of pronounced structural permeability, these magmas were stored in the crust and assimilated substantial amounts of felsic crustal materials (Icanche Formation). Slab-related metasomatism was ongoing through the Eocene, and ultimately drove the oxidation state of the sub-arc cumulates to the point that chalcophile metals could be released into hydration-related partial melts. These were uniquely able to reach the shallow crust and cause porphyry copper mineralisation during the dynamic strain environment offerred by counter-tectonic along arc shear imposed by bending of the Bolivian Orocline.

Chapter 7.

CONCLUSIONS.

7.1 Context

The Collahuasi district of northern Chile (21ºS 68º45'W) is one of four major Eocene-Oligocene porphyry-epithermal camps located along a 650 km-long segment of the central Andean margin. Collahuasi is unique among these districts in that mainly Upper Paleozoic volcano-sedimentary rocks of the Choiyoi Arc (the Peine Group) are the major host to mineralisation. The district contains the largest and most continuous exposure of Peine Group anywhere in northern Chile. Metamorphism is negligible and volcanic textures are well preserved. The district hosts a range of porphyry and epithermal mineral deposit styles that contain substantial economic mineral resources. Widespread exposure of (or access to) mineralised rocks and host sequences is provided by active mining operations at the three major porphyry copper deposits, related infrastructure-related excavations, active exploratory drilling and trenching at La Grande, and steep natural dissection of the Copaquire porphyry copper deposit. Collahuasi is therefore an exceptional district in which to investigate the geological framework of a major continental porphyry copper district.

In this study, the district geology was mapped at 1:10,000, encompassing the Ujina, Rosario-La Grande, and Quebrada Blanca Cu-Mo deposits. Selective mapping was also conducted in valleys that dissect the western margin of the district. Fault and vein arrays were mapped in the major porphyry-high sulfidation copper deposits. Zircon and apatite (U-Th)/He data were collected and compiled to constrain the timing and absolute motion on major faults. The hydrothermal paragenesis of some deposits were revised in light of new observations, and the distribution of peripheral alteration facies was mapped. A new local stratigraphic column for the Peine Group and Cretaceous to Oligocene magmatic rocks was constrained by detailed petrology, 46 new whole rock chemical analyses, 21 new laser ablation ICPMS zircon U-Pb ages and three new 40Ar/39Ar laser step heating ages.

7.2 Stratigraphy and Intrusive History

7.2.1 Permo-Triassic Evolution

Across the district, the Permo-Triassic strata dip broadly northward, effectively revealing a cross-arc section through the stratigraphy, although the base of the section is obscured by plutonic rocks. The Peine Group is here divided into lithostratigraphic members that belong to and define six proposed Formations that are separated by significant depositional hiatuses or unconformities. The Peine Group at Collahuasi records deposition of eight broad facies associations. These associations partly coincide with the lithostratigraphic formations, and reflect periods of distinct style and chemistry of volcanic and sedimentary deposition. The sequence of deposition is constrained by mapping, and the absolute timing and duration of which is constrained by new geochronology; from oldest to youngest:

- 308 – 289 Ma: Reduced subaerial felsic volcanic and volcaniclastic facies association (308* – 289 Ma: Chiclla Formation; *oldest ages from Munizaga et al., 2008).
- Subaqueous bimodal volcano – sedimentary facies association (289 – 285 Ma: Lower La Grande Formation; Miembro Medio Basin subsidence).
- Subaerial volcanic and terrestrial carbonate and evaporitic sedimentary facies association (289 – 285 Ma: Middle La Grande Formation; Miembro Medio Basin infill).
- Oxidised dacitic to rhyolitic volcanic and volcaniclastic facies association (~285 Ma: Upper La Grande Formation and Cascasca Formation; Miembro Medio Basin filled and covered).
- Oxidised felsic volcanic facies association (≥276 Ma: Lower Huinquintipa Formation).
- Reduced rhyolitic – dacitic volcaniclastic facies association (276 – 273 Ma; Upper Huinquintipa Formation and Sallihuinca Formation).
- Oxidised rhyolitic – dacitic volcanic and volcaniclastic facies association (242 – 244 Ma: Lower Yabrociya Formation).
- Andesitic volcanic facies association (?237 Ma: Upper Yabricoya Formation).

In addition, three distinct pre–Middle Triassic intrusive phases are recognised and constrained by the new mapping and geochronology. The three are chemically distinct and are equivalent to contemporaneous volcanic facies:

- Fine grained basaltic andesite dyke swarm (238 – 237 Ma: Cascasca dykes);
- Porphyritic monzogranite dykes (248* – 232 Ma: Collahuasi Porphyry; Characolla Porphyry; Cerro Silvar Porphyry; *additional geochronology 244-248 Ma from Masterman, 2003, and Munizaga et al., 2008);
- Equigranular diorite to granodiorite plutons (270 – 260* Ma: Escorial Diorite; Ceucis Granodiorite; Chara 'Granite'; *geochronology from Huete et al., 1977; Damm et al., 1986).

Several fundamental changes in the accommodation of deposited materials and petrogenesis of the volcanic rocks are recorded by the Peine Group and related intrusions. The lowermost Peine Group records explosive, mostly subaerial eruptions that resulted in the formation of voluminous dacitic to rhyolitic ignimbrites. These crop out in the vicinity of the Monctezuma epithermal vein system, and at the El Colorado prospect SW of Quebrada Blanca. A significant period of creation of sedimentary accommodation space commenced at ~289 Ma, and was accompanied by effusive subaqueous eruption of basaltic andesites in the Rosario – La Grande area, centered on the Rosario Fault and apparently limited in the west by the Monctezuma Fault. Polylithic epiclastic conglomerates and granular sandstones interbedded with the basaltic andesites were deposited as mass flows entered the adjacent subbasin.

By about 285 Ma, the early basin had filled, and creation of accommodation space shifted westward across the Monctezuma Fault. Dacitic and lesser andesitic lavas were erupted, followed by voluminous dacitic and rhyodacitic ignimbrites. During periods of volcanic quiescence, shallow water laminated microbial limestones and minor evaporites were deposited. The same time coincides with a change in the bulk magma chemistry. The older sequences are uniformly black-grey and contain magmatic ilmenite, whereas the upper Peine Group is commonly reddish, contains little magmatic ilmenite, and ferromagnesian phases have strong iron oxide oxidation rims.

A volcanic hiatus between 270 and 260 Ma coincided with intrusion of voluminous equigranular medium grained intermediate to felsic plutons. Disharmonic open, upright 'crumple' folding of the Peine group was associated with the emplacement of these intrusions. The uppermost Peine Group was erupted in the earliest Triassic (~248 Ma) and includes various felsic domes, flows and proximal explosive volcaniclastic facies. These formed at two centres, interpreted to be located on the Domeyko Fault and the northern Monctezuma Fault, respectively. In both areas, volcanic products and related terrigenous sediments were accommodated in local subbasins that formed to the east of the Monctezuma and Quebrada Blanca faults, respectively. At around the same time, rare, thick dykes of porphyritic monzogranite, and abundant narrow basaltic andesite dykes were emplaced in the eastern half of the district.

The chemistry of the Peine Group rocks suggests that they formed from intracrustal sources with some arc-like contributions. Two crustal sources appear to be represented by the felsic and basaltic-andesite compositional modes; an evolved upper crustal source for the most felsic members, and a depleted lower crustal source for the mafic La Grande Formation members. The Triassic intrusions include the most primitive Peine Group rocks and show the strongest arc-like signature. Overall, the Peine Group and related intrusions represent a range of three-component mixtures between primitive arc-related basalt, depleted lower crustal andesite and evolved upper crustal rhyolite.

7.2.2 Jurassic to Recent Evolution

The post-Triassic history of the Collahuasi district can be considered in terms of four broadly-defined facies associations, and three intrusive episodes. The facies associations record, respectively:

- marine sedimentation in the Mesozoic Tarapaca Basin,
- subaqueous magmatism and related intrusion in the Cretaceous magmatic arc,
- subaerial volcanism and two stages of attendant intrusion in the Eocene magmatic arc, and
- terrigenous sedimentation and ignimbrite deposition from the Late Oligocene to Recent.

The Tarapaca Basin. Extension that marked the decline of the Choiyoi Arc was related to marked slab rollback, which drove substantial subsidence during the Jurassic. The back-arc, marine Tarapaca Basin covered the western part of the Collahuasi district at this time, in which thick package of shales and carbonates were deposited throughout the Jurassic and Early Cretaceous (Quehuita Formation). This basin was partially inverted during the late Middle Cretaceous Peruvian Tectonic Phase, after which subsidence was reduced and the basin began to fill, shallowing until a redbed sequence was deposited. Shallow water persisted into the Late Cretaceous basin, which by this time had been partly captured by eastward migration of the magmatic arc. Andesitic and basaltic lavas erupted from ~73 Ma, and the basin was filled with related coarse grained epiclastic materials (Cerro Empexa Formation).

Late Cretaceous Intrusions. Fine grained to weakly porphyritic microsyenite and aplite dykes occur across the Collahuasi district, and a polyphase alkalic intrusive complex occupies the northeastern corner of the District (Tolaun Intrusive Complex). New zircon U-Pb geochronology constrains the timing of emplacement and cooling of these intrusions between 68 and 66 Ma. Locally they represent a discrete stage of magmatism inboard of the main arc front, alkalic arc volcanism, which correlates more regionally with similar events along the Late Cretaceous arc. Some of these rocks resemble younger mineralised intrusions petrographically, but they are not known to be mineralised at Collahuasi or in other porphyry districts in northern Chile. Tectonism at the Cretaceous-Tertiary boundary appears to have caused the end of this retro-arc magmatism, although fertile magmatism occurred sporadically during the next 11 m.y. along the main front of this arc.

Eocene Magmatism. Two stages of Eocene magmatism can be resolved at Collahuasi; a more voluminous pre-mineral stage dominated by equigranular stocks and coeval with the Icanche Formation; and a syn-mineral stage represented by a handful of smaller porphyritic stocks.

Medium to coarse grained, equigranular dioritic to monzonitic stocks are abundant west of the Domeyko Fault, and several are also known further east. The largest of such intrusions in the central part of the District are hosted by an andesite-rhyolite volcanic complex dated here by zircon U-Pb at ~44-41 Ma. This complex, previously assigned a Cretaceous age, therefore represents the Icanche Formation at Collahuasi.

It includes proximal, coherent lava and autobrecciated flow facies, as well as various lithic and pumiceous lapilli and ash volcanclastic facies.

The porphyry copper deposits are uniformly associated with porphyritic monzodiorite to small monzonite dykes and stocks. These are typically weakly polyphase, comprising 2-3 related intrusive stages, among which the syn- or post-mineral intrusions are subtly more mafic than pre-mineral stages. Emplacement of these intrusions between 37 and 34 Ma had largely been established prior to this study by K-Ar, 40Ar/39Ar and Re-Os methods. However, the coincidence of new zircon U-Pb dates with existing ages confirmed that those data record the timing of the magmatic and hydrothermal events within their analytical error, and do not relate to more protracted cooling.

Terrigenous Sedimentation and Ignimbrite Eruption. This study has not directly sought to add to the understanding of these units. Their stratigraphy and geochronology is already well established, most notably by the authors that contributed to Tomlinson et al. (2001). Among this work, the Paleogene sedimentary history along the Domeyko Fault serves as particularly important evidence for the Eocene-Oligocene history of that structure. At a qualitative level, the development of intermontane basins at sinistral releasing bends, e.g., the Quebrada Caya, testify to the sense and extent of Oligocene and younger strike slip displacement along the Domeyko Fault.

7.3 Structural Geology

7.3.1 Architecture

The Domeyko Cordillera at Collahuasi comprises a regional arc-parallel pop-up that exposes the Permo-Triassic stratigraphy (e.g., Amilibia et al., 2008). Internally, the district is divided into a series of approximately arc-parallel slivers by long-lived N- to NNE-trending faults. Stratigraphic relationships across these major faults require that they originated during Peine Group time, when they articulated local basin subsidence. A similar extensional origin is inferred for the Domeyko Fault and the Rio Loa Fault (Prinz et al., 1994; Muñoz et al., 2002). The NW-trending Rosario Fault also appears to have originated at this time. Its location adjacent to the thickest part of the La Grande Formation andesite package is interpreted as indirect evidence

that it may originally have influenced magma ascent as a sinistral dilational splay off the Monctzeuma Fault. Two major, >7 strike-km, NNW-trending dykes (or swarms) are recognised, and post-date the origin of the major arc-parallel growth faults. They represent a discrete phase of WSW-directed extensional strain during latest Peine Group time, during which major new penetrative fracturing occurred. Subsequent tectonism does not appear to have generated new, hard-linked fault zones in the district, with the possible exception of the Huinquintipa Fault. Nonetheless, linear elements in physiographic and geophysical patterns suggest post-Peine Group time development of diffuse zones of ENE-trending fracturing and local faulting. By correlation with shortening events recognised elsewhere in the Central Andes, these are likely to have formed during Earliest Paleocene, or Middle Eocene shortening associated with the ultimate uplift of the Domeyko Cordillera and folding of the flanking Mesozoic stratigraphy.

Spatial Relationships Between Cu Deposits and Structural Elements. Each of the four major porphyry copper deposits at Collahuasi is located on, or close to host sequence growth faults that affect either the Peine Group or Jurassic to Early Cretaceous stratigraphy. The two largest deposits are located at the intersection of these faults with each of the two major Triassic dykes. It is therefore likely that dilatant sites in the pre-Tertiary extensional architecture served as the principal conduits for magma ascent during Eocene magmatic-hydrothermal mineralisation. All four deposits also coincide with corridors of diffuse ENE-trending fracturing, and so emplacement may also have been focused in locations that acquired additional structural permeability during Paleogene deformation.

7.3.2 Structural History of the Mineral Deposits

Patterns of brittle strain accommodation recorded in the deposits are consistent with those evident more generally in the host sequences. These patterns suggest alternation, and eventual switch between arc parallel dextral and sinistral shear, and hence between oblique compression and extension within the arc.

Monctezuma. New $^{40}Ar/^{39}Ar$ geochronology constrains the timing of mineralisation at Monctezuma to ~40 Ma. The vein array suggests that mineralisation accompanied dilation and sinistral shear on the Monctezuma Fault. The veins therefore record

the first Eocene reversal of arc-parallel wrench shear that is recognised at Collahuasi. Across the District the Middle Eocene is characteristed by increased magmatic activity; new zircon U-Pb dates constrain eruption of the main Icanche Formation volcanic package at Cerro Vega and Cerro Sallihuinca to ~44-41 Ma. This magmatic centre was plausible the thermal driver for epithermal fluid circulation.

Copaquire and Quebrada Blanca. The 37-36 Ma Copaquire and Quebrada Blanca (QB) porphyries are located on NNE trending second order faults that splay from the regional Domeyko fault zone, a major subvertical, arc-parallel deformation zone. Lower Priabonian dilation and accommodation of intrusions, breccias, and early stage alteration and mineralisation occurred along these subsidiary faults, as well as on prominent 3rd order ENE-trending splays at QB. This is interpreted to suggest that the NNE-trending faults acted as dextral synthetic shears to the Domeyko fault zone during mineralisation. At Copaquire, main stage quartz-molybdenite-pyrite veins occupy shallowly E-dipping orientations. At QB, early quartz-pyrite-muscovite-biotite veinlets define a conjugate array of shallowly and moderately E-dipping orientations, interpreted to have formed during compression. Therefore, intrusion and early stage mineralisation in both deposits occurred under dextral transpression. This was followed by relaxation of tectonic stresses during main stage copper-bearing vein formation at QB. Approximately two million years later, the QB hydrothermal system was renewed during a period of weak extension and sinistral along-arc shear evidenced by late stage NW-trending breccias, veins and SW-directed normal faults.

Ujina. At ~35 Ma the Ujina intrusive complex was emplaced into the intersection between the Cascasca dyke swarm, the southeastern continuation of the Rosario Fault (subsequently offset along the Collahuasi Fault), and N-trending faults related to the Rio Loa fault. The orientations of dykes around the margins of the Ujina Porphyry imply intrusion occurred under weak directed horizontal stress. However, a conjugate array of chlorite-altered joints and faults in the marginal alteration facies have kinematic indicators consistent with main stage hydrothermal activity accompanying weak ENE-directed extension. The main and intermediate-stage vein arrays are dominated by radial and concentric geometries and widespread re-use of fault-related fracture networks. Hydraulic forces associated with intrusion and the hydrothermal system dominated fracture development during mineralisation. Tectonically-imparted

differential horizontal stresses were probably very low.

Rosario-La Grande. The greater Rosario-La Grande alteration system encompasses a structurally-defined block that is largely limited by major NNE-trending faults; on the west by the Monctezuma Fault, and on the east by the Lulu Fault.Main stage (~34 Ma) stockwork veins generally dip steeply and strike NNW and NW parallel to major faults. Shallowly dipping veins are uncommon. During mineralisation, the northern Lulu Fault appears to have become hard-linked with strands of the Monctezuma Fault by hijacking short segments of the Rosario fault and the Triassic Collahuasi Porphyry dyke. In doing so it created a sinistral dilational jog into which the Rosario porphyry was emplaced. Dilational strain on those orientations occurred during WSW-directed extension. Sinistral wrench became the principal mode of brittle strain accommodation by ~32.6 Ma, at which time the La Grande epithermal veins formed. By that time, southward escape of the La Grande block had unroofed the Rosario porphyry and permitted juxtaposition of the porphyry and epithermal environments at Rosario.

7.4 Thermochronometry and Tectonic Evolution

New zircon (U-Th)/He data were collected for samples of intrusive rocks across a wide range of elevations on both sides of the Domeyko, Quebrada Blanca and Monctezuma faults. In conjunction with existing apatite (U-Th)/He data, the results demand 300-500 m of post-30 Ma west-side-up displacement across the Domeyko Fault, and smaller offsets for the other two faults studied. Interpretation of the thermochronometry results was constrained by detailed stratigraphic and structural mapping.

The implied Oligocene displacement along the Domeyko Fault is contrary to exposure of older rocks along the core of the Domeyko Cordillera, but is consistent with similar studies elsewhere in Chile. The results are best explained by at least two stages of distinct strain along the Domeyko Fault. An early (i.e. Incaic) stage of oblique reverse dextral strain drove the uplift of the Domeyko Cordillera, and is recorded by ductile fault materials mapped in the field. Partitioning of dextral strike-slip strain into the Domeyko Fault was associated with emplacement of mineralised

intrusions at Copaquire and Quebrada Blanca. Subsequently, the kinematic environment changed and sinistral slip occurred along the Domeyko Fault. This manifested at surface as brittle strike slip faults with striae that plunge shallowly to the north. Tens of kilometres of sinistral displacement (for which there is abundant external evidence) would therefore have caused W-side up offset of 10^2-10^3 metres, thereby satisfying the post-30 Ma offsets implied by thermochronometry data. By correlation with the vein and fault arrays at Ujina and Rosario, the timing of the main change in the sense of along arc strike-slip shear is estimated at ~35 Ma.

7.5 Magmatic Chemistry

The magmatic chemistry of the Tolaun Intrusive complex (TIC), the Icanche Formation and related stocks, and the mineralised intrusions at Collahuasi was investigated in light of a body of existing work toward understanding the chemistry of background and mineralised magmatic rocks in continental and oceanic arc settings. All three suites are unambiguous subduction-related magmatic rocks that have pronounced negative anomalies in Nb, Ta and Ti, and enrichment in alkalis, alkali earths, Pb and the LREE (relative to primitive mantle).

The TIC is an alkaline suite, similar to contemporaneous intrusive complexes along the eastern Domeyko Cordillera. These record a period of deepening of typical subduction-factory processes consistent with their retro-arc position, during which metamorphic reactions in the subducted slab favour the generation of alkaline melts. They evolved primarily via low-pressure fractional crystallisation of clinopyroxene and plagioclase. Production of these alkaline retro-arc magmas was likely coincident with extension along the Preandean Depression, and ceased during the terminal Cretaceous compressional event recognised throughout northern Chile.

Middle Eocene volcanics of the Icanche Formation and related intrusive rocks are chemically similar to most Miocene to Quaternary volcanic rocks of the Central Andes, in most respects. They span a range of compositions from andesite to rhyolite, and show petrographic and chemical evidence of substantial (but variable) crustal assimilation. A compilation of new and published data for the Icanche suite shows one key difference from normal Central Andes magmas; among the REE and

HFSE, a subset of the data are weakly compatible. Within the limitations of available mineral-melt partitioning data, this pattern is apparently unique to magmas generated by the melting of sources containing amphibole and ilmenite. The Icanche suite are therefore interpreted to partly record high degree re-melting of hydrous sub-arc cumulate material.

The same patterns are strikingly developed among the mineralised intrusions at Collahuasi, elsewhere in northern Chile, and in three porphyry copper districts in the SW Pacific. Mineralised intrusions at Collahuasi are depleted relative to normal Miocene-Recent Andean magmas, in the LILE, HFSE, REE, Mn, Fe and Ca. They are subtly enriched in Al. The differentiation trends (Harker diagram) for the LILE, alkali metals and Al demand variable losses and addition of oligoclase-andesine plagioclase late in the magmatic evolution of the mineralised rocks. Differentiation trends for the REE and HFSE are typically weakly compatible through the intermediate to felsic range of bulk composition represented by the mineralised suites. If a contemporaneous suite of unmineralised mafic to intermediate stocks from the Escondida district represents related, less evolved magmas, then patterns for these elements show marked inflexions at andesitic silica contents. Exactly the same patterns are shown by the broader range of compositions represented by mineralised and related background suites in SW Pacific mineral camps. These relationships are interpreted as evidence that the mineralised porphyry magmas were the products of low to moderate degrees of melting of ilmenite-amphibole-bearing sub-arc cumulates (distinct from higher degrees of melting inferred for the Icanche suite). In the Andean case, especially pronounced depletion of the HREE and Y requires the additional involvement of garnet in the cumulate residue as a coincidental result of sufficient crustal thickening prior to the Late Eocene.

7.6 An Integrated Model for Eocene-Oligocene Porphyry Copper Metallogeny in the Central Andes.

The Eocene-Oligocene Andean margin was characterised by a series of partly co-incident, complementary tectonic and structural phenomena that led directly to the formation and efficient ascent of fertile magmas. These magmas are envisaged on chemical bases to have formed at, or below the base of the seismically-defined crust,

albeit among rocks that are genetically related to supra-subduction zone processes and the evolution of the overlying crust. Compression related to the Incaic tectonic phase provided an environment in which amphibole-bearing arc magmatic cumulates formed in the lithospheric mantle above the subduction zone. Tectonic drivers of this compressive event; including upper plate velocity changes and a decrease in sediment load to the trench led ultimately to the establishment of a flattened subduction geometry. By occlusion of the mantle wedge, slab flattening crucially permitted metasomatism of the sub-arc cumulates by slab related fluids, and it is most likely was this hydration prompted melting of the amphibole-bearing cumulates. Initially, magmas reaching the upper crust were either the residual liquids related to the formation of the amphibolitic cumulates, or were derived from moderate to high degrees of melting of this cumulate material. In the absence of pronounced structural permeability, these 'normal' Andean magmas were stored in the crust and assimilated substantial amounts of felsic crustal materials (Icanche Formation and related stocks). Slab-related metasomatism was ongoing through the Eocene, and ultimately drove the oxidation state of the sub-arc cumulates to the point that chalcophile metals could be released into hydration-related partial melts. These volatile- and metal-charged fertile magmas were low-volume, and required a highly specialised structural environment to be able to ascend into the brittle shallow crust without freezing.

At other times in the Andean geological record, such specialised environments appear to have been provided by coincidence of compression and stress perturbation by subducted aseismic ridges or oceanic plateaux. In the Eocene-Oligocene Central Andes, a different structural environment is required by the long arc-segment over which mineralisation was effectively synchronous. Deposit-, and district-scale structural interpretations made on the basis of this study suggest that mineralisation accompanied a proposed change in the sense of along-arc strike slip shear. This change is envisaged to have been driven by lateral escape related to differential shortening along the arc and the resultant bending of the Bolivian Orocline. Sinsitral along-arc shear was in opposition to the lateral component of tectonic convergence, and the transfer was both protracted and stuttered, with multiple reversals in sense of shear before the eventual dominance of sinistral shear after 31 Ma. Fertile magmas were uniquely able to reach the shallow crust and cause porphyry copper mineralisation

during the dynamic strain environment offered the counter-tectonic along-arc shear imposed by bending of the Bolivian Orocline. The absence of magmatic products in the Central Andes between 31 and 27 Ma might reflect either the reduction in dynamism of the strain environment, or a wholesale decrease in magma productivity following establishment of a genuine flat slab subduction geometry.

7.7 Applications in Exploration

This thesis, as well as the broader P765 AMIRA International project was sponsored by mining companies with active exploration divisions. The research themes are a balance between academic and mineral industry goals. The utility of several of the results in mineral exploration are detailed below.

7.7.1 Mapping and Structural Architecture

Mapping is arguably the most under-utilised exploration tool; it is expensive, slow, and demands large amounts of time in the field away from facilities and relationships. This study has shown that substantially pre-mineral extensional faults and dykes are the major control on porphyry copper localisation at Collahuasi. Many of the major structural elements of the Collahuasi district are evident as linear elements or discontinuities in topography, airborne geophysics, or remote imagery (e.g., Landsat). However, the Triassic dykes that coincide with the positions of the Rosario and Ujina deposits are not evident in this data. Likewise, without detailed mapping, the discrimination of basement-age growth faults such as the Quebrada Blanca Fault that localised mineralisation would be impossible. Especially during exploration in terranes with poorer exposure or access, mapping may identify basement extensional elements that can be projected under vegetation or stratigraphic cover. The intersections or discontinuities in these structures would represent blind or hidden targets.

It is also apparent that the two smaller deposits at Collahuasi are located close to the principal arc-parallel fault system (Domeyko Fault), whereas the two larger deposits are located along second-order structures. Whereas the first order regional structures are an obvious (and in the case of Chuquicamata, productive) target, mapping will be key in recognising second order structures that are at least as favourable targets.

7.7.2 Conceptual Structural Targets and Tectonic Evolution

Structural results presented in Chapters 4 and 5 demonstrate that the strain accommodated in the immediate porphyry environment changed dramatically within the timeframe of hydrothermal activity at all four porphyry centres at Collahuasi. Importantly, this variability means that sites on strike-slip faults that were dilational anomalies during broadly transpressional regimes are mineralised regardless of whether they were dilational under dextral or sinistral shear. This came about because of fluctuation in the sense of lateral shear contrary to the net tectonic convergence. Therefore structural targeting that uses a strike slip releasing bend model should include sites interpreted to be restraining under the generalised far field stress condition. Once some independent evidence of alteration has been found, I speculate that these 'counter-intuitive' sites should rank as more favourable since their dilation demands a more dramatic strain anomaly within the magmatic arc.

7.7.3 Sinistral Offset of the Copaquire Porphyry

The location of the Copaquire Porphyry west of the Domeyko Fault poses an immediate possibility of an as yet undiscovered mineral district if one believes that ~37 kms of post-mineralisation sinistral slip has been accommodated on this structure. North of Collahuasi, Miocene to Pliocene ignimbrite cover becomes more extensive, thus increasing the chances that more porphyry copper or high sulfidation systems remain to be discovered in northernmost Chile. Locating other deposits that may have formed roughly east of Copaquire will be complicated by the effects of increased shortening, more chaotic block rotations and related breakdown of the along-arc shear couple that characterised the flanks of the Bolivian Orocline. The net offset at the latitude of Copaquire is likely to be less than the 37 kms estimated from the Chuquicamata district.

7.7.4 Alteration Textures and Mineral Assemblages

Propylitic Alteration. The gross plan-view distribution of alteration zones about porphyry copper deposits has long been established and used effectively in exploration. The results of this study add some detail to that scheme, and also show the extent to which lithology and structure control the distribution of alteration.

Generally, alteration patterns around Rosario-La Grande and Ujina suggest that increases in the proportion of epidote that occur as veins, and in the association of sphalerite, pyrite and/or magnetite with epidote may indicate more proximal alteration subzones. In contrast, the most distal occurrences of epidote N of Rosario and NE of Quebrada Blanca are characterised by highly alkaline oxidising assemblages including red hematite-albite intergrowths. Rock permeability, more than fracture density, controls epidote distribution around Quebrada Blanca. There is strong selective epidote alteration in andesitic epiclastic host units, whereas epidote is restricted to amygdales and minor fracture surfaces in more proximal and Ca-poor lithologies. The Quebrada Blanca example demands that propylitic alteration assemblages can not be interpreted effectively without stratigraphic mapping.

Secondary Copper Minerals. Interpretation of outcropping mineralised structures at La Grande is complex because several generations of pyritic alteration all oxidise to visually similar iron oxide-rich gossans. Discrimination of structures that originally hosted primary Cu-As sulfosalts was possible because they produce secondary arsenate minerals that are easily identified by colour and crystal form. These are a particularly effective targeting tool as they are largely endogenous. In contrast, abundant chrysocolla is distributed over a larger area than hypogene pyritic alteration related to the Rosario-La Grande system, and is almost ubiquitously exogenous.

7.7.5 Magmatic Chemistry

Magmatic fertility criteria are conventionally interpreted as a numeric score (either a bulk value or a ratio) which can be used simply to classify magmatic rocks as ‘fertile’ or ‘infertile’. Since different criteria reflect different aspects of the magmatic evolution, then the ‘fertility’ of samples that satisfy multiple diverse criteria can be interpreted with more confidence than those that satisfy only some. There are problems with this approach however, as the thresholds and the robustness of the discrimination varies between terranes and between calc-alkaline and alkalic magma series. For example, in the Andes, fertile intrusions typically have bulk Y < 10 ppm, but this criterion does not adequately distinguish SW Pacific mineralised suites. Further, the utility of the method is limited since the distinctive characteristics are most evident among the productive intrusions and much less so among widespread

associated suites. In most cases, zones of recognizable hydrothermal alteration at outcrop scale are likely to be apparent long before analytical results are received.

Instead, this study has highlighted trends defined by suites of samples including those produced before main stage mineralisation (and less commonly afterwards). These trends (such as convex REE Harker plots and flat or compatible HFSE Harker plots) can be recognised among new and literature data for the Andes, and among roughly equivalent data for porphyry copper districts in the SW Pacific. I speculate that such trends should be defined by all products in a discrete episode of arc magmatism, where episodes might last tens of millions of years, and are punctuated by major magmatic hiatuses or migration of the arc front. These trends are interpreted to reflect the gross tectonic conditions that led to development of sub-arc ilmenite-amphibolites and their subsequent melting. Using this approach, any suite of arc magmas showing this HFSE and REE behaviour, as well as V/Sc that is stable, or increases with increasing with silica, would generically be considered fertile.

7.8 Directions for Future Research

The breadth of exposure, near-absence of vegetation, and prolific mineral deposits make Collahuasi is a wonderful natural laboratory. Several lines of further investigation were underway prior to-, and during 2009, and I would propose that several others might be valuable:

7.8.1 Relationships between alteration mineralogy/intensity, structural geology and geophysical responses at Rosario-La Grande.

Electrical geophysical methods were used successfully in the original discovery and delineation of the Ujina and Rosario porphyry copper deposits, and more recently in the delineation of the extent of alteration related to the La Grande HS system. Alteration at Rosario and La Grande is imaged in plan as a pronouced polygonal ring-shaped resistivity low/chargeability high centred approximately on Cerro la Grande. Conventional models might lead to interpretation of the ring feature as surrounding a central intrusive source. However, the Rosario porphyry occupies the northern margin of the ring, and the main sub-surface supergene La Grande deposit occupies part of its western margin. I suspect instead that pyritic high sulfidation

alteration, or perhaps the supergene weathering of this material, was focused along a series of faults (clockwise from La Grande: Monctezuma, Rosario, Lulu, Chiclla) that were active together. Closer integration of alteration mapping, structural mapping and 3D modeling of the geophysical response might help mineral explorers to interpret more accurately their early stage surface geophysical results.

7.8.2 Supergene Cu enrichment at La Grande

The northern part of the La Grande HS alteration system partly overlaps the stockwork related to the Rosario Porphyry, but large volumes of pyritic rock up to 3 kms outboard of the porphyry have strong supergene chalcocite development. Simple mass balance calculations suggest that the massive sulfide La Grande veins must have had vertical extent of ~1 km if they were the primary source of this supergene copper. Alternatively, had groundwaters that caused the supergene leaching flower laterally, copper might have been redistributed from Rosario to La Grande. Neither scenario seems likely, and more work is warranted to explain the evolution of the La Grande supergene profile.

7.8.3 Surface manifestation of blind HS vein systems at La Grande

The outcropping gossanous fault zones and veins on Cerro La Grande are apparently not rooted in significant mineralisation at depth. Instead, the most significant bodies of alteration at La Grande are largely blind; and are recognised only as narrow (2-5 m) zones of kaolinitisation in surface trenches. La Grande therefore provides an opportunity to develop and test methods that might help explorers rank HS drill targets based on limited surface exposure and data. A corollary of this would be to investigate vertical changes in the alteration distribution and mineralogy of the La Grande system. P765 touched on both of these topics, but a more thorough approach could be useful.

7.8.4 Hyperspectral responses of porphyry and HSE-related alteration.

During this study, I investigated the hyperspectral (ASTER) response over the entire district. The major mineral deposits are identified as the loci of occurrence of alunite and pyrophyllite, but it is unclear the extent to which this is a response to

dust generated by the mining operations. Critically, false positives were generated from the salt lakes in the eastern edge of the district, and several apparently genuine anomalies were also generated. These may warrant further exploration, but from a technical standpoint, it seems that more work is needed to resolve real alteration-related anomalies from artifacts. Further, while the alteration mineralogy of porphyry copper systems is well known among volcanic host sequences, there may also be value in investigating the spectral response generated in carbonate-clay dominated sedimentary host sequences such as the Quehuita Formation west of the Domeyko Fault.

7.8.5 Extensions to the chemistry of peripheral-facies alteration minerals

The chemistry of epidote and chlorite was one of the major themes of the P765 research project to which this thesis belongs. Initial results suggest far greater transition metal substitution into epidote than previously suspected, and far greater apparent solubility of REE and HFSE in the fluids that cause propylitic alteration (Ireland et al., 2006). Those results open two related avenues for further investigation. Locally, sufficient Pb is present in epidote alteration around the Rosario porphyry that the Pb isotopic composition could be determined. This would add to our understanding of the source of metals precipitated in the edges of porphyry-related hydrothermal systems.

Zirconium, yttrium and most other REE are also abundant in epidote (relative to the whole rocks) at La Grande. These are elements traditionally considered to be effectively immobile in most hydrothermal environments. Resolution of the mobility or immobility of these elements during alteration may therefore impact on the interpretation of the magmatic chemistry of related intrusion.

7.8.6 Constraining fertile petrogenesis

The hypothesis put forward for fertile petrogenesis in this study makes some important assumptions where appropriate experimental data are unavailable. Notably, ilmenite-melt HFSE and LREE partitioning behaviour has only been documented in one study of felsic volcanic rock. No data are available for basaltic and andesitic liquids, nor at pressures more appropriate for the base of the continental crust.

Likewise, there is scant available amphibole-melt LREE- of HFSE partitioning data for felsic liquids (although there is voluminous data for mafic liquids). Experimental studies that address these gaps in mineral-melt partitioning datasets would allow much better evaluation of the hypotheses of arc petrogenesis related to porphyry copper metallogeny.